

# **Ferroelectrets: Heterogenous Polymer Electrets with High Electromechanical Response**

Habilitationsschrift zur Erlangung des akademischen Grades

doctor rerum naturalium habilitatus

(Dr. rer. nat. habil.)

der Mathematisch-Naturwissenschaftlichen Fakultät  
der Universität Potsdam

vorgelegt von

**DR. XUNLIN QIU**

geb. am 21. Juli 1978

Potsdam, 06. November 2016

Published online at the  
Institutional Repository of the University of Potsdam:  
URN urn:nbn:de:kobv:517-opus4-398425  
<http://nbn-resolving.de/urn:nbn:de:kobv:517-opus4-398425>

## Abstract

Ferroelectrets are internally charged polymer foams or cavity-containing polymer-film systems that combine large piezoelectricity with mechanical flexibility and elastic compliance. The term “ferroelectret” was coined based on the fact that it is a space-charge **electret** that also shows **ferroic** behavior. In this thesis, comprehensive work on ferroelectrets, and in particular on their preparation, their charging, their piezoelectricity and their applications is reported.

For industrial applications, ferroelectrets with well-controlled distributions or even uniform values of cavity size and cavity shape and with good thermal stability of the piezoelectricity are very desirable. Several types of such ferroelectrets are developed using techniques such as straightforward thermal lamination, sandwiching sticky templates with electret films, and screen printing. In particular, fluoroethylenepropylene (FEP) film systems with tubular-channel openings, prepared by means of the thermal lamination technique, show piezoelectric  $d_{33}$  coefficients of up to 160 pC/N after charging through dielectric barrier discharges (DBDs). For samples charged at suitable elevated temperatures, the piezoelectricity is stable at temperatures of at least 130 °C. These preparation methods are easy to implement at laboratory or industrial scales, and are quite flexible in terms of material selection and cavity geometry design. Due to the uniform and well-controlled cavity structures, samples are also very suitable for fundamental studies on ferroelectrets.

Charging of ferroelectrets is achieved via a series of dielectric barrier discharges (DBDs) inside the cavities. In the present work, the DBD charging process is comprehensively studied by means of optical, electrical and electro-acoustic methods. The spectrum of the transient light from the DBDs in cellular polypropylene (PP) ferroelectrets directly confirms the ionization of molecular nitrogen, and allows the determination of the electric field in the discharge. Detection of the light emission reveals not only DBDs under high applied voltage but also back discharges when the applied voltage is reduced to sufficiently low values. Back discharges are triggered by the internally deposited charges, as the breakdown inside the cavities is controlled by the sum of the applied electric field and the electric field of the deposited charges. The remanent effective polarization is determined by the breakdown strength of the gas-filled cavities. These findings form the basis of more efficient charging techniques for ferroelectrets such as charging with high-pressure air, thermal poling and charging assisted by gas exchange. With the proposed charging strategies, the charging efficiency of ferroelectrets can be enhanced significantly.

After charging, the cavities can be considered as man-made macroscopic dipoles whose direction can be reversed by switching the polarity of the applied voltage. Polarization-*versus*-electric-field ( $P(E)$ ) hysteresis loops in ferroelectrets are observed by means of an electro-acoustic method combined with dielectric resonance spectroscopy.  $P(E)$  hysteresis loops in ferroelectrets are also obtained by more direct measurements using a modified Sawyer-Tower circuit. Hysteresis loops prove the ferroic behavior of ferroelectrets. However, repeated switching of the macroscopic dipoles involves complex physico-chemical processes. The DBD charging process generates a cold plasma with numerous active species and thus modifies the inner polymer surfaces of the cavities. Such treatments strongly affect the chargeability of the cavities. At least for cellular PP ferroelectrets, repeated DBDs in atmospheric conditions lead to considerable fatigue of the effective polarization and of the resulting piezoelectricity.

The macroscopic dipoles in ferroelectrets are highly compressible, and hence the piezoelectricity is essentially the primary effect. It is found that the piezoelectric  $d_{33}$  coefficient is proportional to the polarization and the elastic compliance of the sample, providing hints for developing materials with higher piezoelectric sensitivity in the future. Due to their outstanding electromechanical properties, there has been constant interest in the application of ferroelectrets. The antiresonance frequencies ( $f_p$ ) of ferroelectrets are sensitive to the boundary conditions during measurement. A tubular-channel FEP ferroelectret is conformably attached to a self-organized minimum-energy dielectric elastomer actuator (DEA). It turns out that the antiresonance frequency ( $f_p$ ) of the ferroelectret film changes noticeably with the bending angle of the DEA.

Therefore, the actuation of DEAs can be used to modulate the  $f_p$  value of ferroelectrets, but  $f_p$  can also be exploited for in-situ diagnosis and for precise control of the actuation of the DEA. Combination of DEAs and ferroelectrets opens up various new possibilities for application.

## Zusammenfassung

Ferroelectrets sind intern geladene Polymerschäume oder Polymerfilmsysteme mit definierten Hohlräumen, die große piezoelektrische Koeffizienten mit guter mechanischer Flexibilität und hoher elastischer Nachgiebigkeit vereinen. Der Begriff "Ferroelectret" weist darauf hin, dass es sich um einen Ladungselectret handelt, der gleichzeitig ferroisches Verhalten zeigt. In der vorliegenden Arbeit werden umfangreiche Untersuchungen an Ferroelectretten, insbesondere zu ihrer Herstellung und Aufladung, ihrer Piezoelektrizität sowie ihren Anwendungen beschrieben und diskutiert.

Für industrielle Anwendungen sind Ferroelectrete mit gut kontrollierten Verteilungen oder sogar einheitlichen Werten von Hohlraumgröße und Hohlraumform und mit hoher thermischer Stabilität der Piezoelektrizität sehr wünschenswert. Mehrere Typen solcher Ferroelectrete werden unter Verwendung von thermisch laminierten Folien, von Schichtaufbauten mit aufeinander haftenden Electretfilmen und von Siebdruck-Verfahren entwickelt. Insbesondere zeigen durch thermisches Laminieren hergestellte Kopolymer-Filmsysteme aus Fluor-Ethylen-Propylen (FEP) mit röhrenförmigen Kanälen parallel zur Oberfläche nach Aufladung durch dielektrische Barrierenentladungen (DBDs) piezoelektrische  $d_{33}$ -Koeffizienten von bis zu 160 pC/N. Bei Proben, die bei erhöhten Temperaturen aufgeladen werden, ist die Piezoelektrizität bis mindestens 130 °C stabil. Die Herstellungsverfahren sind leicht im Labor- oder im Industriemaßstab zu realisieren, und sie sind hinsichtlich der Materialauswahl und der Hohlraumgeometrie sehr flexibel verwendbar. Aufgrund der gleichmäßigen und gut kontrollierbaren Hohlraumstrukturen eignen sich solche Proben auch für Grundlagenuntersuchungen an Ferroelectretten.

Das Aufladen von Ferroelectretten erfolgt über dielektrische Barrierenentladungen (DBDs) innerhalb der Hohlräume. In der vorliegenden Arbeit wird diese Polungstechnik mittels optischer, elektrischer und elektroakustischer Verfahren umfassend untersucht. Das Spektrum des transienten Lichts aus den DBDs in zellulären Polypropylen (PP)-Ferroelectretten bestätigt die Ionisierung von molekularem Stickstoff und ermöglicht die Bestimmung des lokalen elektrischen Felds in der Entladung. Die damit verbundene Lichtemission zeigt nicht nur DBDs bei hoher angelegter Spannung, sondern auch Rückentladungen, wenn die angelegte Spannung auf ausreichend niedrige Werte reduziert wird. Die Rückentladungen werden durch die deponierten Ladungen ausgelöst, da der elektrische Durchschlag in den Hohlräumen durch die Summe des von außen angelegten elektrischen Felds und des elektrischen Felds der deponierten Ladungen bestimmt wird. Die remanente Polarisierung wird durch die Durchschlagsfestigkeit der gasgefüllten Hohlräume begrenzt. Diese Erkenntnisse bilden die Grundlage für effizientere Aufladungsverfahren für Ferroelectrete wie z.B. das Aufladen in Luft unter erhöhtem Druck, das thermische Polen und das Aufladen mit gezieltem Gasaustausch. Mit den vorgeschlagenen Aufladestrategien kann die Effizienz der Aufladung von Ferroelectretten deutlich gesteigert werden.

Die intern geladenen Hohlräume können als makroskopische Dipole betrachtet werden, deren Orientierung durch Umschalten der Polarität der angelegten Spannung umgekehrt werden kann. Hysteresekurven für das Verhalten der elektrischen Polarisierung bei Variation des elektrischen Felds, d.h. sogenannte  $P(E)$ -Hysteresekurven, können in Ferroelectretten mittels eines elektroakustischen Verfahrens in Kombination mit der dielektrischen Resonanzspektroskopie beobachtet werden. Darüber hinaus können  $P(E)$ -Hysteresekurven auch durch direkte Messung des Polarisationsstromes unter Verwendung einer modifizierten Sawyer-Tower-Schaltung erhalten werden. Solche Hystereseschleifen sind ein direkter Nachweis des ferroischen Verhaltens der



Ferroelektrete. Das wiederholte Schalten der makroskopischen Dipole ist jedoch von komplexen physikalisch-chemischen Prozessen begleitet. Der DBD-Ladeprozess erzeugt ein kaltes Plasma mit zahlreichen aktiven Spezies und modifiziert dadurch die inneren Oberflächen der Hohlräume. Dies wirkt sich in erheblichem Maße auf die wiederholte Aufladbarkeit der Hohlräume aus. So führen bei zellulären PP-Ferroelektreten wiederholte DBDs unter normalen atmosphärischen Bedingungen zu einer deutlichen Reduzierung der effektiven Polarisierung und der daraus resultierenden Piezoelektrizität.

Die makroskopischen Dipole in Ferroelektreten sind hoch-kompressibel, daher beruht die Piezoelektrizität im Wesentlichen auf dem primären piezoelektrischen Effekt, d.h. der Veränderung der Dipolmomente. Es wurde festgestellt, dass der piezoelektrische  $d_{33}$ -Koeffizient proportional zur elektrischen Polarisierung und zur elastischen Nachgiebigkeit der Probe ist. Daraus können Folgerungen für die künftige Entwicklung von Materialien mit höherer piezoelektrischer Empfindlichkeit gezogen werden. Aufgrund ihrer hervorragenden elektromechanischen Wandler-Eigenschaften besteht ständiges Interesse an der Anwendung von Ferroelektreten. Die Antiresonanzfrequenzen ( $f_p$ ) von Ferroelektreten hängen von den Randbedingungen des jeweiligen Experiments ab. So wurde ein FEP-Ferroelektret mit röhrenförmigen Kanälen mit einem dielektrischen Elastomer-Aktuator (DEA) in einer sich selbst einstellenden Konfiguration minimaler Energie kombiniert. Es zeigte sich, dass sich die Antiresonanzfrequenz des Ferroelektretfilms mit dem Biegewinkel des DEA merklich ändert. Somit können DEAs zur Modulation des  $f_p$ -Wertes von Ferroelektreten eingesetzt werden, und umgekehrt können piezoelektrische Antiresonanzen für die in-situ-Diagnose und für eine präzise Ansteuerung von DEAs Anwendung finden. Auf diese Weise eröffnet die Kombination von DEAs und Ferroelektreten neue Anwendungsperspektiven nicht nur in der Sensorik und der Aktorik, sondern auch zur Energiegewinnung aus der Umgebung (sogenanntes "energy harvesting").



# Contents

<b>1</b>	<b>Introduction</b>	<b>1</b>
<b>2</b>	<b>A Brief History of Ferroelectrets</b>	<b>3</b>
<b>3</b>	<b>Ferroelectret Systems</b>	<b>5</b>
<b>4</b>	<b>Charging Process</b>	<b>9</b>
4.1	Charging Mechanisms . . . . .	9
4.1.1	Micro-plasma Discharge in Cavities . . . . .	9
4.1.2	Polarization <i>vs.</i> Electric Field Hysteresis . . . . .	12
4.2	Thermal Poling of Ferroelectrets . . . . .	14
4.3	Poling Assisted by Gas Exchange . . . . .	15
<b>5</b>	<b>Piezoelectricity of Ferroelectrets</b>	<b>17</b>
<b>6</b>	<b>Applications</b>	<b>21</b>
<b>7</b>	<b>Conclusions and Outlook</b>	<b>22</b>
	<b>References</b>	<b>24</b>
	<b>Appendix</b>	<b>34</b>
<b>A</b>	<b>Journal and Review Articles</b>	<b>34</b>
	Barrier discharge in ferroelectrets... (J. Appl. Phys. <b>101</b> , 104112 (2007)) . . . . .	37
	Spectroscopic study of ferroelectrets... (Appl. Phys. Lett. <b>91</b> , 132905 (2007)) . . . . .	44
	Influence of gas pressure . . . (Appl. Phys. Lett. <b>92</b> , 052901 (2008)) . . . . .	47
	Effective polarization fatigue . . . (Appl. Phys. Lett. <b>93</b> , 152902 (2008)) . . . . .	50
	Tubular-channel FEP ferroelectrets . . . (J. Appl. Phys. <b>106</b> , 014106 (2009)) . . . . .	53
	Patterned piezo-, pyro-, and ferroelectricity... (J. Appl. Phys. <b>108</b> , 011101 (2010)) . . . . .	58
	Mapping polarization in ferroelectrets . . . (Appl. Phys. Lett. <b>97</b> , 072905 (2010)) . . . . .	78
	Polarization build-up in ferroelectrets... (IEEE TDEI <b>17(4)</b> , 1043 (2010)) . . . . .	81
	Beneficial and detrimental fatigue effects... (J. Appl. Phys. <b>110</b> , 024108 (2011)) . . . . .	88
	DBD charging in ferroelectrets . . . (IEEE TDEI <b>18(1)</b> , 34 (2011)) . . . . .	96
	Combination of elastomer and ferroelectret . . . (Appl. Phys. A <b>107</b> , 583 (2012)) . . . . .	105
	Direct hysteresis measurements . . . (J. Appl. Phys. <b>113</b> , 224106 (2013)) . . . . .	111

Screen printing for ferroelectrets ... (Appl. Phys. A <b>114</b> , 515 (2014)) . . . . .	119
Polarization in FEP ferroelectrets ... (Ferroelectrics <b>472</b> , 100 (2014)) . . . . .	125
Polymer electret and ferroelectret materials ... (Book chapter in <b>Electromechanically Active Polymers</b> (2016)) . . . . .	135
Thermal poling of ferroelectrets ... (Appl. Phys. Lett. <b>108</b> , 252901 (2016)) . . .	164
Efficient charging with gas exchange ... (Appl. Phys. Lett. <b>109</b> , 222903 (2016))	168
<b>B Curriculum Vitae</b>	<b>172</b>
<b>Acknowledgments</b>	<b>173</b>

# 1 Introduction

The demand for advanced functional materials in transducer technology is growing rapidly. Piezoelectric/electrostrictive materials transform mechanical variables (displacement or force) into electrical signals (charge or voltage) and vice versa. They are suitable for a large range of existing or conceivable applications. Some, but not all, piezoelectric materials also exhibit pyroelectricity which transforms temperature variations into electrical currents and is used mainly in sensors, whereas the reverse electrocaloric effect has been more intensively studied only recently [1–3]. Sometimes, piezoelectricity is also connected with ferroelectricity – the existence of a spontaneous and remnant polarization that can be re-oriented in sufficiently high electric fields.

Studies on piezoelectricity started with crystalline polar materials containing intrinsic dipolar units. In 1880 and after, Pierre and Jacques Curie discovered piezoelectricity in natural crystals such as tourmaline, quartz and Rochelle salt. Since then, many fundamental and technological studies were devoted to linear and non-linear electromechanical properties of materials. Lead zirconate titanate (PZT), discovered in the 1940s, has become the most widely used ceramic piezoelectric material because of its high piezoelectric coefficient [4]. Together with other ferro-, pyro- and piezoelectric crystals such as barium titanate or lead niobate, PZT crystallites exhibit perovskite structure with the chemical formula  $ABO_3$ . Below the Curie transition temperature, the titanium cation is shifted along the  $c$  axis of the tetragonal unit cell, which leads to a spontaneous polarization. The crystalline domains are usually randomly oriented, but can be aligned through poling in strong electric fields. Piezoelectricity in PZT stems from deformation of the intrinsic dipoles, *i.e.* the movement of titanium cations along the  $c$  axis upon changes in the mechanical or electrical stress (primary piezoelectricity).

Around 1970, piezo- and pyroelectricity in electrically poled poly(vinylidene fluoride) (PVDF) was first reported [5], which triggered extensive research on ferro-, pyro- and piezoelectric polymers [6, 7]. PVDF (chemical formula  $[CH_2CF_2]_n$ ) is a semi-crystalline fluoropolymer which usually forms spherulites consisting of crystalline  $\alpha$ -phase lamellae in an amorphous matrix. In the crystalline  $\beta$  phase, the molecular chains assume an all-trans (zig-zag) conformation.  $\beta$ -phase molecules exhibit net dipole moments that are parallel in each crystallite and can be reoriented in a sufficiently strong electric field. A macroscopic net polarization is attained when the crystallites are preferentially oriented through poling. At least above the respective glass-transition temperature, the amorphous phase is much softer (hence more compressible) than the crystalline phase, and therefore the piezoelectricity in PVDF originates mainly from changes in the dipole density (secondary piezoelectricity). A number of further ferroelectric polymers have been identified and explored – among them copolymers of VDF and trifluoroethylene (TrFE), tetraflu-

oroethylene (TFE) or hexafluoropropylene (HFP), some odd-numbered polyamides, and aromatic or aliphatic polyureas.

Later, piezoelectric ceramic-polymer composites were developed with the intention of combining desirable material properties of each component. Most piezoelectric composites are di-phasic systems consisting of an active ceramic phase and a passive polymer phase. Newnham *et al.* proposed the concept of connectivity to characterize how each phase is physically self-connected [8]. In their notation for piezoelectric composites, the first number denotes the connectivity of the active ceramic phase, and the second number represents the connectivity of the passive polymer phase. For example, in a so-called 0 – 3 piezoelectric composite, isolated ceramic particles are dispersed in a polymer matrix. Based on this concept, a number of ceramic-polymer piezoelectric composites with improved overall properties compared to each individual component have been designed, prepared and studied [9]. In view of all these concepts, piezoelectricity is often assumed to be possible only in polar – *i.e.* dipole-containing – materials.

During the last two decades, the family of piezoelectric materials has received a new member – the so-called “ferroelectret” [10]. Ferro- or piezoelectrets are internally charged non-polar polymer foams. Polymer foams are widely used in our daily life, for instance, as packaging materials for candies and chocolates. A frequently adopted method to produce polymer foams is stretching filler-loaded polymers. Tiny mineral particles are often employed as fillers that serve as stress concentrators for micro-cracks during stretching of the film. Simultaneous or sequential stretching in two perpendicular directions results in films with lens-like cavities in the case of ferroelectrets. The polymer itself is a space-charge electret that can quasi-permanently store real charges of both polarities [11]. Thus, it came as a big surprise that completely non-polar polymer foams can behave almost like ferroelectrics. It has been found that the cavities inside the material can be internally charged at high electric fields by means of micro-plasma discharges (also known as dielectric barrier discharges or DBDs). The charged cavities form macroscopic dipoles whose orientation can be switched by reversing the polarity of the applied electric field [12]. Figure 1(a) shows a typical scanning electron microscope (SEM) image of the cross section of a cellular PP films [13]. The macroscopic dipoles (internally charged cavities) deform when the film is subjected to mechanical stress. The resultant change of the density of macroscopic dipole moments introduces a voltage (open circuit) or current (short circuit) between the two electrodes (Fig. 1(b)). This is known as direct piezoelectric effect. As for inverse piezoelectric effect, the macroscopic dipoles change their dimension upon the application of an additional voltage to the two electrodes.

Dielectric elastomers (DEs) are another group of electro-active polymers that connect mechanical and electrical signals [14]. They are soft polymeric dielectrics extensively studied for use in artificial muscles. Usually, the elastomer layer is coated on both surfaces with compliant electrodes, thus forming a “rubber capacitor”. Charges of opposite polarity ap-

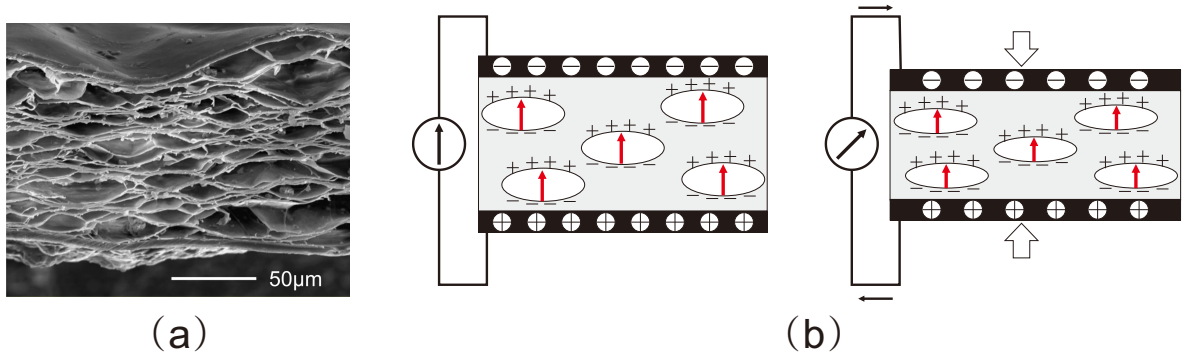


Figure 1: (a) SEM image of the cross-section of a cellular PP film [13]. (b) Schematic representation of the primary piezoelectricity in cellular PP ferroelectrets.

pear on the electrodes when a voltage is applied, causing an electrically induced mechanical stress (“Maxwell stress”) on the DE layer. Consequently, the DE shrinks in thickness and expands in area. The DE material is so soft that actuation strains up to several hundred percent can be achieved. Four types of material are widely used for DE actuators: Acryl polymers such as VHB (3M), silicone elastomers such as poly(dimethylsiloxane) (PDMS), a range of suitable polyurethanes (PUs), and thermoplastic elastomers such as styrene-ethylene/butylene-styrene tri-block copolymer (SEBS).

Advanced sensors and actuators are essential for smart systems that enable a higher quality of life in modern societies. Traditionally, hard solid-state materials have been the prime candidates for sensors and actuators because they are well understood and easily integrated into silicon-based electronic systems. Up to now, commercially available materials with strong piezoelectricity have usually been inorganic single crystals or ceramics. However, they provide only rather narrow ranges of essential properties such as specific acoustic impedance, attainable resonance frequencies and useful frequency range, etc., and do not lend themselves easily to many specific applications. Polymers are advantageous over inorganic materials in respect of some of the essential properties. Therefore, the discovery of piezoelectricity in PVDF aroused intensive research on piezoelectric polymers. The application of piezoelectric polymers is, however, limited by their relatively weak piezoelectricity (for PVDF:  $d_{33}=15\sim 20$  pC/N;  $d_{31}=25\sim 30$  pC/N). Ferroelectrets combine large piezoelectricity with mechanical flexibility and elastic compliance, and thus own some of the respective advantages of piezoelectric ceramics and polymers. The exciting development significantly enlarges the range of piezoelectric materials.

## 2 A Brief History of Ferroelectrets

Cellular polymers (polymer foams) were produced as early as during the 1960s [15]. The voided structure not only renders polymer foams lightweight, but also leads to mechanical,

thermal as well as electrical properties that may be quite different from those of their non-voided counterparts. Thanks to their special properties, polymer foams are now widely used in our daily life for thermal insulation, shock and sound absorption, packaging, etc.

Already during the 1970s, piezo- and pyroelectric effect of noncentrosymmetric electrically charged nonpolar polymers were theoretically predicted and also experimentally studied to some extent [16,17]. However, the research interest faded because of the rather weak piezo- and pyroelectricity obtained at that time. A breakthrough came with the invention of cellular polypropylene films and the investigation of their electromechanical properties in late 1980s [18,19]. In the pioneering works, the electromechanical or electrothermalmechanical cellular PP foams were employed in several applications such as capacitive sensors and electrostatic actuators. The former can detect small pressure- or temperature-induced film-thickness changes, while the latter can generate quite large thickness change upon application of a large electric field. Moreover, it was already pointed out that the foams are charged in such a way that electric charges of opposite polarities are deposited on both sides of the lenslike bubbles.

In 1990s, a number of potential applications of cellular polypropylene (PP) foams were studied such as applications in thermoelectrical energy conversion, in sensing mechanical movements of animals and humans, in actuation of micromovements, etc. Cellular PP foams are highly nonuniform materials. The lenslike cavities have lateral dimensions (usually tens to hundred  $\mu\text{m}$ ) much larger than their thickness (usually several to ten  $\mu\text{m}$ ). Based on this, Paajanen *et al.* and Sessler *et al.* reported a simplified layer-model for the piezoelectricity of cellular PP foams in 1999 [20,21]. The model consists of alternative polymer and air layers. The space charges trapped at the top and bottom polymer surfaces of each air gap are taken to be opposite in polarity and equal in magnitude, since they originate from the dielectric barrier discharges (DBDs) in the air gap during charging. DBDs only lead to charge separation but not to the generation of excess charges of one polarity. Model analysis indicates that the piezoelectricity of cellular PP foams is essentially proportional to the effective polarization (*i.e.* the density of macroscopic dipoles) and the elastic modulus of the material.

While the interest in potential applications of cellular PP foams continued, more and more fundamental studies were also carried out, in which the charging mechanism as well as the direct and converse piezoelectricity are investigated. In 2002, the first review on the topic was published [22]. In 2004, Bauer and colleagues proposed a new term, *i.e.* Ferroelectrets, for the internally charged non-polar polymer foams [23]. The term was coined based on the fact that these are space-charge electrets that also exhibit ferroic behavior.

More recently, much efforts have also been devoted to seeking ferroelectrets from different materials by means of a variety of preparation methods. The aim is to develop ferroelectrets with superior piezoelectric properties and/or with well-controlled uniform cavity



size and cavity shape. A considerable number of cellular polymer foams and polymer film systems containing internal cavities have been developed and identified as ferroelectrets. Following the early example of cellular PP ferroelectret, cellular foam ferroelectrets have been developed from polyesters (polyethylene terephthalate PETP and poly(ethylene naphthalate) PENP), cyclo-olefin copolymer (COC), and fluoroethylenepropylene (FEP). The cellular structure, formed by techniques such as stretching filler-loaded polymer melt or foaming with supercritical CO<sub>2</sub>, can be adjusted and optimized with gas-diffusion expansion process. Besides, the number of ferroelectrets of polymer film systems with internal cavities is rapidly increasing. These are layer structures, composed of hard (solid) and soft (highly porous) polymer layers, and polymer film systems containing regular cavities. Polytetrafluoroethylene (PTFE) (solid or porous) and polycarbonate (PC) are also added to the list of candidate materials for making this type of ferroelectrets. These exciting developments significantly enlarge the range of functional space-charge polymer electrets and bring forth numerous novel applications in, for instance, tactile sensors, ultrasonic devices, vibration energy harvesters, etc. For a more detailed account of the history of ferroelectret research, see Refs. [10, 12, 22, 24–29].

### 3 Ferroelectret Systems

As mentioned in section 2, extensive studies on ferroelectrets were initiated around 1990 by colleagues from Finland using cellular PP. Since then, cellular PP has become the workhorse of ferroelectret research and technology due mainly to its high piezoelectricity, its availability and its ease of processing. However, cellular PP ferroelectrets are not free of problems. First of all, the piezoelectricity of cellular PP ferroelectrets is stable only up to 60 °C, which limits their application [30]. Also, the cavities in cellular PP foams always have a rather wide and not so well-controlled size and shape distribution so that only some of the cavities are optimal for charging and for transducer operation. For industrial applications, films with well-controlled distributions or even uniform values of cavity size and cavity shape are very desirable. Such films may be easily produced on a large scale with good reproducibility. In recent years, a number of ferroelectrets have been developed through different preparation strategies. The current state of available ferroelectrets has been summarized in a recent review [31] (cf. p. 135). Overall, ferroelectrets that are available so far can be classified into three categories.

#### (1) Cellular polymer foams

Numerous lens-shaped cavities are distributed inside the material. The cavities have a thickness of several  $\mu\text{m}$  and a lateral dimension from tens to hundred  $\mu\text{m}$ . Traditionally, polymer foams are produced using chemical or physical nucleating agents in molten polymer [19]. The pressure in extruder, where plastic material is melted, compressed and mixed, is sufficiently high to keep the melt non-foamed. Immediately after the pressure

drop in the head of the extruder or die foam bubbles appear and grow affecting a cellular structure in the polymer.

Another widely used method is stretching filler-loaded polymers under suitable conditions, which has been employed to fabricate cellular PP [32] and cellular cyclo-olefin copolymer (COC) films [33–36]. Tiny mineral particles are often employed as fillers that serve as stress concentrators for micro-cracks during biaxial stretching of the film. Simultaneous or sequential stretching in two perpendicular directions results in films with lens-like cavities. More recently, cellular polyester films, including poly(ethylene terephthalate) (PET) [37,38] and poly(ethylene naphthalate) (PEN) [39,40], and cellular fluorinated ethylene-propylene (FEP) [41] have been fabricated through physical foaming with supercritical carbon dioxide (scCO<sub>2</sub>). In this method, non-voided film is first saturated with scCO<sub>2</sub> at high pressure. Then, the pressure is quickly released, and the film filled with scCO<sub>2</sub> is thermally treated at elevated temperature. Consequently, the scCO<sub>2</sub> inside the film undergoes a phase change into gas, and foams the film. The foamed structure can be further optimized by means of well-controlled biaxial stretching.

With a pressure and temperature treatment, so-called gas-diffusion expansion (GDE) process, the size of the cavities in cellular polymer foams can be adjusted [13,42,43]. The external gas pressure is usually raised and kept at a high value for a certain period of time, so that the internal pressure of the cavities equalizes the external pressure due to gas diffusion. Then the polymer foam is inflated by a sudden release of the external gas pressure. The thickness expansion of the foam is stabilized by heat treatment at elevated temperatures during or right after the pressure treatment.

## (2) Soft/hard-layer systems

Layer sandwiches of space-charge polymer-electret films were already used in early implementations of piezoelectrets. Kacprzyk *et al.* studied piezoelectric double-layer sandwiches of one softer and one harder layer with real charges in between and confirmed the possibility of making piezo- or ferroelectrets in this way [44,45]. In 1999, Xia *et al.* reported that porous polytetrafluoroethylene (PTFE) shows excellent surface-charge storage stability, especially at elevated temperature [46]. The porous films, prepared from commercial PTFE resin by means of unidirectional stretching at high temperature, exhibit open structure of the cavities. Because of its open-cavity structure, porous PTFE by itself is not a good piezoelectric material. During metallization with electrodes that are necessary for electrical contact for measuring the signal, the metallic particles go into the interfaces between the cavities and the dielectric. As a result, the deposited charges are lost and the piezoelectricity of the film becomes extremely low. Nevertheless, porous PTFE is highly suitable for preparation of sandwich-structure ferroelectrets due to its softness and its excellent electret properties. Shortly after, layer stacks of porous and nonporous PTFE films as ferroelectrets were studied [47,48].

Von Seggern *et al.* prepared ferroelectrets by sandwiching a highly porous PTFE, so-called expanded PTFE (ePTFE) consisting of 91% air and 9% fibrous PTFE, between two solid fluoroethylenepropylene (FEP) layers [49–55]. In the study of Zhang *et al.*, laminated PTFE films consisting of a porous PTFE core and two nonporous PTFE cover layers were prepared by sintering or thermal bonding under high pressure [56–58].

### (3) Film systems with regular voided structure

Much effort has been devoted to developing fluoropolymer film systems with regular voided structure by combining fusion bonding and suitable patterning techniques. The film systems are usually bonded above their melting temperature. Altafim *et al.* developed FEP film systems with uniform cavities by thermal fusion combined with vacuum evacuation [59, 60]. In their study, a stack of two FEP films was placed between two cylindrical metal plates which can be independently heated. The top plate is completely solid, while the bottom one has tiny holes that are connected to a vacuum pump. The bottom plate was separated from the stack of FEP films by a metal grid. Most of the air was removed through the holes of the bottom plate by means of the vacuum pump and the adjacent FEP film was sucked into the openings of the metal grid. By heating and pressing the top plate onto the stack, air cavities with the same diameter as the grid openings were created.

For stacks of very thin FEP and PTFE films, void-containing film systems can be obtained by directly pressing a metal mesh with (sub) millimeter spacing [61, 62]. With a thermal treatment at 280 °C, the polymer layers were fused underneath the wires of the metal mesh and cavities were formed between the fused areas because of the thermal expanding of the trapped air and the thermal softening of the fluoropolymer films. In several other works, rigid templates were used to bring forth the desired pattern in the fusion-bonded fluoropolymer film systems [63–65]. FEP film sandwiches with a patterned middle layer can also be bonded locally by means of a laser beam [66].

Using a straightforward lamination process, ferroelectrets with well-controlled and uniform cavities were developed [67] (cf. p. 53). In this process, two polymer electret films are laminated around a template between them. The template, which can be made of metal foils or of polymers with a melting temperature higher than that of the electret films, contains regular openings through which the electret films can be fused with each other. Lamination is implemented at a temperature substantially higher than the melting temperature of the electret films yet lower than that of the template. After the outer layers have been fused, the template is removed, resulting in a polymer-film system with cavities of the designed pattern. Figure 2(a) schematically shows the preparation for tubular-channel FEP ferroelectrets. The template, made of an 100  $\mu\text{m}$  thick PTFE by means of laser cutting, consists of several well-cut stripes with clearly defined and evenly distributed openings between them. The two solid FEP films have a thickness of 50  $\mu\text{m}$  each. After being laminated at 300 °C, the stack is naturally cooled down under laboratory conditions.

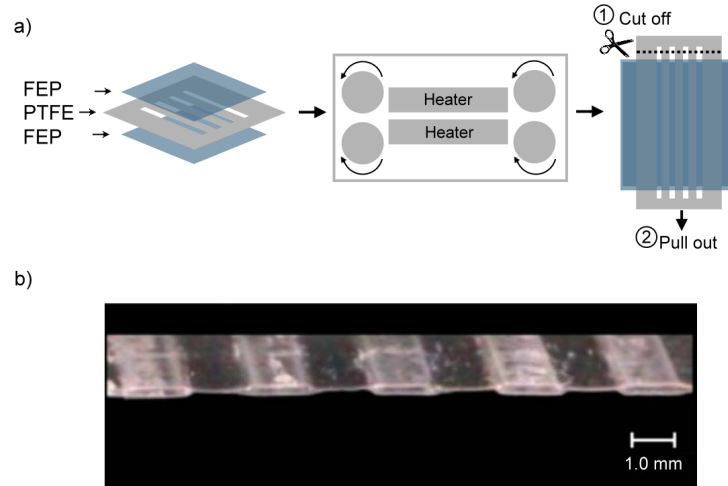


Figure 2: (a) Schematic view of the preparation process for tubular-channel ferroelectrets. (b) Optical micrograph of the cross section of an FEP ferroelectret sample [67].

The two FEP films are permanently fused with each other through the openings of the template. An FEP film system with open tubular cavities is obtained after removal of the PTFE template. Figure 2(b) shows an optical image of the cross section of such an FEP film system. After DBD charging, the tubular-channel FEP film systems show piezoelectric  $d_{33}$  coefficients of up to 160 pC/N. For samples charged at suitable elevated temperatures, the piezoelectricity is stable at temperatures of at least 130 °C. The new technique has the obvious advantages of simplicity and of well-controlled cavity geometries and patterns. Furthermore, it can be easily adopted to continuous industrial fabrication.

Using a sticky template that can tightly bond electret films represents another straightforward technique. In [68], we prepared such a template with a double-sided paste tape (cf. p. 78). Honeycomb-shaped openings were cut into a piece of past tape by means of computer-controlled laser cutting. The openings have a length of 1.5 mm for one side of each hexagon, and the remaining adhesive tape ridges are 0.5 mm in width. A polymer system with well-defined cavities was obtained by sandwiching the template with two uniform polycarbonate films. In another study, we developed polycarbonate ferroelectrets by means of screen printing—a technology that is widely used for the two-dimensional patterning of printed layers [69] (cf. p. 119). For the sample preparation, paste material (ink) was deposited in a pre-designed pattern via screen printing onto the surface of one electret film, and then another electret film is put on top of the ink pattern. Curing under suitable conditions facilitates the bonding between the ink pattern and the electret films, yielding a film system with well-defined cavities.

Cyclo-olefin copolymers (COCs) show good electret properties and excellent mechanical and electrical properties [70], and therefore are promising candidate materials for ferroelectrets. Li *et al.* proposed a scCO<sub>2</sub>-assisted assembly approach for producing COC

film systems with regular cavity structure [71]. When the material is exposed to  $scCO_2$ , the surface glass transition temperature becomes significantly lower than that of the bulk due to strong COC- $CO_2$  interaction. Thus, the interfaces of the COC stack, which consists of two patterned COC films (containing regular openings) sandwiched with three compact COC films, can be bonded at a temperature substantially lower than its melting point.

A quite promising development is the microfabrication of cellular polydimethylsiloxane (PDMS) ferroelectrets reported by Wang *et al.* [72, 73]. The sample fabrication consists multilayer PDMS casting and stacking processes. A photoresist mold is prepared on a silicon wafer. The cellular microstructure is duplicated to a thin PDMS layer that is casted on top of the mold. By bonding the patterned PDMS film to a blank thin PDMS layer, a PDMS foam with closed cavities is obtained. Multilayer structures can be constructed by repeating the casting and bonding processes. The cavities were filled with a solution of Teflon<sup>®</sup> AF. Once the solvent evaporates, a thin layer of AF film deposits which assures good charge storage after internal charging of the cavities. During the processing, chemical or corona treatment is carried out, in order to have easy peeling off or good bonding, respectively.

## 4 Charging Process

### 4.1 Charging Mechanisms

#### 4.1.1 Micro-plasma Discharge in Cavities

In order to render polymer foams or void-containing polymer systems piezoelectric, the cavities inside the material must be internally charged under high electric fields. Charging can be achieved by means of direct contact charging [74]. In this case, the high electric field inside the cavities is induced directly by the external voltage applied to the sample electrodes. Charging can also be carried out through corona discharge at high corona-point voltages without a grid [75] or electron beam charging [76]. The internal electric field of the cavities is induced by the surface potential or the injected electrons, respectively.

Compared with that of ferroelectric polymers, the charging of ferroelectrets is a quite different story. Charging (or poling) of ferroelectric polymers involves the orientation of intrinsic molecular dipoles. Ferroelectrets are, however, non-polar polymers containing no molecular dipoles. Rather, they are space-charge electrets in which “real” charges can be trapped and quasi-permanently stored [77, 78]. The charging process in ferroelectrets is accomplished by a series of dielectric barrier discharges (DBDs) [79]. In DBDs, at least one side of the discharge gap is insulated from the electrodes by a solid dielectric layer [80]. In the context of ferroelectrets, both electrodes are covered with polymer layers.

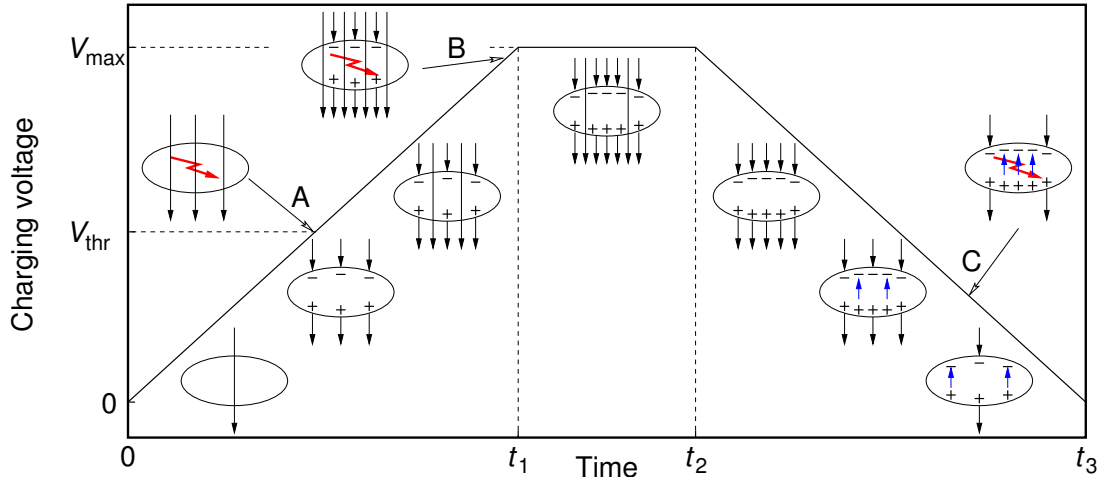


Figure 3: Schematic view of the DBD charging process in a single polymer cavity. When the charging voltage reaches the threshold value  $V_{\text{thr}}$ , Paschen breakdown is ignited (A). At higher voltages, a second discharge may occur (B). During ramping down the voltage, the reverse electric field from the trapped space charges may lead to back discharges (C) [81].

DBDs in ferroelectrets are always accompanied by light emission that can be easily photographed. Based on the investigation of the light emission, a schematic model for the charging process has been proposed, as shown in Fig. 3 [81] (cf. p. 37). Internal breakdown (Paschen breakdown) in the cavities is initiated when the voltage reaches the required threshold value (in this sense, the electric field in the cavities is comparable with the “coercive field” in ferroelectrics). Charges of opposite polarity are separated during the DBDs and are subsequently trapped on the top and bottom surfaces of the cavities, respectively (point A in Fig. 3). The trapped charges induce an electric field opposite to the externally applied field and thus eventually extinguish the discharge. As the applied voltage increases further, a second series of breakdown events may occur, and the density of the internally trapped charges strongly increases (point B in Fig. 3). No breakdown occurs at the plateau of the applied voltage. When the applied voltage is reduced, the electric field of the trapped charges may overcompensate the applied field and may thus be able to trigger back discharges (point C in Fig. 3). Namely, the breakdown inside the cavities is controlled by the sum of the applied electric field and the electric field of the deposited charges. The sustainable maximum charge density  $\sigma$  is determined by the breakdown strength of the gas-filled cavities.

It is widely accepted that the threshold behavior of the charging process is governed by Paschen’s law. According to Townsend’s model, the critical breakdown field of common gases in a uniform electric field is determined by the gas pressure  $p$ , the electrode spacing  $d$  (which in a ferroelectret context is equal to the cavity height), and the Paschen coefficients [82]. Therefore, the dimensions of the cavities, the gas pressure, and the com-

position of the gas inside the cavities all strongly influence the charging process. This partly explains the positive effect on the piezoelectric sensitivity from gas-diffusion expansion treatment with suitable parameters [13,42,43], since cavities with optimal dimensions require lower breakdown voltage and thus have higher charging efficiency. In [83], the transient light emission from the dielectric barrier discharges (DBDs) in cellular polypropylene ferroelectrets subjected to high electric poling fields was spectroscopically measured (cf. p. 44). The spectrum shows strong emission from the second positive system (SPS) of molecular nitrogen,  $N_2(C^3\Pi_u) \rightarrow N_2(B^3\Pi_g)$ , and the first negative system (FNS) of  $N_2^+$ ,  $N_2^+(B^2\Sigma_u^+) \rightarrow N_2^+(X^2\Sigma_g^+)$ , consistent with a DBD in air. The appearance of the FNS of  $N_2^+$  directly confirms the ionization of molecular nitrogen during the DBDs. From selected vibronic band strength ratios, the electric field during the DBDs in cellular PP is found to be between 21 and 28 MV/m, in good agreement with the predicted breakdown strength in air for cavities with heights between 10 and 15  $\mu\text{m}$ . The charging efficiency and in turn the piezoelectric sensitivity can be further improved by charging in a suitable dielectric gas atmosphere at elevated pressure [84–86] (cf. p. 47).

Recently, Mellinger *et al.* adopted a multi-layer electromechanical model to describe the charging process in cellular PP foams [87, 88]. The simulations predict threshold voltages much lower than experimental values. They concluded that the Paschen’s law is not applicable to micrometer-sized cavities, and in this case the standard Paschen coefficients need to be modified. However, the breakdown behavior follows the standard Paschen curves at atmospheric and elevated pressures for cavities with heights on the order of tens of microns [89,90].

The DBDs in air produce a variety of species including energetic and reactive monatomic and diatomic charged gas particles (*i.e.* ions), electrons, and neutral species [80]. During DBDs, the polymer surface is thus exposed to a highly reactive plasma, and both chemical and physical processes occur on the exposed surface areas [91,92]. It is found that repeated DBDs in air result in considerable fatigue of the effective polarization and of the piezoelectricity because of plasma-surface interactions at the internal cavity surfaces [93,94] (cf. p. 50 and p. 88). The fatigue is attributed to plasma-induced chain scission and oxidation of the polymer surface. Conventional DBD treatment of PP leads to the formation of polar water-soluble low-molecular-weight oxidized material (LMWOM) on the surface, containing O–C=O, C=O, and C–O groups. For cellular PP ferroelectrets, chain scission and the formation of polar LMWOM at the internal surfaces during DBDs deteriorate the chargeability of the cavities, resulting in the observed polarization fatigue. A threshold peak-to-peak voltage  $V_{pp}$  of 3 kV for fatigue is in good agreement with the previous finding that the DBDs inside the cavities are initiated when the voltage is higher than 3 kV [81]. The fatigue rate strongly depends on the amplitude and the number of driving-voltage cycles, whereas the frequency and the waveform do not have a strong influence,

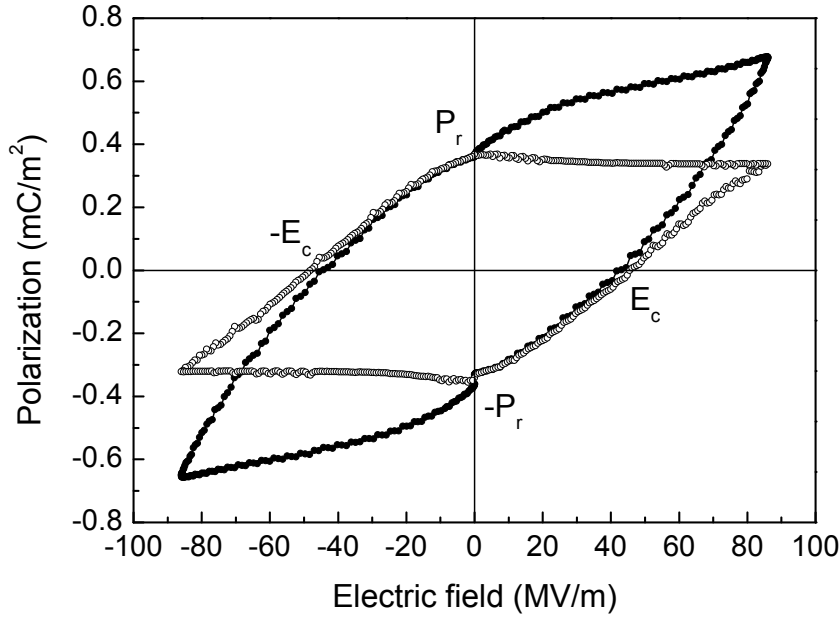


Figure 4: Polarization as a function of the electric field for a cellular PP ferroelectret sample. Solid circles: polarization originated from the dielectric barrier discharges in cavities. Open circles: polarization without component related to back discharges [98].

which indicates the influence of molecular dynamics and physico-chemical processes at the internal polymer surfaces.

#### 4.1.2 Polarization *vs.* Electric Field Hysteresis

In ferroelectrets, the density of the macroscopic dipoles (*i.e.*, the internally charged cavities) forms the effective polarization that is analogous to the polarization in traditional ferroelectrics. Zhang *et al.* and Zhukov *et al.* theoretically and experimentally studied the build-up of effective polarization in ferroelectrets [52, 95]. It was found that the effective polarization is zero when the charging voltage is below the threshold value  $V_{th}$ . Thereafter, the effective polarization linearly increases with  $V$ , and saturates at a voltage of  $2V_{th}$ . The slope of the increase is determined by the material parameters.

The build-up of the effective polarization in cellular PP ferroelectrets was also studied by making use of the converse piezoelectricity [81, 96] (cf. p. 37 and p. 81). The piezoelectric sensitivity of ferroelectrets under external voltages has contributions not only from the effective polarization, but also from the applied voltage due to the Maxwell stress. For measurement, a sinusoidal driving voltage was applied to the sample, and the radiated sound signal was recorded with a microphone. Meanwhile, a dc charging voltage was su-



Table 1: FERROELECTRIC BEHAVIOR: Evidence in various materials classes (Necessary and sufficient conditions) [98].)

<b>Condition for</b>	<b>Single- or Multi-</b>	<b>Semi-Crystalline</b>	<b>Heterogeneous</b>
Ferroelectric Behavior	<b>Crystalline</b> Polar Material	Polymer or Polymer-Based Composite	Material with Interface Charge
Curie Phase Transition	Always Observed	Sometimes Masked	Never Observed
Symmetry Breaking	Induced by Curie Transition (+ Poling)	Induced by Curie Transition + Poling	Induced by Electric Poling
Spontaneous Polarization	Related to Curie Transition	Related to Curie Transition	So Far Not Observed
Remanent Polarization	Related to Frozen Dipole Orientation	Related to Frozen Dipole Orientation	Related to Guest Phase with Interface Charge
Hysteresis Behavior	Dipole Reorientation + Domain Walls	Dipole Reorientation + Crystallite Boundaries	Breakdown Threshold of Internal Guest Phase

perimposed onto the sinusoidal voltage. A “butterfly” curve was obtained for the received microphone signal during charging of a ferroelectret under linearly increasing or decreasing voltages. The acoustic measurements were converted to piezoelectric  $d_{33}$  coefficients by comparing the zero-charging-field microphone signals with the absolute  $d_{33}$  values determined by means of dielectric resonance spectroscopy immediately after charging [97]. A polarization-voltage ( $P$ - $V$ ) hysteresis loop was obtained by analyzing the data according to an existing model for the piezoelectric  $d_{33}$  coefficient of ferroelectrets reported by Paaajanen *et al.* [20] and by Sessler and Hillenbrand [21].

Recently, the  $P(E)$  hysteresis loops for ferroelectrets have been obtained by using a modified Sawyer-Tower (ST) circuit [98] (cf. p. 111). The measured charge has contributions from the sample conductivity, from the sample capacitance and from the DBD charging of the cavities. With a voltage waveform consisting of two positive sine-squared semicycles (1 and 2) followed by two negative ones (3 and 4), the contributions from the sample conductance and the sample capacitance can be deducted from the measured values. Semicycles 1 and 3 constitute directly the  $P(E)$  hysteresis curve of the sample. In addition, semicycles 2 and 4 provide the back-discharge-relevant non-remanent component of the polarization. By subtracting this component, a hysteresis loop containing solely the net remanent polarization is obtained. When the sample conductivity is negligibly small such as tubular-channel ferroelectret systems made of FEP films, hysteresis loops can be obtained by simply applying a bi-polar sinusoidal voltage waveform [99] (cf. p. 125).

Figure 4 shows the hysteresis curves for cellular PP ferroelectrets. As can be seen from Fig. 4, the hysteresis curves of ferroelectrets are phenomenologically undistinguishable from those found on other ferroic materials, although the mechanism is quite different. A few important conditions for ferroelectric behavior in different types of materials are

summarized in Table I. The  $P(E)$ -hysteresis loops not only prove the ferroic behavior of ferroelectrets, but also allow us to determine such parameters as the coercive field and the remanent polarization. Figure 4 also demonstrates that back discharges destroy a large portion of the effective polarization in ferroelectrets. The hysteresis curve without back-discharge-relevant components takes a parallelogram-like shape, in agreement with previous studies on ferroelectrets with uniform cavities [52, 95].

## 4.2 Thermal Poling of Ferroelectrets

A thermal poling scheme is often adopted for ferroelectric polymers such as  $\beta$ -phase PVDF [78]. In this poling technique, the sample is first heated up to a temperature  $T_P$  above the glass transition temperature  $T_g$ , so that the molecular dipoles become more flexible. When the preset poling temperature  $T_P$  is reached, the poling voltage is then applied to align the molecular dipoles. In order to orient the molecular dipoles as completely as possible, the poling voltage remains at  $T_P$  for a period of time ranging from several minutes to several hours. The dipole orientation is frozen by cooling down the sample in the presence of the poling voltage.

It is found that the thermal poling scheme is also useful for charging ferroelectrets, although the charging mechanisms are quite different. As already discussed in the previous section, Paschen breakdown has been identified to be essential for triggering the DBD charging process in ferroelectrets. However, Paschen's law is usually written down for room temperature ( $T_0 = 293$  K). The inception of gas breakdown is caused by the acceleration of electrons in the applied electric field  $E$ . The energy gain of electrons is proportional to the product  $El$  where  $l$  represents the mean free path, *i.e.* the mean distance that electrons travel between two consecutive collisions. Since  $l$  strongly depends on temperature, Paschen's law must be modified for different temperatures [101–104]. According to the so-called Peek correction [101], the breakdown voltage of gas is inversely proportional to the gas temperature. Thus, the threshold voltage of the ferroelectret sample at a gas temperature  $T$  is given by

$$V_{\text{th}} = \frac{T_0}{T} V_{\text{th}0}, \quad (1)$$

where  $V_{\text{th}0}$  is the threshold voltage for the sample at room temperature of  $T_0 = 293$  K. Hysteresis measurements on tubular-channel FEP ferroelectrets show that the temperature dependence of the threshold voltage agrees reasonably well with Eq. (1).

The threshold voltage  $V_{\text{th}}$  is a critical parameter for the charging of ferroelectrets. In [52] and [95], the build-up of the polarization during charging was studied for ferroelectrets having a single void height. When a fresh sample is charged with a voltage  $V$ , the effective polarization  $P_{\text{eff}}$ , *i.e.* the density of the macroscopic dipoles, in the presence

of the voltage  $V$  is given by [52, 95]

$$P_{\text{eff}} = \begin{cases} 0 & (V < V_{\text{th}}) \\ k(V - V_{\text{th}}) & (V \geq V_{\text{th}}) \end{cases}, \quad (2)$$

where  $k$  is a sample-specific parameter. The effective remanent polarization (*i.e.* the polarization after the voltage has been turned off) can be expressed as

$$P_{\text{rem}} = \begin{cases} 0 & (V < V_{\text{th}}) \\ k(V - V_{\text{th}}) & (V_{\text{th}} \leq V \leq 2V_{\text{th}}) \\ kV_{\text{th}} & (V > 2V_{\text{th}}) \end{cases}. \quad (3)$$

From Eqs. (2) and (3),  $P_{\text{rem}}$  is equal to  $P_{\text{eff}}$  when the charging voltage is smaller than  $2V_{\text{th}}$ .  $P_{\text{rem}}$  reaches its maximum of  $kV_{\text{th}}$  when  $V = 2V_{\text{th}}$  and saturates for charging voltages higher than  $2V_{\text{th}}$  [52, 95]. Before saturation is reached, a decrease in  $V_{\text{th}}$  will lead to increases in  $P_{\text{eff}}$  and  $P_{\text{rem}}$ . However, when  $V > 2V_{\text{th}}$ , a decrease in  $V_{\text{th}}$  would still lead to an increase in  $P_{\text{eff}}$ , but will also cause a decrease in  $P_{\text{rem}}$ .

With increasing  $T_{\text{p}}$ , the threshold voltage for triggering dielectric barrier discharges in ferroelectrets decreases. Thus, increasing the temperature facilitates the charging of ferroelectrets. However, a lower threshold voltage reduces the attainable remanent polarization because back discharges occur at lower charge levels, as soon as the charging voltage is turned off. Thus, the charging or poling temperature is an important parameter that affects the coercive field, the polarization and the observed hysteresis, even though the charging/poling mechanisms and the ferroelectric behaviors of ferroelectrics and ferroelectrets are quite different. A thermal poling scheme is proposed for more efficient charging of ferroelectrets [100] (*cf.* p. 164). The ferroelectret sample to be charged is first heated up to a suitable elevated temperature in order to lower the threshold voltage. The charging voltage is applied when the preset charging temperature  $T_{\text{p}}$  is reached. Then the sample is cooled down, and the charging voltage is not switched off until the temperature returns to its initial value, so that a higher remanent polarization is attained.

### 4.3 Poling Assisted by Gas Exchange

Charging of ferroelectrets depends on electrical breakdown of the gas inside the cavities. Thus, the breakdown strength of the gas strongly influences the charging process of ferroelectrets. Different gases may have quite different breakdown strength. For instance, it is reported that the electrical strength of helium at atmospheric pressure is only 15% of that of nitrogen under similar conditions [105]. Gas with a lower breakdown strength also has a lower threshold voltage, thus decreasing the onset voltage for DBD charging of the

cavities. However, a lower threshold voltage also leads to a lower value for the remanent polarization because back discharges take place at lower charge levels.

The threshold behavior of tubular channel FEP ferroelectrets was studied through measurements of the hysteresis loops [98,99] and dynamic  $d_{33}$  coefficients [106]. In atmospheric air, a threshold voltage of about 1.3 kV is observed. For charging voltage below the threshold, the polarization is nearly zero. Then, the polarization increases with charging voltage. While the polarization at maximum voltage  $P_{\max}$  keeps increasing with the voltage, the remanent polarization  $P_{\text{rem}}$  saturates at about 0.1 mC/m<sup>2</sup> for voltage higher than 3 kV.

Because of the lower breakdown strength of helium, a threshold voltage of about 500V is determined, more than two times lower compared with charging in air. A  $P_{\max}$  of about 0.1 mC/m<sup>2</sup> can be found at a maximum voltage of 1.3 kV when the sample is charged in helium. Unfortunately, the polarization is partly destroyed by back discharges when the voltage is reduced from its maximum back to zero, and  $P_{\text{rem}}$  saturates at about 0.46 mC/m<sup>2</sup> for voltages higher than 1.0 kV.

Dynamic  $d_{33}$  measurements show similar threshold behavior. In order to achieve higher  $d_{33}$  coefficients, the sample should be charged to higher  $P_{\text{rem}}$  values. Hysteresis measurements suggest that the  $P_{\max}$  of 0.1 mC/m<sup>2</sup> in helium at a voltage of 1.3 kV can be retained if helium is replaced with air. On this basis, a charging strategy is proposed where the DBDs start in a gas with lower (in the present case, helium) and are completed at a higher breakdown strength (*e.g.*, nitrogen or atmospheric air) [107] (cf. p. 168). Compared with charging only in helium at atmospheric pressure, a significant increase of the  $d_{33}$  coefficient is achieved without the need for high charging voltages (cf. the vertical arrow in Fig. 5). The sample is charged to saturation with a significantly lower voltage compared with charging solely in atmospheric air (cf. the horizontal arrow in Fig. 5). Thus, the exchange of gas in the cavities during charging can significantly enhance the charging efficiency of ferroelectrets.

An earlier study on the dielectric strength of N<sub>2</sub>-He mixtures showed that the breakdown voltage rises rapidly when the He content decreases from 100 to 95% [108]. Therefore, relatively high purity of helium (higher than 99.5%, for instance) is desired in order to have low threshold voltage. However, complete removal of helium before switching off the charging voltage is not necessary, since N<sub>2</sub>-He mixture has a dielectric strength close to that of pure N<sub>2</sub> when the He content is lower than about 10%. In previous studies, gas exchange between the cavities and the surroundings was reported for ferroelectrets with closed foam structures. As confirmed by measurements of the sample capacitance, gas molecules diffuse through the polymer walls when the sample is subjected to vacuum or high-pressure gas. As a result, the internal and the external pressures equalize after sufficient waiting times [86,109]. Therefore, the proposed charging scheme is also appli-

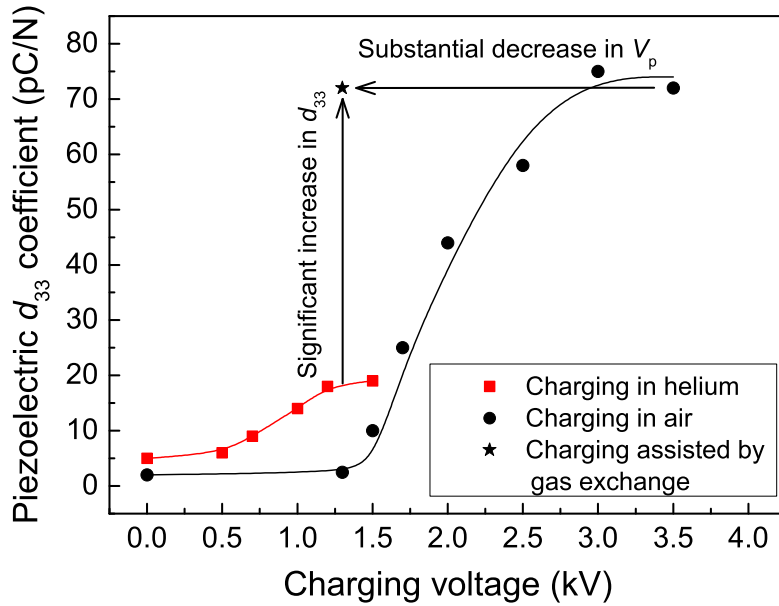


Figure 5: Piezoelectric  $d_{33}$  coefficient of a tubular-channel FEP ferroelectret sample as a function of the charging voltage. Solid squares: Sample was charged in helium at atmospheric pressure. Solid star: Sample was first charged at a voltage of 1.3 kV in helium at atmospheric pressure, then helium was replaced with atmospheric air, while the charging voltage was maintained. Charging voltage was turned off after the gas exchange. Solid circles: Sample was charged in atmospheric air. Lines are only guides for the eye.

cable to cellular-foam ferroelectrets, provided that sufficient time is allowed for the gas exchange.

With the proposed charging scheme, ferroelectrets are charged to saturation with a voltage even lower than the threshold in atmospheric air! The study not only deepens the understanding of the underlying physical process in ferroelectrets, but also is of great importance from a practical point of view. The substantially lowered charging voltage reduces the high-voltage related complication and cost in the preparation of ferroelectrets. Furthermore, development of new ferroelectrets is often restrained by insufficient charging efficiency, either because extremely high charging voltage that is not easily available is required, or because the charging voltage is so high that destructive electrical breakdown of the material occurs. Therefore, the proposed charging scheme increases significantly the flexibility in developing new ferroelectrets.

## 5 Piezoelectricity of Ferroelectrets

In Greek piezo means to squeeze or press. Piezoelectricity is the ability to generate electric charge in response to applied mechanical stress, and vice versa. It is the property of

certain materials that are noncentrosymmetrical. In the most general picture, piezoelectricity is observed when a material contains internally separated charges of opposite sign (requirement 1) and exhibits a non-affine mechanical deformation behavior (requirement 2). In addition, a linear relationship between the input and output signals is required. The piezoelectric materials mentioned in the previous section are just examples that fulfill the basic requirements.

Recently, a quite intuitive charge-spring model was proposed to describe the piezoelectric response of dielectric materials [110]. The model consists of a two-phase system with a dipole phase “D” and a matrix phase “M”. It applies to different types of piezoelectric materials, since they all fulfill the two above-mentioned requirements. However, the length scale of the phases might be quite different for different piezoelectric materials. For instance, the macroscopic dipoles in ferroelectrets (*i.e.*, the internally charged cavities) have a dimension in the range from  $\mu\text{m}$  to  $\text{mm}$ , substantially bigger than the molecular dipoles in ferroelectric polymers such as  $\beta$ -phase poly(vinylidene fluoride) (PVDF) which are in the sub-nanometer range.

Without loss of generality, the piezoelectric  $d_{33}$  coefficient (the longitudinal direct piezoelectricity in the thickness direction) is considered. It expresses the ratio of either the charge generated on the surface electrode to the force applied perpendicularly to the film surface (direct piezoelectric effect) or the change in the film thickness to the voltage applied across the film (converse piezoelectric effect). According to the charge-spring model, the  $d_{33}$  coefficient is expressed by [110]:

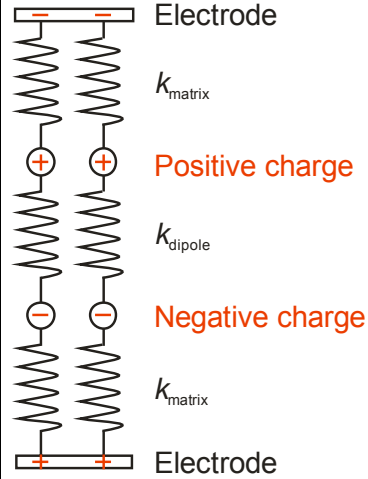
$$d_{33} = -\frac{P_3}{Y_M} + \frac{P_3}{Y_D}, \quad (4)$$

where  $P_3$  is the overall polarization,  $Y_M$  and  $Y_D$  are the elastic modulus of the matrix and the dipole phase, respectively. The first term on the right-hand side of the equation denotes the contribution from the deformation of the matrix with stiff dipoles (secondary piezoelectricity), while the second term the deformation of the dipoles themselves within a stiff matrix (primary piezoelectricity). In [99], it is found that the  $d_{33}$  coefficient of tubular-channel FEP ferroelectrets linearly increases with increasing polarization with a slope approximately equal to the sample compliance (cf. p. 125). As proved by data from our previous studies and from the literature, the approximation between the ratio of the piezoelectric coefficient to the respective remanent polarization and the sample compliance is also observed for cellular PP ferroelectrets and several piezoelectric polymers. By correcting the spring length of the dipole phase with the tetragonality, the charge-spring model is also applicable for ferroelectric perovskites [111].

A schematic diagram of the charge-spring model and different types of electromechanical coupling in materials are summarized in Table 2. According to Equation (4), it is obvious that no piezoelectricity is observed when the matrix and dipole phases have the

same elastic modulus (affine deformation). In ferroelectrets, the gas-filled cavities are much softer than the polymer matrix. When a negative force is applied in the thickness direction, the thickness decrease of the film mainly arises from the compression of the air-filled cavities. Consequently, the macroscopic dipole moment decreases and so does the electrode charge. Thus,  $d_{33}$  is positive (primary piezoelectricity). In ferroelectric polymers, a negative force mainly shortens the distance between the chains, due to the relatively weak van der Waals and electrostatic interactions between chains in comparison with the strong covalent bonds within the chain. As a result, the dipole moment density increases, giving a negative  $d_{33}$  coefficient (secondary piezoelectricity). Similarly, the transverse piezoelectric coefficients ( $d_{31}$  and  $d_{32}$ ) are negative for ferroelectrets, also opposite to those of ferroelectric polymers. The piezoelectric coefficients of ferroelectrets are of the same sign as those of typical ferroelectric ceramics, such as lead zirconate titanate (PZT).

Table 2: Electromechanical coupling in materials systems.

Schematic view	Conditions	Examples
	(1) $k_{\text{matrix}} = k_{\text{dipole}}$ : Affine deformation ( <i>i.e.</i> no piezo-effect)	Space charge electrets with isotropic mechanical properties such as PTFE, FEP, PP, etc.
	(2) $k_{\text{matrix}} < k_{\text{dipole}}$ : Dipole-density change (secondary piezoelectricity)	Ferroelectric polymers such as $\beta$ -PVDF and copolymers; Composites of polymer+hard particles and of elastomer+polymer granules.
	(3) $k_{\text{matrix}} > k_{\text{dipole}}$ : Dipole-moment change (primary piezoelectricity)	Ferroelectric ceramics such as PZT; Composites of polymer/elastomer+gas and of polymer+liquid.

The pyroelectric coefficient of ferroelectrets also has opposite sign to those of ferroelectric polymers. The sample thickness thermally expands with increasing temperature, which leads to increases of the macroscopic dipole moment and of the charge on the electrodes, yielding a positive pyroelectric  $p_3$  coefficient.

Take cellular PP ferroelectrets as examples. The cavities are highly compressible in the thickness direction due to the large anisotropy, whereas in the transverse directions the materials are much stiffer. Thus, cellular PP ferroelectrets show very large piezoelectric  $d_{33}$  coefficient. Values of hundreds of pC/N are often achieved, more than one order of magnitude greater than those found in conventional ferroelectric polymers. The transverse piezoelectric coefficient ( $d_{31}$  or  $d_{32}$ ) is typically around 2 pC/N, two orders of magnitude lower than the  $d_{33}$  coefficient. This feature renders cellular PP ferroelectrets ideal candidates for flexible piezoelectric sensors, since they are almost insensitive to the

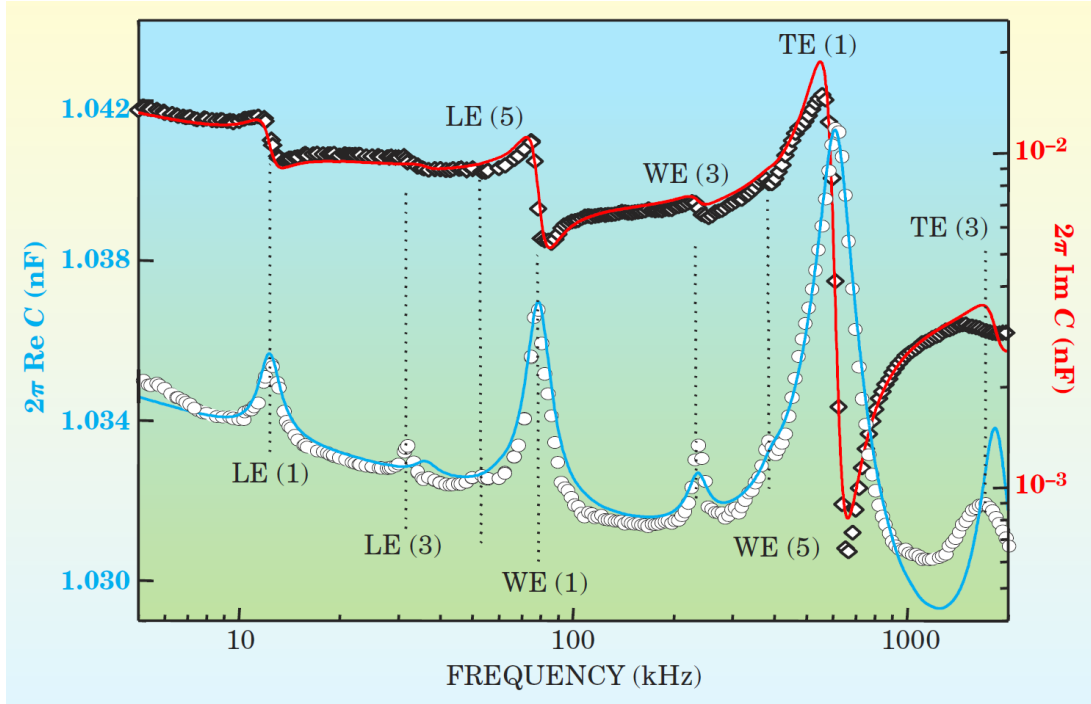


Figure 6: Dielectric resonance spectroscopy as a tool for characterizing the piezoelectric properties of ferroelectrets [112, 113]. The spectra show length- (LE), width- (WE), and thickness-extension (TE) resonances. Shown in the figure are measured curves of the real ( $\diamond$ ) and the imaginary part ( $\circ$ ) of the sample capacitance. Mechanical and electromechanical properties are obtained by a least squares fit of the measured curves (solid lines) with theoretical formula.

bending during operation. The pyroelectric coefficient of cellular PP ferroelectrets ( $0.25 \mu\text{C}/\text{m}^2\text{K}$ ) is much smaller than that of polar polymers such as PVDF ( $27 \mu\text{C}/\text{m}^2\text{K}$ ) [112]. For this reason, there have been only very few investigations of pyroelectricity in cellular ferroelectrets.

As traditional piezoelectric materials, ferroelectrets exhibit resonance behavior in their dielectric spectra. Figure 6 shows the piezoelectric resonances of a rectangular cellular PP ferroelectret sample with a length of 10 cm, a width of 1 cm and a thickness of  $70 \mu\text{m}$  [112, 113]. The sample is mechanically free during the measurement. Resonance peaks for the length- (LE), width- (WE), and thickness-extension (TE) modes are clearly seen. As is often the case with such spectra, the figure also shows some higher harmonics. Piezoelectricity in cellular PP ferroelectrets was also confirmed by measurements of the converse piezoelectric effect using an interferometric method [114]. Below the resonance frequency, the converse piezoelectric response is more or less flat with increasing frequency. A slight decrease is attributed to the increase of the Young's modulus of the material. At higher frequencies, the response starts to rise and reaches the maximum at the resonance frequency as a consequence of the electromechanical resonance.



## 6 Applications

Ferroelectrets combine large piezoelectricity with elastic compliance and mechanical flexibility and have potential for use in numerous applications. Based on ferroelectret films, the fabrication of flexible sensors is possible if the electronics are separated from the sensor film and connected via cables. The sensors can be easily made into almost any shape, and can be conformably attached to uneven surfaces. Sensors can also be manufactured in large area. Applications of ferroelectrets in micromovement actuators, in flexible control panels and keyboards, in sensors for motion control and pressure measurement, in electroacoustic transducers such as microphones, musical pickups and hydrophones, etc. have been discussed in previous reviews [10, 22, 24–27, 29].

Ferroelectret films are suitable for tactile sensors such as thin control panels, keyboard pushbuttons and prosthetic skin sensors, etc. The principle is simple. Changing the mechanical pressure on a ferroelectret film (with a load of certain weight, for instance) leads to a pulse-like sensor signal which can be easily detected with standard electronics. Due to the very small piezoelectric  $d_{31}$  and  $d_{32}$  coefficients, ferroelectret films are highly suitable for rollable and bendable keyboards and tactile sensors. A piece of rectangular cellular PP ferroelectret film can be used as a flexible large area sensor for touch point localization [115]. The two film surfaces are coated with electrodes. The highly conductive electrode is grounded, and piezoelectric signals are detected from the four corners of the other electrode with large sheet resistance. The touch position is determined by analyzing the shapes and amplitudes of the four signals. Kogler *et al.* reported ultrathin flexible keyboards by making use of the different polarization states in ferroelectrets [116]. The polarization in ferroelectret films has two states (*i.e.* up (+1) and down (-1)), which, together with the inactive state (*i.e.* unpoled (0)), can be patterned into a ferroelectret film using suitable poling methods. With reading electronics, different regions in the pattern can be identified with different sensor signals. By combining several layers to a multilayer stack, the number of identifiable regions is increased. The challenge in this concept is to achieve effective polarization with good edge-resolutions between alternating regions in the pattern.

The use of ferroelectrets as sensor skin was also explored. By embedding ferroelectret films into a dielectric elastomer, highly stretchable sensors as large-area prosthetic skin for robotics or wearable electronics were fabricated [117, 118]. Fang *et al.* reported that ferroelectret skin sensors can detect both touching and slipping signals [119, 120]. The two types of signals can be distinguished from each other according to their different signal characteristics. Such thin-film ferroelectret sensors might be employed to produce sensation for prosthetic hands.

Another promising area of applications is achieved by combining dielectric elastomer actuators (DEAs) and ferroelectrets into a single device. When a prestretched DE film is

fixed to a flexible plastic frame, the frame changes its shape upon release of the DE film from the prestretch, leading to a complex structure with minimum of free energy that can be used as a bending actuator [121–123]. A tubular-channel FEP ferroelectret film is glued to the plastic frame prior to the formation of minimum-energy DEA structure. It turns out that the antiresonance frequency ( $f_p$ ) of the ferroelectret film, which can be easily detected through dielectric resonance spectroscopy [97], changes noticeably with the bending angle of the DEA. Thus, combination of DEAs and ferroelectrets opens up various new possibilities for application. The  $f_p$  of ferroelectrets can be taken for *in-situ* diagnosis and precise control of the actuation of DEA devices. Also, the actuation of DEAs can be used to modulate the  $f_p$  of ferroelectrets in order to meet the requirements of given applications [124] (cf. p. 105).

Energy harvesting for powering low-energy electronics such as wireless sensors and wearable devices is one of the traditional applications of electrets [125]. The application of ferroelectrets as low frequency vibration energy harvesters has also been explored more recently. In 2012, Anton and Farinholt demonstrated the feasibility of vibration energy harvesting with ferroelectrets, albeit the output power is quite low, only in the range from 2.5 to 40 nW with mechanical excitation over a 2.54 cm×2.54 cm sample area [126]. The output power may be enhanced with larger piezoelectric sensitivity and/or larger harvester volume. Thanks to the low density, it is not a big problem to increase the volume of the ferroelectret harvester. With larger or multi-layered samples, the output power was significantly increased to typically several to tens of  $\mu\text{W}$  [127–134]. Luo *et al.* reported a flexible energy harvesting insole containing a 80-layer ferroelectret stack in the heel [135]. The insole harvests about 100  $\mu\text{J}$  energy per footstep of an 80 kg person. It was shown that the energy harvested from every 3 to 4 footsteps is enough to power an 8-bit wireless data transmission.

## 7 Conclusions and Outlook

Internally charged polymer foams and void-containing polymer systems (so-called ferroelectrets) are a new class of electromechanically active materials. In this thesis, comprehensive work on ferroelectrets, and in particular on their preparation, their charging, their piezoelectricity and their applications is reported. Novel ferroelectrets with well-controlled cavity structures have been prepared using techniques including straight forward thermal lamination, sandwiching sticky templates with electret films and screen printing. After charging through dielectric barrier discharges (DBDs), the newly developed ferroelectrets show promising piezoelectricity. In particular, laminates of fluoroethylenepropylene (FEP) films with tubular-channel openings show large piezoelectricity ( $d_{33}$  up to 160 pC/N) that is stable at temperatures of at least 130 °C. The preparation methods reported here are easy to implement at laboratory or industrial scales, and are quite flexible in terms of

material selection and cavity geometry design. Due to the uniform and well-controlled cavity structures, samples are also very suitable for fundamental studies on ferroelectrets.

The DBD charging process of ferroelectrets is comprehensively studied by means of optical, electrical and electro-acoustic methods. Such investigations reveal details of the onset of charging and back discharge, ionization species, and fatigue effects due to repeated switching. Polarization-*versus*-electric-field ( $P(E)$ ) hysteresis loops in ferroelectrets are observed by means of an electro-acoustic method combined with dielectric resonance spectroscopy or by more direct measurements using a modified Sawyer-Tower circuit. Hysteresis loops of ferroelectrets are phenomenologically undistinguishable from those found on other ferroic materials, proving the ferroic behavior of ferroelectrets. Based on these intriguing findings, a number of procedures are proposed for significantly higher charging efficiency of ferroelectrets, such as charging with high-pressure air, thermal poling and charging assisted by gas exchange.

After DBD charging, the gas-filled cavities are turned into macroscopic dipoles. The macroscopic dipoles are highly compressible, and hence the piezoelectricity in ferroelectrets is essentially the primary effect. It turns out that the piezoelectric  $d_{33}$  coefficient is proportional to the polarization and the elastic compliance of the sample, providing hints for developing ferroelectrets with higher piezoelectric sensitivity in the future. Due to their outstanding electromechanical properties, there has been constant interest in the application of ferroelectrets. In the present work, it is found that the antiresonance frequency ( $f_p$ ) of a ferroelectret is sensitive to the boundary conditions during measurement. This effect can be utilized for a number of interesting applications.

In recent years, the knowledge of ferroelectrets has significantly advanced. Also, numerous techniques for preparing novel ferroelectrets have been proposed, attempting to acquire ferroelectrets with superior electromechanical properties and/or with easier and more economic processing. It is very likely that ferroelectrets with much broader ranges of the relevant electromechanical (and other) properties will become available within the next few years. With the advancement of science and technology in the field, it might even be possible to design and tune ferroelectrets according to specific device requirements. Furthermore, interest in the application of ferroelectrets will certainly continue. A few products based on cellular PP ferroelectrets are already on the market, and more and more work on the laboratory prototypes is reported. With the development of new ferroelectrets with better electromechanical properties, more intensive research on the applications of ferroelectrets and the emergence of more products on the market are foreseeable.

## References

- [1] A. S. Mischenko, Q. Zhang, J. F. Scott, R. W. Whatmore, and N. D. Mathur, “Giant Electrocaloric Effect in Thin-Film  $\text{PbZr}_{0.95}\text{Ti}_{0.05}\text{O}_3$ ”, *Science*, 311, 1270–1271 (2006).
- [2] B. Neese, B. Chu, S. Lu, Yong Wang, E. Furman, Q. Zhang, “Large Electrocaloric Effect in Ferroelectric Polymers Near Room Temperature”, *Science*, 321, 821–823 (2008).
- [3] S. P. Alpay, J. Mantese, S. Trolier-McKinstry, Q. Zhang, and R. W. Whatmore, “Next-generation electrocaloric and pyroelectric materials for solid-state electrothermal energy interconversion”, *MRS Bull.*, 39, 1099–1111 (2014).
- [4] A. S. Bhalla, R. Y. Guo, and R. Roy, “The perovskite structure – a review of its role in ceramic science and technology”, *Mat. Res. Innovat.*, 4(1), 3–26 (2000).
- [5] H. Kawai, “The Piezoelectricity of Poly (vinylidene Fluoride)”, *Jpn. J. Appl. Phys.* 8, 975–976 (1969).
- [6] G. M. Sessler, “Piezoelectricity in polyvinylidene fluoride”, *J. Acoust. Soc. Am.*, 70(6), 1596–1608 (1981).
- [7] A. J. Lovinger, “Ferroelectric polymers”, *Science*, 220(4602), 1115–1121 (1983), and references therein.
- [8] R. E. Newnham, D. P. Skinner, and L. E. Cross, “Connectivity and piezoelectric-pyroelectric composites”, *Mat. Res. Bull.*, 13(5), 525–536 (1978).
- [9] E. K. Akdogan, M. Allahverdi, and A. Safari, “Piezoelectric composites for sensor and actuator applications”, *IEEE Trans. UFFC*, 52(5), 746–775 (2005).
- [10] S. Bauer, R. Gerhard, and G. M. Sessler, “Ferroelectrets: Soft electroactive foams for transducers”, *Phys. Today*, 57(2), 37–43 (February 2004).
- [11] R. Kressmann, G. M. Sessler, and P. Günther, “Space-charge electrets”, *IEEE Trans. DEI*, 3(5), 607–623 (1996).
- [12] X. Qiu, R. Gerhard, and A. Mellinger, “Turning polymer foams or polymer-film systems into ferroelectrets: dielectric barrier discharges in voids”, *IEEE Trans. Dielectr. Electr. Insul.*, 18(1), 34–42 (2011).
- [13] M. Wegener, W. Wirges, J. Fohlmeister, B. Tiersch, and R. Gerhard-Mulhaupt, “Two-step inflation of cellular polypropylene films: void-thickness increase and enhanced electromechanical properties”, *J. Phys. D: Appl. Phys.*, 37(4), 623–627 (2004).
- [14] P. Brochu and Q. Pei, “Advances in Dielectric Elastomers for Actuators and Artificial Muscles”, *Macromol. Rapid Commun.*, 31(1), 10–36 (2010).
- [15] L. Gibson and M. Ashby, *Cellular solids: structure and properties*, New York: Cambridge U. Press, 1999.
- [16] Y. Wada and R. Hayakawa, “Piezoelectricity and Pyroelectricity of Polymers”, *Jpn. J. Appl. Phys.*, 15, 2041–2057 (1976).

- [17] J. J. Crosnier, F. Micheron, G. Dreyfus, and J. Lewiner, “Pyroelectricity induced by space-charge injection in polymer electrets”, *J. Appl. Phys.*, 47, 4798–4799 (1976).
- [18] K. Kirjavainen, Electromechanical film and procedure for manufacturing same”, US Patent 4,654,546 (31 Mar. 1987).
- [19] A. Savolainen and K. Kirjavainen, Electrothermomechanical Film. Part I. Design and Characteristics”, *J. Macromol. Sci. Part A*, 26(2), 583–591 (1989).
- [20] M. Paaajanen, H. Välimäki, and J. Lekkala, “Modeling the sensor and actuator operations of the ElectroMechanical Film EMFi”, *IEEE 10th Intern. Sympos. Electrets*, IEEE Service Center, Piscataway, NJ, USA, pp. 735–738 (1999).
- [21] G. M. Sessler and J. Hillenbrand, “Electromechanical response of cellular electret films”, *Appl. Phys. Lett.*, 75, 3405–3407 (1999).
- [22] R. Gerhard-Multhaupt, “Less can be more: Holes in polymers lead to a new paradigm of piezoelectric materials for electret transducers”, *IEEE Trans. Dielectr. Electr. Insul.*, 9, 850-859 (2002).
- [23] M. Lindner, H. Hoislbauer, R. Schwödiauer, S. Bauer-Gogonea, and S. Bauer, Charged cellular polymers with ”ferroelectretic” behavior”, *IEEE Trans. Dielectr. Electr. Insul.*, 11(2), 255–263 (2004).
- [24] M. Wegener, and S. Bauer, “Microstorms in cellular polymers: A route to soft piezoelectric transducer materials with engineered macroscopic Dipoles”, *Chem. Phys. Chem.*, 6, 1014-1025 (2005).
- [25] S. Bauer, “Piezo-, pyro- and ferroelectrets: soft transducer materials for electromechanical energy conversion”, *IEEE Trans. Dielectr. Electr. Insul.*, 13, 953–962 (2006).
- [26] X. Qiu, “Patterned piezo-, pyro-, and ferroelectricity of poled polymer electrets”, *J. Appl. Phys.*, 108, 011101 (2010).
- [27] S. Rajala and J. Lekkala, “Film-Type Sensor Materials PVDF and EMFi in Measurement of Cardiorespiratory Signals– A Review”, *IEEE Sens. J.*, 12(3), 439–446 (2012).
- [28] Y. Wan and Z. Zhong, “Effective electromechanical properties of cellular piezoelectret: A review”, *Acta Mech. Sin.*, 28(4), 951–959 (2012).
- [29] F. Carpi (Ed.) “Electromechanically Active Polymers, Polymers and Polymeric Composites: A Reference Series”, Springer International Publishing Switzerland 2016.
- [30] A. Mellinger, M. Wegener, W. Wirges, R. R. Mallepally, and R. Gerhard-Multhaupt, “Thermal and temporal stability of ferroelectret films made from cellular polypropylene/air composites”, *Ferroelectrics*, 331, 189–199 (2006).
- [31] X. Qiu, “Polymer Electrets and Ferroelectrets as EAPs: Materials”, Book chapter in “Electromechanically Active Polymers, Polymers and Polymeric Composites: A Reference Series” (Edited by Federico Carpi, Springer International Publishing Switzerland 2016), pp. 1-29.

- [32] J. Raukola, N. Kuusinen, and M. Paaajanen, “Cellular electrets – From polymer granules to electromechanically active films”, Proc. 11th Int Symp. Electrets, Melbourne, Australia, 195–198 (2002).
- [33] A. M. Savijärvi, M. Paaajanen, E. Saarimäki, and H. Minkkinen, “Novel heat durable electromechanical films: Cellular film making from cyclic olefin polymers”, IEEE 12th Intern. Sympos. Electrets (ISE 12), IEEE Service Center, Piscataway, NJ, 75–78 (2005).
- [34] E. Saarimäki, M. Paaajanen, A.-M. Savijärvi, and H. Minkkinen, “Novel heat durable electromechanical film processing: Preparations for electromechanical and electret applications”, IEEE 12th Intern. Sympos. Electrets (ISE 12), IEEE Service Center, Piscataway, NJ, 220–223 (2005).
- [35] M. Wegener, M. Paaajanen, O. Voronina, R. Schulze, W. Wirges, and R. Gerhard-Multhaupt, “Voided cyclo-olefin polymer films: Ferroelectrets with high thermal stability”, IEEE 12th Intern. Sympos. Electrets (ISE 12), IEEE Service Center, Piscataway, NJ, 47–50 (2005).
- [36] E. Saarimäki, M. Paaajanen, A. M. Savijävi, H. Minkkinen, M. Wegener, O. Voronina, R. Schulze, W. Wirges, and R. Gerhard(-Multhaupt), “Novel Heat Durable Electromechanical Film: Processing for Electromechanical and Electret Applications”, IEEE Trans. Dielectr. Electr. Insul., 13(5), 963–972 (2006).
- [37] M. Wegener, W. Wirges, J. P. Dietrich, and R. Gerhard(-Multhaupt), “Polyethylene terephthalate (PETP) foams as ferroelectrets”, IEEE 12th Intern. Sympos. Electrets (ISE 12), IEEE Service Center, Piscataway, NJ, 28–30 (2005).
- [38] W. Wirges, M. Wegener, O. Voronina, L. Zirkel, and R. Gerhard-Multhaupt, “Optimized preparation of elastically soft, highly piezoelectric cellular ferroelectrets from nonvoided poly(ethylene terephthalate) films”, Adv. Funct. Mater., 17, 324–329 (2007).
- [39] P. Fang, M. Wegener, W. Wirges, and R. Gerhard, “Cellular polyethylenenaphthalate ferroelectrets: Foaming in supercritical carbon dioxide, structural and electrical preparation, and resulting piezoelectricity”, Appl. Phys. Lett., 90, 192908 (2007).
- [40] P. Fang, X. Qiu, W. Wirges, R. Gerhard, and L. Zirkel, “Polyethylene-naphthalate (PEN) ferroelectrets: Cellular structure, piezoelectricity and thermal stability”, IEEE Trans. Dielectr. Electr. Insul., 17(4), 1079–1087 (2010).
- [41] O. Voronina, M. Wegener, W. Wirges, R. Gerhard, L. Zirkel, and H. Münstedt, “Physical foaming of fluorinated ethylene-propylene (FEP) copolymers in supercritical carbon dioxide: single film fluoropolymer piezoelectrets”, Appl. Phys. A: Mater. Sci. Process., 90, 615–618 (2008).
- [42] M. Paaajanen, H. Minkkinen, and J. Raukola, “Gas diffusion expansion-increased thickness and enhanced electromechanical response of cellular polymer electret films”, Proc. 11th Int Symp. Electrets, Melbourne, Australia, 191–194 (2002).

- [43] X. Zhang, J. Hillenbrand, and G. M. Sessler, “Piezoelectric  $d_{33}$  coefficient of cellular polypropylene subjected to expansion by pressure treatment”, *Appl. Phys. Lett.*, 85, 1226–1228 (2004).
- [44] R. Kacprzyk, E. Motyl, J. B. Gajewski, and A. Pasternak, “Piezoelectric properties of nonuniform electrets”, *J. Electrostat.*, 35(2-3), 161–166 (1995).
- [45] R. Kacprzyk, A. Dobrucki, and J. B. Gajewski, “Double-layer electret transducer”, *J. Electrostat.* 39 (1), 33–40 (1997).
- [46] Z. Xia, R. Gerhard(-Mulhaupt), W. Künstler, A. Wedel, and R. Dan, “High surface-charge stability of porous polytetrafluoroethylene electret films at room and elevated temperatures”, *J. Phys. D: Appl. Phys.*, 32, L83–L85 (1999).
- [47] W. Künstler, Z. Xia, T. Weinhold, A. Pucher, and R. Gerhard-Mulhaupt, “Piezoelectricity of porous polytetrafluoroethylene single- and multiple-film electrets containing high charge densities of both polarities”, *Appl. Phys. A: Mater. Sci. Process.*, 70(1), 5–8 (2000).
- [48] R. Gerhard-Mulhaupt, W. Künstler, T. Goerne, A. Pucher, T. Weinhold, M. Seiß, Z. Xia, A. Wedel, and R. Danz, “Porous PTFE Space-Charge Electrets for Piezoelectric Applications”, *IEEE Trans. Dielectr. Electr. Insul.*, 7(4), 480–488 (2000) .
- [49] Z. Hu, and H. von Seggern, “Air-breakdown charging mechanism of fibrous polytetrafluoroethylene films”, *J. Appl. Phys.*, 98, 014108 (2005).
- [50] Z. Hu, and H. von Seggern, “Breakdown-induced polarization buildup in porous fluoropolymer sandwiches: a thermally stable piezoelectret”, *J. Appl. Phys.*, 99, 024102 (2006).
- [51] S. Zhukov and H. von Seggern, “Breakdown-induced light emission and poling dynamics of porous fluoropolymers”, *J. Appl. Phys.*, 101, 084106 (2007).
- [52] S. Zhukov and H. von Seggern, “Polarization hysteresis and piezoelectricity in open-porous fluoropolymer sandwiches”, *J. Appl. Phys.*, 102, 044109 (2007).
- [53] H. von Seggern, S. Zhukov, and S. Fedosov, “Poling Dynamics and Thermal Stability of FEP/ePTFE/FEP Sandwiches”, *IEEE Trans. Dielectr. Electr. Insul.*, 17(4), 1056–1065 (2010) .
- [54] S. Zhukov, S. Fedosov, and H. von Seggern, “Piezoelectrets from sandwiched porous polytetrafluoroethylene (ePTFE) films: influence of porosity and geometry on charging properties”, *J. Phys. D: Appl. Phys.*, 44(10), 105501 (2011).
- [55] H. von Seggern, S. Zhukov, and S. Fedosov, “Importance of Geometry and Breakdown Field on the Piezoelectric  $d(33)$  Coefficient of Corona Charged Ferroelectret Sandwiches”, *IEEE Trans. Dielectr. Electr. Insul.*, 18(1), 49–56 (2011) .
- [56] J. Huang, X. Zhang, Z. Xia, and X. Wang, “Piezoelectrets from laminated sandwiches of porous polytetrafluoroethylene films and nonporous fluoroethylenepropylene films”, *J. Appl. Phys.*, 103, 084111 (2008).

- [57] X. Zhang, X. Wang, G. Cao, D. Pan, and Z. Xia, “Polytetrafluoroethylene piezoelectrets prepared by sintering process”, *Appl. Phys. A: Mater. Sci. Process.*, 97, 859–862 (2009).
- [58] X. Zhang, X. Zhang, G. M. Sessler, and X. Gong, “Quasi-static and dynamic piezoelectric responses of layered polytetrafluoroethylene ferroelectrets”, *J. Phys. D: Appl. Phys.*, 47, 015501 (2014).
- [59] R. A. C. Altafim, H. C. Basso, L. Gonçalves Neto, L. Lima, R. A. P. Altafim, and C. V. de Aquino, “Piezoelectricity in Multi-Air Voids Electrets”, *IEEE Conf. Electr. Insul. Dielectr. Phenomena*, IEEE Service Center, Piscataway, NJ, 669–672 (2005).
- [60] R. A. C. Altafim, H. C. Basso, R. A. P. Altafim, L. Lima, C. V. de Aquino, L. Gonçalves Neto, and R. Gerhard(-Mulhaupt), “Piezoelectrets from thermo-formed bubble structures of fluoropolymer-electret films”. *IEEE Trans. Dielectr. Electr. Insul.*, 13(5), 979–985 (2006).
- [61] X. Zhang, J. Hillenbrand, and G. M. Sessler, “Thermally stable fluorocarbon ferroelectrets with high piezoelectric coefficient”, *Appl. Phys. A: Mater. Sci. Process.*, 84, 139–142 (2006).
- [62] X. Zhang, J. Hillenbrand, and G. M. Sessler, “Ferroelectrets with improved thermal stability made from fused fluorocarbon layers”, *J. Appl. Phys.*, 101, 054114 (2007).
- [63] X. Zhang, G. Cao, Z. Sun, and Z. Xia, “Fabrication of fluoropolymer piezoelectrets by using rigid template: structure and thermal stability”, *J. Appl. Phys.*, 108, 064113 (2010).
- [64] Z. Sun, X. Zhang, Z. Xia, X. Qiu, W. Wirges, R. Gerhard, C. Zeng, C. Zhang, and B. Wang, “Polarization and piezoelectricity in polymer films with artificial void structure”, *Appl. Phys. A: Mater. Sci. Process.*, 105, 197–205 (2011).
- [65] X. Zhang, J. Hillenbrand, G. M. Sessler G M, S. Haberzettl, and K. Lou, “Fluoroethylenepropylene ferroelectrets with patterned microstructure and high, thermally stable piezoelectricity”, *Appl. Phys. A: Mater. Sci. Process.*, 107, 621–629 (2012).
- [66] P. Fang, F. Wang, W. Wirges, R. Gerhard, and H. C. Basso, “Three-layer piezoelectrets from fluorinated ethylene-propylene (FEP) copolymer films”. *Appl. Phys. A: Mater. Sci. Process.*, 103, 455–461 (2011).
- [67] R. A. P. Altafim, X. Qiu, W. Wirges, R. Gerhard, R. A. C. Altafim, H. C. Basso, W. Jenninger, and J. Wagner, “Template-based fluoroethylenepropylene piezoelectrets with tubular channels for transducer applications”, *J. Appl. Phys.*, 106, 014106 (2009).
- [68] X. Qiu, L. Holländer, R. F. Suárez, W. Wirges, and R. Gerhard, “Polarization from Dielectric-Barrier Discharges (DBDs) in ferroelectrets: Mapping of the electric-field profiles by means of Thermal-Pulse-Tomography (TPT)”, *Appl. Phys. Lett.*, 97, 072905 (2010).
- [69] M. Sborikas, X. Qiu, W. Wirges, and R. Gerhard, W. Jenninger, and D. Lovera, “Screen printing for producing ferroelectret systems with polymer-electret films and well-defined cavities”, *Appl. Phys. A: Mater. Sci. Process.*, 114, 515–520 (2014).



- [70] G. M. Sessler, G. M. Yang, and W. Hatke, “Electret properties of cycloolefin copolymers”, *Electrical Insulation and Dielectric Phenomena*, 1997. IEEE Ann. Rep. Conf. Electr. Insul. Dielectr. Phenomena, IEEE Service Center, Piscataway, NJ, 467–470 (1997).
- [71] Y. Li and C. Zeng, “Low-Temperature CO<sub>2</sub> -Assisted Assembly of Cyclic Olefin Copolymer Ferroelectrets of High Piezoelectricity and Thermal Stability”, *Macromol. Chem. Phys.*, 214, 2733–2738 (2013).
- [72] J. Wang, T. Hsu, C. Yeh, J. Tsai, and Y. Su, “Piezoelectric polydimethylsiloxane films for MEMS transducers”, *J. Micromech. Microeng.*, 22, 015013 (2012).
- [73] J. Wang, J. Tsai, and Y. Su, “Piezoelectric rubber films for highly sensitive impact measurement”, *J. Micromech. Microeng.*, 23, 075009 (2013).
- [74] R. Gerhard(-Mulhaupt), W. Wegener, W. Wirges, J. A. Giacometti, R. A. C. Altafim, L. E. Santos, R. M. Faria, and M. Paaajanen, “Electrode poling of cellular polypropylene films with short high-voltage pulses”, *IEEE Conf. Electr. Insul. Dielectr. Phenomena*, IEEE Service Centre, Piscataway, NJ, 299–302 (2002).
- [75] M. Wegener, M. Paaajanen, W. Wirges, and R. Gerhard(-Mulhaupt), “Corona-induced partial discharges, internal charge separation and electromechanical transducer properties in cellular polymer films”, *IEEE 11th Intern. Sympos. Electrets*, IEEE Service Center, Piscataway, NJ, 54–57 (2002).
- [76] M. Paaajanen, J. Lekkala, and H. Välimäki, “Electromechanical Modeling and Properties of the Electret Film EMFi”, *IEEE Trans. Dielectr. Electr. Insul.*, 8(4), 629–636 (2001).
- [77] R. Kressmann, G. M. Sessler, P. Gunther, “Space-charge electrets”, *IEEE Trans. Dielectr. Electr. Insul.*, 3(5), 607–623 (1996).
- [78] G. M. Sessler (ed.) (1998) *Electrets*, 3rd edn., Laplacian, Morgan Hill.
- [79] M. Lindner, S. Bauer-Gogonea, S. Bauer, M. Paaajanen, and J. Raukola, “Dielectric barrier microdischarges: Mechanism for the charging of cellular piezoelectric polymers”, *J. Appl. Phys.*, 91, 5283–5287 (2002).
- [80] U. Kogelschatz, “Dielectric barrier discharges:-Their history, discharge physics and industrial applications”, *Plasma Chem. Plasma Process.*, 23, 1–46 (2003).
- [81] X. Qiu, A. Mellinger, M. Wegener, W. Wirges, and R. Gerhard, “Barrier discharges in cellular polypropylene ferroelectrets: how do they influence the electromechanical properties?”, *J. Appl. Phys.*, 101, 104112 (2007).
- [82] E. M. Bazelyan and Y. P. Raizer, *Spark Discharge* (CRC, Boca Raton, FL, 1998).
- [83] X. Qiu, A. Mellinger, W. Wirges, and R. Gerhard, “Spectroscopic study of dielectric barrier discharges in cellular polypropylene ferroelectrets”, *Appl. Phys. Lett.*, 91, 132905 (2007).
- [84] M. Paaajanen, W. Wegener, and R. Gerhard(-Mulhaupt), “Understanding the role of the gas in the voids during corona charging of cellular electret films – a way to enhance their piezoelectricity”, *J. Phys. D: Appl. Phys.*, 34, 2482–2488 (2001).

- [85] X. Qiu, M. Wegener, W. Wirges, X. Zhang, J. Hillenbrand, Z. Xia, R. Gerhard(-Mulhaupt), and G. M. Sessler, “Penetration of sulfur hexafluoride into cellular polypropylene films and its effect on the electric charging and electromechanical response of ferroelectrets”, *J. Phys. D: Appl. Phys.*, 38, 649–654 (2005).
- [86] X. Qiu, A. Mellinger, and R. Gerhard, “Influence of gas pressure in the voids during charging on the piezoelectricity of ferroelectrets”, *Appl. Phys. Lett.*, 92, 052901 (2008).
- [87] A. Mellinger and O. Mellinger, “Breakdown Threshold of Dielectric Barrier Discharges in Ferroelectrets: Where Paschen’s Law Fails”, *IEEE Trans. Dielectr. Electr. Insul.*, 18(1), 43–48 (2011).
- [88] S. Harris and A. Mellinger, “Pressure dependence of space charge deposition in piezoelectric polymer foams: simulations and experimental verification”, *Appl. Phys. A: Mater. Sci. Process.*, 107, 553–558 (2012).
- [89] S. Harris and A. Mellinger, “Towards a Better Understanding of Dielectric Barrier Discharges in Ferroelectrets: Paschen Breakdown Fields in Micrometer Sized Voids”, *J. Appl. Phys.*, 115, 163302 (2014).
- [90] S. M. Harris and A. Mellinger, “Nitrogen and Air Paschen Curves for Dielectric Barrier Discharges in  $\mu\text{m}$ -Sized Voids”, *IEEE Conf. Electr. Insul. Dielectr. Phenomena*, IEEE Service Centre, Piscataway, NJ, 2015.
- [91] C. M. Chan, T. M. Ko, H. Hiraoka, “Polymer surface modification by plasma and photos”, *Surf. Sci. Rep.*, 24, 1–54 (1996).
- [92] F. S. Denes, S. Manolache, “Macromolecular plasma-chemistry: an emerging field of polymer science”, *Prog. Polym. Sci.*, 29, 815–885 (2004).
- [93] X. Qiu and R. Gerhard, “Effective polarization fatigue from repeated dielectric barrier discharges in cellular polypropylene ferroelectrets”, *Appl. Phys. Lett.*, 93, 152902 (2008).
- [94] X. Qiu, W. Wirges, and R. Gerhard, “Beneficial and detrimental fatigue effects of dielectric barrier discharges on the piezoelectricity of polypropylene ferroelectrets”, *J. Appl. Phys.*, 110, 024108 (2011).
- [95] P. Zhang, Z. Xia, X. Qiu, F. Wang, and X. Y. Wu, “Influence of charging parameters on piezoelectricity for cellular polypropylene film electrets”, *IEEE 12th Intern. Sympos. Electrets*, IEEE Service Center, Piscataway, NJ, 39–42 (2005).
- [96] X. Qiu, R. Gerhard, and A. Mellinger, “In-situ acoustical investigation of the polarization build-up in cellular polypropylene ferroelectrets”, *IEEE Trans. Dielectr. Electr. Insul.*, 17, 1043–1049 (2010).
- [97] A. Mellinger, “Dielectric Resonance Spectroscopy: a Versatile Tool in the Quest for Better Piezoelectric Polymers”, *IEEE Trans. Dielectr. Electr. Insul.*, 10(5), 842–861 (2003).
- [98] X. Qiu, L. Holländer, W. Wirges, R. Gerhard, and H. C. Basso, “Direct hysteresis measurements on ferroelectret films by means of a modified Sawyer-Tower circuit”, *J. Appl. Phys.*, 113, 224106 (2013).

- [99] X. Qiu, W. Wirges, and R. Gerhard, “Polarization and Hysteresis in Tubular-Channel Fluoroethylenepropylene-Copolymer Ferroelectrets”, *Ferroelectrics*, 472(1), 100–109 (2014).
- [100] X. Qiu, W. Wirges, and Reimund Gerhard, “Thermal poling of ferroelectrets: How does the gas temperature influence dielectric barrier discharges in cavities?”, *Appl. Phys. Lett.*, 108, 252901 (2016).
- [101] F. W. Peek, “Dielectric Phenomena in High Voltage Engineering”, McGraw-Hill Book Comp., New York, 1915, 1920, and 1929.
- [102] W. G. Dunbar, J. W. Seabrook, “High Voltage Design Guide for Airborn Equipment”, Boeing Aerospace Comp., Seattle, WA, Report AFAPL-TR-76-41, 1976.
- [103] H. S. Uhm, S. J. Jung, and S. Kim, “Influence of Gas Temperature on Electrical Breakdown in Cylindrical Electrodes”, *J. Korean Phys. Soc.*, **42**, S989–S993 (2003).
- [104] E. Sili, F. Koliatene and J. P. Cambronne, “Pressure and temperature effects on the Paschen curve”, *Annu. Rep., IEEE Conf. Electr. Insul. Dielectr. Phenomena*, IEEE Service Centre, Piscataway, NJ, 464–467 (2011).
- [105] A. K. Vijn, “Intermolecular bonding and the electric strength of dielectric gases”, *J. Mater. Sci.*, 11, 1374–1375 (1976).
- [106] P. Fang, L. Holländer, W. Wirges and R. Gerhard, “Piezoelectric  $d_{33}$  coefficients in foamed and layered polymer piezoelectrets from dynamic mechano-electrical experiments, electro-mechanical resonance spectroscopy and acoustic-transducer measurements”, *Meas. Sci. Technol.*, 23, 035604 (2012).
- [107] X. Qiu, “Significant enhancement of the charging efficiency in the cavities of ferroelectrets through gas exchange during charging”, *Appl. Phys. Lett.*, **109**, 222903 (2016).
- [108] J. M. Pelletier, Y. Gervais, and D. Mukhedkar, “Dielectric strength of N<sub>2</sub>-He mixtures and comparison with N<sub>2</sub>-SF<sub>6</sub> and CO<sub>2</sub>-SF<sub>6</sub> mixtures”, *IEEE Trans. Power Ap. Syst.*, PAS-100(8), 3861–3869 (1981).
- [109] X. Qiu, W. Wirges, R. Gerhard, and R.A.P. Altafim, “Heterogeneous polymers as capacitive sensors: Differences between foam cells and closed or open tubular channels”, 2016 Intern. Conf. Dielectr., IEEE Service Center, Piscataway, NJ, 872–875 (2016).
- [110] R. Gerhard, “A Matter of attraction: Electric charges localised on dielectric polymers enable electromechanical transduction”, *IEEE Conf. Electr. Insul. Dielectr. Phenomena*, IEEE Service Centre, Piscataway, NJ, 1–10 (2014).
- [111] R. Gerhard, S. Bauer, and X. Qiu, “Charge-spring model for predicting the piezoelectric response of dielectric materials: Considering tetragonality extends validity to ferroelectric perovskites”, *IEEE Conf. Electr. Insul. Dielectr. Phenomena*, IEEE Service Centre, Piscataway, NJ, 81–84(2016).

- [112] G. S. Neugschwandtner, R. Schwödianer, S. Bauer-Gogonea, S. Bauer, M. Paaanen, and J. Lekkala, “Piezo- and pyroelectricity of a polymer-foam space-charge electret”, *J. Appl. Phys.*, 89, 4503–4511 (2001).
- [113] G. S. Neugschwandtner, R. Schwödianer, M. Vieytes, S. Bauer-Gogonea, S. Bauer, J. Hillenbrand, R. Kressmann, G. M. Sessler, M. Paaanen, and J. Lekkala, “Large and broadband piezoelectricity in smart polymer-foam space-charge electrets”, *Appl. Phys. Lett.*, 77 (22), 3827–3829 (2000).
- [114] J. Hillenbrand and G. M. Sessler, “Quasistatic and Dynamic Piezoelectric Coefficients of Polymer Foams and Polymer Film Systems”, *IEEE Trans. Dielectr. Electr. Insul.*, 11(1), 72–79 (2004).
- [115] G. Buchberger, R. Schwödianer, and S. Bauer, “Flexible large area ferroelectret sensors for location sensitive touchpads”, *Appl. Phys. Lett.*, 92, 123511 (2008).
- [116] A. Kogler, G. Buchberger, S. Bauer, and R. Schwödianer, “Heteropolar ferroelectrets for ultrathin flexible keyboards and tactile sensors”, *Proc. Eng.*, 5, 717–720 (2010).
- [117] R. Schwödianer, I. Graz, M. Kaltenbrunner, C. Keplinger, P. Bartu, G. Buchberger, C. Ortwein, and S. Bauer, “Cellular Ferroelectrets for Electroactive Polymer Hybrid Systems: Soft Matter Integrated Devices with Advanced Functionality”, *Proc. of SPIE*, Vol. 6927, 69270Q (2008).
- [118] S. P. Lacour, I. Graz, D. Cotton, S. Bauer, S. Wagner, “Elastic components for prosthetic skin”, 33rd Annual International Conference of the IEEE EMBS, 8373–8376 (2011).
- [119] P. Fang, L. Tian, Y. Zheng, J. Huang, and G. Li, “Using thin-film piezoelectret to detect tactile and slip signals for restoring sensation of prosthetic hands”, *Conf Proc IEEE Eng. Med. Biol. Soc.*, 2565–2568 (2014).
- [120] Q. Zhuo, L. Tian, P. Fang, G. Li, X. Zhang, “A piezoelectret-based approach for touching and slipping detection in robotic hands”, *Cyber Technology in Automation, Control, and Intelligent Systems (CYBER)*, 2015 IEEE International Conference on, 8-12 June 2015, Shenyang, China, 918-921 (2015).
- [121] G. Kofod, M. Paaanen, and S. Bauer, “Self-organized minimum-energy structures for dielectric elastomer actuators”, *Appl. Phys. A: Mater. Sci. Process.*, 85, 141–143 (2006).
- [122] B. O’Brien, T. McKay, E. Calius, S. Xie, and I. Anderson, “Finite element modelling of dielectric elastomer minimum energy structures”, *Appl. Phys. A: Mater. Sci. Process.*, 94, 507–514 (2009).
- [123] G. Kofod, W. Wirges, M. Paaanen, and S. Bauer, “Energy minimization for self-organized structure formation and actuation”, *Appl. Phys. Lett.*, 90, 081916 (2007).
- [124] W. Wirges, S. Raabe, and X. Qiu, “Fluoropolymer piezoelectrets with tubular channels: resonance behavior controlled by channel geometry”, *Appl. Phys. A: Mater. Sci. Process.*, 107, 583–588 (2012).

- [125] S. Boisseau, G. Despesse, and A Sylvestre, “Optimization of an electret-based energy harvester”, *Smart Mater. Struct.*, 19, 075015 (2010).
- [126] S. Anton and K. Farinholt, “An evaluation on low-level vibration energy harvesting using piezoelectret foam”, *Proc. SPIE 8341, Active and Passive Smart Structures and Integrated Systems 2012*, 83410G (April 26, 2012)
- [127] S. Anton, K. Farinholt, and A. Erturk, “Piezoelectret foam-based vibration energy harvesting”, *J. Intell. Mater. Syst. Struct.*, 25(14), 1–12 (2014).
- [128] P. Pondrom, J. Hillenbrand, G. Sessler, J. Bös, and T. Melz, “Vibration-based energy harvesting with stacked piezoelectrets”, *Appl. Phys. Lett.*, 104(17), 172901 (2014).
- [129] P. Pondrom, J. Hillenbrand, G. Sessler, J. Bös, and T. Melz, “Energy harvesting with single-layer and stacked piezoelectret films”, *IEEE Trans. Dielectr. Electr. Insul.*, 22(3), 1470–1476 (2015).
- [130] X. Zhang, G. M. Sessler, Y. Wang, “Fluoroethylenepropylene ferroelectret films with cross-tunnel structure for piezoelectric transducers and micro energy harvesters”, *J. Appl. Phys.*, 116(7), 074109 (2014).
- [131] Y. Wang, L. Wu, and X. Zhang, “Energy Harvesting from Vibration Using Flexible Fluoroethylenepropylene Piezoelectret Films with Cross-tunnel Structure”, *IEEE Trans. Dielectr. Electr. Insul.*, 22(3), 1349–1354 (2015).
- [132] P. Fang, Q. Zhuo, Y. Cai, L. Tian, H. Zhang, Y. Zheng, G. Li, L. Wu, and X. Zhang, “Piezoelectrets and their applications as wearable physiological-signal sensors and energy harvesters”, 2015 IEEE 12th International Conference on Wearable and Implantable Body Sensor Networks (BSN), 9-12 June 2015, Cambridge, MA, USA, 1–6 (2015).
- [133] Z. Luo, D. Zhu, J. Shi, S. Beeby, C. Zhang, Plamen Proynov, and B. Stark, “Energy harvesting study on single and multilayer ferroelectret foams under compressive force”, *IEEE Trans. Dielectr. Electr. Insul.*, 22(3), 1360–1368 (2015).
- [134] X. Zhang, P. Pondrom, L. Wu, and G. M. Sessler, “Vibration-based energy harvesting with piezoelectrets having high  $d_{31}$  activity”, *Appl. Phys. Lett.*, 108, 193903 (2016).
- [135] Z. Luo, D. Zhu, and S. P. Beeby, “Multilayer ferroelectret-based energy harvesting insole”, *J. Phys. Conf. Ser.*, 660, 012118 (2015).

# Appendix

## A Journal and Review Articles

The following journal and review articles and book chapters represent relevant contributions to the field of non-polar ferroelectret polymers. Those marked with an asterisk are enclosed in this thesis.

1. \*X. Qiu, A. Mellinger, M. Wegener, W. Wirges, and R. Gerhard, “Barrier discharges in cellular polypropylene ferroelectrets: How do they influence the electromechanical properties?”, *J. Appl. Phys.*, **101**, 104112 (2007)
2. \*X. Qiu, A. Mellinger, W. Wirges, and R. Gerhard, “Spectroscopic study of dielectric barrier discharges in cellular polypropylene ferroelectrets”, *Appl. Phys. Lett.*, **91**, 132905 (2007).
3. \*X. Qiu, A. Mellinger, and R. Gerhard, “Influence of gas pressure in the voids during charging on the piezoelectricity of ferroelectrets”, *Appl. Phys. Lett.*, **92**, 052901 (2008).
4. \*X. Qiu and R. Gerhard, “Effective polarization fatigue from repeated dielectric barrier discharges in cellular polypropylene ferroelectrets”, *Appl. Phys. Lett.*, **93**, 152902 (2008).
5. \*R. A. P. Altafim, X. Qiu, W. Wirges, R. Gerhard, R. A. C. Altafim, H. C. Basso, W. Jenninger, and J. Wagner, “Fluoroethylenepropylene ferroelectrets with homogeneous voids and patterns: simple preparation and high piezoelectricity”, *J. Appl. Phys.*, **106**, 014106 (2009).
6. P. Fang, X. Qiu, W. Wirges, R. Gerhard, and L. Zirkel, “Polyethylene-naphthalate (PEN) Ferroelectrets: Cellular Structure, Piezoelectricity and Thermal Stability”, *IEEE Trans. Dielectr. Electr. Insul.*, **17(4)** 1079–1087 (2010).
7. \*X. Qiu, R. Gerhard, and A. Mellinger, “In-situ acoustical investigation of the polarization build-up in cellular polypropylene ferroelectrets”, *IEEE Trans. Dielectr. Electr. Insul.*, **17(4)** 1043–1049 (2010).
8. \*X. Qiu, “Patterned piezo-, pyro-, and ferroelectricity of poled polymer electrets”, *Journal of applied physics*, **108**, 011101 (2010).
9. \*X. Qiu, L. Holländer, R. F. Suárez, Werner Wirges, and R. Gerhard, “Polarization from Dielectric-Barrier Discharges (DBDs) in ferroelectrets: Mapping of the electric-field profiles by means of Thermal-Pulse-Tomography (TPT)”, *Appl. Phys. Lett.*, **97**, 072905 (2010).

10. \*X. Qiu, R. Gerhard and A. Mellinger, "Turning Polymer Foams or Polymer-Film Systems into Ferroelectrets: Dielectric Barrier Discharges in the Voids", *IEEE Trans. Dielectr. Electr. Insul.*, **18(1)** 34–42 (2011).
11. Z. Sun, X. Zhang, Z. Xia, X. Qiu, W. Wirges, R. Gerhard, C. Zeng, C. Zhang, and B. Wang, "Polarization and piezoelectricity in polymer films with artificial void structure", *Appl. Phys. A: Mater. Sci. Proc.*, **105**, 197–205 (2011).
12. \*X. Qiu, W. Wirges, and R. Gerhard, "Beneficial and detrimental fatigue effects of dielectric barrier discharges on the piezoelectricity of polypropylene ferroelectrets", *J. Appl. Phys.*, **110**, 024108 (2011).
13. \*W. Wirges, S. Raabe and X. Qiu, "Dielectric elastomer and ferroelectret films combined in a single device: how do they reinforce each other?", *Appl. Phys. A: Mater. Sci. Proc.*, **107** 583–588 (2012).
14. R. A. P. Altafim, R. A. C. Altafim, X. Qiu, S. Raabe, W. Wirges, H. C. Basso, R. Gerhard, "Fluoropolymer piezoelectrets with tubular channels: resonance behavior controlled by channel geometry", *Appl. Phys. A: Mater. Sci. Proc.*, **107(4)** 965–970 (2012).
15. D. Rychkov, R. A. P. Altafim, X. Qiu, and R. Gerhard, "Treatment with orthophosphoric acid enhances the thermal stability of the piezoelectricity in low-density polyethylene ferroelectrets", *J. Appl. Phys.* **111**, 124105(2012).
16. H. C. Basso, X. Qiu, W. Wirges, and R. Gerhard, "Temporal evolution of the re-breakdown voltage in small gaps from nanoseconds to milliseconds", *Appl. Phys. Lett.*, **102**, 012904 (2013).
17. \*X. Qiu, L. Holländer, W. Wirges, R. Gerhard, and H. C. Basso, "Direct hysteresis measurements on ferroelectret films by means of a modified Sawyer-Tower circuit", *J. Appl. Phys.*, **113**, 224106 (2013).
18. \*M. Sborikas, X. Qiu, W. Wirges, R. Gerhard, W. Jeninger, and D. Lovera, "Screen printing for producing ferroelectret systems with polymer-electret films and well-defined cavities", *Appl. Phys. A: Mater. Sci. Proc.*, **114**, 515-520 (2014).
19. \*X. Qiu, W. Wirges, and R. Gerhard, "Polarization and Hysteresis in Tubular-Channel Fluoroethylenepropylene-Copolymer Ferroelectrets", *Ferroelectrics*, **472(1)**, 100-109 (2014).
20. X. Qiu, D. Rychkov, and W. Wirges, "Properties and Applications of Ferroelectrets", Book chapter in "The Nano-Micro Interface: Bridging the Mirco and Nano

Worlds”, Second Edition Volume 1 (Edited by Marcel Van de Voorde, Matthias Werner, and Hans-Jörg Fecht, WILEY-VCH, Weinheim, 2015), pp. 271-285.

21. \*X. Qiu, “Polymer Electrets and Ferroelectrets as EAPs: Materials”, Book chapter in “Electromechanically Active Polymers, Polymers and Polymeric Composites: A Reference Series” (Edited by Federico Carpi, Springer International Publishing Switzerland 2016), pp. 1-29.
22. \*X. Qiu, W. Wirges, and R. Gerhard, “Thermal poling of ferroelectrets: How does the gas temperature influence dielectric barrier discharges in cavities?”, *Appl. Phys. Lett.*, **108**, 252901 (2016).
23. \*X. Qiu, “Significant enhancement of the charging efficiency in the cavities of ferroelectrets through gas exchange during charging”, *Appl. Phys. Lett.*, **109**, 222903 (2016).



## Barrier discharges in cellular polypropylene ferroelectrets: How do they influence the electromechanical properties?

Xunlin Qiu,<sup>a)</sup> Axel Mellinger, Michael Wegener,<sup>b)</sup> Werner Wirges, and Reimund Gerhard

*Applied Condensed-Matter Physics, University of Potsdam, Am Neuen Palais 10, 14469 Potsdam, Germany*

(Received 18 December 2006; accepted 25 March 2007; published online 29 May 2007)

Ferroelectrets (i.e., charged cellular polymers) are rendered piezoelectric by means of barrier discharges inside the air-filled voids. The light emission from barrier discharges in cellular polypropylene ferroelectrets was quantitatively studied. Light emission typically occurs above a threshold voltage of 3 kV and then significantly increases with the applied voltage. Time-resolved images reveal discharge processes in individual voids. In addition, a second “back discharge” emission is observed when the voltage is reduced to zero. The buildup of the “effective polarization” in cellular PP ferroelectrets was studied by an acoustic method and dielectric resonance spectroscopy. A polarization-voltage ( $P$ - $V$ ) hysteresis loop was obtained by analyzing the data with an existing model for the piezoelectric  $d_{33}$  coefficient of ferroelectrets, from which a threshold charging voltage of 3 kV and the back barrier discharges were confirmed and a zero-field “effective polarization” of  $0.5 \text{ mC/m}^2$  was determined. However, charge densities of up to  $2 \text{ mC/m}^2$  were measured under an applied bias voltage, leading to the conclusion that the observed back discharges destroy a significant fraction of the effective charge density. © 2007 American Institute of Physics. [DOI: 10.1063/1.2735410]

### I. INTRODUCTION

In recent years, a number of cellular and voided polymers were discovered to exhibit a strong quasi-piezoelectric response.<sup>1–3</sup> The piezoelectricity is the result of charges deposited on the internal surfaces of the voids with a typical lateral size of tens of  $\mu\text{m}$ , thus forming electrical dipoles. These materials are now more and more often called “ferroelectrets,” because their polarization behavior and other related properties are macroscopically similar to those of typical ferroelectrics, while microscopic charge trapping is the same as in other space-charge electrets.<sup>4</sup>

Ferroelectrets are of considerable interest because they not only broaden the concepts of functional dielectrics, but also show an attractive potential for a variety of applications. The piezoelectricity of ferroelectrets has been theoretically analyzed by means of a model based on charged plane-parallel solid and gaseous layers,<sup>5–8</sup> including finite-element calculations.<sup>9</sup> Work is in progress to develop ferroelectrets based on new polymers with a higher thermal stability.<sup>10–12</sup> Meanwhile, several examples of applications have been reported.<sup>13,14</sup> Much work has recently been done on optimizing the electromechanical properties of ferroelectrets by means of controlled inflation<sup>15–17</sup> and charging in special gas environments.<sup>18,19</sup> It was found that Young’s modulus  $Y$  has a local minimum upon increasing inflation of the voids, corresponding to a maximum of the piezoelectric  $d_{33}$  coefficient. This verifies the proportional relation between  $d_{33}$  and  $1/Y$

predicted by the model. However, little work has been conducted on the charging process of ferroelectrets, which is the topic of this paper.

Electrical charges are deposited in the voids by means of internal Paschen breakdown that is initiated when the charging voltage becomes higher than a threshold value. In the high external electric field, charges are separated and trapped at the top and bottom surfaces of the voids, resulting in macroscopic dipoles. This charging process in ferroelectrets represents a dielectric barrier discharge (DBD, also referred to as barrier discharge).<sup>20,21</sup> In DBDs, the discharge gap is insulated from the electrodes by dielectric layers. Local breakdown in the gap is initiated by applying an electric field larger than the breakdown field, and charges are transferred through the gap and trapped at the dielectric surfaces. The breakdown extinguishes when the local electrical field, determined by the sum of the electrical field of the accumulated charges and the applied field, becomes lower than the breakdown field. DBDs are widely used for ozone generation, for surface treatment, for pollution control, for excimer lamps<sup>22</sup> and for plasma display panels,<sup>23</sup> and have attracted extensive research.<sup>24</sup> It should be pointed out that DBDs in ferroelectrets are different from the commonly studied ones (these studies are usually dedicated to discharge phenomena in a single dielectric-barrier gap) because of the numerous voids in cellular ferroelectrets with their often rather wide size distribution.

The barrier discharge is accompanied by light emission that can be photographed with a digital camera.<sup>25</sup> Recently, a quantitative analysis of the relation between light emission and piezoelectric activity of layered fluoropolymer ferroelectrets (FEP-ePTFE-FEP sandwiches) was reported.<sup>26</sup> The

<sup>a)</sup>Electronic mail: xunlin@canopus.physik.uni-potsdam.de

<sup>b)</sup>Present address: Functional Polymer Systems, Fraunhofer Institute for Applied Polymer Research, Geiselbergstrasse 69, 14476 Potsdam-Golm, Germany.

ePTFE film in such sandwiches has open pores with a size of 1  $\mu\text{m}$ . In this paper, we focus on the charging behavior of cellular PP ferroelectrets under the application of suitable voltage waveforms. The closed voids inside cellular PP ferroelectret have a lateral dimension of tens of  $\mu\text{m}$  and a height of several  $\mu\text{m}$ . The light emission from the barrier discharges was quantitatively measured and compared with the buildup of the effective charge density as determined with an acoustic method and dielectric resonance spectroscopy.

## II. SAMPLE PREPARATION

Samples were prepared from a commercial cellular PP film with the trade name PQ50 (Nan Ya Plastics Corporation, Taiwan, China). It is produced by stretching filler-loaded PP under suitable conditions.<sup>27</sup> The initial thickness and density are 50  $\mu\text{m}$  and 550  $\text{kg}/\text{m}^3$ , respectively. In order to optimize their electromechanical properties, the samples were inflated by gas diffusion expansion in nitrogen and subsequent heat treatment. The samples were then metallized on both sides with semi-transparent gold electrodes having a diameter of 16 mm and a thickness of 20 nm. For optical detection, the edges of the electrodes were covered with silicone rubber to suppress light emission due to corona discharges at the periphery of the electrode layers.

## III. EXPERIMENTS

### A. Charging

The charging voltage was applied directly to the two-side metallized samples by means of a high voltage amplifier (Trek, Model 610) controlled by a function generator (HP 33120a). In addition to amplifying the signal from the function generator, the amplifier is capable of adding a positive or negative dc bias voltage to the ac wave form.

### B. Light emission during charging

The optical emission in the near UV and visible spectral range was studied in a light-tight chamber. The voltage applied to the sample was ramped up at a constant rate, then kept at its maximum value for a certain period of time and finally ramped down at the same rate. The light emission was synchronously measured by a photomultiplier tube (PMT, R7205-01, Hamamatsu) from one side of the sample and by a PC-controlled electron-multiplying charge-coupled device camera (EMCCD, DV887ECS-BV, Andor Technology) from the other side. In order to block any light originating from a corona discharge at the electrode edge, the side of the sample facing the PMT was covered by a mask with a circular hole 8.5 mm in diameter. The PMT signal was captured by a digital storage oscilloscope (Agilent 54833A). The timing of the exposures of the EMCCD camera with respect to the applied voltage ramp was controlled with a delay generator (BNC Model 565, Berkeley Nucleonics).

### C. Acoustic measurements

The measurements were performed in an anechoic chamber. The voltage applied to the sample electrodes con-

sisted of a sinusoidal voltage with a frequency of 1 kHz and an amplitude of 100 V, superimposed on a dc bias voltage. The output sound signal, which is proportional to the amplitude of the vibration of the surface and hence to the actuator sensitivity of the sample, was measured with a microphone (Type 4191, Brüel & Kjaer), connected to a conditioning amplifier (Nexus, Brüel & Kjaer). Both the effective amplitude of the sound signal and its phase shift compared to the applied sinusoidal voltage were recorded with a lock-in amplifier (Model 7280, Ametek Inc.). The recorded sound amplitude is proportional to the inverse piezoelectric  $d_{33}$  coefficient of the ferroelectret film. The  $d_{33}$  values measured in this way were calibrated by means of dielectric resonance spectroscopy (cf. Sec. III D).

### D. Dielectric resonance spectroscopy

In order to obtain absolute  $d_{33}$  values, dielectric resonance spectra were recorded *in situ* using a Novocontrol ALPHA high-resolution dielectric analyzer. The sample was connected to the sample holder via thin silver wires. The dielectric resonance spectrum of a piezoelectric film near the thickness-extension (TE) mode antiresonance frequency is given by<sup>28-30</sup>

$$C(\omega) = \frac{\epsilon_r \epsilon_0 A}{h} \frac{1}{1 - k_t^2 \frac{\tan(\omega/4f_p)}{(\omega/4f_p)}} - - iC_{\text{loss}}, \quad (1)$$

where  $\epsilon_r$  is the relative permittivity of the sample,  $A$  and  $h$  are the electroded sample area and thickness, respectively,  $k_t$  is the complex electromechanical coupling factor, and  $f_p$  is the complex antiresonance frequency of the TE mode. For a free-standing film,  $f_p$  is related to the complex elastic stiffness  $c_{33}$  and the sample density  $\rho$  by

$$f_p = \frac{1}{2h} \sqrt{\frac{c_{33}}{\rho}}. \quad (2)$$

When one side of the piezoelectric film is glued to a glass substrate, the factor 2 in the denominator must be replaced by 4. The coupling factor  $k_t$  is given by

$$k_t^2 = d_{33}^2 c_{33} / (\epsilon_r \epsilon_0). \quad (3)$$

From the frequency-dependent real or imaginary part of the capacitance  $C(\omega)$ , the free parameters  $f_p$ ,  $k_t$ ,  $c_{33}$ , and  $d_{33}$  are determined according to Eqs. (1)–(3) with a least-squares fit.

## IV. RESULTS AND DISCUSSION

### A. Light emission from barrier discharges

The light emission  $L(t)$  under different charging voltages is shown in Fig. 1. The ramp-up and ramp-down rate of the charging voltage is kept constant (1 kV/s). Significant light emission starts when the applied voltage exceeds approximately 3 kV. As expected, the light intensity initially rises with the charging voltage because barrier discharges are initiated in an increasing number of voids. In the discharge, positive and negative charges become separated and trapped at the internal surfaces (point A in Fig. 2), thus shielding the void from the external field and extinguishing the discharge.

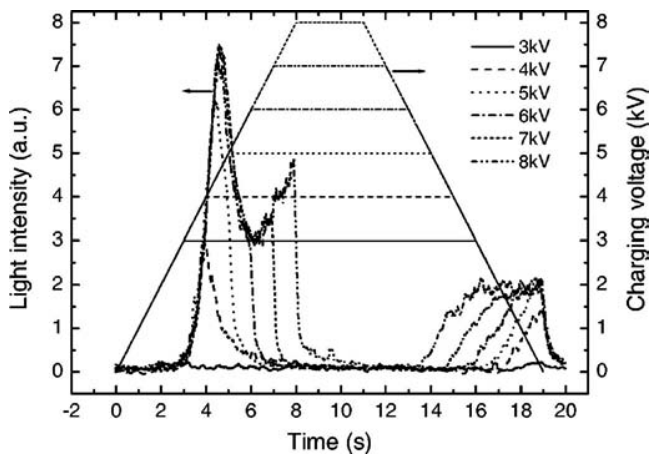


FIG. 1. PMT signal as a function of time under different charging voltages. The voltage ramp rate is  $\pm 1$  kV/s. For each voltage cycle, a fresh, uncharged sample was used.

Above 4.5 kV, a significant fraction of the available voids has already experienced Paschen breakdown, resulting in a decrease in the light intensity. When the voltage exceeds approximately 6 kV, however, the emission starts to increase again. This can be understood if voids having experienced a barrier discharge at lower voltages break down again (point B in Fig. 2). Upon reaching the maximum voltage  $V_{max}$ , the emission decreases sharply to near-zero levels, but starts again during the ramp-down phase when the voltage has dropped to  $\sim 3$  kV below  $V_{max}$ . This emission is attributed to a back discharge (inverse barrier discharge). The charges trapped on the top and bottom surfaces of the voids induce an electric field opposite to that of the applied voltage. When the external voltage is reduced, this field may overcompensate the external field and eventually trigger a back discharge (Fig. 2, point C). It should be noted that the back discharge, also called memory behavior, is well known in conventional DBDs.<sup>21</sup> The extent to which this back discharge affects the electromechanical properties of the ferroelectret material will be discussed in the following sections.

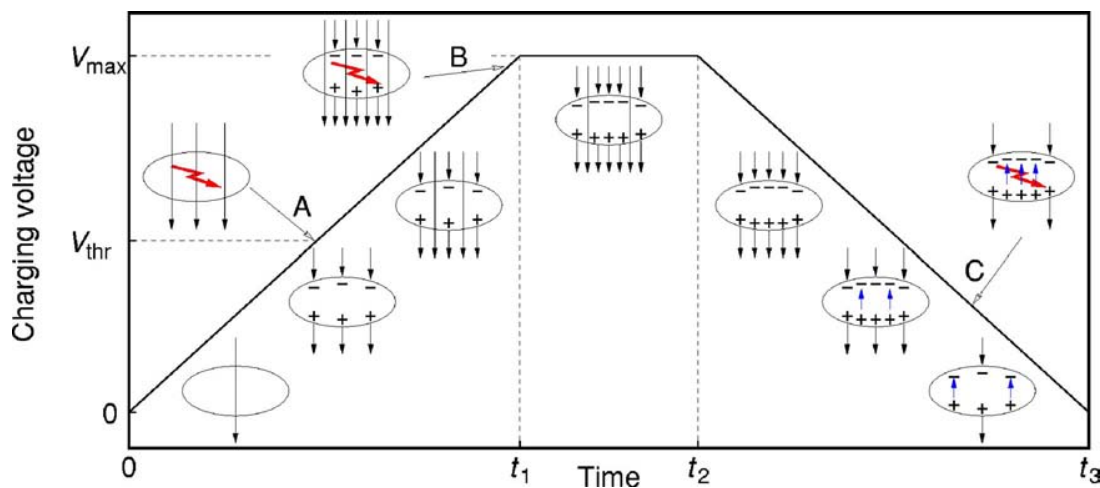


FIG. 2. (Color online) Schematic view of the electric field and trapped space charge in a single polymer void as a function of the applied voltage, which is ramped up from 0 to  $V_{max}$ , then kept constant for a period of time before being ramped down. Upon reaching the threshold voltage  $V_{thr}$ , Paschen breakdown is initiated (a). At high voltages, a second discharge may occur (b). During the ramp-down phase, the trapped charges build up a reverse electric field, leading to a back discharge (c).

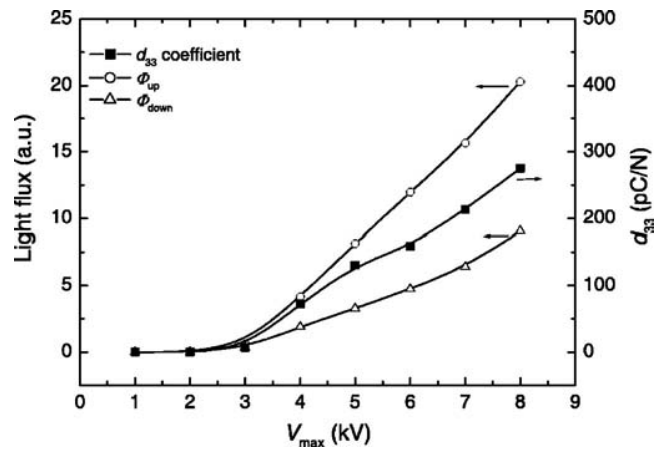


FIG. 3. Light flux during ramping up and during ramping down the charging voltage (experimental data shown in Fig. 1) as a function of the maximum charging voltage. Also shown is the piezoelectric  $d_{33}$  coefficient determined from the dielectric resonance spectrum of each sample.

The total light flux  $\Phi$  can be obtained by integrating the light intensity  $L(t)$  over time. The light flux during the previously discussed “ramp-up–hold–ramp-down” experiment is shown in Fig. 3 as a function of the maximum charging voltage  $V_{max}$ . The ramp-up flux

$$\Phi_{up} = \int_0^{t_1} L(t) dt \tag{4}$$

(where  $t_1$  is defined in Fig. 2) starts at a threshold voltage of approximately 3 kV and monotonically increases with the charging voltage. It is thus strongly correlated with the piezoelectric  $d_{33}$  coefficient, which was calculated from the dielectric resonance spectrum measured immediately after each voltage ramp. Both  $\Phi_{up}$  and  $d_{33}$  exhibit the same threshold behavior. The back-discharge flux



$$\Phi_{\text{down}} = \int_{t_2}^{t_3} L(t) dt \quad (5)$$

(where  $t_2$  and  $t_3$  are again defined in Fig. 2) follows a similar curve, but is significantly weaker, reaching approximately 40% of  $\Phi_{\text{up}}$ .

The piezoelectricity of ferroelectrets is determined by the effective charge density  $\sigma_{\text{eff}}$ , the respective thicknesses of the air gaps  $s_2$  and solid layers  $s_1$  and Young's modulus  $Y$  (cf. Sec. IV B). One should keep in mind that all samples in this study were prepared with the same parameters, so that  $Y$  and  $s_2$  show only slight sample-to-sample variations of 6% and 1%, respectively.  $s_1$  can be considered a constant, since the bulk polymer is nearly incompressible compared to the voids. Therefore, the dependence of  $d_{33}$  on the charging voltage is dominated by  $\sigma_{\text{eff}}$ , which in turn must then be correlated with the light emission  $\Phi$ . In particular, according to the model depicted in Fig. 2, the back discharge is expected to decrease  $\sigma_{\text{eff}}$  from a possibly high value at  $V_{\text{max}}$  to a smaller value in the absence of an external electric field. Verifying this hypothesis required measuring  $d_{33}$  under an applied bias voltage, as described in Sec. IV B.

Additional insight into the charging process of ferroelectrets can be gained from spatially-resolved light-emission maps. Figure 4 shows photographs taken by an EMCCD camera for a maximum charging voltage of  $V_{\text{max}}=6$  kV and a ramp rate of 6 kV/s. The onset of the light emission is at  $t=0.5$  s (corresponding to  $V=3$  kV), which again demonstrates the threshold behavior. Some of the larger voids near the surface facing the camera can be seen to discharge and back-discharge in a specific voltage range. To our knowledge, this represents the first time-resolved imaging of the discharge process in individual voids. Discharges from voids in the bulk of the sample are recorded as well, but, due to strong light scattering in cellular PP, are seen as a diffuse glow, rather than individually resolved point discharges.

By integrating the flux in a 9 mm diameter circle, the time-dependence of the total light emission can be obtained. Figure 5 shows that—as for the PMT data—there is one “charging” and one “back discharge” peak, although their intensity ratio is different in comparison to Fig. 1. Unlike the measurements in Fig. 1, where a fresh sample was used for each “ramp-up–hold–ramp-down” cycle, the samples investigated with the EMCCD camera underwent multiple cycles in order to improve the signal-to-noise ratio. Thus, when the voltage was ramped up from 0 to 6 kV, many voids already carried a charge, and therefore an internal electric field opposite to the applied field. These voids would, if at all, experience a discharge only at much higher charging voltages. Therefore, the intensity of the “charging” peak is reduced, while the “back discharge” peak remains largely unaffected by the history of the sample.

## B. Acoustic investigation of the actuator sensitivity and charge density

The discovery of the back discharge and the observed correlation between light emission and piezoelectric activity prompted the investigation of the piezoelectric  $d_{33}$  coefficient

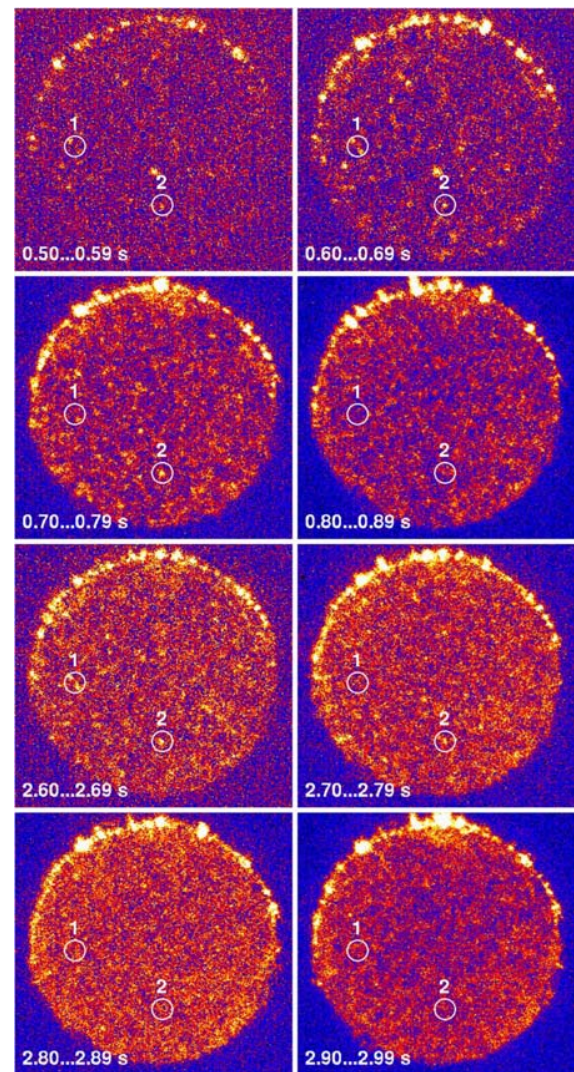


FIG. 4. (Color online) False-color EMCCD images of a cellular PP sample. The applied charging voltage was ramped up at a rate of 6 kV/s, starting at  $t=0$ , kept constant for 1 s and finally ramped down at a rate of  $-6$  kV/s (cf. Fig. 5). Each frame was exposed for 90 ms. The images represent an average over 25 cycles. Circles 1 and 2 indicate light emission from some of the larger voids. The strong emission at the upper rim results from corona discharge at the electrode edge.

during the charging process. An acoustic technique, using the inverse piezoelectric effect, was chosen due to its simplicity and its capability of measuring  $d_{33}$  under an applied bias voltage. The acoustic signal as a function of the external bias voltage  $V_{\text{bias}}$  is depicted in Fig. 6. When the maximum voltage of the cycle is lower than 3 kV, no difference in the sound signal is observed between ramping up and ramping down the external bias voltage. However, when the external bias voltage exceeds 3 kV, the sound signal during ramping up the external voltage is higher than the corresponding value during ramping down, and the difference grows with increasing maximum voltage of the cycle. As the voltage is reduced from its maximum value,  $d_{33}$  reaches a minimum, then increases again as  $V_{\text{bias}}$  passes through zero, forming a characteristic “butterfly” curve.

To understand the origin of this curve, we look at the change in thickness under an external voltage. According to a simplified model of ferroelectrets,  $\Delta s$  can be expressed as<sup>8</sup>

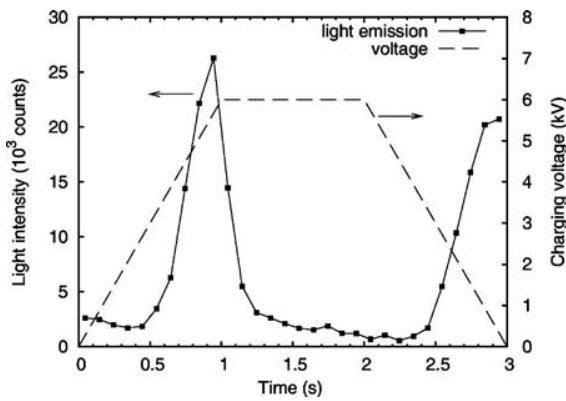


FIG. 5. Light intensity and charging voltage as a function of time. The light intensity was obtained from EMCCD images (cf. Fig. 4) by subtracting dark frames and integrating the flux in a circle of approximately 9 mm diameter, centered on the sample.

$$\Delta s = \frac{s}{Y} \frac{\varepsilon_p s_1 \sigma_{\text{eff}} V - \frac{1}{2} \varepsilon_0 \varepsilon_p^2 V^2}{(s_1 + \varepsilon_p s_2)^2}, \quad (6)$$

where  $V$  is the external voltage applied to the electrodes,  $Y$  is Young's modulus of the sample,  $\varepsilon_0$  and  $\varepsilon_p$  are the permittivity of vacuum and the relative permittivity of PP, respectively.  $s_1$  and  $s_2$  are the total thickness of the solid material layers and the gaseous layers, respectively, with  $s = s_1 + s_2$  being the total film thickness.  $\sigma_{\text{eff}} = \sum s_{2i} \sigma_i / \sum s_{2i}$  is the effective charge density on the PP/air interfaces on both sides of the single air gap, where  $s_{2i}$  is the thickness of the  $i$ th gaseous layer with  $\sum s_{2i} = s_2$ , and  $\sigma_i$  is the charge density on the surface of the  $i$ th layer. In the numerator of Eq. (6), the first term is the piezoelectric contribution from the charged voids while the second term describes the Maxwell stress. The right-hand side of Eq. (6) has the opposite sign compared to that in Ref. 8 due to the fact that  $\sigma_{\text{eff}}$  results from the very barrier discharge caused by the applied voltage  $V$ . Its polarity is such that the piezoelectric term in Eq. (6) makes the

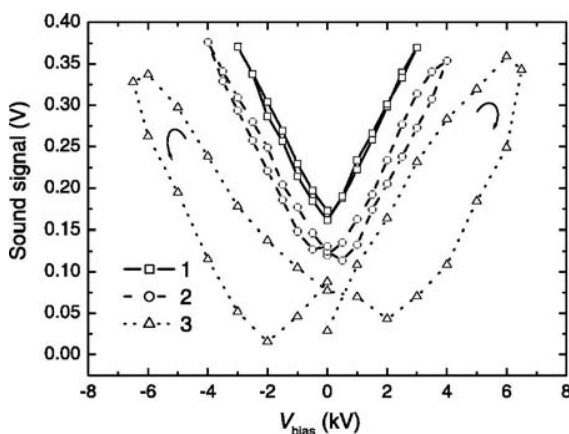


FIG. 6. Sound signal as a function of the external bias voltage applied to the electrodes. The positive half cycle is followed by the negative half cycle (the cycle direction is denoted by two arrows). The maximum voltages for each cycle are: (1) 3 kV, (2) 4 kV, and (3) 6 kV. Measurements were done on the same, previously uncharged sample from cycle 1 to 3. For clarity, the results of cycle (1) and (2) were shifted by 0.15 V and 0.1 V, respectively.

sample expand unless  $V$  is reversed. The Maxwell stress term, on the other hand, always results in a compressive strain.

Applying a voltage  $V = V_{\text{bias}} + V_0 \sin(\omega t)$  where  $V_0 \ll V_{\text{bias}}$ , we obtain from Eq. (6)

$$\Delta s \approx \frac{s}{Y(s_1 + \varepsilon_p s_2)^2} \left\{ -\frac{1}{2} \varepsilon_0 \varepsilon_p^2 V_{\text{bias}}^2 + \varepsilon_p s_1 \sigma_{\text{eff}} V_{\text{bias}} + [-\varepsilon_0 \varepsilon_p^2 V_{\text{bias}} + \varepsilon_p s_1 \sigma_{\text{eff}}] V_0 \sin(\omega t) \right\}, \quad (7)$$

where the term proportional to  $V_0^2$  has been neglected. Inspecting the last term in Eq. (7), we see that the radiated sound amplitude has a contribution not only from the effective charge density  $\sigma_{\text{eff}}$ , but also from the modulated Maxwell stress. The effective piezoelectric coefficient at  $V_{\text{bias}}$  is then given by

$$d_{33} = \frac{s}{Y} \frac{\varepsilon_p s_1 \sigma_{\text{eff}} - \varepsilon_0 \varepsilon_p^2 V_{\text{bias}}}{(s_1 + \varepsilon_p s_2)^2}. \quad (8)$$

The amplitude of the sound signal in Fig. 6 is proportional to the absolute value of  $d_{33}$ . In Ref. 8, an almost linear dependence of the piezoelectric sensitivity on the external voltage was observed within the range from  $-700$  to  $+700$  V. This is the expected behavior according to Eq. (8), since  $\sigma_{\text{eff}}$  can be considered constant at an external voltage much lower than the threshold voltage. In the present work, however, a much higher external voltage was applied, and the actuator response of the sample was synchronously detected by an acoustic method. For cycles where the maximum  $V_{\text{bias}}$  is lower than the threshold voltage, there is no hysteresis in the sound signal (Fig. 6) since the signal results from the reversible effect of the Maxwell stress only. Above a threshold voltage of approximately 3 kV, electric breakdown occurs in the voids, giving rise to an effective charge density  $\sigma_{\text{eff}}$  which contributes to  $d_{33}$  with the opposite sign of the Maxwell stress term in Eq. (8). As a result, the slope in Fig. 6 is reduced as  $V_{\text{bias}}$  increases and a difference of the sound signal between ramping up and ramping down the external bias voltage appears.

The observed minimum in the sound signal vs. bias voltage occurs when the piezoelectric and Maxwell stress terms in Eq. (8) cancel each other. The small residual sound signal at this point can be attributed to a nonuniform spatial distribution of  $\sigma_{\text{eff}}$ . A phase shift of approximately  $180^\circ$  between the sound signal and the stimulating sinusoidal voltage is observed when the sound signal passes through its minimum in the "butterfly" curve due to the reversal of the polarity of the  $d_{33}$  coefficient.

The acoustic measurements, only delivered relative (un-calibrated)  $d_{33}$  values. In order to obtain absolute  $d_{33}$  values, dielectric resonance spectroscopy was performed on the sample immediately after the external voltage cycles. Young's modulus and  $d_{33}$  were determined by fitting the real part of the measured capacitance (inset of Fig. 7) to Eqs. (1)–(3). By comparing this  $d_{33}$  value with the zero-field sound signal, all other sound signal measurements can be converted to piezoelectric  $d_{33}$  coefficients.



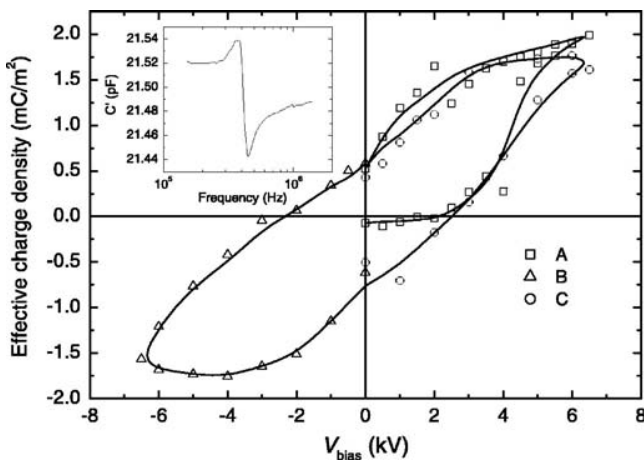


FIG. 7. Calculated effective charge density  $\sigma_{\text{eff}}$  as a function of the bias voltage  $V_{\text{bias}}$ . A fresh, uncharged sample was used for the positive half cycle (a), followed by a negative half cycle (b), and subsequently a second positive half cycle (c). The inset shows a typical dielectric resonance spectrum from which the  $d_{33}$  coefficient and  $\sigma_{\text{eff}}$  were calculated.

Now that absolute  $d_{33}$  values are available,  $\sigma_{\text{eff}}$  can be calculated from  $s_1$ ,  $s_2$ ,  $V_{\text{bias}}$ , and  $Y$  according to Eq. (8). This calculation assumes that  $s_2$  and  $Y$  remain constant. For  $V_{\text{bias}}=6.5$  kV, the first (Maxwell stress) term in Eq. (7) is  $-4.1 \mu\text{m}$ . However, the actual bias thickness change is less than  $-4.1 \mu\text{m}$  because it is partly compensated by the second (piezoelectric) term.  $Y$  can be considered as a constant within such a small thickness change. The quantities  $s_1$  and  $s_2$  were determined from the density of the samples given by the manufacturer and from the measured thickness, because the density of PP is known and the density of air is approximated as zero. The development of  $\sigma_{\text{eff}}$  with  $V_{\text{bias}}$  is clearly visible in Fig. 7, which shows a hysteresis behavior similar to that of traditional ferroelectrics. For a fresh, uncharged sample,  $\sigma_{\text{eff}}$  is nearly zero when the external voltage is below 3 kV. The small negative effective charge density at  $V_{\text{bias}}=0$  (corresponding to  $d_{33} \approx 2$  pC/N) is due to charges deposited during the manufacturing process. Above the threshold voltage,  $\sigma_{\text{eff}}$  increases to a maximum value of  $2.0 \text{ mC/m}^2$ . However, a significant reduction of  $\sigma_{\text{eff}}$  is observed when the external voltage decreases from its maximum to a value below 3 kV, which again proves the back barrier discharge. A zero-field  $\sigma_{\text{eff}}$  value of about  $0.5 \text{ mC/m}^2$  is obtained, analogous to the remanent polarization in ferroelectrics. This value is in very good agreement with values determined by Sessler *et al.*<sup>6</sup> and Paajanen *et al.*<sup>8</sup> on other types of cellular PP ferroelectrets. Somewhat more accurate values could be expected if the thickness change was directly measured by, e.g., an interferometric method.

## V. CONCLUSION

Light emission from barrier discharges in the voids of ferroelectrets shows the same threshold behavior as the piezoelectricity of the respective material. For pressure-inflated PQ50 ferroelectrets, the emission starts above a threshold voltage of 3 kV and then significantly increases with the applied voltage. In addition, a second “back discharge” emis-

sion is observed when the voltage is reduced toward zero. The discharge events in individual voids are revealed by time-resolved images.

Direct contact charging of pressure-inflated PQ50 ferroelectrets with varying voltage leads to a polarization-voltage ( $P$ - $V$ ) hysteresis curve, from which a threshold charging voltage of 3 kV and the back barrier discharges were confirmed and a zero-field “effective polarization” of  $0.5 \text{ mC/m}^2$  was determined. Our results suggest that the piezoelectricity of ferroelectrets would be significantly improved if the back discharge could be suppressed, since it destroys a significant fraction of the effective charge density.

## ACKNOWLEDGMENTS

We thank Dr. Guggi Kofod and Dr. Steffen Bergweiler (both University of Potsdam) for many stimulating discussions. We are also indebted to Professor Martin Ostermeyer and Markus Gregor from the Nonlinear Optics group at the University of Potsdam for providing the EMCCD camera.

- <sup>1</sup>S. Bauer, R. Gerhard-Multhaupt, and G. M. Sessler, *Phys. Today* **57**, 37 (2004).
- <sup>2</sup>M. Wegener and S. Bauer, *ChemPhysChem* **6**, 1014 (2005).
- <sup>3</sup>M. Wegener, *Mater. Sci. Eng., R: Reports* (in press).
- <sup>4</sup>M. Lindner, H. Hoislbauer, R. Schwödäuer, S. Bauer-Gogonea, and S. Bauer, *IEEE Trans. Dielectr. Electr. Insul.* **11**, 255 (2004).
- <sup>5</sup>G. M. Sessler and J. Hillenbrand, *Appl. Phys. Lett.* **75**, 3405 (1999).
- <sup>6</sup>J. Hillenbrand, G. M. Sessler, and X. Zhang, *J. Appl. Phys.* **98**, 064105 (2005).
- <sup>7</sup>M. Paajanen, H. Välimäki, and J. Lekkala, *Proceedings of the 10th International Symposium on Electrets, Delphi, Greece, 22–24 September, 1999* (IEEE Service Center, Piscataway, NJ, 1999), pp. 735–738.
- <sup>8</sup>M. Paajanen, J. Lekkala, and H. Välimäki, *IEEE Trans. Dielectr. Electr. Insul.* **8**, 629 (2001).
- <sup>9</sup>E. Tuncer, *J. Phys. D* **38**, 497 (2005).
- <sup>10</sup>M. Wegener, W. Wirges, and R. Gerhard-Multhaupt, *Adv. Eng. Mater.* **7**, 1128 (2005).
- <sup>11</sup>W. Wirges, M. Wegener, O. Voronina, L. Zirkel, and R. Gerhard-Multhaupt, *Adv. Funct. Mater.* **17**, 324 (2007).
- <sup>12</sup>E. Saarimäki, M. Paajanen, A. Savijärvi, M. Wegener, O. Voronina, R. Schulze, W. Wirges, and R. Gerhard-Multhaupt, *IEEE Trans. Dielectr. Electr. Insul.* **13**, 963 (2006).
- <sup>13</sup>I. Graz, M. Kaltenbrunner, C. Keplinger, R. Schwödäuer, S. Bauer, S. P. Lacour, and S. Wagner, *Appl. Phys. Lett.* **89**, 073501 (2006).
- <sup>14</sup>J. Hillenbrand and G. M. Sessler, *J. Acoust. Soc. Am.* **116**, 3267 (2004).
- <sup>15</sup>X. Zhang, J. Hillenbrand, and G. M. Sessler, *J. Phys. D* **37**, 2146 (2004).
- <sup>16</sup>M. Wegener, W. Wirges, J. Fohlmeister, B. Tiersch, and R. Gerhard-Multhaupt, *J. Phys. D* **37**, 623 (2004).
- <sup>17</sup>M. Wegener, W. Wirges, R. Gerhard-Multhaupt, M. Dansachmüller, R. Schwödäuer, S. Bauer-Gogonea, S. Bauer, M. Paajanen, H. Minkinen, and J. Raukola, *Appl. Phys. Lett.* **84**, 392 (2004).
- <sup>18</sup>M. Paajanen, M. Wegener, and R. Gerhard-Multhaupt, *J. Phys. D* **34**, 2482 (2001).
- <sup>19</sup>X. Qiu, M. Wegener, W. Wirges, X. Zhang, J. Hillenbrand, Z. Xia, R. Gerhard-Multhaupt, and G. M. Sessler, *J. Phys. D* **38**, 649 (2005).
- <sup>20</sup>M. Lindner, S. Bauer-Gogonea, S. Bauer, M. Paajanen, and J. Raukola, *J. Appl. Phys.* **91**, 5283 (2002).
- <sup>21</sup>U. Kogelschatz and J. Salge, in *Low Temperature Plasma Physics, Fundamental Aspects and Applications*, edited by R. Hippler, S. Pfau, M. Schmidt, and K. H. Schoenbach (Wiley VCH, New York, 2001), Chap. 13, pp. 331–357.
- <sup>22</sup>U. Kogelschatz, *Pure Appl. Chem.* **62**, 1667 (1990).
- <sup>23</sup>G. Oversluizen, M. Klein, S. De Zwart, S. Van Heusden, and T. Dekker, *Appl. Phys. Lett.* **77**, 948 (2000).
- <sup>24</sup>U. Kogelschatz, *Plasma Chem. Plasma Process.* **23**, 1 (2003), and references therein.

- <sup>25</sup>M. Wegener, M. Paajanen, W. Wirges, and R. Gerhard-Multhaupt, *Proceedings of the 11th International Symposium on Electrets, Melbourne, Australia, 1–3 October, 2002* (IEEE Service Center, Piscataway, NJ, 2002), pp. 54–57.
- <sup>26</sup>S. Zhukov and H. von Seggern, *J. Appl. Phys.* **101**, 084106 (2007).
- <sup>27</sup>A. Savolainen and K. Kirjavainen, *J. Macromol. Sci., Chem.* **A26**, 583 (1989).
- <sup>28</sup>A. Mellinger, *IEEE Trans. Dielectr. Electr. Insul.* **10**, 842 (2003).
- <sup>29</sup>H. Ohigashi, *J. Appl. Phys.* **47**, 949 (1976).
- <sup>30</sup>G. S. Neugschwandtner, R. Schwödiauer, M. Vieytes, S. Bauer-Gogonea, S. Bauer, J. Hillenbrand, R. Kressmann, G. M. Sessler, M. Paajanen, and J. Lekkala, *Appl. Phys. Lett.* **77**, 3827 (2000).

## Spectroscopic study of dielectric barrier discharges in cellular polypropylene ferroelectrets

Xunlin Qiu,<sup>a)</sup> Axel Mellinger, Werner Wirges, and Reimund Gerhard

*Applied Condensed-Matter Physics, University of Potsdam, Am Neuen Palais 10, 14469 Potsdam, Germany*

(Received 9 August 2007; accepted 29 August 2007; published online 25 September 2007)

The transient light emission from the dielectric barrier discharges (DBDs) in cellular polypropylene ferroelectrets subjected to high electric poling fields was spectroscopically measured. The spectrum shows strong emission from the second positive system of molecular nitrogen,  $N_2(C^3\Pi_u) \rightarrow N_2(B^3\Pi_g)$ , and the first negative system of  $N_2^+$ ,  $N_2^+(B^2\Sigma_u^+) \rightarrow N_2^+(X^2\Sigma_g^+)$ , consistent with a DBD in air. When a dc voltage is applied stepwise to the ferroelectret film, light emission starts above a threshold, coinciding with the threshold voltage in obtaining piezoelectricity. From selected vibronic band strength ratios, the electric field in the discharge was determined and found to agree with Townsend breakdown. © 2007 American Institute of Physics. [DOI: 10.1063/1.2786597]

Cellular polymers (polymer foams) were produced as early as the 1960s.<sup>1</sup> They are now widely used in daily life for thermal insulation, shock and sound absorptions, packaging, etc.<sup>2</sup> In recent years, a number of nonpolar cellular or porous polymers were discovered to exhibit a strong electromechanical (quasipiezoelectric) response. These materials are now more and more called “ferroelectrets”.<sup>3,4</sup> In order to render ferroelectrets piezoelectric, their voids must be internally charged by means of micro-plasma discharges.<sup>5–8</sup> This charging process represents dielectric barrier discharges (DBDs), (also referred to as barrier discharges). In DBDs, at least one side of the discharge gap is insulated from the electrodes by a dielectric layer. DBDs are widely used for ozone generation, for surface treatment, for pollution control, for excimer lamps, and for plasma display panels, and have attracted extensive research.<sup>9</sup> While the theoretical analysis of the piezoelectricity of ferroelectrets, the dependence of the piezoelectricity on the morphology, and the development of ferroelectrets based on new materials have been the subject of numerous publications in recent years, relatively little is known about the DBD process in the voids of ferroelectrets.

DBDs in ferroelectrets during charging are accompanied by light emission that can be photographed with a digital camera.<sup>5,6</sup> This light emission arises from electronically excited and/or ionized gas molecules inside the voids and can be used as a diagnostic tool for characterizing the DBDs.<sup>10</sup> In this letter, the transient light emission from the DBDs in cellular polypropylene (PP) ferroelectrets subjected to high electric fields was quantitatively and spectroscopically analyzed.

Samples were prepared from commercial cellular PP films with the trade name PQ50 (Nan Ya Plastics Corporation, Taiwan, China). They are produced by stretching filler-loaded PP under suitable conditions.<sup>11</sup> The initial thickness and density are 50  $\mu\text{m}$  and 550  $\text{kg}/\text{m}^3$ , respectively. In order to optimize their electromechanical properties, the samples were inflated by a gas diffusion expansion in nitrogen and a subsequent heat treatment.<sup>12</sup> The samples were then metalized on both sides with semitransparent gold electrodes having a diameter of 16 mm and a thickness of 20 nm. The edges of the electrodes were covered with silicone rubber in

order to suppress corona discharges at the periphery of the electrodes. All experiments were performed in a light-tight chamber. Light emission was recorded by a photomultiplier (R7205-01, Hamamatsu) from one side of the sample. The photomultiplier tube (PMT) signal was captured by a digital storage oscilloscope (Agilent 54833A). The charging voltage was supplied by a high voltage amplifier (Trek, Model 610) controlled by an arbitrary waveform function generator (HP 33120A). The optical emission spectra of the light emission were recorded with a fiber-optic charge-coupled device spectrometer (Andor Technology), which consists of an optical fiber, a monochromator, and a charge-coupled device (CCD) camera (Model DU420A-OE). In order to block any light originating from a corona discharge at the electrode edge, the side of the sample facing the PMT (optical fiber) was covered by a plastic mask with a central circular hole 8.5 mm in diameter.

For ferroelectrets, it is known that the curve of the piezoelectric  $d_{33}$  coefficient versus charging voltage shows a threshold behavior.<sup>6</sup> The piezoelectric activity significantly increases with the increase of charging voltage when the latter is higher than the threshold value. The same behavior was found for the light emission during charging, as shown in Fig. 1, in which a stepwise voltage waveform was applied to the sample. Light emission is observed when the charging

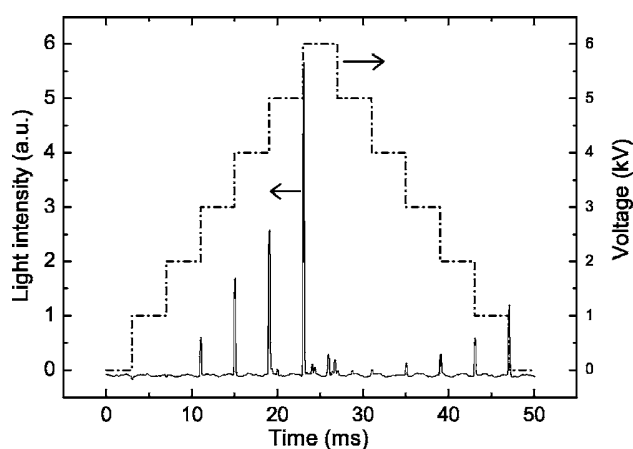


FIG. 1. PMT signal as a function of time under stepwise charging voltages. The charging voltage is increased and then decreased in steps of 1 kV.

<sup>a)</sup>Electronic mail: xunlin@canopus.physik.uni-potsdam.de



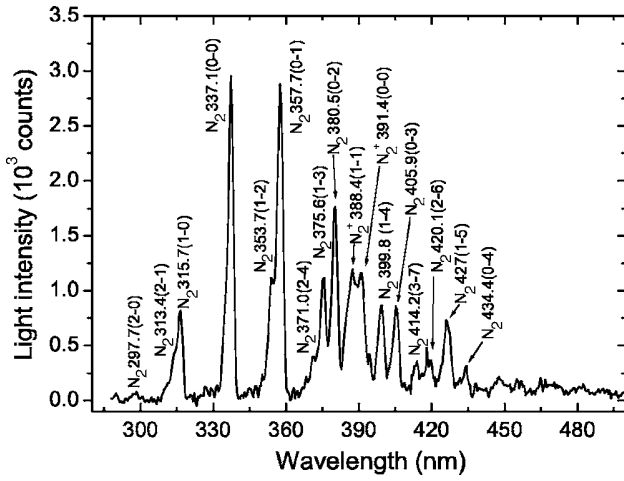
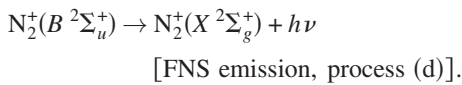
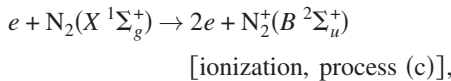
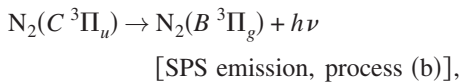
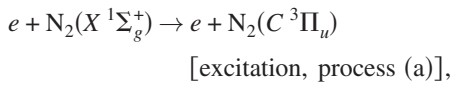


FIG. 2. Optical emission spectra of PQ50 ferroelectret under positively biased sinusoidal voltages with a frequency of 100 Hz and  $V_{pp}$  of 6 kV. The CCD camera is internally triggered with an exposure time of 4 s.

voltage reaches 3 kV, and thereafter the light intensity significantly increases with the increase of voltage. As can be seen from Fig. 1, the light emission occurs only at the beginning of each relevant voltage step and decreases very quickly back to the noise level of the PMT. This is attributed to the choking effect in DBDs.<sup>9</sup> In addition, measurable light emission starts again when the voltage decreases from the maximum of 6 kV back to about 3 kV. This emission is caused by a back discharge.<sup>8</sup>

Analysis of the optical emission spectrum (OES) is an effective method for diagnosing DBDs. The OES of the DBDs in cellular PP ferroelectrets was recorded within the wavelength range of 250–700 nm. A part of the spectrum from samples under positively biased sinusoidal voltages  $V = \frac{1}{2}V_{pp}[1 + \sin(\omega t)]$  is presented in Fig. 2. There is no detectable optical emission when  $V_{pp}$  is lower than 3 kV, which is in agreement with the PMT results. Above 3 kV, the optical emission spectra can be clearly measured. They consist of vibronic bands of the second positive system (SPS) of molecular nitrogen ( $N_2$ ) and the first negative system (FNS) of  $N_2^+$ , which is consistent with DBDs in air.<sup>13</sup>

The optical emission results from the following elementary processes:<sup>13,14</sup>



The SPS of  $N_2$  originates from processes (a) and (b). Obviously, it does not contribute to charge separation, since it only involves electronically excited neutral  $N_2$  molecules, whereas the appearance of the FNS of  $N_2^+$  [processes (c) and (d)] indicates the ionization of molecular nitrogen. Since in-

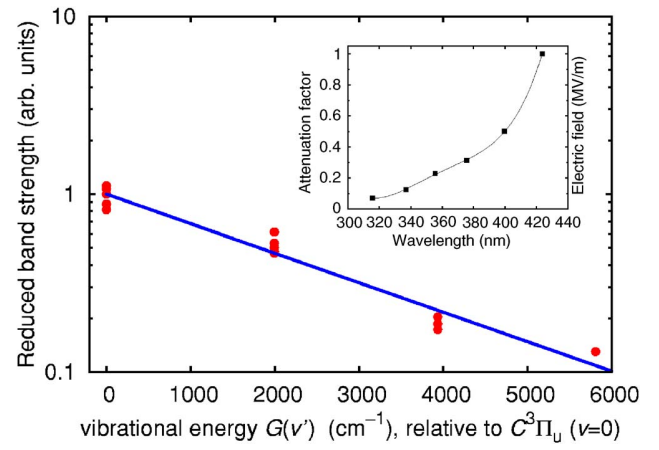


FIG. 3. (Color online) Boltzmann plot of the SPS reduced band strengths [i.e.,  $I/(C_{v'-v''}q_{v'v''}v^3)$ , shown as solid circles] and a least squares fit (straight line) corresponding to a vibrational temperature of 3700 K. The inset shows the optical attenuation coefficient  $C_{v'-v''}$  as a function of wavelength normalized to  $C_{-4}$ .

dividual rotational lines cannot be resolved by the spectrograph, the vibronic band intensity can be written as<sup>15</sup>

$$I = C(v)q_{v'v''}v^3 \exp\left(-\frac{G(v')hc}{kT_{\text{vib}}}\right), \quad (1)$$

where  $I$  is the light intensity in counts,  $T_{\text{vib}}$  is the vibrational temperature, and  $h$ ,  $c$ , and  $k$  are Planck's constant, the speed of light and Boltzmann's constant, respectively. For the SPS, the Franck-Condon factors  $q_{v'v''}$  (where  $v'$  and  $v''$  are the vibrational quantum numbers of the upper and lower level, respectively), the transition frequencies  $\nu$ , and the vibrational term values  $G(v')$  were taken from Ref. 14.  $C(v)$  is a proportionality factor which, for a calibrated spectrometer, should be independent of  $\nu$ . However, a comparison of the experimental spectrum with simulations using Eq. (1) showed a significant intensity decrease toward shorter wavelengths, even though the spectral sensitivity of the apparatus was normalized by means of a calibrated tungsten lamp, and the wavelength-dependent absorption of the semitransparent gold electrodes<sup>16</sup> was taken into account. We attribute this intensity decrease to absorption by UV-absorbing additives which are frequently found in PP, as well as light scattering in the cellular PP film. To determine the attenuation coefficient as a function of wavelength,  $C(v)$  was approximated by a set of attenuation coefficients  $C_{v'-v''}$ . Thus, there is one coefficient for each group of bands with constant  $v'-v''$  (and very similar wavelengths). These coefficients, as well as  $T_{\text{vib}} \approx 3700$  K, were determined by fitting the observed band strengths to Eq. (1). The reduced band strengths [i.e.,  $I/(C_{v'-v''}q_{v'v''}v^3)$ ] are shown in Fig. 3 as a Boltzmann plot; the inset shows the attenuation coefficients (normalized to  $C_{-4}$ ).

With the known attenuation coefficients (interpolated by a fourth order polynomial), absorption-corrected intensities of the  $N_2$  SPS (0→0) and (2→5) bands (at 337.1 and 394.3 nm, respectively) and the  $N_2^+$  FNS (0→0) band at 391.4 nm were calculated. Their ratios, subsequently denoted as  $R_{391/337}$  and  $R_{391/394}$ , have been shown to be an indicator of the electric field in air discharges,<sup>17</sup> as the ionization process (c) of molecular nitrogen is field dependent. Figure 4 shows the intensities of the  $N_2$  SPS (0→0) and  $N_2^+$  FNS (0→0)

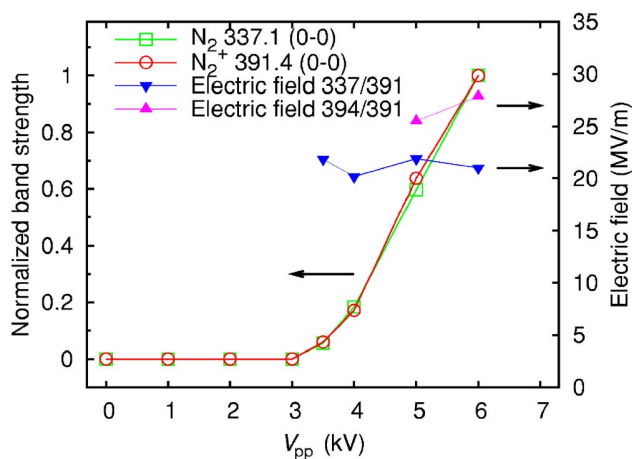


FIG. 4. (Color online) Spectral intensities of the  $N_2$  SPS (0-0) band at 337.1 nm and the  $N_2^+$  FNS (0-0) band at 391.4 nm as a function of  $V_{pp}$  (open squares and circles). The band strengths were normalized to their respective maximum value at  $V_{pp}=6$  kV. Also shown are the electric field strengths calculated from the  $R_{391/337}$  and  $R_{391/394}$  intensity ratios (upward and downward triangles).

bands as a function of  $V_{pp}$ . Both bands appear in the spectrum when  $V_{pp}$  reaches 3 kV and then significantly increase with  $V_{pp}$ , exhibiting a very similar dependence on  $V_{pp}$ . This behavior is in good agreement with the dependence of the piezoelectric  $d_{33}$  coefficient on the charging voltage.<sup>8</sup> Using the empirical equations of Paris *et al.*,<sup>17</sup> the  $R_{391/337}$  and  $R_{391/394}$  ratios were used to determine the electric field in the voids at the moment of discharge (also shown in Fig. 4). Both ratios give an electric field between 21 and 28 MV/m without a significant dependence on  $V_{pp}$ . These values are in good agreement with the breakdown strength in air according to the Townsend breakdown model<sup>18</sup> for air-filled voids with heights between 10 and 15  $\mu\text{m}$ . Smaller voids should have a higher breakdown strength and would therefore experience breakdown at higher values  $V_{pp}$ , suggesting that the observed electric field should rise with  $V_{pp}$ . On the other hand, this dependence would be mitigated by their smaller contribution to the overall light emission (due to their smaller size), and the fact that the larger voids may experience a secondary breakdown at higher applied voltages,<sup>8</sup> which would happen at the same, lower value of the external voltage as the first breakdown. Thus, the spectroscopic measurements of the breakdown field strengths are biased toward larger voids.

In conclusion, the optical emission spectrum of the DBDs in ferroelectrets shows strong UV/visible emission resulting from the second positive system (SPS) of molecular nitrogen  $N_2(C^3\Pi_u \rightarrow B^3\Pi_g)$  and the first negative system (FNS) of  $N_2^+(B^2\Sigma_u^+ \rightarrow X^2\Sigma_g^+)$ , consistent with DBDs in air.

The transient light emission from the DBDs in cellular polypropylene ferroelectrets subjected to high electric fields shows the same trend as the piezoelectricity and is therefore strongly correlated with it. From a spectroscopic analysis of the band strength ratios, the electric field during the discharge process could be determined to be in the range between 21 and 28 MV/m, in good agreement with the Townsend breakdown model. Further studies with an improved spectroscopic setup are expected to yield a better signal-to-noise ratio. These measurements will thus become an important step toward developing a model of the charging process. This in turn will lead to further optimizations of the underlying DBD process and thus also of the poling of cellular ferroelectrets.

We are indebted to Professor Anna Köhler and Dr. Frank Jaiser (University of Potsdam) for providing the access to the spectroscopy setup. One of the authors (X.Q.) thanks the Deutsche Forschungsgemeinschaft (DFG) for providing a Research Fellowship (Reference No. QI 65/1-1).

- <sup>1</sup>L. J. Gibson and M. F. Ashby, *Cellular Solids: Structure and Properties*, 2nd ed. (Cambridge University Press, Cambridge, 1997), Chap. 1.
- <sup>2</sup>*Handbook of Polymeric Foams and Foam Technology*, edited by D. Klemmner and K. C. Frisch (Hanser, Munich, 1991).
- <sup>3</sup>S. Bauer, R. Gerhard-Multhaupt, and G. M. Sessler, *Phys. Today* **57**(2), 37 (2004).
- <sup>4</sup>M. Wegener and S. Bauer, *ChemPhysChem* **6**, 1014 (2005).
- <sup>5</sup>M. Lindner, S. Bauer-Gogonea, S. Bauer, M. Paajanen, and J. Raukola, *J. Appl. Phys.* **91**, 5283 (2002).
- <sup>6</sup>M. Wegener, M. Paajanen, W. Wirges, and R. Gerhard-Multhaupt, *Proceedings of the 11th International Symposium on Electrets, Melbourne, Australia, 1-3 October 2002* (IEEE Service Center, Piscataway, NJ, 2002) pp. 54-57.
- <sup>7</sup>S. Zhukov and H. von Seggern, *J. Appl. Phys.* **101**, 084106 (2007).
- <sup>8</sup>X. Qiu, A. Mellinger, M. Wegener, W. Wirges, and R. Gerhard, *J. Appl. Phys.* **101**, 104112 (2007).
- <sup>9</sup>U. Kogelschatz, *Plasma Chem. Plasma Process.* **23**, 1 (2003).
- <sup>10</sup>I. Graz (private communication).
- <sup>11</sup>A. Savolainen and K. Kirjavainen, *J. Macromol. Sci., Chem.* **A26**, 583 (1989).
- <sup>12</sup>M. Paajanen, H. Minkinen, and J. Raukola, *Proceedings of the 11th International Symposium on Electrets, Melbourne, Australia, 1-3 October 2002* (IEEE Service Center, Piscataway, NJ, 2002), pp. 191-194.
- <sup>13</sup>K. V. Kozlov, H. E. Wagner, R. Brandenburg, and P. Michel, *J. Phys. D* **34**, 3164 (2001).
- <sup>14</sup>A. Lofthuis and P. H. Krupenie, *J. Phys. Chem. Ref. Data* **6**, 113 (1977).
- <sup>15</sup>G. Herzberg, *Molecular Spectra and Molecular Structure. I: Spectra of Diatomic Molecules* (Van Nostrand, New York, 1950), Chap. IV.
- <sup>16</sup>*CRC Handbook of Chemistry and Physics*, edited by David R. Lide and H. P. R. Frederikse, 75th ed. (CRC Press, Boca Raton, 1995), Chap. 12, p. 121.
- <sup>17</sup>P. Paris, M. Aints, F. Valk, T. Plank, A. Haljaste, K. V. Kozlov, and H. E. Wagner, *J. Phys. D* **38**, 3894 (2005).
- <sup>18</sup>John M. Meek and John D. Craggs, *Electrical Breakdown of Gases* (Oxford University Press, London, 1953), Chap. I.

## Influence of gas pressure in the voids during charging on the piezoelectricity of ferroelectrets

Xunlin Qiu,<sup>a)</sup> Axel Mellinger, and Reimund Gerhard

*Applied Condensed-Matter Physics, University of Potsdam, Am Neuen Palais 10, 14469 Potsdam, Germany*

(Received 21 December 2007; accepted 16 January 2008; published online 5 February 2008)

Cellular polypropylene ferroelectrets were subjected to vacuum and high air pressures. The capacitance of the samples was measured as a way to monitor their thickness. It was found that both in vacuum and in high-pressure air, the thickness of the samples recovers to its original value after a sufficient storage time (typically, several hours), indicating that the internal and external pressures equalize as a result of gas diffusion. Optimal piezoelectricity is achieved by charging at a pressure of 170 kPa, which is explained by means of the void-height distribution function in combination with Townsend's model of the Paschen breakdown. © 2008 American Institute of Physics.

[DOI: 10.1063/1.2841037]

In recent years, a number of nonpolar cellular or porous polymers were discovered to exhibit a strong electromechanical (quasipiezoelectric) response and therefore have attracted extensive research.<sup>1,2</sup> These materials are now more and more often called "ferroelectrets." Much work has been done on the theoretical analysis of their piezoelectricity,<sup>3-7</sup> the dependence of the piezoelectricity on the morphology,<sup>8</sup> and the development of ferroelectrets based on new materials.<sup>9-11</sup> The piezoelectricity of ferroelectrets is strongly dependent on their Young's modulus, the size and structure of the voids, and the effective charge density. It should be noted that these factors themselves are closely dependent on each other. For example, the void size could be adjusted by means of controlled gas diffusion/expansion, so that Young's modulus reaches its minimum and the effective charge density is dramatically increased, resulting in optimal piezoelectricity.<sup>12</sup> Zhang *et al.* theoretically and experimentally studied the threshold and saturation phenomenon of the piezoelectricity in ferroelectrets.<sup>13</sup> Later, Zhukov and von Seggern obtained the respective results on open-porous fluoropolymer sandwiches.<sup>14</sup>

It is known that a series of microdischarges occurs in the voids when ferroelectrets are subjected to charging voltages higher than the threshold value.<sup>15-18</sup> These dielectric barrier discharges<sup>19</sup> are interpreted in terms of the Paschen breakdown and are very critical for rendering cellular polymers piezoelectric. The charging efficiency of the voids can be improved by charging in gases with higher breakdown strength.<sup>20,21</sup> In this letter, the influence of the gas pressure inside the voids on the charging efficiency and hence on the piezoelectricity of ferroelectrets is studied.

Samples were prepared from commercial cellular polypropylene (PP) films with the trade name PQ50 (Nan Ya Plastics Corporation, Taiwan, China). They are produced by stretching filler-loaded PP under suitable conditions.<sup>22</sup> The initial thickness and density are 50  $\mu\text{m}$  and 550  $\text{kg}/\text{m}^3$ , respectively. In order to optimize their electromechanical properties, the samples were inflated by gas-diffusion expansion in nitrogen and subsequent heat treatment.<sup>23,24</sup> The samples were then metallized on both sides with gold electrodes having a diameter of 12 mm and a thickness of 20 nm. The final

thickness of the samples is approximately 80  $\mu\text{m}$ . The samples were mounted in a pressure chamber where the atmospheric air was pumped out and dry air at various pressures was fed in. The capacitance of the sample was measured by means of a HP 4284A precision LCR meter. The charging high voltage was supplied by an amplifier (Trek model 610) and controlled by an arbitrary waveform function generator (HP 33120A). The piezoelectric  $d_{33}$  coefficients were determined by means of dynamic mechanical excitation of the sample with a sinusoidal force with an amplitude of 1 N at a frequency of 2 Hz (Brüel&Kjaer model 4810 shaker). In addition, a bias force of 3 N was applied to the sample. The resulting electric response of the sample was amplified by means of a Brüel&Kjaer model 2635 charge amplifier and recorded with an oscilloscope. The piezoelectric  $d_{33}$  coefficients were calculated from the applied force and the resulting electrical signal. The piezoelectric  $d_{33}$  coefficients are average values from six separate measurements on the sample.

Ferroelectrets are extremely compressible due to their voided structure. Measuring their capacitance provides an easy means for the *in situ* monitoring of their thickness change.<sup>25,26</sup> Figure 1 shows the normalized capacitance decay in dry air at different pressures. First, all samples were

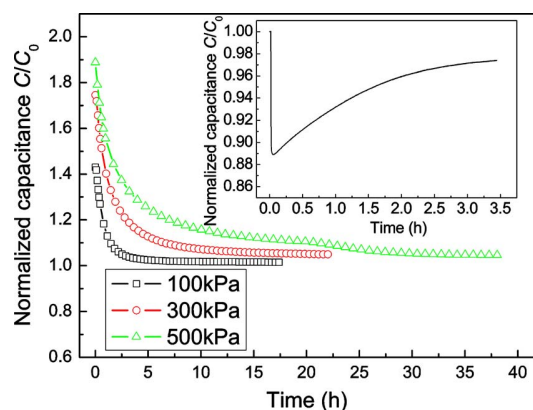


FIG. 1. (Color online) Sample capacitance in high-pressure air, normalized to its initial value  $C_0$  before treatment. Air with the indicated pressures is introduced into the chamber after evacuation to less than 50 Pa. The inset shows the capacitance change during pumping.

<sup>a)</sup>Electronic mail: xunlin@canopus.physik.uni-potsdam.de.



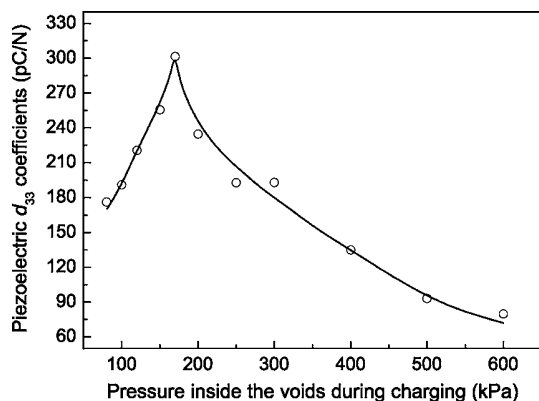


FIG. 2. Piezoelectric  $d_{33}$  coefficient as a function of pressure inside the voids during charging. The line is a guide for the eyes.

subjected to vacuum pumping until the chamber pressure was less than about 50 Pa. The inset of Fig. 1 shows the normalized capacitance change during pumping. A sudden drop of the capacitance is caused by the expansion of the sample due to the relatively high pressure inside the voids, compared to the vacuum environment. Thereafter, the capacitance increases with vacuum treatment time, indicating the diffusion of air from the voids and the recovery of the sample thickness. After 3 h storage in vacuum, the capacitance of the sample recovers back to 97% of its initial value. Next, dry air at different pressures was introduced into the chamber. Due to the compression of the samples, a sudden increase of the capacitance is observed. Higher pressure results in a higher increase, as expected. However, the capacitance decreases back to a value comparable to the initial one (before vacuum pumping) after several hours of exposure to high gas pressure. Therefore, we conclude that dry air fills the voids of the sample and equilibrium is established between the pressure inside the voids and that in the pressure chamber after sufficient storage time.

To charge the ferroelectric films, a voltage of 6 kV was applied to the gold electrodes for 5 s, after the sample capacitance deviated by less than 5% from the initial value. Subsequently, the chamber pressure was brought back to atmospheric pressure, and the samples were removed. Their piezoelectric  $d_{33}$  coefficient was measured 1 day after charging. It should be noted that after the pressure chamber was subjected to laboratory conditions, the thickness of the sample increased to some extent if the treatment pressure was higher than atmospheric pressure (101 kPa). However, without further heat treatment, this expansion is not permanent, and the sample thickness recovers to its initial value of about 80  $\mu\text{m}$  1 day after charging.

Figure 2 shows the piezoelectric  $d_{33}$  coefficient as a function of the pressure inside the voids during charging. The piezoelectric  $d_{33}$  coefficient reaches its maximum at 170 kPa. An improvement of about 58% is achieved at this point, compared to the sample charged in dry air at 100 kPa. As the gas pressure is increased further,  $d_{33}$  decreases again. At 600 kPa, a piezoelectric  $d_{33}$  coefficient of 76 pC/N was measured, approximately 40% of that obtained at 100 kPa.

To understand this behavior, the void heights of the sample were investigated. A distribution function for the void heights was obtained by analyzing cross-sectional scanning electron microscope (SEM) images of the ferroelectric films (Fig. 3). Voids were automatically detected and measured

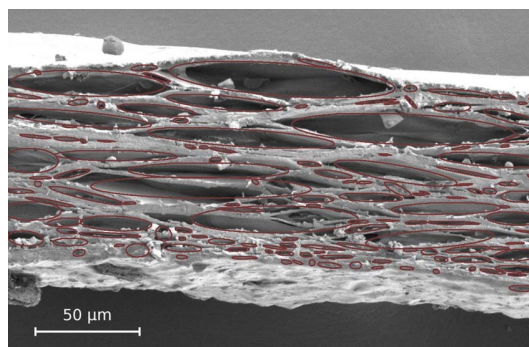


FIG. 3. (Color online) SEM image showing the cross section of a cellular PP sample. The red ellipses indicate voids identified and analyzed by the ImageJ software (Ref. 27).

with the ImageJ (Ref. 27) software package. As can be seen from Fig. 4 a large amount of the voids have a height below 5  $\mu\text{m}$ .

The Paschen breakdown has already been suggested to be responsible for the internal charging of the voids inside ferroelectrets.<sup>3</sup> According to Townsend's model, the critical breakdown field of common gases in a uniform electric field is a function of both gas pressure  $p$  and the electrode spacing  $d$  (which in a ferroelectret context is equal to the void height),<sup>28</sup>

$$E_c = \frac{Ap}{B + \ln(pd)}, \quad (1)$$

where  $B$  is given by

$$B = \ln\left(\frac{C}{\ln(1 + 1/\gamma)}\right). \quad (2)$$

For air,  $A=273.8 \text{ V m}^{-1} \text{ Pa}^{-1}$  and  $C=11 \text{ m}^{-1} \text{ Pa}^{-1}$  are experimentally defined constants and  $\gamma=0.01$  is the so-called second ionization coefficient. Figure 4 shows the breakdown field in air as a function of  $d$  for different gas pressures  $p$ . At constant pressure,  $E_c$  is a monotonic function of  $d$ , indicating that larger voids experience breakdown at lower electric field.

The Paschen breakdown voltage must be reached in the voids in order to initiate microplasma discharges. At low gas pressures, the breakdown field for the majority of the voids is

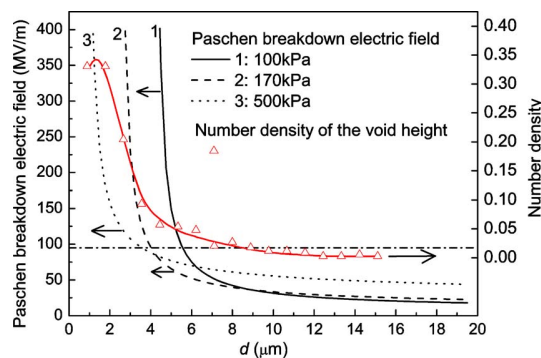


FIG. 4. (Color online) Paschen breakdown field as a function of void height  $d$  for various gas pressures  $p$ . Also shown is the distribution function of the void heights. The dash dot horizontal line indicates the electric field in the voids for an external voltage of 6 kV.

Downloaded 08 Feb 2008 to 141.89.235.172. Redistribution subject to AIP license or copyright; see <http://apl.aip.org/apl/copyright.jsp>

too high to initiate a dielectric barrier discharge. At the applied voltage  $V=6$  kV, the electric field  $E_g$  in the gas-filled voids is given by

$$V = E_g \left( \frac{d_p}{\epsilon_p} + d_g \right), \quad (3)$$

where  $d_p \approx 31 \mu\text{m}$  is the accumulated thickness of the polymer layers,  $d_g \approx 49 \mu\text{m}$  is the accumulated void height along a line perpendicular to the sample surface, and  $\epsilon_p=2.2$  is the permittivity of the solid polymer. Hence,  $E_g$  is estimated as approximately 95 MV/m.

As the gas pressure is increased, more and more voids exhibit a breakdown field lower than  $E_g$  and will thus get electrically charged, leading to a higher piezoelectric  $d_{33}$  coefficient. At the same time, however, the breakdown field for void heights  $d \gtrsim 9 \mu\text{m}$  increases. According to recent studies on the threshold and saturation behavior in ferroelectrets,<sup>13,14</sup> the deposited charge is proportional to the difference  $E_g - E_c$  between the electric field in the gas and the critical breakdown field. Thus, an increase of the latter reduces the amount of charge deposited in the larger voids. Due to their higher compressibility and their larger macroscopic dipole moments, these larger voids contribute substantially to the overall piezoelectricity, despite their relatively small numbers. As their charge is reduced, the piezoelectricity of the sample begins to decrease at pressures above 170 kPa, even though the total number of charged voids is still increasing.

The improved charging efficiency may also be achieved by permanently inflating the sample to higher thickness, but one should keep in mind that the piezoelectricity of ferroelectrets depends not only on the charging efficiency but also on Young's modulus of the polymer film. It was found that the piezoelectricity of ferroelectrets is proportional to  $1/Y$ .<sup>4,12</sup> For inflated PQ50 sample,  $Y$  reaches its minimum at a thickness of about  $80 \mu\text{m}$ ,<sup>29</sup> and similar results have been obtained for a range of other materials.<sup>9</sup> Obviously, optimizing the charging efficiency by modulating the gas pressure inside the voids during charging bears the advantage that it keeps the optimal mechanical properties of the sample nearly unchanged.

In conclusion, the gas composition and pressure inside the voids of ferroelectrets may be changed if the treatment time is long enough. This provides a means for improving the charging efficiency of the voids, which, in turn, will lead to further optimization of the piezoelectricity. The observed peak of the  $d_{33}$  coefficient at a gas pressure of 170 kPa was explained in terms of the Townsend breakdown model, combined with the experimentally obtained distribution function of the void heights. For optimally inflated PQ50 ferroelectrets, the piezoelectricity is improved by 58%.

We are indebted to Dr. Guggi Kofod and Werner Wirges (University of Potsdam) for stimulating discussions. The SEM images were provided by Dr. Brigitte Tiersch (Depart-

ment of Chemistry, University of Potsdam). One of the authors (X.Q.) thanks the Deutsche Forschungsgemeinschaft (DFG) for providing a Research Fellowship (Reference No. QI65/1-1).

- <sup>1</sup>S. Bauer, R. Gerhard-Multhaupt, and G. M. Sessler, *Phys. Today* **57**(2), 37 (2004).
- <sup>2</sup>M. Wegener and S. Bauer, *ChemPhysChem* **6**, 1014 (2005).
- <sup>3</sup>G. M. Sessler and J. Hillenbrand, *Appl. Phys. Lett.* **75**, 3405 (1999).
- <sup>4</sup>J. Hillenbrand, G. M. Sessler, and X. Zhang, *J. Appl. Phys.* **98**, 064105 (2005).
- <sup>5</sup>M. Paajanen, H. Välimäki, and J. Lekkala, *Proceedings of the Tenth International Symposium on Electrets, Delphi, Greece, 22–24 September 1999* (IEEE, Piscataway, NJ, 1999), pp. 735–738.
- <sup>6</sup>M. Paajanen, J. Lekkala, and H. Välimäki, *IEEE Trans. Dielectr. Electr. Insul.* **8**, 629 (2001).
- <sup>7</sup>M. R. Haberman and Y. H. Berthelot, *J. Appl. Phys.* **102**, 124903 (2007).
- <sup>8</sup>E. Tuncer, *J. Phys. D* **38**, 497 (2005).
- <sup>9</sup>M. Wegener, W. Wirges, and R. Gerhard-Multhaupt, *Adv. Eng. Mater.* **7**, 1128 (2005).
- <sup>10</sup>E. Saarimäki, M. Paajanen, A. Savijärvi, M. Wegener, O. Voronina, R. Schulze, W. Wirges, and R. Gerhard-Multhaupt, *IEEE Trans. Dielectr. Electr. Insul.* **13**, 963 (2006).
- <sup>11</sup>W. Wirges, M. Wegener, O. Voronina, L. Zirkel, and R. Gerhard-Multhaupt, *Adv. Funct. Mater.* **17**, 324 (2007).
- <sup>12</sup>M. Wegener, W. Wirges, R. Gerhard-Multhaupt, M. Dansachmüller, R. Schwödiauer, S. Bauer-Gogonea, S. Bauer, M. Paajanen, H. Minkkinen, and J. Raukola, *Appl. Phys. Lett.* **84**, 392 (2004).
- <sup>13</sup>P. Zhang, Z. Xia, X. Qiu, F. Wang, and X. Y. Wu., *Proceedings of the 12th International Symposium on Electrets, Salvador, Brazil, 11–14 September 2005* (IEEE, Piscataway, NJ, 1999), pp. 39–42.
- <sup>14</sup>S. Zhukov and H. von Seggern, *J. Appl. Phys.* **102**, 044109 (2007).
- <sup>15</sup>M. Wegener, M. Paajanen, W. Wirges, and R. Gerhard-Multhaupt, *Proceedings of the 11th International Symposium on Electrets, Melbourne, Australia, 1–3 October 2002* (IEEE, Piscataway, NJ, 2002), pp. 54–57.
- <sup>16</sup>M. Lindner, S. Bauer-Gogonea, S. Bauer, M. Paajanen, and J. Raukola, *J. Appl. Phys.* **91**, 5283 (2002).
- <sup>17</sup>X. Qiu, A. Mellinger, M. Wegener, W. Wirges, and R. Gerhard, *J. Appl. Phys.* **101**, 104112 (2007).
- <sup>18</sup>X. Qiu, A. Mellinger, W. Wirges, and R. Gerhard, *Appl. Phys. Lett.* **91**, 132905 (2007).
- <sup>19</sup>U. Kogelschatz, *Plasma Chem. Plasma Process.* **23**, 1 (2003), and references therein.
- <sup>20</sup>M. Paajanen, M. Wegener, and R. Gerhard-Multhaupt, *J. Phys. D* **34**, 2482 (2001).
- <sup>21</sup>X. Qiu, M. Wegener, W. Wirges, X. Zhang, J. Hillenbrand, Z. Xia, R. Gerhard-Multhaupt, and G. M. Sessler, *J. Phys. D* **38**, 649 (2005).
- <sup>22</sup>A. Savolainen and K. Kirjavainen, *J. Macromol. Sci., Chem.* **A26**, 583 (1989).
- <sup>23</sup>M. Paajanen, H. Minkkinen, and J. Raukola, *Proceedings of the 11th International Symposium on Electrets, Melbourne, Australia, 1–3 October 2002* (IEEE, Piscataway, NJ, 2002), pp. 191–194.
- <sup>24</sup>M. Wegener, W. Wirges, J. Fohlmeister, B. Tiersch, and R. Gerhard-Multhaupt, *J. Phys. D* **37**, 623 (2004).
- <sup>25</sup>J. Leonhartsberger, H. Salhofer, R. Schwödiauer, S. Bauer-Gogonea, S. Bauer, R. Forstner, G. Eder, M. Paajanen, H. Minkkinen, and J. Raukola, *Ferroelectrics* **331**, 181 (2006).
- <sup>26</sup>S. Bauer-Gogonea, F. Camacho González, R. Schwödiauer, B. Ploss, and S. Bauer, *Appl. Phys. Lett.* **91**, 122901 (2007).
- <sup>27</sup>W. S. Rasband, ImageJ, U.S. National Institutes of Health, Bethesda, Maryland, USA, 1996 (<http://rsb.info.nih.gov/ij/>).
- <sup>28</sup>E. M. Bazelyan and Y. P. Raizer, *Spark Discharge* (CRC, Boca Raton, FL, 1998).
- <sup>29</sup>X. Qiu, "The Electret Properties of Cellular PP and Solid PEN Film," Ph.D. thesis, Tongji University, 2006.

## Effective polarization fatigue from repeated dielectric barrier discharges in cellular polypropylene ferroelectrets

Xunlin Qiu<sup>a)</sup> and Reimund Gerhard

*Applied Condensed-Matter Physics, Department of Physics and Astronomy, University of Potsdam, Karl-Liebknecht-Strasse 24-25, 14476 Potsdam-Golm, Germany*

(Received 18 July 2008; accepted 19 September 2008; published online 15 October 2008)

Polarization fatigue is observed when cellular polypropylene (PP) ferroelectrets are subjected to high-voltage cycles. The fatigue rate strongly depends on the amplitude and the number of the applied voltage cycles, whereas the frequency and the waveform of the voltage do not have a strong influence. The much lower piezoelectric activity of significantly fatigued cellular PP ferroelectret films recovers in part after a storage period of typically several hours in ambient air. It is believed that the effective polarization fatigue is mainly caused by the plasma modification of the internal surfaces effected by the repeated dielectric barrier discharges inside the voids. © 2008 American Institute of Physics. [DOI: 10.1063/1.2998597]

Ferroelectrets (i.e., electrically charged polymer foams) have attracted extensive research due to their large piezoelectric activity combined with high mechanical flexibility and compliance.<sup>1,2</sup> In recent years, a significant number of studies have been conducted on optimizing the morphology of ferroelectrets, on the theoretical analysis of their piezoelectricity, and on the development of ferroelectrets from new materials. In order to render polymer foams piezoelectric, the internal void surfaces must be charged by a series of dielectric barrier discharges (DBDs).<sup>3-6</sup> Charges of opposite sign are separated during the DBDs and then trapped at the internal top and bottom surfaces of the voids. The charged voids can thus be considered as macroscopic dipoles, whose direction can be reversed by sufficiently high electric fields, and the resulting electric-displacement-versus-electric-field curves exhibit hysteresis behavior.<sup>4,5</sup> Consequently, the density of the macroscopic dipoles in ferroelectrets (the effective bipolar charge density) can be considered as an effective polarization.

It is known that the piezoelectricity of ferroelectrets can be modeled as a function of the effective charge density (effective polarization), of the average thicknesses of the relevant air gaps and solid layers, and of Young's modulus of the polymer foam.<sup>7,8</sup> Polarization fatigue (the reduction in polarization due to electric stress) is a serious factor for the application of inorganic and polymeric ferroelectrics. A large number of experiments have been carried out on the fatigue in ferroelectrics, and several models have been proposed.<sup>9,10</sup> However, the polarization fatigue in ferroelectrets has not been investigated in detail yet.

In this letter, the polarization fatigue in cellular polypropylene (PP) ferroelectrets is studied. Samples were prepared from commercial cellular PP films (PQ50 from Nan Ya Plastics Corporation, Taiwan, China). They are produced by stretching filler-loaded PP under suitable conditions.<sup>11</sup> The initial thickness and density are 50  $\mu\text{m}$  and 550  $\text{kg}/\text{m}^3$ , respectively. In order to optimize their electromechanical properties, the samples were inflated by gas-diffusion expansion in nitrogen and a subsequent heat treatment for stabilization.<sup>12</sup> The samples were then metallized on both sides

with gold electrodes having a diameter of 12 mm and a thickness of 20 nm. High voltage was supplied by means of an amplifier (Trek Model 610), controlled by an arbitrary waveform function generator (HP 33120A). Dielectric resonance spectra (DRS) around the thickness-extension (TE) resonance of the samples were recorded *in situ* with a Novo-control ALPHA high-resolution dielectric analyzer. The sample was electrically connected to the sample holder via thin silver wires. From the frequency-dependent real and imaginary parts of the capacitance  $C(\omega)$ , the piezoelectric  $d_{33}$  coefficient was determined.<sup>13</sup>

Samples were charged with a voltage of +7 kV for 5 s, followed by a DRS measurement in order to obtain the respective  $d_{33}$  coefficient from the piezoelectric TE resonance peak (called "piezoelectrical measurement" in the following). The observed initial  $d_{33}$  is about 195 pC/N with a variation of about  $\pm 15\%$  from sample to sample due to a broad distribution of void sizes in the samples. The TE resonances are found around a frequency of 370 kHz. Before any piezoelectrical measurement, the samples were always poled again in the same way as detailed above (i.e., with +7 kV for 5 s). Therefore, the polarity reversals of the internal electret charge during cycling and the accompanying switching behavior of the macroscopic polarization were not observed in detail and are not the topic of this letter.

Figure 1 shows the normalized piezoelectric  $d_{33}$  coefficient as a function of the number of cycles ( $N$ ) for bipolar sinusoidal driving voltages with a frequency of 100 Hz and different peak-to-peak ( $V_{pp}$ ) values. The fatigue process was interrupted at predetermined intervals for piezoelectrical measurements. There is no detectable change in the  $d_{33}$  coefficient within the investigated number of cycles when  $V_{pp}$  is lower than 3 kV. However, when  $V_{pp}$  is higher than 3 kV, an obvious decrease in  $d_{33}$  is observed after a certain number of cycles (Fig. 1).

According to a simplified model of ferroelectrets, the  $d_{33}$  coefficient can be expressed as<sup>7,8</sup>

$$d_{33} = \frac{\epsilon s}{Y} \frac{s_1 \sigma_{\text{eff}}}{(s_1 + \epsilon s_2)^2}, \quad (1)$$

where  $\epsilon$  is the permittivity of solid PP,  $Y$  is Young's modulus of the sample, and  $s_1$  and  $s_2$  are the total thicknesses of

<sup>a)</sup>Electronic mail: xunlin@canopus.physik.uni-potsdam.de.



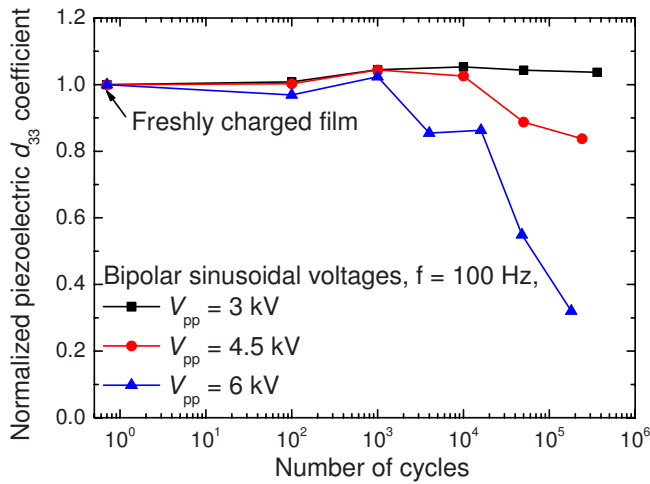


FIG. 1. (Color online) Normalized piezoelectric  $d_{33}$  coefficient as a function of the logarithm of the number of cycles ( $N$ ). Fatigue was achieved by means of a bipolar sinusoidal voltage with a frequency of 100 Hz and an amplitude as indicated. The values for number of cycles below  $10^0$  indicate freshly charged films.

the solid layers and the gaseous layers, respectively, with  $s = s_1 + s_2$  being the total film thickness.  $\sigma_{\text{eff}} = \sum s_{2i} \sigma_i / \sum s_{2i}$  is the effective charge density, where  $s_{2i}$  is the thickness of the  $i$ th gaseous layer with  $\sum s_{2i} = s_2$  and  $\sigma_i$  is the charge density on the surface of the  $i$ th gaseous layer. When  $V_{pp}$  is higher than 3 kV, the measured capacitance of the sample tends to slightly increase with the applied number of cycles. However, this increase is within a range of about 5% of the respective value for the freshly charged film. Therefore, the sample thickness and hence Young's modulus of the film can be considered as constant during the fatigue process. According to Eq. (1), the decrease in the piezoelectric  $d_{33}$  coefficient is mainly caused by the reduction in the effective polarization.

In the polymer industry, DBDs are often used to modify the surface properties of polymers.<sup>3</sup> DBDs produce a variety of species including energetic and reactive monoatomic and molecular diatomic charged particles, electrons, and neutral species. During processing, the polymer surface is thus exposed to a highly reactive plasma, and both chemical and physical changes happen within the exposed surface area.<sup>14</sup> The wettability and the adhesion of the polymer surface are dramatically improved by the treatment due to surface oxidation and chain scission.<sup>15,16</sup> DBD treatment of PP leads to the formation of polar water-soluble low-molecular-weight oxidized material (LMWOM). The LMWOM agglomerates into small topographical mounds, which are visible in atomic-force-microscopy images, leading to an increase in the surface roughness.<sup>17</sup> The investigation on the chemical composition by x-ray photoelectron spectroscopy shows the introduction of O-C=O, C=O, and C-O groups on the surface of PP after DBD treatment, and the O/C ratio indicates the extent to which the polymer surfaces are oxidized.<sup>18</sup> For cellular PP ferroelectrets, chain scission and the formation of polar LMWOM at the internal surfaces during DBDs deteriorate the chargeability of the voids, resulting in the observed polarization fatigue (Fig. 1). A threshold  $V_{pp}$  of 3 kV for the fatigue behavior is in good agreement with the previous finding that the DBDs inside the voids are initiated when the voltage is higher than 3 kV.<sup>5,6</sup> The fatigue rate

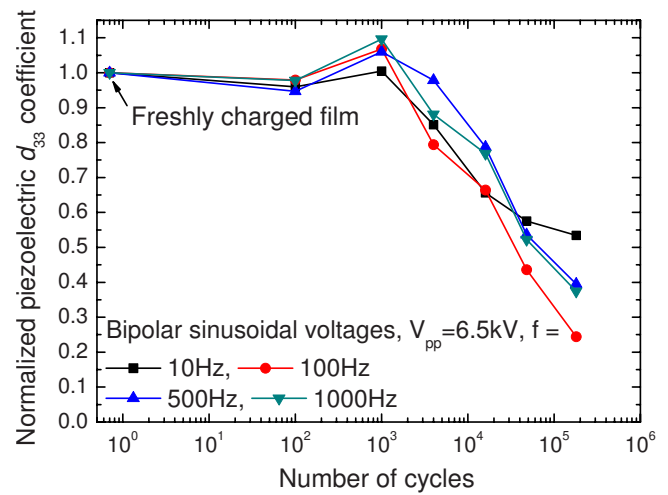


FIG. 2. (Color online) Normalized piezoelectric  $d_{33}$  coefficient as a function of the logarithm of the number of cycles ( $N$ ). Fatigue was achieved by means of bipolar sinusoidal voltages with a  $V_{pp}$  of 6.5 kV and a frequency of 10, 100, 500, and 1000 Hz, respectively.

increases with  $V_{pp}$ , since more and more voids are subjected to DBDs at higher  $V_{pp}$ .

In order to study the frequency dependence of the fatigue behavior, driving voltages with four different frequencies (10, 100, 500, and 1000 Hz) were applied to the sample. As can be seen from Fig. 2, no obvious dependence on the frequency of the driving voltage is observed. This is expected since the same number of identical DBDs are generated per cycle.<sup>3</sup> However, at much lower frequency, for example, 10 Hz, the fatigue rate is slowed down at higher number of cycles, which is caused by a partial recovery between the fatigue processes (cf. Fig. 4 discussed below).

The fatigue behavior for different waveforms is shown in Fig. 3 in which bipolar triangular and sinusoidal waveforms are employed. Again, no significant differences are observed. Also shown in Fig. 3 is the fatigue under unipolar triangular voltage cycles at the same frequency and  $V_{pp}$ . A different polarity of the driving voltage does not yield a significant difference either, since the DBDs rely on  $V_{pp}$  only.

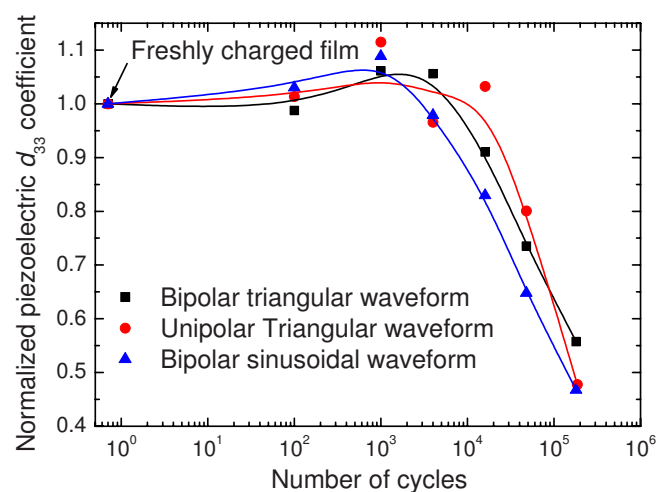


FIG. 3. (Color online) Effect of voltage waveform on the effective polarization fatigue. Fatigue was achieved by means of driving voltages with a frequency of 100 Hz and a  $V_{pp}$  of 5.5 kV. Bipolar triangular, unipolar triangular, and bipolar sinusoidal waveforms were employed. The lines are guides for the eyes only.

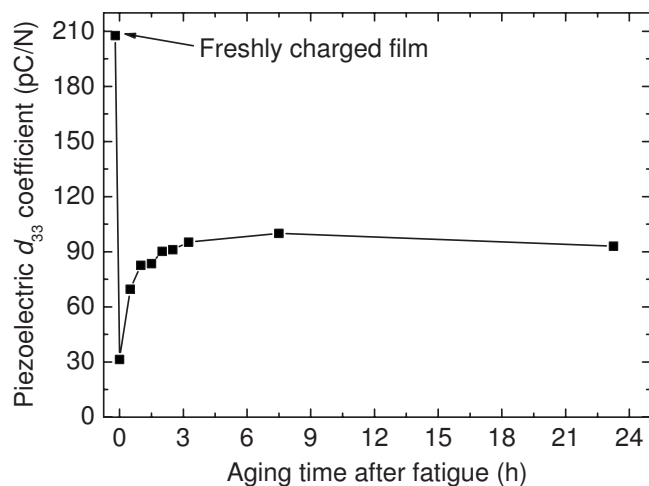


FIG. 4. Piezoelectric  $d_{33}$  coefficient as a function of recovery time in ambient air after the fatigue. Each data point was obtained by piezoelectrical measurements of the same sample. The  $d_{33}$  value for a storage time below zero was taken on the freshly charged film. The  $d_{33}$  value at a storage time of zero was measured immediately after a fatigue process with  $1.8 \times 10^5$  cycles of a bipolar sinusoidal voltage ( $V_{pp}=6.5$  kV;  $f=100$  Hz).

This is further confirmed by spectroscopy: the spectra of the DBDs in cellular PP ferroelectrets are almost independent from an additional dc offset bias (results not shown here).

Figure 4 shows the evolution of the piezoelectric  $d_{33}$  coefficients of a fatigued cellular PP film as a function of storage time in ambient laboratory conditions. A piezoelectric  $d_{33}$  coefficient of 208 pC/N is obtained for the freshly charged film. Thereafter,  $1.8 \times 10^5$  cycles of a bipolar sinusoidal voltage with a frequency of 100 Hz and a  $V_{pp}$  of 6.5 kV were applied to the sample. The  $d_{33}$  coefficient of 31 pC/N immediately after the fatigue process is only about 15% of the initial value. The sample was then stored under ambient laboratory conditions, and its  $d_{33}$  was determined from time to time by means of piezoelectrical measurements. It is found that the  $d_{33}$  coefficient of the fatigued film shows a quick recovery during the first hours of storage. After being stored in ambient laboratory conditions for about 3 h,  $d_{33}$  recovers to 95 pC/N, approximately 46% of the value for the freshly charged film. After longer storage,  $d_{33}$  increases more slowly and finally reaches a plateau value. The partial recovery of the polarization fatigue in cellular PP ferroelectrets can be mainly attributed to the loss of polar LMWOM on the void surfaces and hence the recovery of the chargeability of the voids.<sup>14–18</sup> Morent *et al.*<sup>19</sup> reported that for DBD-treated PP, there is a large O/C atomic ratio decrease in the first hours after DBD treatment, and afterward, the O/C atomic ratio decreases more slowly and finally reaches a plateau value. Due to the same reason, the contact angle for the DBD-treated PP shows a similar fatigue and recovery behavior as the piezoelectric  $d_{33}$  coefficient.

It should be noted that proper DBD treatment might be helpful for improving the chargeability of the voids and hence the piezoelectricity of ferroelectrets. Figures 1–3 all show a slight increase in  $d_{33}$  after  $10^3$  cycles. Künstler

*et al.*<sup>20</sup> showed that a hydrogen- or argon-plasma treatment can improve the charge stability of positively charged polymer electrets. Exploring the beneficial effects of DBDs on the piezoelectricity of ferroelectrets and studying the influence of DBDs in different gas environments on ferroelectrets and their stability will be the next steps of our investigation.

In conclusion, the effective polarization fatigue in cellular PP ferroelectrets has been studied. The fatigue is mainly due to the plasma treatment of the internal surfaces inside the voids during the DBDs. The fatigue rate strongly depends on the amplitude and the number of the applied voltage cycles, and it shows no obvious dependence on the frequency or the waveform of the driving voltages. The significantly decreased piezoelectric activity of fatigued cellular PP ferroelectret films recovers in part after longer periods of storage (typically several hours) in ambient air.

The first author (X.Q.) thanks the Deutsche Forschungsgemeinschaft (DFG) for providing a Research Fellowship (Reference No. QI 65/1-1).

- <sup>1</sup>S. Bauer, R. Gerhard-Mulhaupt, and G. M. Sessler, *Phys. Today* **57**(2), 37 (2004), and references therein.
- <sup>2</sup>M. Wegener and S. Bauer, *ChemPhysChem* **6**, 1014 (2005), and references therein.
- <sup>3</sup>U. Kogelschatz, *Plasma Chem. Plasma Process.* **23**, 1 (2003), and references therein.
- <sup>4</sup>M. Lindner, S. Bauer-Gogonea, S. Bauer, M. Paajanen, and J. Raukola, *J. Appl. Phys.* **91**, 5283 (2002).
- <sup>5</sup>X. Qiu, A. Mellinger, M. Wegener, W. Wirges, and R. Gerhard, *J. Appl. Phys.* **101**, 104112 (2007).
- <sup>6</sup>X. Qiu, A. Mellinger, W. Wirges, and R. Gerhard, *Appl. Phys. Lett.* **91**, 132905 (2007).
- <sup>7</sup>M. Paajanen, H. Välimäki, and J. Leikkala, Proceedings of the Tenth International Symposium on Electrets, Delphi, Greece, 22–24 September 1999 (IEEE Service Center, Piscataway, NJ, 1999), pp. 735–738.
- <sup>8</sup>G. M. Sessler and J. Hillenbrand, *Appl. Phys. Lett.* **75**, 3405 (1999).
- <sup>9</sup>A. K. Tagantsev, I. Stolichnov, E. L. Colla, and N. Setter, *J. Appl. Phys.* **90**, 1387 (2001).
- <sup>10</sup>G. Zhu, Z. Zeng, L. Zhang, and X. Yan, *Appl. Phys. Lett.* **89**, 102905 (2006).
- <sup>11</sup>A. Savolainen and K. Kirjavainen, *J. Macromol. Sci., Chem.* **A26**, 583 (1989).
- <sup>12</sup>M. Paajanen, H. Minkinen, and J. Raukola, Proceedings of the 11th International Symposium on Electrets, Melbourne, Australia, 1–3 October 2002 (IEEE Service Center, Piscataway, NJ, 1999), pp. 191–194.
- <sup>13</sup>A. Mellinger, *IEEE Trans. Dielectr. Electr. Insul.* **10**, 842 (2003).
- <sup>14</sup>G. Borcia, C. A. Anderson, and N. M. D. Brown, *Appl. Surf. Sci.* **221**, 203 (2004).
- <sup>15</sup>R. D. Boyd, A. M. Kenwright, J. P. S. Badyal, and D. Briggs, *Macromolecules* **30**, 5429 (1997).
- <sup>16</sup>S. Ishikawa, K. Yukimura, K. Matsunaga, and T. Maruyama, *Surf. Coat. Technol.* **130**, 52 (2000).
- <sup>17</sup>N. Cui and N. M. D. Brown, *Appl. Surf. Sci.* **189**, 31 (2002).
- <sup>18</sup>V. Jones, M. Strobel, and M. J. Prokosch, *Plasma Processes Polym.* **2**, 547 (2005).
- <sup>19</sup>R. Morent, N. D. Geyter, C. Leys, L. Gengembre, and E. Payen, *Surf. Coat. Technol.* **201**, 7847 (2007).
- <sup>20</sup>W. Künstler, P. Frübing, and R. Gerhard-Mulhaupt, 1998 Annual Report, Conference on Electrical Insulation and Dielectric Phenomena (IEEE Service Center, Piscataway, NJ, 1998), pp. 609–612.



## Template-based fluoroethylenepropylene piezoelectrets with tubular channels for transducer applications

Ruy Alberto Pisani Altafim,<sup>1,a)</sup> Xunlin Qiu,<sup>1,b)</sup> Werner Wirges,<sup>1</sup> Reimund Gerhard,<sup>1,c)</sup> Ruy Alberto Corrêa Altafim,<sup>2</sup> Heitor Cury Basso,<sup>2</sup> Werner Jenninger,<sup>3</sup> and Joachim Wagner<sup>3</sup>

<sup>1</sup>*Applied Condensed-Matter Physics, Institute of Physics and Astronomy, University of Potsdam, Karl-Liebknecht-Strasse 24-25, 14476 Potsdam-Golm, Germany*

<sup>2</sup>*Department of Electrical Engineering, São Carlos School of Engineering, University of São Paulo, Av. Trabalhador São-Carlense 400, 13566-590 São Carlos, SP, Brazil*

<sup>3</sup>*Bayer MaterialScience AG, 51368 Leverkusen, Germany*

(Received 8 May 2009; accepted 1 June 2009; published online 9 July 2009)

We describe the concept, the fabrication, and the most relevant properties of a piezoelectric-polymer system: Two fluoroethylenepropylene (FEP) films with good electret properties are laminated around a specifically designed and prepared polytetrafluoroethylene (PTFE) template at 300 °C. After removing the PTFE template, a two-layer FEP film with open tubular channels is obtained. For electric charging, the two-layer FEP system is subjected to a high electric field. The resulting dielectric barrier discharges inside the tubular channels yield a ferroelectret with high piezoelectricity.  $d_{33}$  coefficients of up to 160 pC/N have already been achieved on the ferroelectret films. After charging at suitable elevated temperatures, the piezoelectricity is stable at temperatures of at least 130 °C. Advantages of the transducer films include ease of fabrication at laboratory or industrial scales, a wide range of possible geometrical and processing parameters, straightforward control of the uniformity of the polymer system, flexibility, and versatility of the soft ferroelectrets, and a large potential for device applications e.g., in the areas of biomedicine, communications, production engineering, sensor systems, environmental monitoring, etc. © 2009 American Institute of Physics. [DOI: 10.1063/1.3159039]

### I. INTRODUCTION

Soft piezoelectric transducer films have a large range of existing and potential applications. In particular, they are useful, e.g., in ultrasonic sensors or in dynamic-pressure transducers for biomedical devices, in microphones, microphone arrays, curved or flat loudspeakers, and headphones for electroacoustical systems, in transmitters and receivers for ultrasonic ranging and inspection, in electromechanical sensors for production engineering and process control, etc. Therefore, several routes have been proposed and demonstrated toward soft piezoelectric materials and devices: Polymers with molecular dipoles such as polyvinylidene fluoride and some of its copolymers, ceramic-polymer nano- and microcomposites, e.g., from lead-titanate particles and epoxy resin, space-charge polymer electrets such as polytetrafluoroethylene (PTFE) and some of its copolymers, etc. Over the past decade, ferroelectrets<sup>1,2</sup> emerged as an additional class of soft transducer films that may be “engineered” by processing or combining suitable materials.

Polymer-based transducers such as electret-condenser microphones or piezoelectric-polymer loudspeakers are usually assembled from several mechanical and electrical components including the active polymer film. In contrast to this

use of active “materials in a device,” ferroelectrets<sup>1,2</sup> may be considered as films with “devices in a material.” In cellular-foam ferroelectrets,<sup>3–5</sup> micrometer-scale voids with electrically charged internal surfaces work as tiny electret transducers. All together, the large number of such active transducerlike voids yield surprisingly high piezoelectric coefficients. Depending on the material and the charging conditions, piezoelectric  $d_{33}$  coefficients of up to 1400 pC/N have been reported.<sup>6</sup> Alternatively, the individual voids with internal charges of both polarities may be viewed as micrometer-scale dipoles whose dipole moments vary significantly under mechanical or electrical stresses. Since the relations between the mechanical and electrical input and output quantities are essentially linear, ferroelectrets show primary piezoelectricity.

Cellular-foam ferroelectrets have the disadvantage that their cellular voids always have a rather wide and not so well-controlled size and shape distribution so that only some of the voids are optimal for charging and for transducer operation.<sup>7,8</sup> In addition, most of the piezoelectric sensitivity is already lost between 60 and 70 °C in polypropylene (PP) ferroelectrets.<sup>9</sup> Consequently, cellular-foam ferroelectrets with higher thermal stability have been developed from polyethylene terephthalate (PET) and polyethylene naphthalate (PEN) by means of physical foaming with supercritical carbon dioxide.<sup>10,11</sup> The polyester ferroelectrets exhibit slightly higher thermal and long-term stabilities that are, however, still not sufficient for many practical applications.

Mainly for these two reasons (wide and not well-

<sup>a)</sup>Present address: Department of Electrical Engineering, São Carlos School of Engineering, University of São Paulo, Av. Trabalhador São-Carlense 400, 13566-590 São Carlos, SP, Brazil.

<sup>b)</sup>Electronic mail: xunlin@canopus.physik.uni-potsdam.de.

<sup>c)</sup>Electronic mail: reimund.gerhard@uni-potsdam.de.

controlled size and shape distribution of the cellular voids, as well as insufficient thermal stability in readily foamable polymers), alternative approaches with thermoformed and relatively large voids between fluoropolymer-electret films<sup>12,13</sup> or with laser-perforated holes in the central layer of a three-layer fluoropolymer sandwich<sup>14</sup> have been suggested more recently. These systems are, however, still difficult to charge optimally and do not lend themselves easily to large-scale production with good reproducibility. Here, we present an approach that avoids these shortcomings and that can serve as a material platform for several types of piezoelectric or even multifunctional ferroelectret films. In order to achieve good thermal stability of the ferroelectret properties, only fluoropolymers with proven stability of the electret properties for both charge polarities were used in the present film systems. The FEP-film ferroelectret systems have well-controlled homogeneous tubular channels due to the template-based fabrication process.

## II. SAMPLE PREPARATION

For sample fabrication in the laboratory, a lamination apparatus (model L-280, Assane®, Brazil) was fitted with a suitable temperature controller (MT-511R, Full Gauge, Germany) so that lamination temperatures up to 300 °C can be attained. The laboratory template consisted of a 100  $\mu\text{m}$  thick Teflon PTFE film with an area of  $30 \times 40 \text{ mm}^2$  and with parallel rectangular openings (area  $1.5 \times 30 \text{ mm}^2$ ) cut into the PTFE films by means of computer-controlled laser ablation. The PTFE separations between adjacent openings also had a width of 1.5 mm. Before lamination, the PTFE template was inserted between two Teflon FEP films with a thickness of 50  $\mu\text{m}$  each. The three-layer fluoropolymer-film sandwich was fed to the lamination apparatus which had been preheated to 300 °C. The chosen lamination temperature is substantially higher than the melting temperature of FEP (about 260 °C), but still well below the melting point of PTFE at 327 °C.

After cooling down under ambient conditions in the laboratory, the two FEP layers are permanently fused to each other through the openings of the PTFE template. Because of the antiadhesive properties of fluoropolymers, the PTFE template can be easily removed after cutting it open at one end. The resulting FEP-film system contains well-defined tubular channels as shown in Fig. 1. Part (a) schematically illustrates the laboratory fabrication process, while an optical micrograph of a typical sample is shown in part (b). Obviously, it is possible to generate uniform channels with a large range of widths, heights, and lengths, as well as arbitrary channel patterns with the present technique. For industrial fabrication, the PTFE templates may be replaced by fixed templates with nonadhesive surfaces around which continuously moving polymer films are laminated in a roll-to-roll process. The laboratory samples were metallized on both sides with circular aluminum electrodes with a diameter of 16 mm and a thickness of 40 nm each.

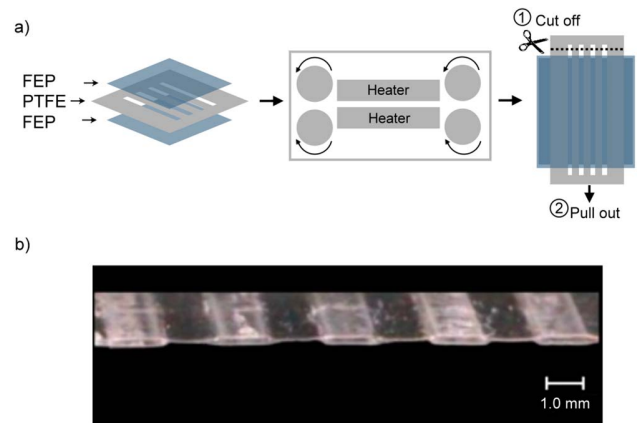


FIG. 1. (Color online) (a) Schematic of the laboratory fabrication process. The ferroelectret system consists of two FEP films that are laminated around a well-designed PTFE template at 300 °C. After lamination, the stack is cooled down to room temperature. (b) Optical micrograph of a typical ferroelectret system with tubular channels. Both the cross section at the end of the film and the film surface are visible.

## III. EXPERIMENTS AND RESULTS

### A. Charging and the resulting piezoelectricity

In order to charge the FEP foams by means of internal dielectric barrier discharges across the tubular channels, a dc voltage was applied to the electrodes for 10 s by means of a high-voltage supply (Trek model 610D).

The resulting piezoelectric  $d_{33}$  coefficient of tubular-channel FEP ferroelectrets as a function of the charging voltage is plotted in Fig. 2. The  $d_{33}$  coefficients were determined by means of dynamic mechanical excitation with a sinusoidal force with an amplitude of 1 N and a frequency of 2 Hz (Brüel&Kjaer model 4810 shaker), superimposed with a static bias force of 3 N. The resulting electric response of the sample was amplified by means of a Brüel&Kjaer model 2635 amplifier and recorded with an oscilloscope. From the applied force and the resulting electrical signal the respective  $d_{33}$  coefficients were calculated. The voltage dependence of the piezoelectric coefficient in the tubular-channel polymer-film systems clearly shows a threshold behavior similar to

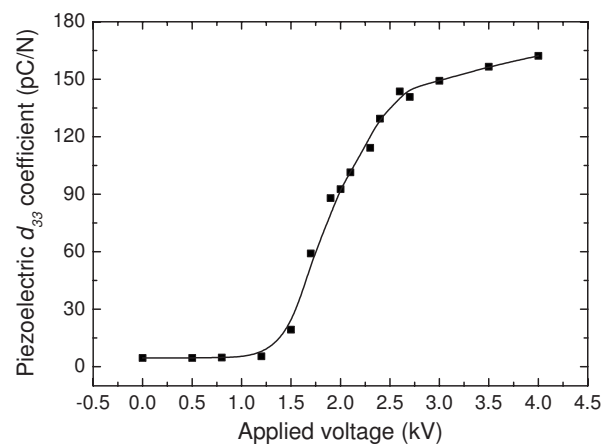


FIG. 2. Piezoelectric  $d_{33}$  coefficient of tubular-channel FEP ferroelectrets as a function of the charging voltage. The line that connects the data points has been drawn as a guide for the eyes only.

that found previously on cellular PP ferroelectrets.<sup>15</sup> For the present samples, the piezoelectric  $d_{33}$  coefficient remains nearly zero for charging voltages below 1.3 kV. Thereafter,  $d_{33}$  increases strongly with charging voltage and finally reaches a saturation value of about 160 pC/N at a charging voltage of about 2.7 kV.

Paschen breakdown in the gas has been suggested as the essential mechanism for the internal charging of the voids inside ferroelectrets.<sup>4,7,16</sup> According to Townsend's model, the critical breakdown field of common gases in a uniform electric field is a function of gas pressure  $p$  and electrode spacing  $d$  (which in our case is equal to the internal void height):<sup>17</sup>

$$E_c = \frac{Ap}{B + \ln(pd)}, \quad (1)$$

where the constant  $B$  is given by

$$B = \ln\left(\frac{C}{\ln(1 + 1/\gamma)}\right). \quad (2)$$

For air,  $A=273.8 \text{ V m}^{-1} \text{ Pa}^{-1}$  and  $C=11 \text{ m}^{-1} \text{ Pa}^{-1}$  are experimentally determined constants, and  $\gamma=0.01$  is the so-called second ionization coefficient. Paschen breakdown must take place inside the voids (i.e., within the tubular channels for the present case), in order to initiate microplasma discharges. For an externally applied voltage  $V$ , the electric field in the tubular channels  $E_g$  is given by

$$V = E_g \left( \frac{d_p}{\epsilon_p} + d_g \right), \quad (3)$$

where  $d_p=100 \text{ }\mu\text{m}$  is the accumulated thickness of the FEP layers,  $d_g=100 \text{ }\mu\text{m}$  is the internal void height, and  $\epsilon_p=2.1$  is the dielectric permittivity of the solid FEP film. From Eq. (1), the breakdown electric field for a  $d$  of  $100 \text{ }\mu\text{m}$  (internal height of the tubular channels between the FEP films) at atmospheric pressure is found to be approximately 8.7 MV/m. Equation (3) yields a corresponding threshold voltage of about 1280 V for the present film system, in very good agreement with the threshold voltage seen in Fig. 2.

The electrical breakdown process inside the tubular channels represents a dielectric barrier discharge (DBD).<sup>18</sup> It is known that DBDs in cellular PP ferroelectrets are accompanied by light emission that can be recorded with a digital camera. The characteristics of the light emission may also be used to investigate the DBDs in more detail.<sup>7,8</sup> Figure 3 shows the spatially resolved light emission from an FEP ferroelectret with tubular channels recorded by means of a PC-controlled electron-multiplying charge-coupled-device camera (EMCCD) (iXon, Andor Technology). For such an investigation, samples are metallized on both sides with semitransparent Au electrodes having a diameter of 16 mm and a thickness of 20 nm each. In order to block any light originating from corona discharges at the electrode edges, the sample is covered by a mask with a circular hole of 8.5 mm diameter. A positively biased sinusoidal voltage  $V = \frac{1}{2}V_{pp}[1 + \sin(\omega x)]$  with a peak-to-peak amplitude  $V_{pp}$  of 3.5 kV and a frequency of 100 Hz is applied to the sample. According to the widely accepted model of the piezoelectric-

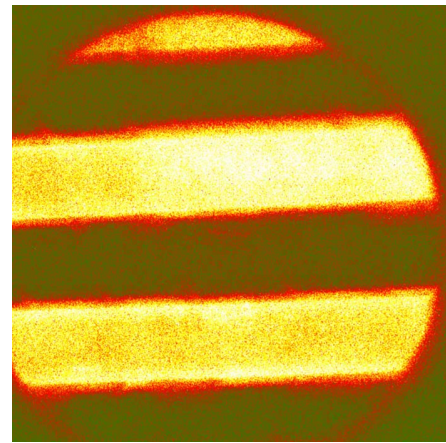


FIG. 3. (Color online) Color-coded EMCCD image of an FEP ferroelectret with tubular channels under positively biased sinusoidal voltages with a frequency of 100 Hz and  $V_{pp}$  of 3.5 kV. The CCD camera is internally triggered with an exposure time of 5 s.

ity in cellular polymer ferroelectrets, charges of opposite sign are trapped at the top and bottom surfaces of the voids during charging by means of DBDs.

A schematic model of the charge distribution in a tubular-channel FEP ferroelectret is shown in Fig. 4. The charged tubular channels, which carry positive charges on one of their inner large surfaces (here on the top surface) and negative charges on the other (here on the bottom surface), can be considered as macroscopic dipoles. The change in the channel height upon mechanical stress leads to a corresponding change of the dipole length and thus also the dipole moment, which results in a change of the induced charges on the electrodes.

Dielectric resonance spectra<sup>19</sup> (DRS) of cellular FEP ferroelectrets with four different channel heights are depicted in Fig. 5. The thickness resonances of the tubular channels are found at frequencies between 20 and 50 kHz. As expected, higher resonance frequencies are observed for thinner ferroelectret systems. The real part of the capacitance of a three-layer FEP ferroelectret well below the resonance frequency can be modeled as parallel arrangement of a three-layer capacitance (FEP-channel-FEP) and a one-layer FEP capacitance (cf. Fig. 4). If it is assumed that the areas of the tubular channels and of the laminated zones between the channels are equal (cf. Figs. 1 and 3), the capacitances of FEP ferroelectrets with a circular electrode and with channel heights of 25, 50, 70, and  $100 \text{ }\mu\text{m}$  are calculated to be 31.0, 27.9, 26.3, and 24.8 pF, respectively, in reasonable agreement with the  $C'$  values found in Fig. 5 at frequencies well below the respective resonance frequency. Figure 5 also illustrates that the resonance frequency of the ferroelectret systems can be adjusted by controlling the height of the tubular channels via

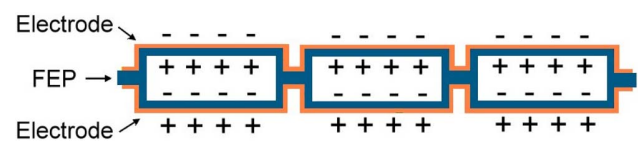


FIG. 4. (Color online) Schematic model of the charge distribution in a tubular-channel FEP-film ferroelectret.



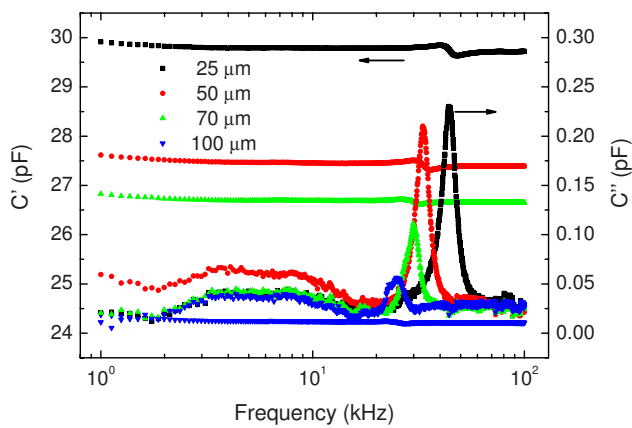


FIG. 5. (Color online) Frequency dependencies of the real part  $C'$  (left ordinate) and the imaginary part  $C''$  (right ordinate) of the capacitance determined on tubular-channel FEP ferroelectrets with four different channel heights as indicated.

PTFE templates of suitable thickness. A detailed analysis of the DRS results is under way and will be published elsewhere.

Optimization of the piezoelectric properties and, in particular, of the piezoelectric thickness coefficient and the resonance frequency is thus possible through adjustments of the geometrical parameters of the tubular-channel fluoropolymer-film ferroelectret system, such as the overall thickness of the materials system and the dimensions and the patterns of the tubular channels in it, and through control of the space-charge levels on the internal top and bottom surfaces of the tubular channels. To this end, polymer layers of the required thickness and PTFE templates of suitable geometry have to be employed together with adequate charging voltages and times.

### B. Thermal stability of the piezoelectricity

A typical example for the thermal stability of the piezoelectricity in the tubular-channel FEP-film ferroelectrets is shown in Fig. 6. A sample was charged at room temperature (RT) under 3 kV for 10 s, and the initial  $d_{33}$  coefficient was determined at RT. Then the sample was stored in an oven at

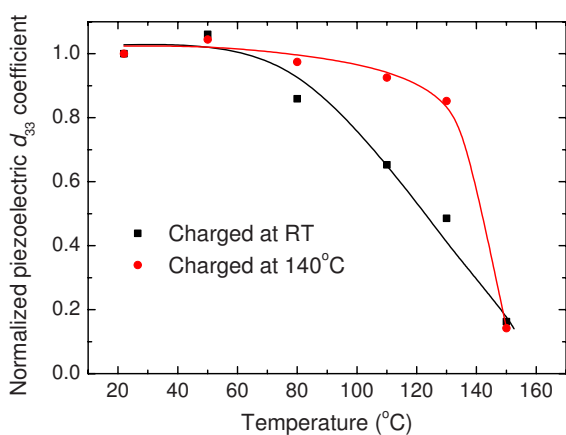


FIG. 6. (Color online) Decay of the piezoelectric  $d_{33}$  coefficient after charging at room temperature or at 140 °C and subsequent annealing at the indicated temperatures for 1 h.

a preset elevated temperature for 1 h. Subsequently, the sample's  $d_{33}$  coefficient was measured again at RT. Figure 6 (solid squares) indicates a slight decay of  $d_{33}$  after a 1 h storage at 80 °C. Storage at 100 °C leads to a significant decay of  $d_{33}$ . Thus the thermal stability of the piezoelectricity of tubular-channel FEP ferroelectrets charged at RT is roughly comparable to that of cellular PEN ferroelectrets.<sup>11</sup> Since the macroscopic dipoles (charged voids or channels) rely on the simultaneous existence of equal amounts of positive and negative charges (trapped on the top and bottom surfaces, respectively), the thermal stability of the piezoelectricity of FEP ferroelectrets is limited by the inferior thermal stability of positive charges on FEP, rather than by the superior thermal stability of the negative charges.

It is well known that charging at elevated temperatures is an effective way to improve the thermal stability of positive charges in FEP.<sup>20</sup> The decay of the  $d_{33}$  coefficient in a sample charged at 140 °C is also shown in Fig. 6 (solid circles). The sample was stored at 140 °C for 30 min and was then charged with 3 kV for 10 min at the same temperature. After charging, the sample was cooled down to RT under ambient conditions in the laboratory within 20 min still under the charging voltage, and the decay of its  $d_{33}$  coefficient was determined in the same way as detailed above. Obviously, the thermal stability of the piezoelectric  $d_{33}$  coefficient of the sample that had been charged at 140 °C is much better than that of the one charged at RT. Only a slight decay of about 15% is observed after annealing at 130 °C. Therefore, the piezoelectricity of properly charged FEP ferroelectrets is much better than that of PP ferroelectrets whose piezoelectricity decays already quite significantly at 60 °C.<sup>9</sup>

### IV. CONCLUSION

Tubular-channel FEP-film ferroelectret systems have been fabricated by laminating two FEP films around a PTFE template at 300 °C, followed by removal of the PTFE template from the laminated stacks. A piezoelectric  $d_{33}$  coefficient of up to 160 pC/N has been obtained. The piezoelectricity of tubular-channel FEP ferroelectrets charged at elevated temperature is thermally stable at temperatures of at least 130 °C. Advantages of the material system include its simplicity, its suitability for small-scale laboratory and large-scale industrial fabrication, and its well-controlled geometry that can be adjusted over a wide range of channel sizes and patterns according to the requirements of the respective device applications. Since the transducer function has been built into the material system, transducer elements or arrays can be cut from a roll of the ferroelectret polymer film and only need to be connected to a suitable amplifier.

### ACKNOWLEDGMENTS

The present work has been partly supported by the Conselho Nacional de Desenvolvimento Científico e Tecnológico (CNPq), Brazil, by the German Academic Exchange Service (Deutscher Akademischer Austauschdienst, DAAD) and by the University of Potsdam, Germany. The second author (X.Q.) thanks the Deutsche Forschungsgemeinschaft (DFG)

for providing a Research Fellowship (Reference No. QI 65/1-1) to him.

- <sup>1</sup>S. Bauer, R. Gerhard-Multhaupt, and G. M. Sessler, *Phys. Today* **57**(2), 37 (2004).
- <sup>2</sup>M. Wegener and S. Bauer, *ChemPhysChem* **6**, 1014 (2005).
- <sup>3</sup>M. Paajanen, H. Välimäki, and J. Lekkala, *Proceedings of the Tenth International Symposium on Electrets*, Delphi, Greece, 22–24 September, 1999 (IEEE Service Center, Piscataway, NJ, 1999), pp. 735–738.
- <sup>4</sup>G. M. Sessler and J. Hillenbrand, *Appl. Phys. Lett.* **75**, 3405 (1999).
- <sup>5</sup>M. Wegener, W. Wirges, J. Fohlmeister, B. Tiersch, and R. Gerhard-Multhaupt, *J. Phys. D: Appl. Phys.* **37**, 623 (2004).
- <sup>6</sup>X. Zhang, J. Hillenbrand, and G. M. Sessler, *J. Phys. D: Appl. Phys.* **37**, 2146 (2004).
- <sup>7</sup>X. Qiu, A. Mellinger, M. Wegener, W. Wirges, and R. Gerhard, *J. Appl. Phys.* **101**, 104112 (2007).
- <sup>8</sup>X. Qiu, A. Mellinger, W. Wirges, and R. Gerhard, *Appl. Phys. Lett.* **91**, 132905 (2007).
- <sup>9</sup>A. Mellinger, M. Wegener, W. Wirges, R. Reddy Mallepally, and R. Gerhard-Multhaupt, *Ferroelectrics* **331**, 189 (2006).
- <sup>10</sup>M. Wegener, W. Wirges, and R. Gerhard-Multhaupt, *Adv. Eng. Mater.* **7**, 1128 (2005).
- <sup>11</sup>P. Fang, M. Wegener, W. Wirges, L. Zirkel, and R. Gerhard, *Appl. Phys. Lett.* **90**, 192908 (2007).
- <sup>12</sup>R. A. C. Altafim, H. C. Basso, R. A. P. Altafim, L. Lima, C. V. de Aquino, L. Gonçalves Neto, and R. Gerhard-Multhaupt, *IEEE Trans. Dielectr. Electr. Insul.* **13**, 979 (2006).
- <sup>13</sup>X. Zhang, J. Hillenbrand, and G. M. Sessler, *Appl. Phys. A: Mater. Sci. Process.* **84**, 139 (2006).
- <sup>14</sup>H. C. Basso, R. A. P. Altafim, R. A. C. Altafim, A. Mellinger, P. Fang, W. Wirges, and R. Gerhard, *Annual Report, Conference on Electrical Insulation and Dielectric Phenomena*, Vancouver, Canada, 14–17 October, 2007 (IEEE Service Center, Piscataway, NJ, 2007), pp. 453–456.
- <sup>15</sup>M. Wegener, M. Paajanen, W. Wirges, and R. Gerhard-Multhaupt, *Proceedings of the 11th International Symposium on Electrets*, Melbourne, Australia, 1–3 October, 2002 (IEEE Service Center, Piscataway, NJ, 2002), pp. 54–57.
- <sup>16</sup>M. Lindner, S. Bauer-Gogonea, S. Bauer, M. Paajanen, and J. Raukola, *J. Appl. Phys.* **91**, 5283 (2002).
- <sup>17</sup>E. M. Bazelyan and Y. P. Raizer, *Spark Discharge* (CRC, Boca Raton, FL, 1998).
- <sup>18</sup>U. Kogelschatz, *Plasma Chem. Plasma Process.* **23**, 1 (2003).
- <sup>19</sup>A. Mellinger, *IEEE Trans. Dielectr. Electr. Insul.* **10**, 842 (2003).
- <sup>20</sup>H. von Seggern and J. E. West, *J. Appl. Phys.* **55**, 2754 (1984).

## APPLIED PHYSICS REVIEWS—FOCUSED REVIEW

## Patterned piezo-, pyro-, and ferroelectricity of poled polymer electrets

Xunlin Qiu<sup>a)</sup>*Department of Physics and Astronomy, Applied Condensed-Matter Physics, University of Potsdam, Karl-Liebknecht-Strasse 24-25, 14476 Potsdam-Golm, Germany*

(Received 29 January 2010; accepted 26 May 2010; published online 12 July 2010)

Polymers with strong piezo-, pyro-, and ferroelectricity are attractive for a wide range of applications. In particular, semicrystalline ferroelectric polymers are suitable for a large variety of piezo- and pyroelectric transducers or sensors, while amorphous polymers containing chromophore molecules are particularly interesting for photonic devices. Recently, a new class of polymer materials has been added to this family: internally charged cellular space-charge polymer electrets (so-called “ferroelectrets”), whose piezoelectricity can be orders of magnitude higher than that of conventional ferroelectric polymers. Suitable patterning of these materials leads to improved or unusual macroscopic piezo-, pyro-, and ferroelectric or nonlinear optical properties that may be particularly useful for advanced transducer or waveguide applications. In the present paper, the piezo-, pyro-, and ferroelectricity of poled polymers is briefly introduced, an overview on the preparation of polymer electrets with patterned piezo-, pyro-, and ferroelectricity is provided and a survey of selected applications is presented. © 2010 American Institute of Physics. [doi:10.1063/1.3457141]

## TABLE OF CONTENTS

I. INTRODUCTION.....	1
II. PIEZO-, PYRO-, AND FERROELECTRICITY IN POLED POLYMER ELECTRETS.....	3
A. Polar polymers.....	4
B. Ferroelectrets.....	4
1. Poling.....	4
2. Piezo- and pyroelectricity.....	5
III. PATTERNING OF POLED PIEZO-, PYRO-, AND FERROELECTRIC POLYMERS.....	6
A. Patterning by selective poling and/or depoling.....	7
1. Corona poling through a mask.....	7
2. Poling with patterned electrodes.....	7
3. Electron-beam poling.....	8
4. Photorelated poling.....	8
5. Suitable combinations of poling techniques.....	10
B. Direct patterning.....	10
1. Direct patterning of single-layer polymer-electret films.....	11
2. Patterned layer structures.....	12
IV. SELECTED APPLICATIONS.....	14
V. CONCLUSION.....	17

## I. INTRODUCTION

Polymers are very widely used in our daily life and in practically all areas of technology. Typical features of poly-

mer materials are flexibility, softness, light weight, relatively low acoustic impedance, low thermal conductivity, etc. Polymer electrets, dielectric materials with a quasipermanent excess charge or dipolar polarization, including semicrystalline ferroelectric polymers and amorphous chromophore-doped nonlinear optical (NLO) polymers have been discussed in this journal for sensors and photonics applications in 1996.<sup>1</sup> For details of the history and the state of the art in 1996 the reader is referred to this review paper and the literature cited therein. Today, semicrystalline poly(vinylidene fluoride) (PVDF) and its copolymers with trifluoroethylene [P(VDF-TrFE)] belong to the electroactive polymers that have been most extensively investigated and applied in numerous practical devices. A number of further ferroelectric polymers have also been discovered and explored, including aromatic and aliphatic polyurea, copolymers of vinylidene cyanide (VDCN), odd-numbered polyamides, poly-L-lactic acid (PLLA), and many bipolymers and synthetic polypeptides, etc.<sup>2-7</sup>

Figure 1 shows the molecular compositions of some ferroelectric polymers. A remarkable and promising development is the emergence of relaxor ferroelectric polymers that can be obtained by introducing additional defects into ferroelectric P(VDF-TrFE) polymer either by means of high-energy irradiation or via copolymerization with a bulky monomer such as chlorofluoroethylene or chlorotrifluoroethylene in order to form a terpolymer. This recent class of soft polymers exhibits extremely large electrostriction response and many features typically also found in relaxor inorganic ferroelectrics.<sup>8</sup> For amorphous chromophore-doped NLO polymers, significant progress has been achieved both in fundamental research and in the development of applications.

<sup>a)</sup>Electronic mail: xunlin@canopus.physik.uni-potsdam.de

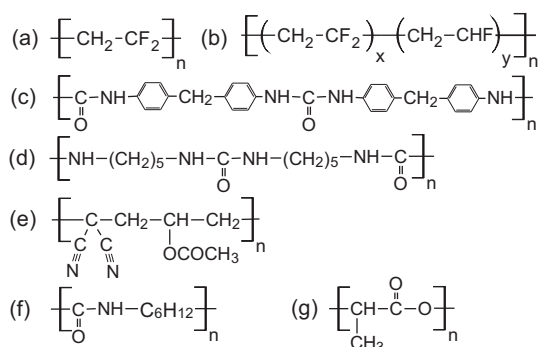


FIG. 1. Molecular compositions of piezoelectric polymers. (a) PVDF, (b) P(VDF-TrFE), (c) aliphatic polyurea, (d) aliphatic polyurea 5, (e) poly(vinylidene-cyanide-co-vinylacetate), (f) Polyamide 7 (PA-7), and (g) PLLA.

For example, the photoinduced motion of chromophores was comprehensively studied both theoretically and experimentally.<sup>9–12</sup> During the last two decades, numerous chromophores have been synthesized, characterized, and incorporated into a polymer matrices by means of physical doping or chemical attachment, in some cases with additional crosslinking.<sup>13–19</sup> Representative chemical compositions of polymers often used as host materials for NLO chromophores are shown in Fig. 2. Additionally, a variety of dendrimers have been prepared in recent years. They are particularly interesting as host materials because of their special well-controlled three-dimensional (3D) architectures.<sup>20,21</sup>

Recently, the family of piezo-, pyro-, and ferroelectric polymers has received a new member called “ferroelectrets” (i.e., internally charged polymer foams). Already during the 1970s, piezo- and pyroelectric properties of noncentrosymmetric electrically charged nonpolar polymers were theoretically predicted and also experimentally studied to some extent.<sup>22,23</sup> However, the research interest faded because of the rather weak piezo- and pyroelectricity obtained at that time. The situation changed substantially over the past one and half decades and a considerable number of cellular and voided electret polymers with strong piezoelectricity were identified and developed. This exciting development<sup>24–27</sup> significantly enlarges the range of piezo- and pyroelectric materials. During electrical poling of cellular or void-containing

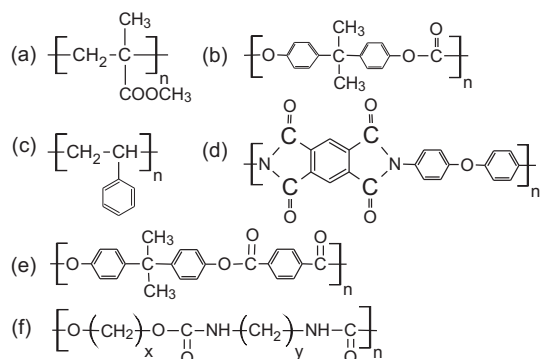


FIG. 2. Molecular compositions of polymers that are often used as matrix materials for chromophores. (a) PMMA, (b) polycarbonate, (c) PS, (d) polyimide, (e) poly(4,4'-isopropylidenediphenylene terephthalate) copolymer (U-100), (f) Polyurethane.

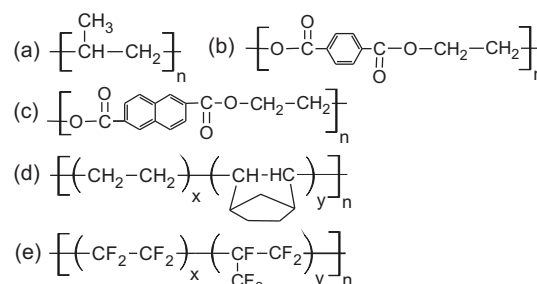


FIG. 3. Chemical compositions of several polymers suitable for ferroelectret preparation. (a) PP, (b) poly(ethylene terephthalate), (c) poly(ethylene naphthalene-2,6-dicarboxylate), (d) cyclo-olefin copolymer, (e) FEP copolymer.

polymer structures, charges of opposite polarity are generated in a dielectric barrier discharge (DBD) and trapped at the internal surfaces of the gas-filled voids.<sup>28–30</sup> The charged voids can be considered as macroscopic dipoles, which—in combination with the macroscopically nonuniform elastic properties of the material—induce the desired piezo- and pyroelectricity. The poled materials are called ferroelectrets because their macroscopic polarization and other related properties are phenomenologically similar to the behavior observed on typical ferroelectrics, while the internal charge trapping is the same as in other space-charge electrets.<sup>31</sup> Figure 3 shows the chemical compositions of several polymers that have been successfully employed to develop ferroelectrets.<sup>32–37</sup> Depending on the structure of the material and the charging conditions, ferroelectrets often show piezoelectric  $d_{33}$  coefficients of hundreds of pC/N, more than an order of magnitude greater than those found in conventional ferroelectric polymers and comparable to the values found in advanced ferroelectric ceramics. Consequently, the new ferroelectrets have attracted considerable interest in research and industry.

The three types of relevant polymer electrets are schematically summarized in Fig. 4. For details on the recent development in this area, the interested reader may consult the respective reviews, such as Refs. 2–7 for ferroelectric polymers, Refs. 9–21 for NLO polymers, and Refs. 24–27 for polymer ferroelectrets, as well as the literature cited therein. Research on piezoelectric composites is also very active. In view of the relatively small piezo- and pyroelectric coefficients of ferroelectric polymers, polymer-ceramic composites—usually ceramic particles embedded in a suitable polymer matrix—are prepared in order to combine the respective advantages of polymers (as above-mentioned) and of ceramics: strong piezo- and pyroelectricity, low dielectric and mechanical loss, a large range of possible dielectric permittivities, etc. Experimental and theoretical studies reveal that the composites possess hybrid properties of the constituents.<sup>38–41</sup> The same basic concept was recently adopted by Ganesan *et al.*<sup>42,43</sup> for a different type of composite. Liquid-crystal (LC) droplets are dispersed in ferroelectric P(VDF-TrFE). After poling of the P(VDF-TrFE) matrix, the local electric field across the LC-filled cavities acts on the LC molecules as a bias field. Due to the piezoelectric effect, the internal electric field of the film changes upon



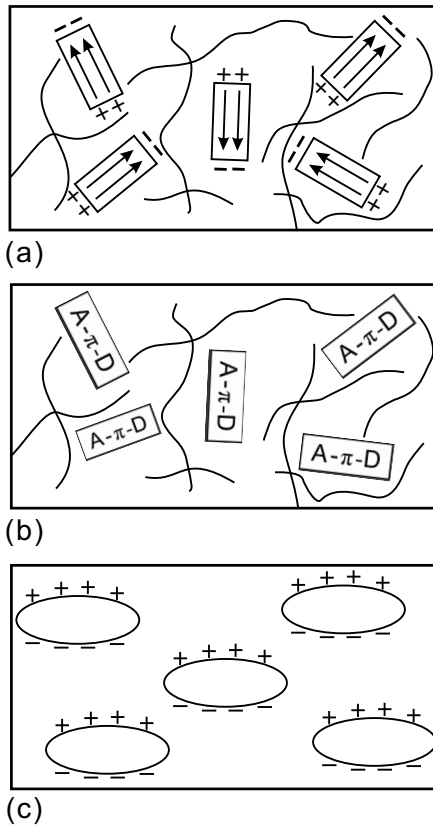


FIG. 4. Schematic view of piezo-, pyro-, and ferroelectric polymer electrets. (a) In semicrystalline ferroelectric polymers, ferroelectric crystallites are dispersed in the amorphous matrix. Space charges trapped at the interfaces between crystallites and amorphous matrix compensate and stabilize the ferroelectric polarization (Ref. 1). (b) Amorphous polymers for photonics applications contain chromophore molecules with large hyperpolarizabilities and large dipole moments (Ref. 1). (c) A new member of the family of piezo-, pyro-, and ferroelectric polymer electrets: internally charged nonpolar cellular polymers with very high piezoelectricity. Charges of opposite sign are deposited on the internal top and bottom surfaces of the voids so that the charged voids can be considered as macroscopic dipoles.

variations in the external mechanical stress, leading to a change in the optical transmission of the composite film. Such a piezo-optical composite may be very attractive for applications e.g., in sensing and visualization but it is also interesting from a fundamental point of view, since the interaction between liquid crystal and ferroelectric polymer can be studied in various ways.

Materials with patterned dipole orientation and thus also patterned piezo-, pyro-, and ferroelectricity are useful for a variety of applications such as sensor arrays with reduced cross talk between individual elements, piezoelectric gratings for direction-sensitive acoustic-wave detection or emission, pyroelectric sensor arrays with complex shapes, etc. For modal-dispersion phase matching within NLO polymer waveguides, steplike dipole orientation profiles across the polymer thickness are usually required.<sup>44</sup> In this paper, we discuss the patterning of piezo-, pyro-, and ferroelectric polymer electrets along their thickness or lateral directions on micro- and macroscopic scales. Obviously, microprocessing and nanofabrication techniques that are widely employed in the manufacture of micro- and optoelectronic devices can also be used for the patterning of functional structures. A

comprehensive survey of these sophisticated techniques is not attempted here. For details, the interested reader may refer to pertinent references such as Refs. 45–49 and to the literature quoted therein. Nevertheless, some of the techniques related to polymer electrets have to be briefly introduced.

The present review starts with a thermodynamic definition of piezo-, pyro-, and ferroelectricity and with a description of the modifications that are necessary in order to account for these effects in poled polymers. The piezo- and pyroelectricity, as well as the NLO properties in polar polymers are briefly reviewed. This is followed by a comprehensive discussion about the poling of ferroelectrets and the resulting piezoelectricity. In Sec. III, suitable techniques for patterning piezo-, pyro-, and ferroelectric polymers are reviewed. It is possible to induce desired polarization patterns into initially homogeneous polymer films by means of selective poling and/or depoling techniques. Patterned polarization can also result from patterned sample structures directly formed during sample preparation. In Sec. IV, several representative applications are shown in order to highlight the applications potential of polymers with patterned piezo-, pyro-, and ferroelectricity. It will become evident from the discussion that suitable combinations of different patterning techniques lead to electroactive polymers with complex polarization patterns, allowing for innovative devices. Conclusions about the topics reviewed here will be drawn in Sec. V.

## II. PIEZO-, PYRO-, AND FERROELECTRICITY IN POLED POLYMER ELECTRETS

Ferroelectricity is based on spontaneous polarization in the material, the direction of which can be switched or modified by external electric fields. An essential criterion for ferroelectricity is the hysteresis behavior of the electric polarization as a function of the electric field. Materials with ferroelectricity are always piezo- and pyroelectric as well.

Defined in a rigorous way according to thermodynamical principles, the macroscopic piezoelectric  $d_{mj}$  coefficient is a tensor component given by the second derivative of the Gibbs free energy  $G$  with respect to the electric field vector  $E$  and the stress tensor  $X$ ,<sup>50</sup>

$$d_{mj} = \left[ \frac{\partial^2 G(E, X, T)}{\partial E_m \partial X_j} \right]_T, \quad (1)$$

where  $T$  is the temperature. Similarly, the pyroelectric  $p_m$  coefficient is defined as

$$p_m = \left[ \frac{\partial^2 G(E, X, T)}{\partial E_m \partial T} \right]_X. \quad (2)$$

The second derivatives in Eqs. (1) and (2) can be taken in any order so that

$$d_{mj} = \left( \frac{\partial D_m}{\partial X_j} \right)_{T,E} = \left( \frac{\partial x_j}{\partial E_m} \right)_{X,T} \quad (3)$$

and



$$p_m = \left( \frac{\partial D_m}{\partial T} \right)_E = \left( \frac{\partial S}{\partial E_m} \right)_T, \quad (4)$$

where  $D$ ,  $x$ , and  $S$  are the electric displacement, the strain, and the entropy, respectively. The first expression in Eq. (3) denotes the direct piezoelectric (transducer) effect, while the second expression describes the inverse piezoelectric (actuator) effect. Thus, the reciprocity of direct and inverse piezoelectricity immediately follows from the theoretical treatment.

For practical purposes, the piezo- and pyroelectric coefficients in polymers can often be defined by a single expression<sup>51</sup>

$$\xi = \frac{1}{A} \left( \frac{\partial Q}{\partial \Xi} \right), \quad (5)$$

where  $\xi$  is either the piezo- or the pyroelectric coefficient,  $\Xi$  is the pressure  $p$  or the temperature  $T$ , and  $A$  and  $Q$  are the electroded area and the charge on the measuring electrode, respectively. In Eq. (5), only commonly measured quantities are involved.

### A. Polar polymers

In a number of reviews on polar polymers with piezo- and pyroelectricity (see for instance, Refs. 1–7), the physical basis, typical experimental results and suggested or implemented applications are extensively discussed.

It is generally accepted that the main contribution to the piezo- and pyroelectricity in polar polymers arises from the dipole-density change as a result of dimensional changes in the sample upon compression (secondary piezoelectricity) or thermal expansion (secondary pyroelectricity). In semicrystalline polymers, dipole libration, reversible changes in crystallinity, and motion of charges necessary for the compensation of the crystallite polarization may also affect the piezo- and pyroelectricity to some extent, while the effect of the affine motion of the dipoles should be taken into account in amorphous polar polymers. Four requirements should be fulfilled for large piezo- and pyroelectricity in polymers:<sup>3</sup> (1) molecular dipoles must be present with a large dipole moment and at a sufficient concentration. (2) The dipoles must be preferentially aligned by a poling procedure and the best results are obtained when saturation is achieved. (3) The dipole alignment, once achieved, must be locked-in, where the best results are obtained in thermodynamically stable states or in frozen states far away from softening temperatures. (4) For piezoelectricity, the material should be easily strained with applied stress, whereas pyroelectricity requires a significant (reversible) temperature dependence of the polarization, often resulting from a relatively large thermal expansion of the relevant phase.

NLO behavior is another important property associated with oriented dipoles in polar polymers. However, it was found that the NLO susceptibility of semicrystalline polar polymer is usually too weak for any practical applications. More recently, a new class of amorphous polymers that contain chromophore molecules with large hyperpolarizabilities and large dipole moments emerged. After the molecular di-

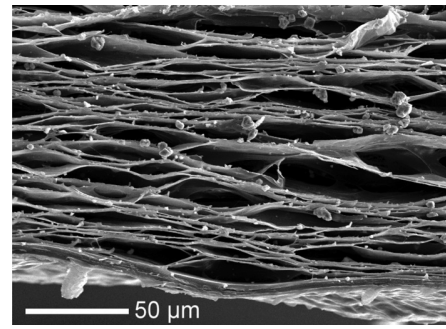


FIG. 5. Scanning electron micrograph of the cross section of a cellular PP foam (Ref. 52).

poles are preferentially oriented by means of poling, the amorphous NLO polymers show significant second-order NLO effects, and therefore, have numerous applications in photonics and optoelectronics.<sup>19,21</sup>

### B. Ferroelectrets

Usually, ferroelectricity is only expected in polar materials. Thus, it came as a big surprise that completely nonpolar polymers with internal space charge of both polarity—the so-called ferroelectrets—behave almost like ferroelectrics! Because of their unusual features, ferroelectrets attract more and more attention both from science and industry. For recent reviews the reader is referred to Refs. 24–27. In this subsection, some new results concerning the poling process in ferroelectrets are discussed. The layer model for the piezoelectricity in ferroelectrets, which consists of alternating polymer and air layers, is also introduced here, since it has not been covered in detail within the above-mentioned review articles.

#### 1. Poling

As seen in the scanning electron microscope (SEM) image of a typical cellular polypropylene (PP) foam in Fig. 5, a large number of voids, with lateral dimensions on the order of 100  $\mu\text{m}$  and vertical dimensions of up to approximately 10  $\mu\text{m}$ , are distributed throughout the bulk of the foamed polymer film.<sup>52</sup> In order to render polymer foams piezoelectric, the voids must be internally charged. The poling process in ferroelectrets is based on DBDs. In DBDs, at least one side of the discharge gap is insulated from the electrodes by a dielectric layer. Based on the investigation of the light emission from the DBDs in ferroelectrets during poling,<sup>28</sup> a schematic model for the poling process has been proposed.<sup>29</sup> Internal breakdown (Paschen breakdown) in the voids is triggered when the electric field in the voids reaches the required threshold value (comparable with the “coercive field” in ferroelectrics). Charges of opposite polarity are separated in the very high electric field inside the DBD and are subsequently trapped on the top and bottom surfaces of the voids, respectively (point A in Fig. 6). The trapped charges induce an internal electric field opposite to the externally applied field and thus extinguish the discharge. As the applied voltage increases further, a second breakdown may occur, and the density of the internally trapped charges strongly increases

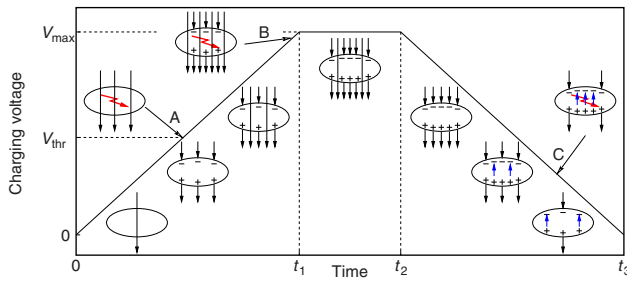


FIG. 6. (Color online) Schematic view of the poling process in a single polymer void. When the poling voltage reaches the threshold value  $V_{thr}$ , Paschen breakdown is initiated (a). At higher voltages, a second series of discharges may occur (b). During ramping down the voltage, the reverse electric field from the trapped space charge may lead to back discharges (c) (Ref. 29).

(point B in Fig. 6). When the applied voltage is reduced, the electric field of the trapped charges may overcompensate the applied field and may trigger back discharges (point C in Fig. 6). An *in situ* acoustical monitoring of the polarization build-up in ferroelectrets shows that the back discharges destroy a significant proportion of the effective charge density.<sup>53</sup> In order to optimize the poling efficiency, the geometry (especially the height) of the voids, the type of gas and its pressure inside the voids are critical factors to be considered and to be optimized.<sup>52,54,55</sup>

A direct proof of the internally trapped charges was obtained by means of SEM images.<sup>56</sup> SEM images of obliquely cut cellular PP ferroelectrets provide a direct visualization of negative charges, because the secondary electron-emission yield and the backscatter from negatively charged areas is higher than that from positively charged areas. Overall, the charged voids can be considered as macroscopic dipoles [see, Fig. 4(c)], the direction of which can be reversed by sufficiently high electric fields. Consequently, the resulting electric-displacement versus electric-field curves exhibit hysteresis behavior. It should be noted that DBDs produce a variety of species including energetic and reactive monoatomic as well as molecular diatomic charged particles (i.e., ions), electrons, and neutral species. Therefore, the inner surfaces of the voids in ferroelectrets are exposed to a highly reactive plasma during DBD poling. Both chemical and physical processes occur on the exposed surface areas. Such effects may be used for surface modification, as shown recently in a simple DBD configuration to improve cell adhesion, by means of labeling of fluorophores.<sup>57</sup> It is also found that repeated DBD poling in air leads to the oxidation of the inner surfaces of the voids in cellular PP ferroelectrets and thus deteriorates their chargeability, resulting in significant fatigue of the effective polarization.<sup>58</sup>

## 2. Piezo- and pyroelectricity

The practical definition of piezo- and pyroelectricity in Eq. (5) holds for ferroelectrets as well. However, the microscopic origin of the piezo- and pyroelectricity in ferroelectrets is significantly different than in polar polymer ferroelectrics. In ferroelectrets, the point symmetry is broken on the macroscopic level with void dimensions on the order of  $100 \times 100 \times 10 \mu\text{m}^3$ , while in polar polymers like PVDF,

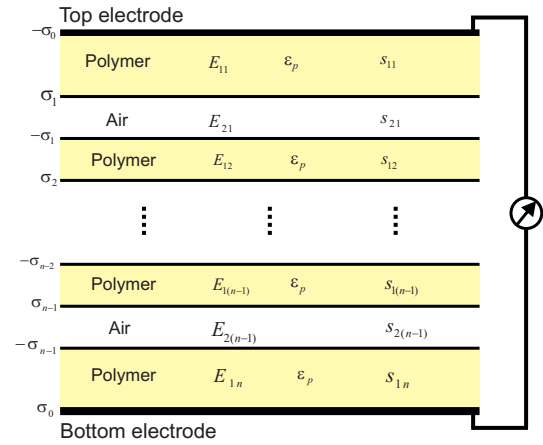


FIG. 7. (Color online) Simplified layer model for ferroelectrets with alternating polymer and air layers (Refs. 59 and 60). Charges of opposite polarity are generated during the DBDs and deposited on the top and bottom air-polymer interfaces, respectively.

the unit cell dimensions are in the order of  $0.9 \times 0.5 \times 0.3 \text{ nm}^3$ . Thus, the basic dipolar unit in ferroelectrets is 15 orders of magnitude larger than that in ferroelectric polymers. Because of the anisotropy of the lenslike voids and the low symmetry of the charge distribution, high piezoelectric sensitivity is only found in the thickness direction ( $d_{33}$  coefficient) and is typically two orders of magnitude larger than the in-plane piezoelectric sensitivity ( $d_{31}$  and  $d_{32}$  coefficients).

Since the lateral dimensions of the voids are much larger than their vertical dimensions (see, Fig. 5), a simplified model has been proposed to describe the piezoelectricity of ferroelectrets, which consists of consecutive polymer and air layers of thicknesses  $s_{1i}$  and  $s_{2j}$ , respectively, with  $i = 1, 2, \dots, n$  and  $j = 1, 2, \dots, n-1$ , where  $n$  is the total number of solid layers.<sup>59,60</sup> Figure 7 schematically shows the layer model. The permanent charges on the two sides of each air gap are taken to be equal in magnitude, since it is assumed that they originate from the DBDs in the air gap during poling (which only leads to charge separation but not to the generation of excess charges of one polarity).

The electric fields in the polymer and air layers may be calculated by use of Gauss' and Kirchhoff's laws. For the top and bottom electrodes, Gauss' law can be written as

$$-\epsilon_0 \epsilon_p E_{11} = -\sigma_0 \quad (6)$$

and

$$\epsilon_0 \epsilon_p E_{1n} = \sigma_0. \quad (7)$$

For the top and bottom interfaces of the  $j$ th air gap,

$$-\epsilon_0 E_{2j} + \epsilon_0 \epsilon_p E_{1j} = \sigma_j \quad (8)$$

and

$$-\epsilon_0 \epsilon_p E_{1(j+1)} + \epsilon_0 E_{2j} = -\sigma_j. \quad (9)$$

Under short-circuit conditions, Kirchhoff's second law is given by

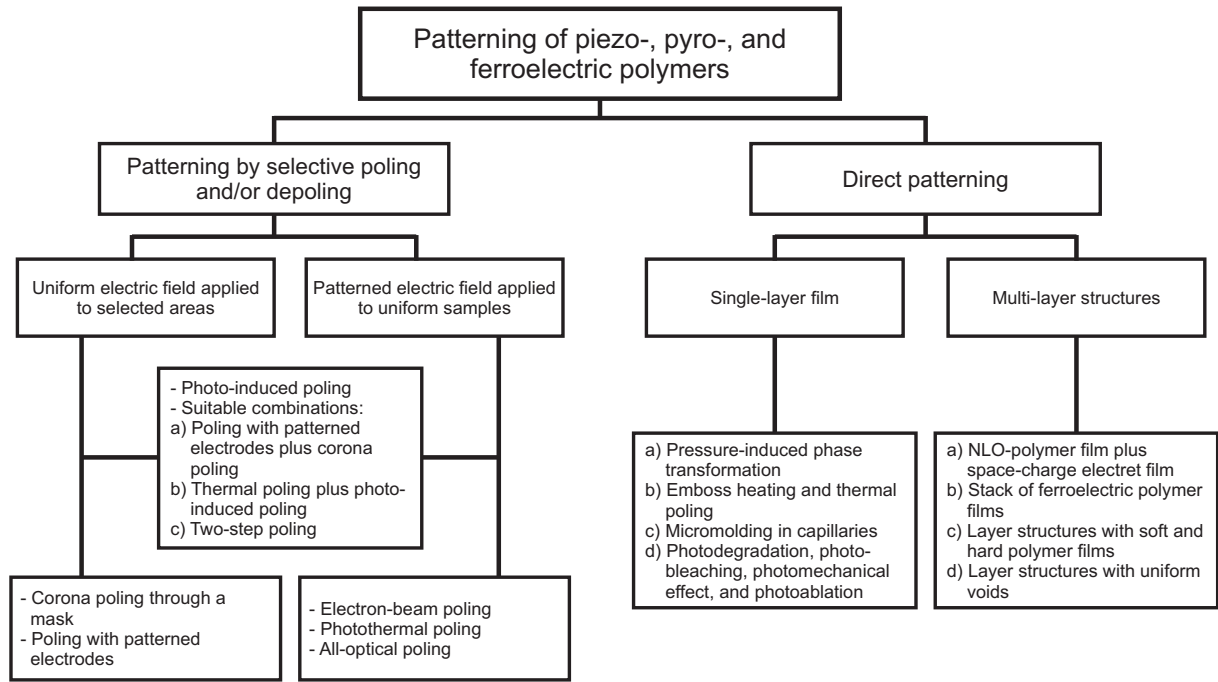


FIG. 8. Schematic illustration of the techniques for patterning piezo-, pyro-, and ferroelectric polymers.

$$\sum_i s_{1i} E_{1i} + \sum_j s_{2j} E_{2j} = 0. \quad (10)$$

Equations (8) and (9) yield

$$E_{11} = E_{12} = \dots = E_1 \quad (11)$$

and

$$E_{2j} = \varepsilon_p E_1 - \frac{\sigma_j}{\varepsilon_0}. \quad (12)$$

Substituting Eqs. (11) and (12) into Eq. (10), one obtains

$$E_1 = \frac{\sum_j s_{2j} \sigma_j}{\varepsilon_0 s_1 + \varepsilon_0 \varepsilon_p s_2} \quad (13)$$

and

$$E_{2i} = \frac{\varepsilon_p \sum_j s_{2j} \sigma_j}{\varepsilon_0 s_1 + \varepsilon_0 \varepsilon_p s_2} - \frac{\sigma_i}{\varepsilon_0}, \quad (14)$$

where  $s_1 = \sum_i s_{1i}$  and  $s_2 = \sum_j s_{2j}$  are the combined total thicknesses of the polymer and air layers, respectively.

When a pressure  $p$  is applied to the electrically charged foam, the thickness changes are primarily due to the compression of the air layers. Therefore, the electrode charge varies according to  $\partial \sigma_0 / \partial s_2$ . If  $\partial s_{2j} / \partial s_2 = s_{2j} / s_2$  is assumed, then

$$\frac{\partial \sigma_0}{\partial s_2} = \frac{\varepsilon_p s_1}{(s_1 + \varepsilon_p s_2)^2} \sigma_{\text{eff}}, \quad (15)$$

where  $\sigma_{\text{eff}} = \sum_j s_{2j} \sigma_j / s_2$  is the effective polarization in the ferroelectret. Together with the stress-strain relation  $\Delta s_2 / s = p / Y$ , where  $s = s_1 + s_2$  and  $Y$  is Young's modulus of the foam, one obtains the piezoelectric coefficient

$$d_{33} = \frac{\varepsilon_p s}{Y} \frac{s_1 \sigma_{\text{eff}}}{(s_1 + \varepsilon_p s_2)^2}. \quad (16)$$

On the other hand, an ac or dc voltage  $\Delta V$  applied to the layer system generates additional fields  $e_1$  and  $e_2$  in the polymer and air layers, respectively. The field  $e_2$  results in an additional force between the two adjacent polymer layers and hence in a thickness change  $\Delta s_{2j}$  of the air layer in between. By analyzing the sum of the thickness changes  $\Delta s_2$  and the applied voltage, one obtains the inverse piezoelectric  $d_{33}$  coefficient of the ferroelectret<sup>61,62</sup>

$$\frac{\Delta d}{\Delta V} = d_{33}, \quad (17)$$

which confirms the reciprocity of the piezoelectric sensor and actuator effects.

For a comparison of the piezo- and pyroelectricity in ferroelectrets and in ferroelectrics, see, Ref. 26. Due to the high compressibility of the voids, very large piezoelectric  $d_{33}$  coefficients of hundreds of pC/N can often be achieved in ferroelectrets. However, the pyroelectric coefficient of ferroelectrets (typically around  $0.25 \mu\text{C}/(\text{m}^2 \text{K})$ ) is much smaller than that of polar polymers such as PVDF [typically around  $27 \mu\text{C}/(\text{m}^2 \text{K})$ ], which is an advantage in electromechanical applications, since the respective devices will be relatively insensitive to temperature changes.<sup>63</sup>

### III. PATTERNING OF POLED PIEZO-, PYRO-, AND FERROELECTRIC POLYMERS

In this section, the techniques for patterning piezo-, pyro-, and ferroelectric polymers will be discussed. An overview of the proposed patterning techniques is given in Fig. 8. Poling under an electric field is necessary in order to render

piezo-, pyro-, and ferroelectric polymer electrets electroactive. Although poling itself means an additional processing step, it also introduces a degree of freedom in the design of devices. Suitable polarization patterns in the film plane and/or across the film thickness are possible through selective poling as well as depoling techniques. Furthermore, patterned piezo-, pyro-, and ferroelectricity in polymers may directly originate from patterned sample structures introduced by means of suitable sample-preparation procedures.

### A. Patterning by selective poling and/or depoling

Poling techniques suitable for breaking the symmetry of polymer electrets have already been reviewed in Ref. 1. In particular, the patterning of piezo-, pyro-, and ferroelectric polymer electrets by means of suitable poling techniques has been discussed in that review. In the following subsections, the possibility of patterning by means of selective poling and/or depoling will be discussed, with a focus on more recent progresses achieved since 1996. A thorough review on the relevant poling techniques themselves will not be given here. Interested readers may refer to the previous review and to the literature cited therein.

#### 1. Corona poling through a mask

Corona discharges have been employed in order to charge the surfaces of electrets since several decades.<sup>64</sup> In addition to established corona-poling procedures for ferroelectric and NLO polymers, corona poling is now also widely used for poling ferroelectrets. In this case, corona poling is often implemented without a grid. The corona ions are deposited onto the surface of the ferroelectret sample and generate a surface potential. Breakdown of the gas inside the voids is triggered when the internal electric field induced by the surface potential reaches the respective threshold. The light emission from the internal breakdown events during corona poling may be recorded with a digital camera.<sup>65</sup> Usually, no thermal treatment is required for triggering the breakdown of the gas inside the voids during corona charging of ferroelectret polymers. This is different from the situation of ferroelectric and NLO polymers, where a simultaneous thermal treatment is usually applied during corona poling in order to reduce the coercive electric field (ferroelectric) or to approach the glass-transition temperature ( $T_g$ ) of the material (NLO polymers). However, a thermal treatment during corona poling influences the charge trapping of the inner surfaces of the voids in ferroelectrets. The charge trapping in shallow traps is suppressed at elevated temperatures, leading to a higher ratio of charges in deep traps to those in shallow traps. Therefore, corona poling at elevated temperatures can improve the thermal stability of the internally charged macroscopic dipoles and hence the piezoelectricity of ferroelectrets.<sup>66</sup> As already discussed in Ref. 1, corona poling through a grounded metal mask is suitable for producing periodic polarization patterns in a polymer film.

#### 2. Poling with patterned electrodes

Another commonly used poling technique to pole piezo-, pyro-, and ferroelectric polymer electrets is electrode poling

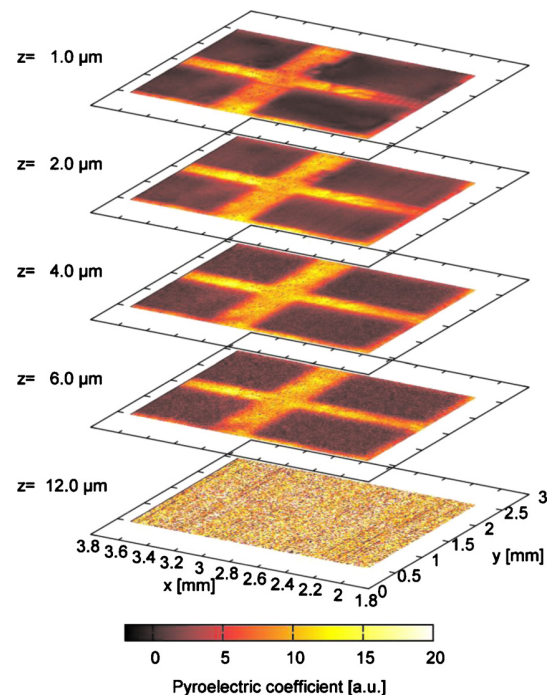


FIG. 9. (Color online) High-resolution 3D polarization map of a P(VDF-TrFE) sample poled with an electrode grating. Details of the electrode grating are very well reproduced (Ref. 74).

with an electric field larger than the coercive field of the film. Basically, there are three ways to generate patterned electrodes: (i) the electrode can be directly deposited onto the sample surface in the desired pattern, (ii) after deposition, a uniform electrode can be patterned by means of lithography and etching, or (iii) a patterned electrode can be fabricated independently and then brought into contact with the sample. The first two approaches may be useful for a variety of applications such as focusing ultrasound generators and receivers or quasiphase-matched second-harmonic generation (QPM-SHG), in which the patterned electrodes are sometimes also required for transducer operation. As already discussed in the earlier review,<sup>1</sup> large periodic deformations of the polymer film surface are caused by the electrostatic forces during poling and by the resulting viscous flow of the polymer in its rubbery state. These effects are usually detrimental but may be minimized by employing periodic poling electrodes on the substrate surface and a large-area continuous electrode on top of the polymer system.<sup>1</sup> Later studies indicated that the width and separation distance of the electrodes must be carefully designed in order to optimize the QPM efficiency.<sup>67-69</sup> The effective nonlinearity contrast can be optimized in ridge-waveguide structures.<sup>70,71</sup>

Patterned electrodes were also used in connection with thermal-pulse tomography (TPT) of ferroelectric polymers. High-resolution 3D polarization mapping of PVDF and P(VDF-TrFE) films poled with well-defined electrode gratings was realized by means of TPT.<sup>72-74</sup> As can be seen from Fig. 9, the polarization profiles reproduce the pattern of the electrode grating very well. In addition, a partial depolarization is observed in particular near the electroded surface. The TPT technique has close relevance to the topic of this paper,



since it provides an efficient way to detect the patterned polarization achieved in piezo-, pyro-, and ferroelectric polymer electrets.<sup>75</sup>

Planar optical waveguides can be fabricated by means of electrical microcontact printing ( $E-\mu\text{CP}$ ), in which the electrode has been implemented through the last of the above-mentioned approaches.<sup>47,48,76,77</sup> A stamp with a suitable pattern, usually prepared from elastomeric poly(dimethylsiloxane) (PDMS) and coated with a thin gold film, is placed in conformal contact with a dielectric film supported on a second electrode. A voltage is applied between the gold layer on the PDMS and the second electrode behind the dielectric film. The resultant current flows predominantly within the intimately contacted regions defined by the stamp pattern and bleaches the chromophores doped in these regions, leading to a change in the local index of refraction of the chromophore-doped polymer. By use of this technique, thin-film waveguides can be patterned in less than 90 s over large areas (more than  $1 \text{ cm}^2$ ).

### 3. Electron-beam poling

In electron-beam poling, the sample is charged by an essentially monoenergetic electron beam in the range between a few and tens of kiloelectron volt. Depending on the electric-field distribution inside the sample, a well-confined space-charge layer is generated, the depth of which depends on the energy of the electron beam. In compact polymers, this dependence is usually given by a power law<sup>78</sup>

$$r = r_0 \left( \frac{E_B}{E_0} \right)^n, \quad (18)$$

where  $E_B$  is the electron-beam energy,  $r_0$  (in  $\mu\text{m}$ ),  $E_0$  (in keV), and  $n$  are constants to be determined from the experimental data. Electron-beam poling of ferroelectrets has also been reported.<sup>61</sup> With the difference that the near-surface charges are injected by means of an electron beam, the high electric field across the voids and the resulting internal breakdown are the same as with corona poling. Electron-beam poling is suitable for patterning piezo-, pyro-, and ferroelectric polymer electrets along both the thickness and the in-plane directions.<sup>1</sup> It should be noted, however, that chemical modifications and some degradation of the material in the irradiated region are usually observed, which—at least in some cases—limits the applicability of electron-beam poling.<sup>78,79</sup>

However, the chemical modification and degradation of the material during electron-beam irradiation may be utilized for patterning in the case of chromophore-doped NLO polymers. These effects may occur with the chromophores within the host polymer. It is found that the chromophores are destroyed, and hence the second-order nonlinearity is erased by electron-beam exposure above a certain dose, while at very low radiation doses, no chromophore destruction is observed.<sup>80</sup> Chemical modification and degradation may also act on the polymer matrix. Electron-beam irradiation of poly(methyl methacrylate) (PMMA) above a certain dose leads to depolymerization of its main chain. The depolymerized layers are completely soluble when the irradiated sample is

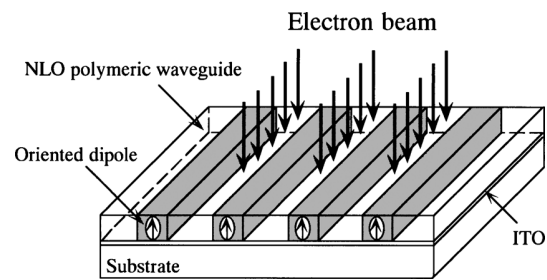


FIG. 10. Geometry of a periodically poled NLO polymer waveguide fabricated by electron-beam irradiation. The sample, spin-coated on a glass slide with a transparent ITO electrode, is irradiated by means of an electron-beam lithography system. The electron-beam irradiation is used to erase the microscopic hyperpolarizability of the chromophores within the exposed area. It may also be used to depolymerize the host polymer or to modify its  $T_g$  within the exposed area, allowing the fabrication of ridge-type optical channel waveguides of high quality in a corona or a two-step poling process (Ref. 80).

treated in isoamyl acetate with ethyl acetate and rinsed with pure water.<sup>80,81</sup> Corona poling is employed after the treatment in order to align the dipoles in the nontreated regions. On a chromophore-doped poly(4,4'-isopropylidenediphenylene terephthalate) copolymer (U-100), the irradiated areas could be removed by means of a thermal development after the electron-beam irradiation.<sup>82,83</sup> Unlike the wet development of PMMA, corona poling can be carried out simultaneously with the thermal development. When polystyrene (PS) is used as the host polymer, the  $T_g$  of the polymer is increased within the exposed area due to the cross-linking caused by the electron-beam irradiation, so that a domain-inversion structure can be generated by means of a two-step poling process (to be discussed later).<sup>83</sup> Based on the above-discussed mechanisms, a ridge-type optical channel waveguide with a high-quality pattern can be obtained by electron-beam irradiation with a suitable arrangement, as schematically shown in Fig. 10. This simple technique is applicable to various types of polymer film for implementing submicrometer patterns with high resolution.<sup>84,85</sup>

### 4. Photorelated poling

As already mentioned above, a simultaneous thermal treatment is often applied during the poling of ferroelectric and NLO polymers in order to enhance the mobility of the dipoles. The thermal treatment can be implemented by means of irradiation of the polymer with light. Using a focused laser beam, the temperature of the sample is increased mainly locally, thus allowing selective poling under a simultaneously applied electric field with suitable waveforms. In order to produce a waveguide with high performance, appropriate laser-beam wavelengths should be selected so that the film can be heated uniformly throughout its thickness. In addition, optimal values of the laser power, of the laser-beam diameter, of the speed of the moving stage, and of the electric-field strength are essential.<sup>86</sup>

Since the  $T_g$  of a ferroelectric PVDF film is well below room temperature (RT), the photothermal poling technique used on NLO polymer films is not suitable for patterning PVDF films. However, poled  $\beta$ -phase PVDF films can be locally depolarized by means of selective heat absorption

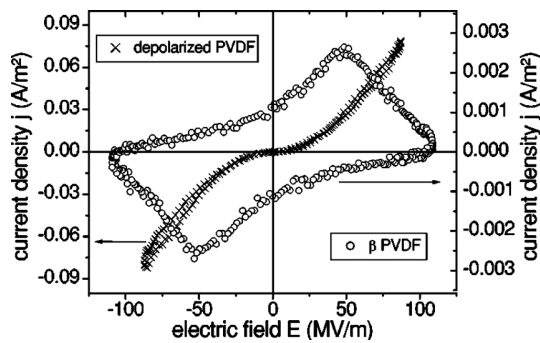


FIG. 11. Poling-field dependence (under a sinusoidal electric field at a frequency of 3 mHz) of the current density during poling of a depolarized PVDF film (left axis) in comparison to a  $\beta$ -phase PVDF film. The depolarization was achieved by controlled scanning of the top sample electrode with a focused laser beam (Ref. 87).

during controlled scanning of a focused laser beam across their top electrodes.<sup>87</sup> With the right processing parameters, an irreversible phase transformation from the  $\beta$  phase to a much less polar phase ( $\alpha$  or  $\alpha_p$ ) occurs throughout the thickness of the poled  $\beta$ -phase PVDF films, without destruction of the film. Figure 11 shows the charging behavior of the depolarized and undepolarized areas of the PVDF film. The current density through the depolarized area under a sinusoidal electric field at a frequency of 3 mHz does not show any peaks.<sup>88</sup> With this technique, depolarized stripes with widths down to 80 to 90  $\mu\text{m}$  can be produced on a 23  $\mu\text{m}$  thick  $\beta$ -PVDF film.

For chromophore-doped NLO polymers, the dipole mobility can be increased through a photoisomerization process. Most chromophore molecules used in NLO polymers contain double bonds around which the molecules undergo a reversible so-called *trans-cis* transformation when they absorb light of a suitable wavelength, leading to a change in the shape of the dipolar molecule and an increase in its mobility.<sup>9-12</sup> Consequently, the molecular dipoles can sometimes be oriented by means of a simultaneously applied electric field even well below the  $T_g$  of the respective NLO polymer (photoinduced orientation, PIO), while light irradiation alone can destroy any previous orientation (photoinduced deorientation or depoling, PID).

Combined with appropriately designed schemes of electric field application, both PIO and PID can be employed to pattern the dipole polarization in NLO polymers.<sup>89-92</sup> Most recently, a new efficient approach was proposed for PIO patterning by means of scanning-probe microscopy.<sup>93</sup> The probe acts both as an electrode for applying an electric field [atomic force microscopy (AFM)] and as a sensor for detecting the polarization *in situ* [electrostatic force microscopy (EFM)]. Both, dipole orientation and contact electrification (CE) can occur during the interaction between probe and sample surface, generating heterocharges and homocharges, respectively. However, the CE effect is negligible if the AFM is operated in the tapping mode, which reduces the friction force and the time period of physical contact during poling. Figure 12(a) shows the fundamental principle: the dipoles are oriented by the electric field from the probe across the sample. In combination with illumination by a linearly po-

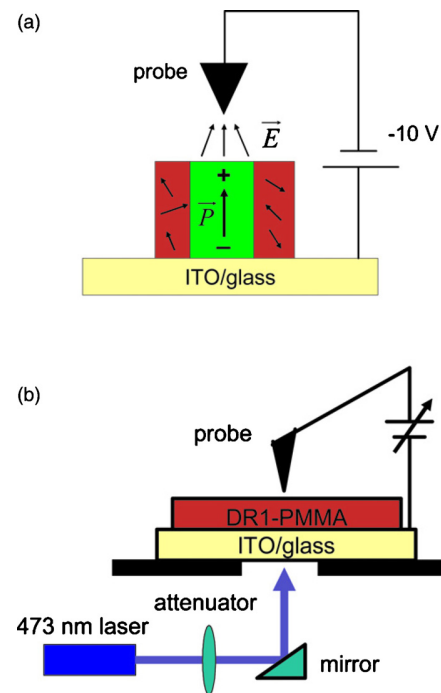


FIG. 12. (Color online) (a) Schematic/view of the relationship between the probe bias and the dipole polarization/bound charges resulting from local poling with a negatively biased probe. (b) Selective PIO/PID during illumination with a laser source from the rear side (Ref. 93).

larized diode-pumped solid-state laser [Fig. 12(b)], dipole polarization is generated or erased locally.<sup>93</sup>

Photoinduced poling (PIP) still requires the presence of a dc electric field, while in all-optical poling (AOP) only light fields are involved.<sup>94-96</sup> During AOP, a polymer film is irradiated simultaneously by two superimposed coherent beams, one at frequency  $\omega$  and the other at frequency  $2\omega$ . Under these conditions, the average of the cubic power of  $\langle E^3 \rangle$  is nonzero (although the mean electric field  $\langle E \rangle = \langle E_\omega + E_{2\omega} \rangle$  is zero), which results in selective polar excitation of the molecules. This technique allows for the orientation not only of dipolar molecules but also of molecules exhibiting octupolar symmetry.<sup>97</sup> Although only light fields are involved in AOP, an induced second-order susceptibility as high as that achieved by means of electric-field poling was obtained by optimizing the seeding conditions.<sup>98,99</sup> In order to optimize the charging efficiency, an appropriate intensity ratio of the two seeding beams is required, and the trade-off between the optical seeding efficiency and the transparency of the polymer should be taken into account.<sup>100-104</sup>

Advantages of patterning by means of PIP are the feasibility of generating complex patterns for integrated circuits and devices through appropriate masks and the good repeatability of the process. Whereas AOP is a promising technique that can be applied for the fabrication of photonic devices also with several advantages: The molecular-dipole orientation has a period exactly satisfying the phase-matching conditions for SHG, there is no need for poling electrodes, and patterning for optimal SHG can be easily achieved by scanning the focal area across the sample surface in a well-controlled manner. In addition, both PIP and AOP permit the

absence of thermal degradation of the chromophores that would be unavoidable during thermal poling at high temperatures. Unfortunately, the dipole orientation induced by PIP and AOP has a inferior thermal stability compared to thermal poling.<sup>105,106</sup> However, the stability of the orientation can be improved by means of a suitable thermal treatment under an applied field (PIP) or during seeding (AOP).<sup>107–110</sup> Another efficient way to improve the temporal stability of the orientation is using side-chain polymers with high  $T_g$  or thermally crosslinkable polymer systems as polymer matrices.<sup>111–115</sup>

### 5. Suitable combinations of poling techniques

Suitable combinations of different poling techniques may be utilized to generate highly special and more complicated polarization patterns. One example is the combination of poling with patterned electrodes and corona poling reported by Jung and Kinoshita.<sup>116</sup> In their study, a periodic electrode on a NLO polymer film is prepared by means of photolithography of a continuous aluminum layer, while a uniform indium-tin-oxide (ITO) layer is used as the second electrode. First, the dipoles underneath the patterned aluminum electrode are oriented by means of electrode poling. Then both the patterned aluminum electrode and the ITO electrode are grounded and corona poling is used to orient the dipoles within the remaining areas in the opposite direction. With this technique, a periodically domain-inverted poled-polymer waveguide for QPM-SHG can be fabricated.

Bimorph or multimorph polarization can be achieved in NLO polymer films through the combination of thermal poling and PIP. First, the whole film is uniformly poled by means of thermal poling, and afterwards, selective poling is achieved with PIP which reorients the dipoles only within the penetration depth of the irradiated light under an electric field opposite to that of the first poling step.

Two-step poling is proposed to prepare bimorph polarization in double layers of two ferroelectric or amorphous polymers with two different Curie or glass-transition temperatures.<sup>44</sup> With proper poling schemes, it is also possible to separately polarize different components within a sample. Rollik *et al.*<sup>117</sup> investigated the contributions of the crystalline and the amorphous phases, as well as the interface between them to the pyroelectricity of PVDF by selecting appropriate poling temperatures below and/or above  $T_g$  as well as poling fields lower and/or higher than the coercive field. In a semicrystalline ferroelectric polymer such as PVDF, there are three possible types of polarization, namely in the crystalline phase, in the amorphous phase, and at the crystalline-amorphous interface (Maxwell–Wagner or interface-charge polarization, MWI polarization). In a special strategy for selective and combined poling of these three contributions, the crystalline phase is poled with an electric field  $E_{PC}$  higher than the coercive field (for PVDF,  $E_C > 80$  MV/m at RT). After this first poling step, all three kinds of polarization may be found in the polymer film. Then the sample is cooled down below  $T_g$  (for PVDF,  $T_g \approx -42$  °C). The polarization of the amorphous phase can be erased if the electrodes are short-circuited before the temperature drops to  $T_g$ . The polarization of the amorphous

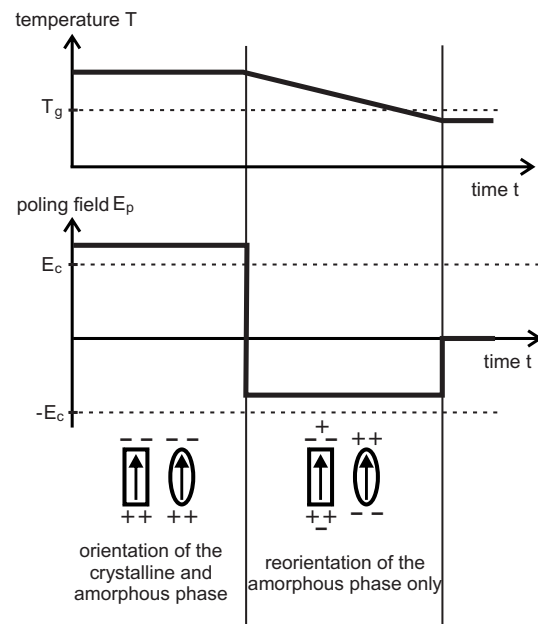


FIG. 13. Selective poling schemes for polar semicrystalline ferroelectric polymers. The resultant polarization of the amorphous phase is in antiparallel with that of the crystalline phase (Ref. 117).

phase can also be induced parallel ( $E_{PA} < E_C$  with the same sign as  $E_{PC}$  during cooling) or antiparallel ( $E_{PA} < E_C$  opposite to  $E_{PC}$  during cooling, as shown in Fig. 13) to that of the crystalline phase. If the sample is solely poled with  $E_{PA}$  and the electrodes are short-circuited before the temperature drops below  $T_g$ , only the MWI polarization is present after poling.

In the case of ferroelectric composites of ceramic nanoparticles in a ferroelectric polymer matrix, the orientation of the polarization in the two components can be poled to be either parallel or antiparallel by means of a similar two-step poling technique.<sup>118,119</sup> It is known that the pyroelectric coefficients  $p_3$  of perovskite ceramics and ferroelectric polymers have the same sign (both negative), while the piezoelectric  $d_{33}$  coefficients have opposite sign (positive and negative for ceramics and ferroelectric polymers, respectively) because of the difference between primary and secondary (i.e., dipole-density) piezoelectricity, respectively. Thus, polymer-ceramic composites with enhanced pyroelectricity but greatly reduced piezoelectricity (when the orientation of the polarization in the two constituents is parallel) or vice versa (when the orientation of the polarization is antiparallel) can be obtained.<sup>119,120</sup> Such composites are of much interest for sensor applications, since a strong influence of temperature changes (or mechanical vibration) on a piezoelectric (respectively, pyroelectric) sensor can be avoided.<sup>120,121</sup>

### B. Direct patterning

As already mentioned, patterned piezo-, pyro-, and ferroelectricity in poled polymer electrets may also originate from patterned sample structures, although poling is always necessary for rendering these polymer electrets electroactive. Conventional techniques for patterning polymer films in-



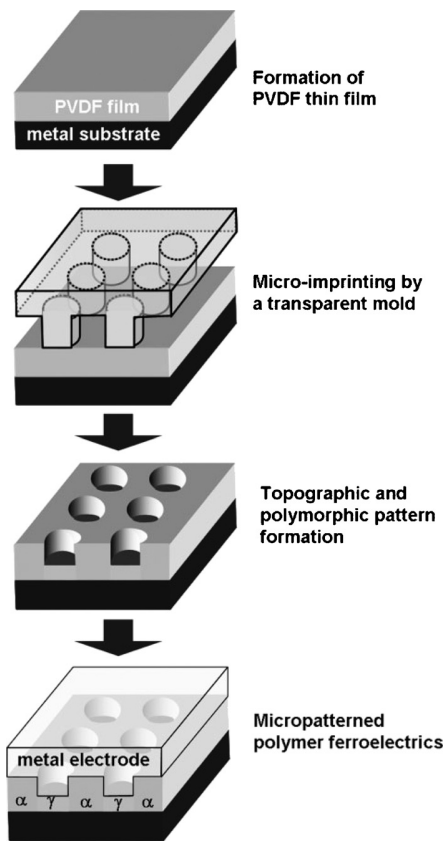


FIG. 14. A schematic view of the fabrication of micropatterned PVDF ferroelectrics. The localized pressure applied in microimprinting lithography leads to a polymorphic transition from the nonpolar  $\alpha$  phase to the ferroelectric  $\gamma$  phase (Ref. 126).

clude laser ablation, numerically controlled drilling or punching, wet etching (with chemicals), dry etching (by means of plasma or reactive-ion etching), hot embossing lithography, photolithography, etc.<sup>122</sup> In this subsection, methods suitable for patterning the sample structure of piezo-, pyro-, and ferroelectric polymer films are discussed.

### 1. Direct patterning of single-layer polymer-electret films

It has been demonstrated that the crystallization of PVDF depends significantly on the hydrostatic pressure applied and that a pressure higher than 500 MPa, combined with specific thermal treatment, can yield a polar crystalline form in PVDF films that can be up to hundreds of micrometers thick.<sup>123–125</sup> Kang *et al.*<sup>126</sup> prepared patterned arrays of isolated ferroelectric  $\gamma$ -type domains embedded in the nonpolar  $\alpha$  phase of thin PVDF films by means of microimprinting of a spin-cast  $\alpha$ -type PVDF film. The thin PVDF film was melted and recrystallized after spin-casting in order to eliminate its initial surface roughness. Then a transparent elastic mold fabricated from PDMS with a topographic array pattern was compressed uniaxially onto the film for (sub)micrometer scale patterning, as shown in Fig. 14. This technique was also used to pattern  $\beta$ -phase ferroelectric P(VDF-TrFE) copolymer films. It is found that the remnant polarization of the P(VDF-TrFE) sample is dramatically enhanced by imprinting at a suitable temperature due to the

increased crystallinity of the film. Various patterns have been created with good pattern transfer from the imprinting molds to the polymer films.<sup>127</sup> Nonlinear surface relief grating (SRG) in NLO polymer film was obtained by means of a simple technique using simultaneous process of emboss heating and thermal poling. In this case, a pressure-induced phase transformation does not occur. For master grating fabrication, a PI film with high thermal stability and high mechanical strength was prepared onto a metal plate and then the desired pattern on the PI film was achieved by a holographic method. The master grating was stamped under pressure into the NLO polymer at elevated temperature and a high voltage was applied between the metal plate and the ground. The film was cooled down with the pressure and the electric field and finally the master grating was removed. This simple technique is applicable to most of the NLO polymer films with short process time and low cost.<sup>128</sup>

Another patterning method that also relies on a PDMS mold is micromolding in capillaries (MIMIC).<sup>129–131</sup> In MIMIC, a PDMS stamp with a suitable surface-relief structure is conformally laid onto the substrate, thus, generating a network of capillaries between the two layers. A liquid prepolymer is sucked into this network by capillary action. Micropatterning of a semicrystalline PVDF solution was performed by means of temperature-controlled MIMIC.<sup>132</sup> O<sub>2</sub>-plasma-treated PDMS molds with micrometer-scale relief features in their surfaces were conformally pressed onto the surface of polished single crystal silicon wafers, which were in turn placed on a temperature-controlled metal substrate. The polar solvent dimethylformamide was used because it produced predominantly  $\gamma$ -phase PVDF crystals and showed almost no swelling of PDMS. The PVDF solution injected into the inlets of the PDMS channels drained rapidly to the outlet of PDMS due to capillary force and filled the interconnected channels between the molds and the substrates. After the solvent has fully evaporated, the PDMS stamp can be easily separated from the patterned microstructures because of its very low interfacial free energy. Well-defined micropatterns of PVDF were generated during fast directional evaporation at 120 °C.

It is well known that PVDF undergoes dehydrofluorination upon irradiation with x-rays, excimer lasers or ion beams.<sup>133–140</sup> These irradiation effects bring new possibilities of patterning. Morikawa *et al.* reported direct pattern transfer onto PVDF using x-ray photons from a synchrotron radiation source.<sup>141,142</sup> In this technique, a PVDF film is exposed to x-rays through an absorbing mask with the desired pattern. As a result of the photodegradation, a maximum etch depth of more than 9  $\mu\text{m}$  is achieved within the exposed area, thus, transferring the pattern into the PVDF film. *In situ* mass spectrometry reveals that the major degradation process is dehydrofluorination, while no carbon-containing species are detected. The photoemission spectra, in combination with *ab initio* molecular-orbital calculations, indicate the formation of fully conjugated C=C double bonds during photodegradation of the polymer. Therefore, the main effects of the photodegradation in PVDF seem to be the shrinking of the irradiated polymer region because of dehydrofluorination and the generation of conjugated bonds. The technique is



also used to directly pattern very thin P(VDF-TrFE) films.<sup>143</sup> A nickel wire-mesh mask is employed for patterning. The residual material within the exposed region is carbon rich because of the formation of double bonds in the polymer chain and crosslinking between chains. In contrast to the case of pure PVDF, the main photofragments include carbon-containing species such as CHF, CH<sub>2</sub>, and CF<sub>2</sub>, which is attributed to the presence of the TrFE monomer species.

Various patterned structures in chromophore-doped NLO polymers can be achieved through photobleaching and photoablation induced by selective light irradiation. As mentioned above, under irradiation at a suitable wavelength, a reversible *trans-cis* photoisomerization occurs in chromophore molecules. However, under irradiation with an energy density higher than that required for photoisomerization, an irreversible photobleaching occurs, during which the double bonds in the chromophores are broken and their non-linearity is easily erased.<sup>144–147</sup> Thus, patterning can be done by locally bleaching the chromophores with such irradiation through a suitable photomask, while poling of the non-bleached areas can be carried out before or after the photobleaching. In the case of chromophore-doped NLO polymers based on photopolymerizable resins, photopatterning takes place mostly in the polymer matrix.<sup>148,149</sup> The polymerization process induced by an exposure to visible light hardens the initially soft matrix material and freezes the orientation of the chromophore molecules. After irradiation with a periodic illumination pattern, the film was charged in a static electric field. The chromophores within the nonpolymerized zones were oriented along the poling field, while those in previously polymerized areas remained oriented at random. Thus, a periodic polarization structure defined by the illumination pattern was created.

A photomechanical effect associated with the photoisomerization of azochromophores is identified and used to pattern NLO polymers.<sup>12,150–152</sup> The isomerization process generates pressure in the polymer matrix and thus also a localized photomechanical deformation of the material. There is a crossover temperature (normally much lower than  $T_g$ ), below and above which photoexpansion and photocontraction are observed, respectively. For patterning, the sample is illuminated with a sinusoidal light intensity (or polarization) pattern generated by two coherent laser beams. Patterning can be realized by either photoexpansion or photocontraction, where the pattern phase is in opposite in the two cases. A sinusoidal grating (SRG) without any defects is obtained on the film surface with a depth of hundreds of nanometers.<sup>151</sup>

For most NLO polymer films, such a spontaneous surface patterning occurs already at relatively low laser powers up to a saturation value without destructive ablation. The resulting SRG can be erased by heating the sample above  $T_g$ . However, laser irradiation at much higher energy density leads to photoablation of NLO polymer films. Laser ablation of polymers is an established technique in the electronic industry.<sup>153</sup> The photoablation of NLO polymers is due to the evaporation of the material and the ablation depth is proportional to the irradiation energy.<sup>147,154–156</sup> The SRG fabricated through photoablation is thermally stable up to a temperature

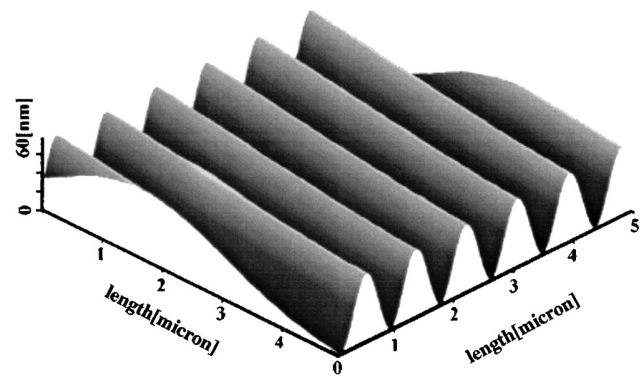


FIG. 15. AFM surface profile of a grating on a urethane-urea copolymer developed by laser interferometry. After fabrication, the grating was heat-treated for 60 min at 150 °C, i.e., above the  $T_g$  (141 °C) of the copolymer (Ref. 155).

higher than the  $T_g$  of the polymer. Figure 15 shows the surface profile of a typical SRG on a urethane-urea copolymer observed by means of AFM. By means of laser interferometry, the grating period can be adjusted from a submicrometer to a millimeter scale by adjusting the incidence angle between the two writing beams.

## 2. Patterned layer structures

Very often, bi- or multilayer structures exhibit useful additional functions that are not possible with any of the constituents alone. The above-discussed double-layer structures of ferroelectric or amorphous polymers with two different  $T_c$  or  $T_g$  parameters are typical examples. These layer structures were, however, included in Sec. III B 2, since the implementation of their functions requires specifically designed poling schemes. A double-layer system that consists of an amorphous fluoropolymer (Teflon-AF) film plus a NLO polymer film was proposed in order to improve the polarization stability in the NLO polymer. The stack was corona poled from the Teflon-AF side so that the dipole orientation in the NLO polymer can be stabilized by the electric field from the space charge in the Teflon-AF layer. Because Teflon-AF can provide very good thermal stability of the space charge, the stability of the dipole polarization and hence also of the NLO effects in the double-layer system is significantly improved in comparison to a single film of the same NLO polymer.<sup>157</sup>

Multilayer ferroelectric polymer stacks are designed and prepared in order to improve the sensitivity of the resulting transducers. Ferroelectric polymer stacks are widely used in ultrasonic transducers. In the case of folded multilayer structures, the ferroelectric polarizations of adjacent layers have opposite signs and are oriented along the thickness direction. The electrodes of folded structures are also alternating so that all even-numbered and all odd-numbered electrodes are connected together, respectively. For an actuator, the output amplitudes of the individual layers are added, while both the resonance frequency and the electrical impedance are reduced in comparison to an individual layer.<sup>158,159</sup> The resonance frequency of the multilayer stack can be adjusted by choosing the thickness of each single layer.<sup>160</sup> In order to obtain a bandwidth comparable to that of a single layer, a

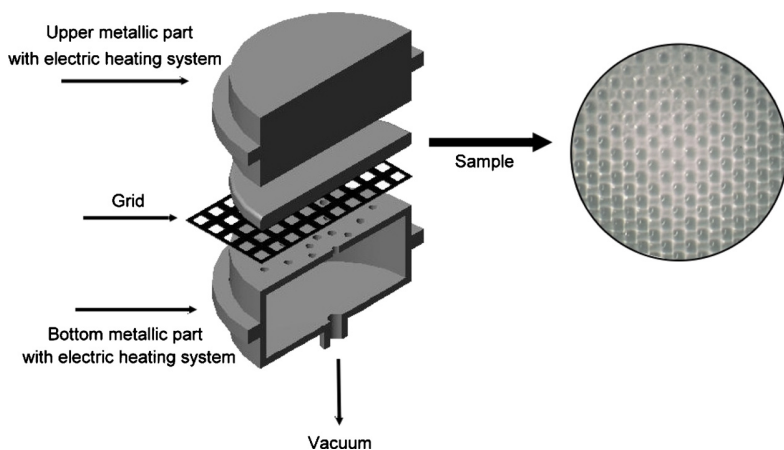


FIG. 16. (Color online) Schematic view of the setup for preparation of thermoformed bubble structures between two polymer films (Ref. 176).

switchable Barker-code stack design is adopted in which the electrodes of the transducer can be connected in parallel or in series for the transmitting and the receiving mode, respectively.<sup>158,161</sup>

Recently, miniaturized monolithic multilayer cantilevers were fabricated from P(VDF-TrFE) on a substrate by means of alternating spin-coating and electrode-evaporation processes. In the multilayer structures, polymer layers with a thickness of several micrometers are separated by aluminum electrodes with a thickness of hundreds of nanometer. After cutting the stack with a dicing saw or etching with an inductively coupled plasma, the internal electrodes of the multilayer structure are exposed, which allows for the electrical connection of alternate electrodes. An actuator consisting of three multilayered P(VDF-TrFE) cantilevers was fabricated. It shows high performance with respect to force, deflection, and motion even at relatively low driving voltages.<sup>162-164</sup>

Layer sandwiches of space-charge polymer-electret films were already used in early implementations of piezoelectrets. Kacprzyk *et al.*<sup>165-167</sup> reported piezoelectric double-layer sandwiches of one softer and one harder layer with electret charges in between and confirmed the possibility of making piezo- or ferroelectrets in this way. Porous polytetrafluoroethylene (PTFE) is very attractive for use as piezoelectric transducer material in such hard/soft electret sandwiches, because of high surface-charge stability and softness.<sup>168-171</sup> Fluoropolymer ferroelectrets were produced by sandwiching a highly porous PTFE [so-called expanded PTFE (ePTFE) consisting of 91% air and 9% fibrous PTFE] between two solid fluoroethylenepropylene (FEP) layers.<sup>172,173</sup> The FEP layers form structurally and electrically dense layers, whereas the fibrous ePTFE layer keeps the two FEP layers apart, forming air-filled cavities. Upon corona charging, breakdown occurs within the cavities when the electric field strength exceeds the Paschen-breakdown threshold value of air. Charges of both polarities are separated during plasma formation and some of them are trapped on the internal surfaces of the top and bottom FEP layers. After bipolar charging of their internal surfaces, the cavities can be considered as macroscopic dipoles. The piezoelectric  $d_{33}$  coefficient is thermally stable if the sample is charged at elevated temperatures. However,  $d_{33}$  decays from 800 to 400 pC/N under

atmospheric pressures within six days, and repeated mechanical loading leads to a similar loss of piezoelectricity, apparently related to mechanical fatigue in the highly porous ePTFE.

For industrial applications, ferroelectrets with well-controlled distributions or even uniform values of void size and void shape and with good thermal stability of the piezoelectricity are very desirable. Such ferroelectrets may be easily produced on a large scale with good reproducibility and they also promise long lifetimes. Several strategies were proposed for preparing ferroelectrets of this kind. A stack of two FEP films was placed between two cylindrical metal plates which can be independently heated. One plate is completely solid, while the other one has tiny holes that are connected to a vacuum pump. An additional metal grid was placed between the stack of FEP films and the bottom plate. Most of the air was removed through the holes of the bottom plate by means of the vacuum pump and the adjacent FEP film was sucked into the openings of the metal grid. By heating and pressing the upper plate onto the stack, air cavities with the same diameter as the grid openings were created.<sup>174-176</sup> Figure 16 schematically shows the setup and the preparation procedure. After corona charging, novel piezo- or ferroelectrets with regular arrays of millimeter-sized dome-shaped bubbles between Teflon-FEP films had been generated.

More recently, this method was modified and further improved by Zhang *et al.*<sup>177</sup> In their study, a metal mesh with (sub)millimeter spacing was pressed on stacks of alternating FEP and PTFE films. With proper thermal treatment, the polymer layers were fused underneath the wires of the metal mesh and cavities were formed between the fused areas because of the thermally expanding trapped air and the thermal softening of the fluoropolymer films. In the ferroelectrets thus obtained, strong piezoelectricity is measured only within the highly compressible areas of the air-filled cavities. Thus, large variations in the piezoelectricity are observed across the sample surface. Nevertheless, such structures are very attractive for applications in piezoelectric sensors and actuators, since active areas of at least several square millimeter are usually available, and also, since averaging of the piezoelectric  $d_{33}$  coefficient can often be exploited.

The aforementioned techniques for fabricating ferroelectrets suffer, however, from the difficulties of processing

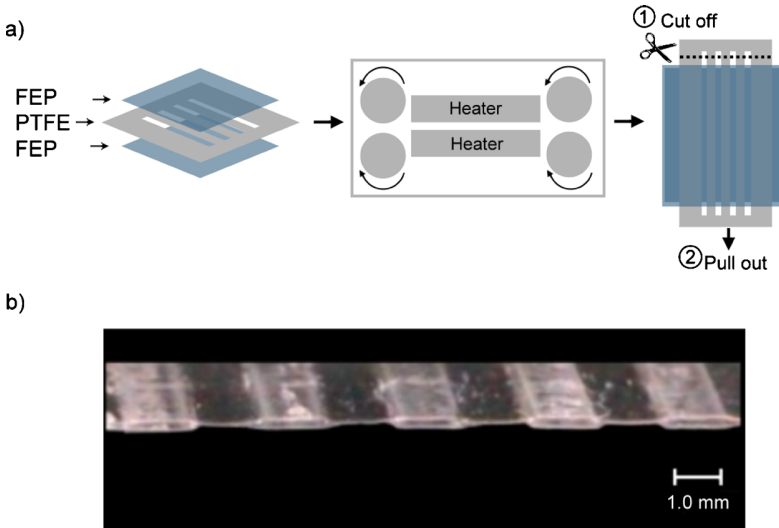


FIG. 17. (Color online) (a) Schematic view of the preparation process for tubular-channel ferroelectrets. A sandwich consisting of two solid FEP films with a well-designed PTFE template between them is laminated at 300 °C. After lamination, the stack is cooled down to RT. An FEP system with open channels is obtained after removing the non-sticking PTFE template from the stack. (b) Optical micrograph of the cross section of a sample together with one of its surfaces (which is seen because of a small angle between sample surface and illuminating light (Ref. 178)).

and/or of melting the soft and hard layers. Very recently, FEP ferroelectrets with well-controlled and uniform voids have been produced by a straightforward lamination process.<sup>178</sup>

The preparation setup is based on a lamination device with a suitable temperature controller. For sample preparation, a PTFE template consisting of several well-cut stripes with clearly defined and evenly distributed openings between them is sandwiched between two solid films of Teflon FEP. The three-layer sandwich is fed to the lamination machine, whose operating temperature was set to 300 °C. This temperature is chosen, since it is substantially higher than the melting temperature of FEP (about 260 °C) but still well below the melting point of PTFE at 327 °C. After lamination, the stack is naturally cooled down under laboratory conditions so that the two FEP layers are intimately bonded to each other through the openings in the PTFE template. A cellular FEP structure with tubular voids is obtained after removal of the PTFE template. Figure 17(a) schematically illustrates the preparation, while a typical cross section of the resulting layer system is shown in Fig. 17(b). With this novel technique that may also be adapted to continuous roll-to-roll processing, it is possible to create uniform channels with a large range of widths, heights, lengths, as well as arbitrary channel patterns.

When a voltage  $V$  is externally applied to such a two-layer FEP system, the electric field inside the tubular channels  $E_g$  is given by

$$V = E_g \left( \frac{d_p}{\epsilon_p} + d_g \right), \quad (19)$$

where  $d_p$  is the combined thickness of the FEP layers,  $d_g$  is the internal void height, and  $\epsilon_p=2.1$  is the dielectric permittivity of the solid FEP films. According to Townsend's model, the critical breakdown field of common gases in a uniform electric field is a function of gas pressure  $p$  and electrode spacing  $d$  (which in our case is equal to the internal void height)<sup>179</sup>

$$E_c = \frac{Ap}{B + \ln(pd)}, \quad (20)$$

where the constant  $B$  is given by

$$B = \ln \left[ \frac{C}{\ln(1 + 1/\gamma)} \right]. \quad (21)$$

For air,  $A=273.8 \text{ V m}^{-1} \text{ Pa}^{-1}$  and  $C=11 \text{ m}^{-1} \text{ Pa}^{-1}$  are experimentally determined constants and  $\gamma=0.01$  is the so-called second ionization coefficient. Uniform DBDs inside the tubular voids could be confirmed with images from an electron-multiplying charge-coupled-device camera with high sensitivity. It is observed that the threshold voltage for uniform DBDs is in very good agreement with the value calculated from Eqs. (19)–(21). During the DBDs, the inner top and bottom surfaces of the tubular voids were charged positively and negatively, respectively. In preliminary studies, a piezoelectric  $d_{33}$  coefficient of 160 pC/N was obtained. After charging at suitable elevated temperatures, the piezoelectricity is stable at temperatures up to at least 130 °C. The new technique has the obvious advantages of simplicity and of well-controlled void geometries and patterns. Furthermore, it can be easily adopted to continuous industrial fabrication.

#### IV. SELECTED APPLICATIONS

Patterning of piezo-, pyro-, and ferroelectric polymer electrets may either improve their piezo-, pyro-, and ferroelectricity, or lead to new functionalities for a range of innovative applications. In order to highlight the applications potential of patterned polymer electrets, several examples will be discussed in this section.

A very interesting application of ferroelectric polymers is in rewritable data-storage devices.<sup>180–186</sup> Recording of a binary optical image was achieved by means of AOP.<sup>181</sup> Either the  $\omega$  beam or the  $2\omega$  beam may carry the image information. In order to obtain high polar order, an appropriate intensity ratio between the  $\omega$  and the  $2\omega$  beams is required. The image written during AOP does not erase the optical information that was previously recorded by means of photo-

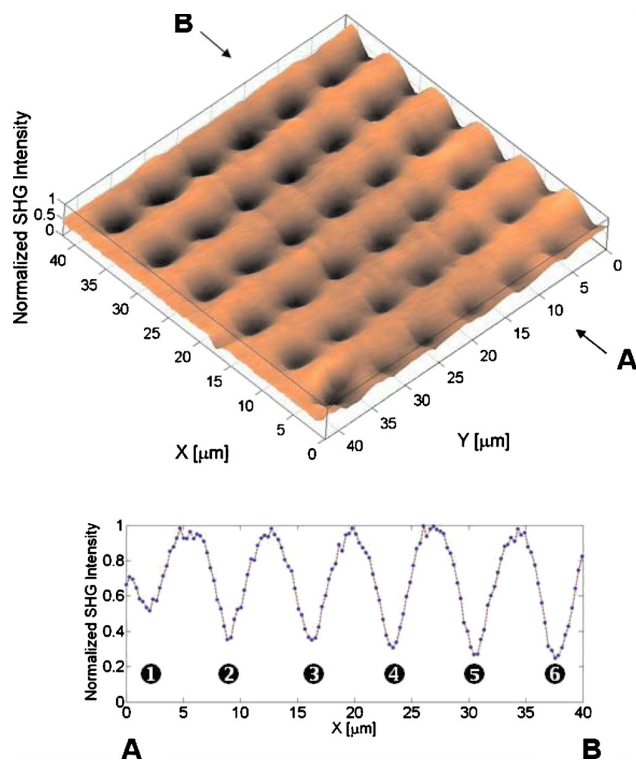


FIG. 18. (Color online) SHG image of the sample after PID recording of a pattern. Top: 3D tomography over an area of  $40 \times 40 \mu\text{m}^2$ . Bottom: SHG profile along a line from A to B across the sample, showing the change in SHG contrast at a constant mean power of 30 mW and for increments of 30 ms in irradiation time. The full width at half maximum of the holes is about  $2.8 \mu\text{m}$  (Ref. 185).

induced birefringence or dichroism. Therefore, a rather large storage capability is available when the two methods are combined.<sup>99</sup> The localized loss in SHG efficiency during PID was also exploited for optical data storage.<sup>185</sup> A spin-coated film of PMMA grafted with 10% Disperse Red 1 (DR1) was first uniformly corona-poled and then put on an X-Y-Z- $\theta$  stage, which was placed in the focal point of a  $50\times$  objective lens from a microscope. The sample can be regularly repositioned by the XYZ stage, and a femtosecond-pulse near-IR laser source was used for local depoling. A 3D tomography of the SHG signal of the sample after the recording process is shown in the upper part of Fig. 18, while the lower part depicts a profile of the depth in the contrast across the SHG signal. Performed with appropriate intensities, a given patterned area can be imaged repeatedly without detectable losses in either contrast or resolution, indicating that this technique is suitable for a rewritable data storage device.

A simple device for focusing air-borne ultrasound was fabricated using a Fresnel zone plate (FZP) or a Fresnel phase plate (FPP) electrode pattern.<sup>187,188</sup> Figure 19 schematically shows an FZP electrode pattern on piezoelectric film which may be prepared by means of standard photolithography, while the other side of the film carries a continuous electrode. Since the acoustic signals are generated under the patterned electrodes only, the emitted ultrasonic radiation interferes at some points determined by the zone radii. The intensity and resolution of an FZP transducer can be improved by using an FPP pattern instead. In an FPP, alternate

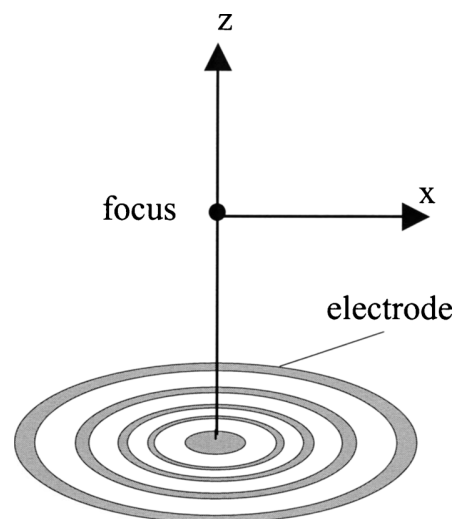


FIG. 19. Schematic view of a FZP for focusing ultrasound (Ref. 31).

zones are poled in opposite directions and both sides of the film are finally coated with continuous electrodes.<sup>187</sup>

Piezoelectric polymers are very suitable for such applications due to their low acoustic impedances that can be close to those of water or even air. For PVDF, the impedance match can be further improved with epoxy (or metal-loaded epoxy) backings. The focal-plane profile of the ultrasonic emission from an epoxy-backed three-zone FZP prepared with PVDF was found to be in good agreement with the theoretically predicted one.<sup>188</sup> Cellular PP ferroelectrets with an FZP electrode provide sound focusing even without any backing, again in excellent agreement with theoretical predictions from the Fresnel theory.<sup>31,189</sup> An accessible frequency of up to 1 MHz is sufficient for most applications in air-borne ultrasound.<sup>31</sup>

Layer structures can be very efficient for enhancing the sensitivity of ferroelectret-transducer devices. In early studies, micromovement actuators were manufactured with multilayer ferroelectret stacks in order to add the voltage-induced thickness variations in the individual films.<sup>32,190</sup> Sensitivity improvements of piezoelectric microphones from cellular polymer ferroelectrets were also achieved in this way.<sup>191</sup> Microphones consisting of a single well-prepared cellular PP ferroelectret typically have a sensitivity of about 2.2 mV/Pa and an equivalent noise level of 37 dB(A) at 1 kHz. A five-layer stacked PP ferroelectret microphone exhibited a sensitivity of approximately 10 mV/Pa and an equivalent noise level of 26 dB(A), well comparable to the respective values of traditional electret condenser microphones.<sup>191</sup> Figure 20 shows the frequency responses of microphones with one and with five cellular PP ferroelectrets, respectively. A flat frequency response is observed over the whole audio-frequency range. Unlike in electret condenser microphones, miniature air gaps are not necessary in ferroelectret microphones, allowing for a much simpler design. Additionally, the ferroelectret microphones have low harmonic distortion and high resonance frequencies. These features make such microphones very suitable for a wide range of applications.

Some applications require complex piezo-, pyro-, or fer-



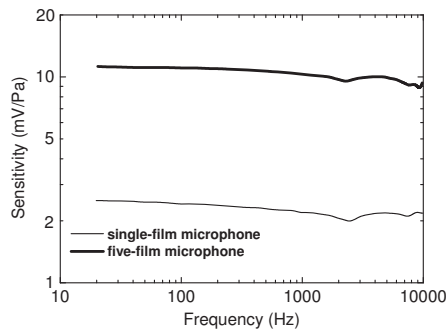
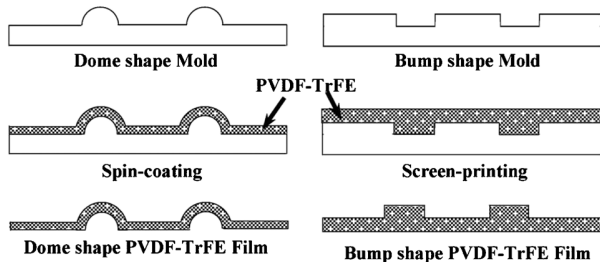


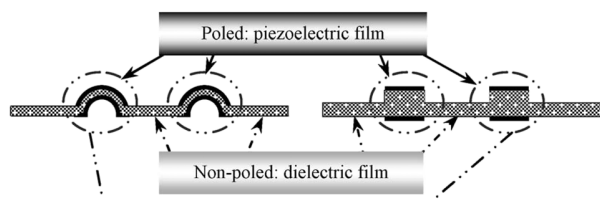
FIG. 20. Frequency response of cellular-PP piezoelectret microphones with a single film and with a stack of five films, determined by means of a comparison method in an acoustic coupler (Ref. 191)

roelectricity patterns which may be achieved by a suitable combination of different patterning techniques. Piezoelectric P(VDF-TrFE) films were patterned by means of a new mold-transfer technique in order to form novel dome and bump shapes. The resulting transducers were assembled on a microcatheter to yield flexible tactile sensors.<sup>192</sup> For sample preparation, a micromachined mold with domes (wells) on a micrometer-to-millimeter scale was fabricated. A piezoelectric polymer solution was spin-coated (screen-printed) onto the mold, followed by a suitable thermal treatment. Samples were deposited with patterned electrodes and dome- or bump-shaped piezoelectric tactile sensors were obtained after dc poling at elevated temperatures. Figure 21 schematically

#### [Mold-transfer Method]



#### [Localized DC Poling]



#### [Assembled Sensors]

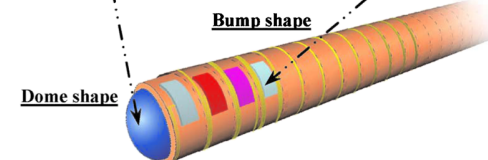


FIG. 21. (Color online) Schematic view of a new mold-transfer technique to pattern P(VDF-TrFE) films and of the new dome- and bump-shaped tactile-sensor modules for smart microcatheters which can detect forces as small as 25 mN and 40 mN, respectively (Ref. 192).

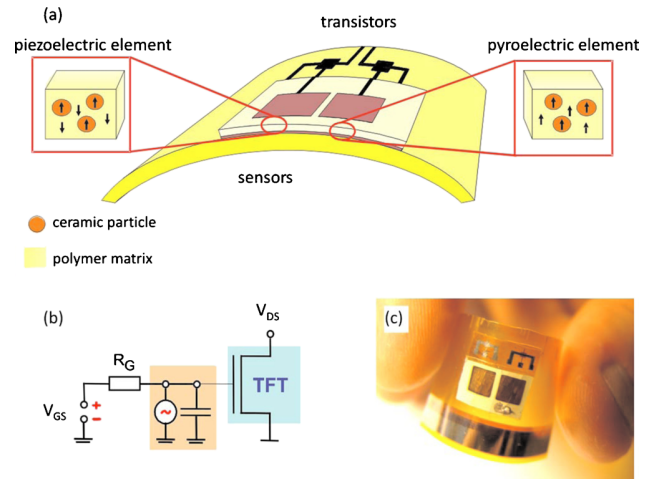


FIG. 22. (Color online) (a) Schematic view of a bifunctional sensor array where the flexible polymer-ceramic sensor frontplane is laminated onto a flexible transistor backplane. The piezoelectric subcell has an antiparallel orientation of the polarizations in the ceramic nanoparticles and the ferroelectric polymer matrix, while the pyroelectric subcell has a parallel orientation of the two polarizations. (b) The equivalent circuit for the subcells. (c) A digital photograph of the sensor prototype (Ref. 121).

shows this technique and a “smart” microcatheter with a dome-shaped piezoelectric film at its tip and a bump-shaped film array along its tube wall. Obviously, this technique represents a combination of direct patterning and patterning by selective poling. The tactile sensors were able to detect forces as small as 40 mN for the bump-shaped sensors and 25 mN for the dome-shaped sensors. The response of the sensors was very stable over a frequency range from 1 to 100 Hz and a temperature range from RT to 45 °C. The sensors are easy to fabricate, to miniaturize, and to pole selectively with standard microelectromechanical-systems technology. They may find numerous applications in micro-catheters or other minimally invasive biomedical devices.

Another example for the combination of direct patterning and patterning by selective poling was reported by Graz *et al.*<sup>121</sup> very recently. A bifunctional polymer-ceramic nanocomposite that can be used for either pressure or temperature sensing was prepared. Piezoelectric lead-titanate nanoparticles were dispersed in a ferroelectric P(VDF-TrFE) polymer matrix during sample preparation. Since the Curie temperature of lead titanate is higher than that of P(VDF-TrFE), the polarizations in the ceramic particles and in the ferroelectric polymer matrix can be oriented either parallel or antiparallel by means of an area-selective two-step poling sequence.<sup>44</sup> As already mentioned, the pyroelectric coefficients  $p_3$  of lead titanate and P(VDF-TrFE) have the same sign, while the piezoelectric  $d_{33}$  coefficients have opposite sign. Therefore, proper parallel (antiparallel) orientation of the polarization leads to a vanishing piezoelectric (pyroelectric) effect and an enhanced pyroelectric (piezoelectric) effect.<sup>121</sup> Figure 22(a) schematically illustrates a bifunctional sensor cell, in which the subcell with an antiparallel orientation of the polarizations in the ceramic nanoparticles and in the ferroelectric polymer matrix is sensitive to pressure changes, while the other subcell with parallel orientation of the polarizations is sensitive to temperature variations. The

two subcells are laminated, respectively, to two transistors on the backplane. The equivalent circuit for the two sensor elements is shown in Fig. 22(b), and Fig. 22(c) represents a photographic image of a sensor prototype. The subcells essentially respond linearly to the input variables they are designed for and exhibit only small cross-talk.

## V. CONCLUSION

Semiconducting ferroelectric polymers, amorphous polymers containing chromophore molecules, and cellular polymer ferroelectrets belong to the family of electroactive polymers. They are attractive from both fundamental scientific and applications-oriented points of view, because of their significant piezo-, pyro-, and ferroelectricity, in combination with the intrinsic features of polymers such as low permittivity, low thermal conductivity, softness and flexibility, good acoustic impedance matching to air and water, relatively low cost, etc. Appropriate patterning of such materials may lead to improved or innovative macroscopic piezo-, pyro-, and ferroelectric or NLO properties and to devices that are useful for a range of applications. Special patterns may be achieved by means of suitable poling techniques and/or appropriate sample-preparation procedures. Various patterning techniques such as selective poling, including corona poling through a mask, poling with patterned electrodes, electron-beam poling, photothermal poling, AOP, PIP, as well as suitable combinations of poling techniques have been reviewed. Patterning of a single film or of layered structures by means of suitable sample-preparation procedures has been discussed, with special emphasis on new results from the author's team. Finally, a survey of selected applications is presented.

## ACKNOWLEDGMENTS

The author gratefully acknowledges Dipl.-Ing. Werner Wirges (University of Potsdam, Germany), Professor Axel Mellinger (Central Michigan University, Mt. Pleasant, Michigan, USA), and Professor Siegfried Bauer (Johannes Kepler University, Linz, Austria) for many stimulating and fruitful discussions on the topics of this paper. He is particularly indebted to Professor Reimund Gerhard (University of Potsdam) for several useful suggestions and for a critical reading of the manuscript. Last, but not least, the author thanks the Deutsche Forschungsgemeinschaft (DFG) for providing a Research Fellowship (Reference No. QI 65/1-1) to him and the European Commission for co-funding some of the equipment used in his own work.

<sup>1</sup>S. Bauer, *J. Appl. Phys.* **80**, 5531 (1996).

<sup>2</sup>G. Eberle, H. Schmidt, and W. Eisenmenger, *IEEE Trans. Dielectr. Electr. Insul.* **3**, 624 (1996).

<sup>3</sup>G. M. Sessler, *Electrets*, 3rd ed. (Springer, New York, 1999).

<sup>4</sup>E. Fukada, *IEEE Trans. Ultrason. Ferroelectr. Freq. Control* **47**, 1277 (2000).

<sup>5</sup>V. V. Kochervinskiĭ, *Crystallogr. Rep.* **48**, 649 (2003).

<sup>6</sup>S. B. Lang and S. Muenst, *Appl. Phys. A: Mater. Sci. Process.* **85**, 125 (2006).

<sup>7</sup>E. Fukada, *IEEE Trans. Dielectr. Electr. Insul.* **13**, 1110 (2006).

<sup>8</sup>V. V. Kochervinskiĭ, *Crystallogr. Rep.* **54**, 1146 (2009) and references therein.

<sup>9</sup>M. Dumont and A. E. Osman, *Chem. Phys.* **245**, 437 (1999).

<sup>10</sup>A. Natansohn and P. Rochon, *Chem. Rev.* **102**, 4139 (2002).

<sup>11</sup>R. H. El Halabieh, O. Mermut, and C. J. Barrett, *Pure Appl. Chem.* **76**, 1445 (2004).

<sup>12</sup>K. G. Yager and C. J. Barrett, *J. Photochem. Photobiol., A* **182**, 250 (2006).

<sup>13</sup>J. A. Delaire and K. Nakatani, *Chem. Rev.* **100**, 1817 (2000).

<sup>14</sup>P. Günter, *Nonlinear Optical Effects and Materials* (Springer, New York, 2002).

<sup>15</sup>H. Ma, A. K. Y. Jen, and L. R. Dalton, *Adv. Mater. (Weinheim, Ger.)* **14**, 1339 (2002).

<sup>16</sup>F. Kajzar, K. S. Lee, and A. K. Y. Jen, *Adv. Polym. Sci.* **161**, 1 (2003).

<sup>17</sup>Y. V. Pereverzev, O. V. Prezhdo, and L. R. Dalton, *ChemPhysChem* **5**, 1821 (2004).

<sup>18</sup>S. K. Yesodha, C. K. S. Pillai, and N. Tsutsumi, *Prog. Polym. Sci.* **29**, 45 (2004).

<sup>19</sup>C. C. Chang, C. P. Chen, C. C. Chou, W. J. Kuo, and R. J. Jeng, *J. Macromol. Sci., Polym. Rev.* **45**, 125 (2005).

<sup>20</sup>H. Ma, S. Liu, J. Luo, S. Suresh, L. Liu, S. H. Kang, M. Haller, T. Sassa, L. R. Dalton, and A. K. Y. Jen, *Adv. Funct. Mater.* **12**, 565 (2002).

<sup>21</sup>M. J. Cho, D. H. Choi, P. A. Sullivan, A. J. P. Akelaitis, and L. R. Dalton, *Prog. Polym. Sci.* **33**, 1013 (2008).

<sup>22</sup>Y. Wada and R. Hayakawa, *Jpn. J. Appl. Phys.* **15**, 2041 (1976).

<sup>23</sup>J. J. Crosnier, F. Micheron, G. Dreyfus, and J. Lewiner, *J. Appl. Phys.* **47**, 4798 (1976).

<sup>24</sup>R. Gerhard-Multhaupt, *IEEE Trans. Dielectr. Electr. Insul.* **9**, 850 (2002).

<sup>25</sup>S. Bauer, R. Gerhard-Multhaupt, and G. M. Sessler, *Phys. Today* **57**(2), 37 (2004).

<sup>26</sup>M. Wegener and S. Bauer, *ChemPhysChem* **6**, 1014 (2005).

<sup>27</sup>S. Bauer, *IEEE Trans. Dielectr. Electr. Insul.* **13**, 953 (2006).

<sup>28</sup>M. Lindner, S. Bauer-Gogonea, S. Bauer, M. Paajanen, and J. Raukola, *J. Appl. Phys.* **91**, 5283 (2002).

<sup>29</sup>X. Qiu, A. Mellinger, M. Wegener, W. Wirges, and R. Gerhard, *J. Appl. Phys.* **101**, 104112 (2007).

<sup>30</sup>X. Qiu, A. Mellinger, W. Wirges, and R. Gerhard, *Appl. Phys. Lett.* **91**, 132905 (2007).

<sup>31</sup>M. Lindner, H. Hoislbauer, R. Schwödiauer, S. Bauer-Gogonea, and S. Bauer, *IEEE Trans. Dielectr. Electr. Insul.* **11**, 255 (2004).

<sup>32</sup>A. Savolainen and K. Kirjavainen, *J. Macromol. Sci., Chem.* **A26**, 583 (1989).

<sup>33</sup>M. Wegener, W. Wirges, and R. Gerhard-Multhaupt, *Adv. Eng. Mater.* **7**, 1128 (2005).

<sup>34</sup>W. Wirges, M. Wegener, O. Voronina, L. Zirkel, and R. Gerhard-Multhaupt, *Adv. Funct. Mater.* **17**, 324 (2007).

<sup>35</sup>P. Fang, M. Wegener, W. Wirges, R. Gerhard, and L. Zirkel, *Appl. Phys. Lett.* **90**, 192908 (2007).

<sup>36</sup>E. Saarimäki, M. Paajanen, A. M. Savijärvi, H. Minkinen, M. Wegener, O. Voronina, R. Schulze, W. Wirges, and R. Gerhard-Multhaupt, *IEEE Trans. Dielectr. Electr. Insul.* **13**, 963 (2006).

<sup>37</sup>O. Voronina, M. Wegener, W. Wirges, R. Gerhard, L. Zirkel, and H. Müstedt, *Appl. Phys. A: Mater. Sci. Process.* **90**, 615 (2008).

<sup>38</sup>C. J. Dias and D. K. Das-Gupta, *IEEE Trans. Dielectr. Electr. Insul.* **3**, 706 (1996).

<sup>39</sup>A. K. Batra, M. D. Aggarwal, M. E. Edwards, and A. Bhalla, *Ferroelectrics* **366**, 84 (2008).

<sup>40</sup>S. F. Mendes, C. M. Costa, V. Sencadas, J. S. Nunes, P. Costa, R. Gregorio, Jr., and S. Lanceros-Méndez, *Appl. Phys. A: Mater. Sci. Process.* **96**, 899 (2009).

<sup>41</sup>D. A. van den Ende, B. F. Bory, W. A. Groen, and S. van der Zwaag, *J. Appl. Phys.* **107**, 024107 (2010).

<sup>42</sup>L. M. Ganesan, P. Frübing, A. Mellinger, and R. Gerhard, *J. Phys. D: Appl. Phys.* **42**, 092006 (2009).

<sup>43</sup>L. M. Ganesan, W. Wirges, A. Mellinger, and R. Gerhard, *J. Phys. D: Appl. Phys.* **43**, 015401 (2010).

<sup>44</sup>S. Bauer-Gogonea, S. Bauer, and R. Gerhard-Multhaupt, *Braz. J. Phys.* **29**, 306 (1999) and references therein.

<sup>45</sup>Y. Xia, J. A. Roger, K. E. Paul, and G. M. Whitesides, *Chem. Rev.* **99**, 1823 (1999).

<sup>46</sup>L. J. Guo, *J. Phys. D: Appl. Phys.* **37**, R123 (2004).

<sup>47</sup>A. P. Quist, E. Pavlovic, and S. Oscarsson, *Anal. Bioanal. Chem.* **381**, 591 (2005).

<sup>48</sup>B. D. Gates, Q. Xu, M. Stewart, D. Ryan, C. G. Willson, and G. M. Whitesides, *Chem. Rev.* **105**, 1171 (2005).

<sup>49</sup>C. Liu, *Adv. Mater. (Weinheim, Ger.)* **19**, 3783 (2007).

<sup>50</sup>D. A. Berlincourt, D. R. Currand, and H. Jaffe, in *Physical Acoustics*,

- edited by W. P. Mason (Academic, New York, 1967) Vol. I, Pt. A.
- <sup>51</sup>H Dvey-Aharon and P. L. Taylor, *Ferroelectrics* **33**, 103 (1981).
- <sup>52</sup>X. Qiu, M. Wegener, W. Wirges, X. Zhang, J. Hillenbrand, Z. Xia, R. Gerhard-Multhaupt, and G. M. Sessler, *J. Phys. D: Appl. Phys.* **38**, 649 (2005).
- <sup>53</sup>X. Qiu, A. Mellinger, and R. Gerhard, "In-situ Acoustical Investigation of the Polarization Build-up in Cellular Polypropylene Ferroelectrets," *IEEE Trans. Dielectr. Electr. Insul.* (to be published).
- <sup>54</sup>M. Paajanen, M. Wegener, and R. Gerhard-Multhaupt, *J. Phys. D: Appl. Phys.* **34**, 2482 (2001).
- <sup>55</sup>X. Qiu, A. Mellinger, and R. Gerhard, *Appl. Phys. Lett.* **92**, 052901 (2008).
- <sup>56</sup>J. Hillenbrand and G. M. Sessler, *Annual Report Conference on Electrical Insulation and Dielectric Phenomena*, Victoria, Canada, 15–18 October 2000 (IEEE Service Center, Piscataway, NJ, 2000), pp. 161–165.
- <sup>57</sup>I. Graz, A. Ebner, S. Bauer, C. Romanin, and H. Gruber, *Appl. Phys. A: Mater. Sci. Process.* **92**, 547 (2008).
- <sup>58</sup>X. Qiu and R. Gerhard, *Appl. Phys. Lett.* **93**, 152902 (2008).
- <sup>59</sup>M. Paajanen, H. Välimäki, and J. Lekkala, *Proceedings of the Tenth International Symposium on Electrets*, Delphi, Greece, 22–24 September 1999 (IEEE Service Center, Piscataway, NJ, 1999), pp. 735–738.
- <sup>60</sup>G. M. Sessler and J. Hillenbrand, *Appl. Phys. Lett.* **75**, 3405 (1999).
- <sup>61</sup>M. Paajanen, J. Lekkala, and H. Välimäki, *IEEE Trans. Dielectr. Electr. Insul.* **8**, 629 (2001).
- <sup>62</sup>J. Hillenbrand, and G. M. Sessler, *IEEE Trans. Dielectr. Electr. Insul.* **7**, 537 (2000).
- <sup>63</sup>G. S. Neuschwandtner, R. Schwödauer, S. Bauer-Gogonea, S. Bauer, M. Paajanen, and J. Lekkala, *J. Appl. Phys.* **89**, 4503 (2001).
- <sup>64</sup>J. A. Giacometti, S. Fedosov, and M. M. Costa, *Braz. J. Phys.* **29**, 269 (1999).
- <sup>65</sup>M. Wegener, M. Paajanen, W. Wirges, and R. Gerhard-Multhaupt, *Proceedings of the 11th International Symposium on Electrets*, Melbourne, Australia, 1–3 October 2002 (IEEE Service Center, Piscataway, NJ, 2002), pp. 54–57.
- <sup>66</sup>P. Fang, X. Qiu, W. Wirges, R. Gerhard, and L. Zirkel, "Polyethylenephthalate (PEN) Ferroelectrets: Cellular Structure, Piezoelectricity and Thermal Stability," *IEEE Trans. Dielectr. Electr. Insul.* (to be published).
- <sup>67</sup>J. Kim, J. J. Ju, and M. Kim, *Jpn. J. Appl. Phys., Part 1* **42**, 7304 (2003).
- <sup>68</sup>M. Jäger, G. I. Stegeman, W. Brinker, S. Yilmaz, S. Bauer, W. H. G. Horsthuis, and G. R. Möhlmann, *Appl. Phys. Lett.* **68**, 1183 (1996).
- <sup>69</sup>V. Taggi, F. Michelotti, M. Bertolotti, G. Petrocco, V. Foglietti, A. Donval, E. Toussaere, and J. Zyss, *Appl. Phys. Lett.* **72**, 2794 (1998).
- <sup>70</sup>J. J. Ju, J. Kim, J. Y. Do, M. Kim, S. K. Park, S. Park, and M. Lee, *Opt. Lett.* **29**, 89 (2004).
- <sup>71</sup>J. J. Ju, S. K. Park, S. Park, J. Kim, M. Kim, M. Lee, and J. Y. Do, *Appl. Phys. Lett.* **88**, 241106 (2006).
- <sup>72</sup>R. F. Suárez, A. Mellinger, M. Wegener, W. Wirges, and R. Gerhard-Multhaupt, *IEEE Trans. Dielectr. Electr. Insul.* **13**, 1030 (2006).
- <sup>73</sup>A. Mellinger, R. Flores Suárez, R. Singh, M. Wegener, W. Wirges, R. Gerhard, and S. B. Lang, *Int. J. Thermophys.* **29**, 2046 (2008).
- <sup>74</sup>C.-D. Pham, A. Petre, L. Berquez, R. Flores Suárez, A. Mellinger, W. Wirges, and R. Gerhard, *IEEE Trans. Dielectr. Electr. Insul.* **16**, 676 (2009).
- <sup>75</sup>R. F. Suárez, X. Qiu, L. Holländer, R. A. P. Altafim, W. Wirges, R. Gerhard, W. Jenninger, and J. Wagner, *Annual Report Conference on Electrical Insulation and Dielectric Phenomena*, Virginia Beach, USA, 18–20 October 2009 (IEEE Service Center, Piscataway, NJ, 2009).
- <sup>76</sup>H. O. Jacobs and G. M. Whitesides, *Science* **291**, 1763 (2001).
- <sup>77</sup>D. B. Wolfe, J. C. Love, B. D. Gates, G. M. Whitesides, R. S. Conroy, and M. Prentiss, *Appl. Phys. Lett.* **84**, 1623 (2004).
- <sup>78</sup>B. Gross, R. Gerhard-Multhaupt, A. Berraissoul, and G. M. Sessler, *J. Appl. Phys.* **62**, 1429 (1987).
- <sup>79</sup>R. V. Rao, P. M. Rao, and M. H. Shridhar, *Nucl. Instrum. Methods Phys. Res. B* **187**, 331 (2002).
- <sup>80</sup>H. Nakayama, O. Sugihara, and N. Okamoto, *Opt. Lett.* **22**, 1541 (1997).
- <sup>81</sup>O. Sugihara, Y. Che, N. Okamoto, H. Fujimura, C. Egami, and S. Umegaki, *Appl. Phys. Lett.* **73**, 3028 (1998).
- <sup>82</sup>H. Nakayama, O. Sugihara, and N. Okamoto, *Appl. Phys. Lett.* **71**, 1924 (1997).
- <sup>83</sup>H. Nakayama, H. Fujimura, C. Egami, O. Sugihara, R. Matsushima, and N. Okamoto, *Appl. Opt.* **37**, 1213 (1998).
- <sup>84</sup>W. H. Wong, J. Zhou, and E. Y. B. Pun, *Appl. Phys. Lett.* **78**, 2110 (2001).
- <sup>85</sup>H. Sun, A. Chen, B. C. Olbricht, J. A. Davies, P. A. Sullivan, Y. Liao, and L. Dalton, *Opt. Express* **16**, 6592 (2008).
- <sup>86</sup>H. Kobayashi, M. Kubo, T. Tsukada, and M. Hozawa, *Int. J. Heat Mass Transfer* **45**, 865 (2002).
- <sup>87</sup>M. Wegener, J. Hesse, T. Wegener, and R. Gerhard-Multhaupt, *J. Appl. Phys.* **91**, 3193 (2002).
- <sup>88</sup>B. Dickens, E. Balizer, A. S. DeReggi, and S. C. Roth, *J. Appl. Phys.* **72**, 4258 (1992).
- <sup>89</sup>E. Toussaere and P. Labbé, *Opt. Mater. (Amsterdam, Neth.)* **12**, 357 (1999).
- <sup>90</sup>J. H. Jung, T. Kato, and T. Kinoshita, *J. Appl. Phys.* **90**, 801 (2001).
- <sup>91</sup>G. Martin, S. Ducci, R. Hierle, D. Josse, and J. Zyss, *Appl. Phys. Lett.* **83**, 1086 (2003).
- <sup>92</sup>J. H. Lin, N. D. Lai, C. H. Chiu, D. Y. Lin, G. W. Rieger, J. F. Young, F. S. Chien, and C. C. Hsu, *Opt. Express* **16**, 7832 (2008).
- <sup>93</sup>F. S. Chien, C. Y. Lin, and C. C. Hsu, *J. Phys. D: Appl. Phys.* **41**, 235502 (2008).
- <sup>94</sup>Y. Atassi, J. Chauvin, J. A. Delaire, J. F. Delouis, I. Fanton-Maltesy, and K. Nakatani, *Pure Appl. Chem.* **70**, 2157 (1998).
- <sup>95</sup>J. M. Nunzi, C. Fiorini, A. C. Etilé, and F. Kajzar, *Pure Appl. Opt.* **7**, 141 (1998).
- <sup>96</sup>X. Liu, G. Xu, J. Si, P. Ye, Z. Li, and Y. Shen, *J. Appl. Phys.* **88**, 3848 (2000).
- <sup>97</sup>N. Tsutsumi and C. Odane, *J. Opt. Soc. Am. B* **20**, 1514 (2003).
- <sup>98</sup>W. Chalupczak, C. Fiorini, F. Charra, J. M. Nunzi, and P. Raimond, *Opt. Commun.* **126**, 103 (1996).
- <sup>99</sup>C. Fiorini, F. Charra, J. M. Nunzi, and P. Raimond, *J. Opt. Soc. Am. B* **14**, 1984 (1997).
- <sup>100</sup>C. Fiorini, F. Charra, P. Raimond, A. Lorin, and J.-M. Nunzi, *Opt. Lett.* **22**, 1846 (1997).
- <sup>101</sup>K. Kitaoka, J. Si, T. Mitsuyu, and K. Hirao, *Appl. Phys. Lett.* **75**, 157 (1999).
- <sup>102</sup>V. M. Churikov, M. F. Hung, C. C. Hsu, C. W. Shiau, and T. Y. Luh, *Chem. Phys. Lett.* **332**, 19 (2000).
- <sup>103</sup>J. Guo, J. Si, G. Qian, J. Qiu, M. Wang, and K. Hirao, *Chem. Phys. Lett.* **381**, 677 (2003).
- <sup>104</sup>Y. Jia, G. Wang, B. Guo, W. Su, and Q. Zhang, *J. Opt. A: Pure Appl. Opt.* **6**, 833 (2004).
- <sup>105</sup>X. L. Jiang, L. Li, J. Kumar, and S. K. Tripathy, *Appl. Phys. Lett.* **69**, 3629 (1996).
- <sup>106</sup>X. Liu, G. Xu, J. Si, P. Ye, Z. Li, and Y. Shen, *Appl. Phys. B: Lasers Opt.* **71**, 539 (2000).
- <sup>107</sup>J. Si, T. Mitsuyu, P. Ye, Y. Shen, and K. Hirao, *Appl. Phys. Lett.* **72**, 762 (1998).
- <sup>108</sup>J. Si, K. Kitaoka, T. Mitsuyu, P. X. Ye, and K. Hirao, *J. Appl. Phys.* **85**, 8018 (1999).
- <sup>109</sup>J. Si and K. Hirao, *Appl. Phys. Lett.* **91**, 091105 (2007).
- <sup>110</sup>A. Apostoluk, J. M. Nunzi, V. Boucher, A. Essahlaoui, R. Seveno, H. W. Gundel, C. Monnerau, E. Blart, and F. Odobel, *Opt. Commun.* **260**, 708 (2006).
- <sup>111</sup>Z. Sekkat, P. Prêtre, A. Knoesen, W. Volksen, V. Y. Lee, R. D. Miller, J. Wood, and W. Knoll, *J. Opt. Soc. Am. B* **15**, 401 (1998).
- <sup>112</sup>G. Xu, J. Si, X. Liu, Q. Yang, P. Ye, Z. Li, and Y. Shen, *J. Appl. Phys.* **85**, 681 (1999).
- <sup>113</sup>G. Xu, J. Si, X. Liu, Q. Yang, P. Ye, Z. Li, and Y. Shen, *Opt. Commun.* **153**, 95 (1998).
- <sup>114</sup>G. Xu, X. Liu, J. Si, P. Ye, Z. Li, and Y. Shen, *Appl. Phys. B: Lasers Opt.* **68**, 693 (1999).
- <sup>115</sup>B. Guo, W. Su, Y. J. Jia, Z. C. Li, Q. J. Zhang, and G. M. Wang, *Phys. Status Solidi B* **242**, 1081 (2005).
- <sup>116</sup>J. H. Jung and T. Kinoshita, *Jpn. J. Appl. Phys., Part 1* **41**, 1587 (2002).
- <sup>117</sup>D. Rollik, S. Bauer, and R. Gerhard-Multhaupt, *J. Appl. Phys.* **85**, 3282 (1999).
- <sup>118</sup>B. Ploss, W. Y. Ng, H. L. W. Chan, B. Ploss, and C. L. Choy, *Compos. Sci. Technol.* **61**, 957 (2001).
- <sup>119</sup>B. Ploss, B. Ploss, F. G. Shin, H. L. W. Chan, and C. L. Choy, *IEEE Trans. Dielectr. Electr. Insul.* **7**, 517 (2000).
- <sup>120</sup>B. Ploss, B. Ploss, F. G. Shin, H. L. W. Chan, and C. L. Choy, *Appl. Phys. Lett.* **76**, 2776 (2000).
- <sup>121</sup>I. Graz, M. Krause, S. Bauer-Gogonea, S. Bauer, S. P. Lacour, B. Ploss, M. Zirkel, B. Stadlober, and S. Wagner, *J. Appl. Phys.* **106**, 034503 (2009).
- <sup>122</sup>S. A. Wilson, R. P. J. Jourdain, Q. Zhang, R. A. Dorey, C. R. Bowen, M. Willander, Q. Ul Wahab, M. Willander, S. M. Al-hilli, O. Nur, E. Quandt, C. Johansson, E. Pagounis, M. Kohl, J. Matovic, B. Samel, W. van der Wijngaert, E. W. H. Jager, D. Carlsson, Z. Djinic, M. Wegener, C.



- Moldovan, R. Iosub, E. Abad, M. Wendlandt, C. Rusu, and K. Persson, *Mater. Sci. Eng. R.* **56**, 1 (2007).
- <sup>123</sup>R. Hasegawa, Y. Tanabe, M. Kobayashi, H. Tadokoro, A. Sawaoka, and N. Kawai, *J. Polym. Sci., Part A: Polym. Chem.* **8**, 1073 (1970).
- <sup>124</sup>J. Scheinbeim, B. Nakafuku, B. A. Newman, and K. D. Pae, *J. Appl. Phys.* **50**, 4399 (1979).
- <sup>125</sup>T. Hattori, M. Kanaoka, and H. Ohigashi, *J. Appl. Phys.* **79**, 2016 (1996).
- <sup>126</sup>S. J. Kang, Y. J. Park, J. Hwang, H. J. Jeong, J. S. Lee, K. J. Kim, H. Kim, J. Huh, and C. Par, *Adv. Mater. (Weinheim, Ger.)* **19**, 581 (2007).
- <sup>127</sup>L. Zhang, S. Ducharme, and J. Li, *Appl. Phys. Lett.* **91**, 172906 (2007).
- <sup>128</sup>M. Nakanishi, H. Yamaji, O. Sugihara, H. Fujimura, C. Egami, and N. Okamoto, *Mol. Cryst. Liq. Cryst.* **349**, 15 (2000).
- <sup>129</sup>E. Kim, Y. Xia, and G. M. Whitesides, *Nature (London)* **376**, 581 (1995).
- <sup>130</sup>X. Zhao, A. Stoddart, S. P. Smith, E. Kim, Y. Xia, M. Prentiss, and G. M. Whitesides, *Adv. Mater. (Weinheim, Ger.)* **8**, 420 (1996).
- <sup>131</sup>Y. Xia, E. Kim, and G. M. Whitesides, *Chem. Mater.* **8**, 1558 (1996).
- <sup>132</sup>Y. J. Park, Y. S. Kang, and C. Park, *Eur. Polym. J.* **41**, 1002 (2005).
- <sup>133</sup>S. S. Chebotaryov, E. M. Baitinger, A. A. Volegov, I. G. Margamov, I. V. Gribov, N. A. Moskvina, V. L. Kuznetsov, S. E. Evsyukov, and L. A. Pesin, *Radiat. Phys. Chem.* **75**, 2024 (2006).
- <sup>134</sup>M. D. Duca, C. L. Plosceanu, and T. Pop, *J. Appl. Polym. Sci.* **67**, 2125 (1998).
- <sup>135</sup>E. Katan, M. Narkis, and A. Siegmann, *J. Appl. Polym. Sci.* **70**, 1471 (1998).
- <sup>136</sup>Y. Izumi, S. Kawanishi, S. Hara, D. Yoshikawa, and T. Yamamoto, *Bull. Chem. Soc. Jpn.* **71**, 2721 (1998).
- <sup>137</sup>S. R. George, J. A. Leraas, S. C. Langford, and J. T. Dickinson, *Appl. Surf. Sci.* **255**, 9558 (2009).
- <sup>138</sup>L. Torrisi and R. Percolla, *Nucl. Instrum. Methods Phys. Res. B* **117**, 387 (1996).
- <sup>139</sup>S. Han, W. K. Choi, K. H. Yoon, and S. K. Koh, *J. Appl. Polym. Sci.* **72**, 41 (1999).
- <sup>140</sup>S. Okuji, H. Boldryeva, Y. Takeda, and N. Kishimoto, *Nucl. Instrum. Methods Phys. Res. B* **267**, 1557 (2009).
- <sup>141</sup>H. M. Manohara, E. Morikawa, J. Choi, and P. T. Sprunger, *J. Microelectromech. Syst.* **8**, 417 (1999).
- <sup>142</sup>E. Morikawa, J. Choi, H. M. Manohara, H. Ishii, K. Seki, K. K. Okudaira, and N. Ueno, *J. Appl. Phys.* **87**, 4010 (2000).
- <sup>143</sup>J. Choi, H. M. Manohara, E. Morikawa, P. T. Sprunger, P. A. Dowben, and S. P. Paltó, *Appl. Phys. Lett.* **76**, 381 (2000).
- <sup>144</sup>G. L. J. A. Rikken, C. J. E. Seppen, S. Nijhuis, and E. W. Meijer, *Appl. Phys. Lett.* **58**, 435 (1991).
- <sup>145</sup>O. Watanabe, M. Tsuchimori, and A. Okada, *J. Mater. Chem.* **6**, 1487 (1996).
- <sup>146</sup>M. Nakanishi, O. Sugihara, N. Okamoto, and K. Hirota, *Appl. Opt.* **37**, 1068 (1998).
- <sup>147</sup>O. Sugihara, M. Nakanishi, Y. Che, C. Egami, Y. Kawata, and N. Okamoto, *Appl. Opt.* **39**, 5632 (2000).
- <sup>148</sup>F. Gillot, L. Mager, K. D. Dorkenoo, S. Méry, C. Carré, and A. Fort, *Chem. Phys. Lett.* **379**, 203 (2003).
- <sup>149</sup>J. P. Bombenger, L. Mager, D. Gindre, J. P. Vola, K. D. Dorkenoo, A. Fort, and C. Carré, *Opt. Commun.* **280**, 192 (2007).
- <sup>150</sup>M. Saphiannikova and D. Neher, *J. Phys. Chem. B* **109**, 19428 (2005).
- <sup>151</sup>C. J. Barrett, J. Mamiya, K. G. Yager, and T. Ikeda, *Soft Matter* **3**, 1249 (2007).
- <sup>152</sup>V. Toshchevikov, M. Saphiannikova, and G. Heinrich, *J. Phys. Chem. B* **113**, 5032 (2009).
- <sup>153</sup>T. Lippert and J. T. Dickinson, *Chem. Rev.* **103**, 453 (2003).
- <sup>154</sup>C. Egami, Y. Kawata, Y. Aoshima, H. Takeyama, F. Iwata, O. Sugihara, M. Tsuchimori, O. Watanabe, H. Fujimura, and N. Okamoto, *Opt. Commun.* **157**, 150 (1998).
- <sup>155</sup>Y. Che, O. Sugihara, C. Egami, H. Fujimura, Y. Kawata, N. Okamoto, M. Tsuchimori, and O. Watanabe, *Jpn. J. Appl. Phys., Part 1* **38**, 6316 (1999).
- <sup>156</sup>Y. Che, O. Sugihara, H. Fujimura, N. Okamoto, C. Egami, Y. Kawata, M. Tsuchimori, and O. Watanabe, *Opt. Mater. (Amsterdam, Neth.)* **21**, 79 (2003).
- <sup>157</sup>G. Chen, Z. Xia, Y. Zhang, and H. Zhang, *IEEE Trans. Dielectr. Electr. Insul.* **6**, 831 (1999).
- <sup>158</sup>Q. Zhang, P. A. Lewin, and P. E. Bloomfield, *IEEE Trans. Ultrason. Ferroelectr. Freq. Control* **44**, 1148 (1997) and references therein.
- <sup>159</sup>M. Nakazawa, M. Tabaru, K. Nakamura, S. Ueha, and A. Maezawa, *Jpn. J. Appl. Phys., Part 1* **46**, 4466 (2007).
- <sup>160</sup>K. Sakaguchi, T. Sato, K. Koyama, S. Ikeda, S. Yamamizu, and Y. Wada, *Jpn. J. Appl. Phys.* **25**, 91 (1986) Suppl. 25-1.
- <sup>161</sup>P. E. Bloomfield, *IEEE Trans. Ultrason. Ferroelectr. Freq. Control* **49**, 1300 (2002).
- <sup>162</sup>N. Snis, E. Edqvist, U. Simu, and S. Johansson, *Sens. Actuators A* **144**, 314 (2008).
- <sup>163</sup>E. Edqvist, N. Snis, and S. Johansson, *J. Micromech. Microeng.* **18**, 015007 (2008).
- <sup>164</sup>E. Edqvist and E. Hedlund, *J. Micromech. Microeng.* **19**, 115019 (2009).
- <sup>165</sup>R. Kacprzyk and E. Motyl, *Proceedings of the 8th International Symposium on Electrets*, Paris, France, 7–9 September 1994 (IEEE Service Center, Piscataway, NJ, 1994), pp. 703–708.
- <sup>166</sup>R. Kacprzyk, E. Motyl, J. B. Gajewski, and A. Pasternak, *J. Electrostat.* **35**, 161 (1995).
- <sup>167</sup>R. Kacprzyk, A. Dobrucki, and J. B. Gajewski, *J. Electrostat.* **39**, 33 (1997).
- <sup>168</sup>Z. Xia, R. Gerhard-Multhaupt, W. Künstler, A. Wedel, and R. Danz, *J. Phys. D: Appl. Phys.* **32**, L83 (1999).
- <sup>169</sup>R. Gerhard-Multhaupt, W. Künstler, T. Görne, A. Pucher, T. Weinhold, M. Seif, and Z. Xia, *IEEE Trans. Dielectr. Electr. Insul.* **7**, 480 (2000).
- <sup>170</sup>M. Wegener, W. Wirges, K. Richter, W. Künstler, and R. Gerhard-Multhaupt, *Proceedings of the fourth International Conference on Electric Charges in Non-Conductive Materials*, Société Française du Vide, Paris, France, 1–6 July 2001, pp. 257–260.
- <sup>171</sup>M. Wegener, W. Wirges, W. Künstler, R. Gerhard-Multhaupt, B. Elling, M. Pinnow, and R. Danz, *Annual Report Conference on Electrical Insulation and Dielectric Phenomena*, Kitchener, Canada, 14–17 October 2001 (IEEE Service Center, Piscataway, NJ, 2001), pp. 100–103.
- <sup>172</sup>Z. Hu and H. von Seggern, *J. Appl. Phys.* **98**, 014108 (2005).
- <sup>173</sup>Z. Hu and H. von Seggern, *J. Appl. Phys.* **99**, 024102 (2006).
- <sup>174</sup>R. A. C. Altafim, C. Dias, L. Gonçalves Neto, H. C. Basso, C. Murakami, P. R. Veronese, and E. F. Rodrigues, *Annual Report Conference on Electrical Insulation and Dielectric Phenomena*, New Mexico, USA, 19–22 October 2003 (IEEE Service Center, Piscataway, NJ, 2003), pp. 225–228.
- <sup>175</sup>R. A. C. Altafim, H. C. Basso, L. Gonçalves Neto, L. Lima, R. A. P. Altafim, and C. V. de Aquino, *Annual Report Conference on Electrical Insulation and Dielectric Phenomena*, Tennessee, USA, 16–19 October 2005 (IEEE Service Center, Piscataway, NJ, 2005), pp. 669–672.
- <sup>176</sup>R. A. C. Altafim, H. C. Basso, R. A. P. Altafim, L. Lima, C. V. de Aquino, L. Gonçalves Neto, and R. Gerhard-Multhaupt, *IEEE Trans. Dielectr. Electr. Insul.* **13**, 979 (2006).
- <sup>177</sup>X. Zhang, J. Hillenbrand, and G. M. Sessler, *Appl. Phys. A: Mater. Sci. Process.* **84**, 139 (2006).
- <sup>178</sup>R. A. P. Altafim, X. Qiu, W. Wirges, R. Gerhard, R. A. C. Altafim, H. C. Basso, W. Jenninger, and J. Wagner, *J. Appl. Phys.* **106**, 014106 (2009).
- <sup>179</sup>E. M. Bazelyan and Y. P. Raizer, *Spark Discharge* (CRC, Boca Raton, FL, 1998).
- <sup>180</sup>N. Yamauchi, *Jpn. J. Appl. Phys., Part 1* **25**, 590 (1986).
- <sup>181</sup>G. Xu, Q. G. Yang, J. H. Si, X. C. Liu, P. X. Ye, Z. Li, and Y. Q. Shen, *Opt. Commun.* **159**, 88 (1999).
- <sup>182</sup>S. H. Lim, A. C. Rastogi, and S. B. Desu, *J. Appl. Phys.* **96**, 5673 (2004).
- <sup>183</sup>R. C. G. Naber, C. Tanase, P. W. M. Blom, G. H. Gelinck, A. W. Marsman, F. J. Touwslager, S. Segayesh, and D. M. de Leeuw, *Nature Mater.* **4**, 243 (2005).
- <sup>184</sup>K. N. N. Unni, S. Dabos-Seignon, and J. M. Nunzi, *J. Phys. D: Appl. Phys.* **38**, 1148 (2005).
- <sup>185</sup>D. Gindre, A. Boeglin, A. Fort, L. Mager, and K. D. Dorkenoo, *Opt. Express* **14**, 9896 (2006).
- <sup>186</sup>Q. Ling, D. Liaw, C. Zhu, D. S. Chan, E. Kang, and K. Neoh, *Prog. Polym. Sci.* **33**, 917 (2008).
- <sup>187</sup>M. Mortezaie and G. Wade, in *Acoustic Imaging*, edited by M. Kaveh, R. K. Mueller, and J. F. Greenleaf (Plenum, New York, 1984), Vol. 13, pp. 345–354.
- <sup>188</sup>M. Z. Sleva, W. D. Hunt, and R. D. Briggs, *J. Acoust. Soc. Am.* **96**, 1627 (1994).
- <sup>189</sup>H. Hoislbauer, R. Schwödauer, S. Bauer-Gogonea, and S. Bauer, *Proceedings of the 11th International Symposium on Electrets*, Melbourne, Australia, 1–3 October 2002 (IEEE Service Center, Piscataway, NJ, 2002), pp. 58–61.
- <sup>190</sup>M. K. Hämäläinen, J. K. Parviainen, and T. Jaaskelainen, *Rev. Sci. Instrum.* **67**, 1598 (1996).
- <sup>191</sup>J. Hillenbrand and G. M. Sessler, *J. Acoust. Soc. Am.* **116**, 3267 (2004).
- <sup>192</sup>C. Y. Li, P. M. Wu, S. Lee, A. Gorton, M. J. Schulz, and C. H. Ahn, *J. Microelectromech. Syst.* **17**, 334 (2008).

## Erratum: “Patterned piezo-, pyro-, and ferroelectricity of poled polymer electrets” [J. Appl. Phys. **108**, 011101 (2010)]

Xunlin Qiu<sup>a)</sup>

*Applied Condensed-Matter Physics, Department of Physics and Astronomy, University of Potsdam, Karl-Liebknecht-Strasse 24-25, 14476 Potsdam-Golm, Germany*

(Received 25 July 2011; accepted 24 August 2011; published online 13 September 2011)

[doi:10.1063/1.3638069]

In the original manuscript, Fig. 1 contained two typographical errors, which made the molecular compositions (b) and (c) disagree with the text. The figure and the text are corrected below. This correction affects no other part of the article.

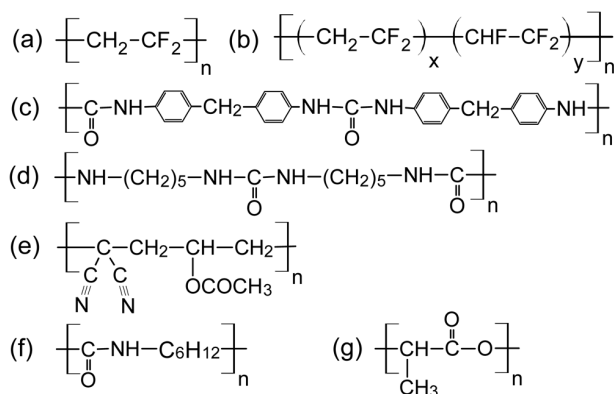


FIG. 1. Molecular compositions of piezoelectric polymers. (a) PVDF, (b) P(VDF-TrFE), (c) aromatic polyurea, (d) aliphatic polyurea 5, (e) poly(vinylidene-cyanide-co-vinylacetate), (f) polyamide 7 (PA-7), and (g) PLLA.

<sup>a)</sup>Electronic address: xunlin@canopus.physik.uni-potsdam.de

## Polarization from dielectric-barrier discharges in ferroelectrets: Mapping of the electric-field profiles by means of thermal-pulse tomography

Xunlin Qiu,<sup>a)</sup> Lars Holländer, Rosaura Flores Suárez, Werner Wirges, and Reimund Gerhard

*Applied Condensed-Matter Physics, Faculty of Science, University of Potsdam, Karl-Liebknecht-Strasse 24-25, 14476 Potsdam-Golm, Germany*

(Received 25 June 2010; accepted 3 August 2010; published online 20 August 2010)

A polymer-ferroelectret system is fabricated by attaching two uniform polycarbonate films to a grid produced from double-sided adhesive tape by means of computer-controlled laser cutting. The openings of the grid structure result in well-defined voids inside the three-layer system, which can be internally charged through dielectric barrier discharges. The negatively charged internal void surfaces can be made visible by means of xerographical toner, and the electric-field distribution inside such ferroelectrets can be studied with thermal-pulse tomography. Both techniques exhibit polarization patterns that are consistent with the grid structure. Possible reasons for the observed non-uniform charge distributions are discussed. © 2010 American Institute of Physics.

[doi:10.1063/1.3481802]

Polymer foams and layer systems with internally charged voids (so-called ferroelectrets) exhibit high piezoelectric activity combined with high mechanical flexibility and compliance.<sup>1-5</sup> So far, the standard material in ferroelectret studies and applications has been cellular polypropylene (PP), which is usually produced by means of blow extrusion or by stretching filler-loaded polymer sheets under suitable conditions.<sup>6,7</sup> Depending on the structure and the charging conditions, cellular PP ferroelectrets often show piezoelectric  $d_{33}$  coefficients of several hundred picocoulomb per newton. However, a wider application of cellular PP ferroelectrets is hindered by the relatively low thermal stability of their piezoelectricity, which decays dramatically between 60 and 80 °C.<sup>8</sup> In addition, cellular PP ferroelectrets have a void structure with a broad distribution of void sizes and shapes, and therefore only a limited number of the voids are optimal for charging and for transducer operation. In order to achieve ferroelectrets with better thermal stability of the piezoelectricity and/or with more uniform void structures, various other polymers have been employed recently as ferroelectrets.<sup>5</sup>

On the other hand, the understanding of the fundamental properties of ferroelectrets is still not sufficiently complete. It is known that the voids must be internally charged by means of dielectric barrier discharges (DBDs) in order to render cellular or void-containing polymer structures piezoelectric. Charges of both polarities are generated in the plasma of a DBD and subsequently trapped at the internal surfaces of the dielectric polymer.<sup>9,10</sup> The charged voids can be considered as macroscopic dipoles that consist of charges of opposite polarity on the internal surfaces. Theoretical analysis indicates that the piezoelectricity of ferroelectrets is linearly related to the effective polarization (i.e., the density of the macroscopic dipoles).<sup>11,12</sup> Early on, the existence of injected near-surface homocharge and of DBD-generated internal heterocharge in corona-poled cellular-PP ferroelectret films was confirmed by means of thermal-wave experiments (sometimes also called laser-intensity modulation method or

LIMM).<sup>13</sup> A direct proof of the internal charges was obtained with scanning electron microscope (SEM) images.<sup>14</sup> SEM images of obliquely cut cellular PP ferroelectrets show the negative charges, because the secondary electron emission yield from negatively charged areas is higher than that from positively charged areas. However, this technique requires cutting of the sample and is thus destructive. For developing new ferroelectrets and for optimizing their properties, a non-destructive technique for assessing the effective polarization is highly desired.

In this paper, a new technique for the fabrication of ferroelectrets is proposed, and the electric-field profiles in the resulting ferroelectret samples are mapped by means of thermal-pulse tomography (TPT). TPT is a nondestructive thermal time-domain technique for detecting three-dimensional (3D) profiles of space charge and dipole polarization.<sup>15-17</sup> Electric-field maps resulting from TPT were shown to agree with those obtained by means of the focused LIMM (FLIMM).<sup>18</sup> In a preliminary study, TPT experiments on the same ferroelectret system revealed electric-field patterns that are closely related to the honeycomb structure of the sample.<sup>19</sup> Here, the earlier investigations were re-examined and re-evaluated as well as supplemented by new experiments and interpretations.

For sample preparation, polycarbonate (PC) films (Makrofol DE 6-2, BMS) with a thickness of 30 or 50  $\mu\text{m}$  were metallized on one surface with either 50 nm thick aluminum or 20 nm thick gold electrodes. A grid of double-sided adhesive tape (468MP 200MP Adhesive, 3M) with a thickness around 100  $\mu\text{m}$  was prepared by means of computer-controlled laser cutting. After peeling off the nonadhesive protective layers (which also have a thickness of about 100  $\mu\text{m}$ ), the adhesive-tape grid was sandwiched with two PC films via their nonmetallized surfaces. In this way, well-defined voids are formed at the openings of the adhesive-tape grid. Figure 1(a) schematically shows the sample preparation, while Fig. 1(b) is a digital image of part of such a sample in which the adhesive tape grid has a honeycomb structure with a length of 1.5 mm for one side of each hexa-

<sup>a)</sup>Electronic mail: xunlin@canopus.physik.uni-potsdam.de.

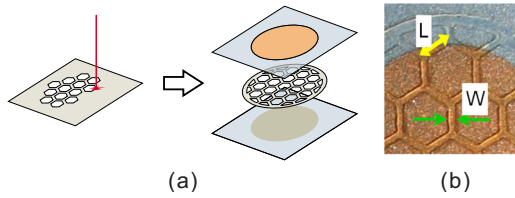


FIG. 1. (Color online) (a) Sample preparation: A grid of double-sided adhesive tape is produced by means of computer-controlled laser cutting. PC films are metalized on one side. The nonmetalized surfaces of two PC films stick to both sides of the adhesive-tape grid, respectively, forming well-defined voids. (b) A digital photo of part of a sample. The PC films are metalized with 20 nm thick semitransparent gold electrodes. The honeycomb structure of the adhesive-tape grid is clearly visible.

gon and with a width of 0.5 mm for the remaining adhesive-tape stripes.

In order to charge the sample by means of DBDs across the voids, a dc voltage is applied between the sample electrodes for 30 s by means of a high-voltage supply (Trek model 610D). The  $d_{33}$  coefficient of the sample as a function of the charging voltage is plotted in Fig. 2. The  $d_{33}$  coefficients were determined dynamically as described in more detail elsewhere.<sup>20</sup> The voltage dependence of  $d_{33}$  clearly shows a threshold behavior similar to that found previously on cellular-PP ferroelectrets.<sup>21</sup> For the present samples,  $d_{33}$  remains nearly zero for charging voltages below 1 kV. Thereafter,  $d_{33}$  increases strongly with the charging voltage and reaches a saturation value of about 30 pC/N at about 2 kV.

It is known that the DBDs in ferroelectrets are accompanied by light emission that can be recorded with a digital camera. Figure 3(a) shows the spatially resolved light emission from a sample under a positively biased sinusoidal voltage with a peak-to-peak value  $V_{pp}$  of 3 kV and a frequency of 100 Hz. The image was recorded by means of a computer-controlled electron-multiplying charge-coupled-device camera (EM-CCD, iXon, Andor Technology). For the measurement, the sample was metalized on both sides with semi-transparent Au electrodes. In order to block any light emission from corona discharges at the electrode edges, the sample was covered by a mask with a circular hole of 8.5 mm diameter. In the image, the honeycomb structure is clearly visible, while the difference between the light intensities of individual voids might be caused by small differ-

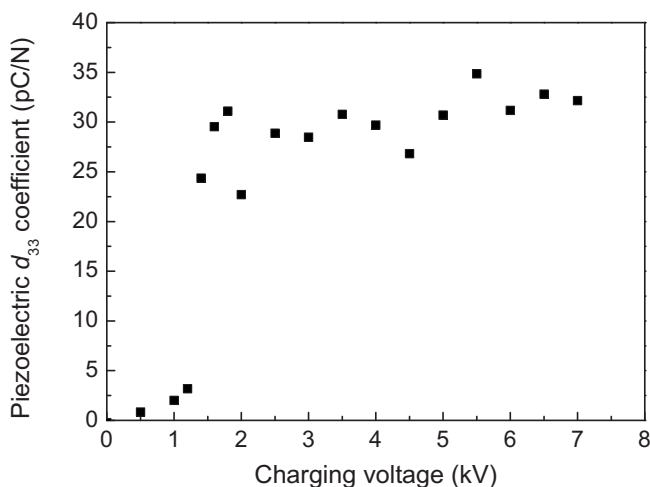


FIG. 2. The piezoelectric  $d_{33}$  coefficient of PC ferroelectrets as a function of the charging voltage.

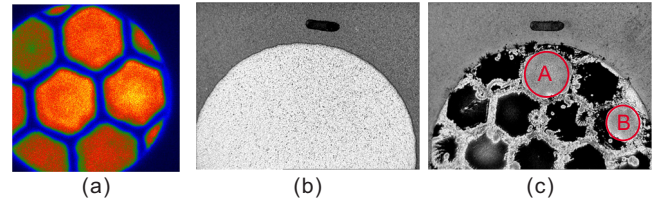


FIG. 3. (Color online) (a) Color-coded EM-CCD image of a PC ferroelectret with honeycomb voids under positive sinusoidal voltages. The EM-CCD camera was internally triggered with an exposure time of 5 s. (b) Digital photograph of the PC film serving as negatively charged internal void surface. The double-sided adhesive-tape template is removed after charging with a dc voltage of 3 kV for 30 s. The uniform aluminum electrode deposited on the other side of the film is clearly seen. (c) Toner pattern obtained by developing the latent charge image on the surface shown in (b) by means of xerographic toner. The negative charges deposited during the DBDs attract the toner, thus revealing the honeycomb void structure. Circles A and B represent areas with positive charges induced by back discharges.

ences in the void parameters that cannot be avoided in the laboratory.

In order to visualize the charge pattern deposited on the inner surfaces of the voids, an adhesive-tape template with its protective layers was used so that the PC films did not stick to the template. The PC-template-PC sandwich was charged with +3 kV for 30 s. According to a widely accepted model, the two internal surfaces of the charged voids carry positive and negative charges, respectively. After charging, the sandwich layers were separated, and the non-metalized surface of the PC film whose electrode was connected with the positive side of the high voltage during charging was photographed [Fig. 3(b)]. The uniform aluminum electrode on the back side is seen through the transparent PC film. The latent charge image on the non-metallized surface of the PC film was developed with xerographic toner from a laser-printer cartridge, and a photograph was taken. The negative charges deposited during the DBDs attract the toner, thus exposing the honeycomb structure of the voids [Fig. 3(c)]. It is also seen in the figure that the surfaces of some of the voids (marked as circles A and B) did not attract the toner. With the same procedure, an inverse toner pattern was obtained on the other PC film, i.e., only the areas facing A and B attract the toner, while the other areas do not. Our results agree with the fact that the xerographic toner is positively charged.

The polarity reversal of areas A and B is attributed to back discharges during and after DBD charging (also known as choking effect in conventional DBDs). The internally deposited charges induce an electric field opposite to the externally applied one. Back discharges may be triggered when the charging voltage is turned off, leading to drastic reduction of the effective polarization and to a polarity reversal of some of the voids.<sup>10</sup>

The electric-field profiles in the resulting ferroelectret samples are mapped by means of TPT with a setup described in Ref. 16. For each beam pointing, the data from 30 laser-pulse experiments were averaged. A map of the electric-field distribution measured 87 days after charging is shown in Fig. 4. A rather high electric-field strength is seen very near to the electrode (depth  $z=0.5 \mu\text{m}$  from the laser-heated electrode). For depths beyond  $z=1 \mu\text{m}$ , however, the electric field does not change much with depth anymore. As can be seen from the figure, the honeycomb shapes of the voids are reproduced by the electric-field patterns. The difference between the



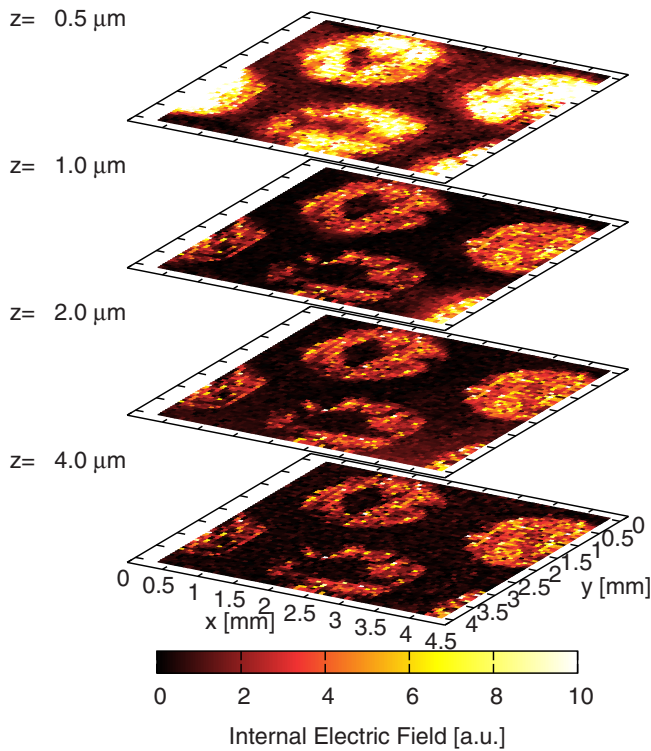


FIG. 4. (Color online) 3D electric-field profile in a three-layer PC-spacer-PC ferroelectret.

electric-field strengths at depths of  $z=0.5$  and of  $1 \mu\text{m}$  indicates a certain amount of space charge that partially compensates the electric field between the macroscopic dipoles and the electrode. The existence of this space-charge layer indicates a rather high conductivity of the PC films at high electric fields, while there seems to be a blocking layer near the electroded PC surface. The charge layer did stabilize the field distribution inside the sample so that it could still be recorded after almost three months.

Figure 4 also shows that the charge density is not always uniform across a honeycomb cell. Sometimes, the charge density is much higher near the edges of a honeycomb than at its center, which might be caused by void-height differences that cannot be avoided in the laboratory, but should be overcome in an industrial-scale production. Near the adhesive-tape stripes, there seems to be almost no charge. These observations probably indicate that both the internal surfaces of the polymer films at the top and the bottom of each void and the adhesive tape forming the side walls of the voids are too conductive for stable ferroelectret systems.

The relatively high conductivity of the double-sided adhesive tape was confirmed in surface-potential-decay measurements. A piece of the adhesive tape was charged in a point-to-grid corona setup with a point voltage  $V_p$  of 15 kV and a grid voltage  $V_g$  of 2 kV. A surface potential  $V_s$  of about 1 kV is found right after charging. Then the decay of the  $V_s$  was monitored under laboratory conditions. It is observed that  $V_s$  decreases to nearly zero within 10 min. Therefore, adhesive tape grids with lower conductivity as well as polymer films with better electret properties should be used in order to achieve ferroelectrets with higher stabilities of their piezoelectricity. Comprehensive information on the evolution of the electric field distribution in the polymer layers requires more detailed investigations. Other polymers as well as film

systems with various void patterns are under investigation.

In conclusion, ferroelectret systems have been fabricated by attaching two PC films to a double-sided adhesive-tape grid cut via a computer-controlled laser. The space-charge or effective-polarization patterns produced during charging by means of internal DBDs were demonstrated through exposure to xerographic toner and via three-dimensional mapping of the electric field by means of TPT, both revealing the honeycomb structure of the voids. From the electric-field profiles, we suspect that the charge stability on the top and bottom polymer films of the voids is deteriorated by conduction on and within the polymer films and the adhesive-tape stripes. Furthermore, it seems that a heterocharge layer may have formed near the top metalization of the electrode-poled three-layer PC-spacer-PC ferroelectrets because of the high conductivity of the polymer. Following and extending the early example of L IMM experiments on ferroelectrets,<sup>13</sup> it could thus be shown that TPT is a very useful method for investigating electric-field profiles at least in the uniform layers of ferroelectret systems and for drawing conclusions about space-charge distributions.

- <sup>1</sup>R. Gerhard-Multhaupt, *IEEE Trans. Dielectr. Electr. Insul.* **9**, 850 (2002).
- <sup>2</sup>S. Bauer, R. Gerhard-Multhaupt, and G. M. Sessler, *Phys. Today* **57**(2), 37 (2004).
- <sup>3</sup>M. Wegener and S. Bauer, *ChemPhysChem* **6**, 1014 (2005).
- <sup>4</sup>S. Bauer, *IEEE Trans. Dielectr. Electr. Insul.* **13**, 953 (2006).
- <sup>5</sup>X. Qiu, *J. Appl. Phys.* **108**, 011101 (2010).
- <sup>6</sup>K. Kirjavainen, "Electromechanical film and procedure for manufacturing same," U.S. Patent No. 4654 546 (March 31, 1987).
- <sup>7</sup>J. Raukola, N. Kuusinen, and M. Paajanen, *Proceedings of the 11th International Symposium on Electrets, Melbourne, Australia*, 1–3 October 2002 (IEEE Service Center, Piscataway, NJ, 2002), pp. 195–198.
- <sup>8</sup>A. Mellinger, M. Wegener, W. Wirges, R. Reddy Mallepally, and R. Gerhard-Multhaupt, *Ferroelectrics* **331**, 189 (2006).
- <sup>9</sup>M. Lindner, S. Bauer-Gogonea, S. Bauer, M. Paajanen, and J. Raukola, *J. Appl. Phys.* **91**, 5283 (2002).
- <sup>10</sup>X. Qiu, A. Mellinger, M. Wegener, W. Wirges, and R. Gerhard, *J. Appl. Phys.* **101**, 104112 (2007).
- <sup>11</sup>M. Paajanen, H. Välimäki, and J. Lekkala, *Proceedings of the 10th International Symposium on Electrets, Delphi, Greece*, 22–24 September 1999 (IEEE Service Center, Piscataway, NJ, 1999), pp. 735–738.
- <sup>12</sup>G. M. Sessler and J. Hillenbrand, *Appl. Phys. Lett.* **75**, 3405 (1999).
- <sup>13</sup>J. van Turnhout, R. E. Staal, M. Wübbenhorst, and P. H. de Haan, *Proceedings of the 10th International Symposium on Electrets, Delphi, Greece*, 22–24 September 1999 (IEEE Service Center, Piscataway, NJ, 1999), pp. 785–788.
- <sup>14</sup>J. Hillenbrand and G. M. Sessler, *Annual Report, Conference Electrical Insulation and Dielectric Phenomena, Victoria, Canada*, 15–18 October 2000 (IEEE Service Center, Piscataway, NJ, 2000), pp. 161–165.
- <sup>15</sup>A. Mellinger, R. Singh, M. Wegener, W. Wirges, R. Gerhard-Multhaupt, and S. B. Lang, *Appl. Phys. Lett.* **86**, 082903 (2005).
- <sup>16</sup>A. Mellinger, R. Flores-Suárez, R. Singh, M. Wegener, W. Wirges, R. Gerhard, and S. B. Lang, *Int. J. Thermophys.* **29**, 2046 (2008).
- <sup>17</sup>R. Flores Suárez, A. Mellinger, M. Wegener, W. Wirges, R. Gerhard-Multhaupt, and R. Singh, *IEEE Trans. Dielectr. Electr. Insul.* **13**, 1030 (2006).
- <sup>18</sup>C.-D. Pham, A. Petre, L. Berquez, R. Flores-Suárez, A. Mellinger, W. Wirges, and R. Gerhard, *IEEE Trans. Dielectr. Electr. Insul.* **16**, 676 (2009).
- <sup>19</sup>R. F. Suárez, X. Qiu, L. Holländer, R. A. P. Altafim, W. Wirges, R. Gerhard, W. Jenninger, and J. Wagner, Annual Report, *Conference on Electrical Insulation and Dielectric Phenomena, Virginia Beach, USA*, 18–20 October 2009 (IEEE Service Center, Piscataway, NJ, 2009).
- <sup>20</sup>R. A. P. Altafim, X. Qiu, W. Wirges, R. Gerhard, R. A. C. Altafim, H. C. Basso, W. Jenninger, and J. Wagner, *J. Appl. Phys.* **106**, 014106 (2009).
- <sup>21</sup>M. Wegener, M. Paajanen, W. Wirges, and R. Gerhard-Multhaupt, *Proceedings of the 11th International Symposium on Electrets, Melbourne, Australia*, 1–3 October 2002 (IEEE Service Center, Piscataway, NJ, 2002), pp. 54–57.

# In-situ Acoustical Investigation of the Polarization Build-up in Cellular Polypropylene Ferroelectrets

Xunlin Qiu<sup>1</sup>, Reimund Gerhard<sup>1</sup> and Axel Mellinger<sup>1,2</sup>

<sup>1</sup>Institute of Physics and Astronomy, University of Potsdam, 14476 Potsdam-Golm, Germany

<sup>2</sup>Department of Physics, Central Michigan University, Mount Pleasant, MI 48859, USA

## ABSTRACT

The build-up of the effective polarization in ferroelectrets under suitable voltage waveforms was studied by means of acoustical measurements and dielectric resonance spectroscopy. The radiated sound from ferroelectrets under external voltage signals has contributions not only from the effective charge density, but also from the Maxwell stress. Therefore, a “butterfly” curve was obtained for the received microphone signal during charging of a ferroelectret under linearly increasing or decreasing voltages. The microphone-signal measurements were converted to piezoelectric  $d_{33}$  coefficients by comparing the zero-charging-field microphone signals with the absolute  $d_{33}$  values determined by means of dielectric resonance spectroscopy immediately after charging. A polarization-voltage ( $P$ - $V$ ) hysteresis loop was obtained by analyzing the data in the light of an existing model for the piezoelectric  $d_{33}$  coefficient of ferroelectrets.

Index Terms — Ferroelectret, acoustical investigation, effective polarization, piezoelectricity.

## 1 INTRODUCTION

**FERROELECTRETS** (voided polymers with internal charges) have attracted considerable interest in research and applications because they not only exhibit strong piezoelectricity (their piezoelectric  $d_{33}$  coefficient can be comparable to or even higher than that of the best piezoelectric ceramics), but also have the intrinsic advantages of polymers [1,2]. Significant theoretical [3-7] and experimental [8-18] work has been published in this area. It was found that the piezoelectric properties of ferroelectrets are determined by the effective charge densities (effective polarization), by the respective thicknesses of the air gaps and the solid layers, and by Young’s modulus  $Y$ .  $Y$  has a local minimum upon increasing inflation of the voids, corresponding to a maximum of the piezoelectric  $d_{33}$  coefficient [8]. This confirms the proportionality between  $d_{33}$  and  $1/Y$  predicted by the model. However, it is still not known how the effective polarization develops in cellular PP ferroelectrets during charging. Such knowledge would be critical for a better understanding and for a possible improvement of the piezoelectricity.

It is known that the micro-discharges inside the voids of ferroelectrets are initiated when the charging voltage is higher than a threshold value. The micro-discharge process is a kind of dielectric barrier discharge (DBD, also referred to as barrier

discharge) [19-22]. Time-resolved measurements of light emission have shown that an individual barrier discharge process in the voids takes place on a time scale of a few ns [19]. In a study on the layered fluoropolymer ferroelectrets (FEP-ePTFE-FEP multi-layer samples), the light emission was measured to indicate the onset and termination of the breakdown inside the pores, while a quantitative analysis of the electric polarization-versus-field hysteresis was performed by measuring the poling current during corona poling [23, 24]. The ePTFE film in such sandwiches has open pores with a size of 1  $\mu\text{m}$ . In this paper, we study the development of the effective polarization of cellular PP ferroelectrets under suitable voltage waveforms by means of acoustical measurement and dielectric resonance spectroscopy. The closed voids inside cellular PP ferroelectrets have a lateral dimension of tens of  $\mu\text{m}$  and a height of several  $\mu\text{m}$ . The sound signal emitted from the sample under a bias voltage, superimposed with a sinusoidal stimulating voltage, was measured with a microphone. The near-field microphone signal is proportional to the amplitude of the surface vibrations and hence to the inverse piezoelectric  $d_{33}$  coefficients of the sample. Dielectric resonance spectroscopy [25-27] around the thickness-extension (TE) resonance of the samples was used to determine their electromechanical parameters. Unlike in [24], where an indirect variable to the piezoelectric effect (i.e. charging current) is measured, and the voltage which produces this current (namely the surface potential during corona charging) is out of control to some

Manuscript received on 1 May 2009, in final form 7 December 2009.

1070-9878/10/\$25.00 © 2010 IEEE

extend, in the acoustical technique, we see directly the development of the relative piezoelectric effect (a butterfly curve is obtained), and the voltage applied to the sample can be controlled precisely.

## 2 LINEAR AND QUADRATIC ELECTROMECHANICAL RESPONSE FROM CELLULAR FERROELECTRETS

According to a simplified model which considers a stack of alternating plane-parallel solid and gaseous layers, the thickness change  $\Delta s$  of ferroelectrets under an external voltage can be expressed as [3-5]

$$\Delta s = \frac{s}{Y} \frac{\varepsilon_p s_1 \sigma_{\text{eff}} V - \frac{1}{2} \varepsilon_0 \varepsilon_p^2 V^2}{(s_1 + \varepsilon_p s_2)^2} \quad (1)$$

where  $V$  is the external voltage applied to the electrodes,  $Y$  is Young's modulus of the sample, and  $\varepsilon_0$  and  $\varepsilon_p$  are the permittivity of free space and the relative permittivity of the polymer, respectively.  $s_1$  and  $s_2$  are the total thickness of the solid material layers and the gaseous layers, respectively, with  $s = s_1 + s_2$  being the total film thickness.  $\sigma_{\text{eff}} = \sum s_{2i} \sigma_i / \sum s_{2i}$  is the effective charge density on the PP/air interfaces on both sides of a single air gap, where  $s_{2i}$  is the thickness of the  $i$ th gaseous layer with  $\sum s_{2i} = s_2$ , and  $\sigma_i$  is the charge density on the surface of the  $i$ th layer. In the numerator of equation (1), the first term is the piezoelectric contribution from the charged voids while the second term describes the Maxwell stress. The right-hand side of equation (1) has the opposite sign compared to [5] due to the fact that  $\sigma_{\text{eff}}$  results from the very barrier discharge caused by the applied voltage  $V$ . Its polarity is such that the piezoelectric term in equation (1) makes the sample expand unless  $V$  is reversed. The Maxwell stress term, on the other hand, always results in a compressive strain.

Applying a voltage  $V = V_{\text{bias}} + V_0 \sin(\omega t)$ , we obtain from equation (1)

$$\Delta s \approx \frac{s}{Y(s_1 + \varepsilon_p s_2)^2} \left\{ -\frac{1}{2} \varepsilon_0 \varepsilon_p^2 (V_{\text{bias}}^2 + \frac{1}{2} V_0^2) + \varepsilon_p s_1 \sigma_{\text{eff}} V_{\text{bias}} + \left[ -\varepsilon_0 \varepsilon_p^2 V_{\text{bias}} + \varepsilon_p s_1 \sigma_{\text{eff}} \right] V_0 \sin(\omega t) + \frac{1}{4} \varepsilon_0 \varepsilon_p^2 V_0^2 \cos(2\omega t) \right\}, \quad (2)$$

where the first and the second term denote the thickness change due to the bias voltage (including the constant part of the Maxwell stress), the third term arises from the piezoelectric effect, and the last term is the second harmonic term from the Maxwell stress. Inspecting the third term in equation (2), we see that the radiated sound amplitude at the fundamental frequency has a contribution not only from the effective charge density  $\sigma_{\text{eff}}$ , but also from the modulated

Maxwell stress. The effective piezoelectric coefficient at  $V_{\text{bias}}$  is then given by

$$d_{33} = \frac{s}{Y} \frac{\varepsilon_p s_1 \sigma_{\text{eff}} - \varepsilon_0 \varepsilon_p^2 V_{\text{bias}}}{(s_1 + \varepsilon_p s_2)^2} \quad (3)$$

while the second harmonic is quadratically dependent on the amplitude of the stimulating sinusoidal voltage, and is independent of  $\sigma_{\text{eff}}$  and  $V_{\text{bias}}$ .

## 3 EXPERIMENTAL DETAILS

### 3.1 SAMPLE PREPARATION

Samples were prepared from commercial cellular polypropylene (PP) films with the trade name PQ50 (Nan Ya Plastics Corporation, Taiwan, China). They had been produced by stretching filler-loaded PP under suitable conditions [28]. The initial thickness and density are 50  $\mu\text{m}$  and 550  $\text{kg/m}^3$ , respectively. In order to optimize their electromechanical properties, the samples were inflated by means of gas diffusion expansion in nitrogen and a subsequent heat treatment [11]. The samples were then metalized on both sides with gold electrodes.

### 3.2 ACOUSTIC-EMISSION ANALYSIS

The measurements were performed in an anechoic chamber. Figure 1 is a schematic view of the setup. The high charging voltage was supplied directly to the two electrodes of the sample from a suitable amplifier (Trek, Model 610). In addition to amplifying the signal from the function generator (HP33120a), the amplifier is capable of adding a positive or negative dc bias voltage to the AC waveform. In this study, the frequency of the sinusoidal stimulating voltage is 1 kHz. The output sound signal was measured with a microphone (Type 4191, Brüel & Kjaer) in the near field (distance to the sample surface no more than 1 cm). Near field acoustical measurements are always difficult to interpret and analyse, but can be used in the present analysis since the geometry is fixed. The microphone was connected to a conditioning amplifier (Nexus, Brüel & Kjaer), which has comprehensive high- and

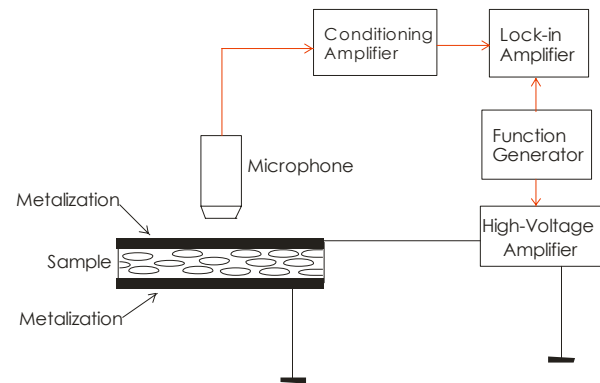
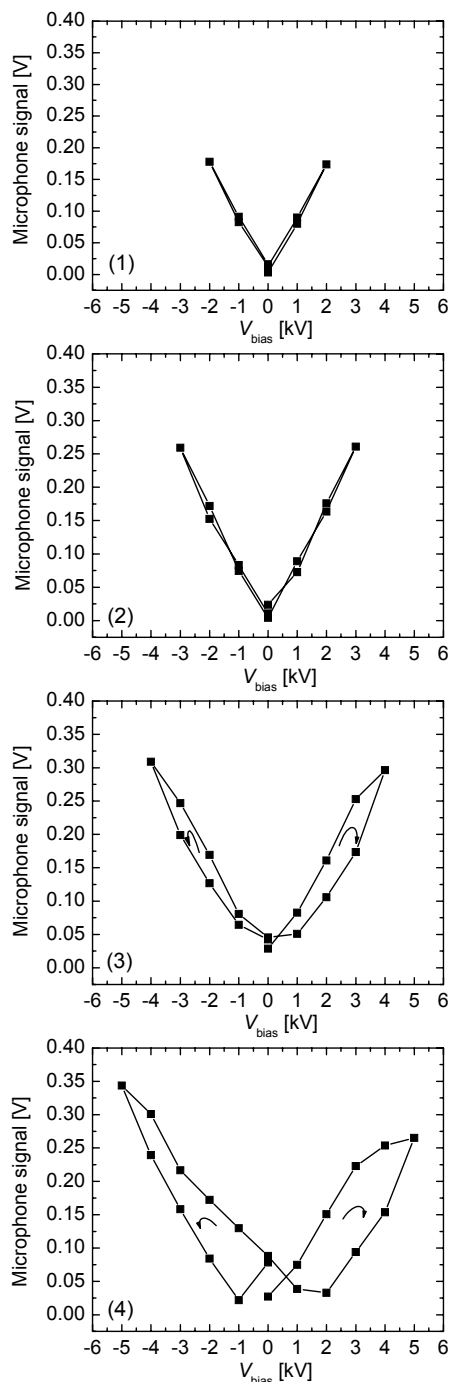


Figure 1. Schematic view of the experimental setup.



low-pass filtering facilities, and is suitable for applications where very high charge inputs can occur [29]. Both the effective amplitude of the microphone signal and its phase shift compared to the applied sinusoidal voltage were recorded with a lock-in amplifier (Model 7280, Ametek Inc.). The microphone-signal amplitude is proportional to the converse

piezoelectric  $d_{33}$  coefficient of the ferroelectret film. In this study, the microphone signal is only used to obtain relative (uncalibrated)  $d_{33}$  values. Direct (calibrated) measurements of the sound-pressure level in the near field above ferroelectrets are under way. The  $d_{33}$  values measured in this way were calibrated by means of dielectric resonance spectroscopy.



**Figure 2.** Microphone signal as a function of  $V_{bias}$  applied to the electrodes. The positive half cycle is followed by the negative half cycle (the cycle direction is denoted by two arrows). The maximum voltages for each cycle are: (1) 2 kV, (2) 3 kV, (3) 4 kV and (4) 5 kV. Measurements were done on the same, previously uncharged sample from cycle 1 to 4 (the thickness of the sample is approx. 80  $\mu\text{m}$ ).

### 3.3 DIELECTRIC RESONANCE SPECTROSCOPY

In order to obtain absolute  $d_{33}$  values, the dielectric resonance spectra of the sample around the thickness-extension (TE) mode anti-resonance frequency were recorded *in situ* using a Novocontrol ALPHA high-resolution dielectric analyzer. The samples were electrically connected to the sample holder via thin silver wires. From the frequency-dependent real or imaginary part of the capacitance  $C(\omega)$  for the thickness-extension mode of a freely vibrating sample, the anti-resonance frequency  $f_p$ , the electromechanical coupling factor  $k_t$ , the elastic modulus  $c_{33}$  and the piezoelectric  $d_{33}$  coefficient are determined from equations (4)-(6) by means of a least-squares fit [25-27]:

$$C(\omega) = \frac{\epsilon_r \epsilon_0 A}{h} \frac{1}{1 - k_t^2 \frac{\tan(\omega / 4f_p)}{(\omega / 4f_p)}} - iC_{loss} \quad (4)$$

$$f_p = \frac{1}{2h} \sqrt{\frac{c_{33}}{\rho}} \quad (5)$$

$$k_t^2 = d_{33}^2 c_{33} / (\epsilon_r \epsilon_0) \quad (6)$$

where  $\epsilon_r$ ,  $A$ ,  $\rho$  and  $h$  are the relative permittivity of the sample, the electroded sample area, the density and the thickness of the sample, respectively.

## 4 RESULTS AND DISCUSSION

### 4.1 ACOUSTICAL INVESTIGATION OF THE ACTUATOR SENSITIVITY

The microphone signal at 1 kHz as a function of the external bias voltage with different maximum voltages is depicted in Figure 2.  $V_{bias}$  was ramped up from zero to the positive maximum value with intervals of 1 kV, then ramped down back to zero with the same intervals. The positive half cycle was followed by a negative half cycle. When the maximum voltage of the cycle is lower than 3 kV, no obvious difference in the microphone signal is observed between ramping up and ramping down  $V_{bias}$ . However, when the maximum voltage of  $V_{bias}$  exceeds 3 kV, the microphone signal during ramping up  $V_{bias}$  is higher than the corresponding value during ramping down, and the difference grows with increasing maximum voltage of the cycle. As  $V_{bias}$  is reduced from its maximum value, the microphone signal reaches a minimum, then increases again as  $V_{bias}$  passes through zero, forming a characteristic “butterfly” curve.

To eliminate the influence of the history of cycles with different maximum voltages,  $V_{bias}$  cycles with a maximum value of 6 kV were applied to a fresh, uncharged sample

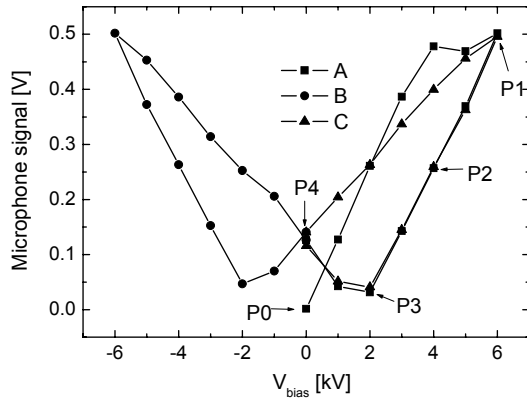


**Figure 3.** Microphone signal as a function of  $V_{\text{bias}}$  applied to the electrodes. The maximum cycle voltage is 6 kV. A fresh, uncharged sample with a thickness of 72  $\mu\text{m}$  was used for the positive half cycle (A), followed by a negative half cycle (B) and subsequently a second positive half cycle (C).

(Figure 3). Again, the positive half cycle was followed by a negative half cycle. There is an obvious difference between the first and the second positive half cycle during ramping up  $V_{\text{bias}}$ . When  $V_{\text{bias}}$  was ramped up from zero, the microphone signal for the first positive half cycle is lower than the corresponding value for the second positive half cycle. However, as  $V_{\text{bias}}$  was increased further, the microphone signal for the first positive half cycle becomes higher than the corresponding value for the second positive half cycle.

The amplitude of the microphone signal is proportional to the amplitude of the surface vibration of the sample and hence to the absolute value of  $d_{33}$ . This is shown in Figure 4, for which the microphone signal was measured as a function of the amplitude  $V_0$  of the stimulating sinusoidal voltage. A perfect linear relationship between the microphone signal and  $V_0$  is observed. Obviously, the slope of each curve is determined by the  $d_{33}$  value at the corresponding  $V_{\text{bias}}$  point. As the  $V_{\text{bias}}$  was ramped from the maximum value back to zero, the slope decreased to the minimum value at  $V_{\text{bias}} = 2$  kV, and then increased again, coinciding with the results shown in Figure 3.

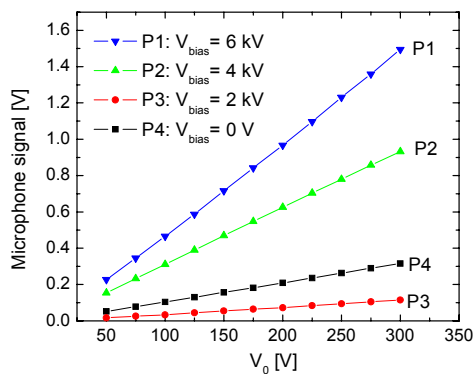


**Figure 4.** Microphone signal at different  $V_{\text{bias}}$  (different points indicated in figure 3) as a function of the amplitude  $V_0$  of the sinusoidal voltage. The slope is proportional to  $d_{33}$  at the respective point.

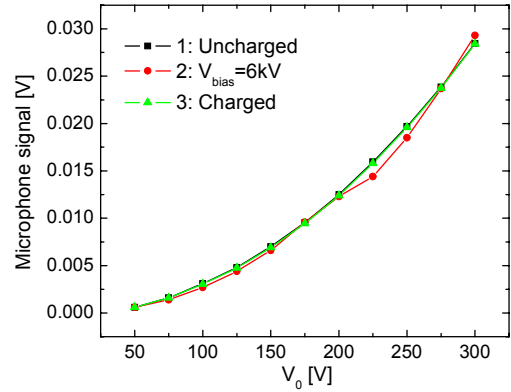


**Figure 5.** The second-harmonic microphone signal as a function of the amplitude  $V_0$  of the sinusoidal voltage. The curves (1), (2) and (3) were measured at the  $V_{\text{bias}}$  positions P0, P1 and P4 indicated in figure 3

For the second harmonic at 2 kHz, a quadratic dependence of the microphone signal on  $V_0$  was observed. As can be seen from Figure 5, the second harmonic is independent of the effective charge density and the external bias voltage, as predicted by equation (2).

According to equation (3), the magnitude of  $d_{33}$  has a contribution both from the external bias voltage applied to the electrodes (Maxwell-stress term) and from the effective charge density (piezoelectric term). The latter depends on the history of the applied  $V_{\text{bias}}$ , which may lead to hysteretic behavior. For cycles with the maximum  $V_{\text{bias}}$  lower than the threshold voltage for breakdown in the voids, there is no hysteresis in the microphone signal (curves (1) and (2) in Figure 2), since the signal results from the reversible effect of the Maxwell stress only. Above a threshold voltage of approx. 3 kV, electric breakdown occurs in the voids, giving rise to an effective charge density  $\sigma_{\text{eff}}$  which according to equation (3) contributes to  $d_{33}$  with the opposite sign to that of the Maxwell-stress term. For higher maximum  $V_{\text{bias}}$  values, barrier discharges occur in more voids, leading to higher charge density  $\sigma_{\text{eff}}$ . As a result, the slope in Figure 2 (curves (3) and (4)) is reduced as  $V_{\text{bias}}$  increases, and a difference of the microphone signal between ramping up and ramping down the external bias voltage appears, and this difference increases with the maximum value of  $V_{\text{bias}}$ .

For a given effective charge density  $\sigma_{\text{eff}}$ , there is a bias voltage where the piezoelectric and Maxwell-stress terms in equation (3) cancel each other, leading to the observed minimum in the microphone signal versus bias voltage near  $\pm 2$  kV (cf. Figure 3). The small residual microphone signal at this point could result from a non-uniform spatial distribution of  $\sigma_{\text{eff}}$ , causing different parts of the sample to reach this minimum at different bias voltages. Note that according to equation (3),  $d_{33}$  should change its sign when passing through the minimum. While the graphs in Figure 2 only indicate the magnitude of  $d_{33}$ , a phase shift of approx.  $180^\circ$  between the

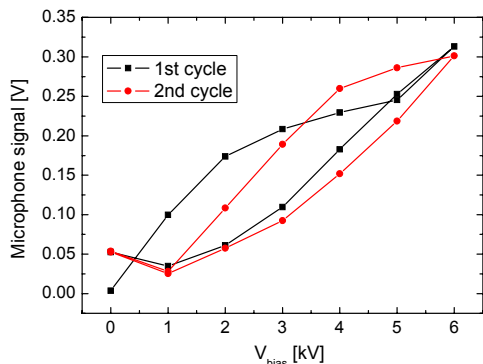


**Figure 6.** Microphone signal as a function of  $V_{\text{bias}}$ . Only positive cycles were subsequently applied. The thickness of the sample is  $60 \mu\text{m}$ .

microphone signal and the stimulating sinusoidal voltage was indeed observed when the microphone signal passes through its minimum in the “butterfly” curve.

When bipolar  $V_{\text{bias}}$  cycles are applied,  $\sigma_{\text{eff}}$  contributes to  $d_{33}$  with the same sign as the Maxwell stress during the subsequent half cycle unless it is reversed, which results in the difference between the first and the second positive half cycle (Figure 3). The microphone signal for the second positive half cycle is higher than the corresponding value for the first positive half cycle when  $V_{\text{bias}}$  was ramped up from zero due to the contribution of  $\sigma_{\text{eff}}$  from the negative half cycle in between. However, as is well-known in conventional DBDs, the  $\sigma_{\text{eff}}$  induced in the negative half cycle promotes the barrier discharge during the subsequent positive half cycle [22]. Therefore, as  $V_{\text{bias}}$  is increased further, the microphone signal for the second positive half cycle becomes lower than the corresponding value for the first positive half cycle due to the larger reversed  $\sigma_{\text{eff}}$  values.

For the results shown in Figure 6, only positive half cycles were applied one by one without negative half cycles. In this case, the  $\sigma_{\text{eff}}$  induced in the previous cycle always gives a contribution with a sign opposite to that of the Maxwell stress. As can be seen from Figure 6, the microphone signal for the second positive cycle decreases when  $V_{\text{bias}}$  is ramped up from zero, and it reaches its minimum at  $V_{\text{bias}} = 1 \text{ kV}$  and then increases again because the Maxwell-stress effect becomes larger than the piezoelectric effect, as  $V_{\text{bias}}$  is ramped up further. As expected, both in Figure 3 and Figure 6, the microphone signal for the first and the second positive voltage half cycle is nearly the same, when  $V_{\text{bias}}$  is ramped down from the maximum back to zero.

#### 4.2 BUILD-UP OF THE EFFECTIVE POLARIZATION IN FERROELECTRETS

According to equation (3),  $\sigma_{\text{eff}}$  can be calculated from  $d_{33}$ ,  $s_1$ ,  $s_2$ ,  $V_{\text{bias}}$ , and  $Y$ . The acoustical measurements only delivered relative (uncalibrated)  $d_{33}$  values. In order to obtain absolute  $d_{33}$  values, dielectric resonance spectroscopy was performed on samples immediately after the external voltage cycles. Young’s modulus and  $d_{33}$  were determined by fitting the real part of the

measured capacitance (inset of Figure 7) to equations (4)-(6). By comparing the zero-field microphone signal with this  $d_{33}$  value, all other microphone signal measurements can be converted to piezoelectric  $d_{33}$  coefficients.

Special attention should be paid to the fact that  $d_{33}$  changes its polarity when a phase shift of approx.  $180^\circ$  between the microphone signal and the stimulating sinusoidal voltage is observed. For  $V_{\text{bias}} = 6 \text{ kV}$ , the first (Maxwell stress) term in equation (2) is  $-3.5 \mu\text{m}$ . However, the actual thickness change is less than  $3.5 \mu\text{m}$  because it is partly compensated by the second (piezoelectric) term. Therefore,  $s_2$  and  $Y$  can be considered as constant during the external bias-voltage cycles. The quantities  $s_1$  and  $s_2$  were determined from the density of the samples given by the manufacturer and from the measured thickness, because the density of PP is known and the density of air can be approximated as zero.

The effective charge density  $\sigma_{\text{eff}}$  as a function of  $V_{\text{bias}}$ , calculated from the experimental data in Figure 3, is depicted in Figure 7, which shows a hysteresis behavior similar to that of ferroelectrics. A  $d_{33}$  of  $127 \text{ pC/N}$  is obtained by means of DRS immediately after the acoustic cycles. For a fresh, uncharged sample,  $\sigma_{\text{eff}}$  is nearly zero when the external voltage is below  $3 \text{ kV}$ . The small negative effective charge density at  $V_{\text{bias}} = 0$  (corresponding to  $d_{33} \approx 2 \text{ pC/N}$ ) is due to charges deposited during the manufacturing process. Above the threshold voltage,  $\sigma_{\text{eff}}$  increases significantly to a maximum value of  $1.6 \text{ mC/m}^2$  at  $V_{\text{bias}} = 6 \text{ kV}$ . However, a significant reduction of  $\sigma_{\text{eff}}$  is observed when the external voltage decreases from its maximum to zero, which is due to the back discharges caused by the over-compensation of the electric field from  $V_{\text{bias}}$  by the space charges trapped at the top and bottom surfaces of the voids [20]. This phenomenon, well-known as “choking behavior” in conventional DBDs [22], is further manifested when we compare  $\sigma_{\text{eff}}$  for the first and second positive half cycles during ramping up the bias voltage  $V_{\text{bias}}$ . For the second positive half cycle, a higher negative

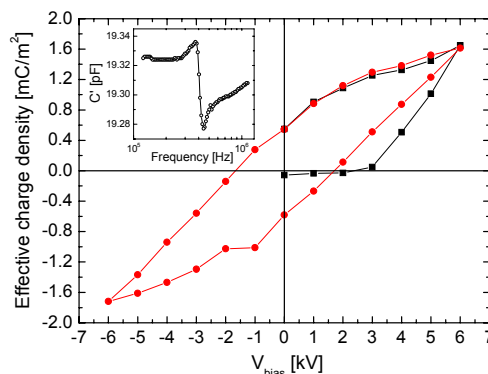


**Figure 7.** Effective charge density  $\sigma_{\text{eff}}$  (calculated from the experimental data shown in figure 3) as a function of  $V_{\text{bias}}$ . The inset shows the dielectric resonance spectrum from which the absolute  $d_{33}$  coefficient corresponding to the zero-field microphone signal was calculated.

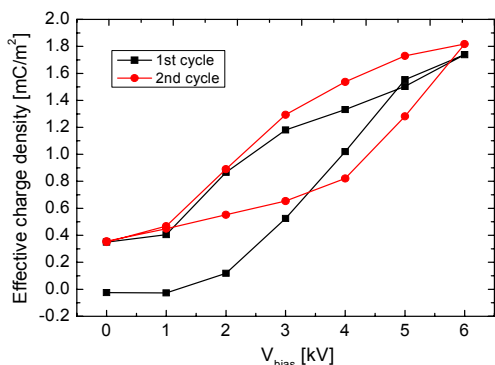


**Figure 8.** Effective charge density  $\sigma_{\text{eff}}$  (calculated from the experimental data shown in figure 6) as a function of the bias voltage  $V_{\text{bias}}$ .

effective charge density, induced by the former negative half cycle, is observed when  $V_{\text{bias}}$  is ramped up from zero. This higher negative  $\sigma_{\text{eff}}$  promotes the barrier discharges in the second positive half cycle, leading to a higher positive  $\sigma_{\text{eff}}$  for the second positive half cycle when  $V_{\text{bias}}$  is ramped up further.

A zero-field  $\sigma_{\text{eff}}$  value of about  $0.5 \text{ mC/m}^2$  is obtained, analogous to the remanent polarization in ferroelectrics. This value is in very good agreement with values determined by Sessler et al [4] and Paajanen et al [5] on other types of cellular PP ferroelectrets.

Figure 8 shows the development of  $\sigma_{\text{eff}}$  when only positive voltage cycles are applied. Again, DRS is performed immediately after the acoustic experiments, and a  $d_{33}$  of  $135 \text{ pC/N}$  is obtained in this case. The effective charge density in the second positive cycle increases again when  $V_{\text{bias}}$  is ramped up to voltages higher than 4 kV, indicating that voids pre-charged in the first positive voltage cycle break down again under high enough external voltage. The influence of the sample thickness on the threshold voltage and the zero-field polarization is not the topic of this paper. However, due to the back discharges, the increase of the  $\sigma_{\text{eff}}$  in the second positive voltage cycle is again not permanent, and it decreases to nearly the same value as that for the first positive voltage cycle when  $V_{\text{bias}}$  is ramped back to zero. Obviously, the effective charge density, and hence the piezoelectricity of ferroelectrets, would be substantially improved if the back discharges could be suppressed.

## 5 CONCLUSION

By means of acoustical measurements, in combination with dielectric resonance spectroscopy, the build-up of the effective polarization of ferroelectrets under suitable voltage waveforms can be monitored. A polarization-voltage ( $P$ - $V$ ) hysteresis loop is obtained by charging pressure-inflated PQ50 ferroelectrets with linearly increasing and/or decreasing voltages, from which the threshold charging voltage and the zero-field effective polarization are determined, and the choking behaviour of space charges trapped at the top and bottom surfaces of the voids is confirmed for the present case.

Our results suggest that the piezoelectricity of ferroelectrets would be significantly improved if the back discharges could be suppressed, since they often destroy a significant fraction of the effective charge density.

## ACKNOWLEDGMENT

We are indebted to Dr. Steffen Bergweiler, to Dr. Guggi Kofod and to Werner Wirges (all University of Potsdam) for many stimulating discussions. The first author (X. Q.) acknowledges a Research Fellowship provided by the Deutsche Forschungsgemeinschaft (DFG, Reference no. Qi 65/1-1).

## REFERENCES

- [1] S. Bauer, R. Gerhard-Multhaupt, and G. M. Sessler, "Ferroelectrets: Soft Electroactive Foams for Transducers", *Phys. Today*, Vol. 57, pp. 37-43, 2004.
- [2] M. Wegener and S. Bauer, "Microstoms in Cellular Polymers: A Route to Soft Piezoelectric Transducer Materials with Engineered Macroscopic Dipoles", *Chem. Phys. Chem.*, Vol. 6, pp. 1014-1025, 2005.
- [3] G. M. Sessler and J. Hillenbrand, "Electromechanical response of cellular electret films", *Appl. Phys. Lett.*, Vol. 75, pp. 3405-3407, 1999.
- [4] J. Hillenbrand, G. M. Sessler, and X. Zhang, "Verification of a model for the piezoelectric  $d_{33}$  coefficient of cellular electret films", *J. Appl. Phys.*, Vol. 98, 064105, 2005.
- [5] M. Paajanen, H. Välimäki, and J. Leikkala, "Modeling the sensor and actuator operations of the ElectroMechanical Film EMFi", *IEEE 10th Intern. Sympos. Electrets*, IEEE Service Center, Piscataway, NJ, USA, pp. 735-738, 1999.
- [6] E. Tuncer, "Numerical calculations of effective elastic properties of two cellular structures", *J. Phys. D: Appl. Phys.*, Vol. 38, pp. 497-503, 2005.
- [7] M. R. Haberman and Y. H. Berthelot, "A differential effective medium model for piezoelectret foams", *J. Appl. Phys.*, Vol. 102, 124903, 2007.
- [8] M. Wegener, W. Wirges, and R. Gerhard-Multhaupt, "Piezoelectric polyethylene terephthalate (PETP) foams - Specifically designed and prepared ferroelectret films", *Adv. Eng. Mater.*, Vol. 7, pp. 1128-1131, 2005.
- [9] E. Saarimäki, M. Paajanen, A. Savijärvi, M. Wegener, O. Voronina, R. Schulze, W. Wirges, and R. Gerhard-Multhaupt, "Novel heat durable electromechanical film: Processing for electromechanical and electret applications", *IEEE Trans. Dielectr. Electr. Insul.*, Vol. 13, pp. 963-972, 2006.
- [10] X. Zhang, J. Hillenbrand, and G. M. Sessler, "Improvement of piezoelectric activity of cellular polymers using a double-expansion process", *J. Phys. D: Appl. Phys.*, Vol. 37, pp. 2146-2150, 2004.
- [11] M. Wegener, W. Wirges, J. Fohlmeister, B. Tiersch, and R. Gerhard-Multhaupt, "Two-step inflation of cellular polypropylene films: void-thickness increase and enhanced electromechanical properties", *J. Phys. D: Appl. Phys.*, Vol. 37, pp. 623-627, 2004.
- [12] M. Wegener, W. Wirges, R. Gerhard-Multhaupt, M. Danschmüller, R. Schwödauier, S. Bauer-Gogonea, S. Bauer, M. Paajanen, H. Minkkinen, and J. Raukola, "Controlled inflation of voids in cellular polymer ferroelectrets: Optimizing electromechanical transducer properties", *Appl. Phys. Lett.*, Vol. 84, pp. 392-394, 2004.
- [13] M. Paajanen, M. Wegener, and R. Gerhard-Multhaupt, "Understanding the role of the gas in the voids during corona charging of cellular electret films—a way to enhance their piezoelectricity", *J. Phys. D: Appl. Phys.*, Vol. 34, pp. 2482-2488, 2001.
- [14] X. Qiu, M. Wegener, W. Wirges, X. Zhang, J. Hillenbrand, Z. Xia, R. Gerhard-Multhaupt, and G. M. Sessler, "Penetration of sulfur hexafluoride into cellular polypropylene films and its effect on the electric charging and electromechanical response of ferroelectrets", *J. Phys. D: Appl. Phys.*, Vol. 38, pp. 649-654, 2005.
- [15] I. Graz, M. Kaltenbrunner, C. Keplinger, R. Schwödauier, S. Bauer, S. P. Lacour, and S. Wagner, "Flexible ferroelectret field-effect transistor for large-area sensor skins and microphones", *Appl. Phys. Lett.*, Vol. 89, 073501, 2006.
- [16] J. Hillenbrand and G. M. Sessler, "Improvement of sensitivity of piezoelectric cellular polymer microphones by expansion and stacking of the films", *J. Acoust. Soc. Amer.*, Vol. 116, pp. 3267-3270, 2004.
- [17] X. Qiu, A. Mellinger, and R. Gerhard, "Influence of gas pressure in the voids during charging on the piezoelectricity of ferroelectrets", *Appl. Phys. Lett.*, Vol. 92, 052901, 2008.



- [18] X. Qiu and R. Gerhard, "Effective polarization fatigue from repeated dielectric barrier discharges in cellular polypropylene ferroelectrets", *Appl. Phys. Lett.*, Vol. 93, 056841, 2008.
- [19] M. Lindner, S. Bauer-Gogonea, S. Bauer, M. Pajanan, and J. Raukola, "Dielectric barrier microdischarges: Mechanism for the charging of cellular piezoelectric polymers", *J. Appl. Phys.*, Vol. 91, pp. 5283-5287, 2002.
- [20] X. Qiu, A. Mellinger, M. Wegener, W. Wirges, and R. Gerhard, "Barrier discharges in cellular polypropylene ferroelectrets: how do they influence the electromechanical properties?", *J. Appl. Phys.*, Vol. 101, 104112, 2007.
- [21] X. Qiu, A. Mellinger, W. Wirges, and R. Gerhard, "Spectroscopic study of dielectric barrier discharges in cellular polypropylene ferroelectrets", *Appl. Phys. Lett.*, Vol. 91, 132905, 2007.
- [22] U. Kogelschatz, "Dielectric barrier discharges: Their history, discharge physics and industrial applications", *Plasma Chem. Plasma Process.*, Vol. 23, pp. 1-46, 2003.
- [23] S. Zhukov and H. von Seggern, "Breakdown-induced light emission and poling dynamics of porous fluoropolymers", *J. Appl. Phys.*, Vol. 101, 084106, 2007.
- [24] S. Zhukov and H. von Seggern, "Polarization hysteresis and piezoelectricity in open-porous fluoropolymer sandwiches", *J. Appl. Phys.* Vol. 102, 044109, 2007.
- [25] A. Mellinger, "Dielectric Resonance Spectroscopy: a Versatile Tool in the Quest for Better Piezoelectric Polymers", *IEEE Trans. Dielectr. Electr. Insul.*, Vol. 10, pp. 842-861, 2003.
- [26] H. Ohigashi, "Electromechanical properties of polarized polyvinylidene fluoride films as studied by the piezoelectric resonance method", *J. Appl. Phys.*, Vol. 47, pp. 949-955, 1976.
- [27] G. S. Neugschwandtner, R. Schwödauer, M. Vieytes, S. Bauer-Gogonea, S. Bauer, J. Hillenbrand, R. Kressmann, G. M. Sessler, M. Pajanan, and J. Lekkala, "Large and broadband piezoelectricity in smart polymer-foam space-charge electrets", *Appl. Phys. Lett.* Vol. 77, pp. 3827-3829, 2000.
- [28] A. Savolainen and K. Kirjavainen, "Electrothermomechanical film. Part I. Design and characteristics", *J. Macromol. Sci., Chem.*, Vol. A26, pp. 583-591, 1989.
- [29] See data sheet "Brüel & Kjær Nexus Conditioning Amplifier for Very High Input", <http://www.bksv.com/pdf/Bp1976.pdf>



**Xunlin Qiu** WAS born on 21 July 1978. From 1996 to 2000, he studied physics at Tongji University and received the degree of B.Sc. From 2000 to 2006 he majored in condensed matter physics in the Pohl Institute of Solid State Physics at Tongji University and received the degree of M.Sc. in 2003 and the degree of D.Sc. in 2006. His main research work is functional polymer dielectrics and electrets. From July 2003 to October 2003 he worked on cellular polymer ferroelectret in the Institute of Communications Technology, Darmstadt University of Technology, Germany, and from November 2003 to January 2004, he worked on the same topic in Applied Condensed-Matter Physics group at the University of Potsdam, Germany. From June 2006 until now, he works as a postdoc at the University of Potsdam, Germany.



**Reimund Gerhard** (S'80-M'84-SM'85-F'93) studied mathematics and physics at the Darmstadt University of Technology in Germany from 1972 until 1978. After graduating as Diplom-Physiker, he spent one year as research fellow at the Collège Militaire Royal in St-Jean, Québec, Canada. From 1979 until 1985, he did his Ph.D. thesis with Professor Gerhard M. Sessler in Darmstadt. From 1985 until 1994, he was a research scientist and project manager at the Heinrich-Hertz Institute for Communications Technology in Berlin. Since 1994 he has been an associate professor and since 1997 a full professor in the Department of Physics and Astronomy of the University of Potsdam in Germany. Presently, he is Dean of the Science Faculty at his university. The main research areas of Prof. Gerhard are polymer electrets and ferroelectrets, in particular the mechanisms of space-charge storage and dipole polarization in dielectric polymers and polymer composites, their ferro-, pyro- and piezoelectrical properties, and their applications in sensors and actuators, as well as the nonlinear optical properties of polymers, and more recently also the physics of musical instruments. From 1974 until 1979, he was a fellow of the Studienstiftung des Deutschen Volkes. In 1988, he was awarded an ITGPreis by the Informationstechnische Gesellschaft im VDE. In 1989, he received a Silver medal from the Stiftung Werner-von-Siemens-Ring. In 2001, he was awarded the first Technologietransfer-Preis by the Technologie-Stiftung Brandenburg and the Prof.-Adalbert-Seifriz-Preis by the Verein Technologie-Transfer Handwerk for his technological collaborations with small industrial companies. Reimund Gerhard is a member of the American, European and German Physical Societies. From 2002 to 2009 he serves as Digest Editor of the IEEE Dielectrics and Electrical Insulation.



**Axel Mellinger** was born in Munich, Germany, on 25 August 1967. He studied physics at the Technical University in Munich, where he obtained his diploma and Ph.D. degrees in 1992 and 1995, respectively (his Ph.D. work was performed at the Max-Planck-Institute for Extraterrestrial Physics). In 1996/7 he held a two year postdoctoral position at UC Berkeley in the Department of Chemistry. From December 1997 until July 2008 he was a senior staff member at the University of Potsdam, Germany, where he obtained the highest German university degree, the Habilitation, in September 2005. Since August 2008 he is an Assistant Professor in the Physics Department at Central Michigan University. His present work focuses on charge storage mechanisms in polymer electrets, optically induced charge-detraping, and multi-dimensional mapping of polarization and space-charge distributions. From 1987 until 1992 he was a scholar of the German National Academic Foundation. He received the 2004 VDE/ITG award for a publication on dielectric resonance spectroscopy and the 2006 "Best Paper Award" by the German IEEE Instrumentation & Measurements chapter for his work on polarization tomography. In his spare time, he enjoys taking high-resolution mosaic images of astronomical objects for use in planetariums around the world.

# Beneficial and detrimental fatigue effects of dielectric barrier discharges on the piezoelectricity of polypropylene ferroelectrets

Xunlin Qiu,<sup>a)</sup> Werner Wirges, and Reimund Gerhard

*Applied Condensed-Matter Physics, Department of Physics and Astronomy, Faculty of Science, University of Potsdam, Karl-Liebknecht-Strasse 24-25, 14476 Potsdam-Golm, Germany*

(Received 1 April 2011; accepted 11 June 2011; published online 25 July 2011)

Cellular polypropylene (PP) ferroelectrets combine a large piezoelectricity with mechanical flexibility and elastic compliance. Their charging process represents a series of dielectric barrier discharges (DBDs) that generate a cold plasma with numerous active species and thus modify the inner polymer surfaces of the foam cells. Both the threshold for the onset of DBDs and the piezoelectricity of ferroelectrets are sensitive to repeated DBDs in the voids. It is found that the threshold voltage is approximately halved and the charging efficiency is clearly improved after only  $10^3$  DBD cycles. However, plasma modification of the inner surfaces from repeated DBDs deteriorates the chargeability of the voids, leading to a significant reduction of the piezoelectricity in ferroelectrets. After a significant waiting period, the chargeability of previously fatigued voids shows a partial recovery. The plasma modification is, however, detrimental to the stability of the deposited charges and thus also of the macroscopic dipoles and of the piezoelectricity. Fatigue from only  $10^3$  DBD cycles already results in significantly less stable piezoelectricity in cellular PP ferroelectrets. The fatigue rate as a function of the number of voltage cycles follows a stretched exponential. Fatigue from repeated DBDs can be avoided if most of the gas molecules inside the voids are removed via a suitable evacuation process. © 2011 American Institute of Physics. [doi:10.1063/1.3610507]

## I. INTRODUCTION

Internally charged polymer foams or void-containing polymer-film systems (so-called ferro- or piezoelectrets) have been added to the family of piezo-, pyro-, and ferroelectric polymers only quite recently.<sup>1-4</sup> They combine a large piezoelectricity with the intrinsic advantages of polymers, such as low density, mechanical flexibility, elastic compliance, suitability for large-area thin film applications, relatively low cost, a rather small acoustic impedance that is quite well matched to air and other fluids, etc. Depending on the structure of the material and the charging conditions, ferroelectrets often show piezoelectric  $d_{33}$  coefficients of hundreds of pico-Coulombs per Newton, comparable with or even higher than the values found in inorganic ferroelectric ceramics. Consequently, ferroelectrets attract more and more attention from science and industry.

In order to render polymer foams or void-containing polymer-film systems piezoelectric, the voids must be internally charged.<sup>5</sup> The charging process represents a dielectric barrier discharge (DBD), which is triggered when the applied voltage exceeds a threshold value.<sup>6-13</sup> During DBDs, charges of opposite polarity are generated and trapped at the internal surfaces of the gas-filled voids. The charged voids form macroscopic dipoles that can be easily deformed under mechanical or electrical stress, leading to the desired direct or inverse piezoelectricity, respectively. It should be noted that the macroscopic dipoles are by no means any intrinsic dipoles. Rather, they are voids carrying space charges on their

internal surfaces. The density of the macroscopic dipoles determines the effective polarization in ferroelectrets. Theoretical analysis shows that the piezoelectricity of ferroelectrets is directly related and essentially proportional to the effective polarization.<sup>14,15</sup> Thus, the effective polarization in polymer ferroelectrets is analogous to the polarization in ferroelectric polymers. However, the mechanism is quite different: The polarization in ferroelectrics relies on the orientation of intrinsic dipoles, whereas the effective polarization in ferroelectrets requires charge separation by means of DBDs and charge trapping on the internal surfaces of the voids.

With sufficiently high electric fields, the direction of macroscopic dipoles can be reversed, and the resulting electric-displacement-versus-electric-field curves exhibit hysteresis behavior.<sup>10,13,16</sup> Polarization fatigue, i.e., the reduction in the number and/or the magnitudes of reversible dipoles due to electric stress, is a serious concern in the application of ferroelectric materials. The bulk of experiments have been carried out on the fatigue in inorganic ferroelectrics, and a number of models have been proposed.<sup>17,18</sup> Polarization fatigue in ferroelectric polymers has also been studied by several groups.<sup>19-23</sup> It is widely accepted that polarization fatigue in ferroelectric polymers is mainly caused by the injection of space charge through the electrodes. The charges are often trapped at the boundaries of crystallites and at defects in the polymer films. Trapped charges can immobilize dipoles and lower the possibility of polarization reversal, and the interaction between dipoles and space charge might prevent the latter from being de-trapped.

Considering the big differences in the polarization mechanisms, fatigue in ferroelectrets might have a very

<sup>a)</sup>Author to whom correspondence should be addressed. Electronic mail: xunlin@canopus.physik.uni-potsdam.de.

different origin as compared with ferroelectric polymers. DBDs generate a cold plasma that produces a variety of energetic and active species including electrons, ions, excited metastable species, photons, etc. As a consequence, light emission from the DBDs in ferroelectrets can be easily measured.<sup>10–13</sup> The light emission originates from electronically excited and/or ionized gas molecules inside the voids. Therefore, the inner polymer surfaces of the voids are exposed to a highly reactive plasma during the DBDs, and numerous physico-chemical processes take place. DBDs in air are often used to modify the surface of polypropylene (PP) films in order to improve their wetting and adhesion properties.<sup>24,25</sup> Surface oxidation and chain scission during the DBDs lead to the formation of a layer of low-molecular-weight oxidized materials. As a result, the surface energy of the polymer film is improved dramatically.

In polymer electrets, traps for charge carriers are closely correlated with molecular chains, inter-chain interactions, and crystallite-amorphous interfaces.<sup>26</sup> Therefore, DBDs will certainly alter the electret properties at least of the polymer surface, which in turn will change the piezoelectricity of ferroelectrets, because charges are trapped at the inner surfaces of the voids. In order to better understand the underlying physico-chemical processes during DBDs and to optimize the relevant properties, systematic studies of polarization fatigue in ferroelectrets are desired. Our previous study showed that repeated DBDs in air result in significant deterioration of the chargeability of the voids, leading to fatigue in the piezoelectricity in ferroelectrets.<sup>27</sup>

In this paper, we present new experimental results to confirm and further illustrate the plasma-polymer interactions during repeated DBDs in the voids as the mechanism of polarization fatigue. We show that the repeated microplasma discharges modify the internal polymer surfaces of cellular ferroelectrets and thus facilitate the charging process, but they also deteriorate the chargeability of the voids, as well as the stability of the piezoelectricity in the cellular polymer, which demonstrates the influence of molecular dynamics and physico-chemical processes. In addition, an approach is proposed with which to avoid polarization fatigue by removing most of the gas molecules from the voids.

## II. EXPERIMENTS

Samples were prepared from commercial cellular PP films with the trade name PQ50 (Nan Ya Plastics Corporation, Taiwan, China). The commercial films were produced by stretching filler-loaded PP under conditions as detailed in Ref. 28. The initial thickness and density are 50  $\mu\text{m}$  and 550  $\text{kg}/\text{m}^3$ , respectively. In order to optimize the electromechanical properties, the samples were inflated via gas-diffusion expansion in nitrogen and a subsequent heat treatment.<sup>29</sup> The samples were then metallized on both sides with gold or aluminum electrodes 12 mm in diameter.

For charging, the samples were mounted in a pressure chamber connected to a vacuum pumping system. The sample capacitance was measured with a HP 4284 A precision LCR meter. High voltages for the charging and fatigue processes were applied to the sample electrodes by means of an amplifier (Trek model 610 D) controlled by an arbitrary-

waveform function generator (HP 33120 A). In the fatigue experiments, a bipolar sinusoidal voltage with a frequency of 100 Hz was employed. Unless otherwise specified, the peak-to-peak value ( $V_{pp}$ ) of the voltage during the fatigue experiments was 6.5 kV.

Dielectric resonance spectra (DRS) around the thickness-extension (TE) resonance of the samples were recorded by means of a Novocontrol ALPHA high-resolution dielectric analyzer or a precision impedance analyzer (Agilent 4294 A). From the frequency-dependent real or imaginary part of the capacitance  $C(\omega)$  of a freely vibrating sample, the anti-resonance frequency  $f_p$ , the electromechanical coupling factor  $k_t$ , the elastic modulus  $c_{33}$ , and the piezoelectric  $d_{33}$  coefficient can be determined by use of Eqs. (1)–(3) and a least-squares fit<sup>30–32</sup>:

$$C(\omega) = \frac{\epsilon_r \epsilon_0 A}{h} \frac{1}{1 - k_t^2 [\tan(\omega/4f_p)/(\omega/4f_p)]} - iC_{\text{loss}}, \quad (1)$$

$$f_p = \frac{1}{2h} \sqrt{\frac{c_{33}}{\rho}}, \quad (2)$$

$$k_t^2 = d_{33}^2 c_{33} / (\epsilon_r \epsilon_0), \quad (3)$$

where  $\epsilon_r$ ,  $A$ ,  $\rho$ , and  $h$  are the relative permittivity, the electrode area, the density, and the thickness of the sample, respectively.

## III. RESULTS AND DISCUSSION

### A. Self-healing of the DBD-induced damage over time: Partial recovery of the piezoelectricity

Partial recovery of the piezoelectricity in significantly fatigued cellular PP ferroelectrets had already been observed in our previous study and was attributed to the loss of polar

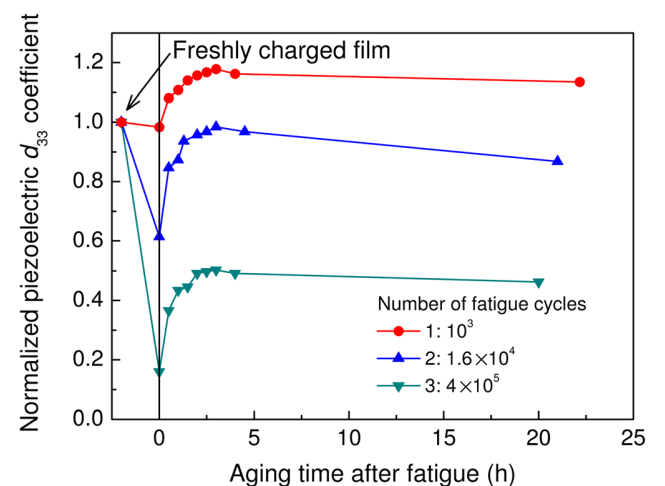


FIG. 1. (Color online) Recovery of the piezoelectric  $d_{33}$  coefficient after fatigue as a function of storage time under laboratory conditions. Each data point was obtained by a piezoelectrical measurement (i.e., charging plus dielectric resonance spectroscopy scan).  $d_{33}$  values for storage times below zero indicate the results on the respective films before fatigue.  $d_{33}$  values at time zero represent the status immediately after fatigue. Fatigue was achieved by means of a bipolar sinusoidal voltage with a  $V_{pp}$  of 6.5 kV, a frequency of 100 Hz, and a number of cycles as indicated.



low-molecular-weight oxidized material from the internal surfaces of the voids.<sup>27</sup> Figure 1 shows the evolution of the piezoelectric  $d_{33}$  coefficients as a function of storage time in ambient laboratory conditions for cellular PP films subjected to slight and moderate fatigue. For comparison, the results for one severely fatigued sample are also shown. First, three fresh samples were charged with +7 kV for 5 s, followed by a DRS measurement of the respective initial  $d_{33}$  coefficients. The combined charging plus DRS procedure is called “piezoelectrical measurement” and was performed for each data point in Fig. 1. Subsequently, the samples were subjected to slight, moderate, and significant fatigue with  $10^3$ ,  $1.6 \times 10^4$ , and  $4 \times 10^5$  cycles of a bipolar sinusoidal driving voltage ( $V_{pp} = 6.5$  kV;  $f = 100$  Hz), respectively. Immediately after fatigue, the  $d_{33}$  coefficients were found to be 98%, 61%, and 16% of the respective initial values for slightly, moderately, and significantly fatigued samples, respectively.

The samples were then stored in the laboratory, and their  $d_{33}$  coefficients were determined from time to time by means of piezoelectrical measurements (i.e., charging with +7 kV for 5 s plus DRS). A quick recovery of  $d_{33}$  values during the first hours of storage is observed for all three sample types. Compared to that of the significantly fatigued sample (curve 3 in Fig. 1), the  $d_{33}$  coefficients of the slightly and moderately fatigued samples recover to much higher values. For example, the  $d_{33}$  coefficient of the moderately fatigued sample recovers to 98% of the initial value after 3 h (curve 2 in Fig. 1). In particular, the  $d_{33}$  value of the slightly fatigued sample recovers to about 120% of the initial value after the same period of storage (curve 1 in Fig. 1). The obvious increase of the  $d_{33}$  coefficient is attributed to a plasma-enhanced charging efficiency of the voids, as confirmed by the reduced threshold after slight fatigue, which is discussed in the following sub-section.

## B. Reducing the threshold voltage for ferroelectret charging: Controlling and employing fatigue processes

It is known that the voltage dependence of the piezoelectric  $d_{33}$  coefficient of ferroelectrets exhibits a threshold behavior.<sup>7–13</sup> Figure 2 shows the threshold curves for a cellular PP sample before and after slight fatigue. Experiments were done on the same sample for all of the curves in Fig. 2 in order to avoid inconsistencies in the results because of different distributions of void sizes. First, a fresh sample was charged again and again with stepwise increasing voltage. Each voltage was applied for 5 s, followed by a DRS measurement in order to obtain the corresponding  $d_{33}$  coefficient. As can be seen from curve 1 in Fig. 2, a threshold voltage of about 3 kV is observed for the fresh sample, consistent with previous findings.<sup>10,11</sup> For voltages lower than 3 kV,  $d_{33}$  is set as zero because no resonance peak can be detected by means of DRS. Above the threshold,  $d_{33}$  increases strongly with increasing charging voltage.

After completion of curve 1, the sample was subjected to a slight fatigue process consisting of  $10^3$  cycles with the sinusoidal fatigue voltage ( $V_{pp} = 6.5$  kV;  $f = 100$  Hz). A resonance peak cannot be detected after the fatigue process,

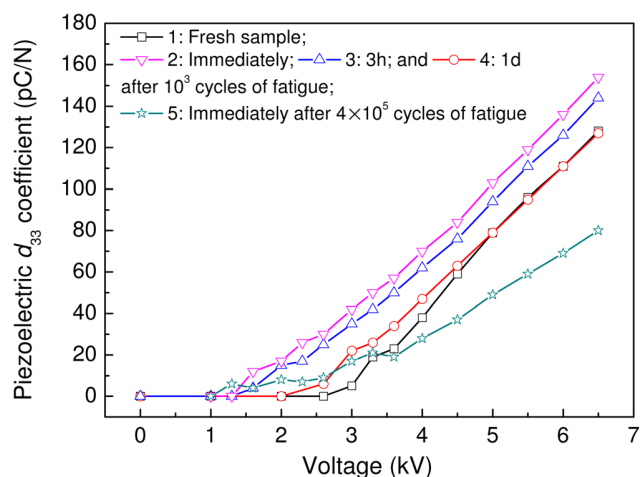


FIG. 2. (Color online) Piezoelectric  $d_{33}$  coefficient as a function of the direct-contact charging voltage. All curves were obtained on the same sample. First, a fresh sample was charged with stepwise increasing voltages. Each voltage was applied for 5 s, followed by a DRS measurement to obtain the respective  $d_{33}$  value via a fitting procedure (squares). Then the sample was subjected in three successive runs to  $10^3$  cycles of fatigue each with a bipolar sinusoidal voltage ( $V_{pp} = 6.5$  kV;  $f = 100$  Hz). The  $d_{33}$  coefficient was measured as a function of the direct-contact voltage immediately after the first run (inverted triangles), 3 h after the second run (triangles), and 1 day after the third run (circles) of the fatigue process. Finally, the sample was subjected to  $4 \times 10^5$  cycles of the same fatigue voltage, and the  $d_{33}$  coefficient was measured as a function of the direct-contact charging voltage (stars).

which indicates that the effective polarization previously induced in the sample has been destroyed. Then the threshold curve was determined again in the same way as before. The observed threshold voltage of 1.6 kV is only about 50% (curve 2 in Fig. 2) of that of the fresh sample. Above the threshold, the  $d_{33}$  coefficient increases with increasing charging voltage with a slope almost the same as that of curve 1. Thus, a higher charging efficiency of the sample after the slight fatigue process is obvious.

In DBDs, energetic and active species induced in the previous cycle influence the following cycle; this is known as memory effect.<sup>33</sup> DBDs in ferroelectrets are Townsend-breakdown events governed by the emission of electrons from negatively biased surfaces and by ionization of the gas in the voids. During the fatigue process, electrons and ions are trapped on the inner surfaces of the voids. The trapped electrons can be relatively easily emitted due to mechanisms such as thermodesorption and, especially, collisions with active metastables, leading to an enhancement of the  $\gamma$  emission from the inner surfaces of the voids.<sup>34</sup> In addition, the existence of metastables in the internal gas after repeated DBDs represents a reservoir of energy that considerably facilitates bulk ionization of the gas during the following DBD charging event. Consequently, the threshold charging voltage is reduced and the charging efficiency is improved after the sample has been subjected to a slight fatigue process, as can be seen from curve 2 in Fig. 2.

Physico-chemical processes still take place after the slight fatigue processes have been terminated. The density of the electrons trapped on the inner surfaces decreases due to the mechanisms mentioned above. The electrons can also diffuse along the inner surfaces and finally recombine with

positive charges.<sup>34</sup> In addition, the density of metastable species inside the voids also decays with time—in particular in the present case, in which the voids contain atmospheric air containing numerous oxygen molecules that can act as quenchers. Therefore, the improvement of the charging efficiency by repeated DBDs should be dependent on the waiting period after the fatigue process. In order to verify this hypothesis, the same slight fatigue process was applied to the sample again after curve 2 had been obtained, and this was followed by 3 h of storage under laboratory conditions. Then the threshold curve was determined (curve 3 in Fig. 2). As can be seen from the figure, the threshold curve shifts back toward that of a fresh sample. When the time of storage under laboratory conditions is extended to 1 day, the threshold curve obtained afterward shows characteristics very similar to the behavior of a fresh sample (curve 4 in Fig. 2), indicating that the positive effect of repeated DBDs on the charging process has been almost completely lost.

For further investigation, the threshold curve was also determined immediately after a significant fatigue of  $4 \times 10^5$  cycles (curve 5 in Fig. 2). Again, for the reasons discussed above, an obvious decrease of the threshold charging voltage is observed in comparison to that of a fresh sample. However, the  $d_{33}$  coefficient is now lower than that of a fresh sample at higher charging voltages because the chargeability of the voids has obviously been reduced significantly. Our results indicate that the piezoelectricity of ferroelectrets might be optimized if an air plasma could be fed into the voids during charging, so that a higher charging efficiency were achieved without destroying the chargeability of the voids. This is particularly feasible for ferroelectrets with open tubular channels,<sup>35</sup> for which the gas inside the channels can be easily exchanged.

### C. Reduced stability of the piezoelectricity: A detrimental effect of fatigue

The stability of the piezoelectricity in ferroelectrets is a critical issue for most applications. Therefore, the influence of the fatigue process on the stability of the piezoelectricity in ferroelectrets is of great interest. It is known that the piezoelectricity of cellular PP ferroelectrets exhibits good temporal stability in ambient atmosphere.<sup>36</sup> Figure 3 shows the decay of the piezoelectric  $d_{33}$  coefficient under laboratory conditions for samples fatigued with different numbers of cycles ( $N$ ). The initial  $d_{33}$  coefficients were obtained by means of piezoelectrical measurements on fresh samples. Subsequently, the samples were subjected to fatigue processes with different  $N$  values as indicated in the figure. After fatigue, the samples were stored under laboratory conditions for 1 day. The samples were then charged with +7 kV for 5 s, and their  $d_{33}$  coefficients were determined from time to time by means of DRS.

It should be noted that Figs. 3 and 1 are quite different, although the samples are subjected to slight, moderate, and severe fatigue in both cases. In Fig. 1, the  $d_{33}$  coefficient of the fatigued samples is shown as a function of the storage time immediately after the fatigue process by means of piezoelectrical measurements (i.e., charging with +7 kV for 5 s plus DRS). In this case, the recovery of the chargeability of

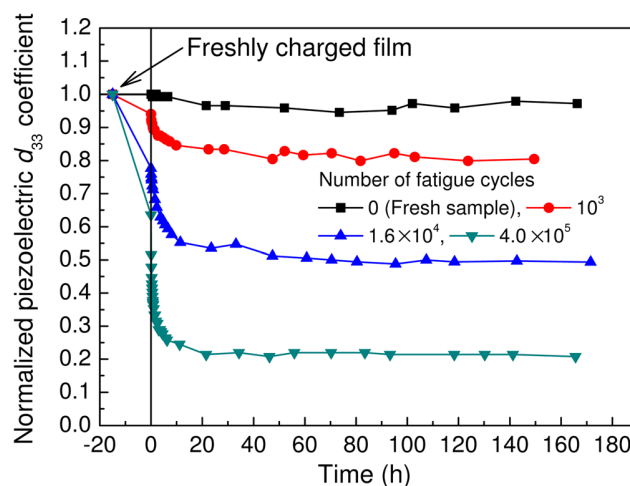


FIG. 3. (Color online) Decay of the normalized piezoelectric  $d_{33}$  coefficient under laboratory conditions.  $d_{33}$  coefficients for storage times below zero belong to freshly charged specimens. Samples were subjected to fatigue processes by means of a bipolar sinusoidal voltage ( $V_{pp} = 6.5$  kV;  $f = 100$  Hz) with a certain number of cycles ( $N$ ) as indicated, followed by 1 day of storage under laboratory conditions. Samples were then charged with +7 kV for 5 s. Thereafter, samples were again stored under laboratory conditions, and their remaining  $d_{33}$  coefficients were determined from time to time by means of DRS.

the voids after fatigue has been investigated. For the results shown in Fig. 3, however, samples had been stored under laboratory conditions for 1 day after the fatigue process. According to Fig. 1, this provides a period of time that is sufficiently long for a recovery of the chargeability of the voids. The samples were then charged with +7 kV for 5 s. Thereafter, the samples were stored under laboratory conditions, and their  $d_{33}$  coefficients were measured as a function of storage time by means of DRS only (without any further charging). Thus, the stability of the piezoelectricity of fatigued samples is illustrated in Fig. 3.

After sufficient recovery, the  $d_{33}$  coefficients obtained by means of piezoelectrical measurement are 94%, 78%, and 64% of their initial values for samples subjected to  $10^3$ ,  $1.6 \times 10^4$ , and  $4 \times 10^5$  cycles of the fatigue voltage, respectively. As can be seen from Fig. 3, the  $d_{33}$  coefficient of fatigued samples shows a quick decrease during the first day of storage. Even for the sample with only  $10^3$  cycles of fatigue,  $d_{33}$  decreases to about 83% of its initial value after 1 day of storage under laboratory conditions. The higher the number of fatigue cycles applied to the sample, the worse the stability of the  $d_{33}$  coefficient. After the same period of storage,  $d_{33}$  decays to about 53% and 24% of the respective initial values for samples subjected to  $1.6 \times 10^4$  and  $4 \times 10^5$  cycles of the fatigue voltage, respectively. For longer storage times,  $d_{33}$  decreases more slowly and finally reaches a stable value. For comparison, the  $d_{33}$  decay of a freshly charged film is also shown in Fig. 3. In this case, a fresh sample, charged once with +7 kV for 5 s, was stored under laboratory conditions, and its  $d_{33}$  was determined by means of DRS from time to time. The  $d_{33}$  coefficient remains at about 97% of its initial value after one week of storage. Thus, good temporal stability is confirmed for freshly charged films, in good agreement with previous studies.<sup>36</sup>

Although the effective polarization and other related properties of ferroelectrets are phenomenologically similar to those of typical ferroelectrics, the internal charge trapping and de-trapping are the same as in non-voided space-charge electrets. A good space-charge electret usually has extremely high resistivity because of (1) very high chemical purity and (2) the existence of numerous deep trapping centers. In polymer electrets, deep traps are associated with intra-chain interactions and other internal chain modifications (primary forces, “chemical traps”), whereas shallow traps are related to inter-chain interactions and other external effects (secondary forces, “physical traps”).<sup>37</sup> It is known that structural defects such as carbonyl groups or double bonds yield shallow or intermediate trapping levels.<sup>26</sup> During the fatigue process, chain scission and surface oxidation caused by plasma-polymer interactions result in the destruction of intrinsic and relatively deep traps and introduce shallower traps at the inner surfaces of the voids. In addition, the formation of polar low-molecular-weight oxidized material on the inner surfaces of the voids leads to a decrease of the surface resistivity in those voids. Kumar *et al.* found that the surface resistivity of PP decreases by more than 3 orders of magnitude after a plasma treatment in air.<sup>38</sup> Consequently, the charges can diffuse along the surface more easily after they have been de-trapped, and they eventually recombine with charges of opposite polarity. Because the space charges are trapped at the inner surfaces of ferroelectrets, these mechanisms explain the deterioration of the chargeability of voids and the inferior stability of the  $d_{33}$  coefficient on fatigued films. Further investigations are under way in order to determine which of the aforementioned or possible other mechanisms are relevant and to which extent each one contributes to the observed behavior.

#### D. Plasma-polymer interaction: Dependence of the fatigue rate on the applied electric field and the number of cycles

In order to determine the dependence of the fatigue rate on the driving voltage and the number of fatigue cycles, a series of samples were fatigued with different driving voltages  $V_{pp}$ . The recovery of the chargeability of the voids and the instability of the  $d_{33}$  coefficients in ferroelectret films after fatigue should be taken into consideration. Experimental procedures similar to those illustrated in Fig. 3 were carried out, i.e., the initial  $d_{33}$  coefficients were determined by means of piezoelectrical measurements, fatigue processes with preset  $V_{pp}$  and  $N$  values were implemented, and the samples were charged 1 day after the fatigue process. According to Fig. 1, 1 day of storage under laboratory conditions after fatigue is sufficient for a recovery of the chargeability of the voids. After charging, the samples were stored under laboratory conditions for 1 week, and the  $d_{33}$  coefficients were then determined solely by means of DRS. According to Fig. 3, the  $d_{33}$  coefficients thereby obtained represent stable values that the fatigued samples can hold for long times. Figure 4 shows the  $d_{33}$  coefficient as a function of the number of cycles for different  $V_{pp}$  values as indicated. For ferroelectric polymer films, the polarization fatigue follows a universal scaling

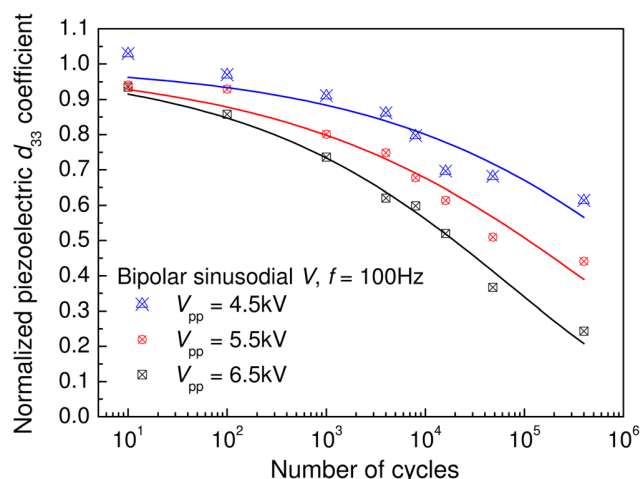


FIG. 4. (Color online) Normalized piezoelectric  $d_{33}$  coefficient as a function of the logarithm of the number of driving-voltage cycles ( $N$ ). Fatigue was achieved by means of a bipolar sinusoidal voltage with a frequency of 100 Hz and various amplitudes as indicated. The solid lines are fitted to a stretched exponential as presented in Eq. (4).

behavior with  $N/f$ , indicating that the fatigue rate is proportional to the total time of exposure to the driving voltage.<sup>21</sup> There, a stretched exponential function with two parameters—a characteristic decay time  $\tau$  and a stretching factor  $\beta$ —is used to fit the experimental data. For films made from ferroelectric ceramics, the frequency dependence of fatigue is more complex. Scaling behavior with  $N/f$  or with  $N/f^2$  was reported, but in some other cases no frequency dependence was observed for the fatigue.<sup>17</sup> However, the fatigue rate of cellular PP ferroelectrets depends mainly on the amplitude and the number of cycles of the driving voltage, and the frequency and the waveform do not have a strong influence.<sup>27</sup> This prompts us to fit the experimental data using an empirical stretched exponential of the form

$$d_{33} = d_{33}^{\text{ini}} e^{-(N/N_0)^\beta}, \quad (4)$$

where  $d_{33}^{\text{ini}}$  is the initial  $d_{33}$  coefficient of a freshly charged film,  $\beta$  is a stretching factor that lies between 0 and 1, and  $N_0$  is the number of cycles for which the  $d_{33}$  coefficient has fallen to  $1/e$  of its initial value. Stretched exponentials, also known as Kohlrausch-Williams-Watts functions, are invoked in a wide range of physical phenomena.<sup>39,40</sup> As can be seen from Fig. 4, at least up to the number of cycles studied here, the experimental data can be fitted reasonably well with the proposed equation, especially for  $V_{pp} = 6.5$  kV. From the fits, values of  $N_0 = 3.6 \times 10^6$ ,  $5.1 \times 10^5$ , and  $7.5 \times 10^4$ , and of  $\beta = 0.26$ ,  $0.24$ , and  $0.27$ , are determined for  $V_{pp}$  values of 4.5, 5.5, and 6.5 kV, respectively.  $N_0$  decreases with  $V_{pp}$  as expected, because more and more voids are subjected to DBDs at higher  $V_{pp}$  values.  $\beta$  does not vary much with  $V_{pp}$ , because the same physical mechanisms are expected to be responsible for the fatigue in all three cases.

Figure 4 also shows that the effect of the number of fatigue cycles on the deterioration of cellular PP ferroelectrets is quite severe. With a voltage sufficiently high for charging—for instance, 5.5 kV—the number of cycles for the onset of fatigue, defined as the number of cycles at which



$d_{33}$  has been reduced to 90% of its initial value, is only about 100 or less. This number of cycles is extremely low as compared to the corresponding number for ferroelectric thin films. The number of cycles for the onset of fatigue, in particular in thin inorganic ferroelectrics, is usually about  $10^5$ ,<sup>17</sup> a number at which most of the piezoelectricity would already have been lost in cellular PP ferroelectrets. Therefore, we have to conclude that cellular PP ferroelectrets are not good candidates for applications involving polarization reversal, at least in an ambient atmospheric environment. In recent years, a number of polymers have been employed in ferroelectrets. So far, ferroelectrets have been successfully developed with poly(ethylene terephthalate),<sup>41,42</sup> poly(ethylene naphthalene-2,6-dicarboxylate),<sup>43,44</sup> cyclo-olefine copolymers,<sup>45</sup> and fluoropolymers.<sup>35,46–49</sup> The consequences of plasma-polymer interactions might be different for different polymers. For example, an oxygen-plasma treatment of polytetrafluoroethylene can improve the stability of a negative charge.<sup>50</sup> Therefore, studies similar to the present investigation should be carried out on ferroelectrets made of different polymers if they are intended for applications that require polarization reversal.

### E. Avoiding fatigue in device operation: Removal of the internal gas

In applications such as sensors and actuators, effective polarization fatigue in ferroelectret polymers might lower the sensitivity of the devices, in particular for higher signal amplitudes, and should thus be avoided. Because effective polarization fatigue in cellular PP ferroelectrets is caused by plasma-polymer interactions at the inner surfaces of voids, it should be absent when the voids are essentially empty, i.e., when the voids contain a vacuum. One of our previous studies shows that air molecules can diffuse through the polymer walls around the voids.<sup>51</sup> Consequently, vacuum or air at a preset pressure can be introduced into the voids.

In order to check the consequences of evacuating cellular polymer ferroelectrets, PP samples were placed in a pressure chamber connected to a pumping system and subjected to consecutive vacuum and atmospheric-air environments. Here, a two-stage oil-sealed rotary-vane vacuum pump from Oerlikon Leybold Vacuum was used to provide a vacuum below 10 Pa in the test chamber. The electrical capacitance of the sample was measured *in situ* during vacuum pumping of the chamber (period  $t_I$ ) and the subsequent restoration to laboratory conditions (period  $t_{II}$ ) in order to monitor thickness changes in the sample.<sup>52,53</sup> A sudden drop (or increase) of the capacitance is observed upon evacuation (or restoration to laboratory conditions) of the chamber due to the pressure difference between the voids and the chamber. However, after a sufficient waiting time (typically several hours), the capacitance recovers approximately to the initial value in both cases. This clearly shows that the internal and external pressures equalize due to gas diffusion.

In order to study the effective polarization fatigue under vacuum and atmospheric conditions, respectively, two samples were subjected to the above-mentioned vacuum pumping followed by restoration to atmospheric-air conditions,

and their respective initial  $d_{33}$  coefficients were obtained via piezoelectrical measurements. For one of the samples, a preset number of driving-voltage cycles (at a frequency of 100 Hz and a  $V_{pp}$  of 5.5 kV) were applied at the time  $t = t_I$  (i.e., the voids contain vacuum). The  $d_{33}$  coefficient was determined by means of a piezoelectrical measurement after  $t = t_I + t_{II}$ . For the other sample, the fatigue voltage was applied at  $t = t_I + t_{II}$  (i.e., the voids contain atmospheric air), and then the  $d_{33}$  coefficient was measured via a piezoelectrical measurement. The normalized  $d_{33}$  coefficient as a function of the number of voltage cycles is shown in Fig. 5 for both samples.

Obviously, the  $d_{33}$  coefficient does not deteriorate if the driving voltage is applied under vacuum. This is expected, as the reason for the effective polarization fatigue, as discussed above, is the plasma-polymer interaction caused by repeated DBDs inside the voids. Under vacuum, no DBDs are generated by the application of the driving voltage, and thus the  $d_{33}$  coefficient is not reduced. In this case, the electrical aging of PP itself under the driving voltage plays a dominant role. The electrical aging of polymers is a gradual degradation of the chemical structure resulting from electrical stresses.<sup>54</sup> Prior studies show that electrical aging of PP is not observed during the first 10 h of exposure to an ac electric field of 83.3 MV/m at 50 Hz (i.e.,  $1.8 \times 10^6$  cycles).<sup>55,56</sup> For the cellular PP samples used in this study, a  $V_{pp}$  of about 11.6 kV, corresponding to the above-mentioned electric field, can be calculated as follows:<sup>51</sup>

$$V = E_p(d_p + \epsilon_p d_g), \quad (5)$$

where  $d_p \approx 31 \mu\text{m}$  is the accumulated thickness of the PP layers,  $d_g \approx 49 \mu\text{m}$  is the accumulated height of the voids, and  $\epsilon_p = 2.2$  is the dielectric permittivity of the solid (non-cellular) polymer. More detailed discussions of the electrical aging in PP itself are, however, beyond the scope of this paper.

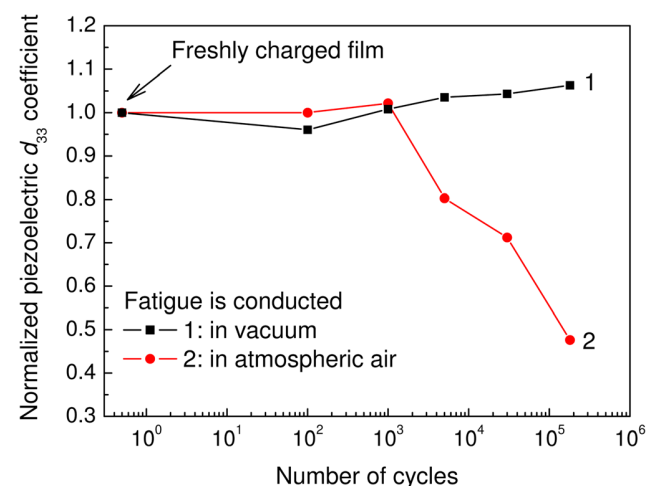


FIG. 5. (Color online) Normalized piezoelectric  $d_{33}$  coefficient as a function of the number of driving-voltage cycles. The squares indicate the sample to which the driving-voltage cycles were applied when the voids had been evacuated, and the circles represent the sample to which the driving-voltage cycles were applied when the voids were filled with atmospheric air. The  $d_{33}$  values for cycle numbers below  $10^0$  were observed on freshly charged films.

It should be pointed out that the experimental procedures for curve 2 in Fig. 5 are different from those for Fig. 4 because of the vacuum treatment. For the results shown in Fig. 5, fatigue processes with increasing numbers of driving-voltage cycles are consecutively applied to the same sample, and for each  $N$ , the  $d_{33}$  coefficient is determined by means of a piezoelectrical measurement immediately after the fatigue process. Therefore, the recovery of the chargeability of the voids and the deterioration of the stability of the piezoelectricity after fatigue are not taken into account in Fig. 5. Nevertheless, from curve 2 in Fig. 5, one can see obvious fatigue of the piezoelectricity when more than  $10^3$  fatigue cycles are applied in atmospheric air. Our results indicate that effective polarization fatigue from repeated DBDs can be avoided if ferroelectrets are used in vacuum environments, such as, for example, in outer space or in vacuum-related devices.

#### IV. CONCLUSION

In this paper, some additional light was shed on the advantages and disadvantages of fatigue processes caused by the repeated charging or poling of cellular polymer ferroelectrets. Dielectric barrier discharges in the voids of ferroelectrets generate a physico-chemically active plasma. Due to memory effects, repeated DBDs can facilitate the charging process in cellular PP ferroelectrets. For example, it was found that the threshold voltage can be reduced by up to 50% and that the charging efficiency is obviously improved after only  $10^3$  DBD cycles. However, the micro-plasma phenomena of the DBDs modify the inner polymer surfaces through chain scission and surface oxidation, and thus deteriorate the chargeability of the voids, leading to polarization fatigue. After storage of the samples for significant time periods under laboratory conditions, the chargeability of the voids might recover at least partially. However, after even a moderate number of fatigue cycles, the stability of the piezoelectricity in cellular PP ferroelectrets can be much worse than that of freshly charged film. The piezoelectric  $d_{33}$  coefficient that fatigued films can hold quasi-permanently decays according to a stretched exponential function that directly depends on the number of alternating cycles of the driving voltage. Effective polarization fatigue from repeated DBDs can be avoided if the air molecules inside the voids are removed by means of vacuum pumping. In total, the results presented here will help not only to improve the applications-relevant behavior of cellular ferroelectrets, but also to provide a deeper understanding of the underlying physico-chemical processes.

#### ACKNOWLEDGMENTS

We are indebted to the European Union for co-funding some of the essential equipment used in our work.

<sup>1</sup>R. Gerhard(-Mulhaupt), *IEEE Trans. Dielectr. Electr. Insul.* **9**, 850 (2002).

<sup>2</sup>S. Bauer, R. Gerhard(-Mulhaupt), and G. M. Sessler, *Phys. Today* **57**(2), 37 (2004).

<sup>3</sup>M. Wegener and S. Bauer, *ChemPhysChem* **6**, 1014 (2005).

<sup>4</sup>X. Qiu, *J. Appl. Phys.* **108**, 011101 (2010).

- <sup>5</sup>X. Qiu, R. Gerhard, and A. Mellinger, *IEEE Trans. Dielectr. Electr. Insul.* **18**, 34 (2011).
- <sup>6</sup>M. Lindner, S. Bauer-Gogonea, S. Bauer, M. Paajanen, and J. Raukola, *J. Appl. Phys.* **91**, 5283 (2002).
- <sup>7</sup>M. Wegener, M. Paajanen, W. Wirges, and R. Gerhard(-Mulhaupt), in *Proceedings of the 10th International Symposium on Electrets, Delphi, Greece, 22–24 September 1999* (IEEE, New York, 1999), pp. 54–57.
- <sup>8</sup>R. Gerhard(-Mulhaupt), W. Wegener, W. Wirges, J. A. Giacometti, R. A. C. Altafim, L. E. Santos, R. M. Faria, and M. Paajanen, in *Annual Report Conference on Electrical Insulation and Dielectric Phenomena, Cancun, Mexico, 20–24 October 2002* (IEEE, New York, 2002), pp. 299–302.
- <sup>9</sup>P. Zhang, Z. Xia, X. Qiu, F. Wang, and X. Wu, in *Proceedings of the 12th International Symposium on Electrets, Salvador, Brazil, 11–14 September 2005* (IEEE, New York, 2005), pp. 39–42.
- <sup>10</sup>X. Qiu, A. Mellinger, M. Wegener, W. Wirges, and R. Gerhard, *J. Appl. Phys.* **101**, 104112 (2007).
- <sup>11</sup>X. Qiu, A. Mellinger, W. Wirges, and R. Gerhard, *Appl. Phys. Lett.* **91**, 132905 (2007).
- <sup>12</sup>S. Zhukov and H. von Seggern, *J. Appl. Phys.* **101**, 084106 (2007).
- <sup>13</sup>S. Zhukov and H. von Seggern, *J. Appl. Phys.* **102**, 044109 (2007).
- <sup>14</sup>M. Paajanen, H. Välimäki, and J. Leikkala, in *Proceedings of the 10th International Symposium on Electrets, Delphi, Greece, 22–24 September 1999* (IEEE, New York, 1999), pp. 735–738.
- <sup>15</sup>G. M. Sessler and J. Hillenbrand, *Appl. Phys. Lett.* **75**, 3405 (1999).
- <sup>16</sup>X. Qiu, R. Gerhard, and A. Mellinger, *IEEE Trans. Dielectr. Electr. Insul.* **17**, 1043 (2010).
- <sup>17</sup>X. J. Lou, *J. Appl. Phys.* **105**, 024101 (2009).
- <sup>18</sup>D. C. Lupascu, *Fatigue in Ferroelectric Ceramics and Related Issues* (Springer, Berlin, 2010).
- <sup>19</sup>I. L. Guy, A. Limbong, Z. Zheng, and D. K. Das-Gupta, *IEEE Trans. Dielectr. Electr. Insul.* **7**, 489 (2000).
- <sup>20</sup>T. Furukawa, T. Nakajima, and Y. Takahashi, *IEEE Trans. Dielectr. Electr. Insul.* **13**, 1120 (2006).
- <sup>21</sup>G. Zhu, Z. Zeng, L. Zhang, and X. Yan, *Appl. Phys. Lett.* **89**, 102905 (2006).
- <sup>22</sup>Z. Zeng, G. Zhu, R. Liu, Q. Zhang, and X. Yan, *Microelectron. Eng.* **85**, 2187 (2008).
- <sup>23</sup>K. Zaitso, S. Lee, K. Ishibe, T. Sekitani, and T. Someya, *J. Appl. Phys.* **107**, 114506 (2010).
- <sup>24</sup>G. Borcia, C. A. Anderson, and N. M. D. Brown, *Plasma Sources Sci. Technol.* **12**, 335 (2003).
- <sup>25</sup>F. Leroux, C. Campagne, A. Perwuelz, and L. Gengembre, *J. Colloid Interface Sci.* **328**, 412 (2008).
- <sup>26</sup>G. M. Sessler, *Electrets*, 3rd ed. (Springer, New York, 1999).
- <sup>27</sup>X. Qiu and R. Gerhard, *Appl. Phys. Lett.* **93**, 152902 (2008).
- <sup>28</sup>A. Savolainen and K. Kirjavainen, *J. Macromol. Sci., Chem. A* **26**, 583 (1989).
- <sup>29</sup>M. Wegener, W. Wirges, J. Fohlmeister, B. Tiersch, and R. Gerhard (-Mulhaupt), *J. Phys. D: Appl. Phys.* **37**, 623 (2004).
- <sup>30</sup>G. S. Neugschwandtner, R. Schwödauier, M. Vieytes, S. Bauer-Gogonea, S. Bauer, J. Hillenbrand, R. Kressmann, G. M. Sessler, M. Paajanen, and J. Leikkala, *Appl. Phys. Lett.* **77**, 3827 (2000).
- <sup>31</sup>H. Ohigashi, *J. Appl. Phys.* **47**, 949 (1976).
- <sup>32</sup>A. Mellinger, *IEEE Trans. Dielectr. Electr. Insul.* **10**, 842 (2003).
- <sup>33</sup>F. Massines, N. Gherardi, N. Naudé, and P. Ségur, *Eur. Phys. J.: Appl. Phys.* **47**, 22805 (2009).
- <sup>34</sup>Y. B. Golubovskii, V. A. Maiorov, J. Behnke, and J. F. Behnke, *J. Phys. D: Appl. Phys.* **35**, 751 (2002).
- <sup>35</sup>R. A. P. Altafim, X. Qiu, W. Wirges, R. Gerhard, R. A. C. Altafim, H. C. Basso, W. Jenninger, and J. Wagner, *J. Appl. Phys.* **106**, 014106 (2009).
- <sup>36</sup>A. Mellinger, M. Wegener, W. Wirges, R. Reddy Mallepally, and R. Gerhard(-Mulhaupt), *Ferroelectrics* **331**, 189 (2006).
- <sup>37</sup>F. Camacho González, “Charge-storage mechanisms in polymer electrets,” Ph.D. dissertation, University of Potsdam, 2006.
- <sup>38</sup>R. Kumar, R. K. Singh, M. Kumar, and S. K. Barthwal, *J. Appl. Polym. Sci.* **104**, 767 (2007).
- <sup>39</sup>A. C. Campbell and B. G. Streetman, *Appl. Phys. Lett.* **54**, 445 (1989), and references therein.
- <sup>40</sup>A. K. Jonscher, *Universal Relaxation Law* (Chelsea Dielectrics, London, 1996).
- <sup>41</sup>M. Wegener, W. Wirges, and R. Gerhard(-Mulhaupt), *Adv. Eng. Mater.* **7**, 1128 (2005).
- <sup>42</sup>W. Wirges, M. Wegener, O. Voronina, L. Zirkel, and R. Gerhard(-Mulhaupt), *Adv. Funct. Mater.* **17**, 324 (2007).

- <sup>43</sup>P. Fang, M. Wegener, W. Wirges, R. Gerhard, and L. Zirkel, *Appl. Phys. Lett.* **90**, 192908 (2007).
- <sup>44</sup>P. Fang, W. Wirges, M. Wegener, L. Zirkel, and R. Gerhard, *e-Polymers* **43** (2008).
- <sup>45</sup>E. Saarimäki, M. Paajanen, A. M. Savijärvi, H. Minkkinen, M. Wegener, O. Voronina, R. Schulze, W. Wirges, and R. Gerhard(-Mulhaupt), *IEEE Trans. Dielectr. Electr. Insul.* **13**, 963 (2006).
- <sup>46</sup>O. Voronina, M. Wegener, W. Wirges, R. Gerhard, L. Zirkel, and H. Münstedt, *Appl. Phys. A* **90**, 615 (2008).
- <sup>47</sup>R. A. C. Altafilm, H. C. Basso, R. A. P. Altafilm, L. Lima, C. V. de Aquino, L. Gonçalves Neto, and R. Gerhard(-Mulhaupt), *IEEE Trans. Dielectr. Electr. Insul.* **13**, 979 (2006).
- <sup>48</sup>X. Zhang, J. Hillenbrand, and G. M. Sessler, *J. Appl. Phys.* **101**, 054114 (2007).
- <sup>49</sup>X. Zhang, G. Cao, Z. Sun, and Z. Xia, *J. Appl. Phys.* **108**, 064113 (2010).
- <sup>50</sup>Q. Chen, *J. Phys. D: Appl. Phys.* **35**, 2939 (2002).
- <sup>51</sup>X. Qiu, A. Mellinger, and R. Gerhard, *Appl. Phys. Lett.* **92**, 052901 (2008).
- <sup>52</sup>J. Leonhartsberger, H. Salhofer, R. Schwödauer, S. Bauer-Gogonea, S. Bauer, R. Forstner, G. Eder, M. Paajanen, H. Minkkinen, and J. Raunkola, *Ferroelectrics* **331**, 181 (2006).
- <sup>53</sup>S. Bauer-Gogonea, F. Camacho González, R. Schwödauer, B. Ploss, and S. Bauer, *Appl. Phys. Lett.* **91**, 122901 (2007).
- <sup>54</sup>K. C. Kao, *J. Appl. Phys.* **55**, 752 (1984).
- <sup>55</sup>D. Liufu, X. S. Wang, D. M. Tu, and K. C. Kao, *J. Appl. Phys.* **83**, 2209 (1998).
- <sup>56</sup>Z. Li, Y. Yin, X. Wang, D. M. Tu, and K. C. Kao, *J. Appl. Polym. Sci.* **89**, 3416 (2003).



# Turning Polymer Foams or Polymer-Film Systems into Ferroelectrets: Dielectric Barrier Discharges in Voids

**Xunlin Qiu, Reimund Gerhard**

Institute of Physics and Astronomy, University of Potsdam,  
Karl-Liebknecht-Strasse 24-25, 14476 Potsdam-Golm, Germany

and **Axel Mellinger**

Department of Physics, Central Michigan University,  
Mount Pleasant, MI 48859, USA

## ABSTRACT

Polymer foams and void-containing polymer-film systems with internally charged voids combine large piezoelectricity with mechanical flexibility and elastic compliance. This new class of soft materials (often called ferro- or piezoelectrets) has attracted considerable attention from science and industry. It has been found that the voids can be internally charged by means of dielectric barrier discharges (DBDs) under high electric fields. The charged voids can be considered as man-made macroscopic dipoles. Depending on the ferroelectret structure and the pressure of the internal gas, the voids may be highly compressible. Consequently, very large dipole-moment changes can be induced by mechanical or electrical stresses, leading to large piezoelectricity. DBD charging of the voids is a critical process for rendering polymer foams piezoelectric. Thus a comprehensive exploration of DBD charging is essential for the understanding and the optimization of piezoelectricity in ferroelectrets. Recent studies show that DBDs in the voids are triggered when the internal electric field reaches a threshold value according to Townsend's model of Paschen breakdown. During the DBDs, charges of opposite polarity are generated and trapped at the top and bottom internal surfaces of the gas-filled voids, respectively. The deposited charges induce an electric field opposite to the externally applied one and thus extinguish the DBDs. Back discharges may eventually be triggered when the external voltage is reduced or turned off. In order to optimize the efficiency of DBD charging, the geometry (in particular the height) of the voids, the type of gas and its pressure inside the voids are essential factors to be considered and to be optimized. In addition, the influence of the plasma treatment on the internal void surfaces during the DBDs should be taken into consideration.

Index Terms — Ferroelectret, piezoelectret, dielectric barrier discharge (DBD), effective polarization, man-made dipole.

## 1 INTRODUCTION

**CELLULAR** polymers (polymer foams) were first produced during the 1960s [1]. They are now widely used for thermal insulation, shock and sound absorption, packaging, etc. Over the past 15 years, a considerable number of cellular or void-containing polymer-electret systems with significant piezoelectricity have been identified and developed. This novel class of polymer materials not only presents new challenges and chances for materials and device engineering, but also represents a new paradigm of piezo-, pyro- and ferroelectricity in soft matter. The new electroactive materials

have been named ferroelectrets. They attract considerable attention in fundamental research and are considered or employed for applications in e.g. ultrasonic receivers and transmitters, microphones and microphone arrays, curved or flat loudspeakers, electromechanical sensors and actuators, etc. For details of the history and of the recent development in this field, the reader may consult relevant review papers and the original literature cited therein [2-6].

The microscopic origin of piezo-, pyro- and ferroelectricity in ferroelectrets is significantly different from that of polar polymer ferroelectrics containing intrinsic dipoles. In order to render polymer foams piezoelectric, the voids must be internally charged under high electric fields. The charging process in ferroelectrets requires dielectric barrier discharges

---

*Manuscript received on 9 August 2010, in final form 14 September 2010.*

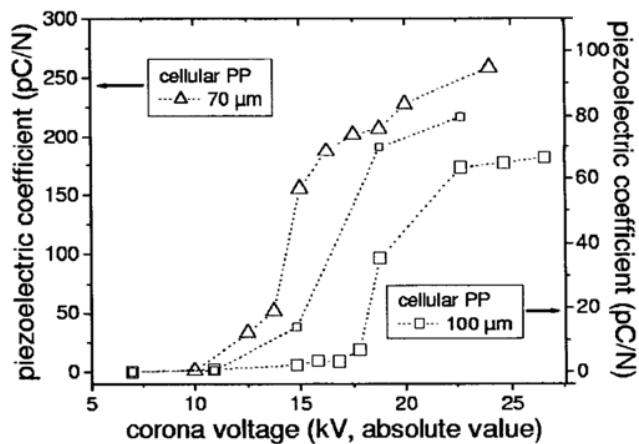


**Figure 1.** Piezoelectric  $d_{33}$  coefficient as a function of corona-charging voltage for positively charged 70  $\mu\text{m}$  thick (triangles) cellular PP as well as for positively (larger symbols) or negatively (smaller symbols) charged 100  $\mu\text{m}$  thick (squares) cellular PP [9].

(DBDs). In DBDs, at least one side of the discharge gap is insulated from the electrodes by a dielectric layer [7]. It is found that charges of opposite polarity are separated during charging and then trapped, respectively, at the internal top and bottom surfaces of the voids. Each charged void can thus be considered as a man-made macroscopic dipole, whose direction can be reversed by sufficiently high electric fields [8]. The macroscopic dipoles can be easily deformed under mechanical and electrical stresses, resulting in very large direct and inverse piezoelectricity, respectively. Depending on the material structures and the charging conditions, ferroelectrets often show piezoelectric  $d_{33}$  coefficients of hundreds of pC/N.

It has become evident that a comprehensive exploration of DBD charging is critical for understanding and optimizing the piezoelectricity of ferroelectrets. In recent years, the knowledge about the charging process in ferroelectrets has significantly advanced. Here, a brief overview on DBD charging of ferro- and piezoelectrets is provided, and recent results concerning the light emission from the DBDs in ferroelectret systems are reported and discussed.

## 2 THRESHOLD BEHAVIOR AND MODEL OF THE INTERNAL ELECTRICAL BREAKDOWN

The voltage dependence of the DBD charging process and the resulting piezoelectric  $d_{33}$  coefficient in ferroelectrets shows a threshold behavior as clearly seen in Figure 1, where the  $d_{33}$  coefficients of cellular-polypropylene (PP) ferroelectrets with different thicknesses are plotted as a function of the corona-charging voltage [9]. In corona charging, the internal electric field in the voids is controlled by the surface potential of the sample. The  $d_{33}$  coefficients remain nearly zero for corona voltages below the threshold. For positively charged 70  $\mu\text{m}$  thick cellular PP, a threshold voltage above 10 kV is observed. For positively and negatively charged 100  $\mu\text{m}$  thick cellular PP, the threshold corona voltages are above +17.5 and below -11 kV,

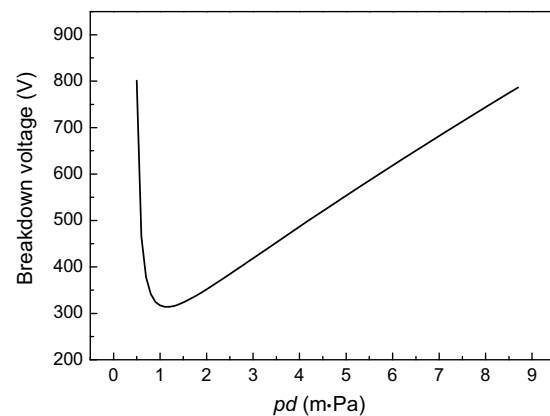


**Figure 2.** Paschen breakdown voltage of air as a function of the product  $pd$ .

respectively. The  $d_{33}$  coefficients increase dramatically with increasing corona voltage above the threshold. The threshold behavior is also confirmed in direct-contact charging experiments on the same types of cellular PP [10]. In direct-contact charging, the internal electric field in the voids is induced directly by the external voltage applied to the sample electrodes that had been deposited by vacuum evaporation prior to charging. For direct-contact charging, threshold voltages of -6 and -6.5 kV are observed on 70 and 100  $\mu\text{m}$  thick cellular PP films, respectively.

The threshold behavior can be explained with Paschen's law which describes the breakdown voltage between parallel plates in a gas as a function of pressure and gap height. According to Townsend's model, the critical breakdown voltage of common gases in a uniform electric field is a function of both gas pressure  $p$  and electrode spacing  $d$  (which is equal to the void height in the present context) [11]

$$V = \frac{Apd}{B + \ln(pd)} \quad (1)$$

where  $V$  is the breakdown voltage in Volt,  $p$  is the pressure in Pascal, and  $d$  is the gap height in m. The parameter  $B$  is given by

$$B = \ln\left(\frac{C}{\ln(1+1/\gamma)}\right) \quad (2)$$

The constants  $A$  and  $C$  depend on the composition of the gas. For air, the values  $A = 273.8 \text{ Vm}^{-1}\text{Pa}^{-1}$  and  $C = 11 \text{ m}^{-1}\text{Pa}^{-1}$  are experimentally determined.  $\gamma = 0.01$  is the so-called second ionization coefficient. Figure 2 shows the breakdown voltage in air as a function of the product  $pd$ . The Paschen breakdown voltage must be reached in the voids in order to ignite dielectric barrier discharges. Consequently, there exists a threshold charging voltage for inducing piezoelectricity in polymer foams. The effective charging field at the threshold is an analogue to the coercive field in ferroelectric materials. However, the mechanism for polarization is quite different: The polarization in ferroelectrics relies on the orientation of intrinsic dipoles, while the polarization in ferroelectrets requires charge separation during the DBDs and charge trapping on the internal surfaces of the voids.

The charging process was theoretically analyzed with a simplified model for the piezoelectricity of ferroelectrets [12, 13]. The model consists of  $n$  layers of polymer separated by  $(n-1)$  layers of gas [14, 15]. The relative dielectric constants, thicknesses and the electric fields of the polymer and the gas layers are  $\epsilon_{pr}$ ,  $d_{pi}$ ,  $E_{pi}$  and  $\epsilon_{gr}$ ,  $d_{gi}$ ,  $E_{gi}$ , respectively. The equivalent charge densities at the interfaces of gas and polymer are  $\pm\sigma_i$ , while  $\sigma_0$  and  $-\sigma_0$  are the charge densities induced on the electrodes. For simplicity, the thickness of each gas layer as well as the charges trapped at the gas/polymer interfaces are assumed not to vary across the sample ( $d_{g1} = d_{g2} = \dots = d_{g(n-1)}$  and  $\sigma_1 = \sigma_2 = \dots = \sigma_n$ ). The piezoelectric  $d_{33}$  coefficient calculated from such a simplified model is given by [14]

$$d_{33} = \frac{\epsilon_{gr}\epsilon_{pr}d}{Y} \frac{d_p \sum d_{gi}\sigma_i}{d_g(\epsilon_{gr}d_p + \epsilon_{pr}d_g)^2}. \quad (3)$$

When an external voltage  $V$  is applied, the electric field in the  $i^{\text{th}}$  gas layer is given by [15]

$$E_{gi} = \frac{\epsilon_0\epsilon_{pr}V - \sigma_i d_p}{\epsilon_0\epsilon_{gr}d_p + \epsilon_0\epsilon_{pr}d_g}, \quad (4)$$

where  $d_p = \sum_{i=1}^n d_{pi}$  and  $d_g = \sum_{i=1}^{n-1} d_{gi}$  are the total thicknesses of all the polymer layers and all the gas layers, respectively.

We consider the case where a linearly increasing voltage  $V$  is applied to a fresh sample [12, 13]. Initially,  $\sigma_i = 0$  when  $E_{gi}$  is lower than the threshold for Paschen breakdown  $E_{th}$ .  $E_{gi}$  increases with increasing  $V$ , and Paschen breakdown is ignited when the field becomes higher than  $E_{th}$ , leading to a non-zero  $\sigma_i$ . The voltage corresponding to  $E_{th}$  is

$$V_{th} = E_{th} \left( \frac{\epsilon_{gr}}{\epsilon_{pr}} d_p + d_g \right). \quad (5)$$

During Paschen breakdown inside the voids, separated charges of opposite polarity are trapped on the internal top and bottom surfaces of the voids, respectively. The trapped charges partly compensate the applied electric field, and the breakdown is extinguished when  $E_{gi}$  decreases back to  $E_{th}$ , which is known as choking effect in conventional DBDs. When  $V$  is further increased, however, the breakdown process continues and  $\sigma_i$  increases continuously until the extinguishing condition  $E_{gi} = E_{th}$  is again met. At this point,  $\sigma_i$  is still determined by Equation (4). Substitution into Equation (3) yields the piezoelectric coefficient

$$d_{33} = \frac{\epsilon_{gr}\epsilon_{pr}d}{Y} \frac{\epsilon_0\epsilon_{pr}(V - V_{th})}{(\epsilon_{gr}d_p + \epsilon_{pr}d_g)^2}. \quad (6)$$

If the electric field generated by the trapped charges is higher than  $E_{th}$ , it is obvious that DBDs in the opposite direction (back discharges) will be triggered when the external voltage is turned off. The minimum voltage required for the occurrence of back discharges is

$$V = 2E_{th} \left( \frac{\epsilon_{gr}}{\epsilon_{pr}} d_p + d_g \right) = 2V_{th} \quad (7)$$

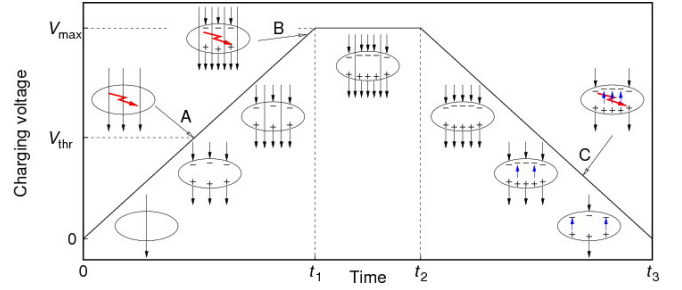


**Figure 3.** Schematic view of the DBD charging process in a single polymer void. When the charging voltage reaches the threshold value  $V_{th}$ , Paschen breakdown is ignited (A). At higher voltages, a second discharge may occur (B). During ramping down the voltage, the reverse electric field from the trapped space charges may lead to back discharges (C) [17].

Again, the back discharges are extinguished when  $E_{gi} = E_{th}$ . Note that  $E_{gi}$  now has opposite sign and direction as the previous  $E_{gi}$  under the externally applied voltage. Thus,  $E_{th}$  determines the maximum value of  $\sigma_i$  that can be attained after charging with a given external voltage  $V$ . From these considerations, the piezoelectric  $d_{33}$  coefficient to be found in ferroelectrets after charging is described by

$$d_{33} = \begin{cases} 0, & (V < V_{th}) \\ k(V - V_{th}), & (V_{th} \leq V \leq 2V_{th}) \\ kV_{th}, & (V > 2V_{th}) \end{cases} \quad (8)$$

where the factor  $k$  is given by

$$k = \frac{\epsilon_0\epsilon_{gr}\epsilon_{pr}^2 d}{Y(\epsilon_{gr}d_p + \epsilon_{pr}d_g)^2} \quad (9)$$

As can be seen from Equation (8), the  $d_{33}$  coefficient of ferroelectrets remains zero when the charging voltage  $V$  is lower than the threshold value  $V_{th}$ . For voltages above the threshold,  $d_{33}$  increases linearly with  $V$  until the latter reaches  $2V_{th}$ . For charging voltages  $V$  higher than  $2V_{th}$ , the  $d_{33}$  coefficient does not increase anymore. It always assumes the constant saturation value. Our experimental results show

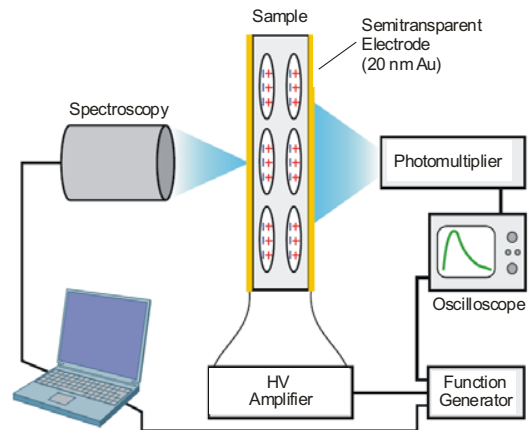


**Figure 4.** Schematic setup for a spectroscopic analysis of the dielectric barrier discharges (DBDs) in the voids of ferroelectrets [20, 21].

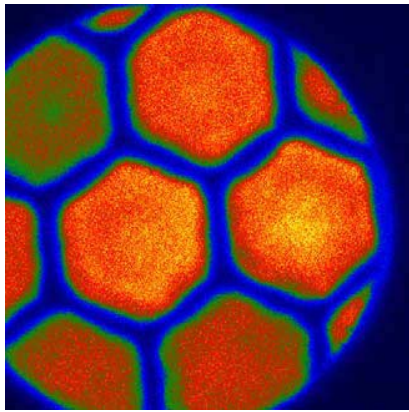


**Figure 5.** Color-coded EM-CCD image of a polycarbonate ferroelectret system with hexagonal voids under a positive sinusoidal voltage (frequency of 100 Hz and peak-to-peak value  $V_{pp}$  of 3 kV). The EM-CCD camera is internally triggered with an exposure time of 5 s [22].

reasonable agreement with the theoretical analysis, while a small deviation is attributed to the wide distribution of void sizes and shapes [12]. Zhukov and von Seggern suggested a similar analysis for layered fluoropolymer ferroelectrets (FEP-ePTFE-FEP sandwiches) [16].

More recently, a schematic model for the DBD charging process in ferroelectrets has been proposed, as shown in Figure 3 [17]. Internal breakdown (Paschen breakdown) in the voids is initiated when the voltage reaches the required threshold value (in this sense, the electric field in the voids is comparable with the “coercive field” in ferroelectrics). Charges of opposite polarity are separated during the DBDs and are subsequently trapped on the top and bottom surfaces of the voids, respectively (point A in Figure 3). The trapped charges induce an electric field opposite to the externally applied field and thus eventually extinguish the discharge. As the applied voltage increases further, a second series of breakdown events may occur, and the density of the internally trapped charges strongly increases (point B in Figure 3). When the applied voltage is reduced, the electric field of the trapped charges may overcompensate the applied field and may thus be able to trigger back discharges ((point C in Figure 3)).

### 3 LIGHT EMISSION FROM THE DIELECTRIC BARRIER DISCHARGES

The DBDs in ferroelectrets are always accompanied by light emission that can be easily photographed [9, 18]. The light emission originates from electronically excited and/or ionized gas molecules inside the voids and can be used as a diagnostic tool for characterizing the DBDs [17, 19]. The setup used for the spectroscopic analysis of the DBDs in ferroelectrets is schematically shown in Figure 4 [20, 21]. The sample, metalized on both sides with semitransparent gold electrodes (diameter of 16 mm and thickness of 20 nm), is mounted in a light-tight chamber. High voltages with suitable waveforms are applied directly to the sample electrodes by means of a high-voltage amplifier controlled by a function generator.

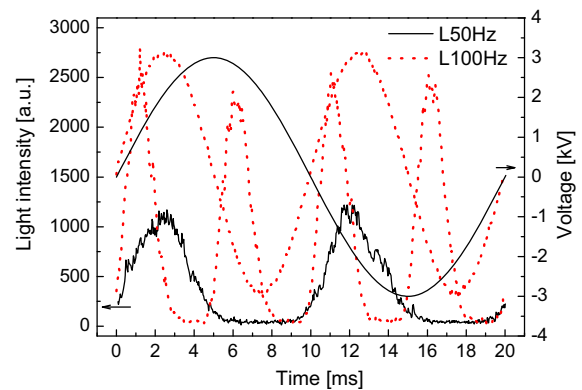


**Figure 6.** Transient light emission from a cellular PP ferroelectret under sinusoidal voltages at two different frequencies (black and red curves).

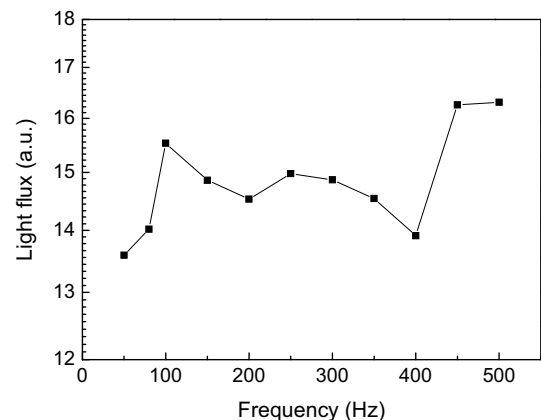


**Figure 7.** Light flux for one cycle of the sinusoidal voltage as a function of frequency.

The light emission is synchronously measured by a photomultiplier tube (PMT) from one side of the sample and by a spectroscopic system from the other side. The spectroscopic system consists of an optical fiber, a grating monochromator, and a PC-controlled electron-multiplying charge-coupled device (EM-CCD) camera. Spatially resolved images of the samples during charging are taken by the EM-CCD camera connected to the chamber via a lens. In order to suppress light emission from corona discharges at the periphery of the electrodes, either the edges of the electrodes are covered with silicon rubber, or the electrode areas of the sample are covered by a plastic mask with a central circular opening (open diameter of 8.5 mm).

Figure 5 shows the spatially resolved light emission from a void-containing polycarbonate ferroelectret system under a positively biased sinusoidal voltage with a peak-to-peak amplitude  $V_{pp}$  of 3 kV and a frequency of 100 Hz [22]. The sample is fabricated by sticking two polycarbonate films to a grid produced from double-sided adhesive tape by means of computer-controlled laser cutting. The hexagonal openings of the grid structure lead to honeycomb-shaped voids inside the three-layer system, which can be internally charged by DBDs under high voltages. In Figure 5, the hexagonal structure is clearly seen. The difference between the light intensities of individual voids is attributed to small differences in the void geometries which cannot be avoided with samples that are prepared individually in the laboratory.

The time-dependent light emission from a cellular PP sample under a sinusoidal voltage with a peak-to-peak amplitude  $V_{pp} = 6$  kV and frequencies of 50 or 100 Hz is shown in Figure 6. Two light-emission peaks are observed for each voltage cycle regardless of the frequency. As can be seen from the figure, light emission starts shortly before the voltage changes sign because of the choking effect in the DBDs. Experimental results show that the repeated light emission is not influenced by an additional dc offset bias voltage superimposed onto the sinusoidal voltage waveforms. This is reasonable, since DBDs are extinguished very quickly by the choking effect under dc voltages, and repeated DBDs are controlled only by the voltage variations, i.e. by the sinusoidal components in this case. The total light flux can be obtained by integrating the light intensity over time. The total light flux during one cycle of the sinusoidal voltage is plotted in Figure 7 as a function of frequency. No obvious dependence on the frequency of the time-dependent voltage is observed for the light flux per cycle, which is expected, since always the same number of practically identical DBDs is generated during each cycle. For the same reason, the power of conventional DBDs in a given configuration and under a fixed peak voltage is directly proportional to the frequency [7].

Analysis of the optical emission spectrum (OES) is an effective method for diagnosing DBDs [23–26]. The OES of the DBDs in cellular PP ferroelectrets under positively biased sinusoidal voltages  $V = \frac{1}{2}V_{pp}[1 + \sin(2\pi ft)]$  with a frequency

of 100 Hz and different  $V_{pp}$  values has been recorded within the near-UV and visible spectral range. There is no detectable OES when  $V_{pp}$  is lower than 3 kV, which is in agreement with the PMT results [17]. Above 3 kV, an OES can be clearly detected. Part of the spectrum for a peak-to-peak voltage  $V_{pp}$  of 6 kV is shown in Figure 8 [19]. The spectrum shows strong emission from the second positive system (SPS) of molecular nitrogen,  $N_2(C^3\Pi_u \rightarrow N_2(B^3\Pi_g)$ , and from the first negative system (FNS) of  $N_2^+$ ,  $N_2^+(B^2\Sigma_u^+ \rightarrow N_2^+(X^2\Sigma_g^+)$ , consistent with a DBD in air.

The appearance of the FNS of  $N_2^+$  directly confirms the ionization of molecular nitrogen during the DBDs. The  $V_{pp}$

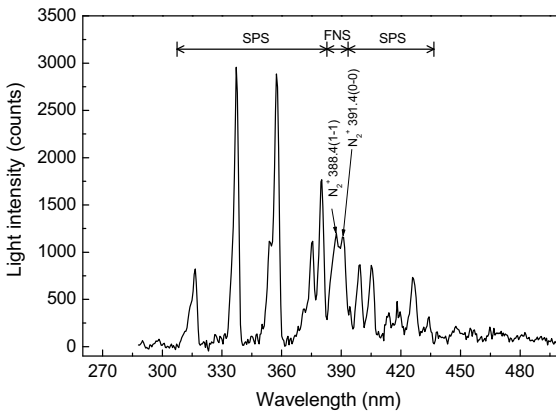


**Figure 8.** Optical emission spectrum of a cellular PP ferroelectret under a positive sinusoidal voltage (frequency of 100 Hz and  $V_{pp}$  of 6 kV). The EM-CCD camera is internally triggered with an exposure time of 4 s. [19]

dependence of the intensity of the spectral bands, e.g. the  $N_2$  SPS ( $0 \rightarrow 0$ ) and  $N_2^+$  FNS ( $0 \rightarrow 0$ ) bands (located at 337.1 and 391.4 nm, respectively) shows the same trend as the charging-voltage dependence of the piezoelectric  $d_{33}$  coefficient [17]. Therefore, light emission from the DBDs in ferroelectrets is strongly correlated with their piezoelectricity. In addition, the band strength ratios in the spectrum provide information on the electric field inside the DBDs [27]. From a spectroscopic analysis, the electric field during the DBDs in cellular PP ferroelectrets is found to be between 21 and 28 MV/m. The values are in good agreement with the breakdown strength in air for voids with heights between 10 and 15  $\mu\text{m}$ , as predicted by the Townsend breakdown model.

#### 4 ACOUSTICAL AND PIEZOELECTRICAL RESPONSE OF THE POLARIZATION

The build-up of the effective polarization in ferroelectrets under suitable voltage waveforms has been studied by means of acoustical measurements in combination with dielectric resonance spectroscopy [28]. In order to generate a sound signal, a sinusoidal voltage with a frequency of 1 kHz and a peak-to-peak voltage  $V_{pp}$  of 100 V is applied to cellular PP foams. An additional dc bias voltage is superimposed onto the sinusoidal voltage, and the sound signal emitted from the sample is measured with a microphone. Under laboratory conditions, the amplitude of the sound signal emitted from the sample is proportional to the absolute value of  $d_{33}$ . According to the common model for ferroelectrets, the  $d_{33}$  coefficient under a dc bias voltage is given by [15]

$$d_{33} = \frac{d}{Y} \frac{\epsilon_{pr} d_1 \sigma_{\text{eff}} - \epsilon_0 \epsilon_{pr}^2 V_{\text{bias}}}{(d_1 + \epsilon_{pr} d_2)^2} \quad (10)$$

where  $V_{\text{bias}}$  is the external voltage applied to the electrodes, and  $\sigma_{\text{eff}} = \sum d_{2i} \sigma_i / \sum d_{2i}$  is the effective charge density on the polymer/air interfaces on both sides of a single air gap. According to equation (10), the sound signal radiated from the sample under a dc bias voltage has contributions not only from the effective charge density (the first term in the equation), but also from the Maxwell stress (the second term in the equation). At low bias voltage  $V_{\text{bias}}$ , the piezoelectricity of ferroelectrets is proportional to the external voltage [29], since  $\sigma_{\text{eff}}$  can be considered constant at a dc bias voltage well below the threshold for DBD inception.

However, when the dc bias voltage is higher than the threshold voltage, DBDs are triggered in the voids, which in turn change the effective charge density  $\sigma_{\text{eff}}$ . Therefore, a “butterfly” curve is obtained for the microphone signal under linearly increasing and then decreasing dc bias voltages if their maximum value exceeds the threshold (Figure 9a).

The absolute values of the piezoelectric  $d_{33}$  coefficients under zero-charging-field have been obtained by means of dielectric resonance spectroscopy (DRS) immediately after the voltage cycles with an external dc bias. Young’s modulus and  $d_{33}$  were determined by fitting the real part of the measured capacitance (inset of Figure 9b) to the relevant theoretical formula [30, 31]. By comparing the microphone signals



without a charging field with the absolute  $d_{33}$  values determined by means of DRS immediately after charging, the microphone-signal measurements could be calibrated and converted into piezoelectric  $d_{33}$  coefficients. The quantities  $d_1$  and  $d_2$  are determined from the density of the samples and from the measured sample thicknesses, since the density of solid PP is known and the density of air can be approximated as zero. A polarization-voltage ( $P$ - $V$ ) hysteresis loop is obtained by evaluating the data according to equation (10). Figure 9b shows the build-up of the effective polarization in a cellular PP ferroelectret as a function of the applied dc-bias voltage. Its features are similar to those typically found in hysteresis curves of ferroelectrics. From the figure, the threshold voltage and the remanence of the effective polarization can be determined. It should be noted that a significant reduction of  $\sigma_{\text{eff}}$  is observed when the dc bias voltage decreases from its maximum to zero, which is due to back discharges. The back discharges originate from the over-compensation of the external electric field from the bias voltage  $V_{\text{bias}}$  by the internal field of the space charges trapped

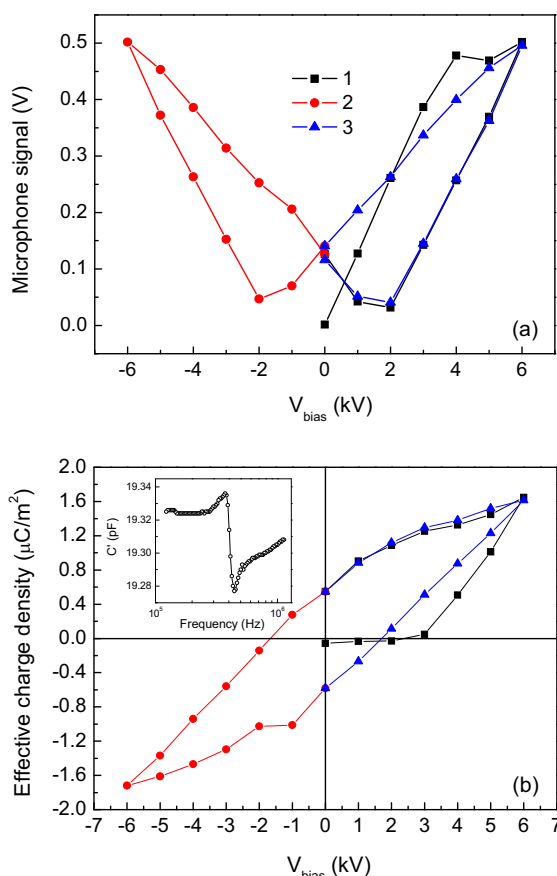


**Figure 9.** (a) Microphone signal as a function of the bias voltage  $V_{\text{bias}}$  applied to the sample electrodes. The maximum absolute voltage is 6 kV. A fresh, uncharged sample with a thickness of 72  $\mu\text{m}$  was used for the positive half cycle (curve 1), followed by a negative half cycle (curve 2) and subsequently a second positive half cycle (curve 3). (b) Effective charge density  $\sigma_{\text{eff}}$  (calculated from the experimental data shown in (a) as a function of  $V_{\text{bias}}$ ). The inset shows the dielectric resonance spectrum from which the absolute  $d_{33}$  coefficient corresponding to the zero-field microphone signal was calculated [28].

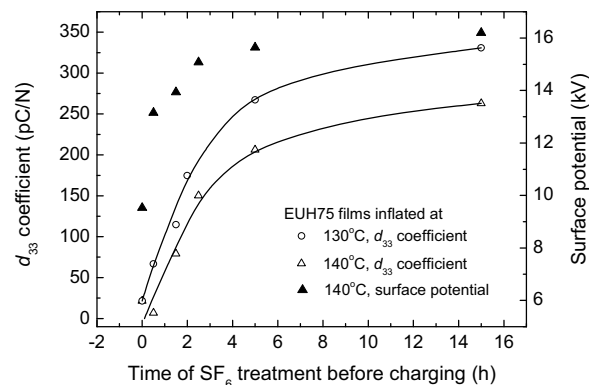


**Figure 10.** Pre-inflated EUH75 cellular PP film: Surface potential and piezoelectric  $d_{33}$  coefficient after charging as a function of the  $\text{SF}_6$  treatment time before charging. The lines are guides for the eye only [33].

at the top and bottom surfaces of the voids [17]. The experimental results indicate that suppressing the back discharges could provide a pathway to a significantly enhanced piezoelectricity.

### 5 INFLUENCE OF GAS TYPE AND GAS PRESSURE ON THE CHARGING PROCESS

As already mentioned, the macroscopic dipoles in ferroelectrets are produced by means of the DBDs inside the voids. Therefore, the gas compositions inside the voids as well as the gas pressures have significant influence on the charging process. In corona discharges used for electret charging, the ambient gas environment also plays a crucial role, since it determines the maximum corona voltage that can be applied and the maximum surface potential that can be obtained. Paajanen *et al.* studied the effect of gas compositions on the corona charging of cellular PP foams in different gases at elevated pressures [32]. It was found that higher corona voltages can be employed with various gases of higher electrical breakdown strength, which results in more efficient charge separation inside the voids and thus also higher piezoelectricity. Especially, piezoelectric  $d_{33}$  coefficients of up to 790 pC/N were obtained when the voids of the sample had been filled with  $\text{N}_2$  gas under high pressure. This  $d_{33}$  value is more than four times that of samples charged under standard laboratory conditions. The large enhancement was attributed to the higher dielectric strength of  $\text{N}_2$  and to its lower moisture content compared to atmospheric air.

In reference [32], it was reported that large  $\text{SF}_6$  molecules were not able to penetrate into the voids of the 70  $\mu\text{m}$  thick cellular PP foams used in the experiments. However, the penetration of  $\text{SF}_6$  into the sample as well as the beneficial effect on the charging efficiency during DBDs depends on the microscopic void structure of the respective samples [33]. For cellular PP foams with larger void dimensions and a low Young's modulus of around 1 MPa, the penetration of  $\text{SF}_6$  into the cellular voids is possible after a long-term pressure treatment, as confirmed by *in-situ* thickness measurements. Figure 10 shows the piezoelectric  $d_{33}$  coefficient as a function

of the treatment time in SF<sub>6</sub>. The  $d_{33}$  coefficient increases with increasing treatment time. An improvement by a factor of up to 1.5 is achieved for a treatment time of 15 h. For cellular PP foams with smaller void sizes and a higher Young’s modulus of about 5.8 MPa, the sample thickness keeps decreasing with increasing treatment time, which indicates that the large SF<sub>6</sub> molecules are not able to penetrate into the voids, whereas the air molecules leak out of the voids under the high pressure. However, a much higher corona voltage up to -60 kV can be applied in an SF<sub>6</sub> atmosphere, leading to much higher surface potentials. Consequently, the voids can also be charged to higher levels, and an enhancement factor of 4 and 3 for the  $d_{33}$  coefficient is achieved after short and long treatment times, respectively. In order to exploit the beneficial effects of charging in SF<sub>6</sub> gas, only short treatment times are necessary for stiffer polymer foams with smaller void sizes (where only the level of surface charging is directly enhanced), whereas for softer foams with larger void sizes, longer treatment times are required in order to fill the voids with SF<sub>6</sub> molecules.

According to Paschen’s law, the breakdown voltage at a given void height can be modulated through a pressure change inside the void. The capacitance of the sample is measured as a way to monitor the thickness change [34]. For pre-inflated cellular PP foams (trade name PQ50), a sudden drop (or a sudden increase) of the capacitance is observed when samples are subjected to vacuum (or to high pressure, respectively). The observation indicates thickness changes of the samples caused by the difference between the ambient pressure and that inside the voids. However, the capacitance of the sample recovers to approximately its initial value after sufficient time (typically several hours) has elapsed, which indicates that the internal and external pressures equalize as a result of gas diffusion. If the sample morphology is analyzed on a cross section we find that most of the voids have a height lower than 6 μm. At standard atmospheric pressure of 101 kPa, the Paschen breakdown voltage has its minimum at a height of around 8 μm (cf. Figure 2). Therefore, an increase of the internal pressure lowers the breakdown voltage for voids with heights lower than 8 μm. Unfortunately, the chargeability of

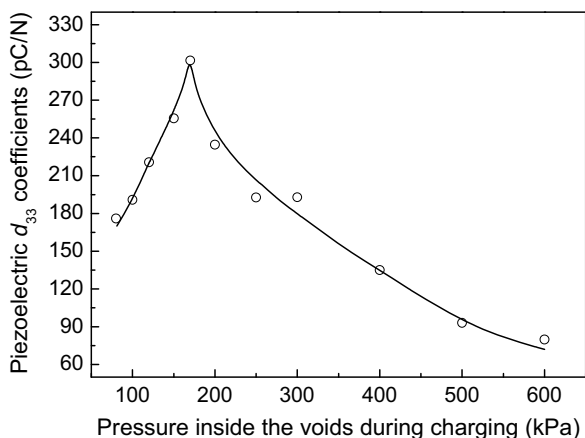


Figure 11. Piezoelectric  $d_{33}$  coefficient as a function of pressure inside the voids during charging (open circles). The line is a guide for the eye only [35].

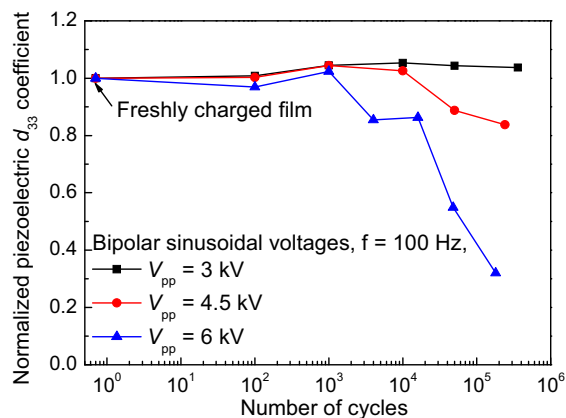


Figure 12. Normalized piezoelectric  $d_{33}$  coefficient as a function of the logarithm of the number of cycles ( $N$ ). Fatigue was observed under a bipolar sinusoidal voltage with a frequency of 100 Hz and an amplitude as indicated. Cycle numbers below 10<sup>0</sup> indicate freshly charged films [38].

the voids with a height larger than 8 μm is reduced at the same time. Thus, the trade-off between the two effects must be considered. For the above-mentioned cellular PP sample, optimal piezoelectricity is achieved by charging at a pressure around 170 kPa (Figure 11) [35].

## 6 FATIGUE UNDER REPEATED DIELECTRIC-BARRIER DISCHARGES

In the polymer industry, non-thermal plasmas found in low-pressure glow discharges as well as in high-pressure (atmospheric) corona discharges and DBDs are often used to modify the surface properties of polymers [7, 36, 37]. DBDs produce a variety of species including energetic and reactive monatomic and diatomic charged gas particles (i.e. ions), electrons, and neutral species. During processing, the polymer surface is thus exposed to a highly reactive plasma, and both chemical and physical processes occur on the exposed surface areas.

It is found that repeated DBDs in air result in considerable fatigue of the effective polarization and of the piezoelectricity because of plasma-surface interactions at the internal void surfaces [38]. The fatigue is attributed to plasma-induced chain scission and oxidation of the polymer surface. Conventional DBD treatment of PP leads to the formation of polar water-soluble low-molecular-weight oxidized material (LMWOM) on the surface, containing O-C=O, C=O, and C-O groups. For cellular PP ferroelectrets, chain scission and the formation of polar LMWOM at the internal surfaces during DBDs deteriorate the chargeability of the voids, resulting in the observed polarization fatigue (Figure 12). A threshold peak-to-peak voltage  $V_{pp}$  of 3 kV for fatigue is in good agreement with the previous finding that the DBDs inside the voids are initiated when the voltage is higher than 3 kV [17]. The fatigue rate strongly depends on the amplitude and the number of driving-voltage cycles, whereas the frequency and the waveform do not have a strong influence, which indicates the influence of molecular dynamics and physico-chemical processes at the internal polymer surfaces.

## 7 CONCLUSION

Internally charged polymer foams and void-containing polymer systems (often called ferro- or piezoelectrets) are new members of the family of piezo-, pyro- and ferroelectric polymer electrets. They have attracted considerable attention due to their large piezoelectricity combined with high mechanical flexibility and good elastic compliance. Although these soft polymer materials are non-polar, they contain gas-filled voids that can be internally charged by means of dielectric barrier discharges (DBDs) under high electric fields. Space charge of opposite polarity is separated during DBDs and deposited at the top and bottom inner surfaces of the voids, respectively. The charged voids can be considered as man-made macroscopic dipoles, whose direction can be reversed under sufficiently high electric fields.

DBD charging of the voids is an essential process for turning polymer foams into ferroelectrets. There is a threshold voltage  $V_{th}$  for triggering the DBDs, which is found from Townsend's model of Paschen breakdown. The DBD charging is a self-extinguishing process because the electric field of the internally trapped charges partly compensates the externally applied field. Above the threshold, the effective polarization  $\sigma_{eff}$  increases with increasing external voltage  $V$ . If the electric field induced by the trapped charges becomes higher than the threshold value, back discharges occur when the charging voltage is sufficiently reduced or completely turned off. Consequently, a saturation of  $\sigma_{eff}$  is observed when the external voltage  $V$  reaches  $2 V_{th}$  (twice the threshold voltage).

From the transient light emission of the DBDs in cellular PP ferroelectrets, a schematic model for the DBD charging process is developed, and the electric field during charging is estimated. The effective polarization (macroscopic dipole density) shows a hysteresis as a function of the charging voltage. The efficiency of DBD charging strongly depends on the geometry (in particular the height) of the voids, the type of gas and the gas pressure inside the voids. Furthermore, the chargeability of the voids is influenced by the plasma treatment of the inner surfaces during the DBDs. At least for cellular PP ferroelectrets, repeated DBDs in atmospheric conditions lead to considerable fatigue of the effective polarization and of the resulting piezoelectricity.

## ACKNOWLEDGMENTS

The authors are indebted to Professor Gerhard M. Sessler (to whom this review is dedicated on the occasion of his 80<sup>th</sup> birthday) for many stimulating discussions on electrets and ferroelectrets and to the European commission for co-funding some of the equipment used in the original research.

## REFERENCES

- [1] L. Gibson and M. Ashby, *Cellular solids: structure and properties*, New York: Cambridge U. Press, 1999.
- [2] R. Gerhard-Multhaupt, "Less can be more: Holes in polymers lead to a new paradigm of piezoelectric materials for electret transducers", *IEEE Trans. Dielectr. Electr. Insul.*, Vol. 9, pp. 850-859, 2002.
- [3] S. Bauer, R. Gerhard-Multhaupt, and G. M. Sessler, "Ferroelectrets: Soft electroactive foams for transducers", *Phys. Today*, Vol. 57, pp. 37-43, 2004.
- [4] M. Wegener and S. Bauer, "Microstorms in cellular polymers: A route to soft piezoelectric transducer materials with engineered macroscopic Dipoles", *Chem. Phys. Chem.*, Vol. 6, pp. 1014-1025, 2005.
- [5] S. Bauer, "Piezo-, pyro- and ferroelectrets: soft transducer materials for electromechanical energy conversion", *IEEE Trans. Dielectr. Electr. Insul.*, Vol. 13, pp. 953-962, 2006.
- [6] X. Qiu, "Patterned piezo-, pyro-, and ferroelectricity of poled polymer electrets", *J. Appl. Phys.*, Vol. 108, 011101, 2010.
- [7] U. Kogelschatz, "Dielectric barrier discharges: Their history, discharge physics and industrial applications", *Plasma Chem. Plasma Process.*, Vol. 23, pp. 1-46, 2003.
- [8] M. Lindner, H. Hoislbauer, R. Schwödauer, S. Bauer-Gogonea, and S. Bauer, "Charged cellular polymers with ferroelectric behavior", *IEEE Trans. Dielectr. Electr. Insul.*, Vol. 11, pp. 255-263, 2004.
- [9] M. Wegener, M. Paajanen, W. Wirges, and R. Gerhard-Multhaupt, "Corona-induced partial discharges, internal charge separation and electromechanical transducer properties in cellular polymer films", *IEEE 11th Intern. Sympos. Electrets*, pp. 54-57, 2002.
- [10] R. Gerhard-Multhaupt, W. Wegener, W. Wirges, J. A. Giacometti, R. A. C. Altafim, L. E. Santos, R. M. Faria, and M. Paajanen, "Electrode poling of cellular polypropylene films with short high-voltage pulses", *IEEE Conf. Electr. Insul. Dielectr. Phenomena*, pp. 299-302, 2002.
- [11] E. M. Bazelyan and Y. P. Raizer, *Spark Discharge* (CRC, Boca Raton, FL, USA, 1998).
- [12] P. Zhang, Z. Xia, X. Qiu, F. Wang, and X. Y. Wu, "Influence of charging parameters on piezoelectricity for cellular polypropylene film electrets", *IEEE 12th Intern. Sympos. Electrets*, pp. 39-42, 2005.
- [13] X. Qiu, *The Electret Properties of Cellular PP and Solid PEN Film*, Ph.D. thesis, Tongji University, Shanghai, China, 2006.
- [14] G. M. Sessler and J. Hillenbrand, "Electromechanical response of cellular electret films", *Appl. Phys. Lett.*, Vol. 75, pp. 3405-3407, 1999.
- [15] M. Paajanen, H. Välimäki, and J. Leikkala, "Modeling the sensor and actuator operations of the ElectroMechanical Film EMFi", *IEEE 10th Intern. Sympos. Electrets*, pp. 735-738, 1999.
- [16] S. Zhukov and H. von Seggern, "Polarization hysteresis and piezoelectricity in open-porous fluoropolymer sandwiches", *J. Appl. Phys.*, Vol. 102, 044109, 2007.
- [17] X. Qiu, A. Mellinger, M. Wegener, W. Wirges, and R. Gerhard, "Barrier discharges in cellular polypropylene ferroelectrets: how do they influence the electromechanical properties?", *J. Appl. Phys.*, Vol. 101, 104112, 2007.
- [18] M. Lindner, S. Bauer-Gogonea, S. Bauer, M. Paajanen, and J. Raukola, "Dielectric barrier microdischarges: Mechanism for the charging of cellular piezoelectric polymers", *J. Appl. Phys.*, Vol. 91, pp. 5283-5287, 2002.
- [19] X. Qiu, A. Mellinger, W. Wirges, and R. Gerhard, "Spectroscopic study of dielectric barrier discharges in cellular polypropylene ferroelectrets", *Appl. Phys. Lett.*, Vol. 91, 132905, 2007.
- [20] A. Mellinger, X. Qiu, M. Wegener, W. Wirges and R. Gerhard, "Charging dynamics of cellular polypropylene ferroelectrets: a combined optical and acoustic study", *Spring Meeting of the German Physical Society, Regensburg, Germany, March 26-30, 2007*.
- [21] A. Mellinger, X. Qiu and R. Gerhard, "Microplasma discharges in polymer foams: a new road to flexible piezoelectric polymer films", *Conf. Fundamentals and Applications of Microplasmas, Organized by Engineering Conferences International (ECI), San Diego, California, USA. Proceedings is not available, 2009*.
- [22] X. Qiu, L. Holländer, R. Flores Suárez, W. Wirges, and R. Gerhard, "Polarization from dielectric-barrier discharges in ferroelectrets: Mapping of the electric-field profiles by means of thermal-pulse tomography", *Appl. Phys. Lett.*, Vol. 97, 072905, 2010.
- [23] S. F. Miralaf, E. Monette, R. Bartnikas, G. Czeremuszkin, M. Latrèche, and M. R. Wertheimer, "Electrical and Optical Diagnostics of Dielectric Barrier Discharges (DBD) in He and N<sub>2</sub> for Polymer Treatment", *Plasma Polym.*, Vol. 5, pp. 63-77, 2000.
- [24] H. Nassar, S. Pellerin, K. Musiol, O. Martinie, N. Pellerin, and J. M. Cormier, "N<sub>2</sub><sup>+</sup>/N<sub>2</sub> ratio and temperature measurements based on the first negative N<sub>2</sub><sup>+</sup> and second positive N<sub>2</sub> overlapped molecular emission spectra", *J. Phys. D: Appl. Phys.*, Vol. 37, pp. 1904-1916, 2004.
- [25] C. O. Laux, T. G. Spence, C. H. Kruger, R. N. Zare, "Optical diagnostics of atmospheric pressure air plasmas", *Plasma Sources Sci. Technol.*, Vol. 12, pp. 125-138, 2003.

[26] D. Staack, B. Farouk, A. F. Gutsol, and A. A. Fridman, "Spectroscopic studies and rotational and vibrational temperature measurements of atmospheric pressure normal glow plasma discharges in air plasmas", *Plasma Sources Sci. Technol.*, Vol. 15, pp. 818-827, 2006.

[27] P. Paris, M. Aints, F. Valk, T. Plank, A. Haljaste, K.V. Kozlov and H-E Wagner, "Intensity ratio of spectral bands of nitrogen as a measure of electric field strength in plasmas", *J. Phys. D: Appl. Phys.*, Vol. 38 pp. 3894-3899, 2005.

[28] X. Qiu, R. Gerhard, and A. Mellinger, "In-situ acoustical investigation of the polarization build-up in cellular polypropylene ferroelectrets", *IEEE Trans. Dielectr. Electr. Insul.*, Vol. 17, pp. 1043-1049, 2010.

[29] M. Paajanen, J. Lekkala, and H. Välimäki, "Electromechanical Modeling and Properties of the Electret Film EMFi", *IEEE Trans. Dielectr. Electr. Insul.*, Vol. 8, pp. 629-636, 2001.

[30] A. Mellinger, "Dielectric Resonance Spectroscopy: a Versatile Tool in the Quest for Better Piezoelectric Polymers", *IEEE Trans. Dielectr. Electr. Insul.*, Vol. 10, pp. 842-861, 2003.

[31] H. Ohigashi, "Electromechanical properties of polarized polyvinylidene fluoride films as studied by the piezoelectric resonance method", *J. Appl. Phys.*, Vol. 47, pp. 949-955, 1976.

[32] M. Paajanen, M. Wegener, and R. Gerhard-Multhaupt, "Understanding the role of the gas in the voids during corona charging of cellular electret films – a way to enhance their piezoelectricity", *J. Phys. D: Appl. Phys.*, Vol. 34, pp. 2482-2488, 2001.

[33] X. Qiu, M. Wegener, W. Wirges, X. Zhang, J. Hillenbrand, Z. Xia, R. Gerhard-Multhaupt, and G. M. Sessler, "Penetration of sulfur hexafluoride into cellular polypropylene films and its effect on the electric charging and electromechanical response of ferroelectrets", *J. Phys. D: Appl. Phys.*, Vol. 38, pp. 649-654, 2005.

[34] J. G. Leonhartsberger, H. Salhofer, R. Schwödiauer, S. Bauer-Gogonea, S. Bauer, R. Forstner, G. Eder, M. Paajanen, H. Minkinen, J. Raukola, "Capacitance dilatometry for the in-situ controlled expansion process of cellular polymer-filler composites (ferroelectrets)", *Ferroelectrics*, Vol. 331, pp. 181-187, 2006.

[35] X. Qiu, A. Mellinger, and R. Gerhard, "Influence of gas pressure in the voids during charging on the piezoelectricity of ferroelectrets", *Appl. Phys. Lett.*, Vol. 92, 052901, 2008.

[36] C. M. Chan, T. M. Ko, H. Hiraoka, "Polymer surface modification by plasma and photos", *Surf. Sci. Rep.*, Vol. 24, PP. 1-54, 1996.

[37] F. S. Denes, S. Manolache, "Macromolecular plasma-chemistry: an emerging field of polymer science", *Prog. Polym. Sci.*, Vol. 29, pp. 815-885, 2004.

[38] X. Qiu and R. Gerhard, "Effective polarization fatigue from repeated dielectric barrier discharges in cellular polypropylene ferroelectrets", *Appl. Phys. Lett.*, Vol. 93, 056841, 2008.



**Xunlin Qiu** was born on 21 July 1978. From 1996 to 2000, he studied physics at Tongji University and received the degree of B.Sc. From 2000 to 2006 he majored in condensed matter physics in the Pohl Institute of Solid State Physics at Tongji University and received the degree of M.Sc. in 2003 and the degree of D.Sc. in 2006. His main research work is functional polymer dielectrics and electrets. In 2003 he worked on cellular polymer ferroelectret in the Institute of Communications Technology, Darmstadt University of Technology, Germany, and he worked on the same topic in Applied Condensed-Matter Physics group at the University of Potsdam, Germany. From June 2006 until now, he works as a postdoc at the University of Potsdam, Germany.



**Reimund Gerhard** (S'80–M'84–SM'85–F'93) studied mathematics and physics at the Darmstadt University of Technology in Germany from 1972 until 1978. After graduating as Diplom-Physiker, he spent one year as research fellow at the Collège Militaire Royal in St-Jean, Québec, Canada. From 1979 until 1985, he did his Ph.D. thesis with Professor Gerhard M. Sessler in Darmstadt. From 1985 until 1994, he was a research scientist and project manager at the Heinrich-Hertz Institute for Communications Technology in Berlin. Since 1994 he has been an associate professor and since 1997 a full professor in the Department of Physics and Astronomy of the University of Potsdam in Germany. Presently, he is Dean of the Science Faculty at his university. The main research areas of Prof. Gerhard are polymer electrets and ferroelectrets, in particular the mechanisms of space-charge storage and dipole polarization in dielectric polymers and polymer composites, their ferro-, pyro- and piezoelectrical properties, and their applications in sensors and actuators, as well as the nonlinear optical properties of polymers, and more recently also the physics of musical instruments. From 1974 until 1979, he was a fellow of the Studienstiftung des Deutschen Volkes. In 1988, he was awarded an ITGPreis by the Informationstechnische Gesellschaft im VDE. In 1989, he received a Silver medal from the Stiftung Werner-von-Siemens-Ring. In 2001, he was awarded the first Technologietransfer-Preis by the Technologie-Stiftung Brandenburg and the Prof.-Adalbert-Seifriz-Preis by the Verein Technologie-Transfer Handwerk for his technological collaborations with small industrial companies. Reimund Gerhard is a member of the American, European and German Physical Societies. From 2002 to 2009 he served as Digest Editor of the IEEE Dielectrics and Electrical Insulation Society (DEIS).



**Axel Mellinger** (M'08–SM'09) was born in Munich, Germany, on 25 August 1967. He studied physics at the Technical University in Munich, where he obtained his diploma and the Ph.D. degrees in 1992 and 1995, respectively (his Ph.D. work was performed at the Max-Planck-Institute for Extraterrestrial Physics). In 1996/7 he held a two year postdoctoral position at UC Berkeley in the Department of Chemistry. From 1997 to 2008 he was a senior staff member at the University of Potsdam, Germany, where he obtained the highest German university degree, the Habilitation, in 2005. Since 2008 he is an Assistant Professor in the Physics Department at Central Michigan University. His present work focuses on optical and electrical properties of polymer micro- and nanocomposites and multi-dimensional mapping of polarization and space-charge distributions. From 1987 to 1992 he was a scholar of the German National Academic Foundation. He received the 2004 VDE/ITG award for a publication on dielectric resonance spectroscopy and the 2006 "Best Paper Award" by the German IEEE Instrumentation & Measurements chapter for his work on polarization tomography. In his spare time, he enjoys taking wide-field mosaic images of astronomical objects for use in planetariums around the world.



# Dielectric elastomer and ferroelectret films combined in a single device: how do they reinforce each other?

Werner Wirges · Sebastian Raabe · Xunlin Qiu

Received: 12 October 2011 / Accepted: 10 February 2012 / Published online: 29 February 2012  
© Springer-Verlag 2012

**Abstract** Dielectric elastomers (DE) are soft polymer materials exhibiting large deformations under electrostatic stress. When a prestretched elastomer is stuck to a flat plastic frame, a complex structure that can be used as an actuator (DEA) is formed due to self-organization and energy minimization. Here, such a DEA was equipped with a ferroelectret film. Ferroelectrets are internally charged polymer foams or void-containing polymer-film systems combining large piezoelectricity with mechanical flexibility and elastic compliance. In their dielectric spectra, ferroelectrets show piezoelectric resonances that can be used to analyze their electromechanical properties. The antiresonance frequencies ( $f_p$ ) of ferroelectret films not only are directly related to their geometric parameters, but also are sensitive to the boundary conditions during measurement. In this paper, a fluoroethylenepropylene (FEP) ferroelectret film with tubular void channels was glued to a plastic frame prior to the formation of self-organized minimum-energy DEA structure. The dielectric resonance spectrum (DRS) of the ferroelectret film was measured in-situ during the actuation of the DEA under applied voltage. It is found that the antiresonance frequency is a monotropic function of the bending angle of the actuator. Therefore, the actuation of DEAs can be used to modulate the  $f_p$  of ferroelectrets, while the  $f_p$  can also be taken for in-situ diagnosis and for precise control of the actuation of the DEA. Combination of DEAs and ferroelectrets brings a number of possibilities for application.

## 1 Introduction

Electromechanically active polymers are extensively studied and are widely used in various applications. Among them, ferroelectrets (i.e., internally charged polymer foams or void-containing polymer-film systems) have attracted considerable interest in research and industry due to their large piezoelectricity combined with mechanical flexibility and elastic compliance [1, 2]. Voids in ferroelectrets can be charged by means of dielectric barrier discharges (DBDs) under high electric fields [3]. After charging, the voids carry space charges of opposite polarities on their top and bottom inner surfaces, respectively, and thus can be considered as macroscopic dipoles. The man-made dipoles can be easily deformed under mechanical or electrical stress, resulting in large piezoelectricity.

Extensive studies on ferroelectrets were initiated about two decades ago by colleagues from Finland using cellular polypropylene (PP) [4]. Since then, cellular PP has become the workhorse of ferroelectret research and technology mainly due to its ease of processing. However, the piezoelectricity of cellular PP ferroelectrets is stable only up to 60°C, hindering their use in more demanding applications [5]. Therefore, polymers with better charge stability have been employed for ferroelectrets. Recently, fluoroethylenepropylene (FEP) ferroelectrets with well defined and uniform voids have been produced by means of a straightforward lamination process [6]. The piezoelectricity is stable at least up to 130°C when the sample is charged at suitable elevated temperatures. Thus, the application range of ferroelectrets is greatly broadened. The lamination process is quite promising with advantages of simplicity and suitability for a wide range of polymers.

Dielectric elastomers (DEs) are another group of electromechanically active polymers. They are soft polymer

W. Wirges · S. Raabe · X. Qiu (✉)  
Applied Condensed-Matter Physics, Department of Physics and Astronomy, Faculty of Science, University of Potsdam,  
Karl-Liebknecht-Strasse 24-25, 14476 Potsdam-Golm, Germany  
e-mail: xunlin@canopus.physik.uni-potsdam.de



dielectrics showing extremely large deformation under Maxwell-stress [7–9]. Usually, the elastomer material is coated on both sides with compliant electrodes, forming a rubber capacitor. When a voltage is applied to the electrodes, the electrostatic stress caused by the capacitive charges is given by

$$p = \varepsilon_0 \varepsilon_r E^2, \quad (1)$$

where  $\varepsilon_0 = 8.85 \times 10^{-12}$  F/m is the permittivity of free space,  $\varepsilon_r$  is the relative permittivity of the polymer material, and  $E$  is the electric field. The DE material is so soft that actuation strains up to several hundred percent can be achieved by the Maxwell-stress. More recently, electrode-free DEs have been experimentally and theoretically studied [10]. In this case, charges from a corona discharge are deposited on both surfaces of the elastomers. Much larger actuation range is allowed and in the mean time, the problems of the electrode degradation and of the pull-in electromechanical instability are avoided.

The large deformation of DEs under applied  $E$  is the basis for a wide range of potential applications such as artificial muscles, microrobots, energy harvesters, adaptive optical elements, etc. As indicated by (1), the actuation of a DE film is dependent on the applied electric field. For more precise control and for possible further optimization of the device performance, an in-situ detection of the actuation is highly desired. One approach to this issue is to employ self-sensing technique in which the electrical variables such as capacitance and leakage current of the DEA are measured directly during operation for characterization of the performance of the device [11–13].

Recently, a variety of operation schemes are explored with DE films for improved and/or novel properties. For example, it has been shown that applying a certain level of prestretch to DE actuators can further improve their performance [14, 15]. When a prestretched DE film is fixed to a flexible plastic frame, the frame changes its shape upon release of the DE film from the prestretch, and finally a complex structure with minimum of free energy is formed [16, 17]. The structure deforms toward the initial planar state when a voltage is applied, and thus can be used as bending actuator [18]. In this paper, the possibility of combining DE and ferroelectret films in a single device is explored. An FEP ferroelectret film was mounted to a DE bending actuator with minimum-energy structure. It is demonstrated that the electromechanical parameters of the FEP ferroelectret film such as the anti-resonance frequency  $f_p$  exhibit monotropic dependence on the bending angle of the DEA. Therefore, combination of DEs and ferroelectrets brings a variety of possibilities for application.

## 2 Experiments

Ferroelectret sample with well-defined tubular channels was prepared by means of a thermal lamination technique described in [6]. In this process, two polymer electret films are laminated around a template between them. The template, which can be made of metal foils or of polymers whose melting temperature is higher than that of the electret films, contains regular openings through which the electret films can be fused with each other. Lamination is performed at a temperature substantially higher than the melting temperature of the electret films yet lower than that of the template. After the outer layers have been fused, the template is removed, resulting in a polymer-film system with open void channels. Here, 25  $\mu\text{m}$  thick FEP films were laminated around a polytetrafluoroethylene (PTFE) template at 300°C. The template was fabricated from a 50  $\mu\text{m}$  thick Teflon PTFE film with an area of 62 mm  $\times$  40 mm. Six parallel rectangular openings (1.5 mm  $\times$  50 mm) were cut by means of a computer-controlled laser system. The PTFE ridges between adjacent openings also had a width of 1.5 mm. After cooling down under laboratory conditions, the FEP layers are permanently fused with each other through the openings of the template. The PTFE template was then removed after cutting it open at one end, and the sample was metallized on both sides in the central areas with aluminum electrodes 10 mm in width (in the direction parallel to the channels) and 20 mm in length (in the direction perpendicular to the channels).

In order to charge the FEP film system with tubular channels, a dc voltage of 4 kV was applied to the Al electrodes for 10 s by a high voltage power supplier (Trek model 610D). The piezoelectric  $d_{33}$  coefficient was determined by means of dynamic mechanical excitation of the sample with a sinusoidal force with an peak-to-peak amplitude of 1 N at a frequency of 2 Hz (Brüel&Kjaer model 4810 shaker), superimposed with a static force of 3 N. The resulting electrical response of the sample was amplified with a Brüel&Kjaer model 2635 charge amplifier. From the applied force and the resulting electrical signal, the piezoelectric  $d_{33}$  coefficient was calculated. Dielectric resonance spectra (DRS) of the FEP ferroelectret film were recorded in situ using a Novocontrol ALPHA high-resolution dielectric analyzer. The sample was connected to the equipment via thin copper wires.

The DE specimen used here were prepared from commercial films with the trade name VHB4910 supplied by 3M. A soft frame with two circular holes (30 mm in diameter each) and a square hole (30 mm in side length) was prepared with 100  $\mu\text{m}$  thick PET (Hostaphan) film (Fig. 1 (top)). Rigid frame was made of 2 mm thick acryl plate. Two circular holes 30 mm in diameter were cut, and then the material in the central of the frame with a width of 10 mm

was removed (Fig. 1 (middle)). The DE film prestretched to  $400\% \times 400\%$  was sandwiched between the soft and the rigid frames. For metallization, the sandwich structure was fixed with rigid masks having two circular holes the same as those in the soft frame. Gold electrodes with a thickness of 50 nm each were vacuum-deposited onto both surfaces of the DE film in the exposed areas. Finally, the DE material within the square area of the soft frame was removed, and the FEP ferroelectret film was mounted into this area. Figure 1 (bottom) shows a digital image of the bending actuator equipped with an FEP ferroelectret film.

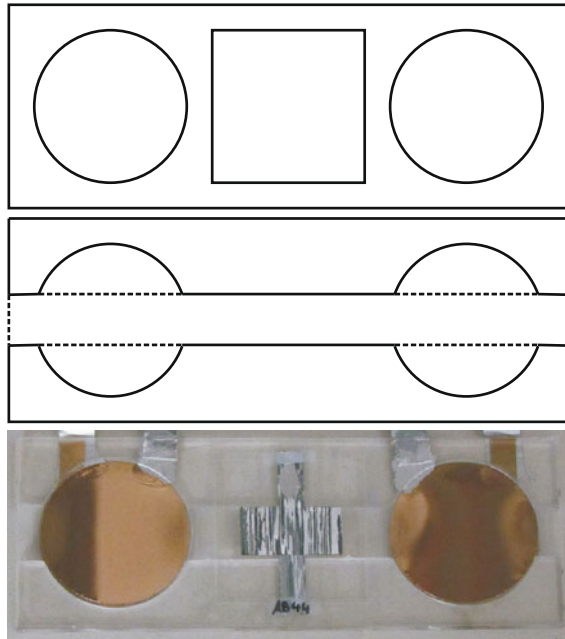
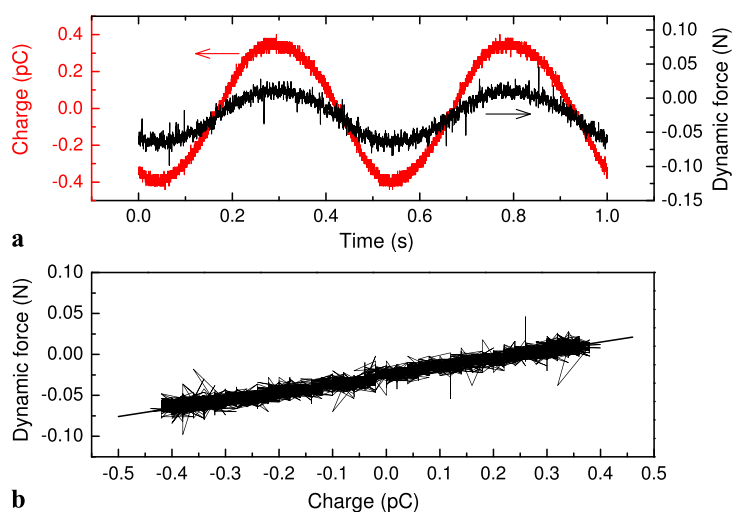


**Fig. 1** A self-organized minimum-energy actuator: thin plastic film frame (*top*), two stiffening frame pieces (*middle*), and a digital image of a sample (*bottom*)

**Fig. 2** (a) Charge and force signals captured with an oscilloscope in the dynamic measurement. (b) A piezoelectric  $d_{33}$  coefficient of 49 pC/N was determined by analyzing the measured charge and force signals with a linear fit



### 3 Results and discussion

#### 3.1 Piezoelectricity of FEP ferroelectret film with tubular channels

To begin with, the piezoelectric activity of the FEP ferroelectret film was characterized before it was mounted to the DE bending actuator. The piezoelectric  $d_{33}$  coefficient was measured by means of the dynamic method detailed above. Figure 2(a) shows the dynamic sinusoidal force applied to the film and the resultant electrical signal. By a linear fit of one of the signals over the other (Fig. 2(b)), a  $d_{33}$  coefficient of about 49 pC/N was determined.

Another manifestation of the piezoelectric activity of a ferroelectret film is the piezoelectric resonances in their dielectric spectra around the respective resonance frequencies [19]. From the frequency dependent real and imaginary parts of the complex capacitance  $C(\omega)$ , several important electromechanical parameters of a piezoelectric film can be determined according to the following equations for the thickness-extension (TE) mode of a free-standing sample [20]

$$C(\omega) = \frac{\varepsilon_r \varepsilon_0 A}{h} \frac{1}{1 - k_t^2 \frac{\tan(\omega/4f_p)}{(\omega/4f_p)}} - iC_{\text{loss}}, \quad (2)$$

$$f_p = \frac{1}{2h} \sqrt{\frac{c_{33}}{\rho}}, \quad (3)$$

$$k_t^2 = d_{33}^2 c_{33} / (\varepsilon_r \varepsilon_0). \quad (4)$$

In (2),  $\varepsilon_r$ ,  $A$ ,  $h$ ,  $k_t$ , and  $f_p$  are the relative permittivity of the sample, the electroded sample area, sample thickness, the complex electromechanical coupling factor, and the complex anti-resonance frequency of the fundamental TE mode, respectively.

Figure 3 shows the measured real and imaginary parts of the complex capacitance of the ferroelectret film and the

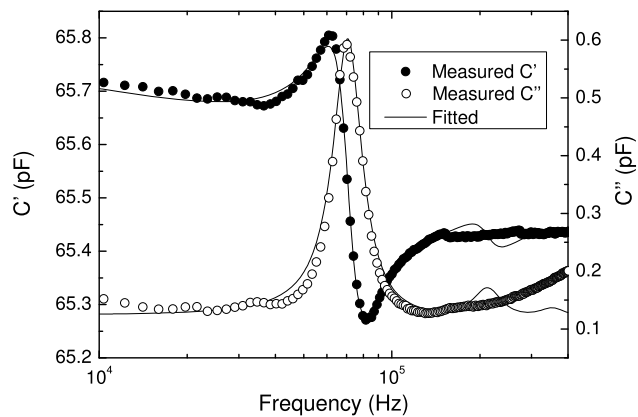


**Fig. 3** Dielectric resonance spectra for the FEP ferroelectret film. The thickness-extension (TE) resonance frequency is located at about 70.5 kHz

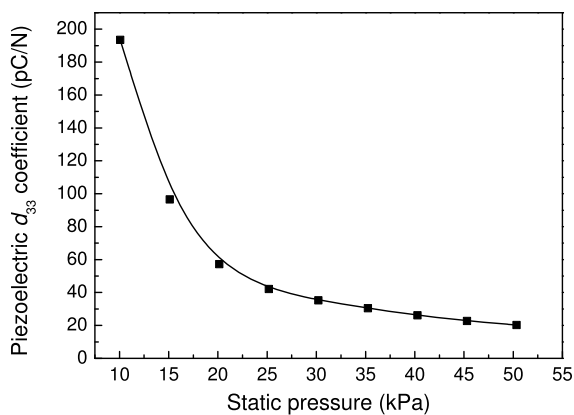


**Fig. 4** Piezoelectric  $d_{33}$  coefficient as a function of the static pressure applied in the dynamic measurement

corresponding fitting curves by means of a least-squares fit based on (2). Several sample parameters such as  $f_p$ ,  $k_t$ ,  $\varepsilon_r$ ,  $c_{33}$ , and  $d_{33}$  can be determined from the fitting. An elastic modulus  $c_{33}$  of about 0.32 MPa is extremely low compared to that of nonvoided polymer films (about 550 MPa for FEP film). This can be attributed to the particular voided structure of the sample. The tubular voids, formed by removing the PTFE template from the fused sandwich system, have open channels so that the air within the channels can flow in and out freely according to the variation of the external stress. Therefore, the sample shows very low  $c_{33}$  for very small external stresses (such as the electrical stresses applied during the DRS measurement) because of the streaming of the air in and out of the void channels. However, with increasing external stress, the  $c_{33}$  of the sample increases substantially due to the volume decrease of the void channels, i.e., the ferroelectrets become stiffer. This is confirmed by the pressure dependence of the  $d_{33}$  coefficient obtained by applying different static force in the dynamic measurement. A fast decay of the  $d_{33}$  with pressure is observed, especially

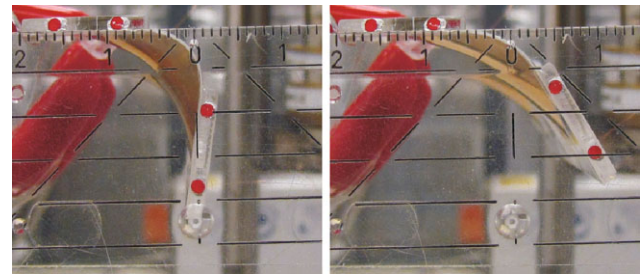


**Fig. 5** Digital images of a minimum-energy bending actuator equipped with an FEP ferroelectret film. For clarity, a goniometer was put in front the actuator, and two red dots were marked on the side of each piece of the rigid frames. As the applied voltage increased from 0 V (left) to 2 kV (right), the actuator unfolded from an bending angle of  $101^\circ$  to  $60^\circ$

at low static pressures (Fig. 4). Consequently, a  $d_{33}$  coefficient of 494 pC/N obtained from the fitting of the DRS is much larger than the value obtained by the dynamic method. The TE antiresonance frequency  $f_p$  of the sample is about 70.5 kHz. As indicated by (3),  $f_p$  is determined by the thickness, the elastic modulus, and the density of the sample. Therefore, it might be modulated by varying the sample structure via, for instance, bending.

### 3.2 Performance correlation between dielectric elastomer and ferroelectret films combined in a single device

After the characterization of its piezoelectricity, the FEP ferroelectret film was mounted to the DE bending actuator (cf. Fig. 1 (bottom)). Then the DE films were released from the prestretch. The central area of the flexible PET frame together with the electroded area of the FEP ferroelectret film, where no rigid acryl frame was stuck, bended because of the elastic energy released by the DE film, while the shape of other area with rigid acryl frame remained unchanged. As a result, a simple bending actuator with self-organized minimum-energy structure shown in Fig. 5 (left) was formed.

The bending angle of the actuator can be controlled by applying a voltage to the electrodes of the DE films [16]. Figure 6 shows the bending angle of the DEA as a function of the applied voltage. The applied dc voltage was increased from 0 to 2 kV with an interval of 0.25 kV. A nonlinear dependence is observed, which is typical for DE actuators. Initially, an equilibrium bending angle of about  $101^\circ$  was measured when no voltage was applied ( $V = 0$  V). With increasing voltage, the bending angle decreases in an accelerating manner. At 1 kV, the bending angle is about  $91^\circ$ ,  $10^\circ$  lower than the initial value, whereas at 2 kV, the bending angle is about  $60^\circ$  (Fig. 5 (right)), i.e., an actuation angle of  $41^\circ$  is achieved. Higher voltages were not tried in our experiments in order to avoid destructive breakdown of the DE films. Such nonlinear behavior results from the input elec-

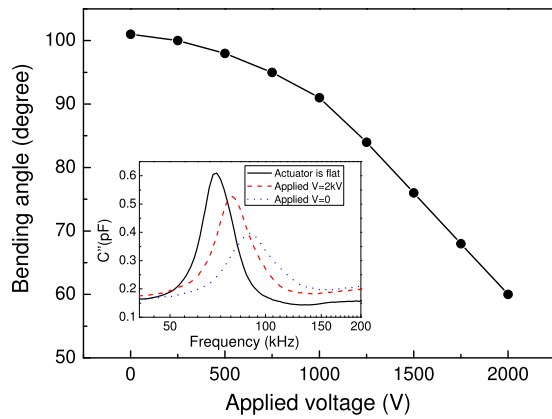


**Fig. 6** Bending angle of the DEA as a function of the applied voltage. *Inset*: Frequency dependence of  $C''$  of the FEP ferroelectret film around its TE resonance when the DEA was flat or voltages as indicated were applied to the bending actuator

trical energy that couples the energy of the bending elastic frame and the DE films [18].

For each applied voltage, the DRS of the FEP ferroelectret film was measured. It is found that the DRS is sensitive to the bending angle. The inset of Fig. 6 shows the imaginary part of the capacitance of the ferroelectret film when the film is flat and when it is bending with the DEA at an applied voltage of 0 V or 2 kV. As can be seen from the figure, the  $f_p$  of the ferroelectret film clearly shifts with the voltage applied to the actuator. At  $V = 0$ , an  $f_p$  of 93 kHz is determined, 22.5 kHz higher than the value obtained when the ferroelectret film is flat. With increasing applied voltage, the bending actuator unfolds towards the flat state, and accordingly,  $f_p$  decreases to about 80 kHz at  $V = 2$  kV.

$f_p$  as a function of the bending angle of the DEA is plotted in Fig. 7. According to (3),  $f_p$  is determined by the thickness, the density as well as the elastic modulus of the ferroelectret film. However, DRS measurements show that the capacitance change of the FEP ferroelectret film is less than 2% over the bending range studied here. Moreover, the contribution to the change of  $f_p$  from the change in thickness is partly compensated by that from the resultant change in density. Therefore, the thickness change of the ferroelectret film during bending can not account for the large change of  $f_p$ . The relatively large change of  $f_p$  must be caused by the variation of the elastic modulus of the ferroelectret film.

As mentioned in the previous subsection, the FEP ferroelectret film exhibits extremely low  $c_{33}$  coefficient during the DRS measurement. With increasing external stress, the  $c_{33}$  increases sharply, leading to substantial decrease of the  $d_{33}$  coefficient (cf. Fig. 4). When the DEA bends, the stress exerted to the ferroelectret film is more complex. In the curved part of the ferroelectret film, there is a so-called neutral surface where the stress is zero, while the outer and the inner part of the film are subjected to tensile and com-

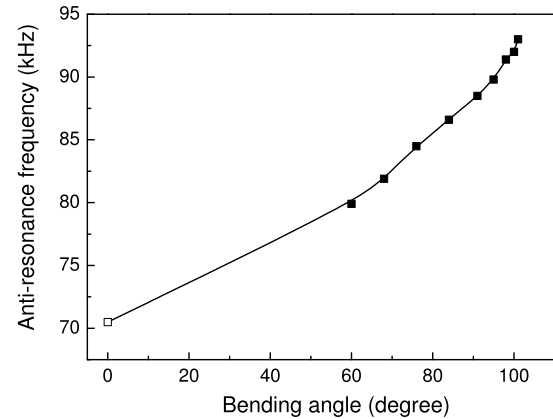


**Fig. 7** Antiresonance frequency  $f_p$  as a function of the bending angle of the minimum-energy DE bending actuator.  $f_p$  was determined from the DRS of the FEP ferroelectret film. *Open square*: DRS was measured when the actuator was flat (i.e., before the DE films were released from the prestretch). *Solid squares*: DRS was measured in situ at certain bending angles under the applied voltage. The voltage applied to the bending actuator was increased from 0 to 2 kV with an interval of 0.25 kV. The line is a guide for the eye

pressive stress, respectively [21]. The bigger the bending angle, the larger are the stresses. Our results show that the  $c_{33}$  coefficient obtained by means of DRS is quite sensitive to the stresses generated during bending. The  $c_{33}$  coefficient increases with increasing bending angle. At a bending angle of  $60^\circ$  (corresponding to an applied voltage of 2 kV), a  $c_{33}$  coefficient of 0.41 MPa was measured, while at  $101^\circ$  ( $V = 0$ ), a  $c_{33}$  of 0.55 MPa was determined from the DRS, which is about 70% higher than the value obtained when the ferroelectret film is flat. Consequently,  $f_p$  increases with increasing bending angle, as can be seen from Fig. 7.

Such a monotropic dependence of the  $f_p$  on the bending angle of the actuator is very promising for potential applications. After calibration, the  $f_p$  of the ferroelectret film can be taken for in-situ diagnosis and for precise control of the DE actuators. This approach has the advantages of low cost, simplicity in manufacture and ease of operation, as compared with the self-sensing method which normally requires an oscillating driving signal carried out using usually expensive high voltage switching. On the other hand,  $f_p$  is one of the most important parameters for the application of ferroelectrets because it directly affects the frequency response of devices. Aided by a DE bending actuator, a single piece of ferroelectret film can have an  $f_p$  covering a certain frequency range. Such a ferroelectret film can be used as a filtering sensor, detecting signals only around the designed frequency range. Also, the  $f_p$  of ferroelectrets can be adjusted according to the requirements of a given practical application by applying a suitable voltage to the combined DEA, so that the devices can be operated either around or far away from the  $f_p$ .



#### 4 Conclusions

The possibility of combining dielectric elastomer actuators (DEA) and ferroelectrets into a single device has been demonstrated. A self-organized minimum-energy structure that can be used as bending actuator was produced by sandwiching a prestretched elastomer between a flexible plastic frame and rigid frame pieces. Such an actuator was equipped with an FEP ferroelectret film containing tubular channel voids. The bending angle of the DEA was controlled by applying a voltage to the electrodes of the DE films, and the dielectric resonance spectrum (DRS) of the ferroelectret film was measured in-situ during the actuation of the DEA. It turns out that the antiresonance frequency is a monotropic function of the bending angle of the actuator. Therefore, combination of DEAs and ferroelectrets opens up various new possibilities for application. The  $f_p$  of ferroelectrets can be taken for in-situ diagnosis and precise control of the actuation of DEA devices. Also, the actuation of DEAs can be used to modulate the  $f_p$  of ferroelectrets in order to meet the requirements of given applications. The concept proposed here has the obvious advantages of low cost, simplicity in manufacture, and ease of operation.

**Acknowledgements** The authors are indebted to Mr. Matthias Kollosche and Mr. Nicolas Marroquin Jacobs (both University of Potsdam) for stimulating discussions and to the European Union for cofunding some of the equipment used in their work.

#### References

1. S. Bauer, R. Gerhard-Multhaupt, G.M. Sessler, *Phys. Today* **57**(2), 37 (2004)
2. R. Gerhard-Multhaupt, *IEEE Trans. Dielectr. Electr. Insul.* **9**, 850 (2002)
3. X. Qiu, R. Gerhard, A. Mellinger, *IEEE Trans. Dielectr. Electr. Insul.* **18**, 34 (2011)
4. K. Kirjavainen, Electromechanical film and procedure for manufacturing same, US Patent No. 4654546 (1987)
5. A. Mellinger, M. Wegener, W. Wirges, R. Reddy Mallepally, R. Gerhard-Multhaupt, *Ferroelectrics* **331**, 189 (2006)
6. R.A.P. Altafim, X. Qiu, W. Wirges, R. Gerhard, R.A.C. Altafim, H.C. Basso, W. Jenninger, J. Wagner, *J. Appl. Phys.* **106**, 014106 (2009)
7. F. Carpi, D. De Rossi, R. Kornbluh, R. Pelrine, P. Sommer-Larsen (eds.), *Dielectric elastomers as electromechanical transducers* (Elsevier, Amsterdam, 2008)
8. F. Carpi, S. Bauer, D. De Rossi, *Science* **330**, 1759 (2010)
9. P. Brochu, Q. Pei, *Macromol. Rapid Commun.* **31**, 10 (2010) and references therein
10. C. Keplinger, M. Kaltenbrunner, N. Arnold, S. Bauer, *Proc. Natl. Acad. Sci. USA* **107**, 4505 (2010)
11. L.A. Toth, A.A. Goldenberg, *Proc. SPIE* **4695**, 323 (2002)
12. C. Keplinger, M. Kaltenbrunner, N. Arnold, S. Bauer, *Appl. Phys. Lett.* **92**, 192903 (2008)
13. T.A. Gisby, S.Q. Xie, E.P. Calius, I.A. Anderson, *Proc. SPIE* **7642**, 764213 (2010)
14. R. Pelrine, R. Kornbluh, Q. Pei, J. Joseph, *Science* **287**, 836 (2000)
15. G. Kofod, *J. Phys. D, Appl. Phys.* **41**, 215405 (2008)
16. G. Kofod, M. Paajanen, S. Bauer, *Appl. Phys. A, Mater. Sci. Process.* **85**, 141 (2006)
17. B. O'Brien, T. McKay, E. Calius, S. Xie, I. Anderson, *Appl. Phys. A, Mater. Sci. Process.* **94**, 507 (2009)
18. G. Kofod, W. Wirges, M. Paajanen, S. Bauer, *Appl. Phys. Lett.* **90**, 081916 (2007)
19. G.S. Neugschwandtner, R. Schwödauer, M. Vieytes, S. Bauer-Gogonea, S. Bauer, J. Hillenbrand, R. Kressmann, G.M. Sessler, M. Paajanen, J. Lekkala, *Appl. Phys. Lett.* **77**, 3827 (2000)
20. A. Mellinger, *IEEE Trans. Dielectr. Electr. Insul.* **10**, 842 (2003)
21. S. Timoshenko, J.N. Goodier, *Theory of Elasticity* (McGraw-Hill, New York, 1951)



## Direct hysteresis measurements on ferroelectret films by means of a modified Sawyer–Tower circuit

Xunlin Qiu,<sup>1,a)</sup> Lars Holländer,<sup>1</sup> Werner Wirges,<sup>1</sup> Reimund Gerhard,<sup>1</sup> and Heitor Cury Basso<sup>2</sup>

<sup>1</sup>Applied Condensed-Matter Physics, Department of Physics and Astronomy, Faculty of Science, University of Potsdam, Karl-Liebknecht-Str. 24-25, 14476 Potsdam-Golm, Germany

<sup>2</sup>Department of Electrical Engineering, São Carlos School of Engineering, University of São Paulo, Av. Trabalhador São-Carlense 400, 13566-590 São Carlos, SP, Brazil

(Received 17 April 2013; accepted 20 May 2013; published online 11 June 2013)

Ferro- and piezo-electrets are non-polar polymer foams or film systems with internally charged cavities. Since their invention more than two decades ago, ferroelectrets have become a welcome addition to the range of piezo-, pyro-, and ferro-electric materials available for device applications. A polarization-*versus*-electric-field hysteresis is an essential feature of a ferroelectric material and may also be used for determining some of its main properties. Here, a modified Sawyer-Tower circuit and a combination of unipolar and bipolar voltage waveforms are employed to record hysteresis curves on cellular-foam polypropylene ferroelectret films and on tubular-channel fluoroethylenepropylene copolymer ferroelectret film systems. Internal dielectric barrier discharges (DBDs) are required for depositing the internal charges in ferroelectrets. The true amount of charge transferred during the internal DBDs is obtained from voltage measurements on a standard capacitor connected in series with the sample, but with a much larger capacitance than the sample. Another standard capacitor with a much smaller capacitance—which is, however, still considerably larger than the sample capacitance—is also connected in series as a high-voltage divider protecting the electrometer against destructive breakdown. It is shown how the DBDs inside the polymer cavities lead to phenomenological hysteresis curves that cannot be distinguished from the hysteresis loops found on other ferroic materials. The physical mechanisms behind the hysteresis behavior are described and discussed. © 2013 AIP Publishing LLC. [<http://dx.doi.org/10.1063/1.4809556>]

### I. INTRODUCTION

Ferroelectrets (sometimes also called piezoelectrets) are internally charged non-polar polymer systems with internal cavities. They combine large piezoelectricity in the thickness direction with high mechanical flexibility and good elastic compliance.<sup>1–4</sup> For the formation of ferroelectrets, an internal charging process in the cavities at high electric fields is necessary. The process consists of a series of dielectric barrier discharges (DBDs). In DBDs, at least one side of the discharge gap is insulated from the respective electrode by a dielectric layer.<sup>5</sup> Charges of opposite polarity are generated during the DBDs and then trapped at the top and bottom internal surfaces of the cavities, respectively.<sup>6</sup> The internally charged cavities form macroscopic dipoles that can be easily deformed under mechanical or electrical stress, leading to the desired direct or inverse piezoelectricity, respectively. In other words, the ferroic behavior in ferroelectrets originates from the nonuniform charge distribution inside the heterogeneous material combined with its nonuniform elastic properties (both on a macroscopic scale). The density of the macroscopic dipoles represents an effective polarization in ferroelectrets, in analogy to the volume polarization in conventional ferroelectrics.

Although the ferroic behavior of ferroelectrets is phenomenologically similar to that observed on typical ferroelectrics,

the mechanism is quite different. The macroscopic dipoles in ferroelectrets are not intrinsic ionic or molecular dipoles, but rather cavities (or more generally heterogeneities) with trapped space charge on internal surfaces. A few important conditions for ferroelectric behavior in different types of materials are summarized in Table I. Here, the existence of a polarization-*versus*-electric-field ( $P(E)$ ) hysteresis is an essential feature of ferroelectric materials. It is often investigated for characterizing some of their properties such as the spontaneous polarization, the coercive field, and the polarization reversal under various conditions. On inorganic ferroelectrics (single crystals and multi-crystalline ceramics), the  $P(E)$  hysteresis is often recorded with a Sawyer-Tower (ST) circuit.<sup>7</sup> An ST circuit is a series connection of the sample and a standard capacitor whose capacitance is much larger than the sample capacitance so that the voltage applied to the circuit is found almost completely across the sample, while the standard capacitor—for continuity reasons—must carry the same displacement charge as the sample.

The ST method is particularly suitable for materials with negligible internal conductivity. For such materials, the applied voltage and the voltage across the standard capacitor are recorded on an oscilloscope, and a hysteresis curve is obtained by plotting the latter *versus* the former (with appropriate scaling). In practice, the recorded curve is often deformed because of the influence of circuit elements and/or the electrical conductivity in the material under test. In this case, it is necessary to modify the ST circuit in order to compensate the

<sup>a)</sup>Electronic mail: xunlin@canopus.physik.uni-potsdam.de

TABLE I. Ferroelectric behavior: Evidence in various materials classes (necessary and sufficient conditions).

Condition for Ferroelectric Behavior	Single- or Multi-Crystalline Polar Material	Semi-Crystalline Polymer or Polymer-Based Composite	Heterogeneous Material with Interface Charge
Curie Phase Transition	Always Observed	Sometimes Masked	Never Observed
Symmetry Breaking	Induced by Curie Transition (plus Poling)	Induced by Curie Transition plus Poling	Induced by Electric Poling
Spontaneous Polarization	Related to Curie Transition	Related to Curie Transition	So Far Not Observed
Hysteresis Behavior	Dipole Reorientation + Domain Walls	Dipole Reorientation + Crystallite Boundaries	Breakdown Threshold of Internal Guest Phase

distortions<sup>8–11</sup> and/or to extract the  $P(E)$  hysteresis from the recorded data by means of suitable numerical processing.<sup>12–14</sup>

Compared with inorganic ferroelectrics, ferroelectric polymers such as  $\beta$ -phase polyvinylidene fluoride (PVDF) and some of its copolymers usually have much higher coercive fields of 50–100 MV/m (about one order of magnitude higher than the typical values for inorganic ferroelectrics) and much longer switching time for the dipoles. In addition, destructive breakdown is often observed in ferroelectric polymer samples under high voltages, in particular at high frequencies. Therefore,  $P(E)$  hysteresis curves of ferroelectric polymers are often determined by measuring and analyzing the poling currents under very slowly AC voltages at frequencies down to the mHz region.<sup>15,16</sup> The recorded current may be separated into three components as follows:<sup>17</sup>

$$i = i_{\text{cap}} + i_p + i_{\text{cond}} = C_s \frac{dV_s}{dt} + A_s \frac{dP_s}{dt} + \frac{V_s}{R_s}, \quad (1)$$

where  $C_s$  is the capacitance of the sample,  $V_s$  is the voltage applied to the sample,  $t$  is the time,  $A_s$  is the sample area, and  $P_s$  and  $R_s$  are the ferroelectric polarization and the electrical resistance of the sample, respectively. The three main contributions to the observed current stem from the charging of the sample capacitance, from the orientation of the dipole polarization and from the conductivity in the sample. By use of a poling scheme with more than one bipolar cycle or with a combination of bipolar and unipolar semicycles, it is possible to separate the contributions of the conduction processes and of the sample-capacitance charging. The remaining current represents only the contribution of the dipole orientation, and consequently, its integration over time allows for the determination of the overall polarization in the sample at any time.<sup>16</sup>

The polarization of ferroelectrets relies on charge separation by means of DBDs and charge trapping on the internal surfaces of the cavities. Paschen's law governs the onset of the DBDs in the cavities. Therefore, the dimensions of the cavities, the composition of the gas inside the cavities, and its pressure all strongly influence the charging process.<sup>18–22</sup> In comparison with the alignment of the dipole polarization in ferroelectric polymers, DBDs in the cavities of ferroelectrets are very fast processes. The transient current pulses of the DBDs are much shorter than the time resolution of the current-voltage mode  $P(E)$  hysteresis measurements that are

usually carried out on ferroelectric polymers. Consequently, measurements in the current-voltage mode are not feasible for studying hysteresis phenomena on ferroelectrets in real time. In our previous work, hysteresis curves on cellular polypropylene (PP) ferroelectrets were obtained by means of acoustic measurements in combination with dielectric resonance spectroscopy (DRS).<sup>23</sup> This method does, however, not lend itself easily to ferroelectrets with non-planar surface topographies such as the fluoroethylenepropylene (FEP) copolymer film systems with tubular channels that we study here.

In this paper, hysteresis curves on ferroelectrets are measured in a voltage-voltage mode—with a setup that is similar to the one we used recently for studying the re-breakdown in thin discharge gaps.<sup>24</sup> In the voltage-voltage mode, the charge flowing through the sample during charging is determined from the voltage across a standard capacitor that is connected in series with the sample. The capacitance of the standard capacitor is much larger than that of the sample. Another standard capacitor, which has a capacitance much smaller than the first standard capacitor, but still substantially larger than the sample, is also connected in series to serve as a high-voltage divider and to protect the electrometer that is employed for the voltage measurements. We also show that the contributions from the sample conductivity and from the charging of its capacitance can be subtracted from the measured charge by use of a voltage waveform that consists of two positive sinusoidal semicycles followed by two negative ones. Evaluation of the resulting data leads to the hysteresis curves of the respective ferroelectret films.

## II. EXPERIMENTS

Cellular PP samples were prepared from commercial films (PQ50<sup>TM</sup> from Nan Ya Plastics Corp., Taiwan, China) industrially produced by stretching filler-loaded PP under suitable conditions.<sup>25</sup> The initial thickness and density are 50  $\mu\text{m}$  and 550  $\text{kg}/\text{m}^3$ , respectively. In order to optimize their electro-mechanical properties, the samples were inflated by gas-diffusion expansion in nitrogen with a subsequent heat treatment for stabilization.<sup>26</sup> The samples were then metalized on both surfaces with aluminum electrodes 20 mm in diameter. The final sample thickness is about 70  $\mu\text{m}$ , determined by means of a mechanical thickness gauge with constant spring loading.

Teflon<sup>TM</sup> FEP film systems with tubular channels were prepared by means of thermal lamination as described before.<sup>27</sup> In this process, two polymer-electret films are laminated around a structured polymer template between them. The template must have a melting temperature higher than that of the electret films, so that the electret films can be fused to each other through the openings in the template. Here, two films of Teflon<sup>TM</sup> FEP with a thickness of 50  $\mu\text{m}$  each were laminated at 300 °C around a 100  $\mu\text{m}$  thick polytetrafluoroethylene (PTFE) template. The template, 35 mm  $\times$  45 mm in area, contained parallel rectangular openings (area 1.5 mm  $\times$  40 mm) that were cut by means of a computer-controlled laser system. The PTFE stripes between neighboring openings also had a width of 1.5 mm. After the outer Teflon<sup>TM</sup>-FEP layers have been fused, the template is removed, which results in a Teflon<sup>TM</sup>-FEP film system with open tubular channels. The samples were also metallized on both sides with aluminum electrodes having a diameter of 20 mm.

Figure 1 schematically shows the measuring circuits. The voltage is applied to the sample by means of a high-voltage (HV) supply (FUG HCB 7-6500) controlled by an arbitrary-waveform function generator (HP 33120 A). Figure 1(a) shows the circuit diagram for hysteresis measurements on ferroelectric polymers in the current–voltage mode.<sup>28</sup> The poling current is recorded with an electrometer (HP3458A) in the current mode. A resistor  $R_1$  of 1.97 M $\Omega$  is connected in series with the sample, in order to protect the electrometer against breakdown in the sample. Figure 1(b) schematically illustrates the modified Sawyer–Tower circuit employed here for hysteresis experiments on polymer ferroelectrets. It consists of a series connection of the sample, an HV capacitor  $C_1$  (3 nF), and a large standard capacitor  $C_m$  (1  $\mu\text{F}$ ). The voltage  $V_{\text{out}}(t)$  across  $C_m$  is probed by means of the same electrometer as before (Fig. 1(a)), but now operated in the voltage mode with an input impedance  $R_m > 10\text{G}\Omega$ . We made sure that all parasitic capacitances are at least ten times smaller than any of the circuit capacitors.

The waveform of the applied voltage is shown in Fig. 2 (left y-axis). One complete voltage loop consists of two positive sine-squared semicycles ( $\sin^2(\omega t)$ ) followed by two negative ones ( $-\sin^2(\omega t)$ ). In the figure, the voltage semicycles are consecutively numbered for clarity and later reference. A computer that controls the voltage source and the multimeter

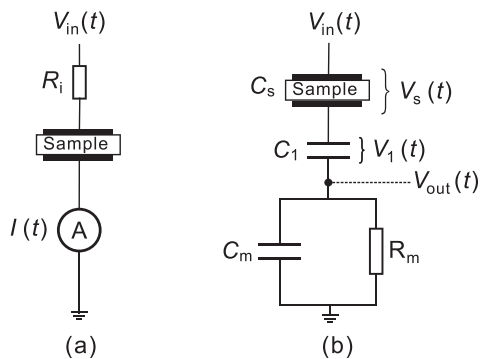


FIG. 1. Schematic view of the circuits employed for (a) hysteresis measurements on ferroelectric polymers in the current–voltage mode and (b) hysteresis experiments on ferroelectrets in the voltage–voltage mode.

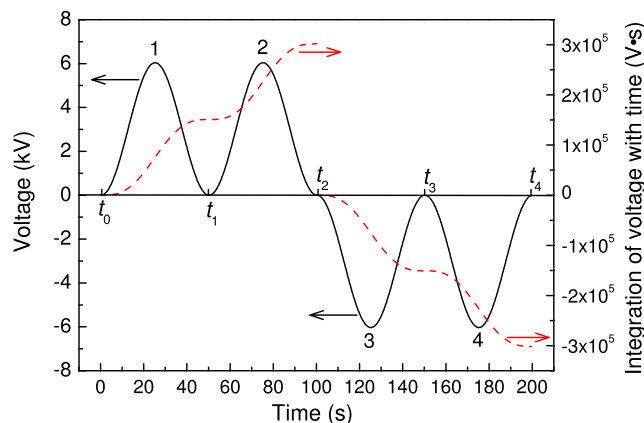


FIG. 2. Temporal waveform of the voltage applied to the ferroelectret samples (solid line, left y-axis) and integral of the voltage over time (dashed line, right y-axis).

also stores  $V_{\text{in}}(t)$  and  $I(t)$  (Fig. 1(a)) or  $V_{\text{out}}(t)$  (Fig. 1(b)), respectively. Two consecutive voltage loops were applied for each measurement (for a total duration of 400 s in each case).

### III. RESULTS AND DISCUSSION

#### A. Current–voltage measurements on cellular and tubular-channel ferroelectrets

The current recorded on a cellular-PP ferroelectret film during the second applied-voltage loop is shown in Fig. 3(a). Because of the charging and discharging of the sample capacitance, the current–versus–voltage curves are essentially elliptical. In addition, several current peaks are observed. They originate from the DBD charging processes inside the sample cavities. As can be seen in the figure, the current measured during semicycles 1 and 3 (*i.e.*, when the applied voltage increases from zero to its maximum) shows very significant peaks, while almost no peaks are observed when the applied voltage decreases from its maximum, and only a limited number of small peaks appear when the voltage approaches zero. In comparison, the currents measured during semicycles 2 and 4, respectively, exhibit quite a different behavior when the applied voltage increases from zero to its maximum, although similar behavior is observed when the voltage decreases from its maximum to zero. Now, only a limited number of peaks are seen when the applied voltage approaches its maximum in its rising phase. This behavior is easily explained by the different sample histories for different semicycles: Immediately before semicycles 1 and 3, the sample had been charged with opposite polarity, while the sample had been previously charged with the same polarity just before semicycles 2 and 4, respectively. The space charges deposited on the inner surfaces of the cavities during the previous voltage semicycle generate an internal electric field that either facilitates (semicycles 1 and 3) or hinders (semicycles 2 and 4) the DBDs in the subsequent voltage semicycle. When the internal electric field is strong enough, back discharges may be triggered when the decreasing applied voltage approaches zero.<sup>29</sup> This is confirmed by the observation of some relatively small current peaks upon the approach to zero in all voltage semicycles.

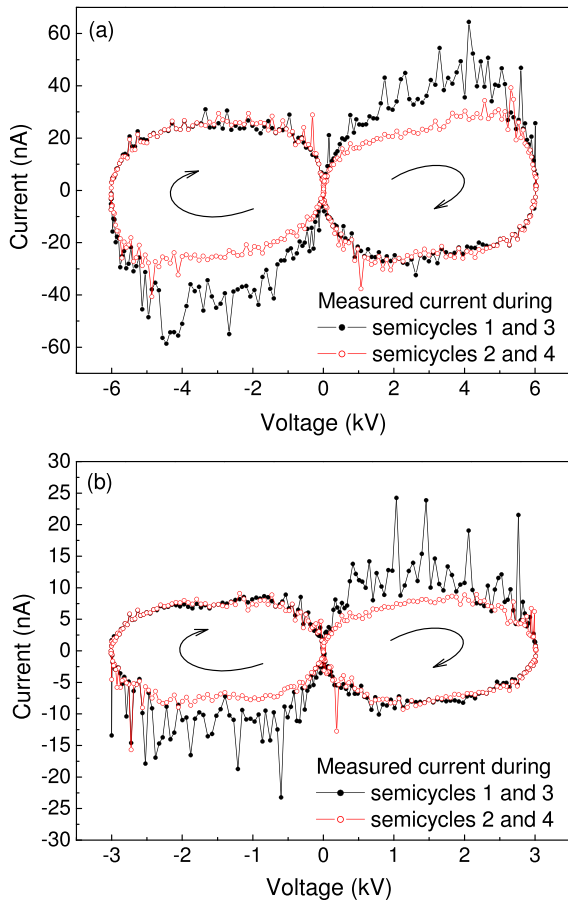


FIG. 3. Charging currents on (a) a cellular PP ferroelectret film and (b) a Teflon™-FEP tubular-channel ferroelectret system recorded during the second complete voltage loop according to Fig. 2 (the respective semicycles are indicated by numbers). The progress of the measurement during the semicycles is illustrated by arrows.

Figure 3(b) shows the current measured on a Teflon™-FEP ferroelectret system with tubular channels. Here, the maximum voltage was set to 3 kV instead of the 6 kV maximum for cellular PP ferroelectrets that is also depicted in Fig. 2. According to a previous study, the polarization saturates around this voltage<sup>27</sup> so that higher voltages would only lead to back discharges upon the return of the applied voltage to zero. Except for the smaller maximum of the applied voltage, Fig. 3(b) indicates the same behavior as Fig. 3(a), even though the sample structure has been quite different (open tubular channels instead of closed ellipsoidal foam cells).

As mentioned before, DBDs in ferroelectrets are extremely fast processes. Time-resolved measurements of the light emission from such a discharge indicate that an individual DBD inside a cavity takes only a few ns.<sup>30</sup> During ferroelectret charging, the DBDs produce numerous transient current pulses, and the individual pulse durations are much shorter than the time resolution that is possible in the current–voltage mode  $P(E)$  hysteresis measurements. Therefore, Figs. 3(a) and 3(b) yield only qualitative information about the occurrence of DBDs in the sample, and a precise quantitative analysis of the amount of charge transported during the DBDs cannot be done by integrating the recorded current over time.

## B. Ferroelectret hysteresis measurements in voltage–voltage mode

As discussed above, hysteresis measurements in the voltage–voltage mode are also indicated for polymer ferroelectrets. To this end, a standard capacitor of 1  $\mu\text{F}$  ( $C_m$  in Fig. 1(b)) has been connected in series with the sample, so that the voltage across the capacitor, which can be easily measured by means of an electrometer, is a scaled integral of the current that flows through the circuit. Another high-voltage capacitor of 3 nF ( $C_1$  in Fig. 1(b)) is also connected in series as a voltage divider that protects the electrometer in case of electrical breakdown in the sample.

Integrating Eq. (1), we obtain the charge flowing through the circuit,

$$\begin{aligned} Q(t) &= Q_{\text{cap}}(t) + Q_p(t) + Q_{\text{cond}}(t) \\ &= C_s V_s(t) + A_s P_s(t) + \frac{1}{R_s} \int_0^t V_s(t') dt'. \end{aligned} \quad (2)$$

A fresh sample was used in each measurement. At the beginning of each measurement,  $C_1$  and  $C_m$  are discharged, so that the voltages can be expressed as

$$V_1(t) = \frac{1}{C_1} \int_0^t i(t') dt', \quad (3)$$

$$V_{\text{out}}(t) = \frac{1}{C_m} \int_0^t i(t') dt' = \frac{C_1}{C_m} V_1(t), \quad (4)$$

and

$$V_{\text{in}}(t) = V_s(t) + V_1(t) + V_{\text{out}}(t). \quad (5)$$

$C_1$  and  $C_m$  are standard capacitors ( $C_m \gg C_1 \gg C_s$ ) so that  $V_s \gg V_1 \gg V_m$  and, from Eq. (5),  $V_{\text{in}} \approx V_s$ , which results in

$$Q(t) = C_s V_{\text{in}}(t) + A_s P_s(t) + \frac{1}{R_s} \int_0^t V_{\text{in}}(t') dt'. \quad (6)$$

Since the decay of  $V_{\text{out}}$  through  $R_m$  (with a time constant  $> 10$  ks) is much slower than the total measuring time, it follows that

$$Q(t) \approx C_m V_{\text{out}}. \quad (7)$$

Finally, as  $C_m \gg C_1 \gg C_s$  and as the capacitors are connected in series,  $C_s$  can be approximated by the equivalent capacitance  $C$  of the circuit and

$$C_m V_{\text{out}} \approx C V_{\text{in}}(t) + A_s P_s(t) + \frac{1}{R_s} \int_0^t V_{\text{in}}(t') dt'. \quad (8)$$

## C. Voltage–voltage hysteresis experiments on cellular polypropylene ferroelectrets

The charge recorded on a cellular PP ferroelectret during the first loop of the applied voltage is shown in Fig. 4(a). Initially, the charge increases from zero almost linearly, as



$V_{in}$  rises according to Fig. 2. When  $V_{in}$  reaches a sufficiently high value, DBDs are triggered inside the cavities and, as a result, the slope of the  $Q$ -versus- $V_{in}$  curve increases. The slope keeps rising, as  $V_{in}$  further increases, and  $Q$  reaches  $0.52 \mu\text{C}$  at the maximum of  $V_{in} = 6 \text{ kV}$ .  $Q$  decreases when  $V_{in}$  is reduced from its maximum. However, the charge during the decrease of the absolute voltage is higher than the corresponding charge during its increase. A remaining charge  $Q$  of about  $0.14 \mu\text{C}$  is measured when  $V_{in}$  reaches zero ( $Q(t_1)$  in Fig. 4(a)). At the beginning of semicycle 2,  $Q$

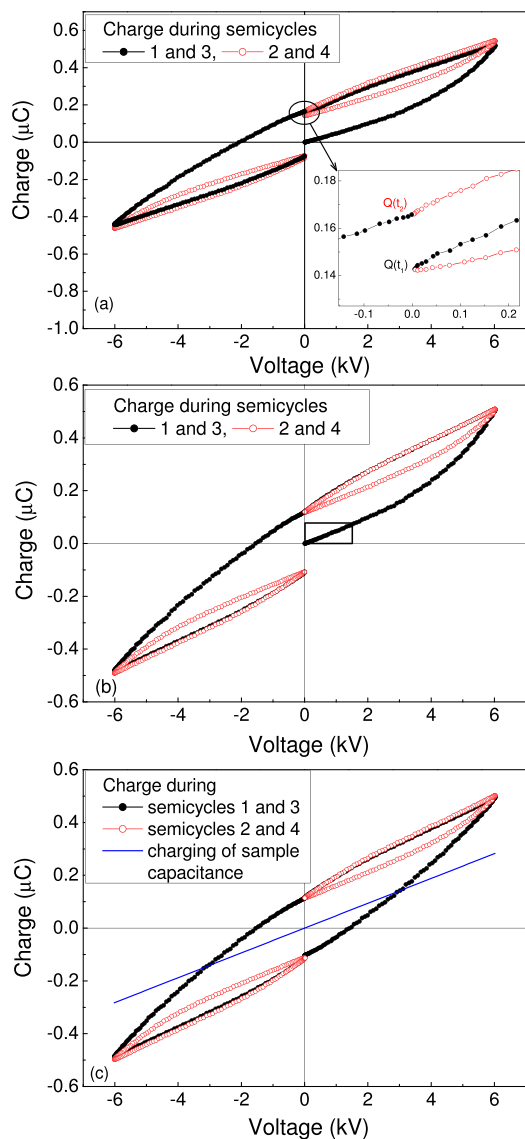


FIG. 4. Measured and calculated charge as a function of the applied voltage for a cellular PP ferroelectret film. (a) Charge measured during the first voltage loop. The sample resistance is determined from the small difference between the ordinates of the last points of two consecutive semicycles with the same polarity (for positive voltage, an enlarged view of the difference is shown in the inset). (b) Calculated charge without the contribution from the sample conductivity during the first voltage loop. The difference between the end points of two subsequent semicycles disappears. A linear fit of the initial part of the curve (highlighted with a rectangular box) yields a sample capacitance of  $49.4 \text{ pF}$ . (c) Calculated charge without the contribution from the sample conductivity during the second voltage loop. The straight line represents the contribution obtained from the charging of the calculated sample capacitance.

again first increases linearly with  $V_{in}$  in the same way as during semicycle 1. The linear increase lasts up to a higher applied voltage than in semicycle 1. Subsequently, the slope increases only slightly, and  $Q$  reaches  $0.54 \mu\text{C}$  at  $6 \text{ kV}$ . The charge curve during the decrease of the applied voltage lies slightly above that of semicycle 1, and ends with a charge  $Q$  of  $0.16 \mu\text{C}$  ( $Q(t_2)$  in Fig. 4(a)). The charge  $Q$  decreases to zero, as  $V_{in}$  is further reduced to negative values (semicycle 3), then changes its polarity and decreases further to negative values, as  $V_{in}$  also becomes more negative. The charge curve upon the decrease of the absolute voltage in semicycle 3 and the curve during semicycle 4 are quite similar to those of semicycles 1 and 2, respectively (but of course inverted with respect to the origin of the coordinate system).

According to a previously developed basic model for the poling process of ferroelectrets,<sup>29</sup> back discharges occur in the same way during a voltage decrease in the voltage semicycles if the polarity and the maximum value are the same. Equation (2) indicates that the differences between the voltage-reduction phases of semicycles 1 and 2 and between the same phases of semicycles 3 and 4 can be attributed to electrical conduction in the sample. The respective sample resistances  $R_{s+}$  and  $R_{s-}$  for the two positive (1 and 2) and the two negative (3 and 4) semicycles can be determined via

$$\Delta Q_+ = Q(t_2) - Q(t_1) = \frac{1}{2R_{s+}} \int_{t_0}^{t_2} V_{in}(t') dt' \quad (9)$$

and

$$\Delta Q_- = Q(t_4) - Q(t_3) = \frac{1}{2R_{s-}} \int_{t_2}^{t_4} V_{in}(t') dt', \quad (10)$$

if they are assumed to be independent of the absolute voltage. In Eqs. (9) and (10),  $Q(t_i)$  ( $i = 1 \dots 4$ ) is the charge measured at the end of the  $i^{\text{th}}$  voltage semicycle. In order to make sure that the difference between subsequent semicycles of the same polarity is only caused by the sample conductivity, additional experiments with a third semicycle for each polarity were performed on PP ferroelectrets under otherwise identical conditions. The additional semicycles yield practically the same charge differences as before, which confirms our assumption.

As can be seen from Fig. 4(a),  $\Delta Q_+$  and  $\Delta Q_-$  are substantially smaller than  $Q(t_i)$ . This is to be expected, since ferroelectret films are highly insulating (a typical feature of non-polar electret polymers). The integration of  $V_{in}(t)$  for both polarities can be easily carried out numerically (Fig. 2 (right y-axis)). Once  $R_{s+}$  and  $R_{s-}$  have been determined, the contribution from the conduction current  $Q_{con}(t)$  in the sample can be calculated and subtracted from the measured charge  $Q(t)$ . Figure 4(b) shows the calculated charge after subtracting the aforementioned contribution from the curve in Fig. 4(a). The phases of absolute-voltage decrease in semicycles 2 and 4 now agree well with those of semicycles 1 and 3, respectively.

If it is assumed that the sample capacitance is also independent of the applied voltage, the charge build-up on the sample capacitance yields a straight line as a function of the



applied voltage regardless of its waveform.<sup>24</sup> The initial part of semicycle 1 in Fig. 4(b) represents such a straight line. A capacitance of 49.4 pF is determined by a linear fit of the part enclosed with a rectangular box in the figure. Obviously, the initial parts of semicycle 2 and of semicycle 4 are two lines that are parallel with the respective part of semicycle 1 and hence carry the same information. Therefore, the sample capacitance can also be evaluated by a linear fit of these two parts. This is particularly useful when a sample with unknown charging history is used, in which case the initial part of semicycle 1 might not be suitable for a linear fit. With the capacitance value, the contribution  $Q_{\text{cap}}(t)$  from the charging of the sample capacitance can be calculated over the whole voltage range, which is shown in Fig. 4(c) (straight blue line). Also shown in Fig. 4(c) is the calculated charge for the second voltage loop without the contribution from the sample conductivity.

By subtracting  $Q_{\text{cap}}$  from the calculated charge shown in Fig. 4(c), we obtain the charge contribution solely from the polarization generated by the DBDs inside the cavities. Taking into account the electrode area and the sample thickness, we finally obtain the polarization in the sample as a function of the applied electric field. Semicycles 1 and 3 then yield directly the  $P(E)$  hysteresis curve (Fig. 5). From the figure, a coercive field  $E_C$  (at which the polarization is zero) of 47 MV/m and a remanent polarization  $P_r$  (defined as the polarization at zero electric field) of 0.35 mC/m<sup>2</sup> are determined, respectively.

In a simplified model of ferroelectrets that consists of alternating polymer and air layers, the effective polarization  $\sigma_{\text{eff}}$  is defined as<sup>31,32</sup>

$$\sigma_{\text{eff}} = \sum s_{2i} \sigma_i / \sum s_{2i}, \quad (11)$$

where  $s_{2i}$  is the thickness of the  $i^{\text{th}}$  gas layer, and  $\sigma_i$  is the charge density on the internal polymer surfaces facing the  $i^{\text{th}}$  gas layer. It should be noted that  $P_s$  determined in this study is not the effective polarization  $\sigma_{\text{eff}}$ . Rather, it is the electric displacement on the sample electrodes that is induced by  $\sigma_{\text{eff}}$ . According to Paaanen *et al.*<sup>31</sup> and Sessler and Hillenbrand,<sup>32</sup>

$$P_s = \frac{\epsilon_p s_2 \sigma_{\text{eff}}}{s_1 + \epsilon_p s_2}, \quad (12)$$

where  $\epsilon_p$  is the relative permittivity of solid PP,  $s_1$  and  $s_2$  are the total thickness of the solid polymer layers and the gas layers, respectively, with  $s = s_1 + s_2$  being the total film thickness. Because the density of PP is known and the density of air can be approximated as zero, the quantities  $s_1$  and  $s_2$  can be determined from the film density provided by the manufacturer and from the measured thickness.  $\epsilon_p$  is assumed to be approximately 2.2. Thus,  $P_r$  in Fig. 5 corresponds to a  $\sigma_{\text{eff}}$  of 0.49 mC/m<sup>2</sup>. In prior studies, a  $\sigma_{\text{eff}}$  of 0.5 mC/m<sup>2</sup> was determined on the same film type.<sup>23,29</sup> For other types of cellular PP ferroelectrets,  $\sigma_{\text{eff}}$  values from 0.36 to 0.86 mC/m<sup>2</sup> were reported.<sup>31,33</sup> Therefore, the  $\sigma_{\text{eff}}$  determined here is in good agreement with previous findings.

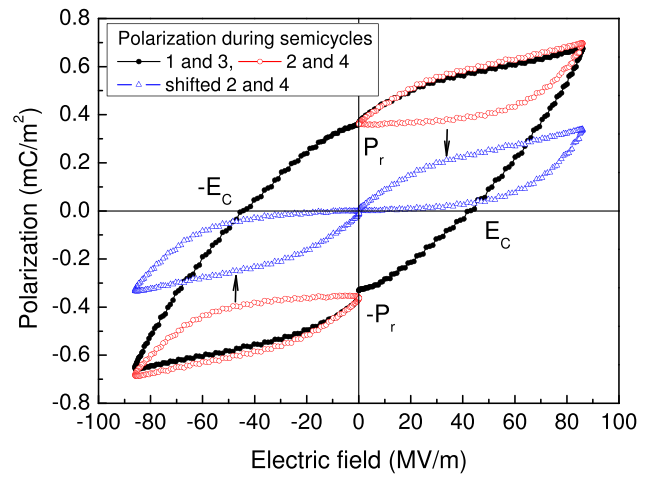


FIG. 5. Polarization as a function of the electric field (calculated from Fig. 4(c) by subtracting the contribution from the charging of the sample capacitance). Subtracting the remaining polarization  $P_r$  from the charge curves of semicycles 2 and 4 yields two curves (blue triangles) containing solely the back-discharge-relevant polarization during the charging process.

Another feature of the  $P(E)$  hysteresis curve composed of semicycles 1 and 3 in Fig. 5 is that  $P_s$  decreases significantly when the absolute value of the applied electric field is reduced from its maximum to zero.  $P_r$  is only about half of  $P_s$  at the maximum electric field. The large decrease of  $P_s$  during reduction of the absolute value of the external electric field is caused by back discharges that are triggered by the internal electric field of the space charge deposited on the air-polymer interfaces inside the cavities.<sup>29</sup>

Semicycles 2 and 4 are quite different from semicycles 1 and 3 because of different sample histories. For both semicycles 2 and 4, the sample has previously been charged during a voltage semicycle of the same polarity. Therefore,  $P_s$  first remains at  $P_r$ , as the electric field increases.  $P_s$  then starts to increase at sufficiently high electric fields, indicating that DBDs are triggered again and some additional polarization is generated.  $P_s$  finally reaches the maximum polarization value of the respective previous cycle (1 or 3). The decreasing phase of semicycles 2 and 4 is, however, almost the same as that of the respective previous semicycles, *i.e.*, the additional polarization generated during the rising phase is again completely lost by the back discharges. Therefore, semicycles 2 and 4 contain information about the back-discharge-relevant non-remanent component of the polarization. The non-remanent component is superimposed on  $P_r$ , which is the initial polarization for semicycles 2 and 4.

Shifting semicycles 2 and 4 towards the  $x$ -axis by  $P_r$  results in two curves containing only the back-discharge-relevant polarization (blue triangles in Fig. 5). This component of the polarization can be subtracted from the hysteresis curve composed of semicycles 1 and 3 in Fig. 5. The resulting parallelogram-like polarization-*versus*-electric-field hysteresis curve contains only the net polarization that is independent of the back discharges (open circles in Fig. 6). With this calculation, the assumption of a voltage-independent sample capacitance is no longer necessary. It is found that the hysteresis curve obtained in this way is very similar to the one theoretically predicted under the assumption of cavities with

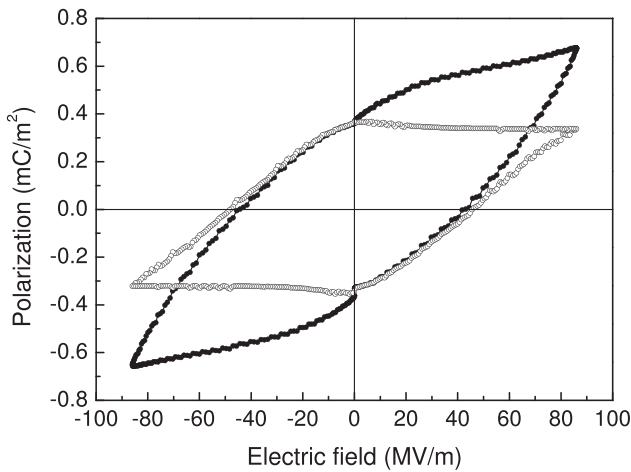


FIG. 6. Polarization as a function of the electric field for the cellular PP ferroelectret film of Fig. 4. Solid circles: polarization originated from the dielectric barrier discharges in cavities. Open circles: polarization without the component related to back discharges.

uniform dimensions.<sup>34,35</sup> With this assumption, back discharges occur only after saturation of the polarization, and consequently, the shape of the hysteresis loop is a parallelogram. For comparison, the hysteresis composed of semicycles 1 and 3 in Fig. 5 is also shown in Fig. 6 (solid circles). The two hysteresis curves in Fig. 6 show the same remanent polarization, and the respective values of the coercive field do also not differ much.

#### D. Voltage–voltage hysteresis experiments on tubular-channel FEP–copolymer ferroelectrets

Using the method proposed here, we also determined the hysteresis loop of the FEP–copolymer ferroelectret system with tubular channels. Figure 7(a) shows the measured charge as a function of the applied voltage during the second voltage loop. It turns out that  $\Delta Q_+$  and  $\Delta Q_-$  are now negligibly small. This is not surprising, since the maximum of the applied voltage is relatively small ( $\pm 3$  kV) and also since Teflon<sup>TM</sup>–FEP is one of the polymers with the best electrical-insulation characteristics. Therefore, we do not need to subtract the contribution from the sample conductivity. The contribution from the sample capacitance  $Q_{\text{cap}}$  is subtracted from the measured charge in the same way as detailed above. Taking into account the electrode area, we obtain the polarization  $P_s$  generated by the DBDs inside the tubular channels. Because of the special cavity structure of the FEP–copolymer film system with tubular channels, the measured value of the sample thickness strongly depends on the external stress applied during the measurement.<sup>36</sup> Consequently, the thickness value measured by means of the thickness gauge might be much smaller than the real thickness during the hysteresis measurement. A precise determination of the sample thickness, e.g., by interferometry, will not be attempted here. In Fig. 7(b), the polarization induced by the DBDs in the channels (solid circles) and the net polarization without the back-discharge-relevant component (open circles) are plotted as a function of the applied voltage. Compared with the cellular PP ferroelectret, both hysteresis curves of the FEP–copolymer film system

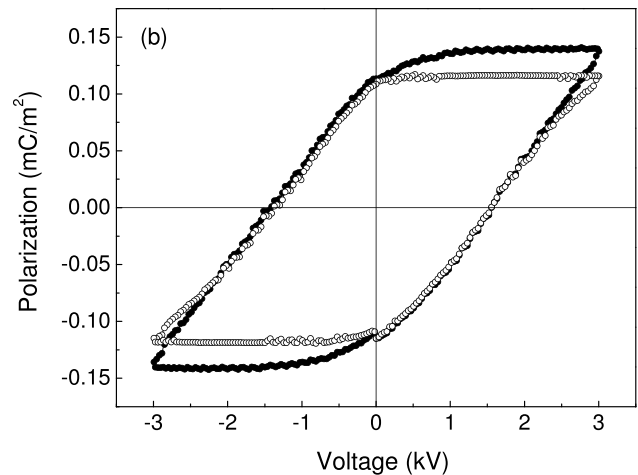
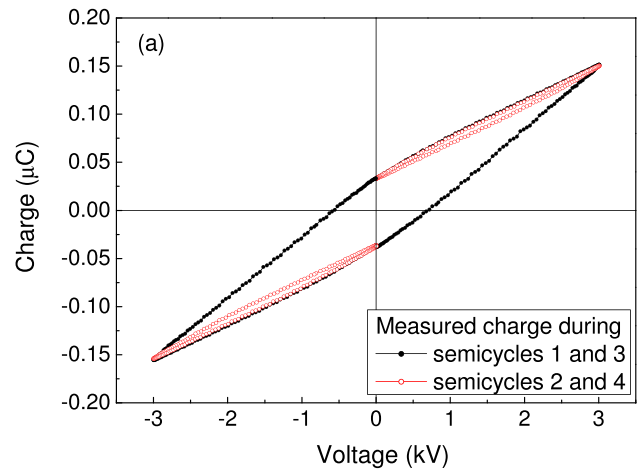


FIG. 7. (a) Measured charge as a function of the applied voltage for a Teflon<sup>TM</sup>–FEP ferroelectret film with tubular channels. (b) Polarization as a function of the applied voltage. Solid circles: polarization originated from the dielectric barrier discharges in tubular channels. Open circles: polarization without the component related to back discharges.

with tubular channels exhibit a much more parallelogram-like shape because of the more uniform cavity structure. The small deviation of the curves from ideal parallelograms might be caused by small differences in the cavity parameters that can not be avoided during the manual preparation of individual samples in our laboratory.

#### IV. CONCLUSION

Measurements in a voltage–voltage mode have been proposed and demonstrated for obtaining hysteresis loops on ferroelectret films. The measuring circuit, which consists of two standard capacitors connected in series with the sample under test, represents a modified Sawyer–Tower circuit. The charge flowing through the circuit is evaluated by measuring the voltage on the large standard capacitor, while the other, somewhat smaller standard capacitor is employed as a voltage divider that protects the electrometer in case of destructive breakdown in the sample. The charge that can be determined in our measurements has contributions from conduction processes in the sample, from the charging of the

sample capacitance, and from the desired internal DBD charging inside the cavities. Using voltage loops composed of two positive sine-squared semicycles (1 and 2) followed by two negative ones (3 and 4), the contributions from the sample conductance and the sample capacitance can be subtracted from the recorded charge values, and the ferroelectric hysteresis curve of the sample is directly obtained from semicycles 1 and 3. From the hysteresis loop, the remanent polarization and the coercive field or voltage can be read. In addition, semicycles 2 and 4 provide the back-discharge-relevant non-remanent component of the polarization. By subtracting this component, a hysteresis loop containing solely the net remanent polarization is obtained.

## ACKNOWLEDGMENTS

Mobility funding from CAPES (Brazil) and DAAD (Germany) (PROBRAL Project 54392969 & 316/09, respectively) is gratefully acknowledged. The German authors are also indebted to the European Union for co-funding some of the equipment used in the study. R.G. thanks the Fundação de Amparo à Pesquisa do Estado de São Paulo (FAPESP) and the Lady Davis Fellowship Trust (LDFT) for granting him Visiting Professorships at the Universidade de São Paulo (USP) and at the Hebrew University of Jerusalem (HUJI), respectively.

- <sup>1</sup>R. Gerhard(-Mulhaupt), *IEEE Trans. Dielectr. Electr. Insul.* **9**, 850 (2002).
- <sup>2</sup>S. Bauer, R. Gerhard(-Mulhaupt), and G. M. Sessler, *Phys. Today* **57**(2), 37 (2004).
- <sup>3</sup>M. Wegener and S. Bauer, *Chem. Phys. Chem.* **6**, 1014 (2005).
- <sup>4</sup>X. Qiu *J. Appl. Phys.* **108**, 011101 (2010).
- <sup>5</sup>U. Kogelschatz, *Plasma Chem. Plasma Process.* **23**, 1 (2003), and references therein.
- <sup>6</sup>X. Qiu, R. Gerhard, and A. Mellinger, *IEEE Trans. Dielectr. Electr. Insul.* **18**, 34 (2011).
- <sup>7</sup>C. B. Sawyer and C. H. Tower, *Phys. Rev.* **35**, 269 (1930).
- <sup>8</sup>H. Roetschi, *J. Sci. Instrum.* **39**, 152 (1962).
- <sup>9</sup>P. Zurcher, R. E. Jones, P. Chu, T. Lii, and S. J. Gillespie, *Integr. Ferroelectr.* **10**, 205 (1995).

- <sup>10</sup>K. Singh, S. S. Limaye, R. U. Tiwari, S. Nath, and S. S. Bhoga, *Ferroelectrics* **189**, 9 (1996).
- <sup>11</sup>J. H. Park, B. K. Kim, J. G. Park, I. T. Kim, H. J. Je, Y. Kim, and S. J. Park, *Ferroelectrics* **230**, 151 (1999).
- <sup>12</sup>R. Bouregba and G. Poullain, *Ferroelectrics* **274**, 165 (2002).
- <sup>13</sup>R. Bouregba, B. Vilquin, G. Le Rhun, and G. Poullain, *Rev. Sci. Instrum.* **74**, 4429 (2003).
- <sup>14</sup>C. K. Wong and F. G. Shin, *J. Appl. Phys.* **98**, 024104 (2005).
- <sup>15</sup>B. Dickens, E. Balizer, A. S. DeReggi, and S. C. Roth, *J. Appl. Phys.* **72**, 4258 (1992).
- <sup>16</sup>M. Wegener *Rev. Sci. Instrum.* **79**, 106103 (2008).
- <sup>17</sup>R. Gerhard(-Mulhaupt) *Ferroelectrics* **75**, 385 (1987).
- <sup>18</sup>M. Paajanen, M. Wegener, and R. Gerhard(-Mulhaupt), *J. Phys. D: Appl. Phys.* **34**, 2482 (2001).
- <sup>19</sup>X. Qiu, M. Wegener, W. Wirges, X. Zhang, J. Hillenbrand, Z. Xia, R. Gerhard(-Mulhaupt), and G. M. Sessler, *J. Phys. D: Appl. Phys.* **38**, 649 (2005).
- <sup>20</sup>P. Fang, M. Wegener, W. Wirges, R. Gerhard, and L. Zirkel, *Appl. Phys. Lett.* **90**, 192908 (2007).
- <sup>21</sup>X. Qiu, A. Mellinger, and R. Gerhard, *Appl. Phys. Lett.* **92**, 052901 (2008).
- <sup>22</sup>S. Harris and A. Mellinger, *Appl. Phys. A* **107**, 553 (2012).
- <sup>23</sup>X. Qiu, R. Gerhard, and A. Mellinger, *IEEE Trans. Dielectr. Electr. Insul.* **17**, 1043 (2010).
- <sup>24</sup>H. C. Basso, X. Qiu, W. Wirges, and R. Gerhard, *Appl. Phys. Lett.* **102**, 012904 (2013).
- <sup>25</sup>A. Savolainen and K. Kirjavainen, *J. Macromol. Sci.: Pt. A - Chem.* **26**, 583 (1989).
- <sup>26</sup>M. Wegener, W. Wirges, J. Fohlmeister, B. Tiersch, and R. Gerhard(-Mulhaupt), *J. Phys. D: Appl. Phys.* **37**, 623 (2004).
- <sup>27</sup>R. A. P. Altafim, X. Qiu, W. Wirges, R. Gerhard, R. A. C. Altafim, H. C. Basso, W. Jenninger, and J. Wagner, *J. Appl. Phys.* **106**, 014106 (2009).
- <sup>28</sup>M. Wegener, W. Künstler, K. Richter, and R. Gerhard(-Mulhaupt), *J. Appl. Phys.* **92**, 7442 (2002).
- <sup>29</sup>X. Qiu, A. Mellinger, M. Wegener, W. Wirges, and R. Gerhard, *J. Appl. Phys.* **101**, 104112 (2007).
- <sup>30</sup>M. Lindner, S. Bauer-Gogonea, S. Bauer, M. Paajanen, and J. Raukola, *J. Appl. Phys.* **91**, 5283 (2002).
- <sup>31</sup>M. Paajanen, H. Välimäki, and J. Lekkala, in *Proceedings of the 10th International Symposium on Electrets, Delphi, Greece, 22–24 September 1999* (IEEE Service Center, Piscataway, NJ, 1999), pp. 735–738.
- <sup>32</sup>G. M. Sessler and J. Hillenbrand, *Appl. Phys. Lett.* **75**, 3405 (1999).
- <sup>33</sup>J. Hillenbrand, G. M. Sessler, and X. Zhang, *J. Appl. Phys.* **98**, 064105 (2005).
- <sup>34</sup>P. Zhang, Z. Xia, X. Qiu, F. Wang, and X. Wu, in *Proceedings of the 12th International Symposium on Electrets, Salvador, Brazil, 11–14 September 2005* (IEEE Service Center, Piscataway, NJ, 2005), pp. 39–42.
- <sup>35</sup>S. Zhukov and H. von Seggern, *J. Appl. Phys.* **102**, 044109 (2007).
- <sup>36</sup>W. Wirges, S. Raabe, and X. Qiu, *Appl. Phys. A* **107**, 583 (2012).

# Screen printing for producing ferroelectret systems with polymer-electret films and well-defined cavities

Martynas Sborikas · Xunlin Qiu · Werner Wirges ·  
Reimund Gerhard · Werner Jenninger · Deliani Lovera

Received: 24 May 2013 / Accepted: 24 September 2013 / Published online: 12 October 2013  
© Springer-Verlag Berlin Heidelberg 2013

**Abstract** We report a process for preparing polymer ferroelectrets by means of screen printing—a technology that is widely used for the two-dimensional patterning of printed layers. In order to produce polymer-film systems with cavities that are suitable for bipolar electric charging, a screen-printing paste is deposited through a screen with a pre-designed pattern onto the surface of a polymer electret film. Another such polymer film is placed on top of the printed pattern, and well-defined cavities are formed in-between. During heating and curing, the polymer films are tightly bonded to the patterned paste layer so that a stable three-layer system is obtained. In the present work, polycarbonate (PC) films have been employed as electret layers. Screen printing, curing and charging led to PC ferroelectret systems with a piezoelectric  $d_{33}$  coefficient of about 28 pC/N

that is stable up to 100 °C. Due to the rather soft patterned layer,  $d_{33}$  strongly decreases already for static pressures of tens of kPa. The results demonstrate the suitability of screen printing for the preparation of ferroelectret systems.

## 1 Introduction

Polymer foams are widely used in daily life. Their void-containing structures lead to mechanical, thermal as well as electrical properties that may be quite different from those of the same polymers in solid form [1]. It has been found that polymer foams or void-containing polymer-film systems can be rendered piezoelectric by means of internal electric charging. The charging process consists of dielectric barrier discharges (DBDs) [2, 3]. In DBDs, one or both electrodes of the discharge gap are insulated by dielectric layers [4]. During the DBD charging process, charges of opposite polarity are separated and then trapped at the internal top and bottom surfaces, respectively, of the gas-filled cavities inside the foams or three-dimensional structures. The internally charged cavities can be considered as man-made macroscopic dipoles. Such dipoles are easily deformed under mechanical or electrical stress, resulting in large direct and inverse piezoelectricity, respectively. The materials are called ferroelectrets because macroscopically they show ferroelectric behavior [5], while microscopically the charge trapping is the same as in other space-charge electrets [6–9].

Ferroelectrets have attracted considerable interest in research and industry due to their large piezoelectricity combined with good mechanical flexibility and high elastic compliance. Extensive studies on ferroelectrets were initiated about two decades ago by Finnish scientists who developed and studied cellular polypropylene (PP) [10]. Since then,

---

The remaining co-authors dedicate this paper to the memory of Dr. Werner Jenninger who contributed so much to ferroelectret research and to this manuscript and who suddenly passed away on 11 January 2012.

---

M. Sborikas · X. Qiu (✉) · W. Wirges · R. Gerhard  
Applied Condensed-Matter Physics, Institute of Physics and  
Astronomy, University of Potsdam, Karl-Liebknecht-Strasse  
24-25, 14476 Potsdam-Golm, Germany  
e-mail: [xunlin@canopus.physik.uni-potsdam.de](mailto:xunlin@canopus.physik.uni-potsdam.de)

*Present address:*

M. Sborikas  
Fraunhofer Institute for Applied Polymer Research (IAP),  
Geiselbergstrasse 69, 14476 Potsdam, Germany

W. Jenninger · D. Lovera  
Bayer MaterialScience AG, 51368 Leverkusen, Germany

*Present address:*

D. Lovera  
Technology and Innovation Division, SABIC Technology Center  
Geleen, Geleen, The Netherlands



cellular PP has become the workhorse of ferroelectret research and technology mainly because of its high piezoelectricity, its availability and its ease of processing.

Cellular PP is usually manufactured via biaxial stretching of foamed or filler-loaded polymer sheets [11, 12]. The size and shape of the voids in such foams are not uniform, and only cavities within a rather narrow range of geometrical parameters are optimal for charging [13, 14]. In addition, the piezoelectricity of cellular PP ferroelectrets is usually stable only up to 60 °C, which prevents their application in more demanding situations [15, 16]. Therefore, polymers with better charge stability have also been employed for ferroelectrets.

Cellular ferroelectrets from polyethylene terephthalate (PETP) and polyethylene naphthalate (PENP) were developed by means of physical foaming with supercritical carbon dioxide [17–19]. The polyester ferroelectrets show slightly better thermal stability up to about 80 °C, which is still not sufficient for many practical applications. Cyclo-olefin copolymer ferroelectrets fabricated by stretching filler-loaded films exhibit a relatively low piezoelectric  $d_{33}$  coefficient of about 15 pC/N, but the piezoelectric response is stable up to 110 °C [20]. It is well known that fluoropolymers such as fluoroethylenepropylene (FEP) and polytetrafluoroethylene (PTFE) show excellent charge stability at elevated temperatures [21]. Fluoropolymer ferroelectrets with good thermal stability of the piezoelectricity have been studied in several research groups. Von Seggern and his colleagues investigated fluoropolymer ferroelectrets consisting of highly porous PTFE (expanded PTFE, or ePTFE) sandwiched with blocking layers of non-porous FEP [22–25]. Fluoropolymer ferroelectrets were also prepared by use of techniques such as spin coating of porous and non-porous layers, sintering of films, thermal fusion under a metal mesh, or thermal lamination [26–30]. With the latter two techniques, well-controlled uniform void structures can be generated. These achievements will significantly broaden the range of ferroelectret applications.

In the present study, ferroelectret films consisting of two polycarbonate (PC) films with well-defined voids between them were prepared by means of screen printing. PC is a durable thermoplastic with high toughness and a large creep modulus, with good heat resistance, high dimensional stability and good electrical insulation properties. Therefore, PC is widely used in electronic applications (e.g. as dielectric in capacitors with high stability). Erhard et al. reported that PC films with additives exhibit excellent charge stability after thermal treatment [31]. Cellular PC foams were successfully prepared by means of foaming and also by stretching films containing low-molecular-weight components that can be subsequently removed through phase extraction. Unfortunately, such PC foams cannot be rendered piezoelectric, as the foam sheets are too thick for efficient charging and/or

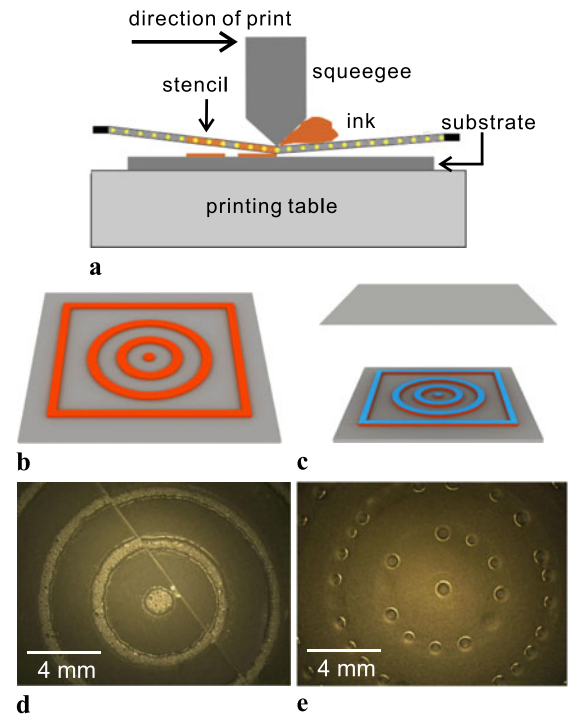


**Fig. 1** Schematic diagrams of the screen-printing process (a), and of the steps for manufacturing void-containing PC polymer systems ((b) and (c)). (d) and (e) Digital photographs of two samples prepared from an ink formulation (type I) consisting of 97.6 % monomer and 2.4 % photo-initiator and from another one (type II) consisting of 83.8 % monomer, 1.9 % photo-initiator and 14.3 % solvent, respectively

the films are too stiff for sufficient deformation under mechanical or electrical stress [32]. Here, we suggest a route to PC ferroelectrets which involves screen printing for producing the required cavities. Screen printing is often used to deposit inks onto substrates ranging from ceramics to plastic materials, fabrics and paper. It is also widely utilized in the electronics industry for the fast and efficient generation of patterned electrodes [33]. Furthermore, screen printing is employed for making solar cells on flexible substrates [34]. In the following, a new process involving screen printing for preparing ferroelectret systems is introduced, and preliminary results on their piezoelectric properties are presented and discussed.

## 2 Sample preparation

Samples were prepared by means of screen printing as schematically shown in Fig. 1(a). A tensioned screen is mounted onto a frame and permanently coated with a layer of ink-blocking stencil that provides open areas with the desired pattern for ink transfer. The screen is filled with ink and brought close to the substrate on the printing table. Upon application of pressure by means of a squeegee, the solution is forced to pass the screen via the open areas and is deposited



onto the substrate in the desired pattern. The printing quality is strongly affected by factors such as the printing speed, the interplay between the squeegee pressure and the distance between substrate and screen (so-called “snap-off”), the diameter of the threads, and the number of threads per unit area. The final thickness of the print layer  $d$  is also dependent on the ink properties such as the concentration of solid material in the ink and the density of the material in the final dry film [34]. Here,  $d$  is of particular importance, since it determines the height of the voids in the ferroelectret systems.

Figure 1(b) illustrates the pattern that was deposited on the first PC film and later covered with the second PC film. Ink formulations for screen printing were prepared as follows: The monomer was loaded into a plastic vessel, followed by the addition of a photo-initiator and/or of a solvent with additives. The chemicals were then mixed in an automatic mixer for 6 min at a rotation rate of 2000 r/min. PC films with a thickness of 50  $\mu\text{m}$  (Makrolon 3108, Bayer MaterialScience) were employed as electret films. First, the polymer ink, represented by the orange-colored pattern in Fig. 1(b), was screen-printed onto the surface of a PC film (dark gray substrate in the figure). The printing step was repeated once, allowing the deposition of a sufficient amount of ink. Afterwards, the printed polymer ink was cured for 4.5 s by means of UV curing at 30 % of the available maximum intensity of 1800  $\text{mJ}/\text{cm}^2$ . A second layer of ink with essentially the same pattern (blue layer in Fig. 1(c)) was printed on top of the cured first ink layer. This serves as an adhesive for the second PC film to be placed on the freshly deposited pattern. The sandwich structure was then thermally annealed for 4 h in an oven at 110  $^\circ\text{C}$ . As a result of this process, two PC films are tightly bonded to each other by the polymer ink pattern between them. Silver-paste electrodes were screen-printed onto both outer surfaces of the samples in order to provide electrical contact during electrical charging (“poling”) and electromechanical characterization of the ferroelectret systems.

The simplest ink formulation that was used here (type I) consists of 97.6 % monomer (Desmolux u680H) and 2.4 % photo-initiator (Darocure 1173). Figure 1(d) shows a digital photograph of a typical sample prepared from this formulation (type I). As can be seen from the figure, a large number of bubbles with diameters between 2 and 70  $\mu\text{m}$  are randomly distributed within the ink pattern. A second formulation (type II) was composed of 83.8 % monomer, 1.9 % photo-initiator, and 14.3 % solvent (Hexanediol Diacrylate, HDDA). A digital photograph of a sample fabricated from the second formulation (type II) with the same screen size as before is shown in Fig. 1(e). Now, the size of bubbles is quite uniform and they are almost uniformly distributed within the ink pattern. The thicknesses of samples from formulations I and II are 220 and 230  $\mu\text{m}$ , corresponding to void heights of 120 and 130  $\mu\text{m}$ , respectively. Microscope images of cross

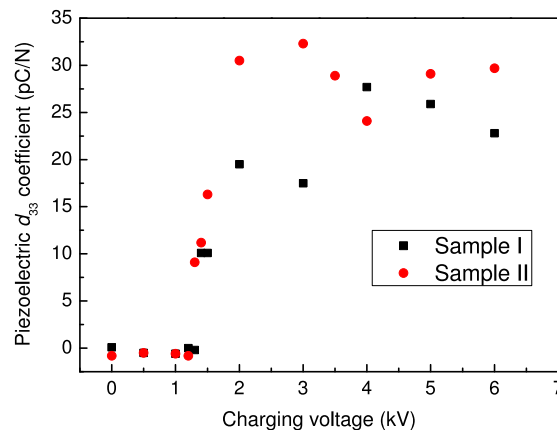


**Fig. 2** Piezoelectric  $d_{33}$  coefficients of samples from formulations I and II as functions of the charging voltage

sections of samples that have been cut by means of a scalpel indicate good bonding between the inner surfaces of the PC films and the ink pattern, which results in well-defined void-containing polymer-film systems.

It should be noted that the presence of bubbles in the ink tracks will not influence the suitability of the samples as ferroelectrets if good bonding between the ink pattern and the inner polymer surfaces is given and if the required internal charge levels in the voids are attainable. In large-scale production, ink patterns with regular bubble distributions or without any bubbles are to be preferred in the interest of good reproducibility. Avoiding bubble formation in the ink pattern might be achieved with formulations containing anti-foaming additives and/or with higher percentages of solvent. Altering the formulation will, however, affect the final thickness of the printed ink pattern. Optimization of sample preparation thus requires more comprehensive investigations on these and other relevant factors that are often inter-related as well.

### 3 Experimental results and discussion

For rendering polymer foams or layer systems piezoelectric, their internal cavities must be electrically charged—positively on one surface and negatively on the other. In order to charge the cavities of the PC systems, a dc voltage was applied to the external electrodes for 5 s by means of a high-voltage power supply (Trek model 610D) controlled by an arbitrary-waveform function generator (HP 33120A). The piezoelectric  $d_{33}$  coefficients of both types of samples are plotted as functions of the charging voltage in Fig. 2. The  $d_{33}$  values were determined by means of a dynamic method as detailed elsewhere [35]. In this method, the sample under test is mounted between a small top electrode and a large bottom electrode. The top electrode has a diameter of 1.1 cm. A sinusoidal force with an amplitude of 1 N and

a frequency of 2 Hz is applied (Brüel & Kjaer model 4810 shaker). In order to ensure good mechanical contact between the sample and the external electrodes, the sinusoidal force is superimposed with a static bias force. For the investigation of the static-pressure dependence of the  $d_{33}$  coefficients, the static force was increased from 1 to 8 N at intervals of 1 N, while it was kept at 3 N for the other measurements. The electrical response of the sample was amplified by means of a Brüel & Kjaer model 2635 charge amplifier and recorded with an oscilloscope. From the applied force and the resulting electrical signal, the  $d_{33}$  coefficients were calculated. For the tests shown in Fig. 2, two fresh samples (type I and type II, respectively) were used, one sample for each curve, as indicated. The samples were charged again and again with stepwise increasing voltage, and the  $d_{33}$  coefficients were measured after charging at the indicated voltages. Figure 2 clearly shows the threshold behavior of both samples which can be rendered piezoelectric after charging with sufficiently high voltages, confirming the suitability of the proposed process for the fabrication of ferroelectrets.

It is known that internal charging of the cavities requires Paschen breakdown [3] so that the threshold charging voltage of the sample is given by

$$V_{\text{th}} = E_{\text{th}} \left( \frac{d_p}{\varepsilon_p} + d_g \right), \quad (1)$$

where  $E_{\text{th}}$  is the threshold breakdown field of air in a uniform electric field,  $d_p = 100 \mu\text{m}$  is the total thickness of the PC films,  $d_g$  is the height of the cavities in the sample, and  $\varepsilon_p = 2.9$  is the permittivity of the solid polymer. According to Townsend's model,  $E_{\text{th}}$  of air under normal conditions in gaps with thicknesses  $d_g$  of 120 and 130  $\mu\text{m}$  is 8.22 and 8.03 MV/m, respectively [36]. From Eq. (1),  $V_{\text{th}}$  values of 1270 and 1320 V are calculated for the sample types I and II, respectively, in good agreement with the threshold voltages found in Fig. 2. For charging voltages above the threshold, the  $d_{33}$  coefficients increase significantly up to saturation values around 28 pC/N in both sample types. Further optimization of the piezoelectricity might be achieved, for instance, by using softer ink material or by adjusting the void height and/or the thickness of the PC films [25].

Figure 2 also shows unexpectedly large scattering of the  $d_{33}$  coefficients at high charging voltages. This can probably be attributed to the fact that it is impossible to place the top electrode again onto exactly the same area of the sample for the measurements after each charging step. Obviously, the  $d_{33}$  value determined in our study is an average over the respective sample area contacted by the top electrode. Because of the highly non-uniform sample structure, large variations in the piezoelectricity can be expected across the sample surface. The areas with air-filled cavities show high piezo-

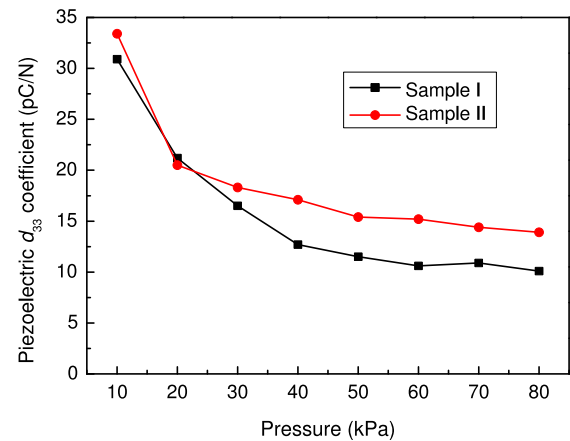


**Fig. 3** Piezoelectric  $d_{33}$  coefficients as functions of the static pressure that was applied during the dynamic measurements

electricity, whereas almost no response is expected from the areas with printed ink material. After charging above the respective saturation voltage, the internal charge of the cavities will trigger back discharges when the charging voltage is turned off [3]. It is conceivable that back discharges occur in a more or less arbitrary manner, so that the final internal charge density is not constant across the sample. Rather, it may assume a value below the saturation level. A clear understanding of the back-discharge behavior requires further investigations.

Figure 3 shows the pressure dependence of  $d_{33}$  which was obtained by applying different static forces during the dynamic measurements. At relatively low static pressures,  $d_{33}$  decays strongly with increasing pressure. For sample types I and II,  $d_{33}$  decreases from 31 and 33 pC/N at a static pressure of 10 kPa to 12 and 15 pC/N at 50 kPa (i.e., to 39 and 45 % of the corresponding initial values), respectively. As the static pressure increases further,  $d_{33}$  decreases more and more slowly. The large reduction of  $d_{33}$  with static pressure can be attributed to the particular structure of the present samples. The rather soft ink material leads to a large sample compression already at relatively low pressures. In addition, the circular cavities are bigger than the top electrode (except the first one around the center of the printed pattern), so that the air under the compressed area flows to the non-compressed area of the same cavity. As a result, the samples are highly compressible at low pressures, and the compressibility strongly decreases with increasing pressure. An even stronger decline of  $d_{33}$  with pressure was reported on FEP ferroelectrets with open tubular channels where the air can flow in or out of the cavities rather freely. There,  $d_{33}$  decreases to about 10 % of its initial value upon a static-pressure increase from 10 to 50 kPa [37]. Such a strong  $d_{33}$  decrease was, however, not observed on ferroelectret systems of fused fluorocarbon polymer layers where the cavities were closed [28].

In practical applications of ferroelectrets, the thermal stability of the piezoelectricity is of great importance. Figure 4 shows the decay of  $d_{33}$  as a function of temperature. Samples were charged at 4 kV for 5 s, and the initial  $d_{33}$  value was determined in dynamic measurements at room temperature. Then, the samples were stored for 1 h in an oven at the temperatures indicated on the abscissa of the figure. The 1-hour storage periods at stepwise increasing temperatures alternated with brief  $d_{33}$  measurements at ambient temperature. The thermal stability of their piezoelectricity is closely related to the temperature dependencies of the mechanical and electret properties of the samples. At elevated temperatures, most ferroelectret samples become softer, while the charges trapped on or in the electret films are released faster upon thermal activation. At relatively low annealing temperatures up to 80 °C, we observed that the  $d_{33}$  coefficient slightly increases with increasing temperature, indicating that the softening is more important than the thermally enhanced charge release. The piezoelectric  $d_{33}$  coefficient starts to decay when the annealing temperatures become higher because de-trapping of the charges becomes dominant. However, even after annealing at 100 °C for 1 h, the  $d_{33}$  coefficient of a sample of type I is still higher than its initial value, and the  $d_{33}$  of a sample of type II remains at 90 % of its initial value. Therefore, the thermal stability of the piezoelectric  $d_{33}$  coefficient in the PC-ink-PC ferroelectret systems prepared here is slightly better than that of polyester ferroelectrets [19] and much better than that of cellular PP ferroelectrets [16].

In the relevant literature, it was reported that PC films modified by incorporating additives plus a thermal treatment can exhibit excellent charge stability [31]. Enhanced thermal stability of  $d_{33}$  is to be expected if such modified PC electret films are employed. In addition, the fabrication process introduced here allows for a large range of materials to be used for the outer electret films and for the screen-printed middle layer(s). In order to achieve ferroelectrets with high thermal stability, ink material with low electrical conductivity and polymers with excellent electret properties should be employed. It should also be noted that the optimal temperature for the thermal treatment of the ink mainly depends on the ink material and is almost independent of the electret films. If the optimal treatment temperature is significantly lower than the melting point of the electret films, thermal degradation of the films during preparation can be avoided—a condition that is easy to fulfill when polymers with good thermal stability such as fluoropolymers are employed. This possibility can be an essential advantage over other preparation techniques such as thermal lamination. There, the samples must usually be heated up to temperatures near or even above the respective melting points of the electret films.

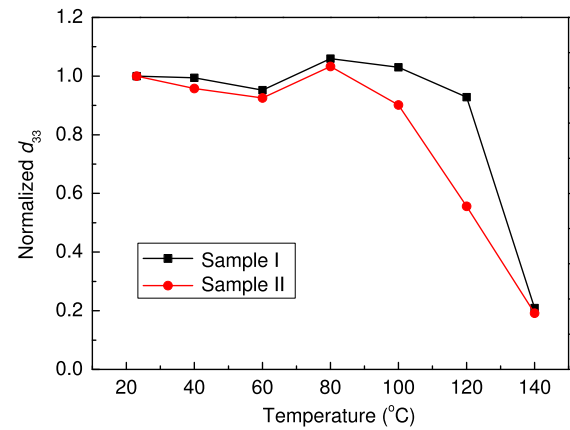


**Fig. 4** Decay of the piezoelectric  $d_{33}$  coefficients in samples of type I and type II after charging at room temperature and subsequent annealing for 1 h at selected temperatures as indicated

#### 4 Conclusions

Screen printing has been demonstrated as a useful technique for preparing polymer-film systems that are suitable as ferroelectrets after charging at sufficiently high voltages. In the preparation process suggested here, paste material (ink) is deposited in a pre-designed pattern via screen printing onto the surface of one electret film, and then another electret film is put on top of the ink pattern. Curing under suitable conditions leads to good bonding between the ink pattern and the electret films, yielding a film system with well-defined cavities. One of the advantages of the process lies in the fact that a large variety of electret-film materials and ink layers may be employed in order to optimize the ferroelectret properties with respect to a given application. In the present paper, polycarbonate (PC) films have been employed as electrets. It was found that the PC-film systems exhibit piezoelectricity after charging, thus confirming the suitability of the proposed process for ferroelectret production. The piezoelectric  $d_{33}$  coefficients obtained so far are around 28 pC/N. With the present ink,  $d_{33}$  strongly depends on static pressures—in particular in the range of tens of kPa. The PC-ink-PC ferroelectrets exhibit thermal stability up to 100 °C.

**Acknowledgements** The authors are indebted to the European Union for co-funding some of the essential equipment used in their work. R.G. wishes to thank the Fundação de Amparo à Pesquisa do Estado de São Paulo (FAPESP) and the Lady Davis Fellowship Trust (LDFT) for granting him visiting professorships at the Universidade de São Paulo (Brazil) and at the Hebrew University of Jerusalem (Israel), respectively.

#### References

1. L.J. Gibson, M.F. Ashby, *Cellular Solids: Structure and Properties*, 2nd edn. (Cambridge University Press, Cambridge, 1997)

2. M. Lindner, S. Bauer-Gogonea, S. Bauer, M. Paajanen, J. Raukola, *J. Appl. Phys.* **91**, 5283 (2002)
3. X. Qiu, R. Gerhard, A. Mellinger, *IEEE Trans. Dielectr. Electr. Insul.* **18**, 34 (2011)
4. U. Kogelschatz, *Plasma Chem. Plasma Process.* **23**, 1 (2003), and references therein
5. X. Qiu, L. Holläder, W. Wirges, R. Gerhard, H.C. Basso, *J. Appl. Phys.* **113**, 224106 (2013)
6. S. Bauer, R. Gerhard(-Mulhaupt), G.M. Sessler, *Phys. Today* **57**(2), 37 (2004)
7. R. Gerhard(-Mulhaupt), *IEEE Trans. Dielectr. Electr. Insul.* **9**, 850 (2002)
8. M. Wegener, S. Bauer, *ChemPhysChem* **6**(6), 1014 (2005)
9. X. Qiu, *J. Appl. Phys.* **108**, 011101 (2010)
10. K. Kirjavainen, Electromechanical film and procedure for manufacturing same, US Patent No. 4654546 (1987)
11. A. Savolainen, K. Kirjavainen, *J. Macromol. Sci. Chem. A* **26**, 583 (1989)
12. J. Raukola, N. Kuusinen, M. Paajanen, in *Proc., IEEE 11th Intern. Symp. Electrets* (2002), pp. 195–198
13. X. Qiu, A. Mellinger, R. Gerhard, *Appl. Phys. Lett.* **92**, 052901 (2008)
14. A. Mellinger, O. Mellinger, *IEEE Trans. Dielectr. Electr. Insul.* **18**(1), 43 (2011)
15. J. Hillenbrand, X. Zhang, Y. Zhang, G.M. Sessler, in *Annual Report of Conference on Electrical Insulation and Dielectric Phenomena* (2003), pp. 40–43
16. A. Mellinger, M. Wegener, W. Wirges, R. Reddy Mallepally, R. Gerhard(-Mulhaupt), *Ferroelectrics* **331**, 189 (2006)
17. M. Wegener, W. Wirges, R. Gerhard(-Mulhaupt), *Adv. Eng. Mater.* **7**, 1128 (2005)
18. W. Wirges, M. Wegener, O. Voronina, L. Zirkel, R. Gerhard (-Mulhaupt), *Adv. Funct. Mater.* **17**, 324 (2007)
19. P. Fang, M. Wegener, W. Wirges, L. Zirkel, R. Gerhard, *Appl. Phys. Lett.* **90**, 192908 (2007)
20. E. Saarimäki, M. Paajanen, A. Savijärvi, H. Minkkinen, M. Wegener, O. Voronina, R. Schulze, W. Wirges, R. Gerhard (-Mulhaupt), *IEEE Trans. Dielectr. Electr. Insul.* **13**, 963 (2006)
21. G.M. Sessler (ed.), *Electrets*, 3rd edn. vol. I (Laplacian Press, Morgan Hill, 1999)
22. Z. Hu, H. von Seggern, *J. Appl. Phys.* **99**, 024102 (2006)
23. S. Zhukov, H. von Seggern, *J. Appl. Phys.* **102**, 044109 (2007)
24. H. von Seggern, S. Zhukov, S. Fedosov, *IEEE Trans. Dielectr. Electr. Insul.* **17**, 1056 (2010)
25. H. von Seggern, S. Zhukov, S. Fedosov, *IEEE Trans. Dielectr. Electr. Insul.* **18**, 49 (2011)
26. A. Mellinger, M. Wegener, W. Wirges, R. Gerhard(-Mulhaupt), *Appl. Phys. Lett.* **79**, 1852 (2001)
27. R.A.C. Altafim, H.C. Basso, R.A.P. Altafim, L. Lima, C.V. de Aquino, L. Gonçalves Neto, R. Gerhard(-Mulhaupt), *IEEE Trans. Dielectr. Electr. Insul.* **13**, 979 (2006)
28. X. Zhang, J. Hillenbrand, G.M. Sessler, *Appl. Phys. A* **84**, 139 (2006)
29. X. Zhang, X. Wang, G. Cao, D. Pan, Z. Xia, *Appl. Phys. A* **97**, 859 (2009)
30. R.A.P. Altafim, X. Qiu, W. Wirges, R. Gerhard, R.A.C. Altafim, H.C. Basso, W. Jenninger, J. Wagner, *J. Appl. Phys.* **106**, 014106 (2009)
31. D.P. Erhard, D. Lovera, W. Jenninger, J. Wagner, V. Altstädt, H. Schmidt, *Macromol. Chem. Phys.* **211**, 2179 (2010)
32. N. Bhrendt, *IEEE Trans. Dielectr. Electr. Insul.* **17**, 1113 (2010)
33. W. Chang, T. Fang, H. Lin, Y. Shen, Y. Lin, *J. Disp. Technol.* **5**, 178 (2009)
34. F.C. Krebs, *Sol. Energy Mater. Sol. Cells* **93**, 394 (2009)
35. P. Fang, L. Holländer, W. Wirges, R. Gerhard, *Meas. Sci. Technol.* **23**, 035604 (2012)
36. E.M. Bazelyan, Y.P. Raizer, *Spark Discharge* (CRC, Boca Raton, 1998)
37. W. Wirges, S. Raabe, X. Qiu, *Appl. Phys. A* **107**, 583 (2012)

# Polarization and Hysteresis in Tubular-Channel Fluoroethylenepropylene-Copolymer Ferroelectrets

X. QIU,\* W. WIRGES, AND R. GERHARD

Applied Condensed-Matter Physics, Institute of Physics and Astronomy,  
Faculty of Science, University of Potsdam, Karl-Liebknecht-Str. 24-25,  
14476 Potsdam-Golm, Germany

*Polarization-vs.-applied-voltage hysteresis curves are recorded on tubular-channel fluoroethylene-propylene (FEP) copolymer ferroelectrets by means of a modified Sawyer–Tower circuit. Dielectric barrier discharges (DBDs) inside the cavities are triggered when the applied voltage is sufficiently high. During the DBDs, the cavities become man-made macroscopic dipoles which build up an effective polarization in the ferroelectret. Therefore, a phenomenological hysteresis curve is observed. From the hysteresis loop, the remanent polarization and the coercive field can be determined. Furthermore, the polarization can be related to the respective piezoelectric coefficient of the ferroelectret. The proposed method is easy to implement and is useful for characterization, further development and optimization of ferro- or piezoelectrets.*

**Keywords** Ferroelectrets; piezoelectrets; tubular-channel polymer systems; dielectric barrier discharge (DBD); fluoroethylenepropylene (FEP) copolymer; piezoelectricity-polarization relation

## Introduction

Ferroelectrets are internally charged non-polar polymer foams or polymer systems with electrically charged internal cavities [1–4]. For the formation of ferroelectrets, the cavities must be charged through a series of dielectric barrier discharges (DBDs) [5–7]. During charging, charges of opposite polarity are generated and then trapped at the top and bottom internal surfaces of the cavities, respectively. The internally charged cavities can be considered as man-made macroscopic dipoles. The macroscopic dipoles easily deform under mechanical or electrical stress, leading to large direct or inverse piezoelectricity, respectively. In addition, the direction of the macroscopic dipoles can be reversed by switching the polarity of the applied voltage. Therefore, the macroscopic dipoles in ferroelectrets behave in close analogy to the molecular dipoles in polymer ferroelectrics or to the ionic dipoles in inorganic ferroelectrics, and constitute a macroscopic electric polarization.

In ferroelectric materials, polarization-versus-electric-field ( $P(E)$ ) hysteresis curves are observed in order to study several important properties such as the spontaneous polarization, the coercive field and the remnant polarization.  $P(E)$  hysteresis curves in inorganic ferroelectric ceramics are often recorded with a Sawyer-Tower (ST) circuit [8]. Compared

---

Received April 2, 2014; in final form May 7, 2014.

\*Corresponding author. E-Mail: xunlin.qiu@uni-potsdam.de

Color versions of one or more of the figures in the article can be found online at [www.tandfonline.com/gfer](http://www.tandfonline.com/gfer).



with their inorganic counterparts, ferroelectric polymers – such as  $\beta$ -phase polyvinylidene fluoride (PVDF) and some of its copolymers – usually have much higher coercive fields of 50–100 MV/m and much longer switching times for the dipoles. Furthermore, destructive breakdown often occurs in ferroelectric polymer films under high voltages, especially at high frequencies. For these reasons,  $P(E)$  hysteresis curves in ferroelectric polymers are usually determined by measuring and analyzing the poling current under very slowly oscillating AC voltages [9].

DBDs in the cavities of ferroelectrets are very fast phenomena [6,10,11]. During charging, the DBDs produce numerous transient current pulses that are too short to be efficiently measured by means of the current-voltage method that is mainly used for ferroelectric polymers. Lindner *et al.* studied the dielectric hysteresis behavior in cellular ferroelectrets and on model systems by use of a conventional ST circuit [6,12]. In the present study,  $P(E)$  hysteresis curves of tubular-channel fluoroethylenepropylene (FEP) copolymer ferroelectrets are investigated by means of a modified Sawyer–Tower circuit. As in a conventional ST circuit, a capacitor whose capacitance is much larger than that of the sample is connected in series with the sample. The charge transferred during the charging process is determined from the voltage on the capacitor by means of an electrometer. Since a high voltage of several kV is required in order to effectively charge the sample, another capacitor, with a capacitance much smaller than that of the former, but still substantially larger than that of the sample, is also connected in series. This capacitor serves as a high-voltage divider. With this modification, the electrometer is protected in case of destructive breakdown in the sample. It turns out that the recorded charge stems mainly from the charging of the sample capacitance and from the DBDs inside the cavities. Subtracting the contribution from the charging of the sample capacitance, we obtain a phenomenological hysteresis curve that is analogous to the hysteresis loops found in other ferroic materials.

## Experiments

Samples with well-defined tubular channels were prepared by means of a thermal lamination technique as described in a previous paper [13]. In this process, two polymer-electret films are laminated around a template which contains openings with the desired pattern. The template must have a melting temperature higher than that of the electret films, so that the films can be fused to each other through the openings in the template. Here, the template was prepared from a 100  $\mu\text{m}$  thick polytetrafluoroethylene (PTFE) film with an area of 35 mm  $\times$  45 mm. Six parallel rectangular openings (area 1.5 mm  $\times$  40 mm each) were cut by means of a computer-controlled laser system. The PTFE stripes between neighboring openings also had a width of 1.5 mm. Two films of Teflon<sup>TM</sup> FEP with a thickness of 50  $\mu\text{m}$  each were laminated at 300°C around the template. During lamination, the two FEP layers were fused with each other through the openings in the template. After the sandwich was cooled down in the laboratory, the template was removed, which resulted in a Teflon<sup>TM</sup>–FEP film system with open tubular channels. The samples were then metallized on both surfaces with aluminum electrodes of 20 mm diameter.

Hysteresis curves were determined by means of a modified Sawyer–Tower circuit as described in [14]. In this circuit, a high-voltage (HV) capacitor  $C_1$  (3 nF) and a large standard capacitor  $C_m$  (1  $\mu\text{F}$ ) are connected in series with the sample (Fig. 1). The voltage was applied to the circuit by an HV supply (FUG HCB 7-6500) controlled by an arbitrary-waveform generator (HP 33120A). A sinusoidal wave ( $V_{\text{in}}$ ) with a frequency of 10 mHz was applied. Since  $C_s \ll C_1 \ll C_m$ , we have  $V_s \gg V_1 \gg V_{\text{out}}$ , where  $V_s$ ,  $V_{\text{out}}$  and  $V_1$  are the voltages across the sample,  $C_1$  and  $C_m$ , respectively. In order to determine the charge

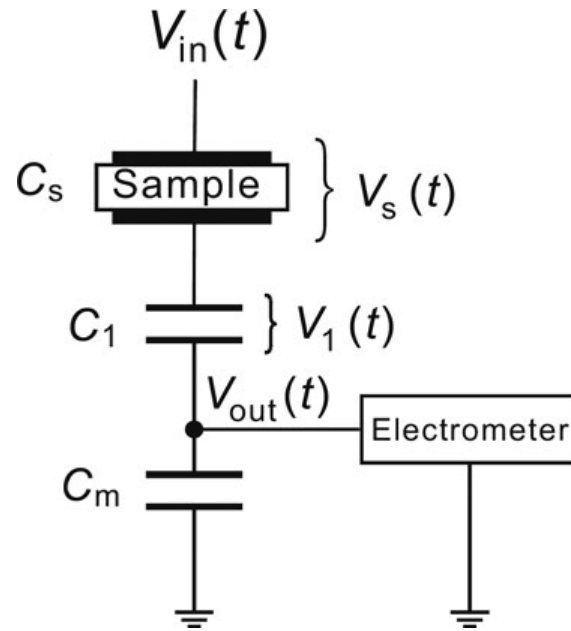


**Figure 1.** Schematic view of the experimental setup.

flowing through the circuit,  $V_{\text{out}}$  was measured with an electrometer (HP3458A), operated in the voltage mode with an input impedance  $R_m > 10 \text{ G}\Omega$ . Since the decay of  $V_{\text{out}}$  through  $R_m$  is much slower than the total measuring time, we have  $Q(t) \approx C_m V_{\text{out}}(t)$ .

The piezoelectric  $d_{33}$  coefficients were determined by means of a dynamic method [13]. Samples were loaded with a sinusoidal force with an amplitude of 1 N at a frequency of 2 Hz (Brüel&Kjær model 4810 shaker). In addition, a static bias force of 3 N was applied to the sample. The resulting electric response of the sample was amplified by means of a charge amplifier (Brüel&Kjær model 2635) and recorded with an oscilloscope. The piezoelectric  $d_{33}$  coefficients were calculated from the applied force and the resulting electrical signal.

## Results and Discussion

Consecutive voltage cycles with an amplitude of 3 kV were applied to a fresh sample.  $C_1$  and  $C_m$  are discharged prior to the measurement, so that  $C_1 V_1 = C_m V_{\text{out}}$ . The charging current includes three components that originate from charging of the sample capacitance, from the DBDs inside the tubular channels and from the conductivity in the sample, respectively. For highly insulating non-polar polymers such as Teflon<sup>TM</sup> FEP, the current from the sample conductivity is negligibly small [14]. Therefore, the current is essentially given by  $i(t) = i_{\text{cap}}(t) + i_p(t)$ . Correspondingly, the charge flowing through the circuit is expressed by  $Q(t) = Q_{\text{cap}}(t) + Q_p(t)$ . Since  $C_s \ll C_1 \ll C_m$ , it follows that:

$$Q(t) \approx C_s V_{\text{in}}(t) + Q_p(t). \quad (1)$$

The charge measured during the first and the second voltage cycle is shown in Fig. 2(a). At the beginning, the charge starts from zero and increases linearly with  $V_{\text{in}}$ , resulting from charging of the sample capacitance (*i.e.* the first term on the right-hand side of Equation (1)). As  $V_{\text{in}}$  increases further, the slope of the  $Q$ -versus- $V_{\text{in}}$  curve increases. This is because DBDs are triggered inside the channel cavities above the threshold voltage, and as a result, the second term in Equation (1) starts to increase.  $Q$  keeps increasing with  $V_{\text{in}}$  until the later

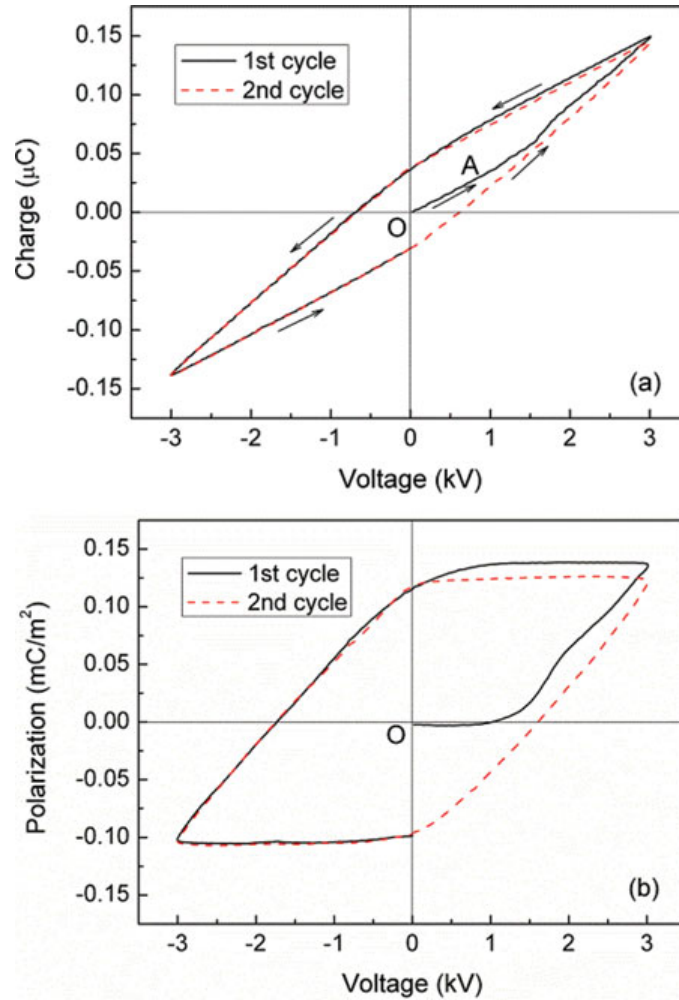


**Figure 2.** (a) Measured charge as a function of the applied voltage. Cycles of a sinusoidal voltage with an amplitude of 3 kV were applied to a fresh sample. The arrows denote the progress of the measurement during the cycles. (b) Polarization as a function of the applied voltage (calculated from (a) by subtracting the contribution from charging of the sample capacitance).

reaches its maximum of 3 kV.  $Q$  decreases when  $V_{in}$  is reduced from its maximum, but the value is higher than the corresponding charge during its increase. A remaining charge  $Q$  of  $0.04 \mu\text{C}$  is observed when  $V_{in}$  is reduced back to zero. The charge  $Q$  decreases to zero and further to negative values, as  $V_{in}$  is running into its negative half-cycle. The charge curve upon the decrease of the absolute voltage in the negative half-cycle is quite similar to that of the positive half-cycle (but of course inverted with respect to the origin of the coordinate system). Thus, a characteristic hysteresis curve is obtained.

As mentioned above, the initial linear part in Fig. 2(a) (segment OA) stems from the charging of the sample capacitance. A linear fit of this part yields a capacitance of 35.4 pF. With this capacitance value, the contribution  $Q_{cap}(t)$  can be calculated over the whole voltage range, assuming the sample capacitance is independent of the applied voltage. By subtracting  $Q_{cap}(t)$  from the recorded charge shown in Fig. 2(a), we find the charge contribution from the polarization that is induced by the DBDs inside the channel cavities. Taking into account the electrode area, we obtain the polarization in the sample as a function of the applied voltage (Fig. 2(b)). The hysteresis curve exhibits a parallelogram-like shape, coinciding with previous theoretical and experimental studies on ferroelectrets with uniform

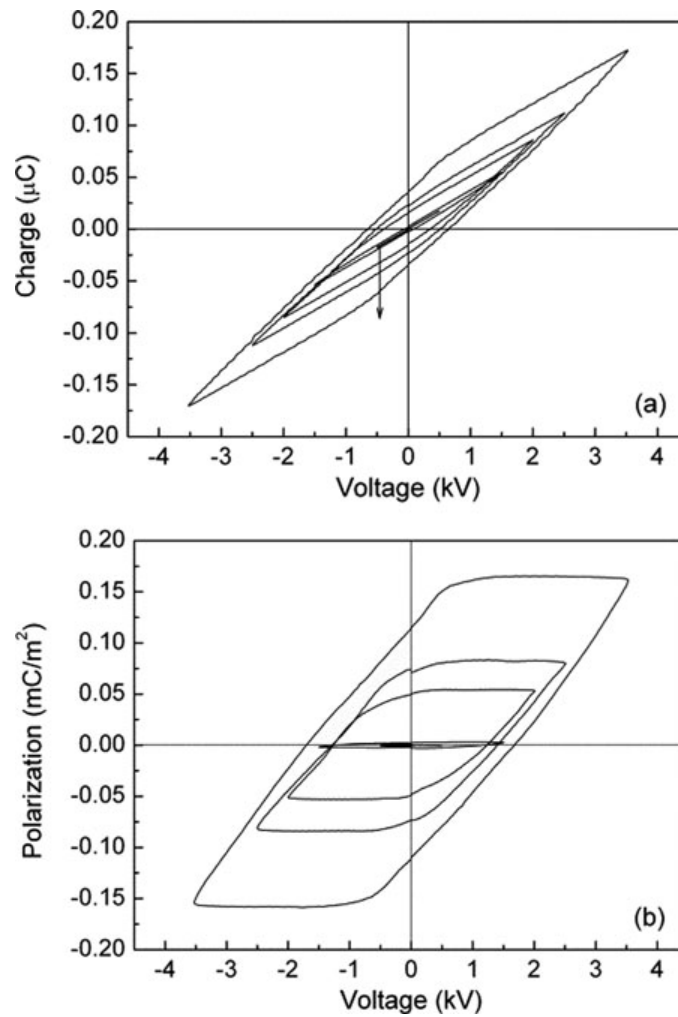


**Figure 3.** (a) Experimentally observed total amount of charge vs. the respective applied voltage of different amplitude. Along the arrow, the voltage amplitudes increase from 0.5 kV via 1.5, 2.0 and 2.5 kV to 3.5 kV. (b) Polarization as a function of the applied voltage (calculated from (a), but without the contribution from the charging of the sample capacitance).

cavity height [15,16]. From the figure, the coercive field  $E_c$  (at which the polarization is zero) and the remanent polarization  $P_r$  (defined as the polarization at zero electric field) can be determined. Obviously, we can determine  $P_r$  directly from Fig. 2(a) (*i.e.*, by scaling the charge values at the intercepts of the curves with the electroded sample area), since there is no contribution from the sample capacitance at zero applied voltage – an easy way of determining the remanent polarization in ferroelectrets!

Noticeable differences are observed between the positive half-cycles of the first and of the second cycle, which can probably be attributed to the different sample history. However, our results show that the hysteresis curves are rather repeatable from the second voltage cycle on, at least up to the sixth cycle.

In order to study the dependence of the hysteresis curve on the voltage amplitude, voltages with increasing amplitude were applied to another fresh sample with tubular channels. For each amplitude value,  $Q-V$  curves were recorded with two cycles of the voltage, followed by the determination of the piezoelectric  $d_{33}$  coefficient by means of the dynamic method. Fig. 3(a) shows the measured  $Q-V$  curves during the second voltage

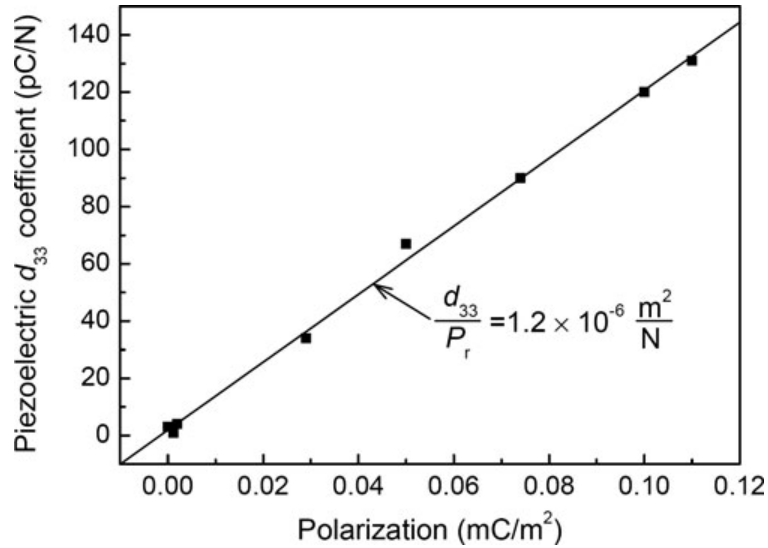


**Figure 4.** Piezoelectric  $d_{33}$  coefficient of tubular-channel FEP ferroelectrets as a function of polarization.

cycle for different amplitudes. In our previous study, a threshold voltage of about 1.3 kV was determined for the DBDs inside the channel cavities [13]. When the voltage amplitude is lower than the threshold for DBDs, no hysteresis is observed. Rather, straight lines are measured, coming from the charging of the sample capacitance. However, a slim hysteresis appears for an amplitude of 1.5 kV. Thereafter, the area enclosed by the hysteresis curve grows with increasing amplitude of the voltage.

The sample capacitance is determined by a linear fit of the straight  $Q-V$  lines for voltages with an amplitude lower than the threshold (e.g. 500 V as shown in Fig. 3(a)). Then the contribution from the sample capacitance is subtracted in the way detailed above. The results are depicted in Fig. 3(b). Above the threshold, the parallelogram-like hysteresis curves expand with increasing voltage amplitude (Fig. 3(b)). For voltages with an amplitude much higher than the threshold, the polarization decreases when the voltage is reduced from its maximum to zero (see, e.g., the curve for 3.5 kV in Fig. 3(b)). This is due to back discharges that are triggered by the charges trapped on the internal channel surfaces [7]. Theoretically, the coercive field should remain unchanged with increasing voltage amplitude, provided the channel height is exactly uniform. The difference between the coercive fields for different curves in Fig. 3(b) might be attributed to the non-uniform channel geometry that cannot be avoided in the laboratory.

In Fig. 4, the piezoelectric  $d_{33}$  coefficient of the sample is plotted as a function of the remnant polarization  $P_r$  determined from Fig. 3(b). A linear dependence is displayed, in agreement with theoretical concepts for the electromechanical behavior of ferroelectrets [17,18]. Such a linear dependence of the piezoelectricity on the remnant polarization  $P_r$  has also been reported for PVDF and for a copolymer of vinylidene cyanide and vinyl acetate P(VDC/VAc) [19,20]. In the present study, we found a slope of  $d_{33}/P_r = 1.2 \times 10^{-6} \text{ m}^2/\text{N}$  for tubular-channel FEP ferroelectrets through a linear fit to the experimental data (Fig. 4). In comparison, a factor of  $4 \times 10^{-10} \text{ m}^2/\text{N}$  is reported for the  $d_{31}/P_r$  ratio of  $\beta$ -PVDF [19]. It is known that the  $d_{33}$  coefficient in PVDF usually has the same order of magnitude as  $d_{31}$ , since both are closely related because PVDF can be considered to be essentially incompressible. Therefore, a value similar to  $d_{31}/P_r$  can be expected for the ratio  $d_{33}/P_r$  in PVDF. The slope factor of ferroelectrets is 3 to 4 orders of magnitude larger



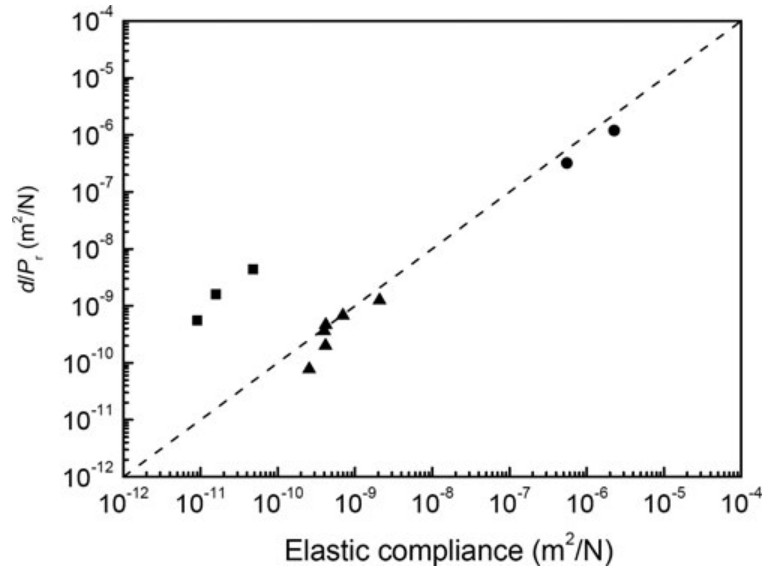


**Figure 5.** Ratio  $d/P_r$  of the observed piezoelectric coefficient and the remanent polarization in ferroelectric materials as a function of the respective tensor component of the elastic compliance in three distinct groups of ferroics. Circles correspond to cellular PP (lower point) [24] and tubular-channel FEP (higher point) ferroelectrets. Triangles indicate ferroelectric polymers: From bottom to top the points refer to the data for Polyamide-11 [25], P(VDCN/VAc) [26], Polyurea-5 [27], PVDF [28], P(VDF-TrFE) [28] and P(VDF-HFP) [29], respectively. Squares denote inorganic ferroelectrics: BaTiO<sub>3</sub> (bottom) [30,31], PZT (middle) [28] and PZN (top) [32]. Values of the piezoelectric  $d_{31}$  coefficient are used for P(VDCN/VAc) and Polyurea-5;  $d_{33}$  values are employed in all other cases. The diagonal of the coordinate system (corresponding to a slope of 1) is shown as a dashed line.

than that of PVDF, resulting mainly from the special sample structure which is highly compressible in the thickness direction (anisotropic compressibility). The slopes of the  $d$ -vs.- $P_r$  lines are closely related to the respective components of the compliance tensor (or inversely related to the respective components of the elasticity tensor). Here, we find that the inverse values of the slopes of  $1.2 \times 10^{-6} \text{ m}^2/\text{N}$  (FEP ferroelectret) and  $4 \times 10^{-10} \text{ m}^2/\text{N}$  (PVDF ferroelectric) are 833 kPa and 2.5 GPa, respectively, which are of the same order of magnitude as the values of the respective elastic-tensor components (Young's moduli of  $c_{33} = 440 \text{ kPa}$  and  $c_{31} = 1.6 \dots 3.2 \text{ GPa}$ , respectively) [21,22]. The agreement means that the piezoelectric coefficients are essentially proportional to the charge densities in the dipole polarization (or to the dipole densities themselves) and to the elastic compliance in the material between the relevant charges (or between the relevant dipoles) (*cf.* the model calculations for polymer ferroelectrets in Refs. [17,18] and for ferroelectric polymers in Ref. [23], respectively).

Figure 5 shows the ratios of the piezoelectric  $d_{33}$  or  $d_{31}$  coefficients to the corresponding values of the remanent polarization as a function of the elastic compliances on several different ferroelectric materials [24–32]. In the new type of plot, ferroelectrets, ferroelectric polymers and inorganic ferroelectric ceramics are located in three distinct parameter regions because of their quite different electromechanical and elastical properties. Nevertheless, the data for polymer ferroelectrets and ferroelectric polymers are distributed close to the diagonal of the plot, in accordance with the above interpretation. The few data points for ferroelectric ceramics that we found in the literature so far lie, however, almost two decades above the diagonal of the plot, which is probably related to the origin of the piezoelectricity in the crystalline lattices of inorganic materials. The piezoelectricity in

ferroelectric ceramics stems from the relative displacement of ions in the crystal lattice, which leads to a deformation of the intrinsic dipoles. The dipole deformation occurs mainly along the polar axis and is not directly correlated with the elastic volume change of the crystalline lattice in ferroelectric ceramics under mechanical load. The new plot of Fig. 5 may eventually be developed into a so-called Ashby materials-property chart [33] for electromechanical transducer materials which may be very helpful for identifying or designing electroactive materials. Work is under way to add relevant data for further ferroic materials in order to arrive at a more complete picture and at a deeper fundamental understanding.

## Conclusion

A modified Sawyer-Tower circuit is proposed for hysteresis measurements on tubular-channel FEP ferroelectrets. The measured charge is mainly caused by the charging of the sample capacitance and by the dielectric barrier discharges (DBDs) inside the channel cavities. We obtain the polarization hysteresis by subtracting the contribution that stems from the charging of the sample capacitance. Clear hysteresis loops are observed when the voltage exceeds the threshold value for DBD charging of the sample. The remnant polarization found in the hysteresis loops is directly related to the resulting piezoelectric  $d_{33}$  coefficient of the respective sample – via the relevant elasticity-tensor component. The same relationship was also found in literature data for cellular-foam ferroelectrets, for ferroelectric polymers and for inorganic ferroelectrics. A unified plot of the relevant data reveals that the underlying mechanisms are not the same so that the three groups of materials occupy three distinct parameter areas in the plot.

## References

1. R. Gerhard(-Mulhaupt), Less can be more: Holes in polymers lead to a new paradigm of piezoelectric materials for electret transducers. *IEEE Trans Dielectr Electr Insul.* **9**, 850–859 (2002).
2. S. Bauer, R. Gerhard(-Mulhaupt), and G. M. Sessler, Ferroelectrets: Soft Electroactive Foams for Transducers. *Phys Today.* **57**, 37–43 (2004).
3. S. B. Lang and S. Muensit, Review of some lesser-known applications of piezoelectric and pyroelectric polymers. *Appl Phys A.* **85**, 125–134 (2006).
4. X. Qiu, Patterned piezo-, pyro-, and ferroelectricity of poled polymer electrets. *J Appl Phys.* **108**, 011101 (2010).
5. M. Paajanen, M. Wegener, and R. Gerhard(-Mulhaupt), Understanding the role of the gas in the voids during corona charging of cellular electret films – a way to enhance their piezoelectricity. *J Phys D: Appl Phys.* **34**, 2482–2488 (2001).
6. M Lindner, S Bauer-Gogonea, S Bauer, M Paajanen, and J Raukola, Dielectric barrier microdischarges: Mechanism for the charging of cellular piezoelectric polymers. *J Appl Phys.* **91**, 5283–5287 (2002).
7. X. Qiu, R. Gerhard, and A. Mellinger, Turning Polymer Foams or Polymer-Film Systems into Ferroelectrets: Dielectric Barrier Discharges in Voids. *IEEE Trans Dielectr Electr Insul.* **18**, 34–42 (2011).
8. C. B. Sawyer and C. H. Tower, Rochelle Salt as a Dielectric. *Phys Rev.* **35**, 269–273 (1930).
9. B. Dickens, E. Balizer, A. S. DeReggi, and S. C. Roth, Hysteresis measurements of remanent polarization and coercive field in polymers. *J Appl Phys.* **72**, 4258–4264 (1992).
10. X. Qiu, A. Mellinger, M. Wegener, W. Wirges, and R. Gerhard, Barrier discharges in cellular polypropylene ferroelectrets: how do they influence the electromechanical properties? *J Appl Phys.* **101**, 104112 (2007).

11. X. Qiu, A. Mellinger, W. Wirges, and R. Gerhard, Spectroscopic study of dielectric barrier discharges in cellular polypropylene ferroelectrets. *Appl Phys Lett.* **91**, 132905 (2007).
12. M. Lindner, H. Hoislbauer, R. Schwödauer, S. Bauer-Gogonea, and S. Bauer, Charged Cellular Polymers with “Ferroelectric” Behavior. *IEEE Trans Dielectr Electr Insul.* **11**, 255–263 (2004).
13. RAP Altafim, X Qiu, W Wirges, R Gerhard, RAC Altafim, HC Basso, W Jenninger, and J Wagner, Template-based fluoroethylenepropylene piezoelectrets with tubular channels for transducer applications. *J Appl Phys.* **106**, 014106 (2009).
14. X. Qiu, L. Holländer, W. Wirges, R. Gerhard, and H. C. Basso, Direct hysteresis measurements on ferroelectret films by means of a modified Sawyer-Tower circuit. *J Appl Phys.* **113**, 224106 (2013).
15. P. Zhang, Z. Xia, X. Qiu, F. Wang, and X. Wu, Influence of charging parameters on piezoelectricity for cellular polypropylene film electrets. *IEEE 12th Intern Symp Electrets* (IEEE Service Center, Piscataway, NJ, USA), 2005: 39–42.
16. S Zhukov and H von Seggern, Polarization hysteresis and piezoelectricity in open-porous fluoropolymer sandwiches. *J Appl Phys.* **102**, 044109 (2007).
17. M. Paaanen, H Välimäki, J Lekkala, Modeling the sensor and actuator operations of the ElectroMechanical Film EMFi. *IEEE 10th Intern Symp Electrets* (IEEE Service Center, Piscataway, NJ, USA), 1999: 735–738.
18. G. M Sessler, J. Hillenbrand, Electromechanical response of cellular electret films. *Appl Phys Lett.* **75**, 3405–3407 (1999).
19. G. M Sessler, R. Gerhard(-Mulhaupt), H. von Seggern, JE West, Spatial and temporal buildup of polarization in PVDF. *Ann. Rep., Conf. Electr. Insul. Dielectr. Phenom.* (IEEE Service Center, Piscataway, NJ, USA), 1984: 393–398.
20. S. Tasaka, K. Miyasato, M. Yoshikawa, S. Miyata, and M. Ko, Piezoelectricity and remanent polarization in vinylidene cyanide/vinyl acetate copolymer. *Ferroelectrics.* **57**, 267–276 (1984).
21. RAP. Altafim, D. Rychkov, W. Wirges, R. Gerhard, H. C. Basso, R. A. Altafim, and M. Melzer, Laminated Tubular-channel Ferroelectret Systems from Low-density Polyethylene Films and from Fluoroethylene-propylene Copolymer Films – A Comparison. *IEEE Trans Dielectr Electr Insul.* **19**, 1116–1123 (2012).
22. Piezoelectric Films Technical Information. Available at (downloaded on 09 April 2014): <http://www.piezotech.fr/image/documents/22-31-32-33-piezotech-piezoelectric-films-leaflet.pdf>
23. M. G. Broadhurst, G. T. Davis, J. E. McKinney, and R. E. Collins, Piezoelectricity and pyroelectricity in polyvinylidene fluoride – A model. *J Appl Phys.* **49**, 4992–4997 (1978).
24. X. Qiu, A. Mellinger, M. Wegener, W. Wirges, and R. Gerhard, Barrier discharges in cellular polypropylene ferroelectrets: how do they influence the electromechanical properties? *J. Appl. Phys.* **101**, 104112 (2007).
25. P. Fröbing, A. Kremmer, W. Neumann, R. Gerhard-Mulhaupt, and I. L. Guy, Dielectric relaxation in piezo-, pyro- and ferroelectric polyamide 11. *IEEE Trans Dielectr Electr Insul.* **11**, 271–279 (2004).
26. S. Tasaka, K. Miyasato, M. Yoshikawa, S. Miyata, and M. Ko, Piezoelectricity and remanent polarization in vinylidene cyanide/vinyl acetate copolymer. *Ferroelectrics.* **57**, 267–276 (1984).
27. T. Hattori, Y. Takahashi, M. Iijima, and E. Fukada, Piezoelectric and ferroelectric properties of polyurea-5 thin films prepared by vapor deposition polymerization. *J Appl Phys.* **79**, 1713–1721 (1996).
28. T. Furukawa and N. Seo, Electrostriction as the origin of piezoelectricity in ferroelectric polymers. *Jpn J Appl Phys.* **29**, 675–680 (1990).
29. M. Wegener, W. Künstler, K. Richter, and R. Gerhard-Mulhaupt, Ferroelectric polarization in stretched piezo- and pyroelectric poly(vinylidene fluoride-hexafluoropropylene) copolymer films. *J Appl Phys.* **92**, 7442–7447 (2002).
30. H. H. Wieder, Electrical Behavior of Barium Titanate Single Crystals at Low Temperatures. *Phys Rev.* **99**, 1161–1165 (1955).

31. G. Hayward, J. Bennett, and R. Hamilton, A theoretical study on the influence of some constituent material properties on the behavior of 1-3 connectivity composite transducers. *J Acoust Soc Am.* **98**, 2187–2196 (1995).
32. S. E. Park and T. R. Shrout, Ultrahigh strain and piezoelectric behavior in relaxor based ferroelectric single crystals. *J Appl Phys.* **82**, 1804–1811 (1997).
33. L. J. Gibson, M. F. Ashby, *Cellular Solids: Structure and Properties*. New York: Cambridge U. Press; 1999.

---

# Polymer Electrets and Ferroelectrets as EAPs: Materials

Xunlin Qiu

## Contents

1	Polymer Electrets .....	2
1.1	Modified Conventional Polymer Electret Materials with Improved Electret Properties	3
1.2	High-Performance Polymer Electrets .....	6
2	Ferroelectrets .....	10
2.1	Polyolefin Ferroelectret .....	12
2.2	Polyester Ferroelectret .....	15
2.3	Cyclo-Olefin Polymer (COP) and Copolymer (COC) Ferroelectret .....	18
2.4	Polycarbonate Ferroelectret .....	19
2.5	Fluoropolymer Ferroelectret .....	20
3	Summary .....	25
	References .....	25

---

## Abstract

Recent progress relating to polymer electret and ferroelectret materials is reviewed. As for polymer electret materials, the development is described in two aspects: (i) Modified conventional polymer electret materials with improved electret properties. The improvement of the electret properties is achieved by incorporating suitable additives, by blending different polymer compounds, or by modifying with certain chemicals. Sometimes, the properties can be further enhanced by physical aging. (ii) Newly introduced high-performance polymer electrets. Parylene HT<sup>®</sup> and CYTOP are two examples. They can not only retain high surface charge densities but also show exceptional high temperature stability. Moreover, they are compatible with MEMS technology and therefore are particularly attractive for applications in micro power electret generators.

---

X. Qiu (✉)

Department of Physics and Astronomy, University of Potsdam, Potsdam-Golm, Germany  
e-mail: [xunlin.qiu@uni-potsdam.de](mailto:xunlin.qiu@uni-potsdam.de)

© Springer International Publishing Switzerland 2016  
F. Carpi (ed.), *Electromechanically Active Polymers*, Polymers and Polymeric  
Composites: A Reference Series, DOI 10.1007/978-3-319-31767-0\_25-1

1



The research of ferroelectret, as a relatively new branch in the field of electret, has been advanced significantly in recent years. A considerable number of cellular polymer foams and polymer film systems containing internal cavities have been developed and identified as ferroelectrets. Following the early example of cellular polypropylene (PP) ferroelectret, cellular foam ferroelectrets have been developed from polyesters (polyethylene terephthalate PETP and poly(ethylene naphthalate) PENP), cyclo-olefin copolymer (COC), and fluoroethylene-propylene (FEP). The cellular structures, formed by techniques such as stretching filler-loaded polymer melt and foaming with supercritical CO<sub>2</sub>, can be adjusted and optimized with gas-diffusion expansion process. Besides, the number of ferroelectrets of polymer film systems with internal cavities is rapidly increasing. These are layer structures, composed of hard (solid) and soft (highly porous) polymer layers, and polymer film systems containing regular cavities. Polytetrafluoroethylene (PTFE) (solid or porous) and polycarbonate (PC) are also added to the list of candidate materials for making this type of ferroelectrets. These exciting developments significantly enlarge the range of functional space-charge polymer electrets and bring forth numerous novel applications.

---

**Keywords**

Electrets • Ferroelectrets • Chemical modification • Physical aging • High performance polymers • polymer foams • polymer films

---

## 1 Polymer Electrets

The research and application of electrets very much rely on the availability of suitable materials. Conventional polymer electrets are discussed in previous books, book chapters, and review articles (Hilczner and Malecki 1986; Sessler 1999, 2001; Gerhard-Multhaupt 1999; Kressmann et al. 1999). In this section, the recent development in polymer electret materials is discussed.

Significant progress has been made in bettering the performance of conventional polymer electrets. This is achieved through, for example, incorporating suitable additives or blending different compounds. Physical aging brings further enhancement. For polymer electrets produced by means of corona charging (a charging method that is widely used in the electret industry), the deposited charges are normally trapped on or near the polymer surface. Therefore, surface modification of polymer electrets will directly affect charge trapping, charge detrapping, and charge transport. Modification can be done by using either reactive gases or chemical solvents. In view of their superior performance, the treated polymer electrets can be considered as “novel” electret materials.

Also, new polymer electret materials have been added to the family of electrets, i.e., parylene HT<sup>®</sup> (referred to as “polymer AF-4”) and the amorphous perfluorinated polymer CYTOP. The development of such high-performance electrets is mainly motivated by the application in micro electret power generators (Suzuki 2011; Yang

et al. 2012). High-performance electrets are required in such applications, in order to have generators with large output and long-standing performance. Fluoropolymer electrets such as polytetrafluoroethylene (PTFE) and fluorinated ethylene propylene (FEP) can provide good long-term and thermal stability. However, PTFE and FEP are not compatible with MEMS fabrication technology, since they are insoluble in solvents. Moreover, their surface charge density is insufficient for generators with high output. Parylene HT<sup>®</sup> and CYTOP are two types of high-performance polymer electrets which to a large extent fulfill the requirements.

## 1.1 Modified Conventional Polymer Electret Materials with Improved Electret Properties

### 1.1.1 Polymer Electrets with Physical Treatment

In recent years, colleagues at the University of Bayreuth have carried out comprehensive studies on the improvement of the properties of conventional polymer electrets, sometimes in collaboration with the Darmstadt University of Technology. Their works are reviewed in Erhard et al. (2010a) and therefore will be only briefly introduced here. The interested reader may refer to the previous review for details.

The materials under investigation are commodity polymers including polypropylene (PP), poly(phenylene ether) (PPE) and polystyrene (PS), and high-performance thermoplastic polyetherimide (PEI). It is demonstrated that the electret properties of PP and PEI can be significantly enhanced by incorporating suitable additives. Certain substituted 1,3,5-benzene based trisamides and bisamides are effective additives for PP electret. The additives create supramolecular charge traps via self-assembly. In order to optimize this effect, the additive concentration has to be low. In the case of PEI, phosphorus-based antioxidants are efficient additives. Pure PEI exhibits very poor charge storage capability. The surface potential decays almost completely in 24 h at 90 °C. By adding 0.5 wt% of organophosphonites Irgafos<sup>®</sup> P-EPQ and Irgafos<sup>®</sup> 126, the surface potential remains at 79 and 86 % of the initial value after being stored at 90 °C for a period of longer than 1400 h, respectively. It is also found that increasing the cooling rate during film process and physical aging prior to charging (Erhard et al. 2010b) lead to further improvement of the electret properties of additive-incorporated PP and PEI, respectively. In another study from the same group, polycarbonate (PC) electrets were improved by incorporating bisimide additives combined with physical aging (Erhard et al. 2010c).

PPE and PS are totally miscible over the entire composition range. Compared with neat PPE and PS, PPE/PS (composition ratio 75/25) blend films exhibit excellent charge stability, even at temperatures up to 120 °C. The superior charge stability of the blend is attributed to (1) increased packing density, which limits segmental motions below  $T_g$  and thus hinders the charge drift, and (2) nanoscale phase boundaries, which might act as charge traps. Physical aging can further reduce the free volume of the blend films, bringing forth beneficial effect on the electrets

properties. Incorporation of charging trapping sites by compounding the blend with the third component, i.e., triblockcopolymer poly(styrene-*b*-isobutylene-*b*-styrene) (SIBS), also leads to an improvement of the electret properties.

In the study of Ko et al., 2-(6-mercaptohexyl) was used as additive to improve the performance of COC polymers. By adding a concentration of 3497 mg/kg, the surface potential increases by 71 %, compared with that of a pure COC film (Ko et al. 2010).

### 1.1.2 Chemically Modified Polymer Electrets

An and colleagues treated low density polyethylene (LLDPE) with fluorine gas (which is diluted with nitrogen) (An et al. 2009a). The direct fluorination of the material deepens the traps in the surface layer. It is found the charges trapped in the deep traps block the injection of charge into the bulk of the material. The same group also reported oxyfluorination treatment on LDPE using gas mixture of F<sub>2</sub>/N<sub>2</sub>/O<sub>2</sub> (1:78:1) (An et al. 2009b). Such treatment leads to the formation of various polar groups in the surface layer. It turns out that the oxyfluorinated LDPE is less influenced by the by-products in the semicon electrode. Thus, the oxyfluorinated surface has deeper traps as compared with the virgin film. Because of the resultant high permittivity and the deeper traps of the surface layer, oxyfluorination significantly suppresses space charge injection into the bulk of LLDE. These results are particularly interesting for the application of LDPE as DC high voltage cables. In this application, the injection and accumulation of space charges is a main factor for the degradation of the material and therefore needs to be suppressed.

Rychkov et al. studied the effect of modification of PE, PTFE, and FEP with various chemical solvents on their electret properties (Rychkov et al. 2011a, b, 2012a, b, c, 2013). The chemicals for modification were used either in gas-phase state as vapors or in liquid state.

Modifications of PE with phosphorus trichloride (PCl<sub>3</sub>) and titanium tetrachloride (TiCl<sub>4</sub>) vapors as well as orthophosphoric acid (H<sub>3</sub>PO<sub>4</sub>) all result in significantly enhanced charge stability. Figure 1 shows thermally stimulated surface potential decay (charge TSD) of positively charged PE with and without PCl<sub>3</sub> modification (Rychkov et al. 2011a). It can be seen that modified PE films exhibit much better charge stability. For instance, the half-value temperature (i.e., the temperature at which the surface potential decays to half of its initial value) is shifted to higher temperature by 55 °C. The modification also eliminates the so-called crossover phenomenon that is often observed with virgin PE electrets (curves 1 and 2 in the figure). Thus, the PCl<sub>3</sub> modification on PE not only improves the charge stability but also increases the magnitude of the stabilized charges. Similar effects were observed for modification of PE with TiCl<sub>4</sub> (Rychkov et al. 2011b, 2012a).

Modification of PE with H<sub>3</sub>PO<sub>4</sub> also leads to significant improvement of the charge stability. As shown in Fig. 2, the thermal stability of both positively and negatively charged PE samples was enhanced by about 60 °C with the modification using H<sub>3</sub>PO<sub>4</sub> (Rychkov et al. 2012b).

Modifications of PTFE and FEP with TiCl<sub>4</sub> vapor yield remarkable improvement of the charge stability as well. For PTFE, the charge TSD curve for positive charge is

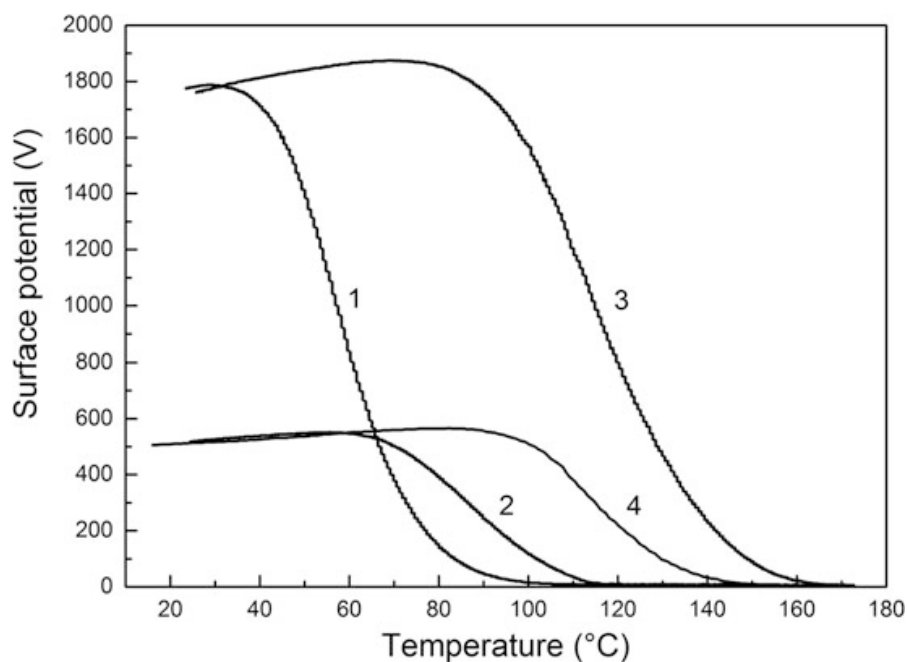


**Fig. 1** Charge TSD in positively charged LDPE films. *1* and *2* virgin samples, *3* and *4* treated with  $\text{PCl}_3$  vapors

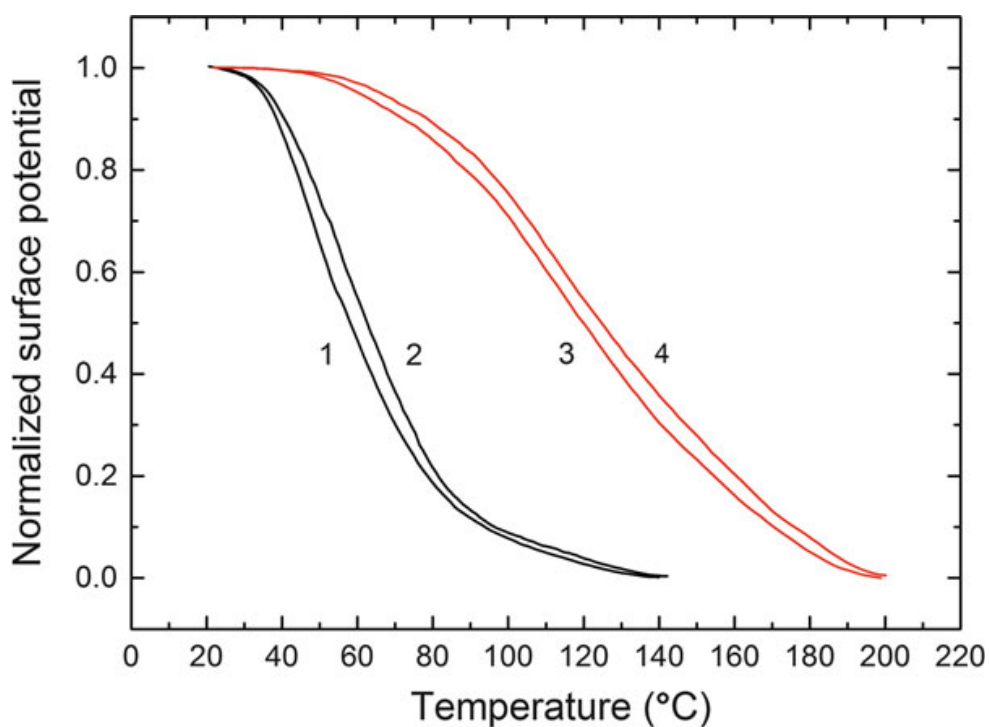


**Fig. 2** Charge TSD in positively (*1* and *3*) and negatively (*2* and *4*) charged LDPE films without (*1* and *2*) and with (*3* and *4*) modification using  $\text{H}_3\text{PO}_4$  (Rychkov et al. 2012b)

shifted to higher temperature by more than  $100\text{ }^\circ\text{C}$  (Rychkov and Gerhard 2011). For FEP, the thermal stability of positive charge is improved by more than  $120\text{ }^\circ\text{C}$  (Rychkov et al. 2013). Unlike PTFE for which the modification almost does not

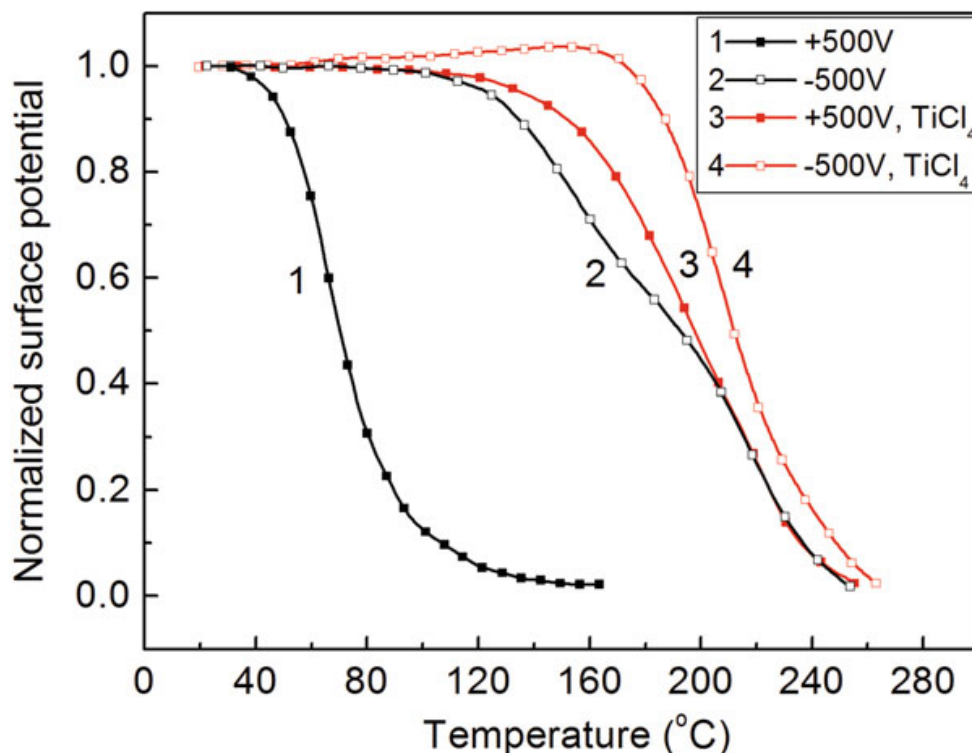


**Fig. 3** Charge TSD of FEP films charged to  $\pm 500$  V. 1 and 2 without treatment, 3 and 4 treated with  $\text{TiCl}_4$  vapor (Rychkov et al. 2013)

influence the negative charge stability, the thermal stability of negative charge in treated FEP is enhanced by about  $20^\circ\text{C}$ . As a result, the asymmetry in the charge stability of both polarities is largely reduced (Fig. 3).

The charge stabilization by the chemical modifications is attributed to the formation of new energetically deep traps on the modified surface. Element analysis reveals that titanium and oxygen are built into the surface after the modification with  $\text{TiCl}_4$  vapor (Rychkov and Gerhard 2011). The scanning electron microscope (SEM) images show that for modification with  $\text{H}_3\text{PO}_4$ , nanoislands, which have chemical compositions different from the polymer substrate, are formed on the polymer surface (Fig. 4) (Rychkov et al. 2012b). This might be the structural origin for the deeper traps formed during the modification. The attachment of new chemical structures to the surface molecules also decreases the molecular mobility, another possible reason for the overall enhancement of the charge stability.

## 1.2 High-Performance Polymer Electrets

### 1.2.1 Parylene

Parylene is the trade name for a number of chemical vapor deposited poly (p-xylylene) polymers. Due to its chemical inertness, conformal coating, and excellent barrier properties, parylene has been used in a wide range of applications, particularly as protective coatings for biomedical devices and microelectronics.



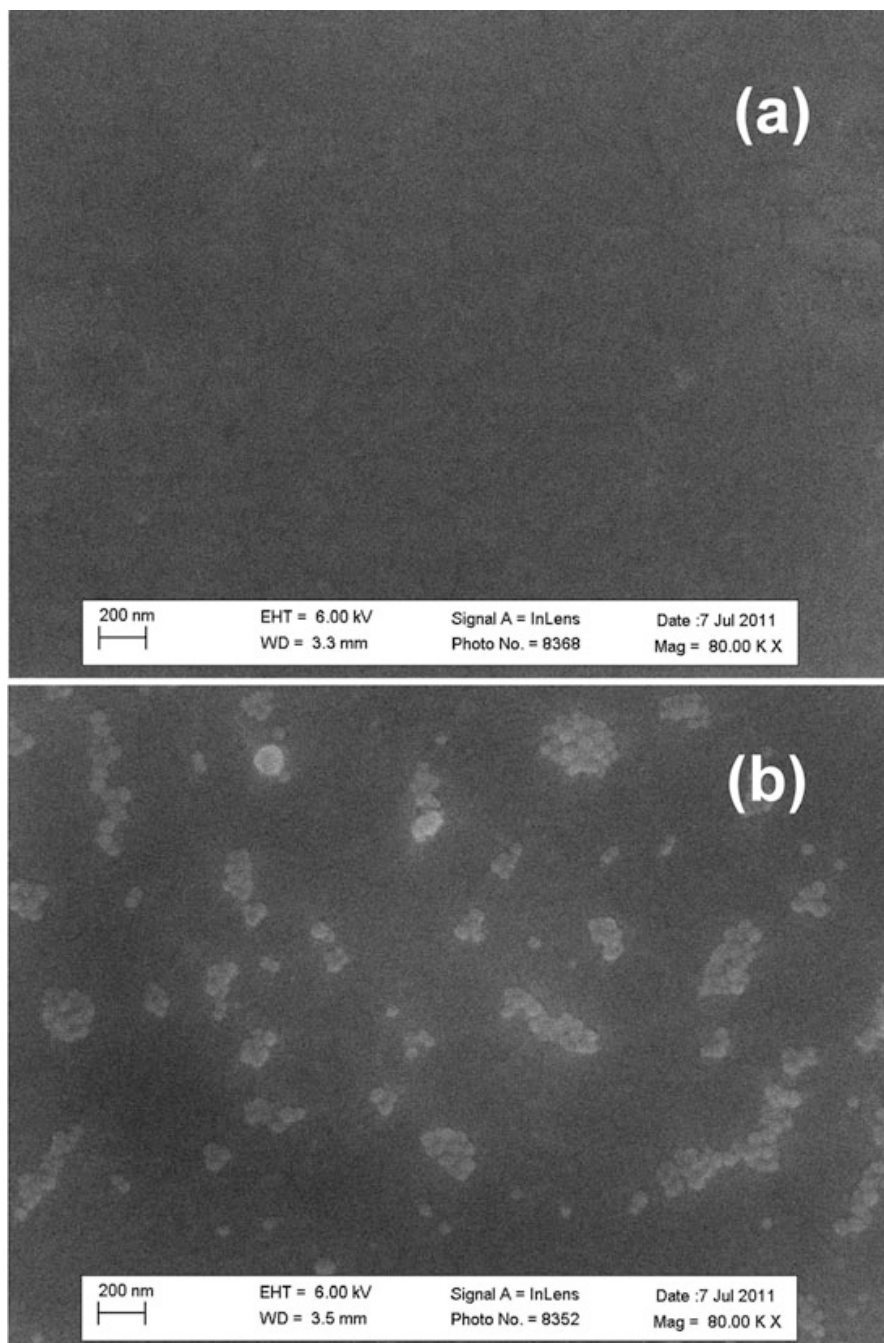


**Fig. 4** SEM images of the surface of LDPE films without (a) and with (b)  $H_3PO_4$  treatment (Rychkov et al. 2012b)

Commonly available parylene variants include parylene C, N, and D. Among them, parylene C is the most popular due to its combination of barrier properties, cost, and other processing advantages. Parylene HT<sup>®</sup> from Specialty Coating System (Indianapolis, IN, USA) is a recent development. Chemical compositions of these parylenes are shown in Fig. 5. Parylene HT<sup>®</sup> has the repeat unit  $-CF_2-$  (the repeat unit of Teflon PTFE) in its aliphatic chemistry, and hence it has superior oxidative and UV stability.

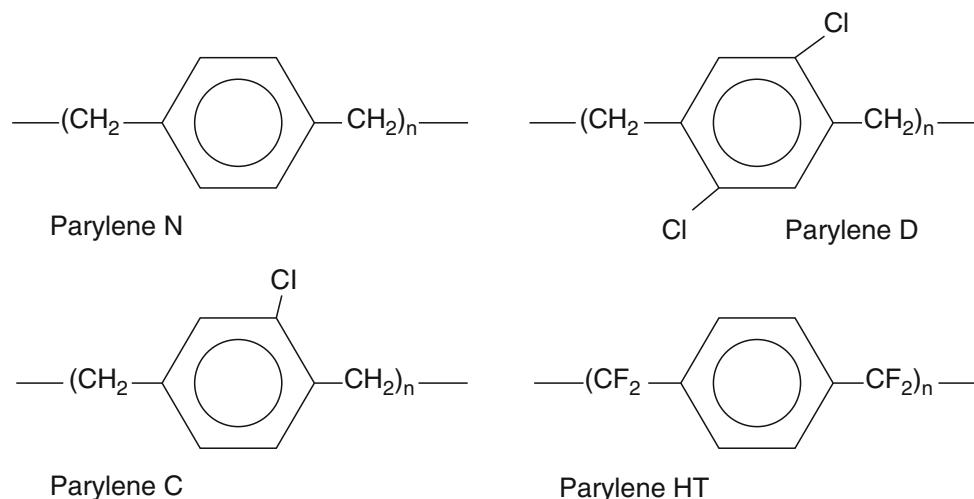


**Fig. 5** Molecular compositions of typical commercially available parylene variants

In 1980, Raschke and Nowlin reported the first study on the electret properties of parylenes (Raschke and Nowlin 1980). They found that parylenes retain surface charge densities greater than or equal to Teflon electrets. In particular, parylene D and parylene HT<sup>®</sup> (referred to as “polymer AF-4”) show exceptional high temperature stability, remarkably better than Teflon electrets. Lo and Tai reported more comprehensive investigations on parylene HT<sup>®</sup> as an electret material (Lo and Tai 2008). The maximum surface potential they obtained is 204.58 V/ $\mu\text{m}$ , corresponding to a surface charge density of 3.69 mC/m<sup>2</sup>. Being stored in ambient conditions of room temperature and 60 % RH, the as-deposited parylene HT<sup>®</sup> shows a relatively large initial drop of the surface potential. However, it maintains a stable value of about 70 % of the initial surface potential after 330 days. It was also found that proper aging treatment can significantly improve the charge stability. When the parylene HT<sup>®</sup> sample is annealed at 400 °C for 1 h before charging, it retains 91 % of the initial surface potential after 330-day storage in ambient conditions.

The thermal stability of parylene HT<sup>®</sup> electrets was studied by means of thermally stimulated discharge measurements. Figure 6 illustrates the TSD surface potential and current of the as-deposited and annealed parylene HT<sup>®</sup> samples. The peak temperatures of the TSD current spectra occur at about 160 °C and 230 °C for the as-deposited and the annealed sample, respectively, higher than those of the TSD spectra of Teflon.

### 1.2.2 CYTOP

CYTOP is a type of perfluorinated polymer. Figure 7 shows the molecular compositions for three types of commercial grade CYTOP (Asahi Glass Co., Ltd). They have different end groups, i.e., trifluoromethyl (CTL-S), carboxyl (CTL-A), and amidosilyl (CTL-M). CYTOP is soluble in perfluorinated solvents and therefore is compatible with MEMS fabrication process. Thick films can be obtained by multiple spin coating. In addition, coated films can be patterned easily with conventional photolithography and O<sub>2</sub> plasma etching.

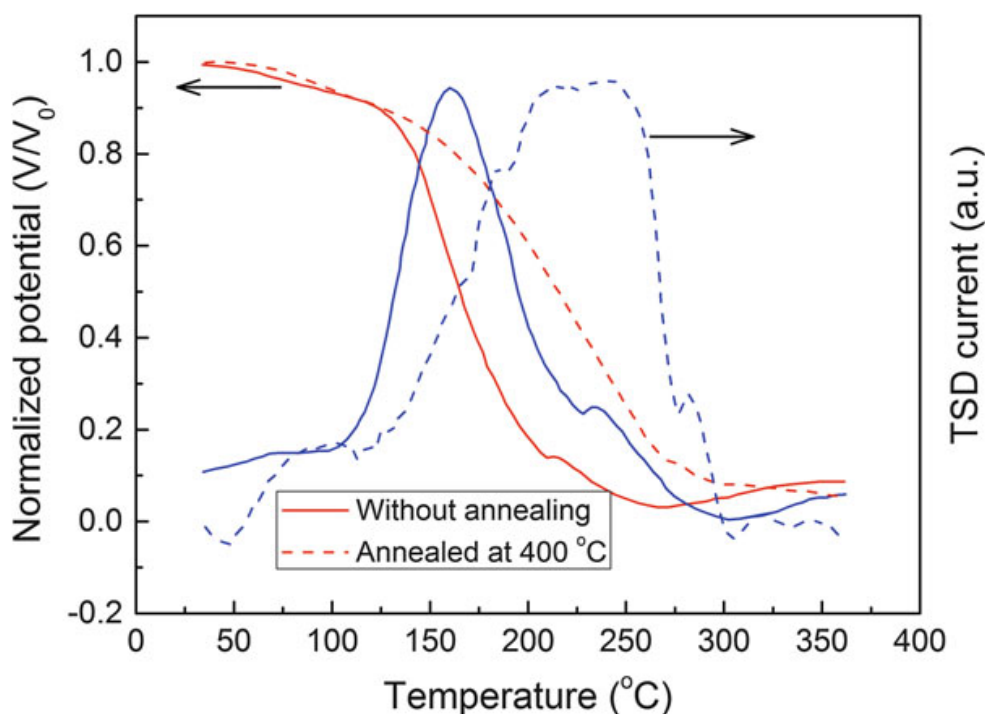


**Fig. 6** Charge TSD and TSD current spectra of parylene HT<sup>®</sup> samples without annealing (*solid*) and annealed at 400 °C for 1 h before charging (*dashed*). The surface potentials are normalized to the initial values, and the TSD current is shown in an arbitrary unit (Lo and Tai 2008)

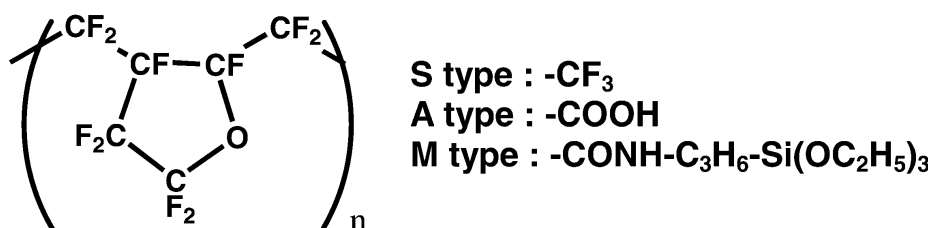


**Fig. 7** Molecular composition and end groups of CYTOP

Suzuki and colleagues studied the electret properties of CYTOP (Arakawa et al. 2004; Tsutsumino et al. 2005, 2006; Sakane et al. 2008; Kashiwagi et al. 2011). It was found that the end groups have strong influence on the electret properties of CYTOP. CTL-A and CTL-M can not only retain high surface charge density but also exhibit good stability. As shown in Fig. 8, the initial surface charge density of CTL-M is as high as  $1.3 \text{ mC/m}^2$  and is stable over a storage time longer than 4000 h. The initial surface charge density of CTL-A is about  $0.8 \text{ mC/m}^2$  also stable over the same period of storage time. In comparison, CTL-S and Teflon AF have much lower surface charge density (Sakane et al. 2008).

The results indicate that the amidosilyl end group plays a critical role in the electret properties of CYTOP. Doping only 0.6–3.0 % of aminosilane into CTL-A can double the surface charge density and improve the thermal stability. CTL-A doped with 3.0 % of aminosilane shows a surface charge density of up to  $1.5 \text{ mC/m}^2$ , higher than that of CTL-M (Fig. 8). By optimizing the charging voltage and the film

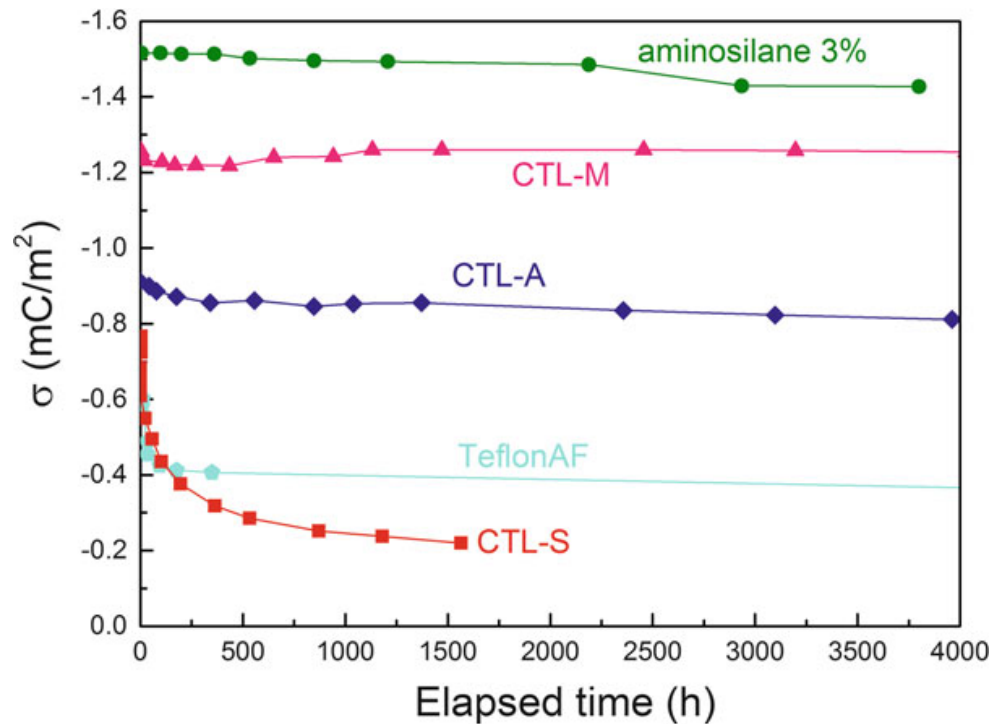


**Fig. 8** Surface charge density as a function of storage time in ambient conditions (Suzuki 2011)

thickness, a surface charge density as high as that of parylene HT<sup>®</sup> (3.7 mC/m<sup>2</sup>) is attainable with an aminosilane-doped CYTOP electret.

## 2 Ferroelectrets

Extensive studies on ferroelectrets were initiated around 1990 by colleagues from Finland using cellular polypropylene (PP). Afterward, cellular PP has become the workhorse of ferroelectret research and technology due mainly to its ease of processing and its high piezoelectricity. However, efforts have been continuously devoted to seeking ferroelectrets from different materials by means of a variety of preparation methods. This is driven mainly by the following two reasons: (i) the piezoelectricity of cellular PP ferroelectrets is stable only up to 60 °C, which limits their application and (ii) the cavities in cellular PP foams always have a rather wide and not so well-controlled size and shape distribution so that only some of the cavities are optimal for charging and for transducer operation. For industrial applications, films with well-controlled distributions or even uniform values of cavity size and cavity shape are very desirable. Such films may be easily produced on a large scale with good reproducibility. As will be demonstrated in this section, a considerable number of cellular polymer films and cavity-containing polymer film systems have been developed as ferroelectrets in recent years. Some of the typical material parameters of polymer ferroelectrets that have been reported so far are given in Table 1.

**Table 1** Material parameters of polymer ferroelectrets, i.e., film thickness  $t$ , resonance frequency  $f_p$ , elastic modulus  $c_{33}$ , piezoelectric  $d_{33}$  coefficient, and continuous service temperature (CST)

Ferroelectrets	$t$ , $\mu\text{m}$	$f_p$ , kHz	$c_{33}$ , MPa	$d_{33}$ , pC/N	CST, $^{\circ}\text{C}$	Reference
Polyolefin	Cellular PP	200 ~ 800	0.9 ~ 10	140 ~ 500	50	Zhang et al. 2004; Wegener et al. 2004
	Cellular PE	–	6 ~ 15	200 ~ 400	–	Tajitsu 2011
Polyester	Cellular PETP	119 ~ 252	0.3 ~ 3.8	~476	–	Wirges et al. 2007
	Cellular PENP	~400	1.4	60 ~ 140	80	Fang et al. 2007, 2008, 2010
COC	Cellular COC	–	–	15	110	Saarimäki et al. 2006
	COC assembly	–	0.3 ~ 270	~1000	110	Li and Zeng 2013
Polycarbonate	220	–	–	30	100	Sborikas et al. 2014
Fluoro-polymer	FEP/ePTFE/FEP sandwich	–	0.3	~500	–	Zhukov et al. 2011; von Seggern et al. 2011
	Cellular AF	9 ~ 60	0.15	600	120	Mellinger et al. 2001
	Cellular FEP	270	–	50	–	Veronina et al. 2008
	Fluoropolymer system (Fusion bonded + patterned)	60 ~ 500	20 ~ 100	0.3 ~ 0.55	160 ~ 500	120
Laser-bonded FEP	~170	31 ~ 53	0.3 ~ 0.8	160 ~ 350	120	Fang et al. 2011
AF + PDMS structure (microfabricated)	300	18	0.3	1000	–	Wang et al. 2012; Wang et al. 2013



## 2.1 Polyolefin Ferroelectret

### 2.1.1 Polypropylene Ferroelectret

Pioneer work on ferroelectrets was done by colleagues from Finland using cellular polypropylene (PP) (Kirjavainen 1987; Savolainen and Kirjavainen 1989; Raukola 1998; Lekkala and Paajanen 1999). Various procedures were adopted in order to produce polymer foams. The traditional way is to use chemical and/or physical nucleating agents in molten polymer. The pressure in extruder, where plastic material is melted, compressed, and mixed, is sufficiently high to keep the melt nonfoamed. Immediately after the pressure drop in the head of the extruder or die foam, bubbles appear and grow, introducing a cellular structure in the polymer. Another widely used method is stretching filler-loaded polymers under suitable conditions (Raukola et al. 2002). Tiny mineral particles are often employed as fillers that serve as stress concentrators for microcracks during stretching of the film. Simultaneous or sequential stretching in two perpendicular directions results in films with lens-like cavities.

Usually, the foamed film is sealed with a thin nonvoided layer on each surface. Thus, the produced polymer foam has an ABA layered structure, where the few microns thick surface layers are smooth and homogeneous, and the thicker midlayer is full of lens-like cavities.

Very often, cavities formed by stretching filler-loaded polymers are too flat for efficient charging by means of microplasma discharges, because the plasma electrons cannot be accelerated sufficiently to ionize the gas molecules. Also, flat cavities give rather stiff films with reduced electromechanical response. With a pressure and temperature treatment, so-called gas-diffusion expansion (GDE) process, the size of the cavities can be adjusted (Paajanen et al. 2002; Zhang et al. 2004; Wegener et al. 2004). The external gas pressure is raised and kept at a high value for a certain period of time so that the gases diffuse into the cavities until the internal pressure of the cavities equalizes the external pressure. The polymer foam is inflated by a subsequent sudden release of the external gas pressure. The thickness expansion of the foam is stabilized by heat treatment at elevated temperatures during or right after the pressure treatment. Figure 9 shows the SEM images for a typical cellular PP foam that is produced by stretching filler-loaded polymer melt before (top) and after (bottom) GDE treatment. It should be noted that the film becomes stiffer again when over expanded, because the cavities are now turned into more stable spherical shapes. Therefore, a medium GDE is required for optimal electromechanical properties.

The cavities in cellular PP are highly compressible in the thickness direction due to the large anisotropy, whereas in the transverse directions the materials are much stiffer. Thus, cellular PP ferroelectrets show very large piezoelectric  $d_{33}$  coefficient. Values of hundreds of pC/N are often achieved, more than one order of magnitude greater than those found in conventional ferroelectric polymers. The transverse piezoelectric coefficient ( $d_{31}$  and  $d_{32}$ ) is typically around 2 pC/N, two orders of magnitude lower than the  $d_{33}$  coefficient. This feature renders cellular PP ferroelectrets ideal candidates for flexible piezoelectric sensors, since they are essentially insensitive to the bending during operation. The pyroelectric coefficient

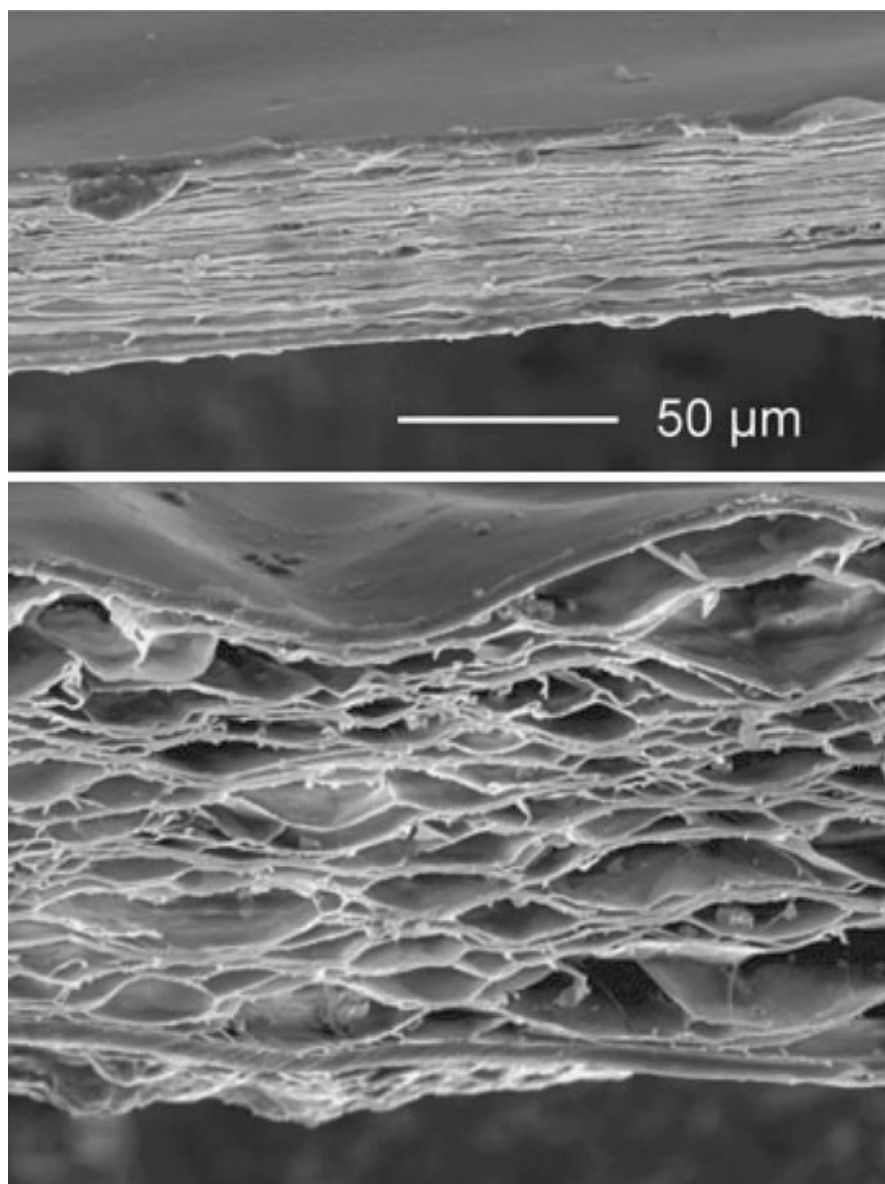


**Fig. 9** SEM of the cross sections of cellular PP films. Top: not expanded. Bottom: expanded at a pressure of 5 MPa with a subsequent heat treatment at 100 °C. The length scale is the same for both micrographs. (Wegener et al. 2004)

of cellular PP ferroelectrets ( $\sim 0.25 \mu\text{C}/\text{m}^2\text{K}$ ) is much smaller than that of polar polymers such as PVDF ( $\sim 27 \mu\text{C}/\text{m}^2\text{K}$ ) (Neugschwandtner et al. 2001). For this reason, there have been so far only very few investigations of pyroelectricity in ferroelectrets.

### 2.1.2 Polyethylene Ferroelectret

Tajitsu and colleagues studied porous polyethylene as ferroelectret (Nakayama et al. 2009; Tajitsu 2011). The porous PE films prepared in their study have a thickness of 30  $\mu\text{m}$  and a porosity ranging from 58 % to 85 %. Pores with a diameter of about 0.3  $\mu\text{m}$  are evenly distributed throughout the sample. In spite of the rather

small pore size, the authors argued that they could charge the samples with corona poling and obtain a piezoelectric  $d_{33}$  coefficient up to 200 pC/N.

It should be noted that the cavities must be internally charged via a series of dielectric barrier discharges (DBDs) in order to render polymer foams ferroelectrets (Qiu et al. 2011). According to Paschen's law, the breakdown voltage of gas in a uniform electric field is a function of gas pressure  $p$  and electrode spacing  $d$  (which in the context of ferroelectret is equal to the cavity height). For air at atmospheric pressure, the breakdown voltage decreases with decreasing  $d$  and reaches its minimum at a spacing of about 8  $\mu\text{m}$  and then increases sharply as  $d$  decreases further. Cavities with a height smaller than 3 or 4  $\mu\text{m}$  require extremely high breakdown voltage and therefore are very difficult to charge with DBDs.

### 2.1.3 Chemically Modified Polyolefin Ferroelectret

From an application point of view, both the sensitivity and the thermal stability of electromechanical transducer materials are critical factors. As for ferroelectrets, the stability of the piezoelectricity is determined by two aspects: stability of the mechanically nonuniform structure and stability of the internally trapped charge. Obviously, the nonuniform structure will collapse at temperatures higher than the melting point  $T_m$  of the material. However,  $T_m$  is usually much higher than the temperature for charge detrapping. Thus, the charge stability usually determines the temperature range for the application of ferroelectrets. For cellular PP ferroelectrets, a significant loss in the piezoelectric sensitivity appears already at 60  $^{\circ}\text{C}$ , resulting from the low long-term thermal stability of the charges stored on the inner surfaces of the cavities (Mellinger et al. 2006). For this reason, the use of cellular PP is restricted in many applications that require thermal stabilities in excess of 60  $^{\circ}\text{C}$  (for example, in the automotive industry). The thermal stability of the piezoelectricity in PE ferroelectrets was not studied in the works of Tajitsu et al. Since PE is inferior to PP in terms of charge storage, a less stable piezoelectricity is to be expected for PE ferroelectrets as compared with cellular PP.

Since space charges are trapped on the surface of the electret material in a ferroelectret (inner surfaces of cavities or interfaces between different material phases), a surface modification can be a promising solution to improve the charge stability and in turn the thermal stability of the piezoelectricity. An et al. modified cellular PP with fluorine gas. It is found the direct fluorination leads not only to higher piezoelectricity but also better thermal stability of the sensitivity (An et al. 2009c). The improvement is more pronounced if the samples were fluorinated under high pressure and were posttreated by nitrous oxide and isothermal crystallization. As shown in Fig. 10, the piezoelectric  $d_{33}$  coefficient of the fluorinated and posttreated sample remains 58 % and 45 % of its initial value after being store at 70  $^{\circ}\text{C}$  for 151 h and at 90  $^{\circ}\text{C}$  for 224 h, respectively. The corresponding value for virgin samples is only 29 and 15 % (An et al. 2012).

In the study of Rychkov et al., ferroelectrets of low-density polyethylene (LDPE) were prepared by means of a template-based lamination technique (Rychkov

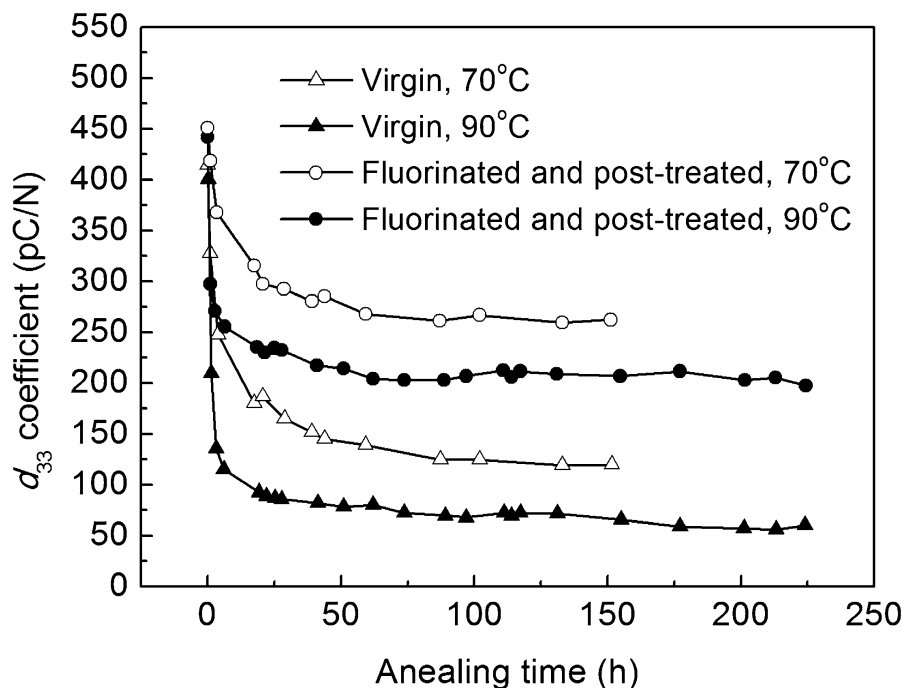


**Fig. 10**  $d_{33}$  decay in fluorinated (solid circles) and virgin (open circles) cellular PP ferroelectrets (An et al. 2012)

et al. 2012b). The as-prepared PE ferroelectrets have low thermal stability of the piezoelectricity, owing to the poor electret properties of PE. A treatment of the samples with orthophosphoric acid results in significantly improved thermal stability of the charges. Consequently, the  $d_{33}$ -decay curves shift to higher temperature by 40 °C (Fig. 11).

Polyolefins have two obvious advantages, i.e., low price and ease processibility. However, the range of application of polyolefin ferroelectrets is limited by their quite low continuous service temperatures (CST). To overcome this limitation, ferroelectrets made from other polymers with higher CST are desired.

## 2.2 Polyester Ferroelectret

The concept and knowledge of ferroelectret, established with cellular PP ferroelectrets, is successfully applied to polyester polymers. At first, polyethylene terephthalate (PETP) foams produced in the industry were studied (Wegener et al. 2005a). It is found that the as-received PET foams are expanded too much and are too stiff to have noticeable piezoelectricity. Annealing at elevated temperatures reduces the thickness of the PET foams substantially. However, the cellular structure is kept as long as the annealing temperature is below 160 °C. By optimizing the annealing parameters, a maximum  $d_{33}$  coefficient of 23 pC/N is obtained. The corresponding elastic modulus of the PET ferroelectret is around 7 MPa.

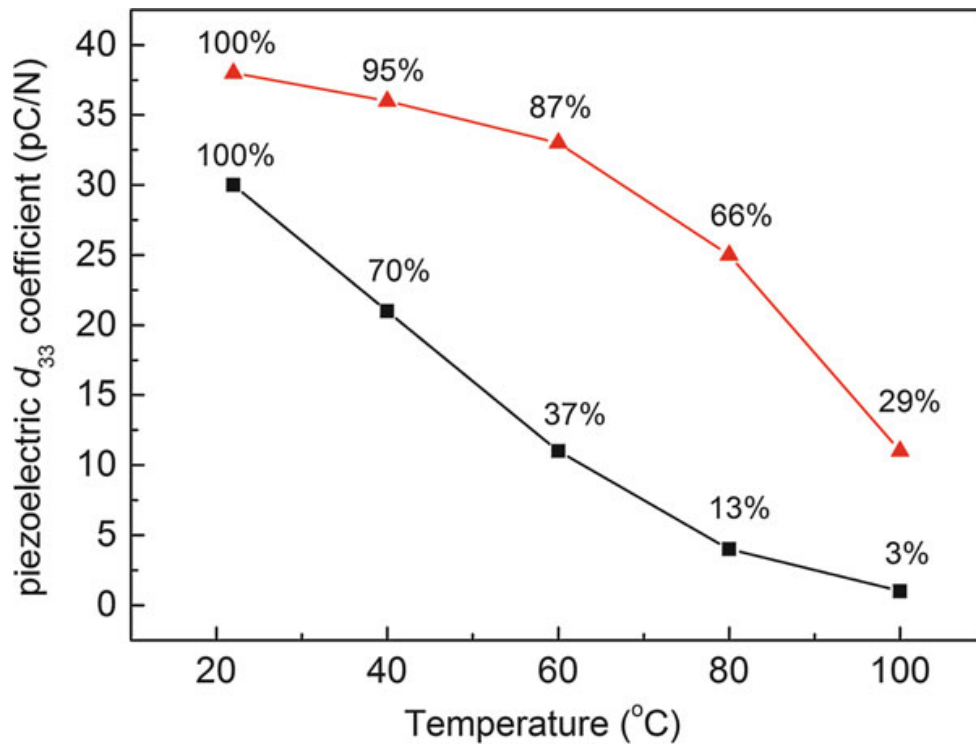


**Fig. 11** Temperature dependence of  $d_{33}$  coefficients in laminated LDPE ferroelectrets (*black squares* – virgin samples; *red triangles* – modified with orthophosphoric acid) (Rychkov et al. 2012b)

Later, the same group reported cellular polyester films, including PETP (Wegener et al. 2005b; Wirges et al. 2007) and poly(ethylene naphthalate) (PENP) (Fang et al. 2007, 2008, 2010), fabricated through physical foaming of nonvoided films with supercritical carbon dioxide (scCO<sub>2</sub>). Sample preparation consists of a sequence of steps as schematically shown in Fig. 12. A nonvoided commercial film is first exposed to pressurized CO<sub>2</sub> at room temperature. At certain high pressures, the CO<sub>2</sub> gas turns into supercritical phase. With storage time, scCO<sub>2</sub> penetrates into the bulk of the polymer film and eventually saturates. Parameters such as the gas pressure and the gas temperature need to be optimized since they strongly affect the penetration of gas molecules. Then the pressure is quickly released (Fig. 12a). This is followed by a thermal treatment on the film filled with scCO<sub>2</sub> at elevated temperature. As a result, the scCO<sub>2</sub> inside the film undergoes a phase change into gas and foams the film (Fig. 12b). The foamed structure can be further optimized by means of well-controlled biaxial stretching and sometimes subsequent gas-diffusion expansion. Figure 13 shows a SEM image of the cross-section of a PEN sample that was foamed, stretched, and expanded.

The optimized PETP and PENP ferroelectrets exhibit high piezoelectric  $d_{33}$  coefficient of 500 and 140 pC/N, respectively. The piezoelectric sensitivity of polyester ferroelectrets is stable at least up to 80 °C, slightly higher than that of cellular PP ferroelectrets. In particular, PENP ferroelectrets are still piezoelectrically active even after storage at 100 °C for 5 days.



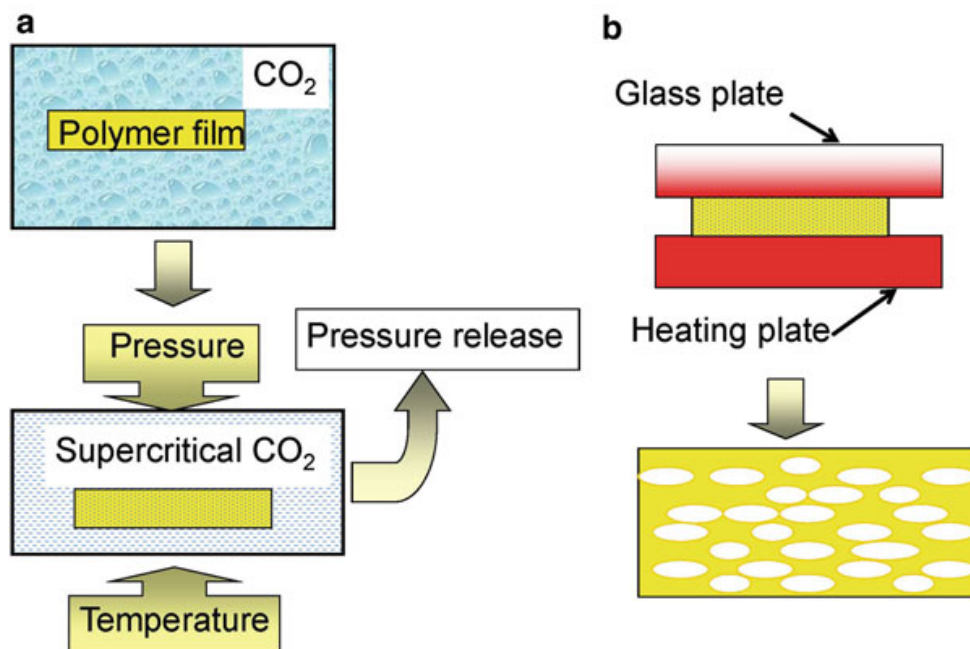


**Fig. 12** Preparation of polymer foams using supercritical CO<sub>2</sub>. (a) Penetration of scCO<sub>2</sub> into the polymer matrix. (b) Foaming of the polymer resulted from the phase change of the scCO<sub>2</sub>

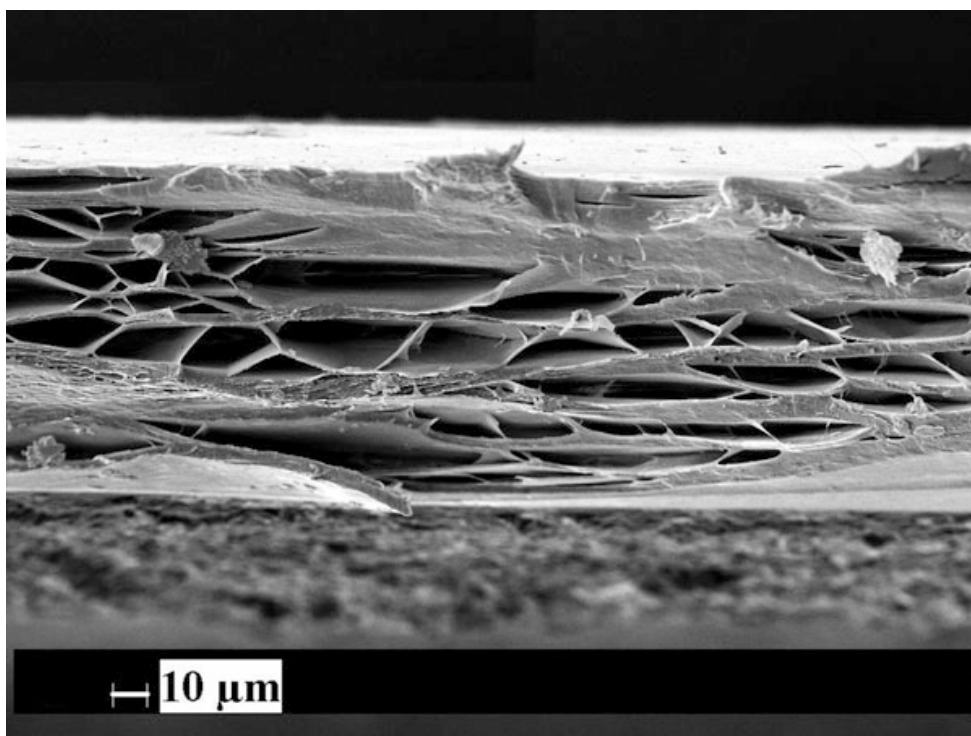


**Fig. 13** SEM image of the cross section of a cellular PEN film. The sample is foamed with scCO<sub>2</sub>, and the foam structure is further optimized by biaxial stretching and gas-diffusion expansion (Fang et al. 2007)

### 2.3 Cyclo-Olefin Polymer (COP) and Copolymer (COC) Ferroelectret

Cyclo-olefin based polymers show good electret properties with outstanding charge stability (Sessler et al. 1997) and therefore are promising candidate materials for ferroelectrets. In the works of Wegener et al. and Savijärvi et al., cyclo-olefin polymers were blended with different olefin polymers with lower glass transition temperature in order to improve the elastic properties (and thus the processability) of the materials (Wegener et al. 2005c; Savijärvi et al. 2005; Saarimäki et al. 2005, 2006). Cellular film structures were formed by stretching filler-loaded polymer compounds. The processing temperature window was very narrow compared with cellular PP foams. Gas diffusion expansion (GDE) procedures were carried out to optimize the cavity dimension. Piezoelectric  $d_{33}$  coefficients about 15 pC/N were obtained with the cellular cyclo-olefin ferroelectrets. The  $d_{33}$  coefficient is relatively small in comparison with that of cellular PP ferroelectrets. Nevertheless, the piezoelectric sensitivity of cyclo-olefin copolymer ferroelectrets exhibits good thermal stability up to 110 °C, markedly better than cellular PP and polyester ferroelectrets.

Recently, a scCO<sub>2</sub>-assisted assembly approach has been proposed for producing COC film systems with regular cavity structure (Li and Zeng 2013). When a COC film is exposed to scCO<sub>2</sub>, the surface glass transition temperature becomes significantly lower than that of the bulk due to strong COC-CO<sub>2</sub> interaction. As a result, the polymer chains near the surface are much more mobile and diffusive. Sample preparation is schematically shown in Fig. 14. Five-layer COC film stacks were employed. Two of the five films contained regular rectangular openings that were cut with a CO<sub>2</sub> laser. The openings had the same length and width and the same spacing between adjacent openings. Three COC films were separated by the two with

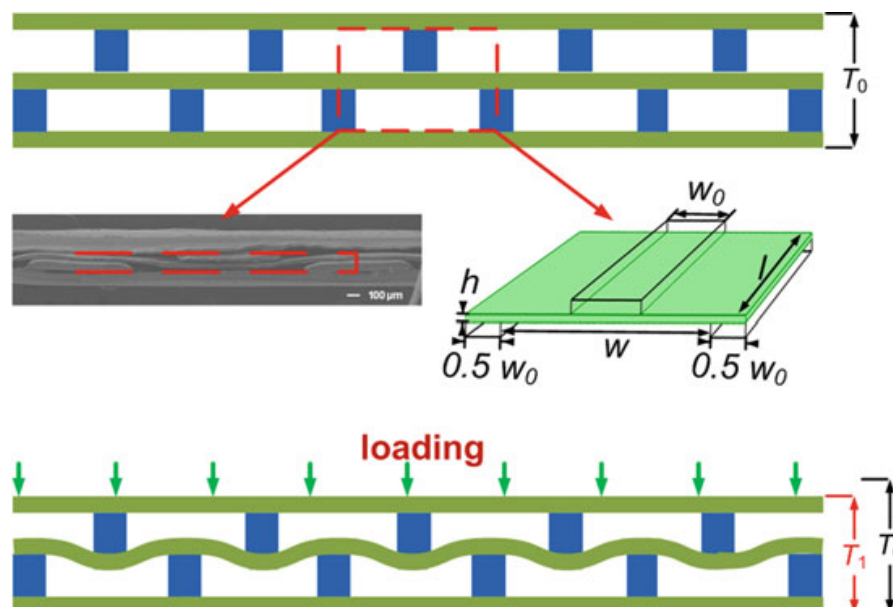


**Fig. 14** Schematic view of the preparation process for COC film systems that contain regular cavity structure. Also shown is a SEM image of a COC ferroelectret sample (LiMCP 2013)

openings, the patterns being shifted by half of the total width of the opening and the spacing. The stack was then treated for 12 h in 10 MPa CO<sub>2</sub> at a temperature of 120 °C (60 °C lower than the glass transition temperature of COC). A good bonding between the interfaces was achieved. In this method, the bulk deformation is prevented since the temperature is much lower than the bulk  $T_g$ . This is a big advantage as compared with techniques using fusion bonding where deformation of the structure and thermal degradation of the material are big concerns.

As shown in Fig. 14, the compression of the sample is realized by the bending of the “unit cell.” Such COC ferroelectrets show significant piezoelectricity. Piezoelectric  $d_{33}$  coefficient of hundreds to 1000 pC/N was reported. Investigations of the thermal stability show that the piezoelectricity is stable at least up to 110 °C.

## 2.4 Polycarbonate Ferroelectret

Polycarbonate (PC) is a durable thermoplastic with high toughness and a large creep modulus, with good heat resistance, high dimensional stability, and good electrical insulation properties. Due to these particular features, PC is widely used in electronic applications, e.g., as dielectric in capacitors with high stability. It was also reported that PC films with additives exhibit excellent charge stability after thermal treatment (Erhard et al. 2010c). Cellular PC foams were successfully prepared by means of foaming with scCO<sub>2</sub> and also by stretching films containing low-molecular-weight components that can be subsequently removed through phase extraction (Bhrendt 2010). The PC foams were charged in a point-to-plate corona with a needle voltage of +32 kV. Unfortunately, the PC foams cannot be rendered piezoelectric in this way, probably because the foam sheets are too thick for efficient charging and/or the films are too stiff for sufficient deformation under mechanical or electrical stress.

New strategies have been proposed for making PC ferroelectrets. One strategy is rather easy to implement. A grid of double-sided adhesive tape with desired opening pattern was prepared by means of a computer-controlled laser cutting. Two polycarbonate (PC) films, which were metalized on one surface, were joined by the grid via their nonmetalized surfaces (Qiu et al. 2010). Thus, well-defined cavities are formed around the openings of the grid. After contact charging with 2 kV, the PC ferroelectrets show a piezoelectric  $d_{33}$  coefficient up to 30 pC/N.

In another strategy, PC ferroelectrets were prepared through the use of screen printing (Sborikas et al. 2014). Screen printing is often employed to deposit inks onto substrates ranging from ceramics to plastic materials, fabrics, and papers. For sample preparation, suitable ink materials are screen printed with desired pattern onto a piece of PC film. Then, the second PC film is placed on top of the ink pattern. With thermal treatment, two PC films are tightly bonded to each other by the polymer ink pattern, leading to a polymer system with well-defined cavities. Silver paste electrodes were screen printed onto both outer surfaces of the samples. After charging, the PC ferroelectrets exhibit  $d_{33}$  coefficient of about 30 pC/N, which is stable up to 100 °C.

## 2.5 Fluoropolymer Ferroelectret

Fluoropolymers, such as several kinds of Teflon (polytetrafluoroethylene [PTFE], fluoroethylenepropylene [FEP], tetrafluoroethylene-per-fluoromethoxyethylene copolymer [PFA], and amorphous Teflon [AF]), are very important electrets due to their excellent charge storage properties. When ferroelectrets are made from fluoropolymers, a good thermal stability of the piezoelectricity is to be expected. However, how to make cellular fluoropolymers is a big challenge because of their poor mechanical properties and severe creep behavior. Initially, porous PTFE was produced by means of unidirectional stretching at high temperature. Such films have open pore structures which is detrimental for the piezoelectricity. Cellular fluoropolymer foams were produced by solvent evaporation technique and foaming with  $scCO_2$ . These techniques require relatively complex processing and lack good reproducibility. More recently, a number of other strategies have been proposed, including fusion bonding combined with patterning, laser bonding, as well as microfabrication.

### 2.5.1 Porous PTFE

Porous PTFE films were prepared from commercial nonporous PTFE plates by means of unidirectional stretching at high temperature. The porous films exhibit open structure of the pores. This is quite different from other types of polymer foams, such as cellular PP, which have closed-cavity structure. Porous PTFE shows excellent surface-charge storage stability, even at elevated temperature (Xia et al. 1999). Because of its open-pore structure, porous PTFE itself is not a promising piezoelectric material. During metallization of electrodes that are necessary for electrical contact for measuring the signal, the metallic particles go into the interfaces between the pores and the dielectric. As a result, the deposited charges are lost and the piezoelectricity of the film becomes extremely low. Nevertheless, porous PTFE is very suitable for preparing sandwich-structure ferroelectrets due to its high softness and excellent electret properties. Shortly after, layer stacks of porous and nonporous PTFE films as ferroelectrets were studied (Künstler et al. 2000; Gerhard-Multhaupt et al. 2000).

Von Seggern and colleagues prepared ferroelectrets by sandwiching a highly porous PTFE consisting of 91 % air and 9 % fibrous PTFE, so-called expanded PTFE (ePTFE), between two solid FEP layers (Hu and von Seggern 2005, 2006; Zhukov and von Seggern 2007a, b; von Seggern et al. 2010, 2011; Zhukov et al. 2011). In order to eliminate any excess air between adjacent layers, samples were subject to an initial evacuation step followed by a slow exposure to lab conditions. Figure 15 shows the cross section of such a fluoropolymer sandwich.

In such sandwiches, the FEP layers form structurally and electrically dense layers, sealing the open porous structure of the ePTFE layer. Upon corona charging, breakdown occurs within the pores when the electric field strength exceeds the Paschen-breakdown threshold value of air inside. Charges of both polarities are

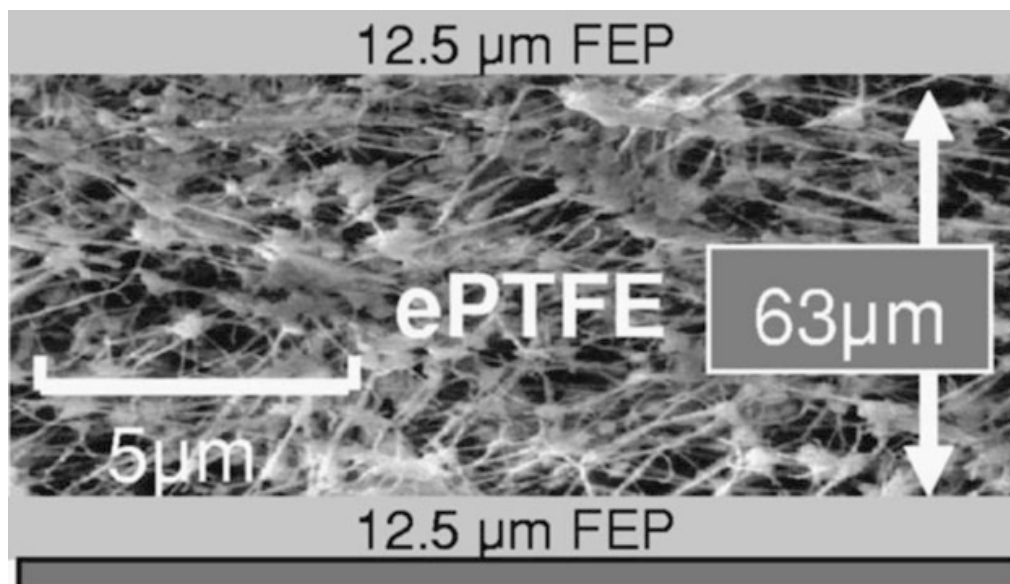


**Fig. 15** FEP/ePTFE/FEP/metal layer system (Zhukov and von Seggern 2007a)

separated, and some of them are trapped on the inner surfaces of the top and bottom FEP layers. After charging, the FEP layers, separated by the ePTFE layer, form macroscopic dipoles, leading to strong piezoelectricity of the sample. The piezoelectric  $d_{33}$  coefficient is thermally stable if the sample is charged at elevated temperatures. However, the  $d_{33}$  decays from 800 to 400 pC/N under atmospheric pressures within 6 days, and repeated mechanical loading leads to a similar loss of piezoelectricity, apparently related to mechanical fatigue in the highly porous ePTFE.

### 2.5.2 Cellular Fluoropolymer Ferroelectret

Teflon AF is easier to process than other fluoropolymers. It can be dissolved in selected perfluorocarbon solvents, which allows the production of AF films by conventional techniques such as drop casting and spin coating. In the work of Mellinger et al., porous Teflon AF films with a thickness of 3–10 μm was obtained by boiling the solvent (Fluorinert FC-77 from 3 M) (Mellinger et al. 2001). Several layers were drop casted on top of each other in order to have the desired overall thickness. The porous film with open pores was sealed with nonporous AF films made by drop casting at room temperature. After corona charging, the Teflon AF ferroelectrets exhibit strong piezoelectricity with a  $d_{33}$  coefficient up to 600 pC/N. The piezoelectric sensitivity is stable at temperatures of at least 120 °C.

Unlike the homopolymer PTFE, FEP is a meltprocessable thermoplastic copolymer. The above described technique of foaming with  $\text{scCO}_2$  was also adopted to make cellular FEP foams (Veronina et al. 2008). The procedures for foaming of the material are similar to the case of polyester polymers. Usually, only one big void



across the film thickness is generated in the FEP foams. After charging and electrode evaporation, the cellular FEP ferroelectrets show  $d_{33}$  coefficients up to 50 pC/N.

### 2.5.3 Cavity-Containing Fluoropolymer Film Systems Prepared by Fusion Bonding

Fluoropolymer film systems containing internal cavities have been prepared by several groups through fusion bonding technique. Altafim et al. developed FEP film systems with uniform cavities by thermal fusion combined with vacuum evacuation (Altafim et al. 2005, 2006). In their study, a stack of two FEP films was placed between two cylindrical metal plates which can be independently heated. The top plate is completely solid, while the bottom one has tiny holes that are connected to a vacuum pump. The bottom plate was separated from the stack of FEP films by a metal grid. Most of the air was removed through the holes of the bottom plate by means of the vacuum pump and the adjacent FEP film was sucked into the openings of the metal grid. By heating and pressing the top plate onto the stack, air cavities with the same diameter as the grid openings were created.

Later, ferroelectrets with well-controlled and uniform cavities were developed by a straightforward lamination process (Altafim et al. 2009). In this process, two polymer electret films are laminated around a template between them. The template, which can be made of metal foils or of polymers with a melting temperature higher than that of the electret films, contains regular openings through which the electret films can be fused with each other. Lamination is implemented at a temperature

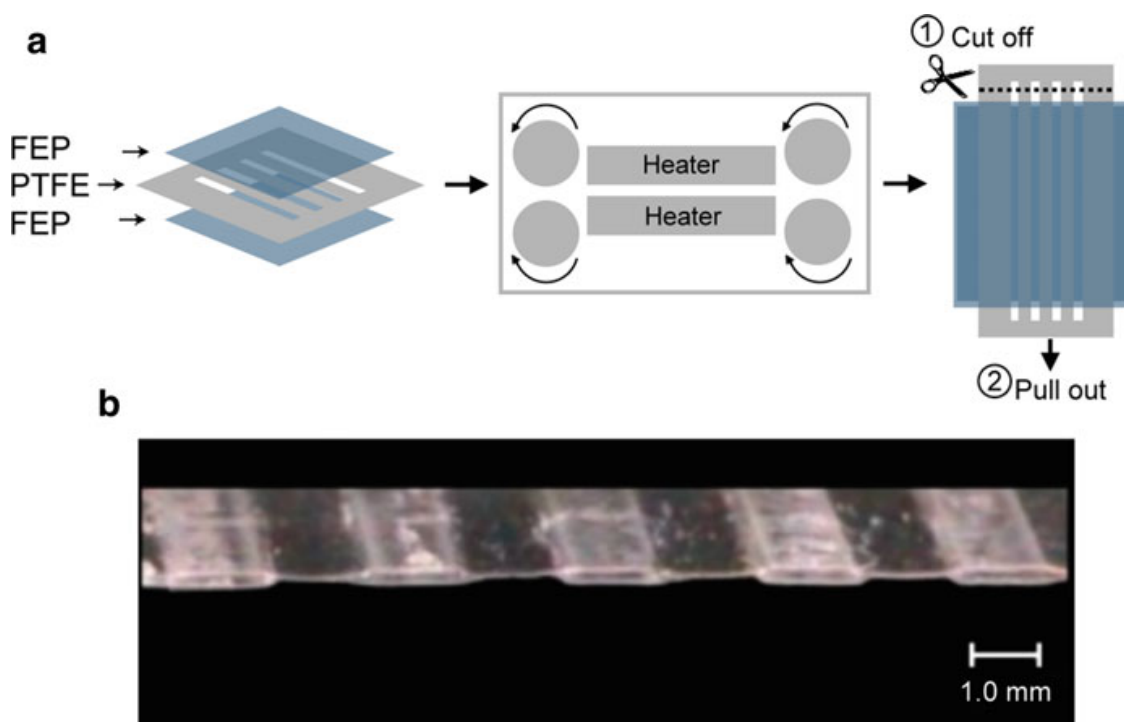


**Fig. 16** (a) Schematic view of the preparation process for tubular-channel ferroelectrets. (b) Optical micrograph of the cross section of an FEP ferroelectret sample (Altafim et al. 2009)

substantially higher than the melting temperature of the electret films yet lower than that of the template. After the outer layers have been fused, the template is removed, resulting in a polymer-film system with cavities of the designed pattern. Figure 16a schematically shows the preparation for tubular-channel FEP ferroelectrets. The template, made of an 100  $\mu\text{m}$  thick PTFE by means of laser cutting, consists of several well-cut stripes with clearly defined and evenly distributed openings between them. The two solid FEP films have a thickness of 50  $\mu\text{m}$  each. After being laminated at 300  $^{\circ}\text{C}$ , the stack is naturally cooled down under laboratory conditions. The two FEP films are permanently fused with each other through the openings of the template. An FEP film system with open tubular cavities is obtained after removal of the PTFE template. Figure 16b shows an optical image of the cross section of such an FEP film system.

For stacks of very thin FEP and PTFE films, void-containing film systems can be obtained by directly pressing a metal mesh with (sub) millimeter spacing (Zhang et al. 2006, 2007). With a thermal treatment at 280  $^{\circ}\text{C}$ , the polymer layers were fused underneath the wires of the metal mesh and cavities were formed between the fused areas because of the thermally expanding trapped air and the thermal softening of the fluoropolymer films. In several other works, rigid templates were used to bring forth the desired pattern in the fusion-bonded fluoropolymer film systems (Zhang et al. 2010, 2012, 2014a; Sun et al. 2011). When porous PTFE film is employed as the middle layer, the step of patterning can be skipped (Huang et al. 2008; Zhang et al. 2009, 2014b). For multilayer system consisting of FEP and porous PTFE, the film systems were bonded at a temperature between the melting point of FEP and that of PTFE. For porous and nonporous PTFE film systems, the film stacks were bonded by means of sintering.

#### 2.5.4 FEP Ferroelectret Prepared by Laser Bonding

In the laser bonding technique, film stacks are locally fused by means of a laser beam (Fang et al. 2011). Commercial Teflon FEP films were used for the sample preparation. Regular square holes are cut into an FEP film separated by FEP stripes. The patterned film was sandwiched with two uniform FEP films. By applying a laser beam at selected points along the FEP stripes, the FEP melted locally and finally fused after the laser is moved away.

#### 2.5.5 Teflon AF Ferroelectret by Microfabrication

Using microfabrication process, Wang et al. produced Teflon AF ferroelectrets built on cellular polydimethylsiloxane (PDMS) structures with micrometer-sized cavities (Wang et al. 2012, 2013). The sample fabrication consists of multilayer PDMS casting and stacking processes (Fig. 17). A photoresist mold is prepared on a silicon wafer. The cellular microstructure is duplicated to a thin PDMS layer that is casted on top of the mold. By bonding the patterned PDMS film to a blank thin PDMS layer, a PDMS foam with closed cavities is obtained. Multilayer structures can be constructed by repeating the casting and bonding processes. The cavities were filled with a solution of Teflon AF. Once the solvent evaporates, a thin layer of AF film deposits which assures good charge storage after internal charging of the cavities.

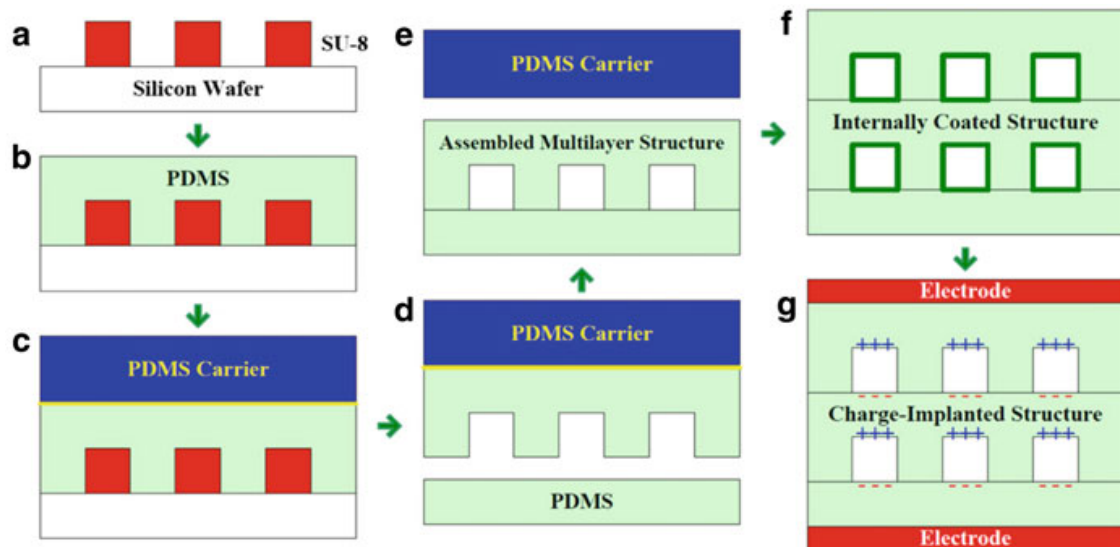


**Fig. 17** Schematic illustration of the microfabrication of PDMS ferroelectrets (Wang et al. 2012)

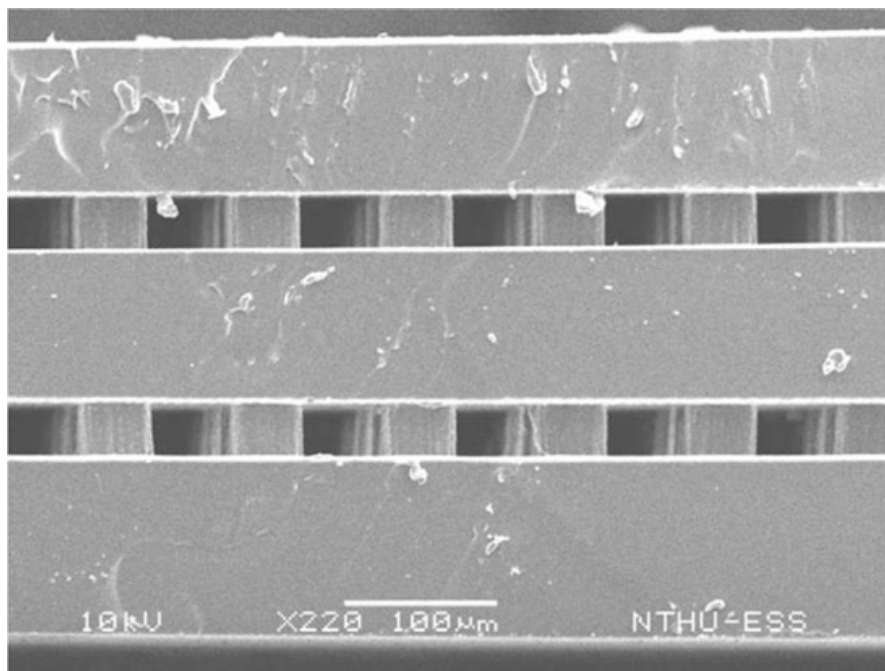


**Fig. 18** Microfabricated cellular PDMS (Wang et al. 2013)

During the processing, chemical or corona treatment is carried out in order to have easy peeling off or good bonding, respectively. Figure 18 shows the SEM image of the cross section of a sample. After electrode deposition and charging, the microfabricated ferroelectrets exhibit a piezoelectric  $d_{33}$  coefficient larger than 1000 pC/N.

### 3 Summary

The development with respect to polymer electret materials has been active over the past years. A number of modified conventional polymer electret materials with superior electret properties have been reported. The improvement of electret properties were achieved by incorporating proper additives, by blending different polymer compounds, by physical aging, and by modifying with certain chemicals. Besides, high-performance polymer electrets, such as Parylene HT<sup>®</sup> and certain types of CYTOP, were introduced to the family of electret materials. They exhibit not only excellent electret properties (high surface charge density with exceptional long-term and thermal stability) but also good compatibility with MEMS fabrication process.

As was also discussed in this chapter, very significant progress has been made in the development of ferroelectrets. A large number of polymer electrets, including polyolefins (PP and PE), polyesters (PETP and PENP), COC, PC, and fluoropolymers, were adopted to prepare ferroelectrets using a variety of techniques. By now, ferroelectrets with excellent electromechanical properties and with well-controlled cavity structures are becoming available.

The development of polymer electret and ferroelectret materials will certainly continue, and numerous novel applications using these new electret materials can be expected in the foreseeable future.

---

### References

- Altafim RAC, Basso HC, Gonçalves Neto L, Lima L, Altafim RAP, de Aquino CV (2005) Piezoelectricity in multi-air voids electrets. In: Proceedings of conference electrical insulation dielectric phenomena, IEEE Service Center, Piscataway, pp 669–672
- Altafim RAC, Basso HC, Altafim RAP, Lima L, de Aquino CV, Gonçalves Neto L, Gerhard-Multhaupt R (2006) Piezoelectrets from thermo-formed bubble structures of fluoropolymer-electret films. *IEEE Trans Dielectr Electr Insul* 13(5):979–985
- Altafim RAP, Qiu X, Wirges W, Gerhard R, Altafim RAC, Basso HC, Jenninger W, Wagner J (2009) Template-based fluoroethylenepropylene piezoelectrets with tubular channels for transducer applications. *J Appl Phys* 106:014106
- An Z, Yang Q, Xie C, Jiang Y, Zheng F, Zhang Y (2009a) Suppression effect of surface fluorination on charge injection into linear low density polyethylene. *J Appl Phys* 105:064102
- An Z, Xie C, Jiang Y, Zheng F, Zhang Y (2009b) Significant suppression of space charge injection into linear low density polyethylene by surface oxyfluorination. *J Appl Phys* 106:104112
- An Z, Zhao M, Yao J, Zhang Y, Xia Z (2009c) Influence of fluorination on piezoelectric properties of cellular polypropylene ferroelectrets. *J Phys D Appl Phys* 42:015418
- An Z, Mao M, Cang J, Zhang Y, Zheng F (2012) Significantly improved piezoelectric thermal stability of cellular polypropylene films by high pressure fluorination and post-treatments. *J Appl Phys* 111:024111
- Arakawa Y, Suzuki Y, Kasagi N (2004) Micro seismic power generator using electret polymer film. In: Proceedings of powerMEMS 2004, Kyoto, pp 187–190

- Bhrendt N (2010) Tailored processing methods for cellular polycarbonate and polyetherimide films – new potentials for electret and piezoelectric applications. *IEEE Trans Dielectr Electr Insul* 17(4):1113
- Erhard DP, Deliani L, von Salis-Soglio C, Giesa R, Alstädt V, Schmidt HW (2010a) Recent advances in the improvement of polymer electret films. In: Müller AHE, Schmidt HW (eds) *Complex macromolecular systems II*, vol 228, Book series: advances in polymer science. Springer, Berlin, pp 155–207
- Erhard DP, Lovera D, Giesa R, Alstädt V, Schmidt HW (2010b) Influence of physical aging on the performance of corona-charged amorphous polymer electrets. *J Polym Sci B Polym Phys* 48:990–997
- Erhard DP, Lovera D, Jenninger W, Wagner J, Alstädt V, Schmidt H (2010c) Tailored additives to improve the electret performance of polycarbonates. *Macromol Chem Phys* 211:2179
- Fang P, Wegener M, Wirges W, Gerhard R (2007) Cellular polyethylene-naphthalate ferroelectrets: foaming in supercritical carbon dioxide, structural and electrical preparation, and resulting piezoelectricity. *Appl Phys Lett* 90:192908
- Fang P, Wirges W, Wegener M, Zirkel L, Gerhard R (2008) Cellular polyethylene-naphthalate films for ferroelectret applications: foaming, inflation and stretching, assessment of electromechanically relevant structural features. *E-Polymers* 8(1):487–495
- Fang P, Qiu X, Wirges W, Gerhard R, Zirkel L (2010) Polyethylene-naphthalate (PEN) ferroelectrets: cellular structure, piezoelectricity and thermal stability. *IEEE Trans Dielectr Electr Insul* 17(4):1079–1087
- Fang P, Wang F, Wirges W, Gerhard R, Basso HC (2011) Three-layer piezoelectrets from fluorinated ethylene-propylene (FEP) copolymer films. *Appl Phys A Mater Sci Process* 103:455–461
- Gerhard-Multhaupt R (ed) (1999) *Electrets*, vol 2, 3rd edn. Laplacian Press, Morgan Hill
- Gerhard-Multhaupt R, Küstler W, Goerne T, Pucher A, Weinhold T, Seiß M, Xia Z, Wedel A, Danz R (2000) Porous PTFE space-charge electrets for piezoelectric applications. *IEEE Trans Dielectr Electr Insul* 7(4):480–488
- Hilczler B, Malecki J (1986) *Electrets*. Elsevier, Amsterdam
- Hu Z, von Seggern H (2005) Air-breakdown charging mechanism of fibrous polytetrafluoroethylene films. *J Appl Phys* 98:014108
- Hu Z, von Seggern H (2006) Breakdown-induced polarization buildup in porous fluoropolymer sandwiches: a thermally stable piezoelectret. *J Appl Phys* 99:024102
- Huang J, Zhang X, Xia Z, Wang X (2008) Piezoelectrets from laminated sandwiches of porous polytetrafluoroethylene films and nonporous fluoroethylenepropylene films. *J Appl Phys* 103:084111
- Kashiwagi K, Okano K, Miyajima T, Sera Y, Tanabe N, Morizawa Y, Suzuki Y (2011) Nano-cluster-enhanced high-performance perfluoro-polymer electrets for energy harvesting. *J Micromech Microeng* 21:125016
- Kirjavainen K (1987) Electromechanical film and procedure for manufacturing same. US Patent 4,654,546
- Ko WC, Tseng CK, Leu IY, Wu WJ, Lee AS, Lee CK (2010) Use of 2-(6-mercaptohexyl) malonic acid to adjust the morphology and electret properties of cyclic olefin copolymer and its application to flexible loudspeakers. *Smart Mater Struct* 19:055007
- Kressmann R, Sessler GM, Günther P (1999) Chapter 9: Space-charge electrets. In: Gerhard-Multhaupt R (ed) *Electrets*, vol 2, 3rd edn. Laplacian Press, Morgan Hill, pp 1–40
- Künstler W, Xia Z, Weinhold T, Pucher A, Gerhard-Multhaupt R (2000) Piezoelectricity of porous polytetrafluoroethylene single- and multiple-film electrets containing high charge densities of both polarities. *Appl Phys A Mater Sci Process* 70(1):5–8
- Lekkala J, Paajanen M (1999) EMFi-new electrets material for sensors and actuators. In: *Proceedings of 10th international symposium electrets*, Delphi, pp 743–746
- Li Y, Zeng C (2013) Low-temperature CO<sub>2</sub>-assisted assembly of cyclic olefin copolymer ferroelectrets of high piezoelectricity and thermal stability. *Macromol Chem Phys* 214:2733–2738



- Lo HW, Tai YC (2008) Parylene-based electrets power generators. *J Micromech Microeng* 18:104006
- Mellinger A, Wegener M, Wirges W, Gerhard-Multhaupt R (2001) Thermally stable dynamic piezoelectricity in sandwich films of porous and non-porous amorphous fluoropolymer. *Appl Phys Lett* 79:1852–1854
- Mellinger A, Wegener M, Wirges W, Mallepally RR, Gerhard-Multhaupt R (2006) Thermal and temporal stability of ferroelectret films made from cellular polypropylene/air composites. *Ferroelectrics* 331:189–199
- Nakayama M, Uenaka Y, Kataoka S, Oda Y, Yamamoto K, Tajitsu Y (2009) Piezoelectricity of ferroelectret porous polyethylene thin film. *Jpn J Appl Phys* 48:09KE05
- Neugschwandtner GS, Schwödiauer R, Bauer-Gogonea S, Bauer S, Paajanen M, Lekkala J (2001) Piezo- and pyroelectricity of a polymer-foam space-charge electret. *J Appl Phys* 89:4503
- Paajanen M, Minkkinen H, Raukola J (2002) Gas diffusion expansion-increased thickness and enhanced electromechanical response of cellular polymer electret films. In: *Proceedings of 11th international symposium electrets*, Melbourne, pp 191–194
- Qiu X, Holländer L, Suárez RF, Wirges W, Gerhard R (2010) Polarization from dielectric-barrier discharges (DBDs) in ferroelectrets: mapping of the electric-field profiles by means of thermal-pulse-tomography (TPT). *Appl Phys Lett* 97:072905
- Qiu X, Gerhard R, Mellinger A (2011) Turning polymer foams or polymer-film systems into ferroelectrets: dielectric barrier discharges in voids. *IEEE Trans Dielectr Electr Insul* 18(1):34–42
- Raschke CR, Nowlin TE (1980) Polyparaxylylene electrets usable at high temperatures. *J Appl Polym Sci* 25:1639–1644
- Raukola J (1998) A new technology to manufacture polypropylene foam sheet and biaxially oriented foam film. Ph.D. thesis, Technical Research Centre of Finland. VTT Publication 361, Espoo
- Raukola J, Kuusinen N, Paajanen M (2002) Cellular electrets – from polymer granules to electro-mechanically active films. In: *Proceedings of 11th international symposium electrets*, Melbourne, pp 195–198
- Rychkov D, Gerhard R (2011) Stabilization of positive charge on polytetrafluoroethylene films treated with titanium-tetrachloride vapor. *Appl Phys Lett* 98:122901
- Rychkov D, Kuznetsov A, Rychkov A (2011a) Electret properties of polyethylene and polytetrafluoroethylene films with chemically modified surface. *IEEE Trans Dielectr Electr Insul* 18:8–14
- Rychkov D, Kuznetsov A, Rychkov A, Goldade V (2011b) Electret properties of polyethylene films modified with titanium tetrachloride vapor. In: *Proceedings of 14th international symposium electrets*, Montpellier, pp 111–112
- Rychkov D, Gerhard R, Ivanov V, Rychkov A (2012a) Enhanced electret charge stability on polyethylene films treated with titanium-tetrachloride vapor. *IEEE Trans Dielectr Electr Insul* 19(4):1305–1311
- Rychkov D, Altafim RAP, Qiu X, Gerhard R (2012b) Treatment with orthophosphoric acid enhances the thermal stability of the piezoelectricity in low-density polyethylene ferroelectrets. *J Appl Phys* 111:124105
- Rychkov D, Yablokov M, Rychkov A (2012c) Chemical and physical surface modification of PTFE films – an approach to produce stable electrets. *Appl Phys A Mater Sci Process* 107(3):589–596
- Rychkov D, Rychkov A, Efimov N, Malygin A, Gerhard R (2013) Higher stabilities of positive and negative charge on tetrafluoroethylene–hexafluoropropylene copolymer (FEP) electrets treated with titanium-tetrachloride vapor. *Appl Phys A* 112:283–287
- Saarimäki E, Paajanen M, Savijärvi AM, Minkkinen H (2005) Novel heat durable electromechanical film processing: preparations for electromechanical and electret applications. In: *Proceedings of 12th international symposium electrets (ISE 12)*, IEEE Service Center, Piscataway, pp 220–223
- Saarimäki E, Paajanen M, Savijärvi AM, Minkkinen H, Wegener M, Voronina O, Schulze R, Wirges W, Gerhard-Multhaupt R (2006) Novel heat durable electromechanical film processing:

- preparations for electromechanical and electret applications. *IEEE Trans Dielectr Electr Insul* 13 (5):963–972
- Sakane Y, Suzuki Y, Kasagi N (2008) The development of a high-performance perfluorinated polymer electret and its application to micro power generation. *J Micromech Microeng* 18:104011
- Savijärvi AM, Paaajanen M, Saarimäki E, Minkkinen H (2005) Novel heat durable electromechanical films: cellular film making from cyclic olefin polymers. In: Proceedings of 12th international symposium electrets (ISE 12), IEEE Service Center, Piscataway, pp 75–78
- Savolainen A, Kirjavainen K (1989) Electrothermomechanical film: Part I. Design and characteristics. *J Macromol Sci A Chem* 26(2&3):583–591
- Sborikas M, Qiu X, Wirges W, Gerhard R, Jenninger W, Lovera D (2014) Screen printing for producing ferroelectret systems with polymer-electret films and well-defined cavities. *Appl Phys A Mater Sci Process* 114:515–520
- Sessler GM (ed) (1999) *Electrets*, vol 1, 3rd edn. Laplacian Press, Morgan Hill
- Sessler GM (2001) Electrets: recent developments. *J Electrostat* 51–52:137–145
- Sessler GM, Yang GM, Hatke W (1997) Electret properties of cycloolefin copolymers. Electrical insulation and dielectric phenomena. In: Annual report conference on electrical insulation dielectric phenomena, IEEE Service Center, Piscataway, pp 467–470
- Sun Z, Zhang X, Xia Z, Qiu X, Wirges W, Gerhard R, Zeng C, Zhang C, Wang B (2011) Polarization and piezoelectricity in polymer films with artificial void structure. *Appl Phys A Mater Sci Process* 105:197–205
- Suzuki Y (2011) Recent progress in MEMS electret generator for energy harvesting. *IEEJ Trans Electr Electron Eng* 6:101–111
- Tajitsu Y (2011) Piezoelectric properties of ferroelectret. *Ferroelectrics* 415:57–66
- Tsutsumino T, Suzuki Y, Kasagi N, Tsurumi Y (2005) High-performance polymer electret for micro seismic generator. In: Proceedings of powerMEMS 2005, Tokyo, pp 9–12
- Tsutsumino T, Suzuki Y, Kasagi N, Sakane Y (2006) Seismic power generator using high-performance polymer electret. In: Proceedings of international conference MEMS'06, Istanbul, pp 98–101
- Voronina O, Wegener M, Wirges W, Gerhard R, Zirkel L, Münstedt H (2008) Physical foaming of fluorinated ethylene-propylene (FEP) copolymers in supercritical carbon dioxide: single-film fluoropolymer piezoelectrets. *Appl Phys A Mater Sci Process* 90:615–618
- von Seggern H, Zhukov S, Fedosov S (2010) Poling dynamics and thermal stability of FEP/ePTFE/FEP sandwiches. *IEEE Trans Dielectr Electr Insul* 17(4):1056–1065
- von Seggern H, Zhukov S, Fedosov S (2011) Importance of geometry and breakdown field on the piezoelectric  $d_{33}$  coefficient of corona charged ferroelectret sandwiches. *IEEE Trans Dielectr Electr Insul* 18(1):49–56
- Wang J, Hsu T, Yeh C, Tsai J, Su Y (2012) Piezoelectric polydimethylsiloxane films for MEMS transducers. *J Micromech Microeng* 22:015013
- Wang J, Tsai J, Su Y (2013) Piezoelectric rubber films for highly sensitive impact measurement. *J Micromech Microeng* 23:075009
- Wegener M, Wirges W, Fohlmeister J, Tiersch B, Gerhard-Multhaupt R (2004) Two-step inflation of cellular polypropylene films: void-thickness increase and enhanced electromechanical properties. *J Phys D Appl Phys* 37(4):623–627
- Wegener M, Wirges W, Gerhard-Multhaupt R (2005a) Piezoelectric polyethylene terephthalate (PETP) foams – specifically designed and prepared ferroelectret films. *Adv Eng Mater* 7:1128–1131
- Wegener M, Wirges W, Dietrich JP, Gerhard-Multhaupt R (2005b) Polyethylene terephthalate (PETP) foams as ferroelectrets. In: Proceedings of 12th international symposium electrets (ISE 12), IEEE Service Center, Piscataway, pp 28–30
- Wegener M, Paaajanen M, Voronina O, Schulze R, Wirges W, Gerhard-Multhaupt R (2005c) Voided cyclo-olefin polymer films: ferroelectrets with high thermal stability. In: Proceedings of 12th international symposium electrets, IEEE Service Center, Piscataway, pp 47–50

- Wirges W, Wegener M, Voronina O, Zirkel L, Gerhard-Multhaupt R (2007) Optimized preparation of elastically soft, highly piezoelectric cellular ferroelectrets from nonvoided poly(ethylene terephthalate) films. *Adv Funct Mater* 17:324–329
- Xia Z, Gerhar-Multhaupt R, Künstler W, Wedel A, Dan R (1999) High surface-charge stability of porous polytetrafluoroethylene electret films at room and elevated temperatures. *J Phys D Appl Phys* 32:L83
- Yang ZH, Wang J, Zhang JW (2012) Research and development of micro electret power generators. *SCIENCE CHINA Technol Sci* 55(3):581–587
- Zhang X, Hillenbrand J, Sessler GM (2004) Piezoelectric  $d_{33}$  coefficient of cellular polypropylene subjected to expansion by pressure treatment. *Appl Phys Lett* 85:1226–1228
- Zhang X, Hillenbrand J, Sessler GM (2006) Thermally stable fluorocarbon ferroelectrets with high piezoelectric coefficient. *Appl Phys A Mater Sci Process* 84:139–142
- Zhang X, Hillenbrand J, Sessler GM (2007) Ferroelectrets with improved thermal stability made from fused fluorocarbon layers. *J Appl Phys* 101:054114
- Zhang X, Wang X, Cao G, Pan D, Xia Z (2009) Polytetrafluoroethylene piezoelectrets prepared by sintering process. *Appl Phys A Mater Sci Process* 97:859–862
- Zhang X, Cao G, Sun Z, Xia Z (2010) Fabrication of fluoropolymer piezoelectrets by using rigid template: structure and thermal stability. *J Appl Phys* 108:064113
- Zhang X, Hillenbrand J, Sessler GM, Haberzettl S, Lou K (2012) Fluoroethylenepropylene ferroelectrets with patterned microstructure and high, thermally stable piezoelectricity. *Appl Phys A Mater Sci Process* 107:621–629
- Zhang X, Sessler GM, Wang Y (2014a) Fluoroethylenepropylene ferroelectret films with cross-tunnel structure for piezoelectric transducers and micro energy harvesters. *J Appl Phys* 116:074109
- Zhang X, Zhang X, Sessler GM, Gong X (2014b) Quasi-static and dynamic piezoelectric responses of layered polytetrafluoroethylene ferroelectrets. *J Phys D Appl Phys* 47:015501
- Zhukov S, von Seggern H (2007a) Breakdown-induced light emission and poling dynamics of porous fluoropolymers. *J Appl Phys* 101:084106
- Zhukov S, von Seggern H (2007b) Polarization hysteresis and piezoelectricity in open-porous fluoropolymer sandwiches. *J Appl Phys* 102:044109
- Zhukov S, Fedosov S, von Seggern H (2011) Piezoelectrets from sandwiched porous polytetrafluoroethylene (ePTFE) films: influence of porosity and geometry on charging properties. *J Phys D Appl Phys* 44(10):105501

## Thermal poling of ferroelectrets: How does the gas temperature influence dielectric barrier discharges in cavities?

Xunlin Qiu,<sup>a)</sup> Werner Wirges, and Reimund Gerhard

*Applied Condensed-Matter Physics, Department of Physics and Astronomy, Faculty of Science, University of Potsdam, Karl-Liebknecht-Str. 24-25, 14476 Potsdam-Golm, Germany*

(Received 25 April 2016; accepted 7 June 2016; published online 20 June 2016)

The influence of the temperature in the gas-filled cavities on the charging process of ferroelectret film systems has been studied in hysteresis measurements. The threshold voltage and the effective polarization of the ferroelectrets were determined as functions of the charging temperature  $T_p$ . With increasing  $T_p$ , the threshold voltage for triggering dielectric barrier discharges in ferroelectrets decreases. Thus, increasing the temperature facilitates the charging of ferroelectrets. However, a lower threshold voltage reduces the attainable remanent polarization because back discharges occur at lower charge levels, as soon as the charging voltage is turned off. The results are discussed in view of Paschen's law for electrical breakdown, taking into account the respective gas temperature and a simplified model for ferroelectrets. Our results indicate that the thermal poling scheme widely used for conventional ferroelectrics is also useful for electrically charging ferroelectrets. Published by AIP Publishing. [<http://dx.doi.org/10.1063/1.4954263>]

Ferroelectrets (sometimes also called piezoelectrets) are relatively new members of the family of piezo-, pyro-, and ferroelectric materials.<sup>1–5</sup> As their name indicates, ferroelectrets are space-charge electrets that show ferroic behavior. They are non-uniform electret materials or materials systems with electrically charged internal cavities. As space-charge electrets, ferroelectrets usually do not contain any molecular dipoles. However, the cavities inside the material can be turned into macroscopic dipoles through a series of microplasma discharges at high electric fields, so-called dielectric barrier discharges (DBDs).<sup>6–8</sup> The gas inside the cavities is ionized when the internal electric field exceeds the threshold for electrical breakdown, generating charges of both polarities.<sup>9</sup> The positive and negative charges travel in opposite directions, and are eventually trapped at the internal top and bottom surfaces of the cavities, respectively. After charging, the cavities may be regarded as macroscopic dipoles that can be switched by reversing the applied voltage.

An electric-polarization-vs.-electric-field ( $P(E)$ ) hysteresis is considered as an essential criterion for ferroelectricity.  $P(E)$ -hysteresis curves are usually characterized by the spontaneous polarization, the coercive field, and the remanent polarization. Recently, we have demonstrated  $P(E)$ -hysteresis loops on two different types of ferroelectrets, namely, cellular polypropylene ferroelectrets and tubular-channel fluoroethylene-polypropylene copolymer ferroelectrets.<sup>10,11</sup> The  $P(E)$ -hysteresis loops not only prove the ferroic behavior of ferroelectrets, but also allow us to determine such parameters as the coercive field and the remanent polarization.

It is widely accepted that Paschen breakdown is the underlying mechanism for the inception of DBDs in ferroelectrets.<sup>12–14</sup> On this basis, the charging behavior and the resulting piezoelectricity of ferroelectrets in different gases at various pressures have been studied.<sup>15–17</sup> Paschen's law

describes the conditions for electrical breakdown in a gas at a constant temperature (usually room temperature), and it needs to be modified for gas breakdown at other temperatures. The temperature stability of the piezoelectricity in ferroelectrets after charging at elevated temperatures was investigated by several researchers.<sup>18–21</sup> Recently, a preliminary report about the effects of the charging temperature on the hysteresis loops in ferroelectrets has been presented.<sup>22</sup>

In this letter, the influence of the gas temperature on the charging of ferroelectret systems is investigated in more detail by means of quasi-ferroelectric hysteresis-loop measurements. Teflon<sup>TM</sup> fluoroethylenepropylene (FEP) copolymer samples with tubular channels were prepared via thermal lamination as described previously.<sup>23</sup> To this end, two FEP films with a thickness of 50  $\mu\text{m}$  each were laminated at 300 °C around a 100  $\mu\text{m}$  thick polytetrafluoroethylene (PTFE) template (total area 35 mm  $\times$  45 mm) that contains parallel rectangular openings (area 1.5 mm  $\times$  40 mm each). After lamination, the template was removed, which results in an FEP film system with open tubular channels. The samples were metallized on both surfaces with aluminum electrodes of 20 mm diameter.

$P(E)$ -hysteresis loops were obtained with a modified Sawyer–Tower (ST) circuit.<sup>10,11</sup> A high-voltage (HV) capacitor  $C_1$  (3 nF) and a large standard capacitor  $C_m$  (1  $\mu\text{F}$ ) were connected in series with the sample. A bipolar sinusoidal voltage with a frequency of 10 mHz was applied from an HV power supply (FUG HCB 7-6500) controlled by an arbitrary-waveform generator (HP 33120a). The voltage  $V_{\text{out}}$  on  $C_m$  is measured by means of an electrometer (HP 3458a), and the charge flowing through the circuit is determined as  $Q(t) = C_m V_{\text{out}}(t)$ . The experiments were carried out at isothermal conditions in a Novocontrol<sup>®</sup> Quatro cryosystem.

With the modified ST circuit,  $Q$ - $V$  loops have been measured on a tubular-channel FEP ferroelectret system at different temperatures. The sample capacitance of about 34.5 pF is determined by a linear fit of the initial part of the  $Q$ - $V$  curve recorded at 20 °C, where the voltage has been

<sup>a)</sup>Electronic mail: xunlin.qiu@uni-potsdam.de

raised up from zero on a fresh sample. The hysteresis loops are obtained from the  $Q$ - $V$  curves by subtracting the contribution that results from charging of the sample capacitance.<sup>10</sup> Figure 1 shows the hysteresis loops of the sample at  $-100$ ,  $0$ , and  $+100$  °C, respectively. According to previous theoretical and experimental studies,<sup>24,25</sup> the length of each of the horizontal sides of the parallelogram-like hysteresis loops is given by  $2V_{th}$  where  $V_{th}$  is the threshold voltage. As the charging temperature decreases, the hysteresis loop becomes wider and less high, i.e., the threshold voltage increases, while the polarization at maximum voltage decreases.

Paschen breakdown has been identified to be essential for triggering the DBD charging process in ferroelectrets.<sup>9</sup> According to Paschen's law, the critical breakdown voltage  $V_B$  of common gases in a uniform electric field is a function of the product of the gas pressure  $p$  and the gap height  $d$  (which inside a ferroelectret is equal to the cavity height).<sup>26</sup> However, Paschen's law is usually written down for room temperature ( $T_0 = 293$  K). The inception of gas breakdown is caused by the acceleration of electrons in the applied electric field  $E$ . The energy gain of electrons is proportional to the product  $El$  where  $l$  represents the mean free path, i.e., the mean distance that electrons travel between two consecutive collisions. Since  $l$  strongly depends on temperature, Paschen's law must be modified for different temperatures.<sup>27-30</sup>

Figure 2 shows the threshold voltage for DBD charging of the tubular-channel FEP copolymer-film system as a function of gas temperature (solid circles). It is found that the threshold voltage strongly depends on the gas temperature. A value of about 2030 V is observed at  $-100$  °C, and the threshold voltage decreases with increasing temperature. At  $0$  and  $100$  °C, the threshold voltages are 1600 and 1200 V, respectively. With increasing temperature, some of the gas molecules leave the open channels. The gas density inside the cavities decreases and thus the mean free path of the electrons increases. Consequently, the threshold voltage decreases because the longer mean free path permits the electrons to gain more energy prior to the next collision.

In our experiments, the internal gas pressure is equal to the external atmospheric pressure because the cavities are

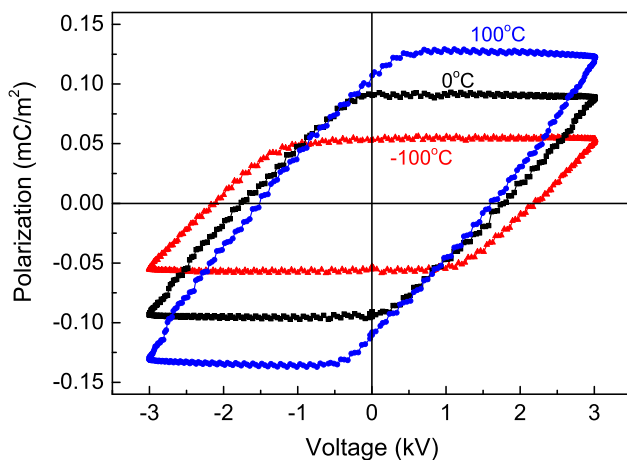


FIG. 1. Hysteresis curves of the tubular-channel FEP ferroelectret system measured at three different temperatures as indicated.

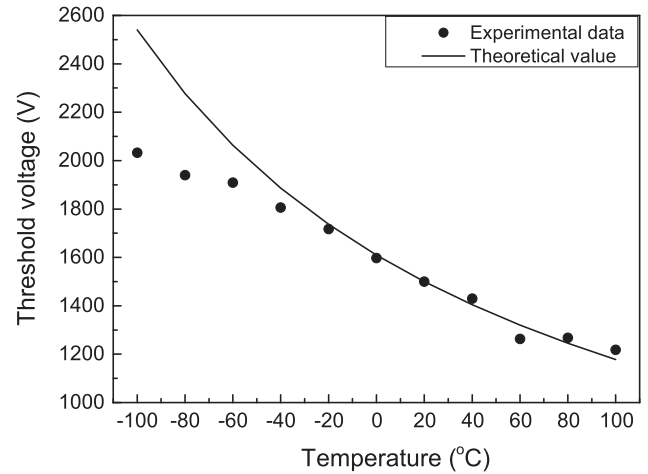


FIG. 2. Experimental and theoretical threshold voltage as functions of the charging temperature.

open. According to the so-called Peek correction,<sup>27</sup> the breakdown voltage of the cavities is inversely proportional to the gas temperature. Thus, the threshold voltage of the sample at a gas temperature  $T$  is given by

$$V_{th} = c \frac{T_0}{T} V_{B0}, \quad (1)$$

where  $c = 1 + 2d_{FEP}/(\epsilon_{FEP}d_g)$  ( $d_{FEP}$  and  $\epsilon_{FEP}$  are the thickness and the relative dielectric permittivity of the FEP films, respectively, and  $d_g$  is the height of the cavities).  $cV_{B0}$  is the threshold voltage for the sample at room temperature of  $T_0 = 293$  K. Making use of the measured threshold voltage at room temperature, the values for other temperatures are calculated from Eq. (1) (solid line in Fig. 2).

As shown in Fig. 2, the theoretical curve agrees reasonably well with the experimental data. At temperatures below  $-60$  °C, however, the experimentally observed threshold voltages are considerably lower than the respective theoretical values. As the Peek correction is based on the ideal gas law, we might expect deviations at low temperatures and/or high pressures along the predictions of the van der Waals equation for real gases if rather constant cavity volumes are assumed. Furthermore, sample and cavity geometries, as well as surface conditions of the electret layers, might change with temperature and DBD exposure and might also lead to lower threshold voltages. Modified surface conditions have been observed in space environments after low-temperature and plasma exposure,<sup>31</sup> and partially reversible surface fatigue was found after long-term DBD experiments.<sup>32</sup> More detailed investigations of these and other contributions to the temperature behavior of ferroelectret charging are desirable, but beyond the scope of the present study.

Figure 2 shows that an increase of the gas temperature leads to a decrease in the threshold voltage, allowing for DBD charging of ferroelectrets at lower poling fields. Thus, we have identified another parameter that behaves phenomenologically in exactly the same manner for ferroelectrets as for ferroelectric polymers such as  $\beta$ -phase poly(vinylidene fluoride) (PVDF). However, the underlying microscopic



mechanism is quite different. In ferroelectric polymers, the lower coercive field at elevated temperature is mainly due to a higher mobility of the molecular dipoles in a thermally softened polymer.<sup>33</sup>

The effective polarization  $P_{\text{eff}}$ , i.e., the density of the macroscopic dipoles, is an essential parameter for the application of ferroelectrets, since the piezoelectric sensitivity of a device is proportional to  $P_{\text{eff}}$ . According to earlier studies, the effective polarization in ferroelectrets strongly depends on the threshold voltage.<sup>24,25</sup> When a fresh sample is charged at a voltage  $V$ , the effective polarization at the respective voltage  $V$  is given by

$$P_{\text{eff}} = \begin{cases} 0 & (V < V_{\text{th}}) \\ k(V - V_{\text{th}}) & (V \geq V_{\text{th}}), \end{cases} \quad (2)$$

where  $k$  is a sample-specific parameter. The effective remanent polarization (the polarization after the voltage has been turned off) can be expressed as

$$P_{\text{rem}} = \begin{cases} 0 & (V < V_{\text{th}}) \\ k(V - V_{\text{th}}) & (V_{\text{th}} \leq V \leq 2V_{\text{th}}) \\ kV_{\text{th}} & (V > 2V_{\text{th}}). \end{cases} \quad (3)$$

From Eqs. (2) and (3),  $P_{\text{rem}}$  is equal to  $P_{\text{eff}}$  when the charging voltage is smaller than  $2V_{\text{th}}$ .  $P_{\text{rem}}$  reaches its maximum of  $kV_{\text{th}}$  when  $V = 2V_{\text{th}}$  and saturates for charging voltages higher than  $2V_{\text{th}}$ .<sup>24,25</sup> Before saturation is reached, a decrease in  $V_{\text{th}}$  will lead to increases in  $P_{\text{eff}}$  and  $P_{\text{rem}}$ . However, when  $V > 2V_{\text{th}}$ , a decrease in  $V_{\text{th}}$  would still lead to an increase in  $P_{\text{eff}}$ , but will also cause a decrease in  $P_{\text{rem}}$ . For tubular-channel FEP ferroelectret systems,  $P_{\text{eff}}$  at a maximum voltage of 3 kV and  $P_{\text{rem}}$  at zero voltage are extracted from the hysteresis loops at different temperatures (Fig. 3). As expected,  $P_{\text{rem}}$  is equal to  $P_{\text{eff}}$  at the maximum charging voltage for temperatures lower than 20°C where saturation cannot be reached. For higher temperatures,  $V_{\text{th}}$  becomes so low that saturation takes place. Now,  $P_{\text{eff}}$  at the maximum

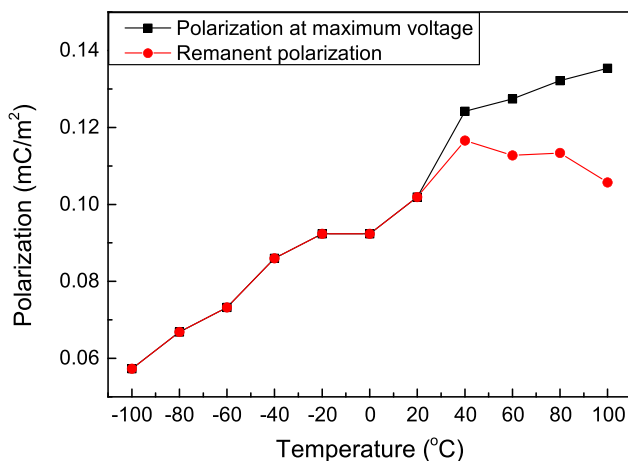


FIG. 3. Polarization  $P_{\text{max}}$  at the maximum charging voltage and remanent polarization  $P_{\text{rem}}$  as functions of charging temperature. For charging temperatures lower than 40°C, saturation of the polarization is not reached, and  $P_{\text{rem}}$  takes the same value as the respective  $P_{\text{max}}$ . For higher charging temperatures,  $P_{\text{max}}$  increases and  $P_{\text{rem}}$  decreases with gas temperature.

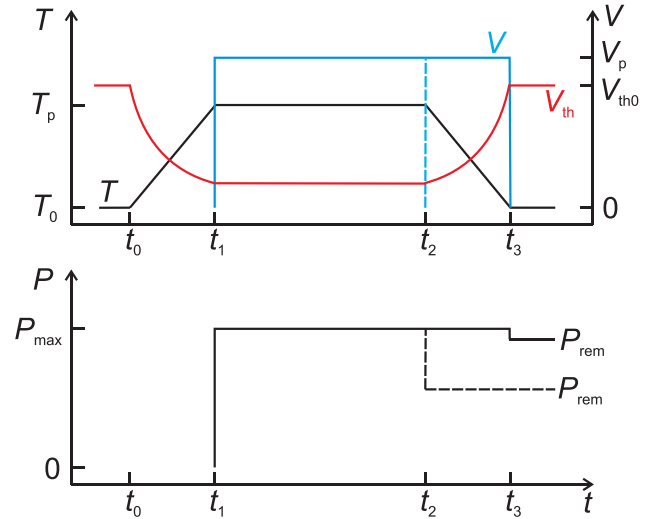


FIG. 4. Thermal poling scheme for ferroelectrets.

charging voltage increases and  $P_{\text{rem}}$  decreases with increasing gas temperature.

Based on our results, we propose a *thermal poling scheme* for ferroelectrets, as schematically depicted in Fig. 4. For charging, the ferroelectret specimen is first heated up (the temperature increases from  $T_0$  at  $t_0$  to  $T_p$  at  $t_1$ ), so that the threshold voltage  $V_{\text{th}}$  is significantly reduced. At  $t_1$  the charging voltage is applied at the preset charging temperature ( $T_p$ ). However, if the saturation of the polarization is exceeded at  $T_p$ , the lower  $V_{\text{th}}$  results in a lower remanent polarization  $P_{\text{rem}}$  when the charging voltage is switched off at  $t_2$  when the temperature is still  $T_p$  (dashed line in the lower part of Fig. 4). In order to achieve a higher  $P_{\text{rem}}$  (solid line in the lower half of Fig. 4), the ferroelectret specimen should be cooled down from  $T_p$  at  $t_2$  to  $T_0$  at  $t_3$  while the voltage is still on, as usually also done during the poling of ferroelectric polymers. As schematically shown in Fig. 4 (bottom part), the polarization builds up almost instantaneously upon application of the charging voltage. This is because DBDs in ferroelectrets are extremely fast events that occur on a time scale of ns.<sup>6</sup> Therefore, one can cool down the ferroelectret sample immediately after the voltage is switched on at  $t_1$ . In the thermal poling of conventional ferroelectrics, the temperature is usually maintained at  $T_p$  for a relatively long period of time ( $t_2 - t_1$  amounts several minutes to several hours), in order to orient the molecular dipoles as completely as possible. Thus, thermal poling can be much more time-efficient on ferroelectrets than on ferroelectric polymers.

The thermal stability of the piezoelectricity is an essential issue for most applications and is mainly governed by the stabilities of both charge polarities on the electret material in the case of ferroelectrets. Above specific elevated temperatures, charges captured in an electret are thermally de-trapped, which leads to a decay of the charge density and consequently also the piezoelectricity in ferroelectrets.<sup>33</sup> The present study, however, indicates that the decay of the piezoelectricity of an already charged ferroelectret at elevated temperature might also be caused, at least in part, by back discharges due to the decrease in  $V_{\text{th}}$ , even if the temperature is not high enough for the de-trapping of some of the internal

electret charges. Thus, we have identified another important factor that needs to be considered for the thermal stability of the piezoelectricity in ferroelectrets.

In conclusion, the charging behavior of ferroelectrets at different temperatures has been studied. Even though the charging/poling mechanisms and the ferroelectric behaviors of ferroelectrics and ferroelectrets are quite different, the charging or poling temperature is an important parameter that affects the coercive field, the polarization, and the observed hysteresis. A thermal poling scheme is proposed for more efficient charging of ferroelectrets. The ferroelectret sample to be charged is first heated up to a suitable elevated temperature in order to lower the threshold voltage. The charging voltage is applied when the preset charging temperature  $T_p$  is reached. Then the sample is cooled down, and the charging voltage is not switched off until the temperature returns to its initial value, so that a higher remanent polarization is attained.

- <sup>1</sup>R. Gerhard-Mulhaupt, *IEEE Trans. Dielectr. Electr. Insul.* **9**, 850–859 (2002).
- <sup>2</sup>S. Bauer, R. Gerhard-Mulhaupt, and G. M. Sessler, *Phys. Today* **57**(2), 37–43 (2004).
- <sup>3</sup>M. Wegener and S. Bauer, *Chem. Phys. Chem.* **6**, 1014–1025 (2005).
- <sup>4</sup>S. Bauer, *IEEE Trans. Dielectr. Electr. Insul.* **13**, 953–962 (2006).
- <sup>5</sup>X. Qiu, *J. Appl. Phys.* **108**, 011101 (2010).
- <sup>6</sup>M. Lindner, S. Bauer-Gogonea, S. Bauer, M. Paajanen, and J. Raukola, *J. Appl. Phys.* **91**, 5283–5287 (2002).
- <sup>7</sup>M. Lindner, H. Hoislbauer, R. Schwödiauer, S. Bauer-Gogonea, and S. Bauer, *IEEE Trans. Dielectr. Electr. Insul.* **11**, 255–263 (2004).
- <sup>8</sup>X. Qiu, A. Mellinger, M. Wegener, W. Wirges, and R. Gerhard, *J. Appl. Phys.* **101**, 104112 (2007).
- <sup>9</sup>X. Qiu, R. Gerhard, and A. Mellinger, *IEEE Trans. Dielectr. Electr. Insul.* **18**, 34–42 (2011).
- <sup>10</sup>X. Qiu, L. Holländer, W. Wirges, R. Gerhard, and H. C. Basso, *J. Appl. Phys.* **113**, 224106 (2013).
- <sup>11</sup>X. Qiu, W. Wirges, and R. Gerhard, *Ferroelectrics* **472**, 100–109 (2014).
- <sup>12</sup>G. M. Sessler and J. Hillenbrand, *Appl. Phys. Lett.* **75**, 3405–3407 (1999).
- <sup>13</sup>M. Wegener, M. Paajanen, W. Wirges, and R. Gerhard-Mulhaupt, in *Proceedings of the 11th International Symposium on Electrets* (IEEE Service Center, Piscataway, NJ, 2002), pp. 54–57.
- <sup>14</sup>S. Harris and A. Mellinger, *J. Appl. Phys.* **115**, 163302 (2014).
- <sup>15</sup>M. Paajanen, M. Wegener, and R. Gerhard-Mulhaupt, *J. Phys. D: Appl. Phys.* **34**, 2482–2488 (2001).
- <sup>16</sup>X. Qiu, M. Wegener, W. Wirges, X. Zhang, J. Hillenbrand, Z. Xia, R. Gerhard-Mulhaupt, and G. M. Sessler, *J. Phys. D: Appl. Phys.* **38**, 649–654 (2005).
- <sup>17</sup>X. Qiu, A. Mellinger, and R. Gerhard, *Appl. Phys. Lett.* **92**, 052901 (2008).
- <sup>18</sup>X. Qiu, Z. Xia, F. Wang, and Z. An, *J. Sichuan Univ. (Nat. Sci. Ed.)* **42**, 159–161 (2005).
- <sup>19</sup>X. Zhang, J. Hillenbrand, and G. M. Sessler, *J. Appl. Phys.* **101**, 054114 (2007).
- <sup>20</sup>P. Fang, X. Qiu, W. Wirges, R. Gerhard, and L. Zirkel, *IEEE Trans. Dielectr. Electr. Insul.* **17**, 1079 (2010).
- <sup>21</sup>J. Zhang, L. Lebrun, B. Guiffard, R. Belouadah, D. Guyomar, L. Garbuio, P. Cottinet, and Q. Liu, *J. Phys. D: Appl. Phys.* **44**, 415403 (2011).
- <sup>22</sup>X. Qiu, M. Steffen, W. Wirges, and R. Gerhard, in *IEEE Conference on Electrical Insulation and Dielectric Phenomena, Annual Report* (IEEE Service Center, Piscataway, NJ, 2015), pp. 644–647.
- <sup>23</sup>R. A. P. Altafim, X. Qiu, W. Wirges, R. Gerhard, R. A. C. Altafim, H. C. Basso, W. Jenninger, and J. Wagner, *J. Appl. Phys.* **106**, 014106 (2009).
- <sup>24</sup>P. Zhang, Z. Xia, X. Qiu, F. Wang, and X. Y. Wu, in *Proceedings of the IEEE 12th International Symposium on Electrets* (IEEE Service Center, Piscataway, NJ, 2005), pp. 39–42.
- <sup>25</sup>S. Zhukov and H. von Seggern, *J. Appl. Phys.* **102**, 044109 (2007).
- <sup>26</sup>E. M. Bazelyan and Y. P. Raizer, *Spark Discharge* (CRC, Boca Raton, FL, 1998).
- <sup>27</sup>F. W. Peek, see <https://archive.org/stream/dielectricphenom00peekrich#page/42/mode/2up> for *Dielectric Phenomena in High Voltage Engineering* (McGraw-Hill Book Company, New York, 1915, 1920, and 1929).
- <sup>28</sup>W. G. Dunbar and J. W. Seabrook, see <http://www.dtic.mil/get-tr-doc/pdf?AD=ADA029268> for *High Voltage Design Guide for Airborne Equipment*, Report No. AFAPL-TR-76-41 (Boeing Aerospace Company, Seattle, WA, 1976).
- <sup>29</sup>H. S. Uhm, S. J. Jung, and S. Kim, *J. Korean Phys. Soc.* **42**, S989–S993 (2003).
- <sup>30</sup>E. Sili, F. Koliatene, and J. P. Cambronne, in *IEEE Conference on Electrical Insulation and Dielectric Phenomena, Annual Report* (IEEE Service Center, Piscataway, NJ, 2011), pp. 464–467.
- <sup>31</sup>J. A. Dever, K. K. de Groh, B. A. Banks, J. A. Townsend, J. L. Barth, S. Thomson, T. Gregory, and W. Savage, *High Perform. Polym.* **12**, 125–139 (2000).
- <sup>32</sup>X. Qiu and R. Gerhard, *Appl. Phys. Lett.* **93**, 152902 (2008).
- <sup>33</sup>G. M. Sessler and R. Gerhard-Mulhaupt, *Electrets*, 3rd ed. (Laplacian Press, Morgan Hill, CA, 1999), Vol. 2.

## Significant enhancement of the charging efficiency in the cavities of ferroelectrets through gas exchange during charging

Xunlin Qiu<sup>a)</sup>

*Applied Condensed-Matter Physics, Department of Physics and Astronomy, Faculty of Science, University of Potsdam, Karl-Liebknecht-Str. 24-25, 14476 Potsdam-Golm, Germany*

(Received 24 September 2016; accepted 17 November 2016; published online 1 December 2016)

Ferroelectrets are non-polar polymer foams or polymer systems with internally charged cavities. They are charged through a series of dielectric barrier discharges (DBDs) that are caused by the electrical breakdown of the gas inside the cavities. Thus, the breakdown strength of the gas strongly influences the charging process of ferroelectrets. A gas with a lower breakdown strength has a lower threshold voltage, thus decreasing the onset voltage for DBD charging. However, a lower threshold voltage also leads to a lower value for the remanent polarization, as back discharges that are caused by the electric field of the internally deposited charges can take place already at lower charge levels. On this basis, a charging strategy is proposed where the DBDs start in a gas with a lower breakdown strength (in the present example, helium) and are completed at a higher breakdown strength (e.g., nitrogen or atmospheric air). Thus, the exchange of the gas in the cavities during charging can significantly enhance the charging efficiency, i.e., yield much higher piezoelectric coefficients in ferroelectrets at significantly lower charging voltages. *Published by AIP Publishing.* [<http://dx.doi.org/10.1063/1.4971259>]

The demand for advanced functional materials in transducer technology is growing rapidly nowadays. As relatively new piezo-, pyro-, and ferroelectric materials, ferroelectrets have attracted more and more attention. They are non-polar polymer foams or polymer systems with internally charged cavities.<sup>1–5</sup> Like in the case of ferroelectric polymers, such as  $\beta$ -phase poly(vinylidene fluoride) (PVDF), charging/poling is a critical step for ferroelectrets. However, the mechanism for charging/poling is completely different. Charging of ferroelectrets is achieved through a series of dielectric barrier discharges (DBDs) inside the cavities.<sup>6,7</sup> In DBDs, at least one side of the discharge gap is insulated from the respective electrode by means of a dielectric layer.<sup>8</sup> DBDs are triggered by applying a voltage that exceeds the threshold for the Paschen breakdown, generating charges of both polarities. Being driven by the applied electric field, the positive and negative charges will travel in opposite directions and finally deposit onto the top and bottom internal surfaces of the cavities, respectively. After DBD charging, the cavities can be considered as macroscopic dipoles. The direction of the macroscopic dipoles can be reversed by changing the polarity of the applied voltage, and hence polarization-versus-electric-field ( $P(E)$ ) hysteresis curves are observed, which are phenomenologically indistinguishable from those found on other ferroic materials.<sup>9,10</sup>

Since DBD charging relies on breakdown of the gas, the breakdown strength of the gas inside the cavities has a strong influence on the charging process in ferroelectrets.<sup>11–14</sup> For a given ferroelectret sample, the threshold voltage  $V_{th}$  is essentially determined by the breakdown strength of the gas inside the cavities. Different gases may have quite different breakdown strengths. For instance, it is reported that the electrical

strength of helium at atmospheric pressure is only 15% that of nitrogen under similar conditions.<sup>15</sup> In this letter, a charging strategy involving the exchange of gases with different breakdown strengths is investigated. The method can significantly enhance the charging efficiency of ferroelectret systems. Teflon<sup>TM</sup> fluoroethylenepropylene (FEP) copolymer film systems with tubular channels were prepared via thermal lamination as described elsewhere.<sup>16</sup> Two FEP films with a thickness of 50  $\mu\text{m}$  each were laminated at 300 °C around a 100  $\mu\text{m}$  thick polytetrafluoroethylene (PTFE) template (total area 35 mm  $\times$  45 mm) that contains parallel rectangular openings (area 1.5 mm  $\times$  40 mm each). After lamination, the template was removed, which results in an FEP film system with open tubular channels. The samples were metallized on both surfaces with circular aluminum electrodes that are 20 mm in diameter.

$P(E)$  hysteresis loops were obtained with a modified Sawyer–Tower (ST) circuit.<sup>9,10</sup> Two high-voltage (HV) capacitors  $C_1$  (3 nF) and  $C_m$  (1  $\mu\text{F}$ ) were connected in series with the sample. A bipolar sinusoidal voltage with a frequency of 10 mHz was applied by means of an HV power supply (FUG HCB 7-6500) controlled by a waveform generator (HP 33120a). The voltage  $V_{out}$  across  $C_m$  is measured by means of an electrometer (HP 3458a), and the charge flowing through the circuit is determined as  $Q(t) = C_m V_{out}(t)$ . The samples were mounted in a pressure chamber that was connected to a pumping system. The gas inside the chamber can be pumped out, and the desired gas at various pressures can be fed in. Direct piezoelectric  $d_{33}$  coefficients were determined by means of a dynamic method.<sup>17</sup> A sinusoidal force with an amplitude of 1 N and a frequency of 2 Hz (Brüel&Kjær model 4810 shaker), superimposed with a static bias force of 3 N, was applied to the sample. The resulting electric response of the sample was amplified

<sup>a)</sup>Electronic mail: xunlin.qiu@uni-potsdam.de

(Brüel&Kjær model 2635 charge amplifier) and recorded on a digital oscilloscope. From the applied force and the resulting electrical signal, the respective  $d_{33}$  coefficients were calculated.

With the modified ST circuit,  $Q$  vs.  $V$  loops of the samples were measured, from which the hysteresis loops were obtained by subtracting the capacitive-charging contribution and by taking into account the electrode area.<sup>10</sup> Figure 1 shows the hysteresis loops measured in atmospheric air on a tubular-channel FEP ferroelectret at increasing voltage amplitudes as indicated. No hysteresis is observed at an amplitude of 1 kV, since the threshold for DBDs in the air-filled cavities has not been reached. A noticeable loop is measured at a voltage amplitude of 1.7 kV. Then, the height of the hysteresis loops increases with the increasing voltage amplitude. Theoretically, the width of the hysteresis loops should remain unchanged with increasing voltage amplitude if the cavities have uniform dimensions.<sup>18,19</sup> Figure 1 shows that the width of the hysteresis loops slightly increases with the growing voltage amplitude, which might be caused by the non-uniform cavity dimensions that cannot be avoided in laboratory experiments.

Hysteresis loops for a tubular-channel FEP ferroelectret, as measured in helium at atmospheric pressure, are depicted in Fig. 2. The sample was first subjected to vacuum pumping for about 15 min, and then helium at atmospheric pressure was fed into the chamber. With the pressure chamber and the vacuum pump employed in the present study, a pressure value inside the chamber lower than 50 Pa is not easily attainable. In order to enhance the purity of the helium in the chamber, the procedure of pumping followed by feeding of helium had been carried out three times. Unlike in the first pumping where atmospheric air was pumped out, the newly introduced helium was removed again together with possible traces of air in the second and in the third pumping cycles. Such a repeated procedure is avoidable with a more efficient pumping system. Then, hysteresis loops at increasing voltage amplitudes were measured as detailed above. Owing to the lower breakdown strength of helium, a noticeable hysteresis loop was already found at a voltage amplitude of 500 V (Fig. 2). For voltage amplitudes higher than 1 kV, an obvious decrease of the

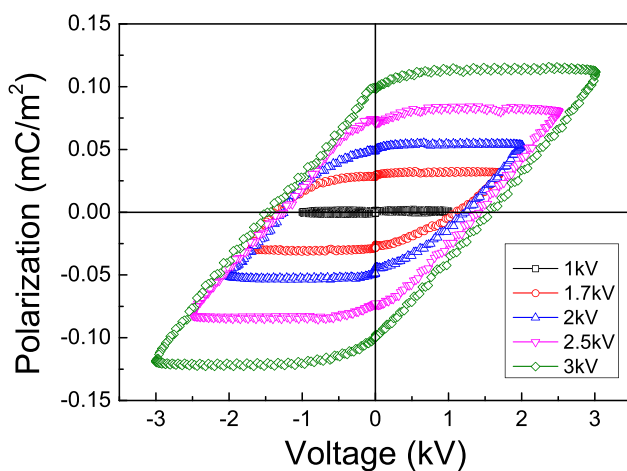


FIG. 1. Hysteresis loops for a tubular-channel FEP ferroelectret sample measured in atmospheric air with voltages of different amplitudes as indicated.

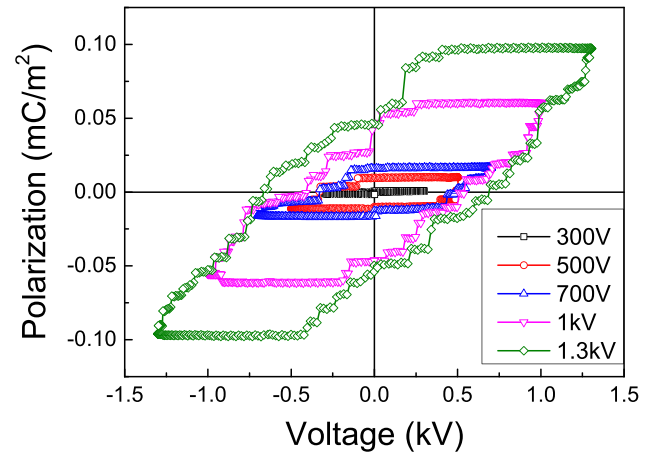


FIG. 2. Hysteresis loops for a tubular-channel FEP ferroelectret sample measured in helium at atmospheric pressure for different voltage amplitudes as indicated.

polarization is observed when the voltage decreases from its maximum back to zero. The decrease results from back discharges caused by the internally deposited charges.<sup>20</sup>

It is known that the DBD charging of ferroelectrets is triggered when the applied voltage exceeds the threshold  $V_{th}$ .<sup>21</sup> When a fresh sample is charged with a voltage  $V$ , the effective polarization  $P_{eff}$  (i.e., the density of the macroscopic dipoles) in the presence of the voltage is given by<sup>18,19</sup>

$$P_{eff} = \begin{cases} 0 & (V < V_{th}) \\ k(V - V_{th}) & (V \geq V_{th}), \end{cases} \quad (1)$$

where  $k$  is a sample-specific parameter. The effective remanent polarization (i.e., the polarization after the voltage has been turned off) may be expressed as

$$P_{rem} = \begin{cases} 0 & (V < V_{th}) \\ k(V - V_{th}) & (V_{th} \leq V \leq 2V_{th}) \\ kV_{th} & (V > 2V_{th}). \end{cases} \quad (2)$$

Figure 3 shows the effective polarizations at maximum voltage ( $P_{max}$ ) and at zero voltage ( $P_{rem}$ ) that are extracted

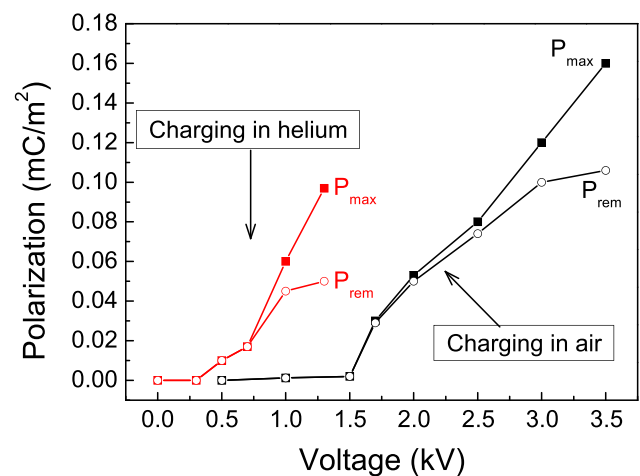


FIG. 3. Effective polarization at the maximum charging voltage ( $P_{max}$ ) and remanent polarization ( $P_{rem}$ ) as a function of the charging voltage.



from the hysteresis loops obtained for different voltage amplitudes. A threshold behavior is clearly observed both in air and in helium. In comparison, the threshold voltage in helium is more than two times lower than that in air. As can be seen from Fig. 3,  $P_{\max}$  and  $P_{\text{rem}}$  are nearly zero when the voltage is lower than the respective threshold voltage  $V_{\text{th}}$ . Above  $V_{\text{th}}$ ,  $P_{\max}$  and  $P_{\text{rem}}$  increase with increasing voltage. For applied voltages higher than about  $2V_{\text{th}}$ ,  $P_{\text{rem}}$  tends to saturate, although  $P_{\max}$  becomes still higher. Thus, the observations are in good agreement with Eqs. (1) and (2).

For applications of ferroelectrets, the piezoelectric  $d_{33}$  coefficient, which is essentially proportional to the remanent polarization  $P_{\text{rem}}$ , is an essential parameter.<sup>22</sup> The threshold behavior of the charging process in ferroelectrets is often investigated by measuring the piezoelectric  $d_{33}$  coefficient as a function of the charging voltage.<sup>21</sup> Here, a fresh tubular-channel FEP sample was employed in order to study the dependence of the  $d_{33}$  coefficient on the charging voltage. A  $d_{33}$  coefficient of about 5 pC/N was measured for the non-charged fresh sample, which might be attributed to charges introduced during the sample preparation. Then, the sample was charged in helium at atmospheric pressure again and again with stepwise increasing voltage. Prior to the charging at each voltage, helium was introduced into the chamber as detailed above. Each voltage was applied to the electrodes for 15 s by means of a high-voltage supply (Trek model 610D), followed by taking out the sample and measuring  $d_{33}$  under laboratory conditions. As seen in Fig. 4 (solid squares), the voltage dependence of the  $d_{33}$  coefficient clearly shows a threshold behavior. Above the threshold voltage of about 500 V, the  $d_{33}$  coefficient increases with increasing charging voltage. A saturation of  $d_{33}$  at about 20 pC/N is reached for voltages above 1.0 kV.

In order to achieve higher  $d_{33}$  coefficients, the sample should be charged to higher  $P_{\text{rem}}$  values. As shown in Fig. 3, a  $P_{\max}$  of about 0.1 mC/m<sup>2</sup> can be found at a maximum

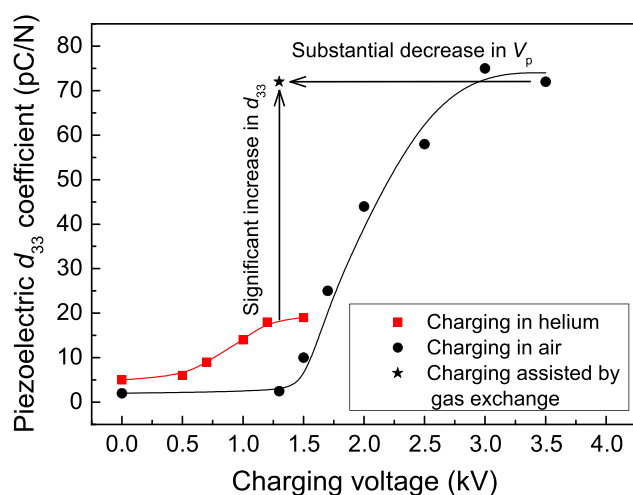


FIG. 4. The piezoelectric  $d_{33}$  coefficient of a tubular-channel FEP ferroelectret sample as a function of the charging voltage. Solid squares: The sample is charged in helium at atmospheric pressure. Solid star: The sample is first charged at a voltage of 1.3 kV in helium at atmospheric pressure, then helium is replaced with atmospheric air, while the charging voltage is maintained. The charging voltage is turned off after the gas exchange. Solid circles: The sample is charged in atmospheric air. Lines are only guides for the eye.

voltage of 1.3 kV when the sample is charged in helium. Unfortunately, the polarization is partly destroyed by back discharges when the voltage is reduced from its maximum back to zero. Figure 3 shows that a  $P_{\text{rem}}$  of 0.1 mC/m<sup>2</sup> can be sustained if the sample is charged in air, although at a much larger charging voltage. This observation suggests that the  $P_{\max}$  of 0.1 mC/m<sup>2</sup> in helium at a voltage of 1.3 kV can be retained (i.e.,  $P_{\text{rem}}$  of 0.1 mC/m<sup>2</sup>), if helium is replaced with air. The gas exchange must be done in the presence of the external electric field, so that back discharges are prevented. In order to confirm this, a voltage of 1.3 kV was applied to the sample in helium at atmospheric pressure. Then, nitrogen gas was fed into the chamber until the pressure reached 4 bar, followed by bringing the chamber back to the atmospheric pressure. In order to have a sufficiently low content of helium, the procedure of feeding in nitrogen at pressures up to 4 bar and subsequently releasing it to atmospheric pressure was repeated five times. Nitrogen gas was used, as it has a breakdown strength similar to that of air. The voltage was switched off only after the gas exchange was completed. Finally, the sample was taken out, and a  $d_{33}$  coefficient of 72 pC/N was observed (solid star in Fig. 4), which is substantially larger than the saturation value of  $d_{33}$  for charging in helium without any gas exchange.

On the same sample,  $d_{33}$  was recorded as a function of the voltage applied in atmospheric air. In order to erase the polarization generated in the previous measurements, the coercive voltage of  $-1.4$  kV in air (read from Fig. 1) was applied to the sample electrodes for 15 s. Afterward, a remaining  $d_{33}$  coefficient of only 0.6 pC/N was measured, indicating that the polarization in the sample had been erased almost completely. Then, the sample was charged in atmospheric air at stepwise increasing voltages, and  $d_{33}$  was measured after each charging step. The voltage dependence of the  $d_{33}$  coefficient is shown in Fig. 4 (solid circles). A threshold value of about 1.3 kV is observed, consistent with previous results.<sup>16</sup> The  $d_{33}$  coefficient saturates at about 73 pC/N for charging voltages above 3 kV. Thus, with the helium-assisted charging scheme proposed here, tubular-channel FEP film ferroelectrets are charged to saturation with a charging voltage less than half of the voltage required by charging only in atmospheric air.

From Fig. 3, a remanent polarization  $P_{\text{rem}}$  of 0.05 and 0.1 mC/m<sup>2</sup> is obtained for charging in helium and in air with atmospheric pressure, respectively. Therefore, the saturation  $d_{33}$  coefficient for charging in helium should be about half of that in air. However, Fig. 4 shows that the saturation  $d_{33}$  for charging in helium is considerably lower than half of that in air. In the present study,  $d_{33}$  coefficients were always measured in lab conditions, during which the helium molecules inside the open channels will be eventually replaced with atmospheric air. This observation probably indicates that further back discharges are triggered when transferring the sample from the helium-filled chamber to the dynamic  $d_{33}$  setup. According to Paschen's law, the critical breakdown voltage of common gases reaches its minimum at certain  $pd$  value ( $pd_{\min}$ ). DBDs in ferroelectrets are extremely fast events, any instantaneous change of the  $pd$  value towards  $pd_{\min}$  might lead to further back discharges.



By charging in air with high pressure, the charging efficiency of a cellular polypropylene (PP) ferroelectret is optimized.<sup>13</sup> In this way, small cavities, which cannot be charged in air with atmospheric pressure, are charged because the  $pd$  values move towards  $pd_{\min}$ . Here, high-pressure nitrogen gas is employed to retain the high polarization (under the charging voltage) introduced by the DBD charging in helium. Since the  $pd_{\min}$  in nitrogen is about 0.75 Pa·m and the channel height is about 100  $\mu\text{m}$ , with a  $p$  above atmospheric pressure, the actual  $pd$  value is already far on the right-hand side of the minimum in Paschen's curve. However, the pressure of helium might strongly influence the breakdown voltage. Further investigations are under way in order to determine the effect of gas pressure on the charging efficiency.

DBD charging is an essential step for the preparation of ferroelectrets. In the charging scheme proposed here, we make use of the lower breakdown strength of helium for easier triggering of DBDs, and we employ nitrogen with relatively higher breakdown strength to retain a higher remanent polarization. Compared with charging only in helium at atmospheric pressure, a significant increase of the  $d_{33}$  coefficient is achieved without the need for high charging voltages (*cf.* the vertical arrow in Fig. 4). The sample is charged to saturation with a voltage as low as the threshold for charging solely in atmospheric air (*cf.* the horizontal arrow in Fig. 4). The results presented here not only deepen the understanding of the underlying physical process in ferroelectrets but also are of great importance from a practical point of view. The substantially lowered charging voltage reduces high-voltage related complications and cost in the preparation of ferroelectrets. In addition, the development of new ferroelectrets is often restrained by insufficient charging efficiency, either because extremely high charging voltage that is not easily available is required, or because the charging voltage is so high that destructive electrical breakdown of the sample occurs. Therefore, the charging scheme proposed here increases significantly the flexibility in developing new ferroelectrets.

An earlier study on the dielectric strength of  $\text{N}_2$ -He mixtures shows that the breakdown voltage rises rapidly when the He content decreases from 100% to 95%.<sup>23</sup> Nevertheless, a He purity of about 99.5% is high enough to have sufficiently low breakdown strength. However, the complete removal of helium before switching off the charging voltage is not necessary, since the  $\text{N}_2$ -He mixture has a dielectric strength close to that of pure  $\text{N}_2$  when the He content is lower than about 10%.<sup>23</sup> In previous studies, gas exchange between the cavities and the surroundings was reported for ferroelectrets with closed foam structures. As confirmed by measurements of the sample capacitance, gas molecules diffuse through the polymer walls when the sample is subjected to vacuum or high-pressure gas. As a result, the internal and the external pressures equalize after sufficient waiting times.<sup>13,24</sup> Hence, the proposed charging scheme is also applicable to cellular-foam ferroelectrets, provided that sufficient time is allowed for the gas exchange.

In conclusion, the effect of a gas exchange during charging (gases with lower (helium) and higher (nitrogen or air) breakdown strengths) on the charging efficiency of ferroelectrets has been studied. Hysteresis measurements show that

filling the cavities with helium reduces the threshold voltage, allowing charging at much lower voltage. However, when the ferroelectret sample is charged to the levels above saturation, the lower threshold voltage leads to a lower remanent polarization because back discharges already occur at lower charge levels. Charging in gases with higher breakdown strengths requires higher voltages but allows for higher values of the remanent polarization. A charging scheme has been presented, during which a gas with lower breakdown strength is replaced by a gas with significantly higher breakdown strength in the presence of the charging voltage. Thus, the cavities are first filled with a gas with lower breakdown strength such as helium, so that DBDs can be easily triggered by applying a relatively low voltage. The charging voltage should not be turned off until the gas inside the cavities has been replaced with a gas having higher breakdown strength such as nitrogen or air, in order to achieve higher remanent polarization. With the charging scheme proposed here, the charging efficiency of ferroelectrets can be significantly enhanced.

The author is indebted to Professor Reimund Gerhard (University of Potsdam) for stimulating discussions and useful comments.

- <sup>1</sup>R. Gerhard-Mulhaupt, *IEEE Trans. Dielectr. Electr. Insul.* **9**, 850 (2002).
- <sup>2</sup>S. Bauer, R. Gerhard-Mulhaupt, and G. M. Sessler, *Phys. Today* **57**(2), 37 (2004).
- <sup>3</sup>M. Wegener and S. Bauer, *Chem. Phys. Chem.* **6**, 1014 (2005).
- <sup>4</sup>S. Bauer, *IEEE Trans. Dielectr. Electr. Insul.* **13**, 953 (2006).
- <sup>5</sup>X. Qiu, *J. Appl. Phys.* **108**, 011101 (2010).
- <sup>6</sup>M. Lindner, S. Bauer-Gogonea, S. Bauer, M. Paaanen, and J. Raukola, *J. Appl. Phys.* **91**, 5283 (2002).
- <sup>7</sup>X. Qiu, R. Gerhard, and A. Mellinger, *IEEE Trans. Dielectr. Electr. Insul.* **18**, 34 (2011).
- <sup>8</sup>U. Kogelschatz, *Plasma Chem. Plasma Process.* **23**, 1 (2003) and references therein.
- <sup>9</sup>X. Qiu, L. Holländer, W. Wirges, R. Gerhard, and H. C. Basso, *J. Appl. Phys.* **113**, 224106 (2013).
- <sup>10</sup>X. Qiu, W. Wirges, and R. Gerhard, *Ferroelectrics* **472**, 100 (2014).
- <sup>11</sup>M. Paaanen, M. Wegener, and R. Gerhard-Mulhaupt, *J. Phys. D: Appl. Phys.* **34**, 2482 (2001).
- <sup>12</sup>X. Qiu, M. Wegener, W. Wirges, X. Zhang, J. Hillenbrand, Z. Xia, R. Gerhard-Mulhaupt, and G. M. Sessler, *J. Phys. D: Appl. Phys.* **38**, 649 (2005).
- <sup>13</sup>X. Qiu, A. Mellinger, and R. Gerhard, *Appl. Phys. Lett.* **92**, 052901 (2008).
- <sup>14</sup>S. Harris and A. Mellinger, *Appl. Phys. A* **107**, 553 (2012).
- <sup>15</sup>A. K. Vijh, *J. Mater. Sci.* **11**, 1374 (1976).
- <sup>16</sup>R. A. P. Altafim, X. Qiu, W. Wirges, R. Gerhard, R. A. C. Altafim, H. C. Basso, W. Jenninger, and J. Wagner, *J. Appl. Phys.* **106**, 014106 (2009).
- <sup>17</sup>P. Fang, L. Holländer, W. Wirges, and R. Gerhard, *Meas. Sci. Technol.* **23**, 035604 (2012).
- <sup>18</sup>P. Zhang, Z. Xia, X. Qiu, F. Wang, and X. Y. Wu, in *IEEE 12th International Symposium on Electrets, IEEE Service Center, Piscataway, NJ* (2005), pp. 39–42.
- <sup>19</sup>S. Zhukov and H. von Seggern, *J. Appl. Phys.* **102**, 044109 (2007).
- <sup>20</sup>X. Qiu, A. Mellinger, M. Wegener, W. Wirges, and R. Gerhard, *J. Appl. Phys.* **101**, 104112 (2007).
- <sup>21</sup>M. Wegener, M. Paaanen, W. Wirges, and R. Gerhard-Mulhaupt, in *IEEE 11th International Symposium on Electrets, IEEE Service Center, Piscataway, NJ* (2002), pp. 54–57.
- <sup>22</sup>G. M. Sessler and J. Hillenbrand, *Appl. Phys. Lett.* **75**, 3405–3407 (1999).
- <sup>23</sup>J. M. Pelletier, Y. Gervais, and D. Mukhedkar, *IEEE Trans. Power Appar. Syst.* **PAS-100**(8), 3861 (1981).
- <sup>24</sup>X. Qiu, W. Wirges, R. Gerhard, and R. A. P. Altafim, in *2016 International Conference on Dielectrics, IEEE Service Center, Piscataway, NJ* (2016), pp. 872–875.

## **B Curriculum Vitae**

Pages 172 (resume) contain personal data and shall thus not be part of the online publication.

# Acknowledgments

This thesis would not have been possible without the support of the “Applied Condensed Matter Physics” group at the Department of Physics and Astronomy, University of Potsdam. First and foremost, I would like to thank Prof. Reimund Gerhard, whose stimulating comments and suggestions were a constant source of encouragement. My thanks also go to our group members. Prof. Axel Mellinger and Dr. Michael Wegener were very helpful discussion partners for everything concerning preparation of electret and ferroelectric materials, poling techniques, and electromechanical measurements. Dr. Peter Fröblich was never tired of being consulted on dielectric spectroscopy results, while Dr. Wolfgang Künstler supported me with his expertise in preparation and characterization of ferroelectric polymers. Dr. Guggi Kofod guided me through elastomers. Dr. Dmitry Rychkov readily shared his knowledge of charge stability in electret materials. Our engineers Andreas Pucher and Werner Wirges provided invaluable help when new equipment had to be designed and built, or broken equipment needed fast repair. I am also grateful to my students MSc. Martynas Sborikas, MSc. Nicolas Marroquin Jacobs, Dipl. Markus Steffen, and other student assistants for their diligent work for acquiring and analyzing the data. Of course, I would like to thank all other (past and present) group members— it was a great pleasure to work with you!

I am grateful to Sandra Zeretzke, Beatrice Unger and Marita Dörrwand, who often helped me dealing with administrative bureaucracy regarding business trips and contracts.

I would also like to thank our national and international cooperation partners. Special thanks go to Prof. Siegfried Bauer (University of Linz, Austria) for his kind support and encouragement, many stimulating discussions and warmly hosting my visits in his group. I am also grateful to Prof. Ruy Alberto Corrêa Altafim, Prof. Heitor Cury Basso (University of São Paulo, Brazil), Prof. Dante Luis Chinaglia (Universidade Estadual Paulista, Brazil), Prof. Ruy Alberto Pisani Altafim (Federal University of Paraíba, Brazil) for the hospitality and fruitful cooperations. I am also indebted to Prof. Wei Ren and his group members (Xi’an Jiaotong University, China) for the hospitality and cooperation in the investigation of the electrical and dielectric properties of ceramic-polymer composites, and Prof. Christian Laurent (University of Toulouse, France) and his group members Dr. Gilbert Teyssède and Eddy Aubert for performing highly sensitive light detection experiments.

Finally, my special thanks go to my wife for her love and support.

